FLUID INCLUSION PLANES IN SELECTED GRANITIC ROCKS OF THE BRITISH ISLES

Jonathan Mark Westerman

A thesis submitted in partial fulfilment of the
requirements of Kingston University
for the degree of Doctor of Philosophy

August 1995

ABSTRACT

When hydrothermal fluids flow through microfractures in quartz, they effectively heal (anneal) them to produce Fluid Inclusion Planes (FIPs). These FIPs are viewed as a three dimensional plane or array of secondary fluid inclusions and may be used to relate brittle deformation associated with tectonic, thermal and hydraulic stresses to contemporaneous hydrothermal events. In this study, FIPs have been interpreted in granitic quartz from various geological settings. Analysis of the FIPs includes recording their orientation, the morphological characteristics of both the FIPs and the inclusions contained within them, together with the thermometric properties of the inclusions. Results show that FIPs may possess a preferential orientation over a wide area, similar to the trend of macrostructures observed in the field. However, local deviations in the stress field, related to the proximity of possible second order faults, may cause local deviations in the orientation of the FIPs. The presence of high FIP abundances has also been linked to the widespread, localised development of kaolinisation (possibly linked to tectonic stresses) and greisenisation (possibly linked to thermal and hydraulic stresses). These phenomena have been identified at several localities in the field areas. It is presumed that intense microfracture networks will allow the wide-spread movement of hydrothermal fluids allowing pervasive alteration.

A classification scheme for FIPs has been devised, whereby FIPs may been classified as tensile, dilatant (*mode 1*) and dilatant shear (*mode 2*) fractures. This classification is based upon the orientation of the FIPs (to macrostructures), their proposed origin and their morphology (both the FIP and the inclusions contained within them). Variation in inclusion morphology has been recorded within selected FIPs. Inclusions have been observed to occur parallel and perpendicular (rare) to the length of the FIP. The presence of a preferred shape orientation in the inclusions has been attributed to a combination of fracturing and subsequent healing process, with controlling parameters including the temperature and chemistry of the fluids (affecting crack lifetimes) together with the geometry of the fracture network.

Acknowledgements

First and foremost my thanks to the big bubble man Prof. Andy Rankin and also to Dr J. Grocott without whose help this thesis would be unreadable.

To lesser known bubble people e.g. Wayne "nice hair-nice jeans" Cox and in the early years Simon "fat controller" Dominy for helpful, if argumentative discussion whose love for fluid inclusions is nearly as great as mine (not). Other post-grads on the mezzanine for the endless hours of Doom playing also need a mention, Jeff (even though he's Scottish) Wilson, Damon "ears" Green, Big Dave Fordam and more recently Steff and Chris.

Thanks also to the technical staff for always being there when needed i.e. Linda, Pat, John, Rob and Gary "I hate southerners" Barker (at times, when he's not at coffee, at lunch, in the surrey playing snooker, study leave/day off lying in bed or generally skiving, shirking, eating, hiding, chatting, smoking, or otherwise generally being somewhere else).

Thanks also to the Kingston University Caving Club for providing those much sought after weekends away in the country, away from the University on a Saturday afternoon, where I can forget all about FIPs, writing-up, and paying the next rent cheque. Those co-conspirators without whose help I would have finished 9 months ago include Mark "the laziest of them all" Morgan, Matt "can we stop at the next services" Light, Martin Allen, Bob, Nic, Si, Lucy, and Gary "sorry" Eisenhauer.

Thanks to Amanda who kept me going in recent times when this thesis seem to obscure the rest of my natural life. Also to Ish "get off this phone" who I seemed to have lived with for the last four years and who has put with my scrounging and general abuse.

Finally thanks to Mum and Dad with whose help and encouragement has paid for all those curries, beers, expensive caving equipment and tins of baked beans.

Cheers, I'm glad its over.

This thesis is dedicated to Alf Hickling who started it all and to Lawrence Webb who was unable to see it finished.

CONTENTS

List of Figures

List of Tables

List of Plates

Symbols and abbreviations used (Chapters in which they first appear)

Chapter 1

Experimental techniques:

FITR	Fourier Transform Infra-Red spectroscopy
PIXE	Proton Microprobe
EPMA	Electron Microprobe
LAMP-ICP-MS	Laser Ablation Microprobe Inductively Coupled Mass Spectrometer

Fluid Inclusions:

FIP	Fluid Inclusion Planes

Deformation:

σ_1	Maximum compressive principal stress
σ_2	Mean compressive principal stress
σ_3	Minimum compressive principal stress

Geological setting

SLFZ	Sticklepath-Lustleigh Fault Zone

Microthermometry

T_{FM}	Temperature of first observed melting
T_{Mice}	Temperature of last ice melting
T_{Mhydro}	Temperature of last hydrohalite melting
T_H	Temperature of homogenisation
T_{Ddiss}	Temperature of dissolution (halite)

Chapter 2

Fracture mechanics:

τ	Shear stress
T	Uniaxial tensile strength
σ_N	Normal stress
P_f or ρ	Fluid pressure
T_O	Tensile strength of rock
K_I	Stress intensity factor
K_{IC}	Critical stress intensity factor
α_V	Volumetric expansivity
σ_y	Thermally induced stress
E	Young's modulus
ΔT	Change in temperature
F_i	Function of facet length
ν	Poisson's ratio
L	Facet length
θ_i	Thermal expansion tensor orientations
$\Delta\alpha_{ki}$	Difference in thermal expansion components
a	Major axis of an elliptical crack
b	Minor axis of an elliptical crack
A	Crack tip tension
σ^r	Remote loading stress
p	Radius of curvature of crack tip
V_p	Seismic velocity primary
V_s	Seismic velocity secondary
V_p	Vapour pressure
L_p	Load pressure
S_t	Surface tension of magmatic bubbles

Inclusion re-equilibration

P_i	Internal pressure
P_c	Confining pressure
MPa	Mega Pascals

Chapter 3

Geological setting:

BVS	Borrowdale Volcanic Group

Deformation:

D_1	First regional deformation phase
D_2	Second regional deformation phase
D_3	Third regional deformation phase
D_4	Fourth regional deformation phase

Chapter 5

Geological setting

BTVP	British Tertiary Volcanic Province
SLFZ	Sticklepath-Lustleigh Fault Zone
BCFZ	Bristol Channel Fault Zone
BCS	Bristol Channel Syncline
DB	Dutson Basin
ECT	Exmoor Cannington Thrust
FBFZ	Flimston Bay Fault Zone
GFZ	Grassholm Fault Zone
LaB	Lamerton Basin
LRH	Lundy Rhomb Horst
NLFZ	North Lundy Fault Zone
SBB	Stanley Banks Basin
SoLFZ	South Lundy Fault Zone
TSFZ	The Smalls Fault Zone
WLB	West Lundy Basin
WLFZ	West Lundy Fault Zone
DG	Dartmoor Granite
HD	Hingston Down
BMG	Bodmin Moor Granite
SAG	St. Austell Granite
CG	Carnmenellis Granite
LEG	Lands End Granite
PDFZ	Prewley Dartmoor Fault Zone
TMFZ	Tavistock Modbury Fault Zone
LRG	Lundy Rhomb Graben

Experimental techniques

SEM-CL	Scanning Electron Microscope Cathodoluminescence

Chapter 6

Thermal expansion

ΔV_{QTZ}	Change in volume of quartz
ΔV_{FELD}	Change in volume of feldspar

CHAPTER 1

INTRODUCTION

1.1 History of Fluid Inclusion analysis and techniques

The study of fluid inclusions in recent years has become increasingly popular among earth scientists. With the development of modern instrumental methods of analysis the amount of information that may be intrinsically derived from fluid inclusions has greatly increased (see Roedder, 1990 for review). This has led to the widespread use of fluid inclusions analysis. Early workers (e.g. Roedder, 1962) determined the approximate trapping temperatures and basic fluid chemistries of a fluid inclusion based upon phase changes using a heating/freezing stage and a simple optical microscope. These early researches were to mostly concentrate on hydrothermal systems and the fluid inclusions provided an invaluable tool for determining the basic chemical and physical properties of those fluids. Even with the advent of modern analytical techniques the use of a heating/freezing stage is still one of the most popular techniques for the investigation of fluid inclusions (Roedder, 1990).

Techniques for the analysis of fluid inclusions can be broadly classified as being destructive or non-destructive. Non-destructive tests include microthermometry; ultraviolet microscopy for the study of hydrocarbon-bearing inclusions (Bodnar, 1989; Guilhaumou *et al.*, 1989); Fourier transform infra-red spectroscopy (FITR) (O'Grady *et al.*, 1989, Vry *et al.*, 1989); laser Raman microspectroscopy for the identification and analysis of polyatomic gas species such as CH_4, CO_2, N_2, H_2 etc. (Seitz *et al.*, 1987) and at low temperatures simple cations may be combined into salt hydrates (Schiffries, 1990) and gas clathrates (Seitz and Pasteris, 1990) together with a series of techniques for specialist application which include proton microprobe (PIXE) (Anderson *et al.*, 1987), electron microprobe (EPMA) (Maaskant, 1986) and cathodoluminescence (CL) (van den Kerkhof and Behr, 1994). Destructive tests include the bulk crush-leach procedure (Bottrell and Yardley, 1987). Other important methods of analysis include Laser Ablation Microprobe attached to a Inductively Couple Plasma Mass Spectrometer (LAMP-ICP-MS) which can open individual inclusions and transfer their contents to a

mass spectrometer for analysis of major and trace element data (Shepherd, 1993), Laser-ICP (Rankin *et al.*, 1992) and Synchrotron-XRF microprobe analysis (Frantz *et al.*, 1988).

1.1.1 What are fluid inclusions?

Detailed reviews of the likely modes of formation of fluid inclusions and their use can be found in Roedder (1984) and Shepherd *et al.*, (1985). This research is concerned with the formation of secondary inclusions in a magmatic/hydrothermal environment. However, for the sake of clarification and completeness, a brief general description of primary and pseudosecondary inclusions and their formation is included. Fluid inclusions generally represent a trapped portion of a fluid phase, and are common in most rock-forming and hydrothermal minerals precipitated or recrystallised in the presence of a fluid phase. However, their use in a majority of cases is limited to minerals in which they are optically visible. The most commonly studied minerals include quartz, fluorite and calcite, occurring in igneous, hydrothermal, metamorphic and sedimentary environments (Alderton *et al.*, 1992; Van Reenen *et al.*, 1994).

Primary vs. secondary inclusions

A fluid inclusion may form at the time of crystal growth, representing the fluid from which the crystal grew. These inclusions are termed primary and may be identified by criteria described by Roedder (1984) but in practical terms are difficult to observe and very rare. Once the crystal has formed, it may undergo brittle fracturing and subsequent healing by fluids of a different provenance to that from which the crystal was formed. The healing of these fractures may leave behind a three dimensional array of fluid inclusions. These inclusions are termed secondary, and are by far the most common type that are observed to exist naturally (Roedder, 1984). A third variety, known as pseudosecondary, also represent healed fractures which have formed during the growth of the crystal, and may thus possess the same thermo-chemical characteristics of the primary inclusions. This research is primarily concerned with the formation of secondary inclusions in quartz from granitic rocks.

1.1.2 Fluid Inclusion Planes

A Fluid Inclusion Plane (or FIP) is the term given to the resulting secondary inclusion array, formed by the healing of microfractures (Plate 1.1). Among the first authors to suggest that the healing of quartz microfractures was the probable origin of FIPs were Hicks (1884) and Van Hise (1890). One of the more interesting properties of FIPs is that they may occur with similar orientations over a very large area. Perhaps the first author to publish an extensive study of this phenomenon was Tuttle (1949), who

described planes of liquid inclusions having a uniform, preferred orientation over an area of 750km^2, in quartz from granitic basement rocks from the Washington D.C., USA, area. Tuttle (*op. cit.*) concluded that the orientation of these inclusion planes was not influenced by the crystallographic orientation of the quartz, which was in disagreement with earlier work by Anderson (1945). Later research by Wise (1964) showed that FIPs in granitic and metamorphic quartz had similar orientations to macrostructures (joints and dykes) observed in the field. More recently, FIPs have been used to relate tectonic and hydrothermal events using the orientations of the FIPs and the thermometric properties of the secondary fluid inclusions contained within them (Pécher *et al.*, 1985; Lespinasse and Pécher, 1986; Cathelineau *et al.*, 1990; Lespinasse and Cathelineau, 1990; Boiron *et al.*, 1991; Lespinasse *et al.*, 1991). These authors used FIPs as stress tensors to reconstruct the regional stress field orientation, and to analyse the movement of fluids during brittle faulting and contact metamorphism. The orientations of the palaeostress trajectories were determined using fault striation analysis, using methods proposed by Etchcopar *et al.*, (1981). An important assumption made by these workers was that FIPs represent healed tensile microfractures, whose orientations are not influenced by the crystallographic orientation of the medium in which they were analysed. Similarly, palaeostress analysis using FIPs in granitic quartz, presumed to have been generated by thermal stresses developed during the cooling of a granite, has been carried out by Kowallis *et al.*, (1987); Jang *et al.*, (1989) and Ren *et al.*, (1989). These workers have shown that a large proportion of the observed FIPs are likely to have been formed during the initial cooling of granite, when high geothermal gradients are coupled with hot, circulating hydrothermal fluids. However, it is also stated that the orientations of these healed microfractures is governed by the regional stress field, again with the presumption that FIPs represent *mode I* tensile fractures, forming parallel to σ_1 and perpendicular to σ_3. *Mode II* fractures represent fractures which show offset of the fracture walls (shear) may form in more complicated orientations. An interesting study by Laubech (1989) showed that microfractures could be healed in shallow buried, quartz-cemented, quartz-arenites by syndiagentic fluids, with healing temperatures as low as 85°C.

More recent work by Vollbrecht *et al.*, (1991) has cast doubt on the assumption that palaeostress directions can be inferred from the orientations of healed microcracks. The possible combination of thermal fracturing and the un-coupling at the grain scale of local stresses leads to the development of two fracture orientations, forming at 90° to each other (normal to σ_2 and σ_3) in granites. This would then require the orientation of the regional stress field to be rotated through 90°. The relationship between FIPs and shear veins was demonstrated by Boullier and Robert (1992). Although it was possible to characterise the orientations of FIPs in extensional veins, preferred orientations in shear veins were not apparent, although one group did tend to form at high angles to the slip

direction. It was presumed that the FIPs resulted from increases in fluid pressure prior to faulting, and were thus characterised as hydraulic fractures, resulting from supralithostatic fluid pressures, in accordance with the fault-valve model proposed by Sibson *et al.*, (1975) and Sibson *et al.*, (1988). However, Meere (1995) showed that fluids may be trapped in healed fractures at sub-lithostatic pressures at depth. Meere (*op. cit.*) proposed that the control of fracture initiation and evolution was due to material anisotropy and stress hetrogenities and not by hydraulic fracturing, and thus tensile failure at depth is the result of far field compressional stresses, resulting in dilation and not locally elevated fluid pressures.

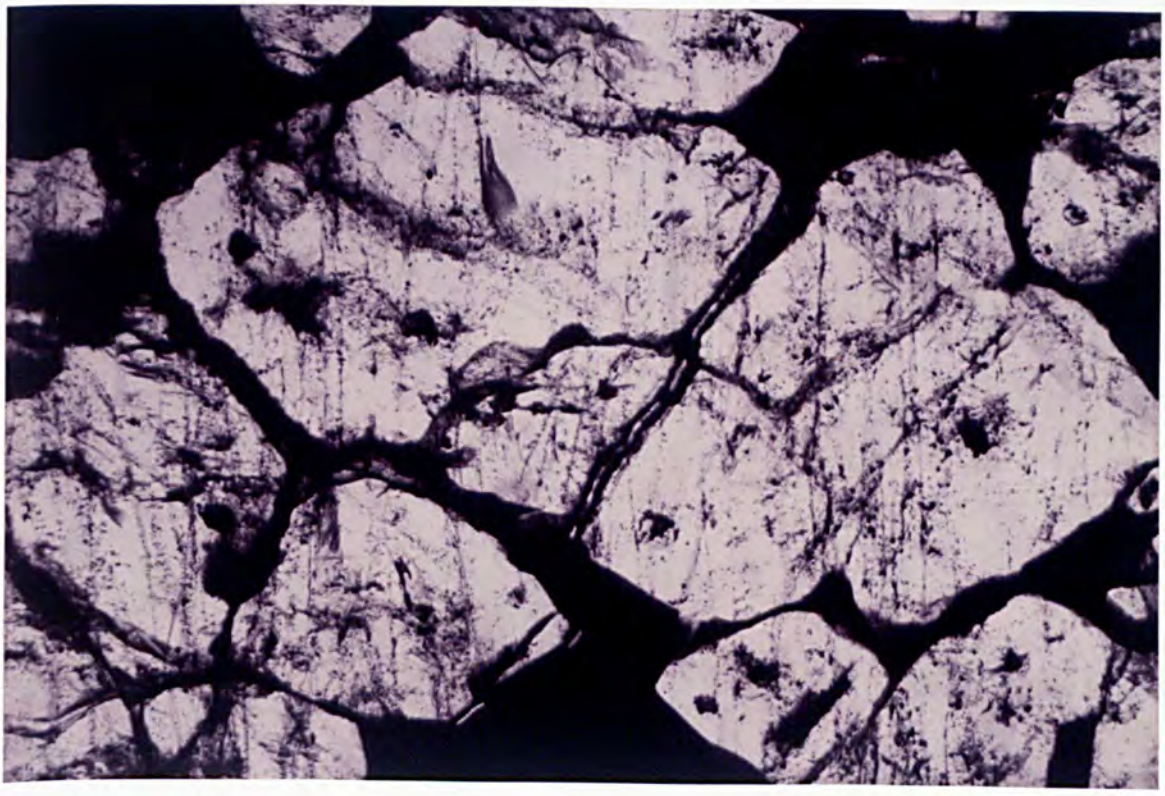

Plate 1.1 Fluid Inclusion Planes showing a strong parallel trend (top to bottom) in granitic quartz from Hingston Down, Devon. Width of frame 7mm.

1.2 Purpose of study

Previous published work has shown that Fluid Inclusion Planes may occur in a wide variety of environments. The origins of these FIPs have previously been simply related to either thermal, hydraulic and tectonic stresses rather than characterising individual FIPs or sets of FIPs. However, within a cooling granite, especially one with a high heat producing potential (e.g. Cornubian batholith) allowing a prolonged cooling history, it is feasible that FIPs may be generated in response to one or all of these stresses occurring within the granite. These stresses may be thermally induced as a result of thermal

contraction, hydraulically generated by high fluid pressures and tectonically produced by subsequent brittle deformation. FIPs may be generated by all these mechanisms as long as the temperatures of the fluids are sufficiently high enough to allow healing of microfractures. Previous authors have shown that a wide temperature range exists for the formation of FIPs, starting with the solidification of the granite and possibly continuing down to temperatures as low as 85°C (Laubech, 1989). It is therefore not unreasonable to expect a diverse population of FIPs related to a variety of processes and fluid types, especially in areas which have been proved to be tectonically and hydrothermally active, over a long period of time.

There has been much discussion in recent years concerning the migration of fluids in granites (Durrance *et al.*, 1982; Rankin and Alderton, 1983; Rankin and Alderton, 1985), and since FIPs are extremely abundant in granite quartz, it may be likely that FIPs are an important indication of this fluid movement. Is it then possible to distinguish between different generations of FIPs, unravelling the hydrothermal fluid history of the granite and illustrating the processes that may be occurring?

An investigation into the origins and causes of FIPs in a variety of settings has been proposed. As a starting point for the research, initial objectives were to test the following hypotheses:

(i) Healed *mode I* extensional microfractures (of which the majority of FIPs are thought to represent) are presumed to form parallel to both σ_1 and σ_2 and perpendicular to σ_3. Thus, although FIPs may be generated by various stresses on the grain scale, their orientation is thought to be governed by the orientation of far-field regional stresses (Ren *et al.*, 1989).

(ii) The majority of workers have considered that FIPs generally represent *mode I* extensional fractures, with the evidence for possible shearing such as off-setting of grain boundaries and other fractures is likely to be too small (possibly 2-3μm) to be observed (Kranz, 1983).

To test the above hypotheses the following questions are posed:

(i) Do FIPs mimic the trend of extensional macrostructures (e.g. extensional veins and normal faults) which may be observed in the field?

(ii) Do the orientations of FIPs reflect the far-field regional stresses. If not, can they be characterised by near field-stresses arising within and between mineral grains? Thus, are the preferred orientations of FIPs similar between adjacent minerals?

(iii) FIPs may be produced by thermal, hydraulic and tectonic stresses. Is it possible to characterise FIPs in relation to these stresses, based upon their orientations and morphologies?

(iv) Can a succession of regional stress fields, that may result in the formation of macrostructures possessing varying orientations, be correlated with the resulting FIP patterns? Thus, can appropriate analysis provide a relative dating of the tectonic and contemporaneous hydrothermal history of a study area, based upon the evolution of the hydrothermal fluids with time?

1.3 Choice of study areas

To test the above hypotheses and answer the questions posed, a series of barren and mineralised "granite" study areas in the U.K. were carefully chosen that filled certain requirements. Requirements for these sampling areas differed to a certain degree as the research proceeded. Certain elements however were essential, which included:

(i) A diverse history of mineralisation and hydrothermal activity which have utilised fluid pathways of varying orientations associated with several tectonic events.

(ii) Published literature concerning the microthermometric properties (temperature and salinity) of the fluids responsible for mineralised events for correlation with data from secondary inclusions. This was especially important at the start of the research to enable rapid evaluation of the initial data without having to perform analysis of primary inclusions in hydrothermal material from the associated mineralisation.

A more complete picture concerning the rationale behind the choice of the study areas is given at the start of each Chapter, together with a full geological background and details the sampling program undertaken. However, brief summaries of the geological setting and reasons for choice of these areas are given below.

1.3.1 Carrock Fell, Cumbria

The Carrock Fell complex is situated in the northern part of the English Lake District. The Skiddaw granite is intruded into Ordovician lavas and slates. Associated with the Skiddaw granite is a series of tungsten and later lead-zinc extensional veins (Shepherd and Waters, 1984; Ball *et al.*, 1985). The mineralising fluids are also responsible for the hydrothermal alteration of the surrounding granite, to form the Grainsgill Greisen. The study was designed to investigate whether FIPs representing healed tensile fractures

would mimic the orientation of the macrostructures, regarded as extensional veins. It should then be possible to illustrate the hydrothermal evolution of the area, especially with regard to the palaeostress field and its re-orientation through time. Furthermore, sampling was designed to illustrate the role of microfractures as pathways for hydrothermal fluids, especially in their role of causing intense, locally developed alteration of the host rocks (Ewart, 1962; Shepherd *et al.*, 1976; Roberts, 1983).

1.3.2 Bodmin-Dartmoor, SW England

The Bodmin-Dartmoor area is the classical mining district of the SW England. The area is characterised by strong regional trends of mineralisation, associated with fluids of diverse origins and properties (Shepherd *et al.*, 1985; Shepherd and Scrivener, 1987). There is a wealth of published literature concerning the mineralisation and alteration processes associated with the alteration of the Cornubian granites (Charoy, 1981; Durrance *et al.*, 1982; Jackson *et al.*, 1982; Alderton and Rankin, 1983; Edmunds *et al.*, 1984). Here sampling procedures were designed to evaluate the preferred orientations which FIPs might possess over a large area which are quite clearly exhibited by macrostructures observed in the field. The sampling procedure was also designed in carefully located areas, to show the possible existence of local deviations from the stress regime. It was also perceived, from the existing literature (Shepherd *et al.*, 1985; Jackson *et al.*, 1989) that fractures associated with mineralising episodes may have resulted from differing origins of stress, whether thermal, hydraulic or tectonic. It was hoped that FIPs associated with these varying styles of mineralisation may also be characterised in relation to the stresses from which the fractures originated.

1.3.3 Lundy Island and the Sticklepath-Lustleigh Fault Zone

Lundy Island is the most southerly expression of the British Tertiary Volcanic Province (BTVP) and lies in the Bristol Channel, approximately 38km due west of Ilfracome on the Devon coast. It lies in proximity to the extension of the NW-SE striking Sticklepath-Lustleigh Fault Zone (SLFZ) (Arthur, 1989). Sampling was undertaken on Lundy, together with an area of the north-easterly part of the Dartmoor granite to further understand results obtained from the Bodmin-Dartmoor area (Chapter 4). Sampling in this location was designed to characterise FIPs in relation to strike-slip faulting associated with NW-SE striking fault zones which are prevalent in SW England (Dearman, 1963; Holloway and Chadwick, 1986), with the SLFZ being the largest and probably exhibiting the most movement. Sampling on Lundy was designed to produce a clearer picture concerning the development of FIPs in relation to stress regimes associated with late-stage movement along the SLFZ. This would provide a greater understanding of the formation and orientation of FIPs related to shearing. Sampling was jointly undertaken on the mainland in area of the Dartmoor granite where brittle

deformation associated with the SLFZ has produced a series of secondary strike-slip and normal faults (Blythe, 1962).

1.4 Order of presentation

The thesis describes the FIP orientations, morphologies and origins from three study areas. The geology of each area is described at the beginning of the next three chapters, together with the aims of the investigation corresponding to that area. Data obtained both in the field and the laboratory are presented, together with a summary of the methods and the rationale for further work in the subsequent sampling areas. A discussion and brief summary of results are included at the end of each chapter. Chapter 6 draws together the results and conclusions from the previous chapters and develops ideas and theories on the origin and significance of FIPs.

1.4.1 Chapter 2

Chapter 2 reviews some of the current ideas relating to various forms of fracturing and the subsequent healing of these fractures. The theories of fracture initiation and propagation in relation to pore pressure and effective stress, fracture mechanics and the 'strength of materials' model (Ingraffea, 1987) are considered. These theories are then discussed in terms of recent work concerning the development of thermal (Wang *et al.*, 1989), hydraulic (Philips, 1972) and tectonic (Hancock, 1985) microfractures in granitic rocks. Mechanisms for the healing of fractures on all scales are discussed, especially with reference to microfracture annealing. Finally, the re-equilibration of fluid inclusions with respect to changes in density and morphology in a variety of situations is examined.

1.4.2 Chapter 3

Initial sampling techniques are undertaken to relate the orientations of FIPs with respect to extensional microfractures observed in the field. Both field data and laboratory data are presented and analysed. Preliminary deductions concerning the variation of FIP abundances and morphologies are presented. Microthermometric analysis of both primary (vein material) and secondary (granite) inclusions is used to constrain hydrothermal evolution with reference to contemporaneous tectonic events.

1.4.3 Chapter 4

Again both field and laboratory data are presented to determine and evaluate regional trends of FIP data, together with local deviations that may also occur close to sampling stations. FIP orientations and morphologies, together with microthermometric data, a used to explain the generation of fractures in relation to thermal, hydraulic and tecto

stresses. Preliminary characterisation of FIPs thought to represent possible healed shear fractures is undertaken. These characteristics are discussed with regard to strike-slip faulting.

1.4.4 Chapter 5

Sampling on Lundy and in NE Dartmoor is designed to investigate the relative movements of the Sticklepath-Lustleigh Fault Zone. This will allow a more detailed analysis and characterisation of FIPs with regard to strike-slip faulting to be illustrated. Variations in FIP morphology and orientation are used to categorise FIPs in relation to their mode of fracturing. Variations in inclusion morphology within and between FIPs are presented. These morphological variations are also used to help infer the origins of FIPs, as either dilatant (*mode I*) or dilatant-shear (*mode II*) microfractures.

1.4.5 Chapter 6

FIP morphologies are categorised in terms of their likely modes of fracturing. The morphologies of secondary inclusions are also related to mode of fracturing. The presence of a preferred shape orientation of inclusions is discussed in relation to the fracture healing process, both naturally and experimentally. The effects of post-healing re-equilibration are then considered especially with regard to changes in inclusion morphology and density and the effect this would have on the preferred orientations of the inclusion shapes.

1.4.6 Chapter 7

A summary of the main conclusions and concluding remarks are presented, together with recommendations for future work.

1.4.7 Appendices and references

Detailed accounts covering all the methods used during the research are presented. These include the collection of oriented samples in the field and the preparation procedures for of thin sections; the collection of microstructural orientation data and the collection of microthermometric data. Calibration techniques, calibration data and error determinations for microthermometry are also included. All data from which interpretations have been drawn is presented together with a complete list of all samples obtained and the locations of sampling stations. Finally a complete bibliography is presented.

1.5 Review of methods

Although a full description of the methods used for data collection and interpretation is presented in the Appendices, a brief review is included here.

1.5.1 Sampling and sample preparation

Generally oriented samples were carefully selected from in-situ, usually fresh granitic material. Orientation markings and preparation for thin sectioning was done using methods published by Prior *et al.*, (1987). The majority of sections were cut in a horizontal orientation since the research was generally interested in FIPs with sub-vertical to vertical orientations. However, several sections were cut with a vertical orientation for completeness.

1.5.2 Orientation analysis

The measurement of FIP orientations was done using a Universal stage attached to a standard petrographic microscope and video printer. Quartz was selected as a medium since it possesses insignificant cleavage that would influence the orientation of fractures and for its abundance of visible fluid inclusions in most environments. Three or four quartz crystals were carefully selected from each specimen. These were then photographed and the healed fracture orientations recorded and mapped for reference. Orientation data were recorded as outlined by Turner and Weiss (1963). Morphological variations of the FIPs were also noted, which included; shape (planar, curvi-planar, sinusoidal etc.); development (inter or intra-crystalline); crack width (or width of healed quartz); abundance and size of secondary inclusions; possible preferred shape orientation of secondary inclusions and the termination/propagation point of the fracture.

1.5.3 Thermometric analysis

After completion of the orientation analysis, the polished wafers (polished both sides) were removed from the glass slides and the quartz crystals separated for thermometric analysis using a Linkham THM600/THMS600 heating/freezing stage attached to petrographic microscope and video printer. Secondary inclusions were carefully selected from FIPs of a known orientation. Phase changes recorded include T_{FM}, T_{Mice}, T_{Mhydro}, T_H, T_{Ddiss}. Generally due to the small size of the inclusions (majority being 3-10μm) only the T_H and T_{LM} (usually ice) were observed. Three or four inclusions were analysed for each FIP where possible.

CHAPTER 2

A REVIEW OF FRACTURING AND FRACTURE HEALING IN CRYSTALLINE ROCKS

2.0 Introduction

The following chapter is a review of the processes concerning the development of fractures on all scales, from small microfractures less than a centimetre in length, to large strike-slip faults, which could be measured in kilometres. The origins of microfractures in granites (predominantly quartz) are specifically reviewed in detail, together with the processes that heal them to produce FIPs, both naturally and experimentally. The relationship between differing scales of fracture development is critical to the understanding of their formation.

2.1 Fracture nomenclature

This section summarises the classification of fractures and outlines the theory behind their formation. All fractures, regardless of scale may be classified as *mode 1* (tensile) or *mode 2* (shear) (Ramsay and Huber, 1987). However, in the field, faults are generally referred to as normal, reverse or strike-slip, whereas fractures on the microscale, are usually classed as tensile or shear.

2.1.1 Normal, reverse and strike-slip faulting.

There is a vast amount of literature concerning the brittle deformation of rocks and the classification of faults in a wide range of geological environments (see Anderson, 1937; Ragan, 1985; Pollard, 1987; Ramsay and Huber, 1987 and Price and Cosgrove, 1990). It is not the intention of this thesis to review all the features of the faulting process, however, a brief classification is needed to clarify the fundamental differences between faults observed in study areas.

Principal compressive stress axes

The formation of faults and fractures (e.g. veins) observed in the field is directly governed by the orientation of the three axes of principal compressive stress, σ_1, σ_2 and σ_3, (where $\sigma_1>\sigma_2>\sigma_3$) (Ramsay and Huber, 1987). The relative orientations of these axes with regard to the Earth's surface will govern the type of fault produced, whether, normal, reverse or strike-slip. It is noted that in anisotropic rocks the mean principal stress axes σ_2 always lies on the failure plane. At depth these stresses are nearly always compressive (Ramsay and Huber, 1987).

Normal faults

Normal faults generally possess a moderately to steeply dipping failure plane, where the dip-slip component is large relative to the strike-slip component, and where the hanging wall moves downwards relative to the foot wall (Fig. 2.1a). These faults are typically found in areas undergoing extensional tectonism (see Gibbs, 1984 for review).

Reverse faults

Reverse faults possess a failure plane which is generally less than 45° from the vertical, where the hanging wall has moved upwards in relation to the foot wall (Fig. 2.1b). Low angled, reverse faults are often termed thrusts. This type of faulting generally occurs in regions undergoing contractional tectonism (see McClay and Price, 1981 for review).

Strike-slip faults

These faults are usually steeply dipping, often vertical and exhibit a predominantly horizontal offset between the fault walls (Fig. 2.1c) (see Sylvester, 1988 for review). For the formation and evolution of strike-slip faults with special reference to granites see Segall and Pollard (1983).

2.1.2 Tensile and shear microfractures

Simmons and Richter (1976) define the term microcrack as:

'an opening that occurs in rocks and has one or two dimensions smaller than the third. For flat microcracks, one dimension is much less than the other two and the width to length ratio, termed the crack aspect ratio, must be less than 10^{-2} and is typically 10^{-3} to 10^{-5}. The length.... typically is of the order of 100μm or less.'

Although cracks are defined by three dimensions, in this study they are essentially veiwed in only two. It is possible to observe the fracture width, when viewed in a vertical position (see Appendix B), however, the largest dimension is then restricted by the

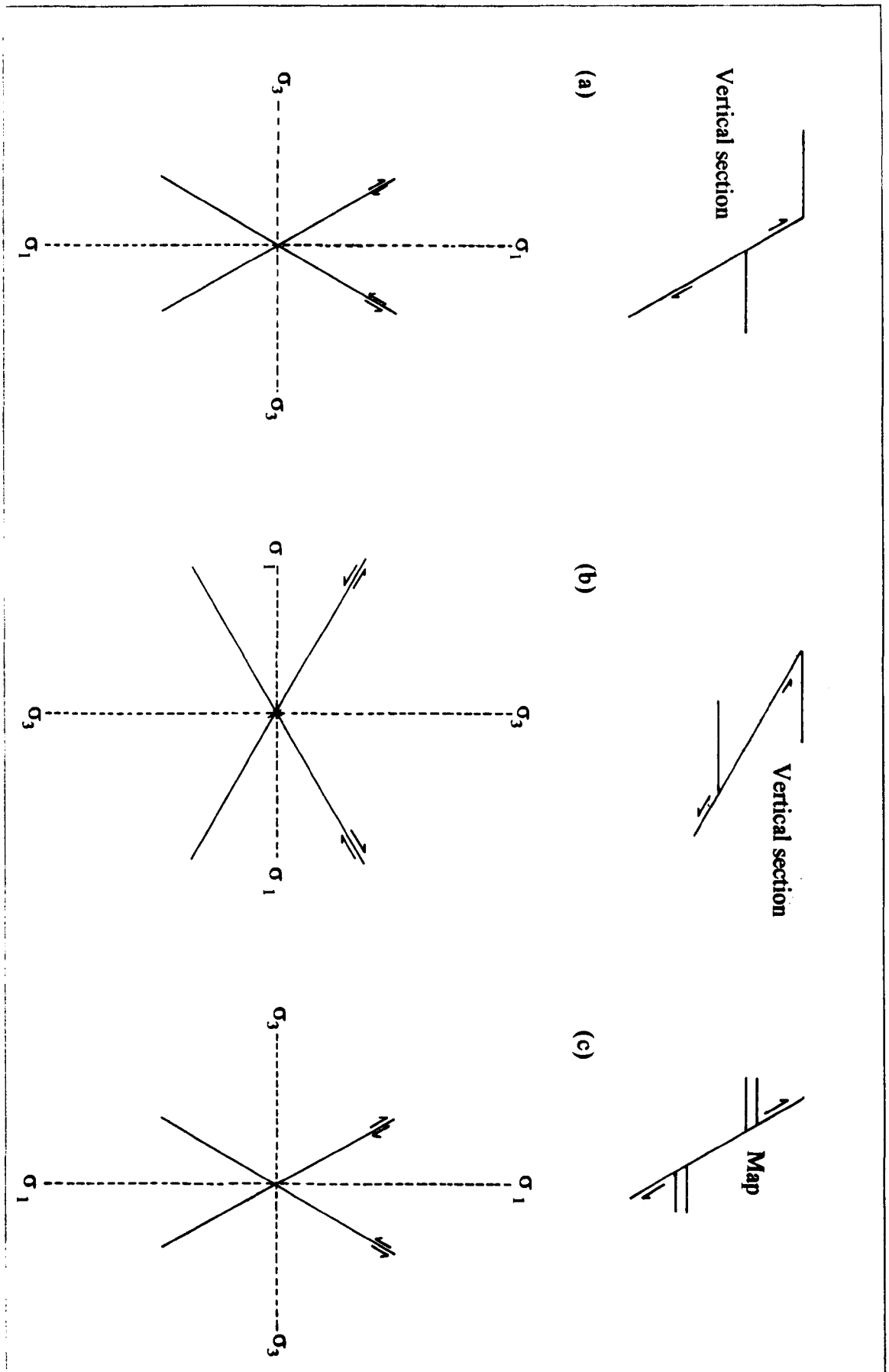

Fig. 2.1. Modes of faulting in relation to the orientation of three axes of principal compressive stress. (a) Normal faulting; (b) Reverse faulting; (c) Strike-slip faulting (after Moore, 1977).

thickness of the slide. The largest dimension of the microfracture is thus usually always observed to be in a horizontal frame as opposed to a vertical one.

In this thesis the terms microcrack and microfracture will be used synonymously. Microfractures can be classified kinematically as tensile or shear, though it must be stated that the vast majority of microfractures observed in rocks are tensile (Kranz, 1983).

Tensile microfractures

Tensile or *mode 1* microfractures form parallel to the maximum principal compressive stress (σ_1) and perpendicular to the minimum principal compressive stress (σ_3). They are likely to form in rocks that are undergoing tectonic extension, and may be associated with macrofractures such as normal faults. However, it must be noted that normal faults are not *mode 1* fractures since they contain a dip-slip component resulting in offset of the fracture walls. Tensile fractures may also be produced by hydraulic and thermal fracturing, both of which are detailed below.

Shear microfractures

Microfractures which exhibit shear, seen by offset of the adjacent fracture walls are termed *mode 2* microfractures. The orientation of this type of fracture in relation to the principal compressive stress axes is not as clear-cut as that of tensile fractures, forming at an angle, rather than parallel to σ_1. A specific type of *mode 2* microfractures are associated with strike-slip faults, recognised from laboratory experiments (Riedel, 1929), and are covered in more detail below. Healed shear fractures may represent hybrid *mode 1* and *mode 2* fractures, since they contain fluid inclusions, formed from a hydrothermal fluid, implying that the fracture has dilated. This type of fracture is termed a dilatant-shear microfracture.

2.1.3 Fracture generation

As stated by Simmons and Richter (1976): "cracks in rocks are produced when the local stress exceeds the local strength", or more precisely, fractures are generated when the differential stress (σ_1 - σ_3) is greater than the tectonic strength of the rock. The differential stress may be thermally or tectonically induced.

Failure criterion

The failure of rocks can be expressed by the Coulomb criterion, based upon the Mohr failure envelope (Fig. 2.2a). However, the important theory of failure developed by Griffith (1920), where the strength of a given rock is directly related to the presence of small flaws or cracks within the rock must be noted. He suggested that when the rock

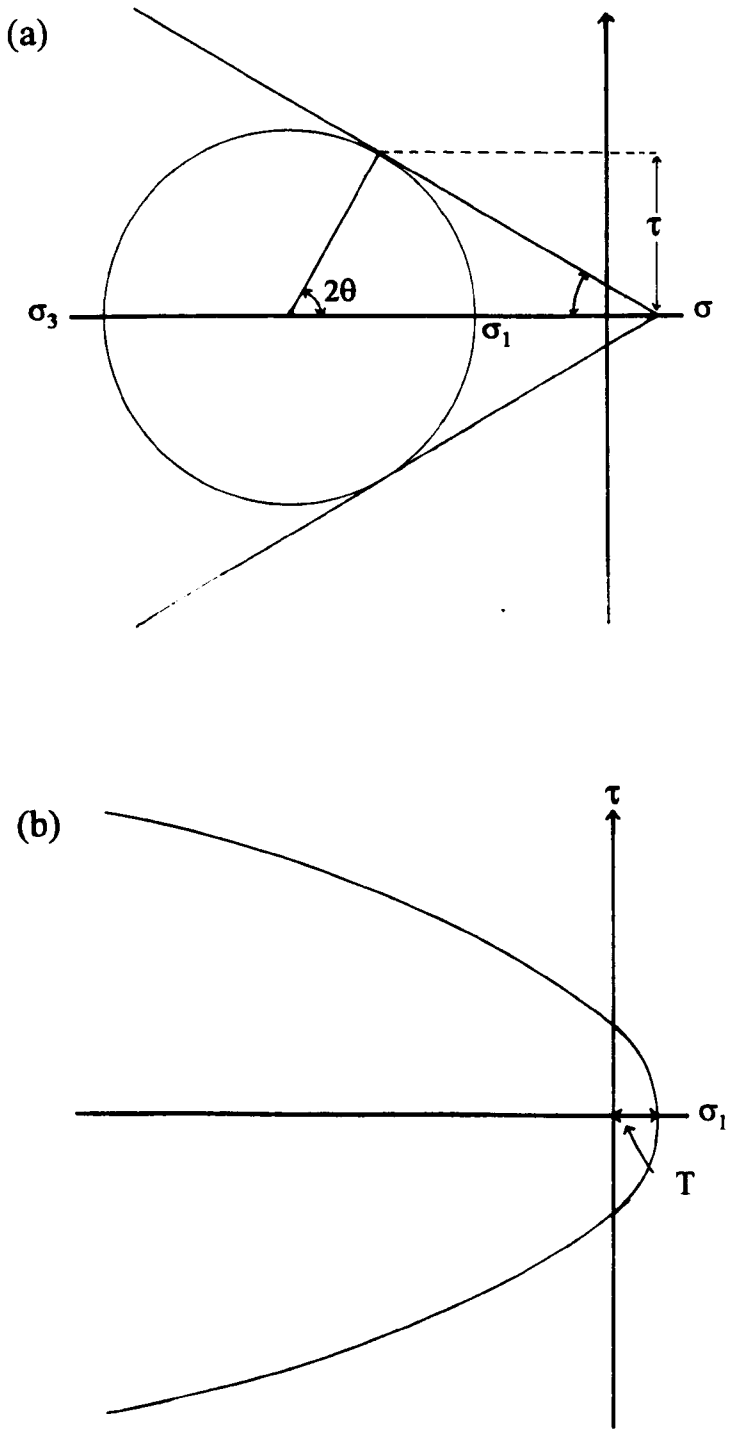

Fig. 2.2. (a) The classical Coulomb criterion for failure; (b) the parabolic Mohr envelope predicted from Griffith crack theory (after Ramsay and Huber, 1987).

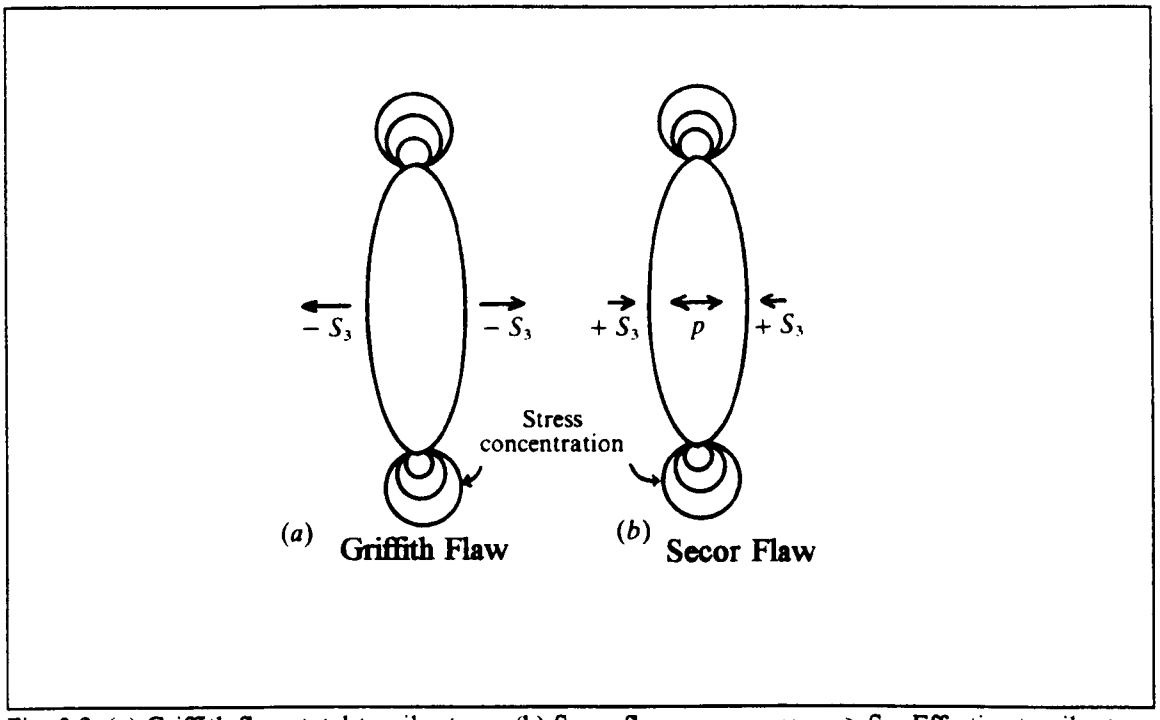

Fig. 2.3. (a) Griffith flaw; total tensile stress; (b) Secor flaw; pore pressure > S_3, Effective tensile stress (after Price and Cosgrove, 1990).

was stressed, very high local stresses occurred at the crack tips (Fig. 2.3a), allowing them to propagate and interconnect, and finally to the development of continuous fracture surfaces. This produces a parabolic form of the Mohr envelope (Fig. 2.2b), with the quadratic relationship:

$$\tau = 4T^2 + 4T\sigma_N \qquad (2.1)$$

where τ is the shear stress, σ_N the normal stress and T is the uniaxial tensile strength of the material. The parabolic failure envelope can now be used to show the differences between the three types of fracturing (Sibson, 1990), *extension fracturing*, *extensional shear*, and *shear fracturing*, (Fig. 2.4).

2.1.4 Pore pressure and effective stress

It is likely that fracturing in rocks generally occurring at depth, is in the presence of a fluid phase. The presence of this fluid (usually water but maybe CO_2 or even magma) will affect the way in which the fracturing process occurs. Since the principal stresses acting within the Earth's crust are almost always compressive, tensile fracturing is only likely to occur when the fluid (hydraulic pressure) becomes greater than the minimum compressive stress (σ_3):

$$P_f \geq \sigma_3 + T_o \qquad (2.2)$$

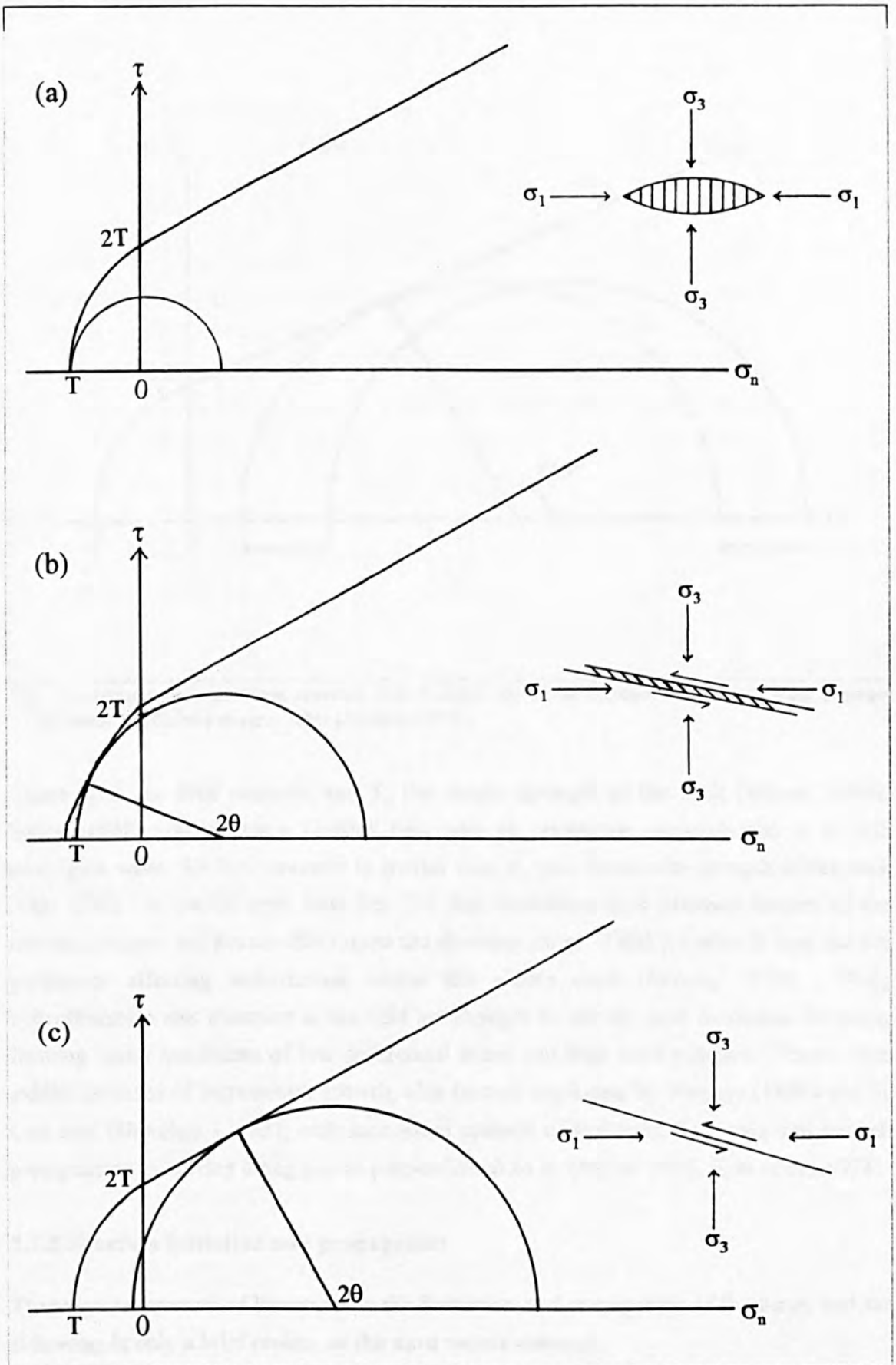

Fig. 2.4. Possible modes of failure in relation to a deviatoric stress field. Mohr diagrams illustrate the general failure envelope for intact rock, the stress conditions for the three modes of brittle failure, and the orientation of the failure surface with regard to the stress field. (a) Extension fracturing; (b) Extensional shear; (c) Shear fracturing (after Sibson, 1990). θ is the angle of σ1 to a normal to the failure plane as defined Means (1976).

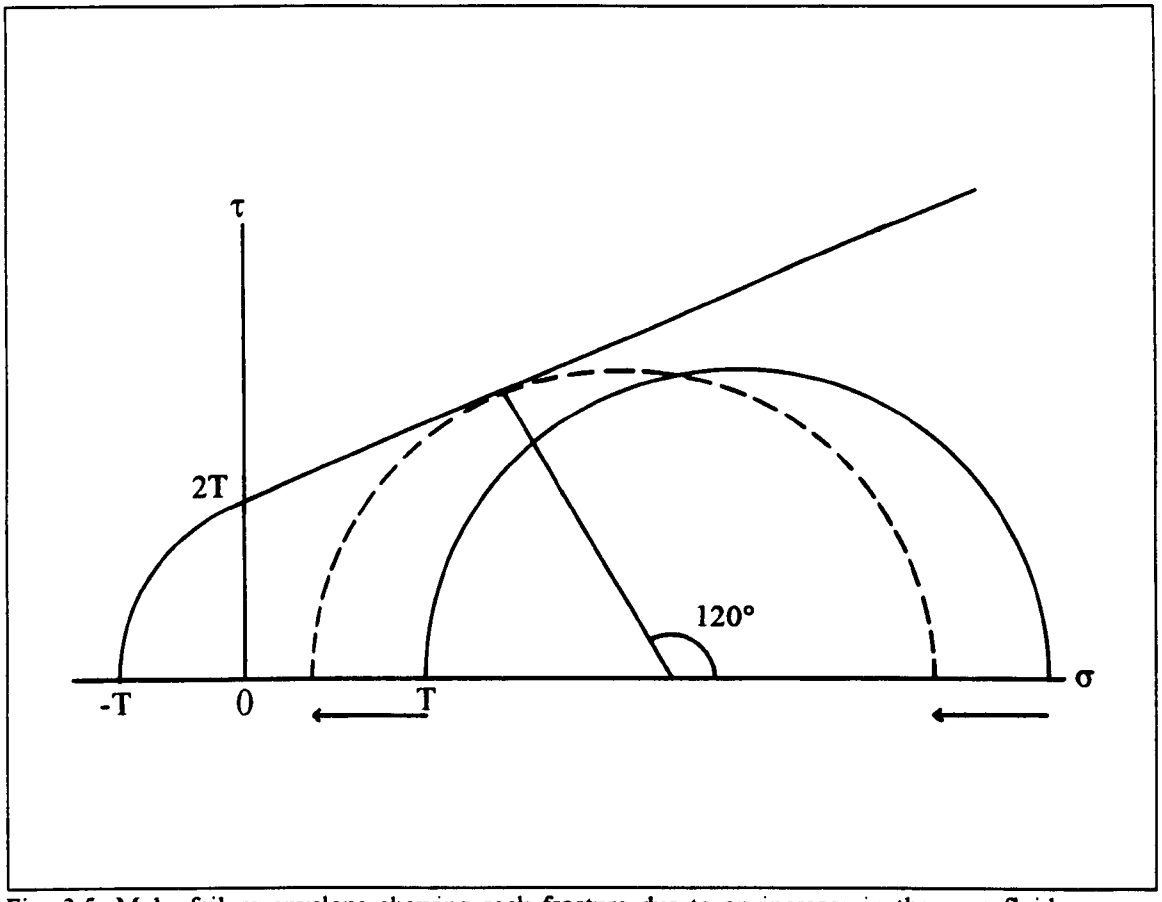

Fig. 2.5. Mohr failure envelope showing rock fracture due to an increase in the pore fluid pressure (increase in effective stress). After Phillips, (1972).

where P_f is the fluid pressure and T_o the tensile strength of the rock (Sibson, 1990). Secor (1968) argued that a 'Griffith' flaw with an orientation perpendicular to σ_3 will propagate when the fluid pressure is greater than σ_3 plus the tensile strength of the rock (Fig. 2.3b). It can be seen from Fig. 2.5 that increasing fluid pressure lowers all the normal stresses, but has no effect upon the shearing stress. Fluid pressure is thus the key parameter affecting deformation within the earth's crust (Sibson, 1990). Many hydrothermal veins observed in the field are thought to occupy pure extension fractures, forming under conditions of low differential stress and high fluid pressure. These veins exhibit textures of incremental growth, also termed crack-seal by Ramsay (1980) and by Cox and Etheridge, (1983), with successive episode of hydraulic fracturing and mineral precipitation occurring along planes perpendicular to σ_3 (Secor, 1965; Fyfe *et al.*, 1978).

2.1.5 Fracture initiation and propagation

There is vast amount of literature on the formation and propagation of fractures, and the following is only a brief review on the most recent research.

Fracture initiation

Crystalline rocks, in general, contain a large number of flaws, which occur naturally as grain defects, such as cleavage planes or, at a molecular scale, these flaws may be

apparent as lattice defects, such as dislocation arrays. The propagation of these flaws may occur due to stresses brought about by thermal or tectonic processes. Microfracturing due to tectonic processes may occur at grain boundaries (Gallagher *et al.*, 1974), around intergranular cavities (Kranz, 1979), or associated with elastic mismatch (Wang and Heard, 1985), kink band and deformation lamellae (Carter and Kirby, 1978) and twin planes (Olsson and Peng, 1976).

Methods for modelling fracture initiation, include several approaches. The elementary concept of the "strength of materials" approach, predicts fracturing to occur when:

$$\sigma_3 = T_o \qquad (2.3)$$

However this approach is unsatisfactory since no information regarding the length of the fracture is included, and that fracturing occurs instantaneously, which it does not. An alternative approach is based upon linear elastic fracture mechanics (Ingraffea, 1987). This involves these basic assumptions:

(i) Associated with the fracture tip is a stress-intensity factor, K_I, assuming that all stresses have been resolved along the fracture walls.

(ii) The material possesses a critical stress-intensity factor, K_{IC}.

(iii) Material behaviour in the fracture-front region, known as the process-zone, is inelastic and non-linear.

Fracturing will thus occur when:

$$K_I = K_{IC} \qquad (2.4)$$

Unfortunately, this approach cannot predict crack initiation, since it is inapplicable to problems without cracks. However, a non-linear fracture mechanics model, taking into account scale effects, especially the size of the process zone in relation to the smallest critical dimension of the fracture, may be suitable (Ingraffea, 1987). To describe the inelastic behaviour in the process zone of crack initiation or propagation in rock, the following assumptions are made:

(i) Stress transfer may still be occurring across the fracture, due to grain bridging and the undulating three dimensional nature of the fracture walls.

(ii) The process zone is localised in the crack front due to rapid softening behaviour of the rock.

A schematic diagram of an initiating fracture and its associated process zone is shown in Fig. 2.6, taken from Ingraffea and Gerstle (1984).

Fracture propagation

In theory, if the stress intensity factor is greater than the critical value, K_{IC}, then fractures will propagate at a velocity similar to that of sound in the medium (Atkinson, 1982).

However, fractures will propagate at stress intensities below K_{IC}; this is called sub-critical crack propagation. Two of the most important factors controlling the rate of sub-critical crack propagation are the rate at which corrosion reactions proceed at the crack tip, and the rate at which the reagents (e.g. water molecules) can be brought to the crack tip area (Kranz, 1983). This process is termed stress corrosion. The pressure, temperature, stress environment and porosity will dictate which is the prime rate-controlling factor.

Generally, a *mode 1* tensile fracture will tend to follow a propagation path that is parallel to the local maximum stress trajectory, deviating from its original path, if necessary, to minimise shear stress effects and maximise the strain energy release rate (Kranz, 1983; Cotterell and Rice 1980). Furthermore, anisotropy within the rock, such as grain boundaries or cleavage planes will influence the fracture path by creating modifications in the local stress field and the cohesive strength of the rock. It is also common for fractures to terminate at grain boundaries as well as be deflected by them (Mosher *et al.*, 1975; Simmons and Richter, 1976; Tapponier and Brace, 1976; Wu *et al.*, 1978; Kranz, 1979).

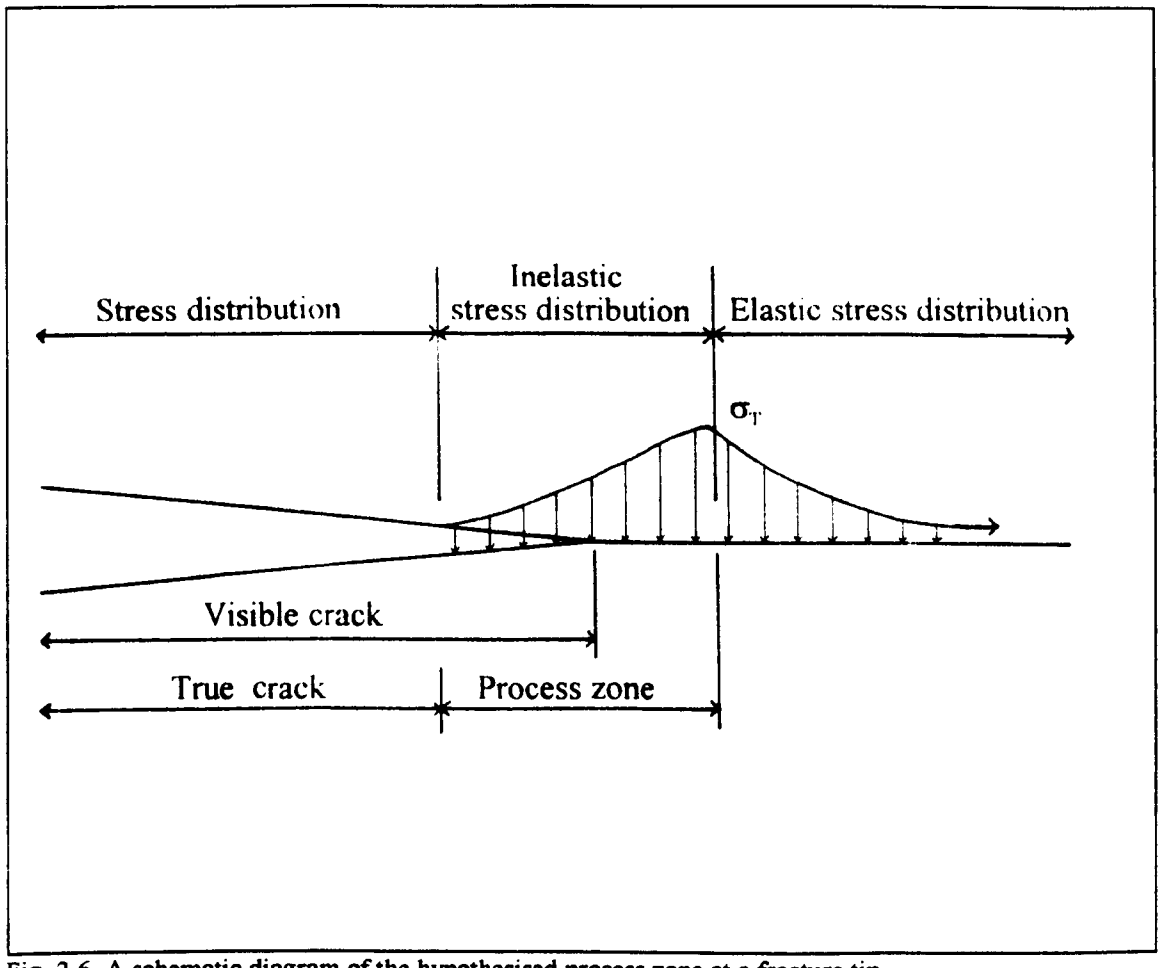

Fig. 2.6. A schematic diagram of the hypothesised process zone at a fracture tip.

2.1.6 Scaling law and fractal geometries

The concept that fracture patterns exhibit a degree of similarity over a wide range in scales has been recognised in geology (Turcotte, 1992). Tchalenko (1970) examined the structure of shear deformation zones ranging from shear box experiments to earthquakes, observing that over a wide range in length scales the formation and evolution of the shear zones involved identical characteristic stages. This self similarity in fracture structure is a characteristic of fractal geometries, in which any portion of the system is a scaled down version of the whole (Mandelbrot, 1983). A feature of a fractal geometry is that the relative numbers of large and small elements remain the same at all scales. This scaling relationship is described by the fractal dimension, which is simply derived from the power-law exponent on a plot of log size *vs.* log cumulative number (Walsh and Watterson, 1993).

Recent workers have shown that some elements of fault systems and fracture patterns have fractal properties. Power-law distributions have been observed in the populations of fault displacements (Walsh *et al.*, 1991), fault trace lengths (Yielding *et al.*, 1992) and fault geometries (Aviles *et al.*, 1987 and Okubo and Aki, 1987). The significance of this work in relation to the development of microfractures is important when considering their morphologies and geometries, particularly in relation to shear fractures. The morphologies of these FIPs are analogous to morphologies of macrostructures observed in the study areas and elsewhere.

2.2 Microfracture development in granites.

As already stated the initiation and propagation of fractures may be induced by thermal or tectonic processes. The process of mechanical fracturing includes cracks formed by brittle deformation of the rock due to deviatoric stresses and hydraulic fractures generated by increases in the pore fluid pressure. Since FIPs contain a fluid they are characterised as hydraulic fractures, although some of these may represent shear fractures, dilated at a later date by an increase in the pore pressure. Also, thermal fractures forming immediately after the solidification of a granite are likely to be in the presence of a fluid phase under high pressure. Thus, the boundaries between these two processes are far from clear-cut. For these reasons fractures have been classified as thermal, hydraulic or tectonic.

2.2.1 Thermal fracturing

The experimental analysis of thermal fracturing has, in recent years, produced a vast amount of literature. The following is a brief review of the causes of thermally induced

fracturing, the formation of the typical fracture modes, morphologies and orientations, with special reference to quartz-feldspar granitic rocks. The formation of thermal or cooling fractures in igneous rocks is due to the differential thermal expansion or contraction between adjacent minerals (Wang *et al.*, 1989). Most intragranular cracking occurs because of thermal expansion and compressibility contrasts between quartz and feldspar, while the preferred orientation of cracks results from external differential stresses on the granite (Rosenfeld and Chase, 1961; Devore, 1969; Nur and Simmons, 1970; Richter and Simmons, 1974; Voight and St. Pierre, 1974; Savage, 1978; Plumb *et al.* 1984). Generally thermal fractures may be classified as grain boundary cracks or as intragranular cracks, with experimental data showing that mode of propagation for the two types of cracks is different (Fredrich and Wong, 1986). Chen and Wang, (1980) demonstrated that heating rates between 0.4°C/min and 12.5°C/min had no appreciable affect on the rate of microfracture generation, suggesting that thermally induced microfracturing is caused by difference in the thermal expansion properties of the constituent minerals, rather than by thermal stress gradients. The induction of thermal stresses is due to either thermal expansion anisotropy, or thermal expansion mismatch.

Thermal expansion anisotropy

Minerals such as feldspar, biotite and quartz will expand or contract upon heating and cooling. However, they contain thermal expansion tensors, which allow the expansion or contraction to vary in different orientations. Thus, tensional or compressional forces may be induced depending upon the orientation of the tensors in adjacent grains in polycrystalline or monocrystalline rocks (Carlson *et al.*, 1990).

Thermal expansion mismatch

Thermal expansion mismatch is independent of the thermal expansion tensor orientation but depends upon the volumetric expansivity, α_v, of each grain, relative to the matrix. Tension or compression may be induced along grain boundaries depending upon the relative thermal expansions of the adjacent minerals (Carlson *et al.*, 1990).

Experimental modelling

Experimental methods have been compared to various models of thermal fracturing to analyse the modes of initiation and propagation of different fractures. Van der Molen (1981) used a spherical solid inclusion model (Wang and Heard, 1985) to explain the pressure shift of thermally induced cracking in granite at the quartz α-β transition temperature. Fredrich and Wong (1986) used a square inclusion which considers both grain boundary and intragranular cracking due to thermal expansion anisotropy and mismatch. Fu and Evans (1985) analysed microcracking in a polycrystalline brittle aggregate using a four grain model and were able to predict microcrack density with

applied loading. This model also gave information regarding the influence of thermal microfracturing on the elastic properties of brittle solids. This allowed the thermally induced stress, σ_y, along the central facet of the four grain model to be derived:

$$\sigma_y(x, \Delta T) = E \Delta T \sum_{i=1}^{4} F_i(x, \nu, L, \Delta\alpha_{ki}, \theta_i) \qquad (2.5)$$

where E is Young's modulus (Pa), ΔT is temperature change (°C), and F_i are the functions of position x, along the central facet, Poisson's ratio ν, facet length L, thermal expansion tensor orientations in each grain, θ_i (i = 1 to 4), and the difference between thermal expansion components in the matrix and each grain, $\Delta\alpha_{ki}$ (k = 1 to 2) (10^{-6}/°C). Jang and Wang (1991) used this model to compare orientations of healed microfractures in the Illinois UPH-3 and the Wolf River granites (Kowallis *et al.*, 1987; Jang *et al.*, 1989) to thermal fractures generated in 1000 randomly oriented grains, during simulated cooling, in a horizontally anisotropic stress field.

Grain boundary fractures

Grain boundary fractures generated by thermal stresses tend to initiate primarily at triple point junctions (Carlson *et al.*, 1990), where the largest stress intensities were generally observed (Evans, 1978) Once initiated they grow unimpeded until encountering a change in geometry of the grain boundary, where they will either stop completely or continue to grow (Fredrich and Wong, 1986). During heating experiments of the granite, it was noted that grain boundary cracks stopped after being heated to a relatively low temperature (approx. 300°C), when it was concluded that thermally-induced internal stresses had opened up a significant proportion of the grain boundaries (Fredrich and Wong, 1986). Carlson *et al.* (1990) noted that quartz-feldspar and quartz-quartz boundaries were more commonly cracked than feldspar-feldspar boundaries. This is likely to be due to differences in thermal expansion between quartz and feldspar and the large differences in the thermal expansion tensors exhibited by quartz (Plumb *et al.*, 1984; Jang and Wang, 1991).

Intragranular fractures

Intragranular fractures may also be produced by differences in thermal expansions of adjacent minerals, though their mode of propagation is different to grain boundary cracks. Tensile fractures may propagate into quartz grains, when they are adjacent to biotite or other quartz crystals (Tapponier and Brace, 1976; Fredrich and Wong, 1986) or from pre-existing natural cavities termed, by Tapponier and Brace, (1976) as low aspect ratio cavities (LARCS). However, intragranular cracks may be arrested before reaching a grain boundary, as their stress intensity decreases with increasing crack length,

and therefore will stabilise and become arrested after a relatively short distance (Fredrich and Wong, 1986; Wang *et al.*, 1989).

2.2.2 Hydraulic fracturing

The following section is a brief outline on the formation of hydraulic induced microfractures, with special reference to granitic rocks and mineralisation (see Phillips, 1972 for detailed review). The role of fluids in respect to crustal deformation and tectonics has been reviewed by Fyfe (1985).

It is well known that hydraulic fracturing is closely linked with disseminated, stockwork and vein-type mineralisation. These include porphyry copper deposits (PCD's) (see Titley and Beane, 1981; Titley, 1982 for reviews), porphyry molybdenum deposits (Wallace, 1991) and stockwork tin/tungsten deposits (Davis and Williams-Jones, 1985), where mineralisation is generally found in arrays of interconnecting hydraulically induced microfractures or as disseminated blobs. The presence of collapse breccias (Evans, 1993) are indicative of hydraulic fracture systems connecting with the surface, and are typical of PCD's. Another form of hydraulic fracturing that has become increasingly important in recent years is the role of fault-related dilatancy as a pre-cursor to seismic failure and earthquake prediction (Spetzler and Mizutani, 1987). Periodic seismic events may represent mineralising episodes, achieved by increases in fluid pressure, forming dilatant microfractures and banded vein textures (Sibson *et al.*, 1975; Ramsay, 1980). The presumption that hydraulic fractures represent dilatant cracks can be used to infer the orientation of the regional stress field. In-situ stress determinations (Bredhoeft *et al.*, 1976; Abou-Sayed and Brechtel, 1978) show that hydraulic fractures form parallel to σ_1, when the minimum and maximum compressive stress axis are not of equal magnitudes.

Propagation of hydraulic fractures

As previously stated, because FIPs represent microfractures, annealed by the hydrothermal fluids, it is not unreasonable to conclude that they may represent hydraulic fractures. For these hydraulic fractures to remain open at depth, it is necessary for the fluid pressure to be equal or greater than the least principal compressive stress. The formation of a hydraulic fracture may also be likened to the intrusion of a dyke, with the fluid pressure being replaced by magma pressure (Delaney *et al.*, 1986). Thus the application of fracture mechanics to the propagation of dykes may also be applied to the propagation of hydraulic fractures, albeit on a much smaller scale.

Inglis (1913) presented the solution for the state of stress of an elliptical hole in an elastic plate, possessing a major axis a and a minor axis b (Fig. 2.7a), with remote uniaxial tensile stress acting at right angles to the major axis. Inglis determined that the tension A

at the crack tip is by far the greatest acting stress. These stress effects show a marked increase as the ratio *a/b* (termed the aspect ratio by Simmons and Richter, 1976) increases. However, natural flaws are seldom elliptical in shape, though the stress at the tip of any slender hole (Fig. 2.7b) may be approximately given as:

$$\sigma^a \approx 2\sigma^r \{a/p\}^{1/2} \qquad (2.6)$$

where p is the radius of the curvature at the end of the hole. The propagation criterion for the crack tip is a function of the applied tensile stress and the crack dimensions, and must be equal to the tensile strength of the material (T_a) at that point (Pollard, 1987):

$$\sigma^a = T^a \qquad (2.7)$$

Combining equations 2.6 and 2.7, the remote stress loading at the crack tip can be given as:

$$\sigma^r \approx Ta/2 \{p/a\}^{1/2} \qquad (2.8)$$

for the crack to begin propagating. However, for a hydraulic fracture, the driving force for propagation is the fluid pressure (ρ). Therefore, replacing σ^r with (σ_3 - ρ) will give the propagation criterion for a hydraulic fracture. Thus, hydraulic fractures with a high aspect ratio, require a driving forces which is only a small fraction of the tensile strength of the rock. Because the stress intensity of the fracture increases with the crack length, propagation may continue at a decreasing pressure (Secor and Pollard, 1975; Pollard, 1976; Pollard and Holzhausen, 1979).

Fault related dilatancy

When a compressive stress is applied to a rock, it tends to cause closure of the fractures contained within it. As the fracture stress is approached, the rock becomes dilatant as fractures start to grow (Brace *et al.*, 1966; Ismail and Murrell, 1976). As discussed above, it is thought that hydraulic microfractures may form as a pre-cursor to seismic failure (Nur and Booker, 1972; Scholz *et al.*, 1973; Sibson, 1990). Sibson also stated that it is unlikely that this type of dilatancy is widespread because the requisite stress levels are unlikely to be maintained around established fault zones. However, the maintenance of high fluid pressures during the cooling of a High Heat Production granite, coupled with large amounts of normal and strike-slip faulting, could result in such microfracture dilatancy. Even more likely to occur are vein scale extension fractures, which are sometimes observable in the vicinity of exhumed faults (Sibson, 1981). Prior to earthquakes, the ratio of the seismic velocities, V_p/V_s decreases due to the lowering of V_p. This may be due to the dilation of rock fractures, producing a

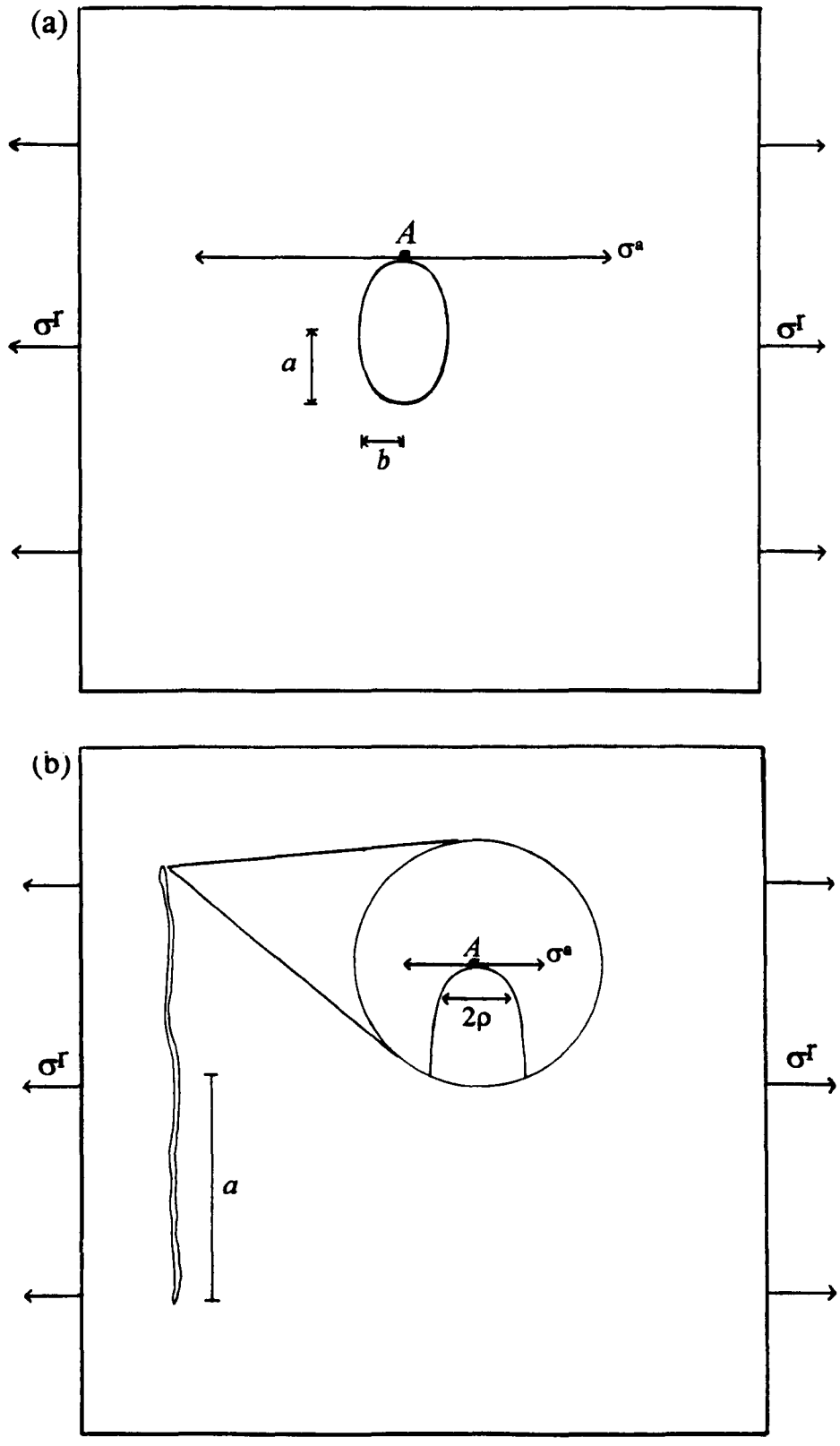

Fig. 2.7. The elastic model of Inglis (1913) (a) Geometry and loading conditions of an elastic plate containing an elliptical hole with semi-major axis a and semi-minor axis b. The remote uniaxial tensile stress σ^r is concentrated at point A (the end of the major axis) where the tension is designated σ^a. (b) Geometry and loading conditions of an elastic plate containing a crack. The radius of curvature of the crack tip is ρ (after Pollard, 1987).

reduction in fluid pressures, therefore increasing the effective stresses and the rock strength. Thus, dilatancy delays the seismic failure, though the increase in fluid pressure and the increased pore volume will inevitably produce critical effective stresses, leading to faulting (Phillips, 1986).

The seismic pumping model suggested by Sibson *et al.*, (1975) is based upon the dilatancy-fluid diffusion model and states that the movement of a fault may be the cause for the intermittent flow of hydrothermal fluids, possibly causing mineralisation. This model will only work when the rate of dilatancy, due to increases in the differential stress, is greater than the flow of fluids into the dilatant zone. Thus hydraulic fracturing may then be produced by the movement of excess fluid.

Further evidence for the wide spread presence of fluid-filled hydraulic fractures can be inferred from shear wave analysis (Shepherd, 1990). Crampin (1986; 1987) postulated the 'extensive dilatancy anisotropy' (EDA) model which explains the presence of shear wave splitting during seismic investigations in varying geological and tectonic environments. The anisotropy can be best explained if the rocks contain sub-parallel, sub-vertical fluid filled microcracks, distributed over a wide area, parallel to the maximum principal stress direction. It may therefore be inferred that FIPs may represent fossil EDA cracks, and although no single inclusion would have an affect upon a seismic wave, the rock sampled by the waves containing many parallel FIPs would be rendered anisotropic.

Hydraulic fractures associated with magmatic intrusions

The formation of hydraulic fractures associated with mineralisation and internal brecciation of porphyry copper deposits through the release of an aqueous phase has been postulated by many authors (Lowell and Guilbert, 1970; Gustafson and Hunt, 1972; Burnham, 1979). The formation of these breccias and fractures has been ascribed to retrograde boiling, during cooling and crystallisation of the magma if the critical condition is reached (Phillips, 1986):

$$V_p > L_p + S_t + T_o \qquad (2.9)$$

where V_p is the vapour pressure, L_p is the load pressure, S_t is the surface tension of the bubbles and T_o is the tensile strength of the rock. Phillips (*op. cit.*) states that during the crystallisation of anhydrous minerals, the vapour pressure associated with the dissolved volatiles increases, because the volatile components are confined to a decreasing volume of liquid.

Another classic example of hydraulic fracturing produced by the intrusion of a magma can be seen in the eroded Tertiary volcanoes of NW Scotland, where spectacular sequences of ring dykes and cone sheets can be observed. The interpretation of the formation of these fluid-filled fractures has presented much controversy. Anderson (1937) postulated that the cone sheets occupied tensile fractures, whereas the ring dykes occupied shear fractures. However, it is unlikely that differential stresses high enough for shear fracturing to occur could accumulate without the high fluid pressure of the magma releasing the stress by hydraulic fracturing. Other authors (Robson and Barr, 1964; Phillips, 1986) have criticised Anderson's hypothesis. Phillips (1986) concludes that the ring dykes are simple hydraulic fractures and the cone sheets were produced by the build up of a shock wave due to fast expansion of the magma. The propagating compressional shock wave would travel faster than the magma, which would then later fill the conical shear fractures produced.

2.2.3 Microfracturing related to faulting

It is postulated that the movement of a fault will produce associated secondary fracturing, on both a macroscopic and microscopic scale. Hancock (1985) used macrofractures to assess the orientation of the stress field around naturally occurring faults, while other authors (Brock and Engelder, 1977; Chernyshev and Dearman, 1991) have shown that the density of macrofractures also decrease away from the fault zone. Similarly microfracture density has also shown to decrease as a function of distance from naturally occurring faults (Freidman, 1969; Engelder, 1974; Brock and Engelder, 1977; Knipe and White, 1979; Kanaori *et al.*, 1991). Furthermore, Brock and Engelder, (1977) state that microfracture development is an early manifestation of faulting, and the generation of microfractures is retarded, everywhere except in the vicinity of the fault zone during the formation of a fault gouge.

The following section attempts to detail the timing and orientation of secondary microfractures that may develop with respect to a primary naturally-occurring fault.

Strike-slip faults

Extensive reviews on strike-slip faults and the secondary structures associated with them (faults, pull-apart basins and *en-echelon* folding) have been given by Christie-Blick and Biddle, (1985), Harding *et al.*, (1985) Sengör *et al.*, (1985) Woodcock and Fischer (1986) and Sylvester (1988). The angular relationships of secondary fractures which may be generated by a right-lateral simple shear, under ideal conditions are shown in Fig. 2.8. The observations are taken from clay cake models as well as geological examples. Riedel shears will form at angles of approximately 15° from the master fault (Tchalenko and Ambraseys 1970), with conjugate Riedels at much greater angles, usually about 70-

80°. Extension fractures will form when the effective stresses become tensile ($P_f \geq \sigma_3 + T_o$), while tension fractures may form when lithostatic loads become negative (Christie-Blick and Biddle, 1985). Much work has been published on the formation of en-echelon fractures (Ramsay and Graham, 1970; Beach, 1975; Ramsay and Huber, 1983; Pollard *et al.*, 1982; Thomas and Pollard, 1993) though it must be noted that Hancock (1972, 1973) has argued that extension fractures may occupy Riedel shears, hybrid fractures or pure extension fractures, based upon crack orientations and the evidence of displacement along some veins. Ramsay (1967) has also stated that if a rock mass contains suitably oriented pre-existing fractures, these are likely to dilate in preference to the formation of new fractures.

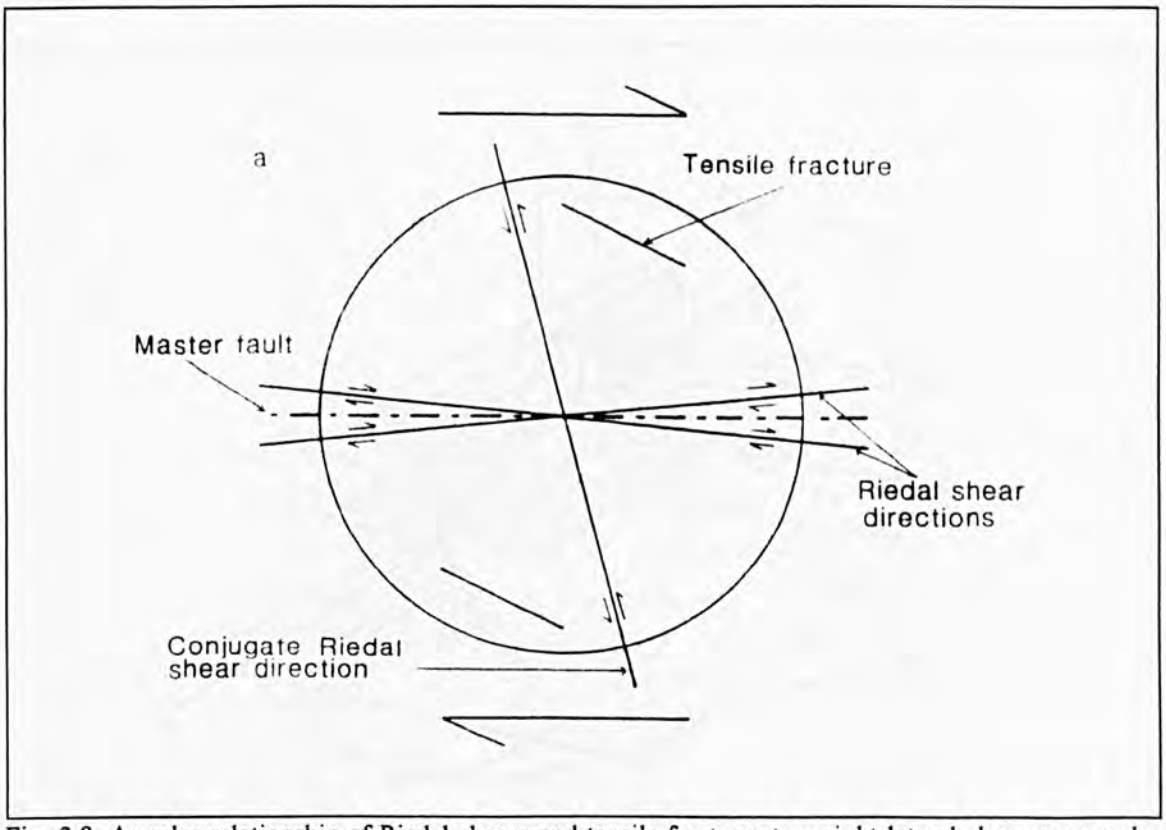

Fig. 2.8. Angular relationship of Riedel shears and tensile fractures to a right-lateral shear zone under ideal conditions, after Biddle and Christie-Blick (1985).

Normal faults

During episodes of normal faulting associated with crustal extension, the formation of tensile microfractures will occur, parallel to the σ_1 plane even in regions of relatively low fluid pressure. These fractures will have orientations similar to the normal faults, but are likely to form with a vertical or sub-vertical dip component, as opposed to a dip of 60° common in most normal faults. The relationships between the angle of faulting (failure surface) and the plane of extension fissures can be seen in Figure 2.9. It should be noted

that normal faults may thus be classified as *mode 2* fractures while the extension fractures are *mode 1*.

Thrust faults

Extension fractures will form in regions undergoing crustal compression, associated with thrusting and reverse faulting only when $P_f > \sigma_3 + T_o$ (Sibson, 1990). The fractures will form with a horizontal or sub-horizontal orientation (parallel to σ_1), only when fluid pressures are supralithostatic. However, Sibson also goes on to state that in normal and strike-slip stress regimes, arrays of vertical hydraulic extension fractures may form at fluid pressures well below lithostatic pressures.

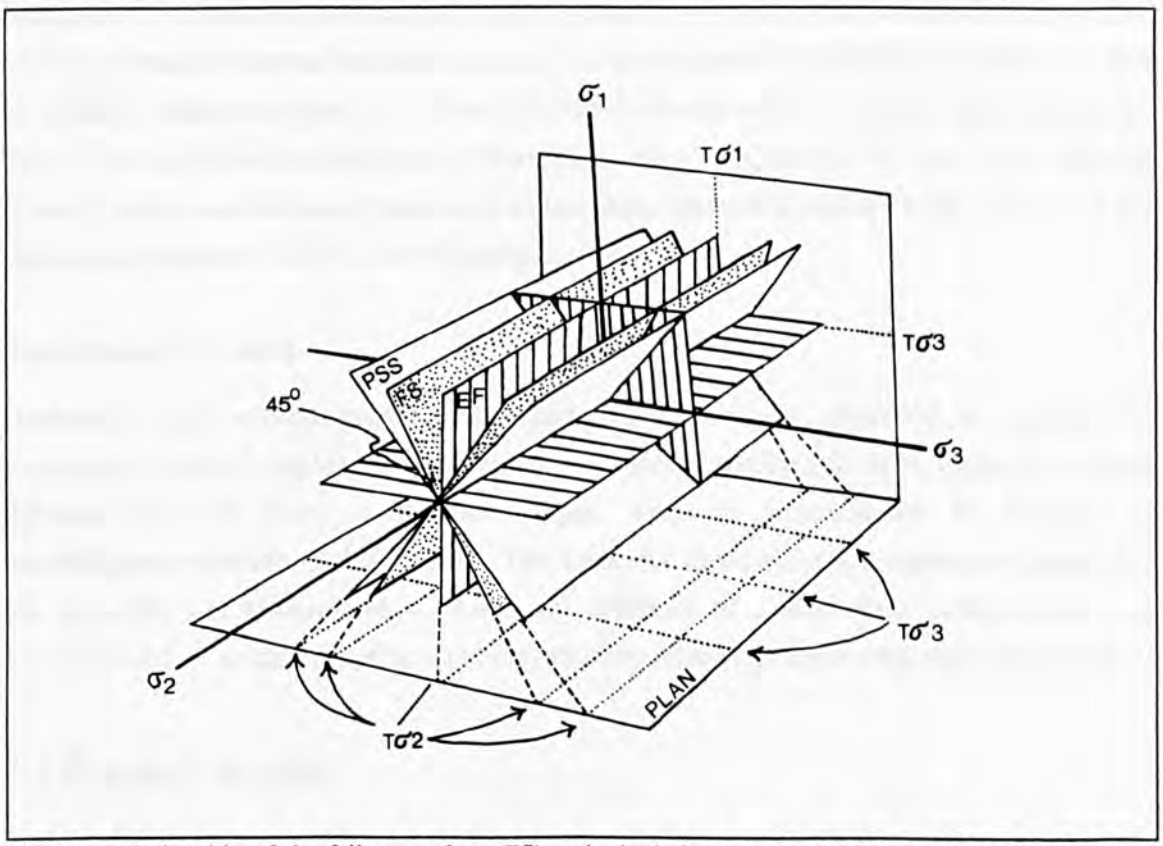

Fig 2.9. Relationship of the failure surface (FS), principal shear surface (PSS) and extension fractures (EF) to the orientation of the three principal compressive stress axis σ_1, σ_2 and σ_3 configuration during normal faulting, after Moore (1975).

Microfracture densities

As demonstrated above, the density of microfractures decreases as a function of distance from the fault and while the kinematics of microfracture development have been well published with relation to experimentally induced failure (Bombokalis, 1964; Brace *et al.*, 1966; Scholz, 1968; Hallbauer *et al,*. 1973; Lockner and Byerlee, 1977), there is still some debate as to whether these microfractures are produced during the initial failure of the rock as the fault propagates, or through subsequent post-failure, fault-slip. Brock

and Engelder (1977) indicate that major fault drag during the early stages of faulting is a major contributor to microfracture formation. However, Anders and Wiltschko (1994) define the region of fracturing produced by the stress field at the time of the earliest formation of a through going fault as a process zone. They distinguish fractures produced in the process zone from those generated after a significant amount of slip has accumulated, which is in agreement with experimental data obtained by Friedman and Logan (1970), Conrad and Friedman (1976) and Teufal (1981).

Macrofractures vs. microfractures

A granite body can be treated as a homogenous body, and apart from the presence of pre-existing fractures, new secondary macrofractures which may form due to primary faulting will possess an orientation directly related to the local and regional stress fields. Likewise, microfractures forming in quartz, which possesses no cleavage planes, will also be oriented relative to the local stress field and also to other secondary microfractures. Thus, although their mechanism of formation may be different for the same faulting episode, both were formed in response to the same stress field, in the same rock, with the same fluid pressure (Anders and Wiltschko, 1994).

Non-tectonic fractures

Horizontal and sub-horizontal joints and fractures were observed at many field exposures, where samples were obtained for studies outlined in later chapters. These fractures do not have a tectonic origin, but are believed to be formed by unroofing/exhumation of the granite. The fractures themselves are expansion joints, and are generally not mineralised or show any evidence of a movement component. The presence of low angle microfractures may thus be related to horizontal expansion joints.

2.3 Fracture healing

So far this review has focused on:
(i) the way in which both macrofractures and microfractures are formed
(ii) the development of an understanding of the mechanisms which are responsible for their generation.

However, the mechanics by which the these fractures are healed are just as important. There is perhaps more of a difference in the way macrofractures are healed with respect to microfractures, than there is in the way they both are formed. Although this present study is specifically concerned with microfractures, a brief summary of the way larger fractures are healed is included for completeness.

2.3.1 Crack-seal mechanisms of macrofractures

Comprehensive reviews for the healing of fractures, generally larger than grain-scale fractures have been given by Ramsay (1980) and Dietrich and Ramsay (1980). The development of oriented layer silicate microstructures with reference to crack-seal mechanisms was demonstrated by Cox and Etheridge (1983).

Healing of large fractures and vein deposition

There are several mechanisms by which hydrothermal fluids may deposit material in open cavity (see Evans, 1993; Barnes; 1967 for reviews). These are generally attributed to changes in fluid temperature, pressure or chemistry. Deposition may be initiated by changes in fluid chemistry due to interaction with the wallrocks, making the metal complexes responsible for the transport of ores in solution unstable. Alternatively, a reduction in fluid pressure may also be responsible for a change in the solubility of the dissolved complexes. However, probably the most common mechanism for the deposition of material from a hydrothermal fluid is a change in temperature, thus resulting in a change in solubility of the ion complexes.

In many instances, ore-fluids may travel considerable distances from the source of the metal to the site of deposition (e.g. mineralisation associated with granites of SW England; Park and Guilbert, 1986). However, in smaller fractures, the source of the material may be locally derived. This is typical in fractures healed by pressure growth (Durney and Ramsay 1973).

Solution transfer

Solution transfer involves the transport of material from an area of high normal stress to one of low normal stress, and typically involves transport over relatively small distances (probably meters). Ramsay (1980) has described the process by which the elongation of a rock takes place by crack-seal growth due to solution transfer (Fig. 2.10). Elastic strain energy reaches a critical level and induces fracturing (Fig. 2.10a). Solution transfer of material takes place from the walls into a microcrack (area of high to low stress) (Fig. 2.10b). Healing of a fracture allows further accumulation of strain energy and repeated fracturing process (Fig. 2.10c-e) which develops into a compound vein with the formation of styolite surfaces, which are perpendicular to the maximum principal compressive stress (Fig. 2.10f).

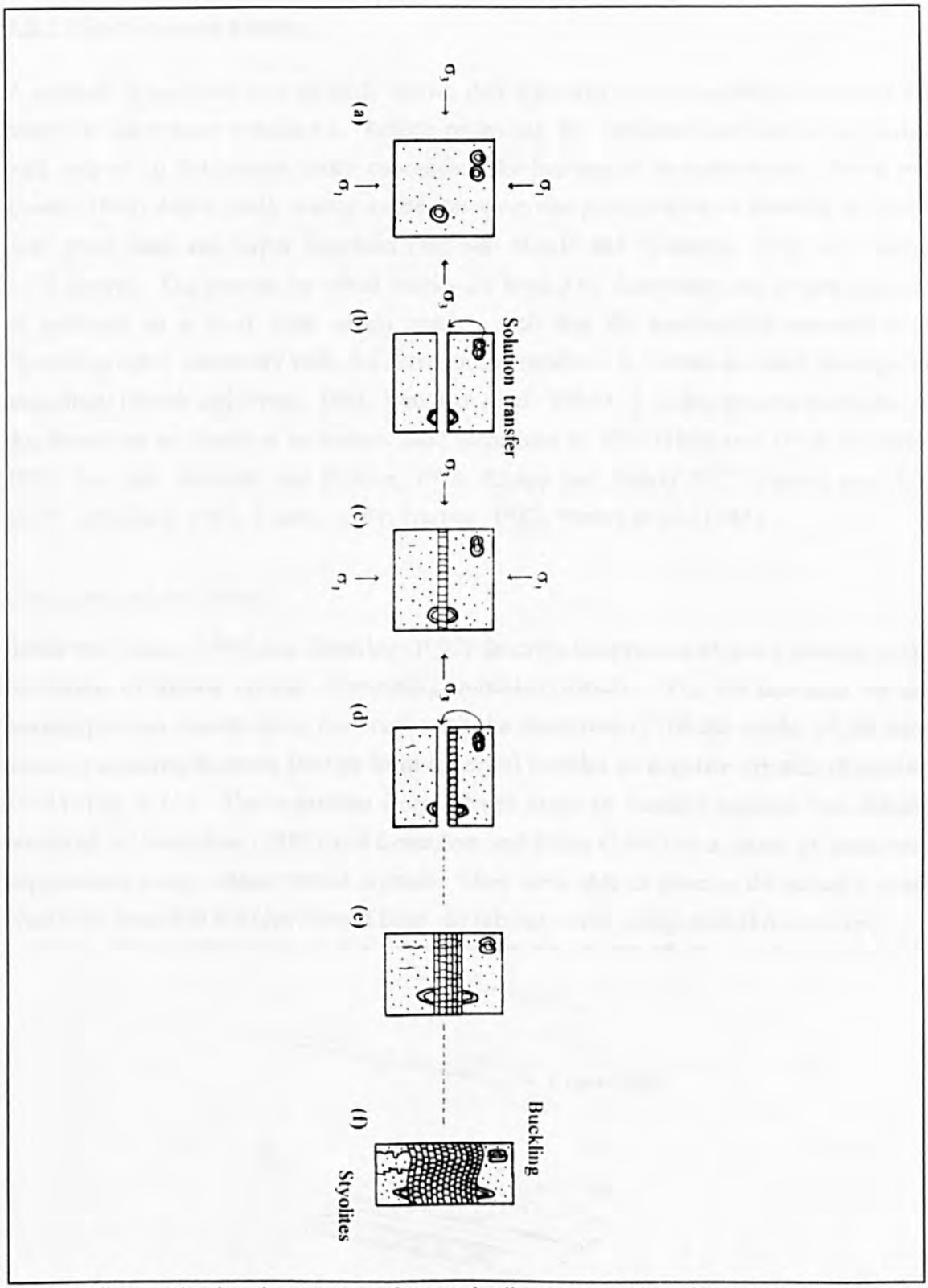

Fig. 10. Diagram showing the sequence of events leading to elongation of a rock by the crack-seal mechanism: (a) elastic strain accumulation (σ_1 and σ_3 are the greatest and least principal tensile stresses); (b) development of first fracture and release of elastic strains in matrix, solution transfer of material from walls into microcrack; (c) seal of vein walls and further elastic strain accumulation; (d) development of second crack and release of elastic strains in vein walls, further solution transfer with development of stylolitic surfaces; (e) repeated crack -seal microcracks forming a compound vein; (f) large finite shortening leading to vein buckling and the formation of stylolites both outside and inside the compound veins (after Ramsay, 1980).

2.3.2 Microfracture healing

A number of workers have recently shown that fractures may be rapidly and effectively healed in laboratory conditions. Before reviewing the evidence clarification is needed with respect to the nomenclature concerning the healing of microfractures. Smith and Evans (1984) define crack sealing as the transport and precipitation of material in cracks over grain scale and larger distances (see also Batzle and Simmons, 1976 and section 2.3.1 above). The process by which cracks are healed by dissolution and re-precipitation of minerals on a local scale within cracks, such that the precipitated material is in crystallographic continuity with the surrounding medium, is known as crack healing (or annealing) (Smith and Evans, 1984: Vaughan *et al.*, 1986). It is this process that leads to the formation of planes of secondary fluid inclusions or FIPs (Hollister, 1981; Roedder, 1981; see also Simmons and Richter, 1976; Knapp and Knight 1977; Sprunt and Nur, 1979; Crawford, 1981; Touret, 1981; Norton, 1982; Pécher *et al.*, 1985).

Crack healing processes

Smith and Evans (1984) and Brantley (1992) describe the process of crack healing as the formation of healed crystal surrounding unhealed islands. The advancement of the healing process occurs along the crack with the formation of tubular voids, which neck down in anisotropic stress field to form spherical bubbles or negative crystals (Roedder, 1981) (Fig. 2.11). This transition from tubular voids to isolated bubbles was initially recorded by Lemmlein (1956) and Lemmlein and Kliya (1960) in a series of laboratory experiments using sodium nitrate crystals. They were able to observe the actual process where the spherical bubbles formed from the tubular voids, using optical microscopy.

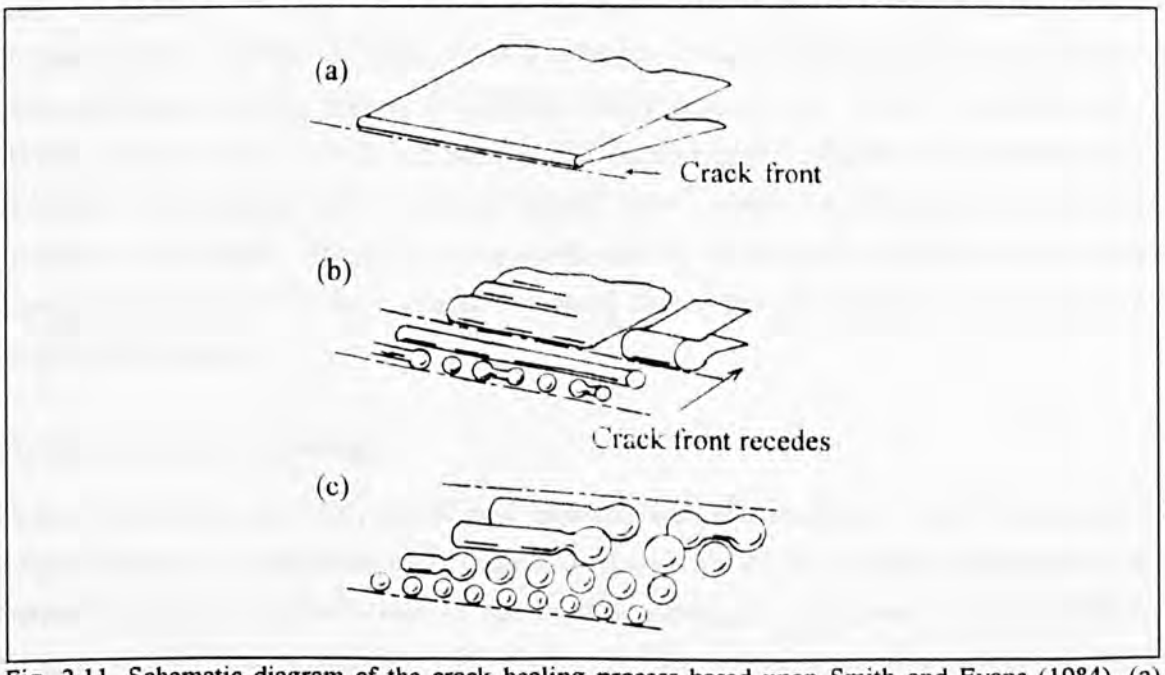

Fig. 2.11. Schematic diagram of the crack healing process based upon Smith and Evans (1984). (a) Crack tip becomes curved due to mass transport produced by a chemical potential gradient. (b) As the process proceeds cylindrical voids are formed, and themselves being unstable, pinch off into spherical bubbles. (c) Bubble planes are formed which are relatively stable to further change.

Shelton and Orville (1980) and Pécher (1981) have demonstrated that crack healing is possible under hydrothermal laboratory conditions at reconstructable temperatures and pressures. Other workers (Pécher, 1981; Smith and Evans, 1984; Brantley *et al.*, 1990; Brantley, 1992) have shown that the factors controlling the rate of healing include the temperature and chemistry of the fluids, the geometry of the microfracture network and the application of non-hydrostatic stresses. Even at temperatures as low as 200°C, microfractures will heal in geologically short periods of time (Brantley, 1992). Smith & Evans (1984) showed that fractures at 400°C in the presence of a fluid were completely healed within 1-2 days.

Probably the most important factors governing the healing of microfractures are the solubility of silica (a function of the PVTX) and the geometry of the fracture network. Moderate increases in NaCl content and increases or decreases in pH could increase the healing rate, whereas dissolution-precipitation inhibitors (e.g. Fe, Al, Zn) and high mole fractions of non-aqueous phases could decrease the healing rate Brantley (1990). These changes in fluid chemistry which increase quartz solubility correlate with increased rates of healing (Brantley, 1992). However, Brantley also states that the geometry of the fracture network, with many small interconnecting fractures will show a greater control over the rate of healing than the fluid chemistry, and may be responsible for the widespread pervasive alteration of the rocks.

2.3.3 Post-healing re-equilibration of fractures and fluid inclusions

It is also well known that re-equilibration of inclusions after they have formed can alter their morphology and the chemistry of the fluids they contain. This has been well documented by Wilkins & Barkas (1978); Pécher (1981); Pécher & Boullier (1984); Binns & Bodnar (1986); Sterner & Bodnar (1986); Bodnar *et al.* (1989); Boullier *et al.*, (1989); Sterner *et al.* (1988) and Sterner & Bodnar (1989). However, to what extent inclusions will change their shape in natural quartz under varying temperatures and pressures is not clear. One of the most stable natural shapes for a fluid inclusions is the negative crystal which is very common in most rocks, but perhaps just as common are irregular inclusions.

Change inclusion morphology

Gratier and Jenatton (1984) established experimental relationships between the rate of length-change of an inclusion with respect to the nature of the crystal, temperature and internal pressure, state of stress of the crystal, geometric characters of the inclusion (length, width), and orientation with respect to the optical axis of the host mineral. Furthermore they define the changes in morphology as two categories:

(i) rapid change from the beginning (after a few hours at the maximum temperature) of heating, likely due to elastic deformations (Eadington and Wilkins, 1980). Also silica solubility of the fluid due an increase in temperature (Leroy, 1979) would dissolve the inclusions walls to a small extent.
(ii) Very slow and regular change over a period of several weeks or months. Usually elongate inclusions become wider and eventually rounder.

These experiments were carried out when the inclusions were subjected to temperatures and pressures greater than those of their growth, i.e. internal overpressure ($P_i > P_c$, internal pressure > confining pressure). Sterner and Bodnar (1989) also carried out a series of experiments on synthetic quartz, with pure H_2O inclusions subjected to an internal overpressure. They also found that inclusions experienced a morphological change towards negative crystal shapes. However, they also noticed a more profound change in the inclusion shape when they subjected the inclusions to an internal underpressure ($P_i < P_c$, internal pressure < confining pressure). A collapse in the parent inclusion into a 'sea' of smaller secondary inclusions was observed. These secondary inclusions are on a scale of a hundred microns and may resemble a planar fracture, though usually they will form a three dimensional array.

Changes in density

In the experiments above, generally, a change in shape was accompanied by a change in density of the fluids within the inclusions. During re-equilibration under conditions of internal overpressure, at 700°C, Sterner and Bodnar (1989) noted that the greatest change in morphology (i.e. inclusions which have become the most regular or euhedral) was accompanied by the greatest decrease in density, together with a decrease in the calculated internal pressure. When the inclusions were submitted to internal underpressures, the densities of the parent inclusions appeared to be randomly distributed within the entire density range of the secondary satellite inclusions as well as for the density range for the entire sample.

Effect of a stress field

Gratier and Jenatton (1984) subjected their synthetic inclusions, which homogenised at temperatures around 265°C, to a uniaxial stress field of 20-65MPa at 265°C for several months without any sign of shape change that could be linked to the stress field. However, Wilkins and Barkas (1978) concluded that fluid inclusions could be introduced during or subsequent to ductile deformation of quartz from recrystallised granites from the Lachlan Fold Belt of eastern Australia. Fluid inclusions disappeared from the cores of sub-grains during recovery and before recyrstallisation.

Results thus show that fluid inclusions will not possess their original densities and shapes if their P-t path has deviated substantially from the isochore corresponding to their conditions of formation (Sterner and Bodnar, 1989). Inclusions will change their shape to approach equilibrium by trying to increase their surface energy. However, if a decrease in the internal pressure has occurred, then the inclusions will tend to change their shape to a lower surface energy configuration to form a negative crystal or sphere (Gratier and Jenatton, 1984). Bodnar and Sterner (1989) further state that under high confining pressures many inclusions show no sign in change of fluid composition, even though they had undergone significant changes in shape and density, and may thus be treated as closed systems. Further discussion regarding the re-equilibration of fluid inclusions, especially with regard to a change in their shape is included in Chapter 6.

2.4 Summary

The purpose of this chapter was to identify the causes of microfracturing, some of the characteristics of the fractures and show relationships to macrostructures, especially with regard to the development of microfractures in granites. Furthermore, a review of the processes controlling the healing of these microfractures by hydrothermal fluids has been included both in naturally occurring and laboratory conditions. This has raised some important questions:

(i) Microfractures may develop in granites in response to a variety of stresses. These stresses may be thermally, tectonically or hydraulically induced. Therefore it can be assumed that these fractures may be thus categorised and it is then possible to determine the origin of healed fractures in quartz based upon the analysis of the fracture orientations, morphologies and analysis of the inclusions contained within them. If so it may be possible to unravel the stress history of a granite, including those with a complicated tectonic and hydrothermal history.

(ii) Fractures have also been kinematically classified as either *mode 1* or *mode 2* fractures. However, previous researchers have considered that healed microfractures are generally *mode 1* in origin, based upon the lack of off-setting of other fractures and grain boundaries. Thus, can all FIPs be used to determine the orientation of the palaeostress field assuming that they represent extension fractures, regardless of the stresses controlled their origin?

(iii) It has been reported that the healing of microfractures may take place during geologically short periods of time, even at temperatures as low as 200°C. If this time period is the same order of magnitude as the fracturing process, then the morphologies of the secondary inclusions contained within them may be influenced. However it is

more likely that stresses applied to the secondary inclusions subsequent to healing of the fracture will influence the inclusion morphologies, possibly by controlling the re-equilibration of the inclusions. Is it then possible to relate the morphologies of secondary fluid inclusions to the kinematics of the fracturing process?

(iv) It has also been shown that inclusions may both re-equilibrate their densities and morphologies under differing conditions of internal and external underpressure or overpressure. Can the morphology of inclusions be influenced by later brittle deformation resulting from a stress field with varying orientations?

(v) Thus, if inclusions exhibit a preferred shape orientation within a healed fracture, is it due to processes governing the healing of the fracture, or is it due to post-trapping deviations from the isochore representing pressure-temperature conditions at the time of formation?

CHAPTER 3

FIP GENERATION ASSOCIATED WITH LOCAL STRESS DEVIATIONS, MINERALISATION AND FAULTING

3.0 Introduction

The area of Carrock Fell lies in the northern part of the English Lake District known as the Caldbeck Fells. The area was selected as a preliminary study area to test the methods and approaches that were developed and outlined as a prelude to their use in more complex geological terranes in Chapters 5 and 6. The features that made the Carrock Fell area an attractive study area were the simple relationships that are present between the mineralisation, alteration and host rocks. Mineralisation is common in the area, and the mining of copper, lead, zinc, antimony and tungsten stretches back several hundred years. However, mining ceased in the area with the closure of the Carrock tungsten mine in the early 80's.

The sampling procedure was designed to investigate several initial questions:

(i) Is it possible to differentiate between generations of FIPs based upon their orientation and the thermometric properties of the secondary fluid inclusions contained within them?

(ii) Can the orientations of these FIPs be related to macrostructures observed in the field?

(iii) Do FIPs show variation in abundance with distance from areas of intense mineralisation and hydrothermal alteration?

The sampling strategy is outlined in greater detail in section 3.2.1 with respect to the scale of the sampling pattern and the material sampled. To investigate these questions initial approaches and techniques were developed that also needed verification. The

main methods of analysis and sampling are detailed in the appendices. These techniques include the following:

(i) Orientation analysis of healed microfracture orientations from oriented samples using a universal stage attached to standard petrographic microscope.

(ii) Optical and thermometric analysis of the fluid inclusion populations specifically with reference to the secondary inclusions continued within the FIPs of a known orientation.

3.1 Geology

The geology of the Lake District dome consists of three broad areas of volcanic and sedimentary rock of Ordovician and Silurian age surrounded by Carboniferous limestone (Fig. 3.1). Shown to be underlying most of the central and northern Lake District is a granite batholith (Bott, 1974) (Fig. 3.2) which may be the southerly extension of the Weardale granite found to the north-east. The deposition of these sediments and lavas is related to the an important period of geological history for the Lake District, with the closure of the Iapetus ocean, resulting in continental collision and the climax of the Caledonian orogeny at the end of the Silurian (Moseley 1978).

The Carrock Fell complex consists of a group of basic and intermediate igneous bodies intruded into a series of lavas and slates. On the border of this igneous complex lies the granite and its associated mineralisation which is the primary interest of this investigation.

3.1.1 Sediments and Volcanics

The Carrock Fell igneous complex is bordered to the north by the Eycott Volcanic Group and to the south by the Skiddaw Slates.

Skiddaw Slates

The oldest rocks in the area are the Skiddaw Slates, which comprise 3000m of graptolitic mudstones (Moseley 1978). They are considered to be mostly distal turbidites deposited on the continental margin of the Lake District island arc during early Ordovician times. The Skiddaw Slates are overlain unconformably by the Borrowdale Volcanic Rocks (BVS) to the south but are thought to be conformable with the Eycott Group to the north, though the boundary is largely a faulted contact (Jackson 1978). Within the thermal aureole of the Skiddaw Granite they have been metamorphosed to form spotted slates, with the development of chlorite and mica, which pass into completely

recrystallised cordierite-biotite-hornfelses closest to the granite contact (Eastwood *et al.* 1968).

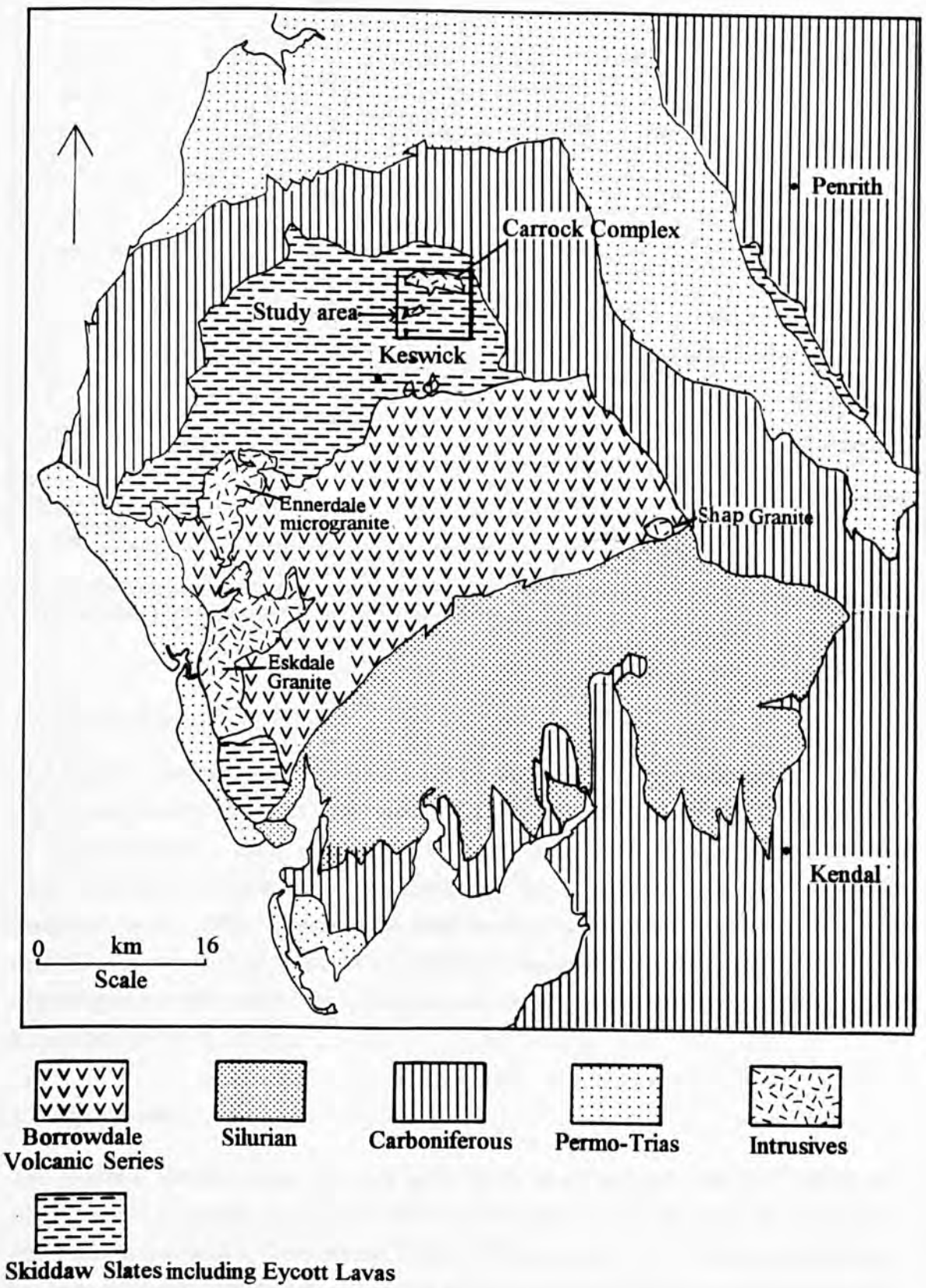

Fig. 3.1. Geological map of the Lake District (after Moseley, 1978). Inset of study area see Figs. 3.3 3.10

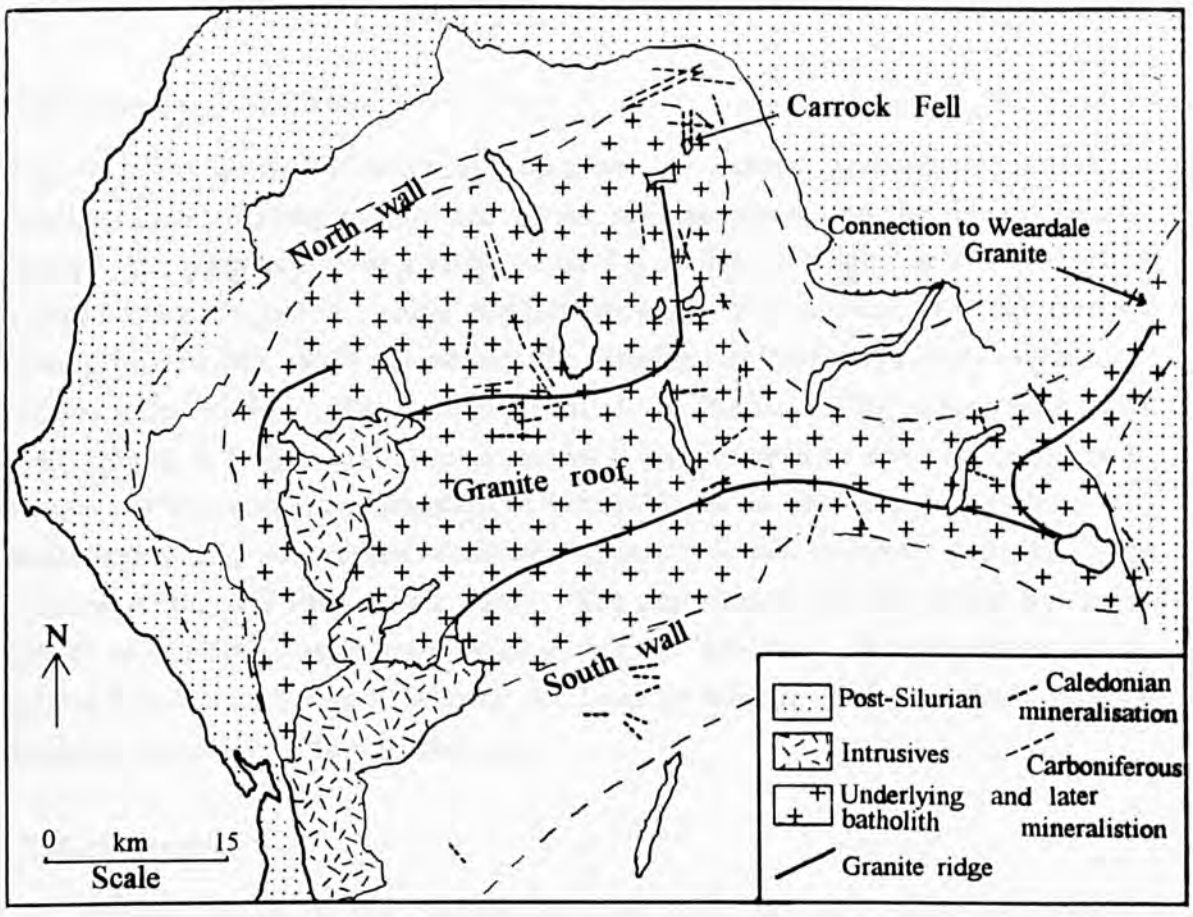

Fig. 3.2. Sketch map showing the roof and wall regions of the postulated Lake District Batholith and its connection to the Weardale Granite (after Bott, 1974).

Eycott Volcanic Group

The Eycott volcanic rocks represent a series of transitional calc-alkaline to tholeiitic basalts and basaltic andesites with some acid flows and tuffs (Fitton and Hughes, 1970) of Ordovician age. These rocks differ both petrographically and chemically from the large exposure of volcanics to the south, the BVS, and are believed to be older (Millward *et al.*, 1978). The tholeiitic trend to these rocks is strong evidence that their deposition occurred in an island arc or continental margin environment during the closure of the Iapetus ocean which was related to a south or south-easterly inclined subduction zone (Bamford *et al.*, 1976).

3.1.2 Intrusives

The Skiddaw Granite which outcrops in the study area, together with the Eskdale and Shap granites is thought to represent the exposed parts of a granite batholith underlying the northern and central Lake District (Bott, 1974), see Fig. 3.2. The Carrock Fell area has been thermally metamorphosed by this granite and is therefore presumed to be older, though its exact age is uncertain. A summary of published isotopic dates for the major intrusions of the Lake District are shown in Table 3.1.

Carrock Fell Igneous Complex

The complex consists of successive intrusions of gabbro, granophyre and diabase (diorite), intruded along the junction of the Skiddaw Slates and the Eycott Volcanic Group. The gabbros possess a crude bilateral symmetry, consisting of a central belt of quartz-hornblende-gabbro, which changes outwards into leucogabbro and marginal melagabbro (Firman, 1978). Previously, the complex was believed to have been intruded sub-vertically (Harker, 1984; Eastwood et al., 1968; Hunter, 1980), though more recent work (Harris & Dagger, 1987) suggests that it was intruded as a sub-horizontal body. Rundle (1979) reports a minimum age of 468±10Ma for the gabbros which together with mineralogical and geochemical evidence suggests they are cogenetic with the Eycott Volcanic Group (O'Brien *et al.*, 1985). The granophyre was also dated by Rundle (1979) at 421±8Ma, appreciably younger than the gabbros. Hornblendisation of the gabbro has occurred, though whether the cause of this are fluids associated with the Skiddaw Granite is not fully understood.

Skiddaw Granite

The Skiddaw Granite is only present as three small outcrops within the study area However the limit of it's thermal aureole suggests it is a much larger intrusion. Surface exposure can be seen at the Carrock tungsten mine, in the Caldew valley and at Sinen Gill. The intrusion is thought to be a steep-sided, flat-topped body, generally homogeneous and approximately 9 by 12km in size (Bott, 1974). The Caldew valley exposure is believed to represent the roof of the intrusion while the Grainsgill mass at the Carrock mine is probably a steep sided cupola (Firman, 1978). The Sinen Gill outcrop was dated by Miller (1961) at 399±14Ma, while more recently Shepherd *et al.*, (1976) have dated the intrusion of the granite at 392±4Ma. This places the intrusion of the granite in 'end-Silurian' times, or possibly early Devonian. Gravity data (Bott, 1974) suggests a connection of the Skiddaw Granite at depth to a large underlying Lake District batholith (Fig. 3.2). However, Rb-Sr whole rock isochron ages for the Eskdale granite in west Cumbria give a date of intrusion at 429±9Ma (Rundle, 1979) and for the Threlkeld microgranite at 445±15Ma. This suggests that emplacement of the granite occurred largely during Ordovician times (Firman & Lee 1986), with final related intrusive events occurring in 'end-Silurian' and early Devonian times.

The Skiddaw Granite consists primarily of biotite, quartz, oligoclase and microcline. Magnetite, apatite, pyrrhotite, ilmenite, zircon, epidote, sphene, rutile and tourmaline also occur as accessory minerals (Firman 1978). The Grainsgill outcrop has undergone various stages of greisenisation, leading to a coarse-grained rock consisting of two thirds quartz and one third muscovite, with accessory tourmaline, apatite, arsenopyrite, pyrite,

molybdenite, pyrrhotite and fluorite. The formation of the greisen and the associated mineralisation will be covered in more detail in section 3.1.4.

O'Brien *et al.* (1985) state that the parental magmas of the Lake District granites had a sub-crustal origin, related to a southerly-dipping subduction zone during and following the closure of the Iapetus ocean.

Table 3.1 Published isotopic dates for the major intrusions of the Lake District (after O'Brien *et al.* 1985)

Intrusion	*Age (Ma)*	*Method*	*Reference*
Skiddaw Granite	392±4	K-Ar (biotite)	Shepherd *et al.* (1976)
Shap Granite	393±3	Rb-Sr	Wadge *et al.* (1976)
Carrock Fell Granophyre	416±20	Rb-Sr	Rundle *et al.* (1979)
Ennerdale Granite	420±4	Rb-Sr	Rundle *et al.* (1979)
Eskdale Granite	429±4	Rb-Sr	Rundle *et al.* (1979)
Threlkeld Microgranite	445±15	Rb-Sr	Wadge *et al.* (1974)
Carrock Fell Gabbro	468±10	K-Ar (biotite)	Rundle *et al.* (1979)

3.1.3 Deformation

The most important period of deformation to affect the Lake District was the Caledonian orogeny. This resulted in polyphase deformation, low grade metamorphism and associated granite emplacement at the end of the Silurian. Three major unconformities in the stratigraphic succession represent periods of uplift, erosion and deformation. The first two are related to the subduction of the Iapetus oceanic plate, while the final and most important coincides with continental plate collision at the end of the Silurian (Soper & Moseley 1978).

End-Silurian polyphase deformation

Roberts (1977) has shown that there were four deformation episodes (D_1-D_4) which have affected the Skiddaw Slates in the study area. D_1 folds are thought to be gravity collapse structures formed before the deposition of the BVS. D_2-D_4 are end-Silurian structures, related to continental-continental collision:

(i) Minor folds, generally only visible within the thermal aureole of the Skiddaw Granite. No associated axial planar cleavage, although the bedding cleavage may have the appearance of a tectonic cleavage, particularly when associated with isoclinal folding.

(i) D_2 represents a period of crustal shortening, closely related in time to the intrusion of the Skiddaw Granite and are formed by the principal Caledonian movements associated with N-S compression. D_2 structures are correlated with E-W trending Caledonian

folding and are generally upright open folds, sometimes with minor overfolding and plunging 10 to 15° along an E-W ENE-WSW trend. An associated slaty cleavage, sub-parallel to bedding but also frequently cutting it is usually the dominant structure in the area and possess a steeply dipping E-W orientation.

(ii) D_3 structures are reclined folds and crenulation cleavage. D_3 deformation post-dates the granite, but coincides with hydrothermal activity associated with the granite intrusion. D_3 structures are generally minor folds and cleavage, more commonly developed outside the thermal aureole of the Skiddaw Granite. Folds are generally sideways closing, refolding both D_1 and D_2 structures with their axial planes and associated cleavage gently inclined. Crenulation cleavage are occasionally well developed. Since D_3 structures have formed in a stress field where σ_1 is vertical, their orientation depends largely upon the existing structures. Thus D_3 possess E-W orientations similar to D_2 structures. An age of end Silurian or very early Devonian is established for D_3.

(iii) D_4 deformation is the last tectonic episode to have any significant effect on the Skiddaw Slates, with D_4 structures themselves being only effected by a non-tectonic joint set. They have developed at right angles to the main structural grain of the area. Minor folds and flexures are formed on limbs of existing folds associated with a strong axial planar fracture cleavage as a result of axial shortening resulting from a relaxation of the major compressive strain after D_2 and D_3 deformations had taken place. The orientation of D_4 structures is consistently N-S.

Caledonian Faulting

Thrust, strike-slip and oblique-slip faults are well developed in the Skiddaw Slates and the BVS. Low angle thrusts are common in the Borrowdale Volcanics close to the boundary with the Skiddaw Slates (Soper & Moseley 1978). Both dextral and sinistral strike-slip faults are also common, with movement occurring before and after folding as they separate different fold patterns (*op. cit.*). To the south of the study area, the Coniston and Brathay faults displace the Coniston Limestone by up to nearly 2km (Norman 1961).

Hercynian Deformation

The Lake District was generally too far north for the Hercynian orogeny to greatly affect it. The underlying granite batholith imparted rigidity to the Lake District, which resulted in the formation of blocks and basins to the west that exerted some control over Carboniferous and later sedimentation (Soper & Moseley 1978). Hercynian faulting did, however, effect Carboniferous and later strata to the north of the study area (Fig. 3.3),

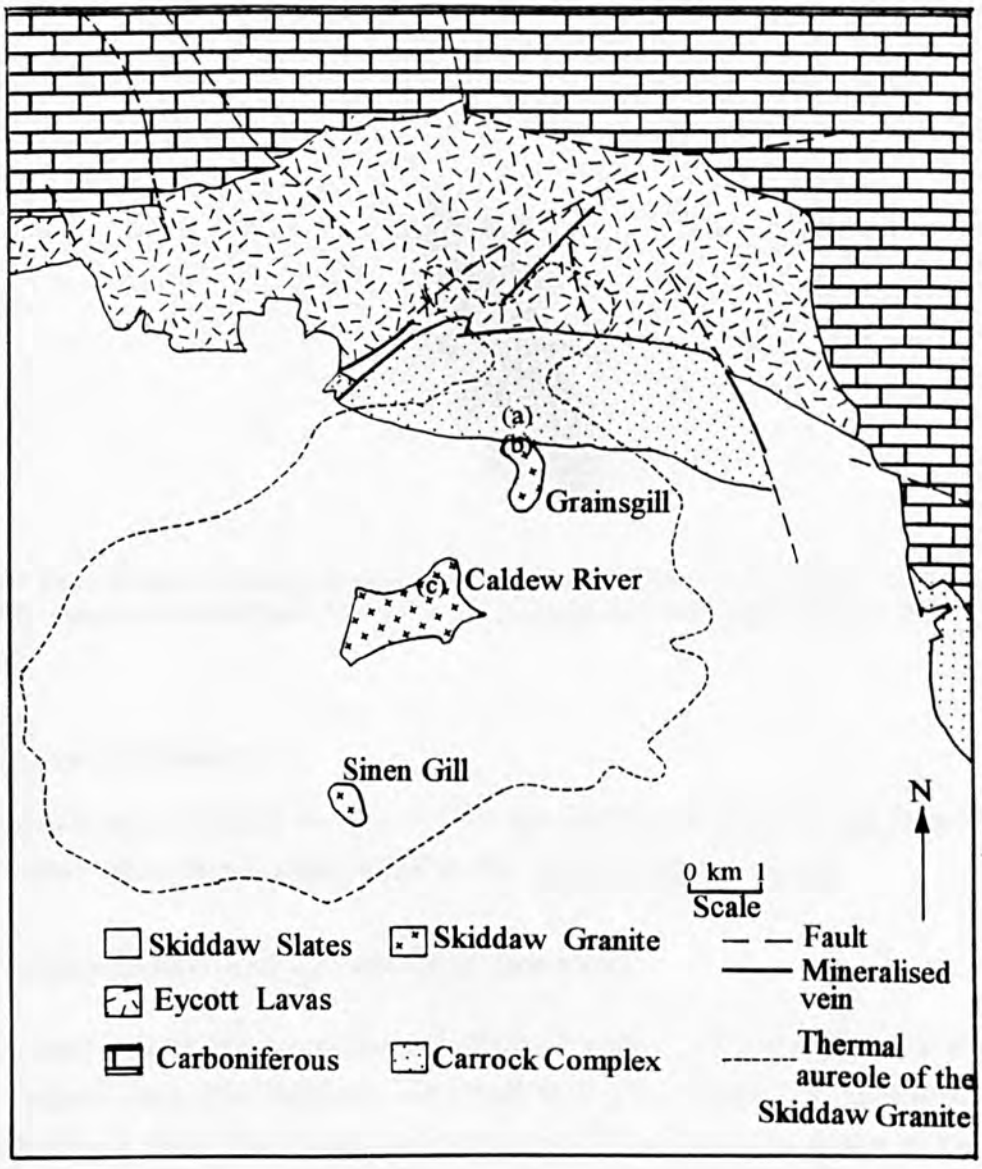

Fig. 3.3. Geology of the study area showing the positions of the three joint surveys: (a) Brandy Gill; (b) Grainsgill and (c) Caldew River (after Ineson and Mitchell, 1974).

forming NW-SE faults, together with minor NE-SW conjugate sets, implying that the principal compressive stress was E-W. The orientations of major faults located in around the study (Fig. 3.3) area are shown in Fig. 3.4.

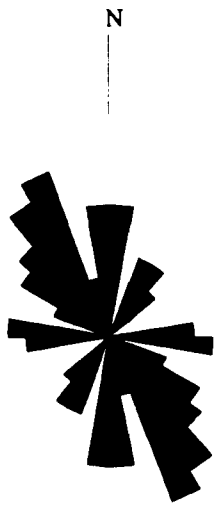

Fig. 3.4 Rose diagram showing the orientation of the major faults in the vicinity of the study area. N=45. Information based upon 1:50 000 solid edition of the Cockermouth sheet 23, BGS.

Post-Triassic deformation

Normal faulting and gentle doming of the Lake District occurred during later Mesozoic and Tertiary times, due to mild tension as the Atlantic Ocean widened.

3.1.4 Mineralisation and hydrothermal alteration

The various mineral deposits of the Lake District show a wide range in their origins and age. Copper, lead, zinc, tungsten and cobalt have all been mined over several hundred years of rich, if somewhat varied, mining history. There does not appear to be a clearly defined lateral zoning, probably due to the close spacing of the emanative centres, producing overlapping zones (Firman & Lee 1986). However, a number of authors (Bott 1974; Dagger 1976; Firman 1978; Stanley & Vaughan 1982) have showed that a close spatial relationship between mineralisation and the underlying Lake District batholith does exist.

Copper, lead, zinc and cobalt mineralisation

Stanley & Vaughan (1982) have classified the copper, lead, zinc and cobalt mineralisation into two groups:

(i) chalcopyrite-pyrite-arsenopyrite mineralisation: lower-Devonian in age, showing a clear relationship with the underlying granite batholith (together with tungsten mineralisation at the Carrock mine).
(ii) galena-sphalerite: early-Carboniferous in age, showing no relationship with the underlying batholith.

The early copper mineralisation was probably associated with the granite intrusions, with convective cycles such as the one set up at Carrock Fell (Shepherd *et al.* 1976) probably also in operation at Coniston and the Vale of Newlands (Firman 1978). These deposits could have formed along fractures opened up during the emplacement of the batholith, after the main period of Caledonian (end-Silurian) deformation (Stanley & Vaughan 1982). Fluids associated with this early Devonian mineralisation were typically 5-10 wt. %. equiv. NaCl brines, with temperatures from 200-400°C (Stanley and Vaughan 1982). The granite is thought by these authors to provide the heat source for remobilising copper and other ore forming elements from the BVS.

The later Carboniferous Pb-Zn mineralisation occurs above the roof region and north and south walls (Bott 1974) of the batholith, generally in N-S and NE-SW fractures implying an E-W tension (Firman 1978). This is in agreement with Russell (1976, 1978) who also hypothesises a tensional tectonic regime in early -Carboniferous times for the Lake District. The high heat flow from within the batholith, or a later thermal pulse may have caused the circulation of these mineralising brines (Firman & Lee 1986), with the ore-

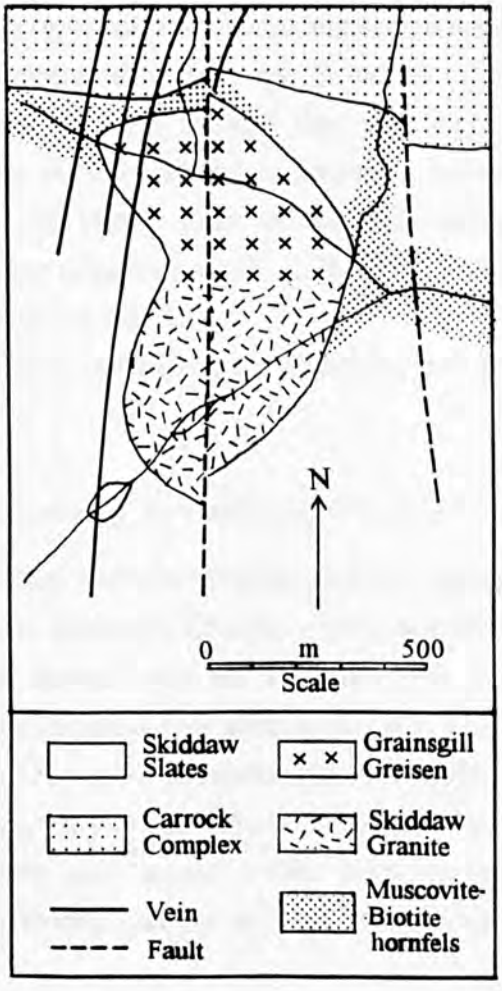

Fig. 3.5. Geology of the Grainsgill outcrop showing the extent of the greisenisation and the associated retrogressive metamorphism of the hornfelsed Skiddaw Slates (after Roberts, 1983).

forming elements being leached from lower Palaeozoic sediments by sea waters drawn into the convective system (Stanley & Vaughan 1982). These fluids were typically 23-25 wt. %. equiv. NaCl brines with temperatures 110-130°C.

Tungsten mineralisation

Tungsten mineralisation occurs at Carrock Fell in three major N-S striking, steeply dipping veins associated with the intrusion of the Skiddaw Granite and its subsequent alteration to the Grainsgill Greisen (Fig. 3.5) Tungsten occurs as wolframite and scheelite, together with arsenopyrite, pyrite, pyrrhotite, sphalerite, ankerite and quartz. The paragenesis of the tungsten mineralisation has been well documented by various authors (Shepherd *et al.* 1976; Shepherd & Waters 1984; Ball *et al.* 1985; Jones 1985). The geology of the area has also been well documented by Finlayson (1910) and Hitchen (1934), while Ewart (1962) and Roberts (1983) have detailed the alteration of the granite and formation of the greisen.

Shepherd (1976) has shown, on the basis of fluid inclusion studies that the temperatures of the fluids responsible for the deposition of tungsten were around 265-295°C (at 800bars pressure), with greisenisation occurring at temperatures around 240-295°C. The fluids were moderately saline (approx. 8 wt. %. equiv. NaCl) and periodically charged in CO_2. Isotope studies showed that they were depleted in ^{18}O relative to magmatic fluids, and are thus considered to contain a major non-magmatic component. More recently, Ball *et al.* (1985) have shown that wolframite deposition may have initiated at slightly higher temperatures (T_h 235-335°C), with a fluid composition of 6 wt. %. equiv. NaCl + 3 wt. % $NaHCO_3$.
The tungsten mineralisation and associated alteration was dated at 385±4Ma (Shepherd *et al.* 1976).

Greisenisation and formation of the Grainsgill Greisen

Late-stage fluids associated with the Skiddaw Granite were responsible for the alteration of the granite to form the Grainsgill Greisen. This resulted in the destruction of feldspar to form muscovite and quartz, with the liberation of K_2O, Na_2O and Al_2O_3 (Roberts 1983). Alteration of the hornfels and gabbro has also occurred over a radius of 200m from the granite intrusion by K metasomatism. Xenoblasts of cordierite have been retrogressed to chlorite, and biotite has been altered to muscovite, (Roberts 1983). Alteration of the gabbro only occurs within close proximity of the tungsten veins. Actinolite is altered to biotite, chlorite and calcite. Feldspar is replaced by calcite and epidote (Ewart 1962).

According to Shepherd *et al.* (1976), the short interval between granite emplacement and the onset of mineralisation and alteration implies a high heat production from the granite which would be capable of sustaining a natural convective system around the intrusion. This would enable groundwater-rock interaction to occur and therefore externally heated fluids is not required.

Chalcopyrite-pyrite-arsenopyrite mineralisation in the Caldbeck Fells

Copper mineralisation lies outside the thermal aureole of the Skiddaw granite, occurring predominantly in N-S and NNW-SSE fractures. No data exists on the fluids responsible for this type of mineralisation, but Cooper & Stanley (1990) suggest that it is of similar age to the tungsten mineralisation (Lr. Devonian) and probably genetically related to copper mineralisation seen at the Vale of Newlands and at Coniston. Tentative data for these fluids suggest temperatures from 200-400°C and salinities from 5-10wt% equiv. NaCl (Stanley & Vaughan 1982). Mineral assemblage consist primarily of quartz, pyrite, chalcopyrite, with or without arsenopyrite.

Manganese mineralisation around Carrock Fell

Manganese mineralisation occurs to the west of Carrock Fell in N-S fractures. It is also seen in the southerly (Wet Swine Gill) and northerly (Brandy Gill) extensions of the tungsten veins (Hitchen 1934; Appleton & Wadge 1976; Shepherd & Waters 1984). Manganese mineralisation occurring to the north of the Carrock tungsten deposits in Dry Gill is thought to be later, signifying more than one episode of this type of mineralisation (Cooper & Stanley 1990).

Antimony mineralisation

A small amount of antimony mineralisation occurs at Wet Swine Gill as Sb-Fe-As-Pb. Fluid inclusion studies by Fortey *et al.*, (1984) indicate homogenisation temperatures of 166-287°C and sailinities from 7-11wt% equiv. NaCl. The fluids are thought to be CO_2-poor but $MgCl_2$-rich, differing from those responsible for tungsten mineralisation at Carrock.

Lead-zinc mineralisation in the Caldbeck Fells

Lead-zinc mineralisation in the Caldbeck Fells occurs generally in E-W or NE-SW striking fractures (Cooper & Stanley 1990). Mineral assemblage consist of galena, sphalerite and chalcopyrite together with quartz. Fluorite only occurs in the E-W vein at Carrock, while barytes occurs as a later infilling of vugs. The Pb-Zn mineralisation is thought to possess an early Carboniferous age (*c.* 360-330Ma) (Stanley & Vaughan 1982). However, isotopic dates from various localities are not in agreement with this.

Table 3.2 Isotopic dates from various localities in the Caldbeck Fells

Locality	*Age (Ma)*	*Method*	*Reference*
Carrock E-W vein	210±70	lead isotope (galena)	Moorbath (1962)
Roughton Gill	220±40	lead isotope (galena)	Moorbath (1962)
Driggith	260±90	lead isotope (galena)	Moorbath(1962)
Carrock E-W vein	197 & 231 (no errors quoted)	K-Ar (illite-chlorite)	Ineson & Mitchell (1974)

However, Cooper & Stanley (1990) suggest that the variability of these ages may be due to the episodic nature of the Pb-Zn mineralisation or the dubious authenticity of isotopic dating using lead isotopes and wall rock illites in areas which have undergone widespread alteration. However, relative ages may be deduced from field evidence, as the N-S veins at Carrock are offset by the E-W vein, showing it to be younger than the tungsten mineralisation.

Stanley (1979) suggests homogenisation temperatures for fluid inclusions from the E-W Carrock vein to be around 120°C. This data is also in agreement with Ball *et al.* (1985) who state that the deposition of fluorite and carbonates were below 150°C. The fluids possessed a high bulk salinity >23 wt. %. equiv. NaCl, and are interpreted to consist of 12 wt. %. equiv. NaCl and 15 wt. % equiv. $CaCl_2$. Cooper and Stanley (1990) envisage sea water as a possible source for the mineralising fluids. However, similar fluids occur in SW England, associated with cross-course mineralisation and may represent basinal brines, expelled from sedimentary basins Shepherd and Scrivener, 1987).

Later mineralisation

Later mineralisation may include the deposition of baryte (*e.g.* Sandbeds mine), by low temperature fluids (below 150°C), possibly utilising fractures generated by Hercynian earth movements (Cooper & Stanley 1990). Faulting of Carboniferous strata is apparent to the north of the field area, although the origin of the mineralising fluids is uncertain.

A summary and classification of the mineralisation of the Carrock area and the surrounding Caldbeck Fells is summarised in Table 3.3.

Table 3.3 Summary and classification of Caldbeck Fell mineral deposits (after Cooper & Stanley 1990).

Tectonic & igneous activity	Age of mineralisation	Typical mineral assemblages	Examples
Tensional regime as Europe and America separate. Post-Triassic earth movements	? Jurassic & later *c.* 190-180Ma	Pyromorphite±mimetite± covelline±malachite± many others	Oxidation assemblages at Potts Gill. Roughton Gill, Driggith, etc.
ESE-WNW faults Uplift due to Hercynian orogeny Olivine dolerite dykes	Upper Carboniferous to Permian *c.* 290-230Ma	Baryte±quartz±calcite± galena	Potts Gill, Sandbeds
E-W to NE-SW normal faults End Devonian-L. Carboniferous earth movements Cockermouth lavas	? Lower Carboniferous *c.* 360-330Ma	Quartz±galena± sphalerite±chalcopyrite± pyrite±antimony±calcite ±baryte±dolomite± fluorite	Roughton Gill, Driggith, Silver Gill, Red Gill, Carrock E-W vein, Brae Fell, etc.
N-S to NE-SW faults	? Lower to Upper Devonian	Quartz±arsenopyrite± stibnite±others	Wet Swine Gill, Grainsgill
N-S faults	? Uncertain	Quartz±'psilomelane'± pyrolusite±other manganese minerals	Brandy Gill, Burdell Gill, Arm o'Grain
N-S (to NNE-SSW & NNW-SSE) faults Intrusion of the Skiddaw Granite at *c.* 400 Ma End of Caledonian orogeny	Lower Devonian *c.* 390-370Ma	Quartz±chlorite± arsenopyrite±pyrite± chalcopyrite±sphalerite± galena Quartz±apatite± wolframite±scheelite± arsenopyrite±bisumuth minerals±many others	Potts Gill Copper vein, Carrock End, Hay Gill Carrock N-S tungsten veins

3.2 Sampling collection and analysis of field data

As discussed in the previous section, the fluids that have deposited ore minerals and associated alteration at Carrock fell and the surrounding area show a distinct temporal and spatial variation. They have been dated (albeit tentatively) over a wide period of geological history. The fluids appear to have originated from a variety of sources, with ore metals being scavenged from both the volcanic and sedimentary pile, as well as from the underlying Lake District batholith. The fractures utilised by these fluids possess various orientations related to different tectonic episodes. However, the precise relationship between fluid source, available pathways for mineral deposition and the governing tectonic regime are far from clear.

The following section details the methodology behind the sampling approach in the study area, together with some of the structural and mineralogical relationships observed in the field.

3.2.1 Sampling approach

The Skiddaw Granite outcrops in three places within the study area. The Grainsgill exposure has been altered to form the Grainsgill Greisen (see above), by fluids utilising a series of N-S fractures, in which the deposition of tungsten has occurred. The other outcrops, both to the south, remain unaltered by the metasomatic fluids, and possess no closely related mineralisation. A sampling approach was adopted to investigate the variation, with distance from the zone of tungsten mineralisation, the orientation and abundance of the FIPs in granite quartz. A change in the abundance of fluid inclusions with respect to the tungsten mineralisation has already been shown to exist by Jones (1985) in mineralised and barren sections of the tungsten bearing veins from the Carrock mine. A variation in abundance of fluid inclusions in the host rocks is expected due to the steam aureole effect (Rankin 1988). It was also expected that samples in proximity to the N-S tungsten veins would show FIPs strongly mimicking their orientation, and that samples within the greisen zone would contain a greater abundance of N-S oriented FIPs than those in the unaltered granite. At greater distances from the mineralisation centre, a return to the background trend to FIP orientations might then be recognisable, according to theory (Rankin *op. cit.*).

Because the granite is clearly older than any of the periods of mineralisation in the area, fluids responsible for all types of ore deposition might be observable within it. It was also presumed that the microstructural evidence would help to explain the tectonic deformation that resulted in the production of open fractures and fissures that were utilised by the ore fluids.

The major control over the location of sampling points was the outcrop pattern of the Skiddaw granite, which can be seen in Fig 3.3 together with the locations of the sampling points. Closely-spaced sampling (~5-10m) of the granite and greisen at the Grainsgill outcrop was possible. However, a change in scale of the sampling (~1-2km) was then imposed by the distance to Caldew River and Sinen Gill outcrops. These distances must be remembered when interpreting changes in FIP orientation and abundances between samples. Un-oriented samples of vein quartz from the N-S tungsten bearing veins (Harding vein) and from the E-W lead bearing cross-course were also obtained to help constrain the fluid inclusion populations specifically associated with the mineralisation.

3.2.2 Joint, fault and vein orientations

Measurements of joint, fault and vein orientations were taken in the study area, especially in the vicinity of the sampling points. However, although the study area is set in a region possessing substantial topography, the exposures of granite at Grainsgill and along the Caldew River are restricted to the valley floor. Thus, the measurements of joint orientations proved to be extremely difficult. The exposure at Sinen Gill is on the side of the valley, but here no joint measurements were obtainable since the granite has been severely affected by weathering, removing all traces of jointing on the surface of the exposure. This also made the sampling procedure extremely difficult.

Joint orientations

Joint surveys were undertaken within the hornfels in Brandy Gill (position 'a' on Fig. 3.3), at Grainsgill (position 'b' on Fig. 3.3) and in the Caldew Valley (position 'c' on Fig. 3.3). Together with the strike and dip of the joint, its form (planar/curvi-planar), mineralisation (if present), development, and border (alteration of the wall rock) were also recorded. The presence of slickenfibres upon the joint surfaces were also recorded, if seen, though this was rare, and no movement direction was detected on any joints.

Fig. 3.6 shows that joints at the Grainsgill outcrop fall into three distinct groups. The E-W (most numerous) and NW-SE joints are both steeply inclined, while a third, smaller group consists of sub-horizontal, flat-lying joints. There does not appear to be any relationship between unmineralised and mineralised joints at this locality.

Joint orientations from the Caldew Valley (Fig. 3.7) exposure show a wide scattering, but a NW-SE striking, steeply dipping group is present, together with a possible sub-horizontal grouping. No mineralised joints were seen at this exposure.

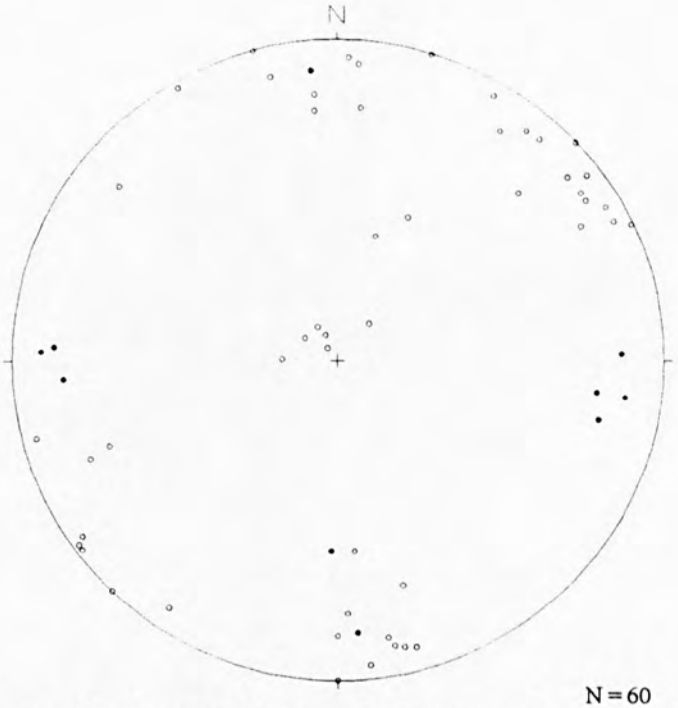

Fig 3.6 Equal area projection showing poles to planes of joint surfaces from the Grainsgill outcrop. Open circles = unmineralised joints, filled circles = qtz and/or muscovite filled joints.

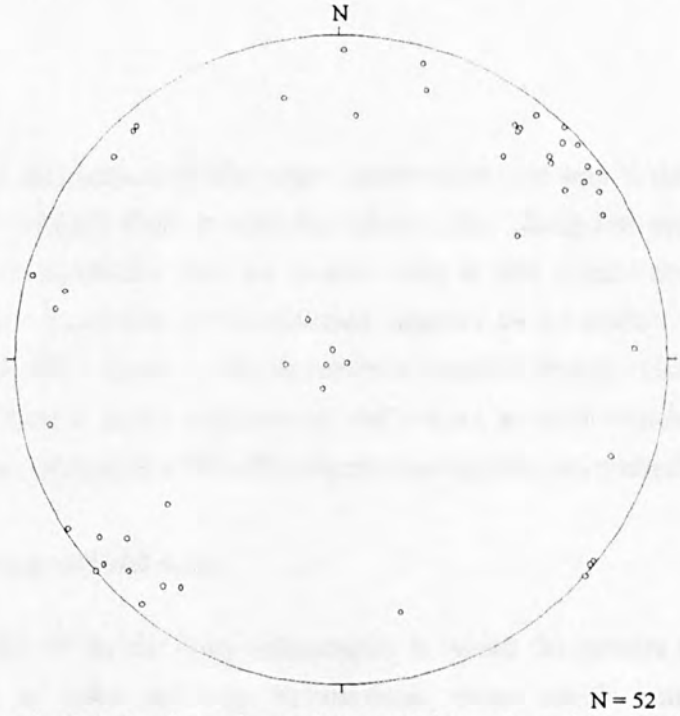

Fig. 3.7 Equal area projection showing poles to planes of joint surfaces from the Caldew River outcrop. Open circles = unmineralised joints.

Joint orientations within the hornfels at Brandy Gill (Fig. 3.8) are generally steeply dipping and show a strong N-S orientation. This orientation is absent in the granite (Fig. 5.7) and only a minor orientation at Grainsgill (Fig.3.6) and their origins are discussed below. Several mineralised joints are present, which are also seen to possess a N-S orientation similar to the tungsten veins at the Carrock mine.

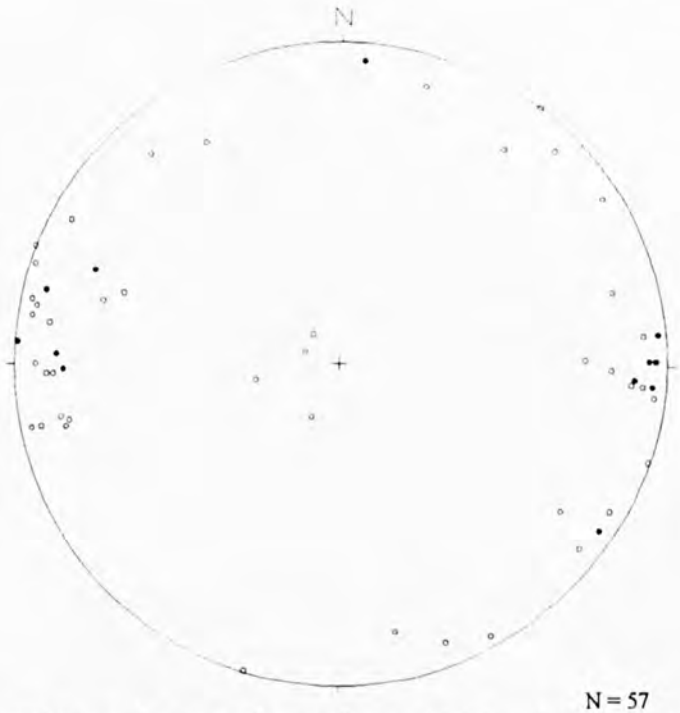

Fig. 3.8 Equal area projection showing poles to planes of joint surfaces from within the hornfels at Brandy Gill. Open circles = unmineralised joints, filled circles = quartz and/or muscovite filled joints.

Vein orientations

Fig. 3.9 shows the orientations of the major mineralised vein sets in the study area and to the north in the Caldbeck Fells around Roughton Gill. Tungsten and manganese veins show a strong N-S orientation and are located only in and around the granite cupola at the Carrock mine. Lead-Zinc mineralisation appears to be mainly restricted to veins striking roughly E-W. These veins occur at Carrock, Brandy Gill and at Dry Gill. Copper mineralisation is more widespread and occurs in veins which a possess a more variable orientation, although a NE-SW orientation may be recognised.

3.2.3 Interpretation of field data

Although the nature of the flat lying topography in which the granite outcrops hampered the measurement of joint and vein orientations, some conclusions can however be reached from the data set. Some mineralised joints (may be called veinlets) were evident in the Grainsgill outcrop and in the hornfels at Brandy Gill. These joints contained quartz, sometimes with muscovite, and show a clear relationship with the tungsten mineralisation and associated alteration. The origins and orientations of joints and veins are summarised in table 3.4.

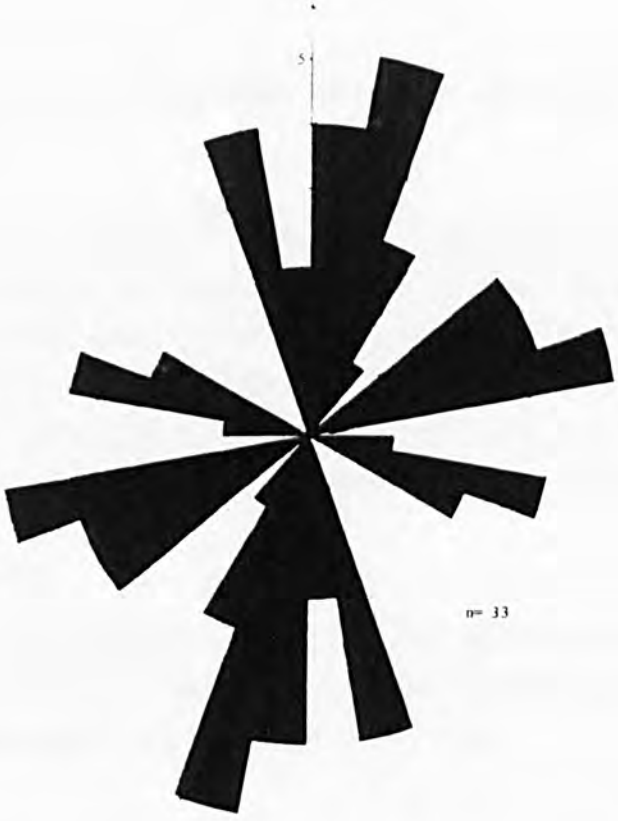

Fig. 3.9. Orientations of the major vein sets in and around the study area.

N-S oriented joints

A strong unmineralised joint set, also oriented N-S was recorded in the hornfels at Brandy Gill, which are thought to be unrelated to the mineralised set. Roberts (1977) states that the D_4 deformation episode at the end of the Caledonian orogeny took place after the effects of the Skiddaw Granite intrusion had ceased, since D_4 structures are found only outside the thermal aureole (Barratt 1968). However, within the thermal aureole, the deformation is manifested by a strong N-S joint set. This deformation is believed to be due to axial shortening, resulting from a relaxation of the major compressive strain, once the D_2 and D_3 deformations had taken place (Robert 1977). D_4 structures are not present within the granite, suggesting that it was to rigid too accommodate D_4 deformation.

Also present are smaller set of mineralised N-S striking joints. These are believed to have the same origins as the N-S tungsten veins.

E-W and NW-SE oriented joints

The origin of the unmineralised E-W and NW-SE joint sets that are apparent within the granite is uncertain. The formation of the E-W set by D_2 and D_3 deformation episodes, which produced E-W striking folds and cleavage in the Skiddaw Slates, is possible. Compression joints formed by N-S compression would not present open fractures, which

could be utilised by hydrothermal fluids, and thus no mineralisation and alteration would occur within them.

Another explanation for the development of the E-W joint set, together with the NW-SE set, is by later, possibly Carboniferous age movements. Field relations support this theory, as these unmineralised joints regularly appear to crosscut the mineralised joints, although no offsetting was observed by the unmineralised joints. A relationship to other structures in the study area, such as E-W, Pb-Zn veins and NW-SE striking, normal faults in Carboniferous and Triassic rocks to the north, could be envisaged.

Sub-horizontal joints

The smallest group of joints is a set of flat lying, sub-horizontal fractures. These are unmineralised, and are thought to be related to cooling (thermal contraction) and/or exhumation of the granite, rather than of tectonic origin.

Vein formation

As stated above, the formation of the N-S tungsten veins was probably due to fluid pressures within the cooling granite exceeding the confining pressure of σ_3, resulting in hydraulic fracturing of the granite (see Chapter 2 concerning hydraulic fracturing and effective stress). This may also explain why tungsten mineralisation occurs only in one place. Shepherd *et al.*, (1976) suggests that there is a major non-magmatic component to the fluids associated with tungsten mineralisation and greisenisation, with the source of the tungsten being outside the granite. The Grainsgill cupola lies above the North Wall (Bott 1974) of the Lake District batholith, and it would appear that only here was the fluid pressure large enough to induce fracturing and vein formation, since N-S fractures and joints are restricted to this area.

Table 3.4 Summary of joint orientations and their origins.

Joint orientation	*mineralisation*	*development*	*origin*
sub-horizontal	none	granite	unroofing / exhumation
NW-SE	none	granite	?Hercynian deformation
E-W	none	granite	?Hercynian deformation
N-S	none	hornfels	D_4 end-Silurian
N-S	qtz±muscovite± arsenopyrite	hornfels, Grainsgill granite	hydraulic fracturing

3.3 Microstructure and microthermometry

The following section concerns an analysis of samples in the laboratory to define the nature of the hydrothermal fluids and the microstructural pathways they utilised. As described in Appendices B and C, this involves a three-stage process:

(i) Orientation analysis of FIPs.
(ii) Optical properties of the fluid inclusion population.
(iii) Microthermometric analysis of the individual fluid inclusions.

A complete catalogue of the data, from which interpretations have been drawn are categorised in Appendix A.

3.3.1 Orientation analysis

The orientations of FIPs have been recorded from seven granite samples within the study area. The orientations of all FIPs encountered in the quartz grains were determined regardless of their likely origin. However, since this study was to relate the orientations of vertical or sub-vertical macrofractures observed in the field which have been utilised by hydrothermal fluids, a preference was given to the analysis of FIPs with a similar orientation. The Universal stage can only analyse fractures which have angles greater than 45° to the section in which they are viewed. Thus, the majority of samples analysed were prepared from horizontal sections, so that sub-vertical to vertical FIPs could be analysed. This method and limitations of the Universal stage technique are discussed in more detail in Appendix B. The orientations of unhealed (open) fractures are not presented. Since it is not possible to characterise the origins of these fractures, their origins may be related to the sampling and sample preparation process and not as a result of tectonic activity.

Summary of orientation results

Approximately 600 FIP orientations were recorded from the seven samples; four from the Grainsgill outcrop (of which three were greisens), two from the Caldew River outcrop, and one from Sinen Gill. Two distinct preferred orientations were observed. These consisted of a strong set of FIPs oriented N-S, and a numerically smaller set which was oriented from NW-SE to NE-SW, but with a general underlying E-W trend. Fig 3.10 shows the sampling locations within the study area and the orientations of FIPs recorded (displayed as rose diagrams, showing strike only). These diagrams show that FIPs with a N-S preferred orientation are only present in samples from the Grainsgill outcrop, whereas FIPs with a general E-W strike, although less abundant within individual samples, are more widely occurring and found in every sample.

It was to be expected that a strong N-S trend of the FIPs would exist within the greisen at Grainsgill, mimicking the strike of the tungsten-bearing veins. However, the orientation of FIPs in the unaltered granite is not so clearly observed. The results clearly show the relationship between microfracturing and the pervasive greisenisation of the granite. An explanation of the mechanisms that produced these N-S FIPs is needed. The origin of the E-W FIPs within the samples is thought to be genetically different from the N-S fractures. Stereonets of the data (Fig. 3.11) from all the sample localities show that the FIPs were generally vertical or sub-vertical. However, a third minor set of horizontal

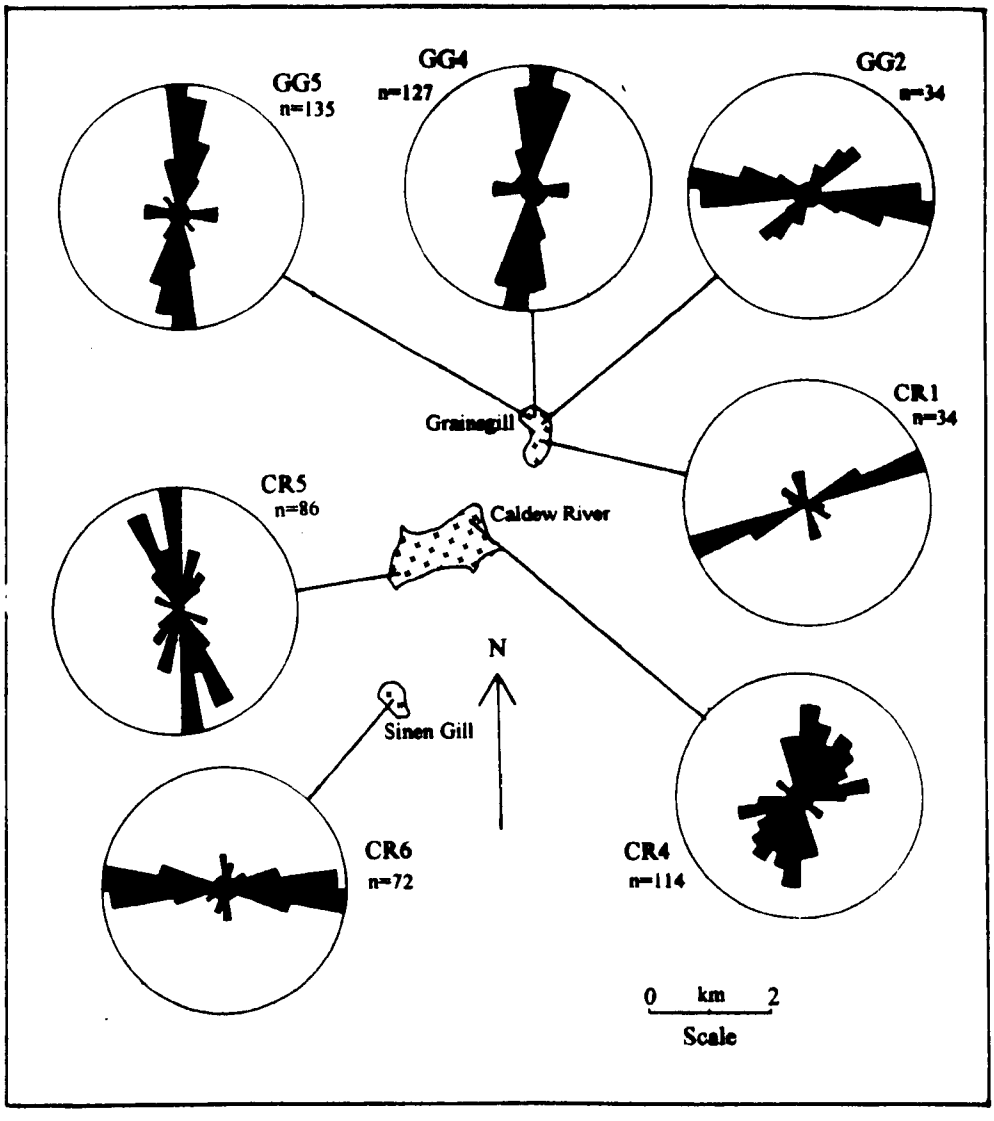

Fig. 3.10. Rose diagrams illustrating the positions of samples from the Grainsgill, Caldew River and Sinen Gill outcrops, together with the orientations of FIPs.

and sub-horizontal FIPs were seen to exist within the granite, recorded in sections prepared in a vertical plane.

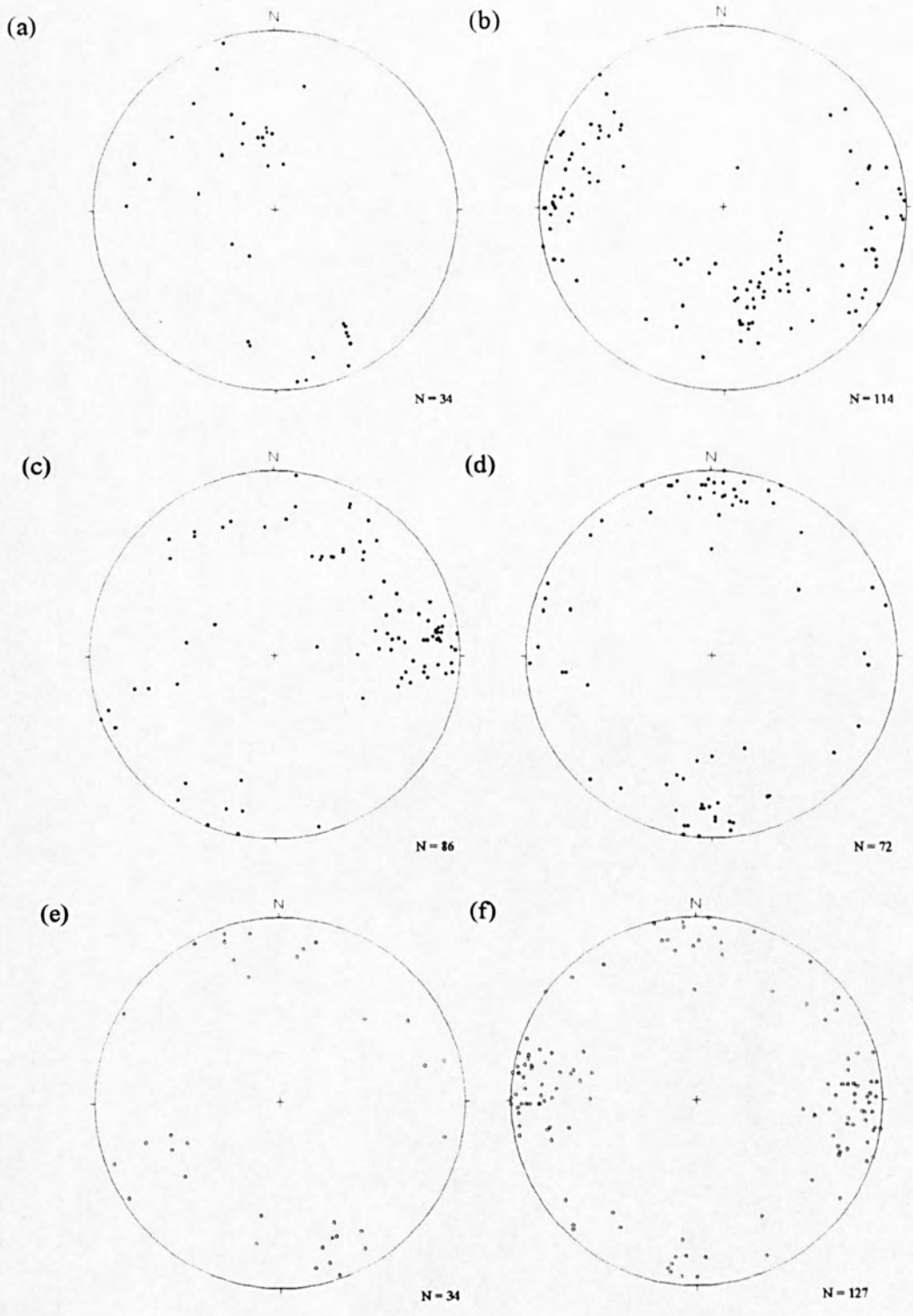
(a)
N
N = 34
(b)
N
N = 114
(c)
N
N = 86
(d)
N
N = 72
(e)
N
N = 34
(f)
N
N = 127

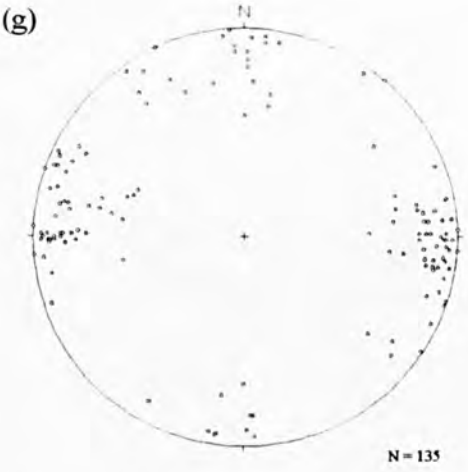

Fig 3.11 Equal area projections showing poles to planes of FIPs. (a) CR1; (b) CR4; (c) CR5; (d) CR6; (e) GG2; (f) GG4; (g) GG5. See Fig. 3.10 for sample locations.

FIP abundances

The abundance of FIPs and therefore inclusions abundance, showed a marked variation between samples. However, the presence of sub-horizontal FIPs within the quartz grain will detract from this correlation, giving anomalously high readings for the inclusions abundance. Measurements were made by counting the total number of FIPs within a grain of quartz within a single plane, not the total thickness of the grain. The area of the quartz grain was calculated, initially using a Site System image analysis software package linked to a standard petrographic microscope and then graphically using images obtained from a videoprinter. Generally three or four quartz grains were selected from each sample. Fig 3.12 shows FIP abundance within the seven samples.

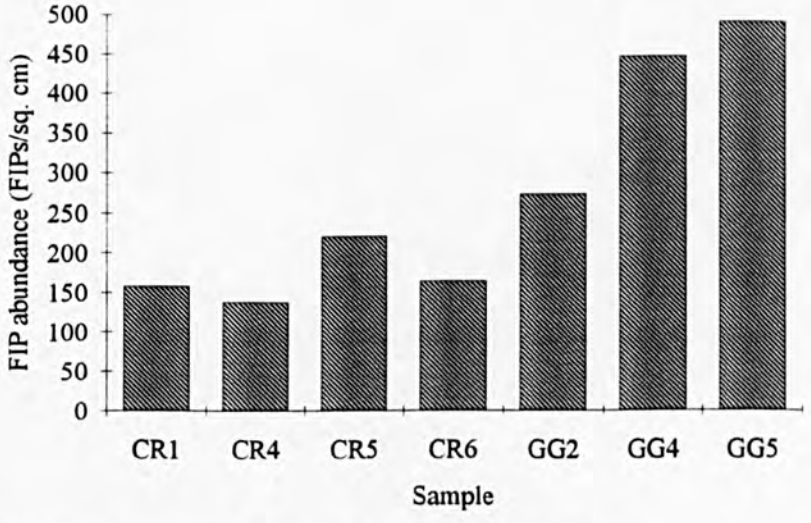

Fig. 3.12 FIP abundance histogram for samples from the Carrock Fell area.

Quartz analysed within the greisen shows a distinct increase in FIP abundance when compared to quartz from the unaltered granite. Sample CR1, obtained close to the granite/greisen boundary shows a marked drop in FIP abundance as compared to sample GG2 and especially samples GG4 and GG5. This signifies the importance of a dense microfracture network in the pervasive alteration of the granite. Although sample CR1 does contains a strong N-S FIP orientation (Fig. 3.10), alteration may only occur when a high quantity of pathways are present for the hydrothermal fluid to percolate through, thus controlling the amount of fluid flux that may pass through the rock over time.

However, sample GG2 shows a relatively low FIP abundance similar to that seen in the granite samples. The cause of this is thought to be recrystallisation of the granitic quartz (Rankin, 1989). Certain quartz crystals within the greisen were almost totally free of FIPs and inclusions. These are thought to have been completely recrystallised by the hydrothermal fluids responsible for the alteration of the granite, and thus removed the presence of all pre-existing FIPs. This phenomena was present in sample GG2, resulting in a lower FIP abundance count.

3.3.2 FIP morphological variations

As outlined in Chapter 2, the processes which are thought to govern the formation of fractures and their subsequent annealing, may result in a large range in morphologies in the resulting FIP population. These variations can thus be used to understand the origins of different FIP's. The morphological variations observed in the Carrock Fell samples include the following:

(i) FIP development: whether inter- or intra- crystalline.
(ii) Propagation points: where the FIP initiates and/or terminates.
(iii) FIP shape: planar, curvi-planar; sinusoidal or irregular.
(iv) FIP width (aspect ratio)
(v) Inclusion size, shape and abundance within FIPs
(vi) FIP definition; a combination of inclusion abundance, size and FIP width. The 'definition' is thought and thought to be related to the degree of annealing of the fracture.

The classification scheme of the FIPs studied was used to help explain the wide variations in morphologies that were observed during the course of the study. It must be noted that the FIPs were studied in essentially two dimensions. Thus, descriptions of FIPs as intracrystalline, or isolated are only with respect to the section in which they are cut. However, in samples which may have quartz grain sizes of upto 4-5mm, it is likely that FIPs with lengths of only a few hundred microns may be completely isloated within the crystal. However, with a large enough data set possible preferred orientations within the two dimensional section may become apparent.

The last three of the above points concern the secondary inclusions found within the fractures and are related to the process which effectively healed them. These will be discussed in section "3.3.3 Optical analysis of the Fluid Inclusion Population".

Inter- and intra- crystalline FIPs

FIPs constrained within a single quartz crystal were by far the most abundant (intracrystalline FIPs). FIPs that clearly crossed grain boundaries, not just terminating or initiating from them, were numerically less important (intercrystalline FIPs). However, these intercrystalline FIPs were generally better developed, with lengths up to several millimetres in the largest cases, than the intracrystalline FIPs whose size range was usually between 100μm and two or three millimetres. Obviously the grain size of the specimen has some control over the number of inter as opposed to intracrystalline FIPs. A large intracrystalline fracture in a coarse-grained granite could be an intercrystalline

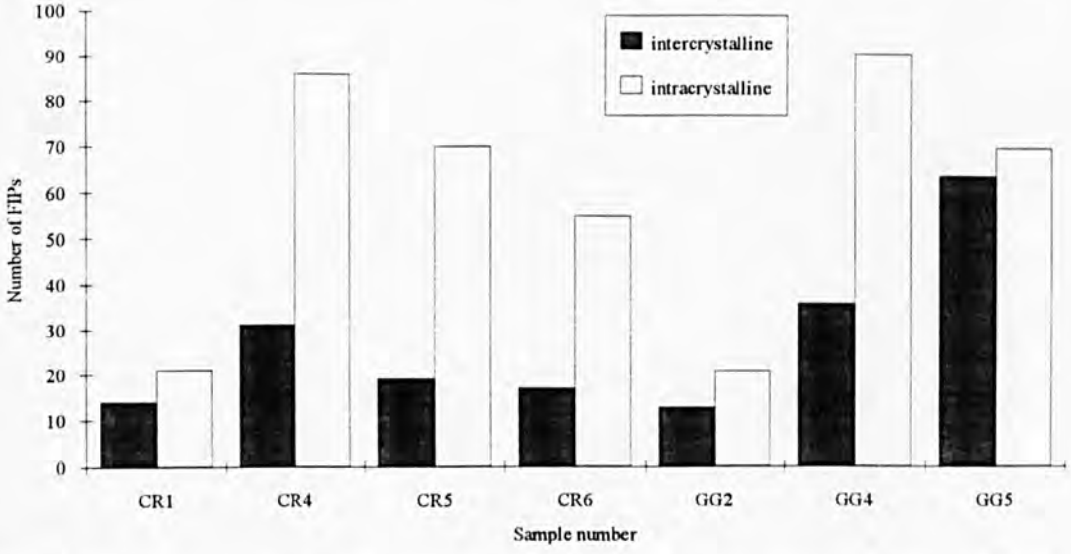

Fig. 3.13 Histogram showing the numerical relationship between inter- and intracrystalline FIPs from the Carrock Fell area.

fracture in a second, finer-grained specimen. The processes which govern the formation of these fracture types are however not thought to be related to grain size, but to the termination and initiation points of the fractures as outlined below. Fig 3.13 shows the numerical proportion of between inter and intracrystalline FIPs within the samples.

It can be seen from Fig 3.13 that both inter- and intracrystalline FIPs are present in all samples. The greisen samples (GG2, GG4 and GG5) show the largest number of intercrystalline FIPs in relation to the total number of FIPs recorded. This is presumed to be a function of the grain size, which was consistently smaller in these samples., as can be seen from Table 3.5.

Table 3.5 Average grain size of quartz crystals from samples from the Carrock Fell area.

Sample	CR1	CR4	CR5	CR6	GG2	GG4	GG5
Average quartz grain size (mm).	4-5	3-4	3-4	4-5	2	2	1-2

A combination of the strike and dip data shows that there is a possible relationship in some samples between orientation and FIP intercrystalline/intracrystalline nature (Fig. 3.14). This was unfortunately masked in the greisen samples due to a fine-grained nature.

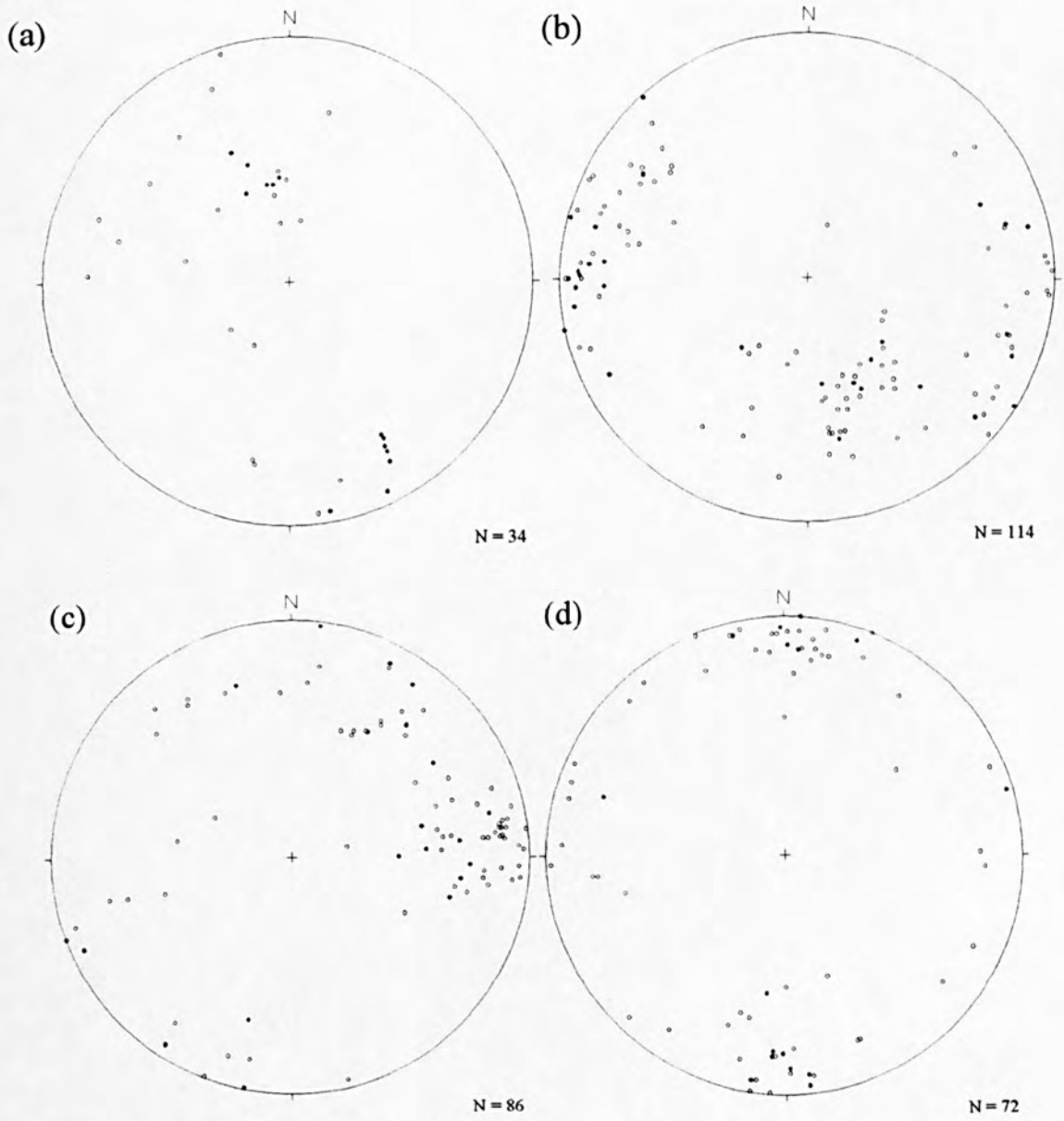

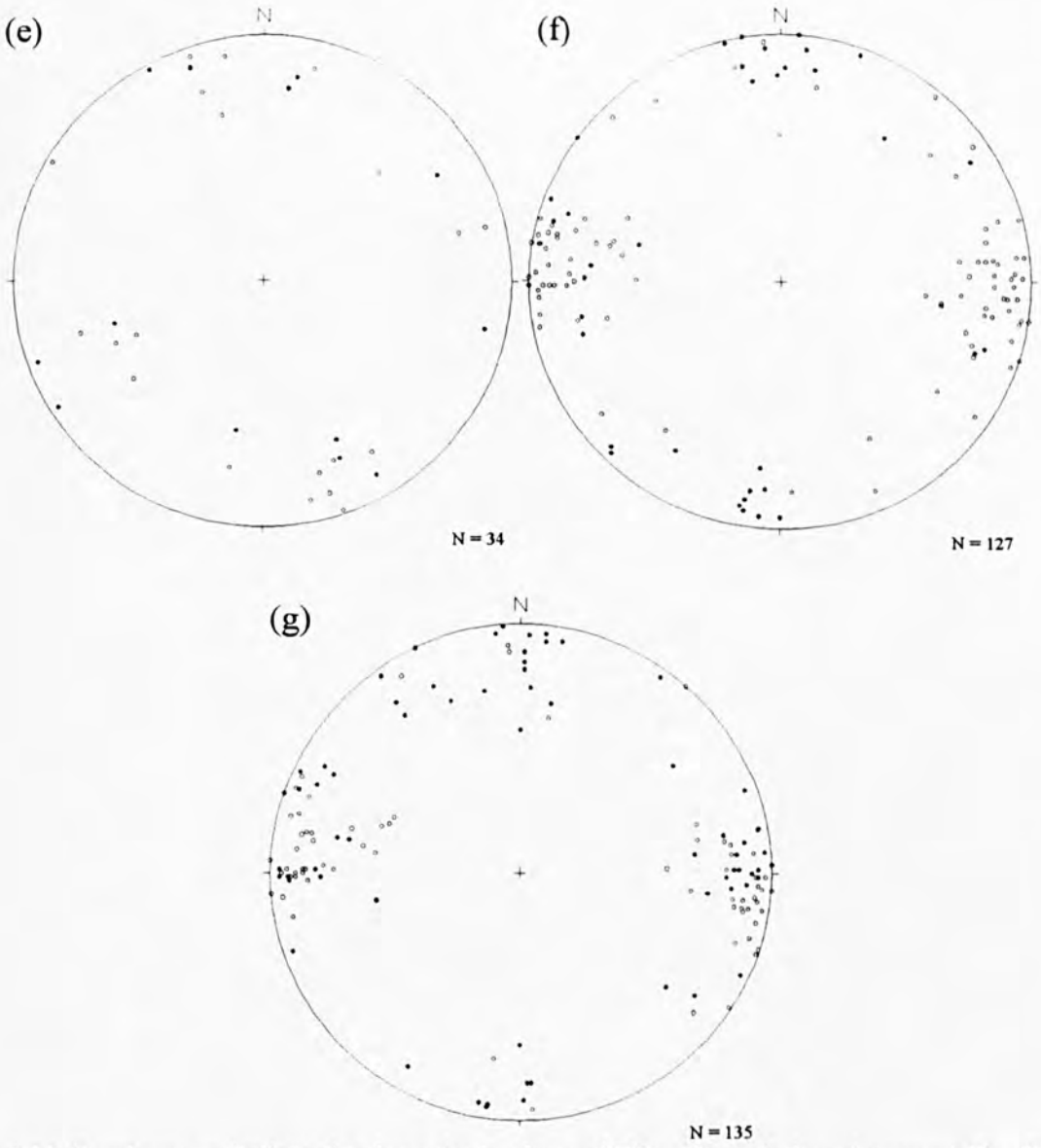

Fig. 3.14 Equal area projections showing poles to planes of FIPs. Open circles = intracrystalline FIPs, filled circles = intercrystalline FIPs. (a) CR1; (b) CR4; (c) CR5; (d) CR6; (e) GG2; (f) GG4; (g) GG5.

From the data it can be seen that where a strong E-W striking set of FIPs occurs, they tend to be intercrystalline fractures (samples CR1 and CR6). Unfortunately the other four samples do not show similar strong trends regarding the intracrystalline FIPs. It is not clear if the grain size of the greisens masked the possible presence of similar strong trends. However the lack of E-W striking FIPs in these samples may be the reason for absence of an intercrystalline FIP grouping.

Fracture propagation

The points from which FIPs appeared to propagate or terminate were also recorded during the study and a classification constructed. It was presumed that groups of FIPs with differing orientations would show variations in their propagation paths, as outlined in Chapter 2. Obviously, some ambiguities exist as it is not always possible to ascertain

the propagation direction of the fracture. FIPs were placed into one of the following classifications:

(i) Intercrystalline: cuts across the entire crystal (see also previous section).
(ii) Grain-boundary: propagates from or terminates at a grain boundary.
(iii) Healed-fracture: propagates from or terminates at another healed fracture.
(iv) Isolated: propagates and terminates within an individual grain with no contact with other fractures.

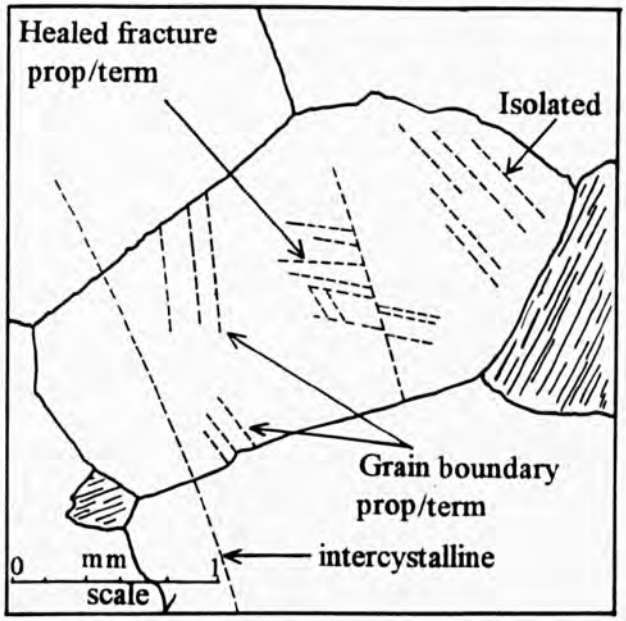

Fig. 3.15. FIP occurrence within quartz grains showing the relationship between the points of fracture propagation/termination.

A diagrammatic sketch of these FIP types is shown in Fig. 3.15. Where an FIP interacts with both a healed fracture and a grain boundary, it was generally classified as a grain boundary fracture. Fig. 3.16 shows strike and dip data combined with the FIP propagation classification. The data show that groups of FIPs with specific orientations may be related to one of the above classes of fracture propagation. Samples GG4 and GG5 show a high concentration of isolated FIPs with a N-S strike, while E-W FIPs are rarely isolated. Isolated FIPs are generally restricted to the greisen samples, with the exception of CR5, which was sampled close to the greisen/granite contact and contains a small proportion of isolated FIPs. Grain-boundary FIPs are seen to occur in both E-W and N-S striking sets and are numerically the most important of the FIPs types recorded. It should be noted that the N-S FIPs in sample CR5 are mainly grain boundary types, as the level of isolated FIPs declines away from the granite/greisen contact. The majority of FIPs that interact with other healed fractures are typically E-W in their orientation.

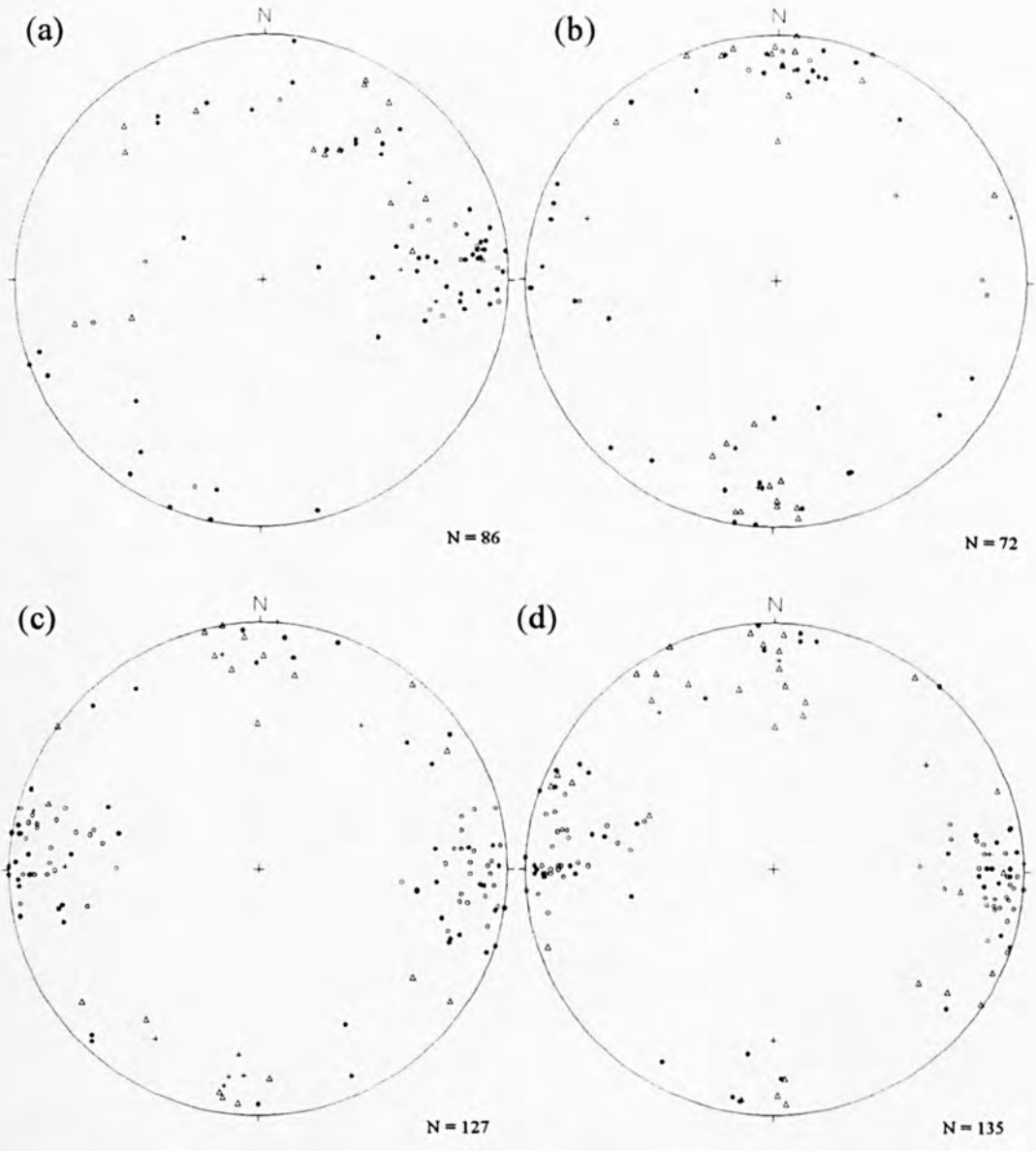

Fig. 3.16 Equal area projections showing poles to planes of FIPs. + = intercrystalline FIPs,• = grain boundary FIPs, Δ = healed fracture FIPs, o = isolated FIPs. (a) CR5; (b) CR6; (c) GG4; (d) GG5.

Samples CR1, CR4 and GG2 showed poor relationships between FIP orientations and the above classification.

FIP morphology

The morphology of all the FIPs measured during the orientation analysis was also recorded. FIPs were classified as follows:

(i) Planar: FIP forms a flat 3-dimensional plane.
(ii) Curvi-planar: FIP detracts from a straight propagation path, forming a curved plane.
(iii) Irregular: FIP forms an irregular propagation path.
(iv) Complex morphology: Kinked, sinusoidal, and splay fractures.

No obvious correlation was observed between the FIP morphology and the orientation. However, as the majority of FIPs were planar (80%), it was presumed that there was not enough data to statistically identify any relationship within these samples. A more complex morphology was observed in a small number of FIPs, examples of which can be seen in Fig. 3.17. A direct relationship between the mode of fracturing of these FIPs and their shape was hypothesised based upon analogies with larger scale structures with the same morphologies (e.g. strike-slip faults). FIPs may possess ramp and flat structures (Fig. 3.17a), which could be viewed as small scale 'duplex' type structures. More difficult to define are FIPs exhibiting an offset, en-echelon type pattern (Fig. 3.17b). These features, although rare, were restricted to FIPs with a approximate E-W orientation, and none were observed to possess a N-S orientation.

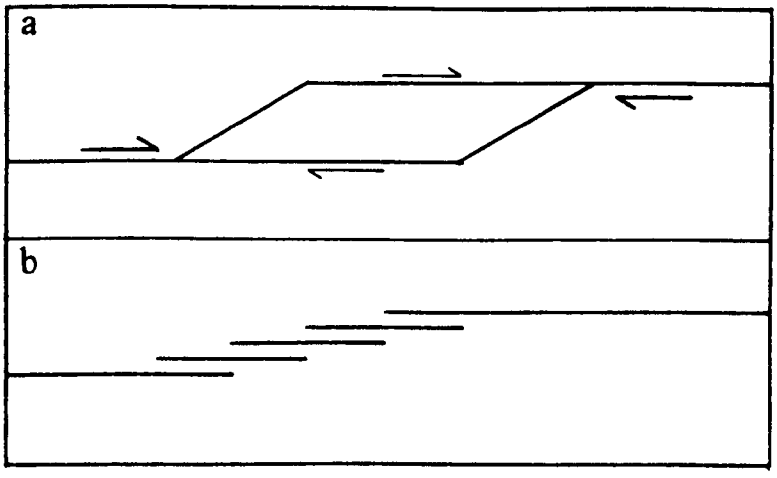

Fig. 3.17. Diagrammatic sketches of complex FIP morphologies (a) Analogous strike-slip duplex (b) *en-echelon* off-setting.

Direct evidence of shearing within FIPs was rare. As stated in Chapter 2, the amount of movement that may occur along a shear fracture may only be a few microns, thus making *mode 2* fractures difficult to observe. However, Plate 3.1 clearly shows an FIP offsetting an earlier healed fracture. Again, these FIPs, of which only two were recorded, were confined to E-W orientations.

3.3.2 Optical analysis of the fluid inclusion population

The following section will describe the morphology, distribution, abundance and other optical properties of the fluid inclusion populations within the samples. For details of the microthermometric analysis see section 3.3.3. Inclusion populations were analysed from both the granite and greisen samples. Quartz from the N-S, tungsten-bearing veins and E-W lead-zinc vein at the Carrock Mine was also examined. Although the main aim of this study is the association of fracturing and the formation of secondary fluid inclusions, primary inclusions have also been included in the results for the sake of comparison and completion. Classifications of inclusion types are summarised in Table 3.5, and are

illustrated by summary sketches in Fig. 3.18. Synoptic sketches of the inclusion populations for each sample, illustrating the major inclusion types, abundances and their modes of occurrence are shown in Fig 3.19.

Inclusion types - quartz from granite/greisen

Five inclusion types have been recognised within quartz from both the granite and the greisen. They exhibit a wide range in morphology, degree of fill, size and origin. They are comprised entirely from mono and two phase ($lH_2O + vH_2O$) inclusions. No chloride daughter minerals were observed, although small specks (approx. 2μm) were recorded on rare occasions type 1 inclusions. These are thought to represent small crystals of mica. The majority of the inclusions, probably over 90% are thought to be secondary or pseudosecondary in origin. No CO_2 rich inclusions were identified.

Inclusion types - vein quartz

Quartz vein material from the N-S bearing tungsten veins and from the E-W lead-zinc-bearing 'cross-course' was also analysed. It is not the object of the present study to provide a 'in-depth' history of ore deposition for the Carrock Fell mineralisation. However, two samples were analysed to provide confirmation regarding the temperatures and salinities associated with tungsten and lead deposition in the vicinity of the Grainsgill outcrop. Readers are referred to Shepherd *et al.* (1976), Shepherd & Waters (1984) and Ball *et al.* (1985) for a complete account of the ore deposition processes (see 3.1.4.).

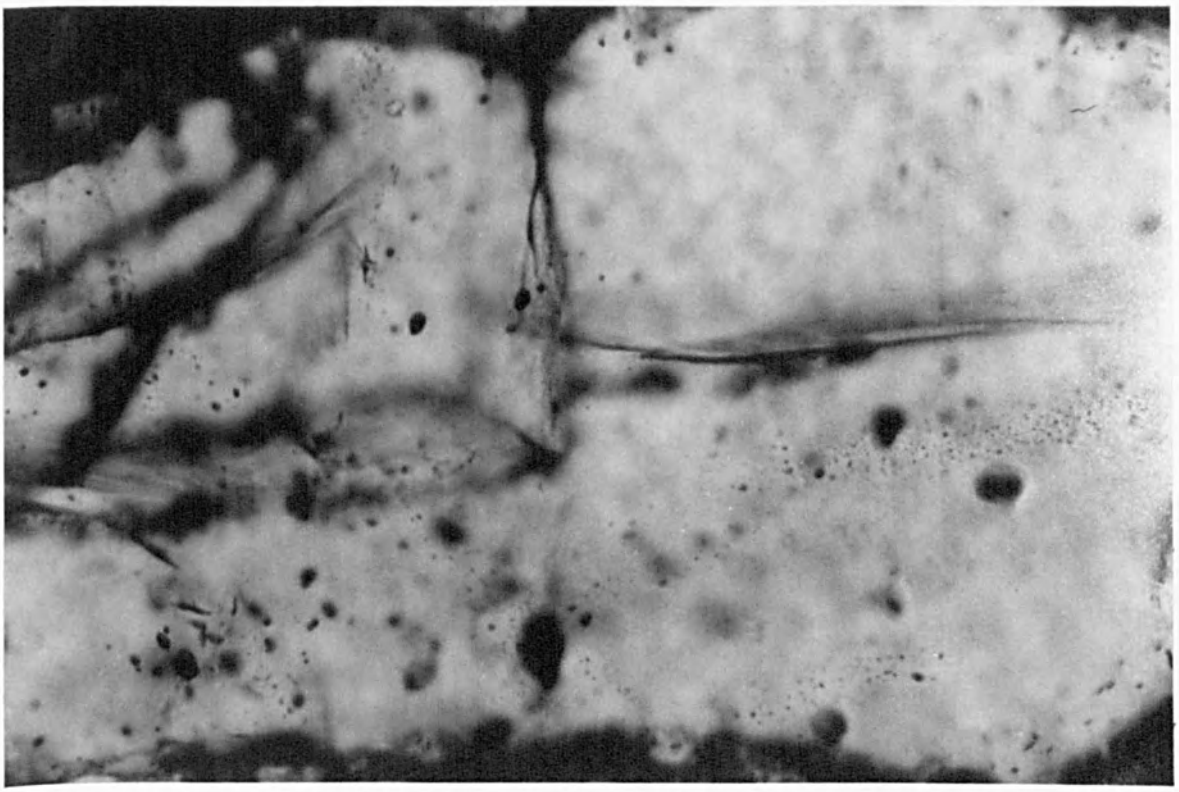

Plate 3.1. Early tensile FIP clearly shown to be off-set by a later dilatant shear (*mode 2*) healed fracture.

Table 3.5 Summary of fluid inclusion types occurring in quartz from the Skiddaw Granite, Grainsgill Greisen, N-S tungsten (Harding) vein and E-W lead vein.

Type and sample	*Size*	*Shape*	*Occurrence*	*Phases*
Type 1 Not present in E-W lead vein	3-20μm	rounded or equant, possible preferred shape orientation	secondary, well defined planes or more rarely as groups	generally two phase, ($l + v$)
Type 2	<3μm	rounded or equant	secondary, well defined planes	generally monophase, (l), rare two phase ($l + v$)
Type 3 Not present in E-W lead vein	5-25μm	irregular or rounded, possibly faceted	secondary / pseudo secondary, poorly defined planes or groups	monophase, gas rich, opaque, or possibly decrepitated
Type 4	5-30μm	very irregular to regular, flattened, necked	secondary, well defined planes or groups	monophase (l) and two phase ($l + v$).
Type 5 Not E-W lead vein	10-20μm	faceted, rounded or equant	isolated or groups	two phase ($l + v$)
Type 6 Only N-S tungsten vein	5-15μm	rounded or equant	pseudosecondary, isolated or in groups	two/three phase ($l H_2O/v CO_2$ and/or $l CO_2$)

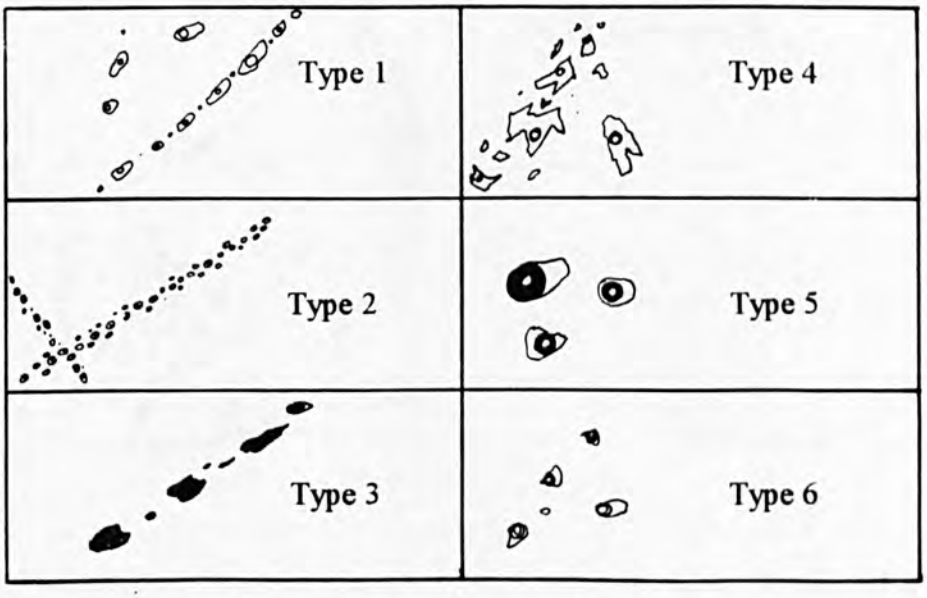

Fig. 3.18. Classification of inclusion types based upon studies of inclusion populations from both granitic and vein quartz.

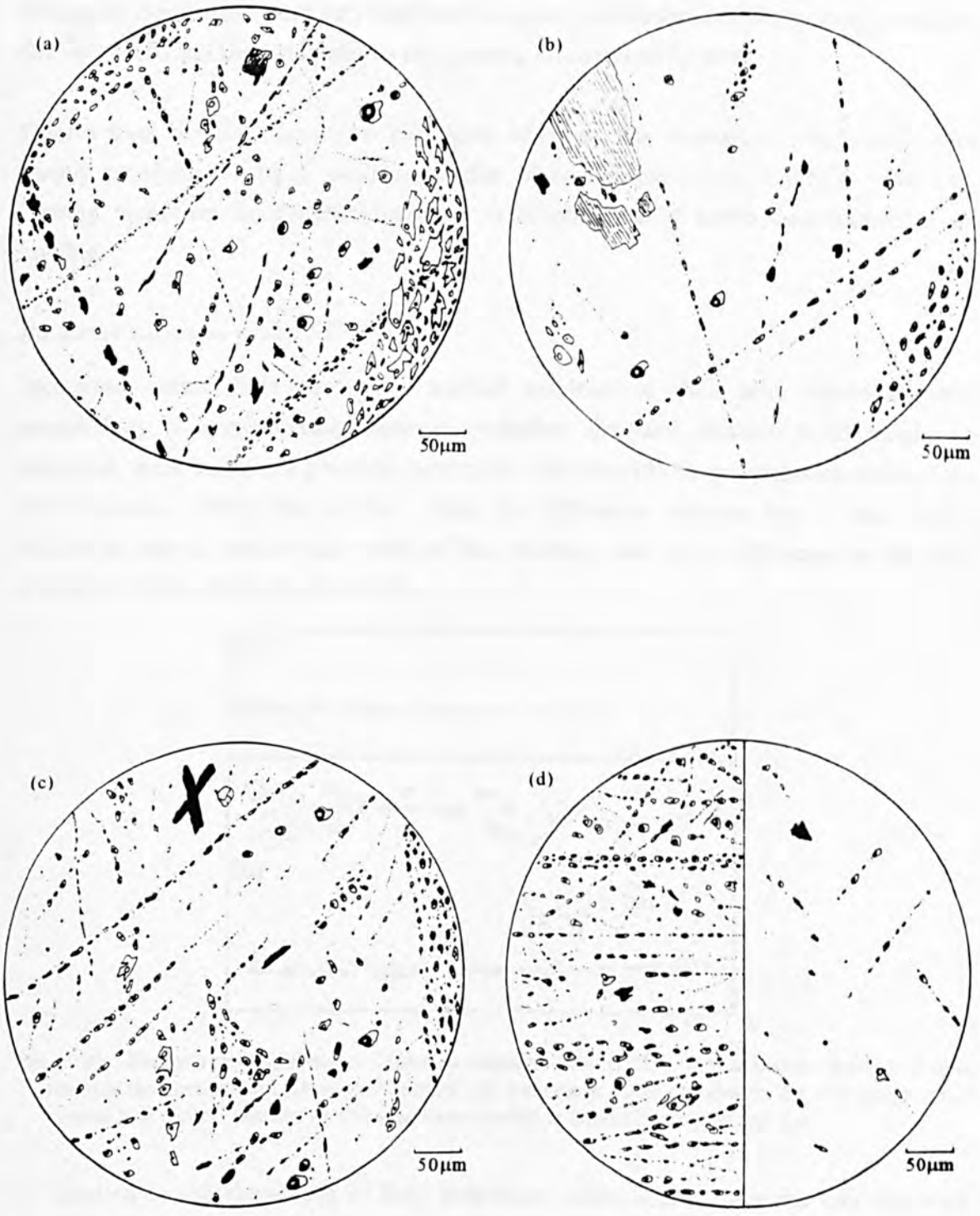

Fig. 3.19. Synoptic sketches of inclusions populations (a) CR1; (b) CR4; (c) CR5; (d) GG2.

Six inclusion types were identified within the tungsten-bearing, quartz veins. Inclusions were single and two phase ($lH_2O + vH_2O$) types. Rare CO_2 bearing inclusions were also identified, containing lCO_2 at room temperature. No daughter minerals were identified. Inclusion abundances were very high with a strong orientation of FIPs evident parallel to the vein walls and perpendicular to the opening direction of the vein.

Quartz from the E-W lead vein contained relatively few inclusions. Inclusions were mainly monophase with a small proportion of two phase ($lH_2O + vH_2O$). No CO_2 bearing inclusions or daughter minerals were observed at room temperature or on cooling.

Inclusion variation within FIPs

Inclusions within FIPs showed a marked variation in their size, abundance and morphology. A relationship between inclusion size and fracture width might be expected, since inclusions generally became smaller towards the propagation front of the FIP (Brantley, 1992) (Fig 3.20a). Thus the difference between type 1 and type 2 inclusions may be due to the width of the fracture, and not a difference in the PVT properties of the fluids that healed it.

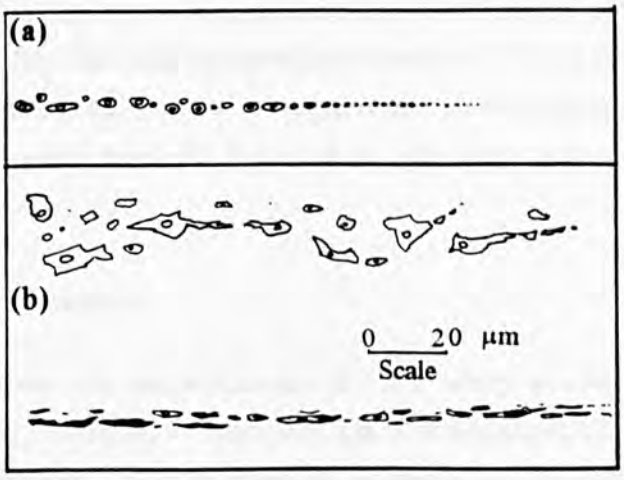

Fig. 3.20. Diagrammatic sketches of inclusion variation within FIPs. (a) Inclusions become smaller towards the propagation tip of the fracture; (b) Inclusions occur parallel to the FIP length when viewed in a vertical position or flattened when viewed in a more horizontal position.

A variation in the abundance of fluid inclusions within healed fractures was observed. However, the measurement of the abundance within FIPs proved difficult to accomplish objectively, so a subjective description was used based upon visual observations. FIPs were termed to be 'inclusion abundant' or 'inclusion poor'. Fig. 3.21 shows the ratios of FIP inclusion abundance recorded.

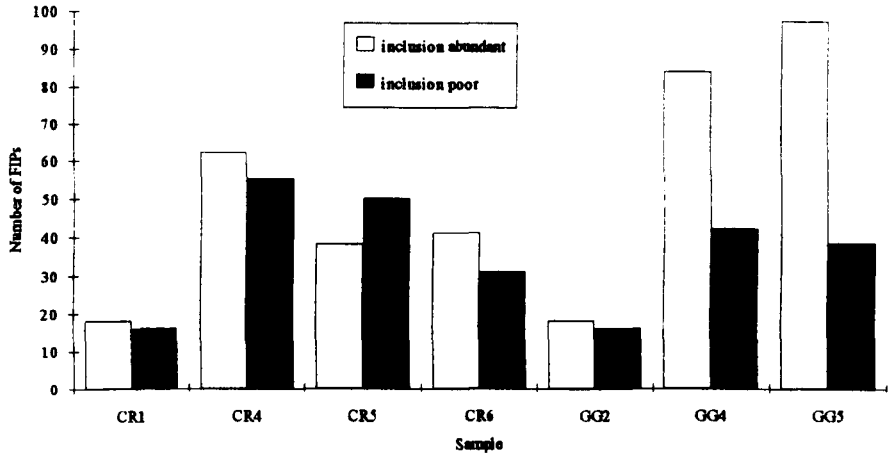

Fig. 3.21 Ratios of inclusion abundant FIPs to inclusion poor FIPs.

Despite the subjectivity involved, it is quite apparent the two greisen samples contain appreciably more FIPs with high inclusion abundance's than those that are classed as inclusion poor. The granite samples contain an approximate equal number of both types.

One of the most interesting, and perhaps most enlightening observations, was the tendency for secondary inclusions to form distinct, preferred orientations within a healed fracture. In several cases, inclusions appeared to have formed parallel to the length of the FIP. Generally this was only observable when the FIP was rotated until it was in a vertical position. Inclusions that were irregular and necked when the FIP was in a sub-vertical orientation, were typically flattened or appeared to be smeared when rotated vertically (Fig. 3.20b).

3.3.3 Thermometric analysis

Thermometric analysis was undertaken on all FIPs, where possible. In many cases the size of the secondary inclusions (<3μm) contained within these FIPs, makes it impossible for data to be obtained. The analysis of primary and pseudosecondary inclusions, although not usually representing well-defined fractures, have also been included in the study. The methodology involved in the thermometric analysis of secondary fluid inclusions is detailed in Appendix C. Data are presented initially as histograms, showing the temperature and salinity of the fluids with the number of inclusions analysed. Bi-variate scatter plots are also included, to characterise the various fluid groups.

Homogenisation temperatures - granite/greisen

Thermometric analysis of four samples was undertaken, CR1, CR4, CR5 and GG4. Homogenisation temperatures were recorded in 379 mainly secondary inclusions from 156 FIPs of various orientations. A wide range in the homogenisation temperatures was recorded (T_h *c.* 110-370°C) as shown in Fig. 3.22.

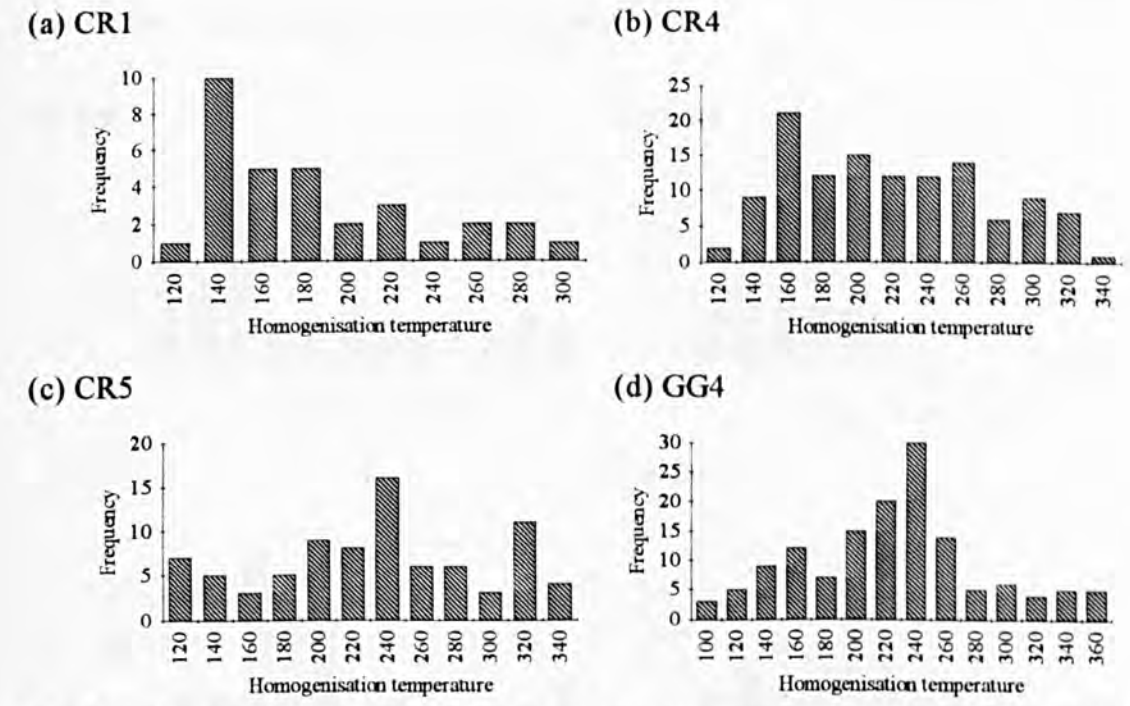

Fig. 3.22. Histograms showing the distribution of homogenisation temperatures. (a) CR1; (b) CR4; (c) CR5; (d) GG4.

Homogenisation temperatures in samples CR5 and GG4 show peaks around 240°C, representing fluids probably related to greisenisation, which is in agreement with Shepherd *et al.* (1976). These peaks are generally absent from samples CR1 and CR4, which were sampled at distance from the alteration halo. High temperature fluids are present in all samples, most likely representing early hydrothermal (magmatic?) fluids in thermal fractures. As the convective system initiated by granite intrusion waned, cooler fluids evolved, which are present in all samples, down to 100-120°C. Modal peaks around 140°C suggest a period of more intense fracturing and subsequent healing.

Bulk salinity - granite/greisen

Bulk salinity measurements were recorded from 302 inclusions. Again the relative size of the smallest inclusions made both the measurement of last ice melting and the freezing of the inclusion (due to supercooling effects) difficult. Salinity distributions are shown in Fig. 3.23., expressed as wt. %. equiv. NaCl. Again a wide spread in the data sets were encountered, as was expected. Fluids were generally low to moderate salinities, but did not show a typical unimodal distribution. A small number of high salinity inclusions were encountered (*c.* 23wt% equiv. NaCl), with ice melting close to the -20.8 eutectic (Shepherd *et al.*, 1985). However first melt data (-40 to -50°C) suggest that the fluids were not solely comprised from NaCl. The exact temperature of the eutectic was difficult to define because of the small size of the inclusions studied. However, the

presence of NaCl-$CaCl_2$-H_2O system is inferred from the crude data, which is in agreement with the data of Cooper & Stanley (1990).

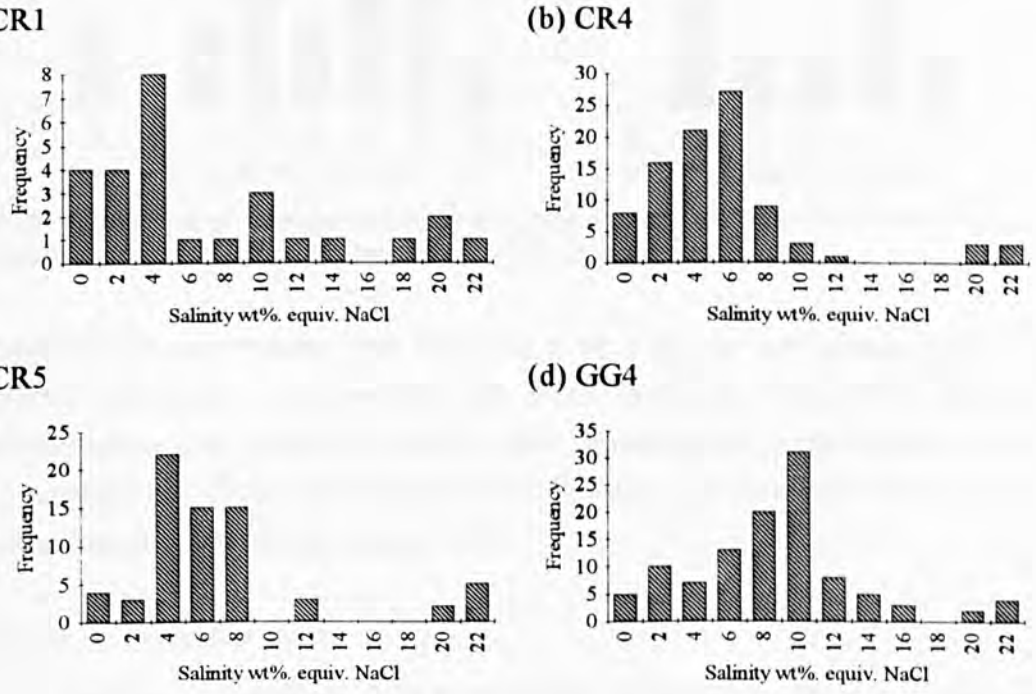

Fig. 3.23. Histograms showing bulk salinity in wt%. equiv. NaCl. (a) CR1; (b) CR4; (c) CR5; (d) GG4. Salinity data based upon last ice melting temperatures (Hall 1989).

Frequency peaks occur at around 8-10 wt. %. equiv. NaCl in sample GG4, representing fluids likely to be associated with greisenisation. These data are similar, to those of Shepherd et al. (1976) who concluded that fluids responsible for greisenisation were approximately 8-10 wt. %. equiv. NaCl. Inclusions possessing salinities up to 16 wt. %. equiv. NaCl, and eutectics around -21°C and may represent early magmatic fluids, with the healing of thermal fractures occurring before mixing with lower salinity fluids could occur.

Homogenisation temperatures - vein quartz

Homogenisation temperatures were measured from 17 inclusions in quartz from the N-S-trending tungsten-bearing, Harding vein, and from 9 inclusions in quartz from the E-W lead bearing cross-course (Fig. 3.24). Although the data sets from the two veins are not statistically large enough to estimate the temperatures of ore deposition accurately, they do confirm that the fluids involved were of significantly different temperatures. Data from the N-S tungsten vein, from mainly primary and pseudo-secondary inclusions shows that homogenisation temperatures varied from 200-250°C, which are similar to those reported by Shepherd *et al.* (1976) (T_h 220-250°C) but not those of Ball *et al.* (1985) (T_h 235-335°C).

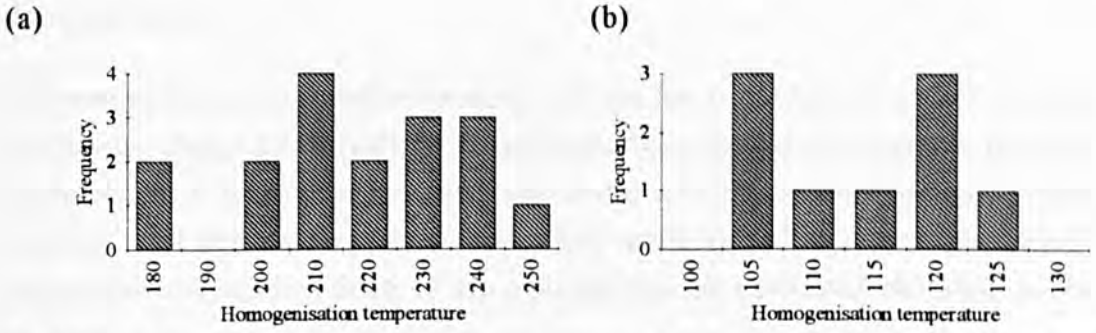

Fig 3.24. Histograms of homogenisation temperatures of inclusions from vein quartz, Carrock Fell tungsten mine. (a) N-S tungsten bearing vein; (b) E-W lead bearing vein

Homogenisation temperature data from the E-W lead vein are mainly from pseudo-secondary inclusions. Temperatures are much lower (*c.* 105-125°C) than in the tungsten-bearing vein, signifying that the two mineralisation events were separated in time. Stanley (1979) found inclusions from fluorite vugs from the same vein yielded homogenisation temperatures around 120°C.

Bulk salinity - vein quartz

Last ice melting temperatures were measured in 15 inclusions from tungsten bearing-quartz and 7 inclusions in quartz from the E-W lead vein. Salinities from the former were typically 8-10 wt. %. equiv. NaCl (Fig. 3.25), in agreement with data from Shepherd et al. (1976), and similar to fluids observed within secondary inclusions from the greisen samples, which were thought to be responsible for the alteration process. Data from the E-W lead vein indicates high salinity fluids (20-22 wt. %. equiv. NaCl), with eutectics similar to high salinity NaCl-$CaCl_2$-H_2O fluids recorded within the greisen samples.

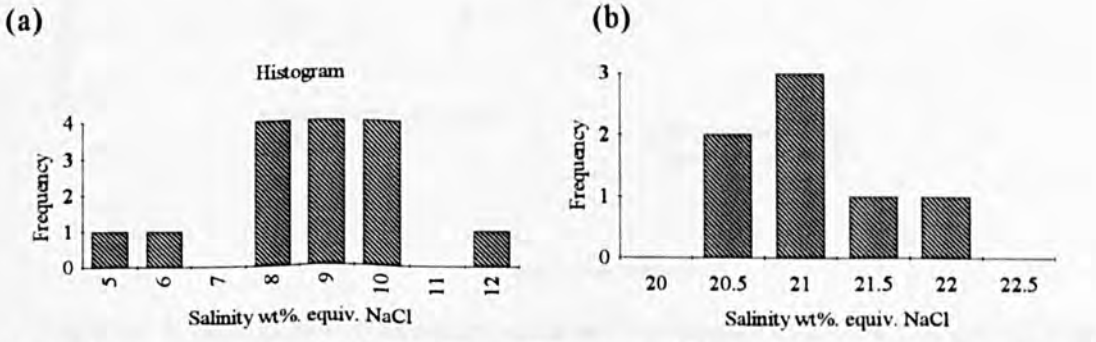

Fig 3.25. Histograms showing bulk salinity in wt %. equiv. NaCl. (a) N-S tungsten bearing vein; (b) E-W lead bearing vein. Salinity data based upon last ice melting temperatures (Hall 1989).

The data show that the fluids responsible for tungsten and lead deposition were genetically different, both in chemistry and temperature.

3.3.4 Discussion

Microstructural and microthermometric analysis has been used to define the pathways utilised by fluids, with a variety of temperatures, salinities and possible origins. The combination of these data however, can reveal how the fracture systems formed and evolved, and furthermore show how fluid evolution of the area may have been responsible for the deposition of ore minerals and the associated alteration of the host rocks.

Fluid evolution

The following speculations are based on previous work by Shepherd *et al.*, (1976), Shepherd and Waters (1984) and Ball *et al.*, (1985) together with the present data collected during this research. The intrusion of the Skiddaw Granite set-up a convective system, circulating magmatic and non-magmatic fluids (Shepherd *et al.*, 1976), and drawing in high salinity $NaCl/CaCl_2$ brines, that led to the deposition of a series of ore and gangue minerals. Major controls over the formation of the mineralisation include the heat produced by the Skiddaw Granite and the presence of an active fracture for deposition. The combination of temperature and salinity data can be used to illustrate the presence of these different fluids, and their evolution.

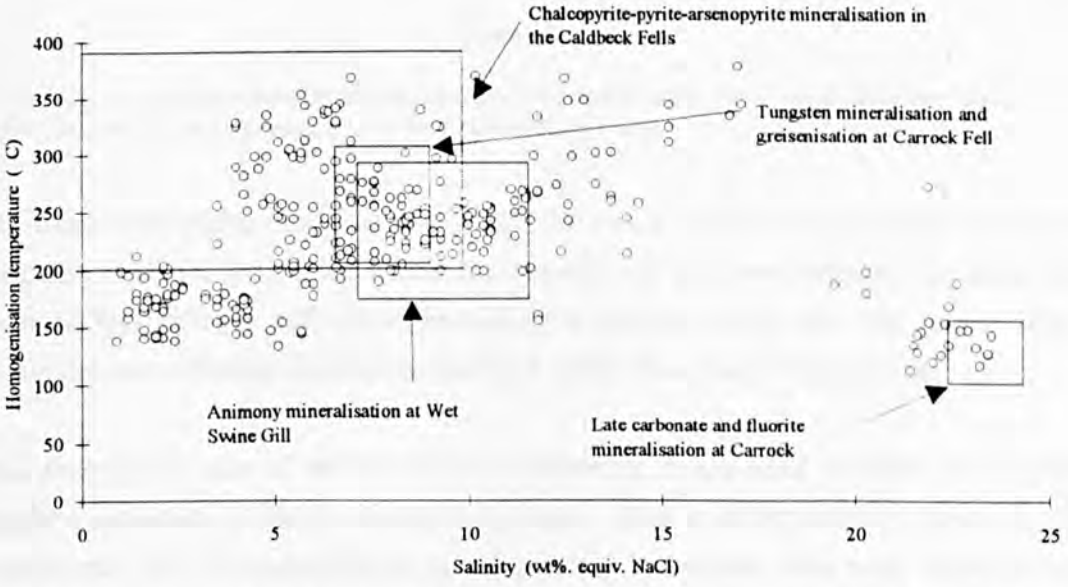

Fig 3.26. T_h-Salinity plot for secondary inclusions from samples CR1, CR4, CR5 and GG4. n= 292

Fig. 3.26. illustrates the evolution of the secondary fluid inclusion population within the granite and greisen samples. High temperature and moderate salinity fluids (probably of magmatic origin) are interpreted to have mixed with cooler less saline (meteoric) fluids. The time interval after granite intrusion, before greisenisation occurred, allowed non-magmatic fluids to be drawn into a convective hydrothermal cell. Thus, fluids

responsible for the greisen, are thought to be cooler and less saline than their magmatic predecessors (Shepherd *et al.*, 1976). As the granite cooled, further meteoric fluids were likely to have been drawn into the system. However, the low temperature/high salinity fluid shown, shows no mixing trend with the other fluids. These fluids are thus likely to have an alternate source. The presence of $CaCl_2$ is typical of fluids expelled from sedimentary basins (Shepherd and Scrivener, 1987; Scrivener *et al.*, 1994) possibly from basins to the west of the Lake District dome and does not appear to be in hydrothermal continuum with the convective cell.

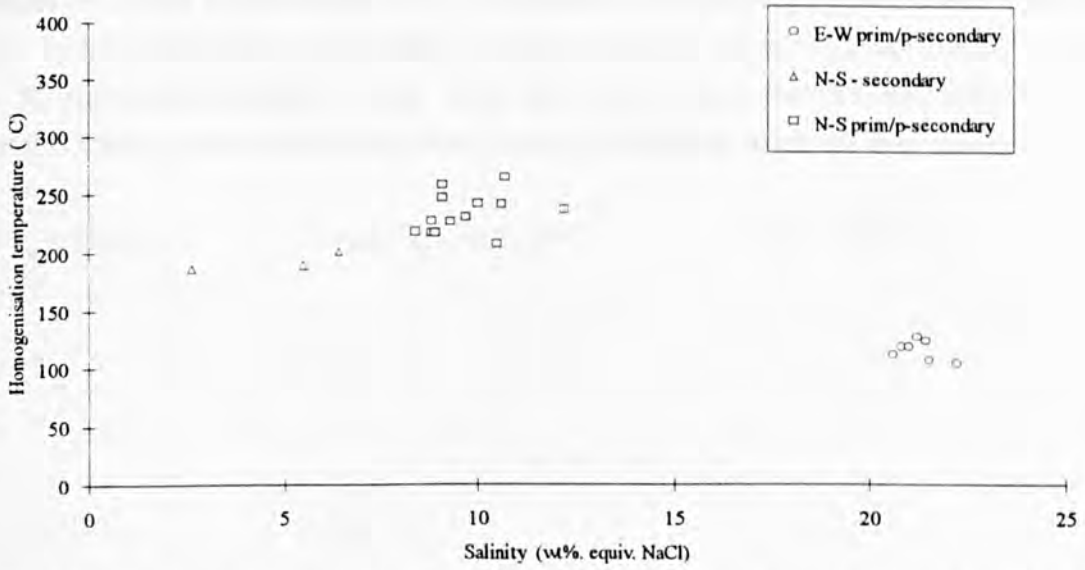

Fig 3.27. T_h-Salinity plot for inclusions from vein quartz from the Carrock tungsten mine. n = 23; A= Tungsten (Harding) vein; B= Pb-Zn ('cross-course') vein

Data from vein quartz from the N-S and E-W veins at the Carrock mine are in good agreement with the data from within the granite and greisens samples. It is therefore proposed that primary and pseudosecondary inclusions within the vein quartz show a genetic link to secondary inclusions recorded within the granite and greisen.

Thus, through the use of secondary fluid inclusions, it has been possible to illustrate a complete evolution of fluids within the granite. This is as opposed to the analysis of discrete episodes of mineralisation using primary inclusions from vein material which may not give a complete picture of the hydrothermal continuum during the evolution of a thermal system.

Fracture evolution

Once the evolution of the hydrothermal fluids has been established, it is possible to constrain the evolution of the fracture system by combining the temperature/salinity data with the orientations of the FIPs they healed. Figs. 3.28 and 3.29 show the orientations

of FIPs with their respective mean homogenisation temperatures and bulk salinities of the inclusions contained within them. FIPs with a N-S orientation contain fluids with moderate to high temperatures (T_h *c.* 200-350°C) and moderate salinities (5-10 wt. %. equiv. NaCl). These FIPs are generally planar, intracrystalline fractures, either isolated or interact with grain boundaries. Their temperatures suggest early, high temperature fluids. They are thought to represent thermal fractures (high temperature fluids, fractures interact with grain boundaries) and hydraulic fractures (moderate temperature fluids, typically isolated fractures). The mechanism of formation of these fracture types is outlined in Chapter 2. The FIPs are presumed to be all tensile fractures, opening parallel to σ_1 and perpendicular to σ_3. However, E-W striking (approximate) FIPs are typically low temperature (T_h >200°C) with low (<5 wt. %. equiv. NaCl) or high (> 17 wt. %. equiv. NaCl) salinity fluids. First melt data suggest that the high salinity fluids contains $CaCl_2$ are therefore likely to be genetically different from the low salinity fluid.

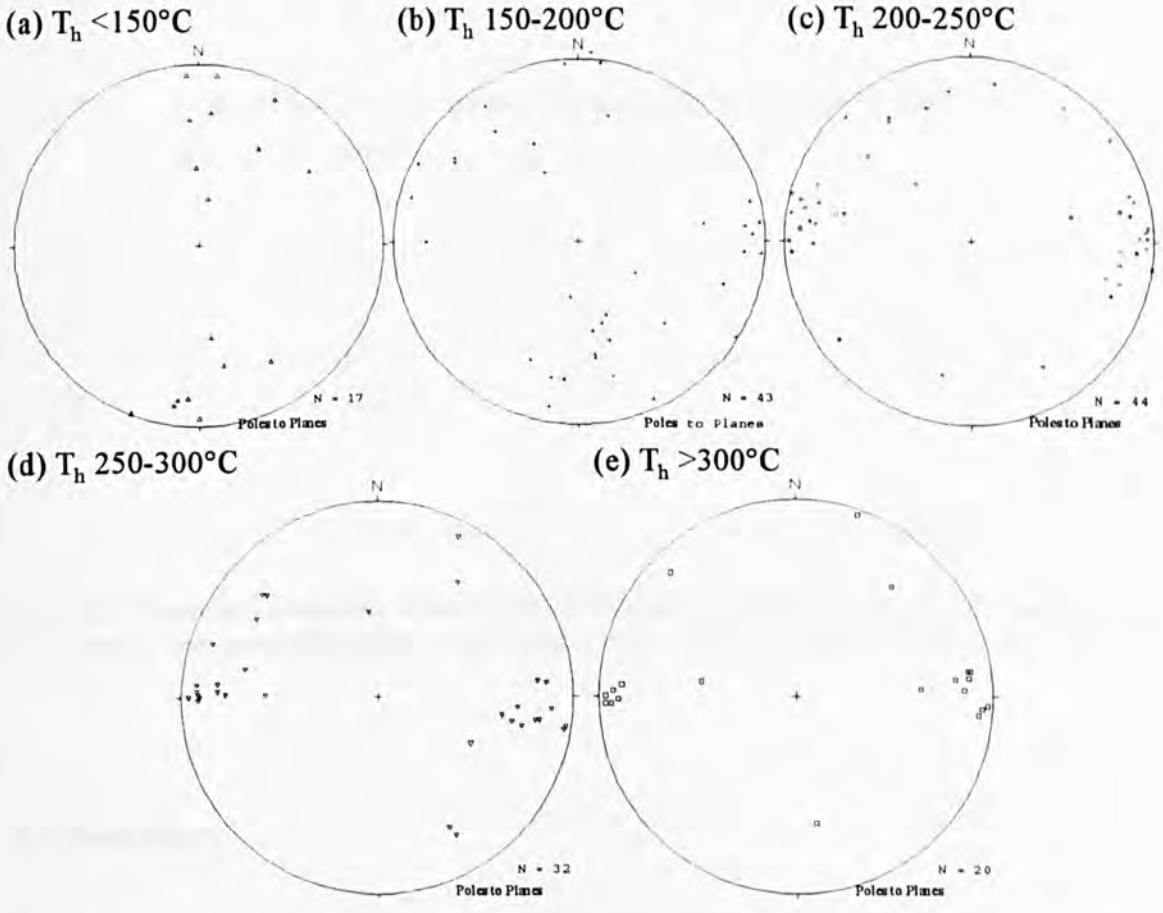

Fig. 3.28. Equal area projection illustrating FIP orientations and T_h of the secondary fluid inclusions contained within them. (a) $\Delta = T_h$ <150°C; (b) + = T_h 150-200°C; (c) O = T_h 200-250°C; (d) $\nabla = T_h$ 250-300°C; (e) □ = T_h >300°C.

Thus, two fluids were in circulation during the evolution of the E-W oriented fracture system. The relatively low abundance of E-W fractures and the low temperature of the fluids that healed suggests that they are unlikely to be thermal to purely hydraulic in

origin. More likely, is that they are associated with periods of brittle deformation that were responsible for the formation of the Pb-Zn bearing veins in the area. This type of mineralisation has similar orientations, and related to fluids with similar properties as the E-W FIPs.

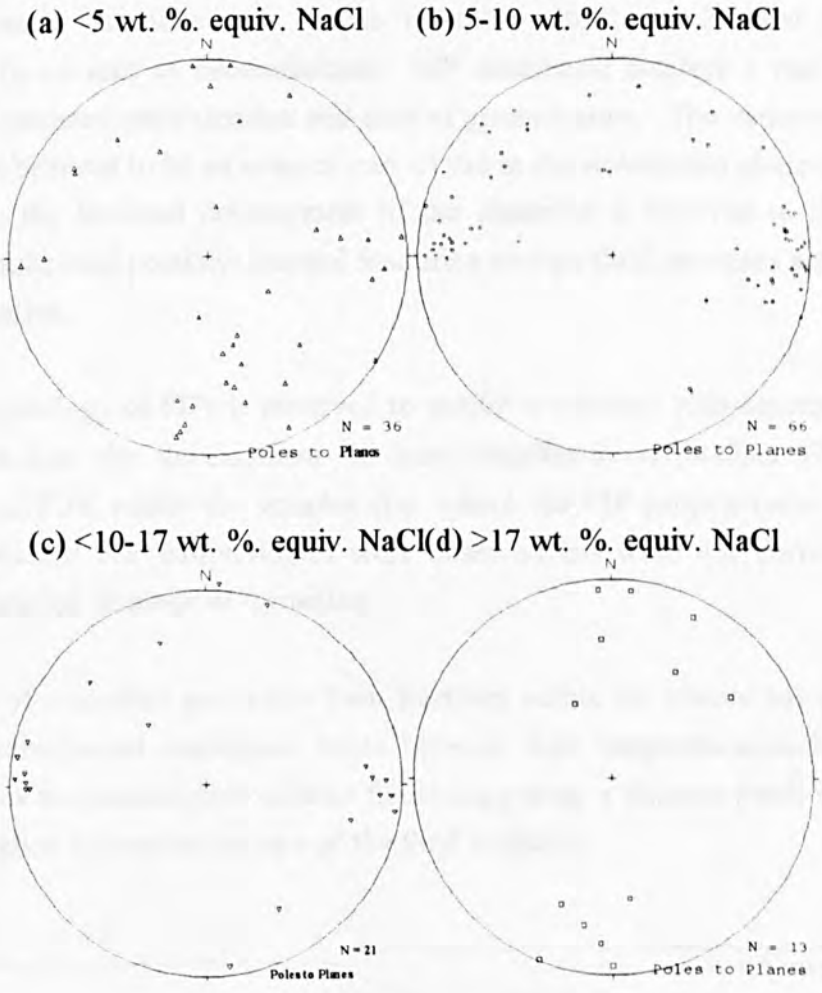

Fig. 3.29. Equal area projection, illustrating FIP orientation and bulk salinity of the secondary fluid inclusions contained within them, in wt%. equiv. NaCl. (a) Δ = <5; (b) O = 5-10; (c) ∇ = 10-17; (d) $\square$ = 17.

3.4 Summary

Fluid Inclusion Planes have been analysed in the Skiddaw Granite from the Carrock Fell area. The data has shown that FIPs may be distinguished through the use of orientation and thermometric data and furthermore by variations in morphology of the FIPs. The following conclusions have been reached:

(i) Different orientations of FIPs may possess differing microthermometric properties.

(ii) FIPs have be shown to have similar orientations to that of macro structures observed in the field. FIPs display a strong N-S orientation in proximity to the N-S tungsten mineralised area, while at distance the major orientation reverts to a typical regional pattern.

(iii) Furthermore, the abundance of the FIPs has also been observed to exhibit a relationship to an area of mineralisation. FIP abundance displays a marked increase towards the tungsten mineralisation and area of greisenisation. The variation in this FIP abundance is believed to be an integral part of the in the widespread alteration of rocks. Furthermore, the localised development of the alteration is believed to be caused by intense hydraulic (and possibly) thermal fracturing by high fluid pressures associated with the mineralisation.

(iv) The morphology of FIPs is observed to exhibit a variation with orientation. These variations include the development of intercrystalline/intracrystalline FIPs and the occurrence of FIPs within the samples (i.e. where the FIP propagates/terminates at). More complicated FIP morphologies were observed but were not correlated to any specific orientation or mode of formation.

(v) The use of secondary inclusions from fractures within the granite has shown that a complete hydrothermal continuum exists between high temperature/moderate salinity fluids and low temperature/low salinity fluids suggesting a dilution (with cooler fluids) trend. This gives a complete picture of the fluid evolution.

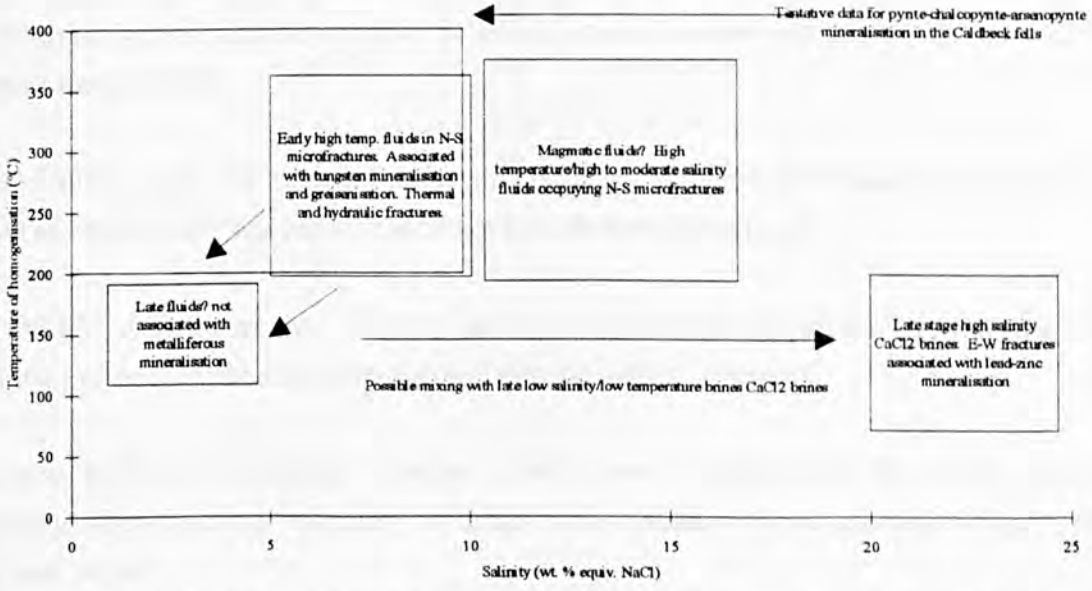

Fig. 3.30 Evolution of fluids within secondary inclusions in quartz from the Skiddaw Granite and Grainsgill Greisen at Carrock Fell. Fluid evolution based upon thermometric data, fracture orientations and possible microfracturing processes.

CHAPTER 4

FIP GENERATION, REGIONAL SCALE MINERALISATION, DEFORMATION AND HYDROTHERMAL EVOLUTION

4.0 Introduction

It has been illustrated in Chapter 3 that FIPs mimic the orientations of macrostructures (e.g. veins) on a local scale, and furthermore they contain fluids of similar thermometric properties. The abundance of FIPs was also observed to increase with proximity to areas of localised mineralisation and more importantly whole rock alteration. The following chapter will illustrate the behaviour of Fluid Inclusion Planes over a wider area (20-25km) and examine the FIP orientations on a more regional scale compared to a more localised study area. It will be shown that a strong trend in the mineralisation occurs, with vein sets exhibiting several well developed regional trends throughout the study area. Thus, together with published data on the hydrothermal evolution of fluids, the study area is an excellent example in which to test several hypothesis related to the orientations of FIPs:

(i) Do FIPs mimic the regional strike of the major vein sets and faults which may be observed in the field between the Bodmin and Dartmoor granites?

(ii) Do FIP abundances vary with respect to distance from mapped faults, mineralisation and the presence of intense hydrothermal mineralisation/alteration?

(iii) Do individual sampling locations exhibit local variations in the stress regime, typically when in close proximity to faults with orientations not corresponding to the regional trend?

(iv) It is presumed that the origins of these macrostructures are related to different tectonic events and are the result of several types of fracturing processes (thermal, hydraulic, mechanical). Can the FIPs, based upon their orientation and the thermometric

properties of the fluids they contain, thus be related to these different fracturing processes?

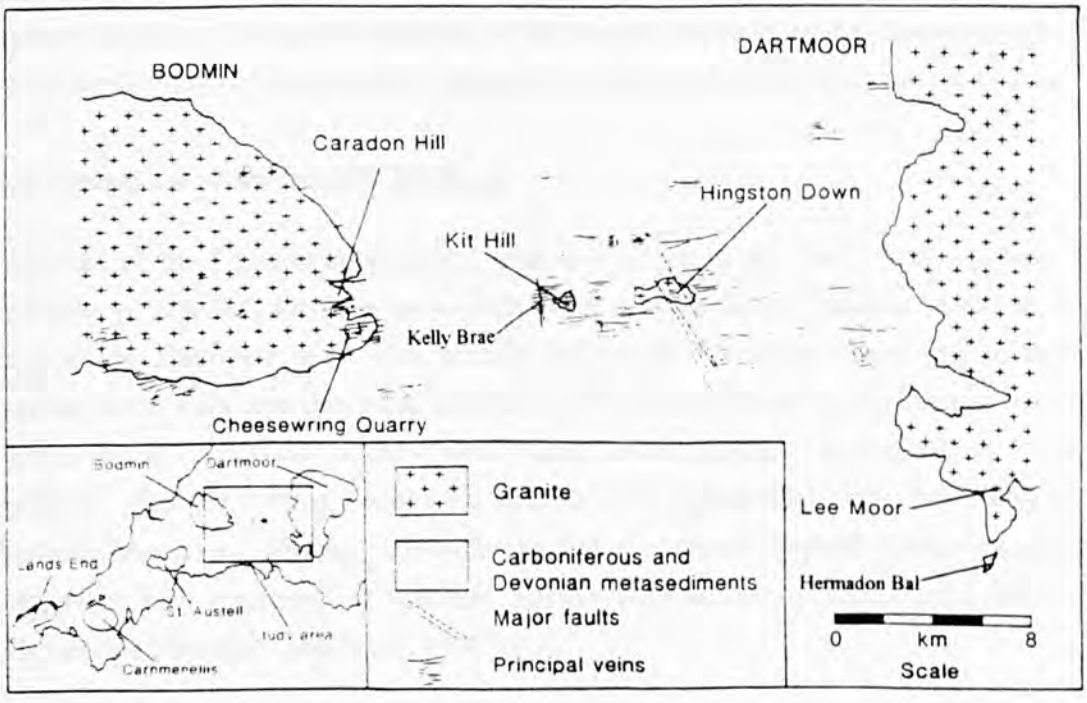

Fig. 4.1 Geology and location of the study area showing sampling localities, major rock types and mineralisation trends. After Dangerfield and Hawkes (1981) and Dines (1956).

One of the most important aspects of the study area is that fluids responsible for the hydrothermal mineralisation and alteration have diverse origins and ages, and also occupy fractures with varying orientations related to more than one tectonic event. It is for these reasons that the study area was chosen, so that fractures of different orientations could be easily characterised by the properties of the fluids that they contain. Thus the position of sampling locations were governed not only by the exposure of the granite batholith, but also by the occurrence of the varying styles of mineralisation and alteration that exist. Samples of fresh granite were thus obtained from localities where varying styles of mineralisation were evident and altered granite from zones of locally developed whole rock alteration. Where possible in-situ material was collected. Hydrothermal vein material (both quartz and fluorite) representing the styles of mineralisation present in the study area was also obtained where possible, especially at localities where oriented granite samples were collected.

4.1 Geological history of SW England and the study area

The Kit Hill - Hingston Down sample area is situated on the Devon - Cornwall border, on either side of the Tamar River. The area is characterised by Devonian and Carboniferous deep and shallow water sedimentary and volcanic and rocks, intruded by

the Cornubian batholith (Fig. 1). The batholith is exposed at the surface forming the Bodmin and Dartmoor granites and the smaller stocks of Kit Hill and Hingston Down. Mineralisation commonly occurs in the study area as vein filling and more rarely as porphyry deposits. Pervasive alteration of the granite and surrounding country rocks has also occurred, and its localised development is widespread throughout the study area.

4.1.1 Geological evolution-SW England

At the end of the Caledonian orogeny, land was raised to the north of the present day Cornubian peninsular, forming semi-desert areas, with deltas draining south into the basins of the Devonian sea. The Middle and Upper Devonian slates and mudstones observed in the field area represent the finer sediments produced as the land to the north is worn down, with local, shallow clear water areas allowing the deposition of reefal limestones (Dineley, 1992). Volcanic activity was widespread with the extrusion of submarine lava flows. During Carboniferous times, rocks are mainly calcareous silts and muds, with great outbursts of volcanic activity represented by lavas, tuffs, ashes and agglomerates (Chandler and Isaac, 1982).

Towards the end of the Carboniferous, sediments deposited in the Devonian - Carboniferous sea were folded along an east-west axis by the Hercynian orogeny. This resulted in the formation of overturned folds, faults and thrust, with the development of a slaty cleavage (Selwood, 1990). During the closing stages of the Hercynian orogeny, the Cornubian batholith was emplaced together with its associated hydrothermal activity. Earth movements from Permian times to recent(?) have resulted in numerous NW-SE striking faults (Dearman, 1963; Holloway and Chadwick, 1986).

4.1.2 Granites

Two large granite plutons, together with the smaller stocks of Kit Hill and Hingston Down are exposed in the field area. They represent part of the Cornubian batholith, a large plutonic complex, found along the entire length of the Cornubian peninsular. Geophysical data (Bott *et al.*, 1958; Bott and Scott, 1964; Willis-Richards and Jackson, 1989) has shown it to be 220km long and between 30-40km in width. The emplacement of the granite is postulated to be related to the progressive subduction of the palaeo-Tethys ocean, climaxing in the Variscan orogeny, with granite emplacement occurring in a extensional back-arc setting (Willis-Richards and Jackson, 1989). The granite is basically an S-type ilmenite, HHP (High Heat Production), two mica, tourmaline-bearing monzogranite. Petrogenesis of the granite is not fully understood, with two schools of thought. Watson *et al.*, (1984) adapted the model of Simpson *et al.*, (1979) and suggested that the granite is mantle derived, via fractional crystallisation and crustal assimilation-hybridisation. However, geophysical data (Willis-Richards and Jackson,

1989) indicates that the batholith does not grade downwards into more basic material. It is therefore likely that it was derived from partial melting of crustal rocks in response to crustal thickening and radiogenic heating of the crust during the Variscan orogeny (Mitchell, 1974; Shackleton *et al.*, 1982; Pearce *et al.*, 1984).

Emplacement depth has been postulated by Floyd (1972) at about 3-4km and by Charoy (1986) at 7-9km. The six major plutons have been emplaced diachronously, between 268±1Ma (Lands End granite) to 290±2Ma (Carnmenellis granite) based upon Rb-Sr whole rock and mineral dating of the coarse grained granites (Chen *et. al.*, 1993). The detailed chronology of granite magmatism in SW England is summarised in Table 1.

Bodmin granite

Ghosh (1927) and Dangerfield and Hawkes (1981) describe the Bodmin granite, distinguishing two types of coarse-grained granite and one fine-grained type, both of which are megacrystic. Rb-Sr dating of mineral separates have yielded an age of 287± 2Ma (Darbyshire and Shepherd, 1985), and 289±2Ma (Chen *et al.*, 1993).

Dartmoor granite

Bramall and Harwood (1923) describe four main phases of granite emplacement: (i) biotite microgranodiorite; (ii) coarse megacrystic biotite granite; (iii) equigranular poorly megacrystic granite; (iv) various aplitic and microgranite bodies. Darbyshire and Shepherd (1985) have inferred an emplacement date of 280±1Ma based upon Rb-Sr whole rock analysis, which is in agreement with Chen *et al.*, (1993) who have presented U-Pb dates 281.4±0.8Ma (coarse grained megacrystic) and 285.7±0.8Ma (poorly megacrystic), indicating at least two episodes of emplacement. This is also in agreement with Ward *et al.*, (1992) who describes the Dartmoor pluton as having a 'marginal' and 'inner' facies, formed by at least two fractionation cycles.

Kit Hill granite

The Kit Hill granite is presumed to represent the surface exposure of the buried granite ridge between the Dartmoor and Bodmin plutons. Darbyshire and Shepherd (1987) have dated it at 290±7Ma (Rb-Sr), which overlaps the date for the Bodmin granite. However, total rock geochemistry does not show a particular affinity to either the Bodmin or Dartmoor granites (*op. cit.*).

Hingston Down microgranite

This intrusion is also thought to be the surface expression of the buried granite ridge. It has been dated by Darbyshire and Shepherd (1987) at 282±8Ma (Rb-Sr whole rock isochron). Bull (1982) has implied that the Hingston Down granite is less differentiated

than its neighbouring intrusions of Dartmoor, Bodmin and Kit Hill, based upon normative compositions and trace element geochemistry.

Table 4.1 Published isotopic dates for the surface exposures of the Cornubian batholith in the study area.

Outcrop	*Method*	*Date (Ma)*	*Reference*
Bodmin	U/Pb monazite	280.8±0.4	Chen *et al.*, (1993)
Bodmin	Ar-Ar muscovite	288.8±0.9	Chen *et al.*, (1993)
Bodmin	Rb-Sr separates	287±2	Darbyshire and Shepherd (1985)
Bodmin	U/Pb monazite	291.4±0.8	Chesley *et al.*, (1993)
Bodmin	Ar-Ar muscovite	287.1±0.9	Chesley *et al.*, (1993)
Dartmoor	U/Pb monazite	278.2±0.8	Chesley *et al.*, (1993)
Dartmoor	Ar-Ar muscovite	280±1.2	Chesley *et al.*, (1993)
Dartmoor	Rb-Sr whole rock	280±1	Darbyshire and Shepherd (1985)
Dartmoor	U/Pb monazite	285±0.6	Chen *et al.*, (1993)
Dartmoor	Ar-Ar muscovite	289.8±0.8	Chen *et al.*, (1993)
Hingston Down	Ar-Ar muscovite	283.1±0.9	Chesley *et al.*, (1993)
Hingston Down	Rb-Sr whole rock	282±8	Darbyshire and Shepherd (1985)
Kit Hill	Rb-Sr whole rock	290±7	Darbyshire and Shepherd (1985)
Kit Hill	Rb-Sr separates	287±4	Darbyshire and Shepherd (1985)
Hemerdon Bal	Rb-Sr whole rock	304±23	Darbyshire and Shepherd (1985)
Hemerdon Bal	Pb/Pb monazite	298.3±2.3	Chesley *et al.*, (1993)
Hemerdon Bal	Ar-AR muscovite	290.2±0.4	Chesley *et al.*, (1993)

4.1.3 Deformation

Deformation in SW England is generally related to the Variscan orogeny, which resulted in folding and thrusting of Devonian and Carboniferous sediments culminating in the intrusion of the Cornubian batholith. The model proposed by Anderton *et al.*, (1979) is based upon the subduction of the Rheic oceanic lithosphere, to the south of the Moldanubian zone of the Hercynides, with a back-arc marginal basin present in the Rheno-Hercynian zone. In SW England, a complex series of folding resulted in the formation of three recognised deformation episodes prior to the intrusion of the batholith (see Dearman *et al.*, 1971; Isaac *et al.*, 1982 and Shackleton *et al.*,. 1982 for reviews). Although this present study is concerned with deformation subsequent to the granite emplacement a brief review of the main Variscan deformation events is outlined below to place the study in a wider context.

Variscan Deformation

Tectonic deformation began in the late Viséan and early Namurian (Isaac *et al.*, 1982) and was followed by a subsequent main thrusting event from late Namurian times

Towards the end of the Namurian and in the Westphalian, the intrusion of the granite batholith may have caused the fold belt to tighten, which resulted in the formation of numerous low angle normal faults (*op. cit.*) which may exhibit listric or ramp and flat geometries together with complex arrangements of secondary faults (Shail and Wilkinson 1994). To summarise, Issac *et al.*, (1982) describes the regime as:

"one of very thin skinned thrust and nappe tectonics with the allochthon probably not exceeding 1km in thickness."

Warr (1988) identifies a subsequent phase of extensional tectonics related to the formation of east-west striking normal faults. Within the study area (the eastern part of the Cornubian batholith, including the St. Austell, Bodmin and Dartmoor granites) normal faults bearing main-stage lodes are east-west striking, whereas in the Lands End and Carnmenellis granites to the east they have a SW-NE strike. Shail and Wilkinson (1994) suggest this variation in orientation is related to differences in pre-Devonian basement fabrics across the Start-Perranporth line. The cause of this end-Variscan period of extensional tectonism has been associated with the onset of crustal rifting (Hawkes, 1982). However, Shail and Wilkinson (1994) assert that the coeval association of late Carboniferous and early Permian potassic volcanicity, with granite magmatism, extensional faulting, and the development of sedimentary basins is the result of Variscan orogenic collapse and consequent relaxation of the associated tectonic forces (Dewey, 1988).

Post-Variscan deformation

Deformation in SW England throughout the Mesozoic and Cenozoic was restricted to substantial displacements along a series of generally NNW-SSE striking, strike-slip faults (Dearman, 1963) (Fig. 4.2). Dearman estimated an approximate total of 34km of dextral offset generated by wrench faulting and related to the compressional forces arising from the Alpine orogeny. Other authors have also envisaged Tertiary fault displacements along approximate NW-SE striking faults in North Devon (Blyth, 1957; Blyth, 1962; Shearman 1967) together with the formation of Tertiary basins related to strike-slip displacements (Bristow and Hughes, 1971; Edwards, 1976; Freshney *et al.*, 1982) in south Devon. However, more recently Holloway and Chadwick (1986) have attributed movements along the Sticklepath-Lustleigh Fault Zone (SLFZ) to late-Variscan and Permo-Triassic times, with sinistral movements occurring in the early Tertiary and only minor dextral movements in late Tertiary times. Turner (1984) concluded that possible wrench faults between the Dartmoor and Bodmin moor granites were reactivated, pre-Variscan basement structures, with little or no evidence of strike-slip displacements.

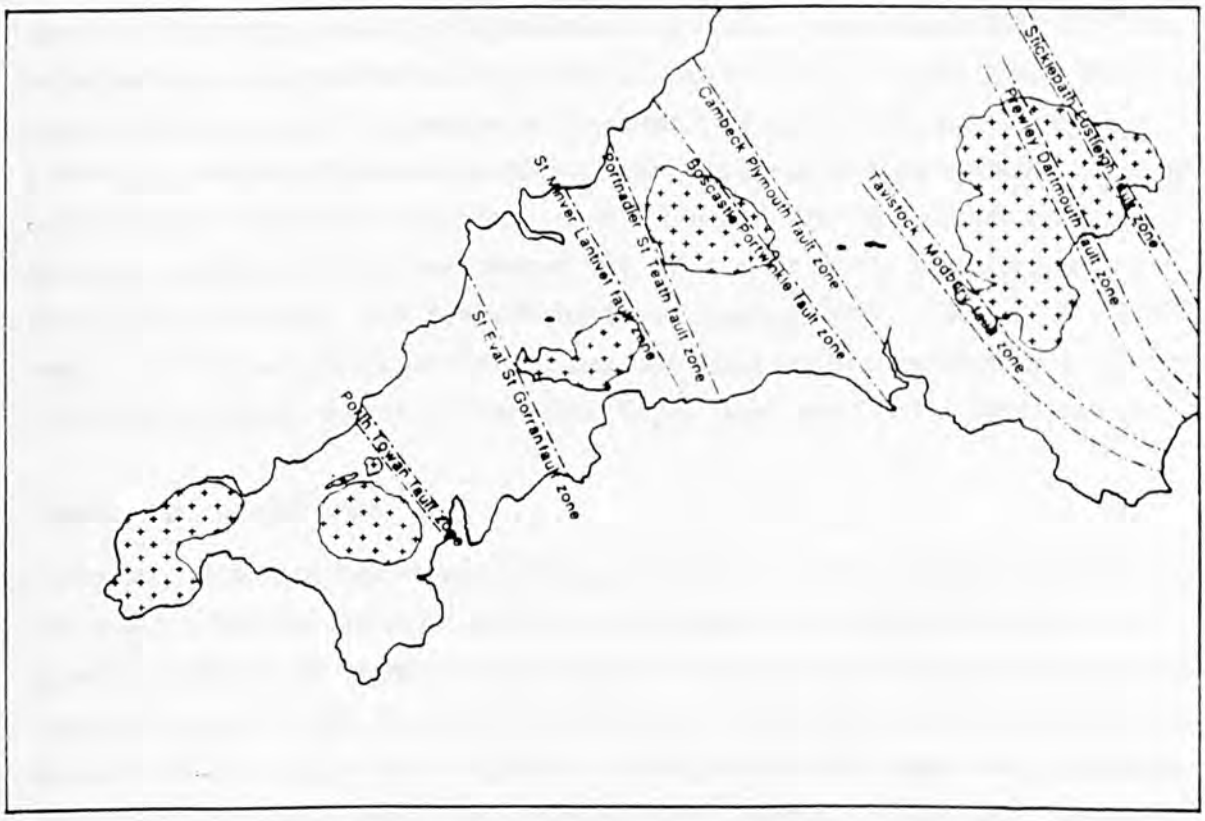

Fig. 4.2 Northwest-southeast striking strike-slip faults and fault zones of the study area and SW England active since post-Variscan times. After Dearman (1963).

4.1.4 Mineralisation and hydrothermal alteration of the study area

Within the study area there is a wide variety of mineralisation and hydrothermal alteration, formed from fluids of diverse origins and related to several tectonic events. Deposits generally occur in high angle fractures (normal faults), and show a classic lateral zonation around the major plutons (Guilbert and Park, 1986). Hydrothermal alteration is extensively locally developed, with economic deposits of china clay being located in the study area. A summary of the published dates for mineralising fluids in the study area is shown in Table 4.2 and the composition of the fluid types responsible is shown in Table 4.3. Based on results from Shepherd *et al.*, (1985), Shepherd and Scrivener (1987) and Scrivener *et al.*, (1994) and from the recent summary by Jackson *et al.*, (1989), the hydrothermal activity in the study area can be classified into four main stages.

Granite-porphyry-hosted, greisen-bordered sheeted vein swarms.

This type of mineralisation is seen at Hemerdon Bal and at Kit Hill. It is typified by tungsten (+ tin) bearing, greisen-bordered, sheeted veins. Fluid inclusions studies by Shepherd *et al.*, (1985) have shown that the fluids responsible for this type of mineralisation are of high temperature but variable salinity. Wolframite-bearing vein

quartz at Hemerdon showed homogenisation temperatures in the range 200-500°C and salinities falling into two discrete groups of 2-12 and 18-25 wt. %. equiv. NaCl. The low salinity fluid phase has been interpreted by Shepherd *et al.*, (1985) and Jackson *et al.*, (1989) as a product of hydraulic fracturing, leading to adiabatic decompression, which in turn triggered wolframite deposition. In SW England, this type of mineralisation is generally considered to have been formed in a single event shortly after emplacement of the batholith (Bromley, 1989; Willis-Richards and Jackson, 1989). Chen *et al.*, (1993) using ^{40}Ar- ^{39}Ar on hydrothermal muscovites have dated similar mineralisation at 281.9± 1.4Ma (St. Michael's Mount), 279.9±0.8Ma (Cligga Head) and 271.2±0.8Ma (Bostraze).

Polymetallic sulphide veins

East-west trending sulphide veins, containing tin, copper, arsenic and zinc are common in the area between the Dartmoor and Bodmin granites. This type of mineralisation is generally found in the sedimentary envelope, or on the edges of the granite plutons. Deposits around Kit Hill, Hingston Down and the Tamar valley have been described in detail by Bull (1982) who recognised a paragenesis with quartz and tourmaline deposition preceding the formation of arsenopyrite, followed by wolframite, cassiterite, chlorite, chalcopyrite, with minor sphalerite, galena, pyrrhotite and stannite. Around Caradon Hill in south east Bodmin and on the western flanks of the Dartmoor granite veins carrying copper, zinc, tin, arsenic and quartz also occur (Dines, 1956; Shepherd *et al.*, 1985).

Fluid inclusion studies reported by Shepherd *et al.*, (1985) have indicated that the fluids responsible for this high temperature mineralisation were formed from partial mixing of two discrete fluids; a low salinity, high temperature magmatic-hydrothermal component (Th 300-380°C; 0.5-12 wt. %. equiv. NaCl) and a lower temperature, moderate salinity component (Th 200-310°C; 12-20 wt. %. equiv. NaCl) thought to have been derived from the surrounding sedimentary rocks. As the system cooled, mixing with a high salinity (19-25 wt. %. equiv. $NaCl/CaCl_2$) fluid become increasingly important. This is in agreement with other data from the east-west polymetallic tin/copper veins throughout SW England (Jackson *et al.*, 1982; Bromley and Holl, 1986).

The mineralisation is restricted to a series of east-west striking normal faults related to a period of north-south extension at the end of the Variscan orogeny (Jackson *et al.*, 1989). Whether this extension is due to the onset of crustal rifting (Hawkes, 1982) or a relaxation of stresses during orogenic collapse (Shail and Wilkinson, 1994) is not clear. Moore (1975) concluded that the host fractures within the granite were produced by hydraulic stresses. Fluids would then emanate outwards along fractures produced by intrusion of the granite, providing a major control on the circulation of fluids around the batholith. Although no dates exist for this style of mineralisation within the study area,

Chen *et al.*, (1993) have dated muscovites directly associated with cassiterite-tourmaline lodes in the South Crofty mine at ≥283.0±1.0Ma (Ar-Ar), which is in disagreement with Chesley *et al.*, (1990, 1991) for fluorite from the same locality.

Late stage lead-zinc cross-courses

A wide variety of late-stage, quartz-carbonate-fluorite veins containing variable amounts of Pb-Zn-Cu-Fe are present throughout SW England and are also in evidence in the study area. These form so called 'cross-course' mineralisation and have varying orientations in the study area from NNW-SSE to N-S. Fluid inclusion studies (Shepherd and Scrivener, 1987) at Kit Hill have shown that the fluids responsible for this type of mineralisation are low temperature (Th 110-170°C) high salinity (18.5-27 wt. %. equiv. NaCl) . This is in agreement with data published by Shepherd *et al.*, (1985) from N-S veins in the Tamar valley and with recent work by Dominy *et al.*, (1994) from 'cross-course' material in the South Crofty mine. Furthermore, these fluids are Na-Ca-Cl brines. with a $NaCl/CaCl_2$ ratio of 1.2:1 (Shepherd and Scrivener, 1987; Dominy *et al.*, 1994). There has been much uncertainty regarding the age of this type of mineralisation, however, recent work by Scrivener *et al.*, (1994) has dated N-S striking veins from the Tamar valley at 236±3Ma using Rb-Sr isotope analysis of fluid inclusions within quartz, placing it in the Triassic which is in agreement with palaemagnetic data (Cox 1995, *pers. comn*) for ferruginous quartz veins from the Goonbarrow china clay pit (SX 008 587). However, the banded nature of the veins indicates an episodic nature to the mineralisation, making a single date open to question. The mineralisation occurs in N-S extensional fractures formed by east-west crustal extension (Scrivener *et al.*, 1994) or may be closely linked to strike-slip faulting as postulated by (Dominy *et al.*, 1994).

Table 4.2 Dating of mineralising events from published sources, mainly within the study area. Dates from localities outside the study area given for mineralisation styles presumed to be of similar age to those undated in the study area.

Location	*Mineralisation*	*Method*	*Age (Ma)*	*Reference*
Old Gunnislake mine	greisen bordered quartz vein	Ar-Ar muscovite	283.2±0.9	Chesley *et al.*, (1993)
Hemerdon	greisen bordered quartz vein	Ar-Ar muscovite	286.2±0.9	Chesley *et al.*, (1993)
Goonbarrow	greisen bordered quartz vein	K-Ar muscovite	273.6±1.1	Bray and Spooner (1983)
South Crofty	Sn-tourmaline	Ar-Ar muscovite	283.0±1.0	Chen *et al.*, (1993)
South Crofty	Sn-free sulphide lodes	Sm-Nd fluorite	259±7	Chesley *et al.*, (1993)
South Crofty	qtz-fluorite vein	Ar-Ar muscovite	269.0±0.8	Chesley *et al.*, (1993)
Tamar Valley	Pb-Zn-Fl	Rb-Sr fluorite-qtz	236±3	Scrivener et al., (1994)

Hydrothermal alteration

Areas of kaolinised granite representing argillic alteration are commonly developed throughout the study area, with large economic deposits occurring at Lee Moor on the south-western flank of the Dartmoor granite (see Dominy, 1993 for review.) The exact origins of kaolinisation in SW England are far from fully understood with a number of theories having been proposed. Sheppard (1977) postulated that kaolin was produced by a type of tropical lateritic weathering. However, Bristow (1977) argued for a hydrothermal origin stating that the deposits had a funnel shape, with depths of alteration greater than 250m, and that up to 250m of granite may overlay the deposit as well. Bristow also noted the close affinity of kaolinisation to greisen-bordered quartz-tourmaline veins. Bray (1980) concluded that it was the high temperature greisenisation, tourmalinisation and hydrothermal mineralisation processes that were responsible for the formation of kaolinite, based upon radiometric dating of muscovites found in kaolinised potassium feldspar. However, it is more likely that the formation of kaolinite is by a two stage process, where initially high temperature fluids 'soften' up the granite which is then altered by the passage of large volumes of low salinity/low temperature meteoric fluids Durrance *et al.*, (1982). Although no data is accessible for this stage of hydrothermal alteration in the study area, Alderton and Rankin, (1983) have shown that fluids of the temperature range 150°C to below 70°C were responsible for the development of economic deposits of china clay in the St. Austell granite.

Table 4.3 Summary of mineralising fluids identified mainly within the study area.

Location	*Type*	*Mineral*	*Th range (°C)*	*Salinity* *wt. % equiv. NaCl*	*Reference*
Hemerdon	greisen bordered sheeted vein	quartz	200-500	2-12 18-25 >29	Shepherd *et al.*, (1985)
Hemerdon	greisen bordered sheeted vein	quartz	360-430	15	Alderton and Harmon (1991)
Wapsworthy	granite	quartz	100->550	40	Alderton and Harmon (1991)
Cheesewring	granite	quartz	100->550	18	Alderton and Harmon (1991)
Birch Tor	Sn-W	quartz	280-330	7	Alderton and Harmon (1991)
Lopez	Cu-Pb-Zn	quartz	257-295	1.5-3.0	Alderton (1978)
Gill	Cu-Pb-Zn	quartz	168-270	1.5-3.5	Alderton (1978)
Bodmin-Dartmoor	(Sn)-Cu-Zn-Pb	quartz	300-380 200-310	0.5-12 12-20	Shepherd *et al.*, (1985)

Collacombe	Cu-Pb-Zn	quartz	210-340	5	Alderton and Harmon (1991)
Capunda	Cu-Pb-Zn	quartz	220-240	2	Alderton and Harmon (1991)
Wheal Lopez	Cu-Pb-Zn	quartz	260-310	5	Alderton and Harmon (1991)
Kit Hill - Gunnislake	Cu-Pb-Zn	fluorite	215-305 110-182	variable salinity 4 & 26 (11 NaCl + 16 $CaCl_2$)	Shepherd and Scrivener (1987)
Wheal Wrey	Pb-Zn-Fl	fluorite	140-175	23	Alderton and Harmon (1991)
Wheal Exmouth	Pb-Zn-Fl	fluorite	110-115	23	Alderton and Harmon (1991)
Kit Hill - Gunnislake area	Pb-Zn-Fl	fluorite	110-170	19-27 (11-15 NaCl + 9-13 $CaCl_2$)	Shepherd and Scrivener (1987)
South Tamar	Pb-Zn-Fl	fluorite	140-146	23.9-24.2	Alderton (1978)
Furzehill	Pb-Zn-Fl	fluorite	138-176	24-24.5	Alderton (1978)
South Crofty	Pb-Zn-Fl	quartz	<100-175	<1-23	Dominy *et al.*, (1994)
Tamar valley	Pb-Zn-Fl	fluorite	105-170	18.5-27 (10 NaCl-13 $CaCl_2$	Shepherd *et al.*, (1985)
Port Issac-St. Endellion	Pb-Zn-Ag	quartz	180-210	0.5-6	Clayton *et al.*, (1990)
Port Issac-St. Endellion	Sb-As-(Au)	quartz	280-315	3-4	Clayton *et al.*, (1990)

4.2 Sampling, collection and analysis of field data

The previous section has provided a brief review of the hydrothermal and tectonic evolution of the study area for the purpose of illustrating the setting in which the generation of FIPs has occurred. The sampling regime was thus undertaken to answer the questions posed in section 4.0, and the locations of the samples were positioned to reflect this. However, one of the major constraints on sampling was the exposure of the granite. As outlined in section 4.1.2, the buried granite batholith is exposed in two major plutons (Dartmoor and Bodmin Moor granites) in the study area, and two minor stocks (Kit Hill and Hingston Down). Therefore, sampling was restricted to exposure in these areas.

4.2.1 Sampling

The mineralisation trend in the study area consists of a strong E-W pattern, with several N-S and NW-SE vein and fault orientations also occurring, albeit less densely. Thus, sampling locations were positioned on the east and west extremities of the study area (west Bodmin and east Dartmoor respectively) in proximity (100-200m) to areas of known hydrothermal mineralisation (Dines, 1956) and within areas of argillic alteration (Dominy, 1993). Further sample stations were located in a more central position at Hingston Down, close (1 to 50m) to known tin and polymetallic sulphide mineralisation. Samples were also obtained from the granite stock at Kit Hill where a small porphyry hosted, greisen bordered sheeted vein wolframite deposit occurs. Shepherd and Scrivener (1987) have shown that the low temperature/high salinity fluids responsible for 'cross-course' mineralisation were present in the Kit Hill area.

Sampling was generally confined to fresh (unaltered) granite (Hingston Down, Caradon Hill, Cheesewring, Kit Hill), although samples of altered granite were obtained on occasion (Lee Moor, Kit Hill). At Lee Moor, semi-altered granites containing $\approx$ 5% kaolinite were obtained, and at Kit Hill where granites with varying degrees of greisenisation were collected. Samples of hydrothermal vein material were collected where they could be obtained in-situ. The use of mine dumps for sampling was avoided However, in-situ, N-S striking, cross-course material could not be obtained and several specimens of Pb-Zn bearing fluorite were collected at disused workings where known production from N-S veins had occurred (e.g., Kelly Brae, near. Kit Hill).

Joint surveys were undertaken at sample locations (Kit Hill, Hingston Down, Caradon Hill and Cheesewring) together with the analysis of surface exposures of vein systems where exposure allowed. Elsewhere, a combination of topography and granite exposure made the collection of field data difficult. Sampling interval was also controlled to an extent by the exposure of the granite. Hingston Down was chosen as an area of more closely spaced sampling (samples obtained at intervals of 50m) to analyse local deviations in the regional stress regime. Hingston Down quarry was selected due to the large degree of exposure and abundance of fracturing and associated hydrothermal mineralisation.

4.2.2 Joint and vein orientations

Joint and vein orientation data were obtained from granites around the sample locations at Caradon Hill, Cheesewring, Hingston Down and Kit Hill quarries, and from sedimentary strata near Gunnislake on the banks of the Tamar river. A joint is defined as a fracture, along which no visible movement has occurred. Data are presented as barren joints (i.e. exhibit no movement or mineralisation) and veins (generally veinlets or

mineralised joints). The presence of slickenfibres, denoting movement was detected in only relatively few cases.

Bodmin granite

Joint orientations are depicted in Fig. 4.3 from the two sample locations on the eastern edge of the Bodmin granite. The data show two distinct groups and a possible third weaker one. A steeply dipping set oriented ENE-WSW is strongly developed at both localities, as is a set of low angle sub-horizontal joints.

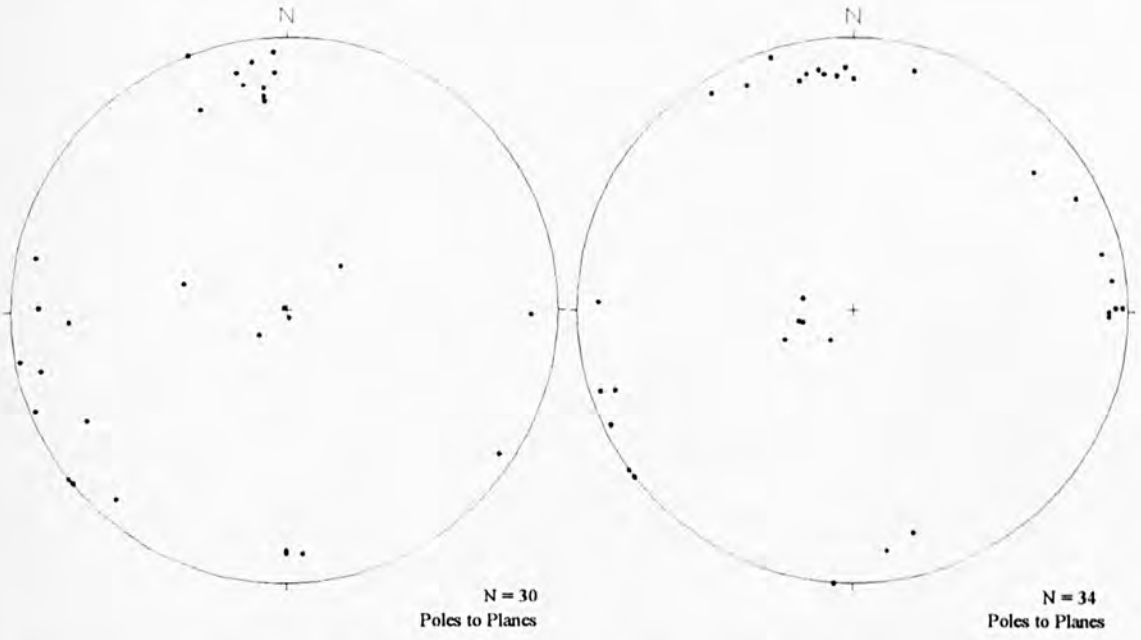

Fig. 4.3 Equal area projection for poles to planes of joint surfaces from (a) Caradon Hill quarry and (b) Cheesewring quarry on the eastern flank of the Bodmin granite. See Fig. 4.1 for locations.

A possible third set with an approximate NNW-SSE orientation is observed at Cheesewring and possibly at Caradon Hill.

Kit Hill-Hingston Down

Fig. 4.4 shows joint and vein orientations from sampling localities at Kit Hill and Hingston Down. The results are similar to those observed in the Bodmin granite, however, the majority of the joints have been used as conduits for mineralising fluids and exhibit a vein filling or alteration.

At Hingston Down the majority of the fractures exhibit alteration of their borders (approximately 1cm on each side of the fracture) to form a greisen. Minor sulphides (chalcopyrite, pyrite and occasionally tourmaline) are sometimes also observed with quartz, indicating a vein filling. These fractures are typically steeply dipping with an E-W orientation. Minor sulphides were not observed in any fractures at Kit Hill, though

again joints exhibiting greisened borders were present. Greisen veins up to 25cm in width were also common. Both these joints and veins had an approximate E-W orientation. A set of N-S striking fractures exhibiting argillic alteration were also identified at Kit Hill. These were generally between 5-10cm in width and were frequently weathered in to the granite

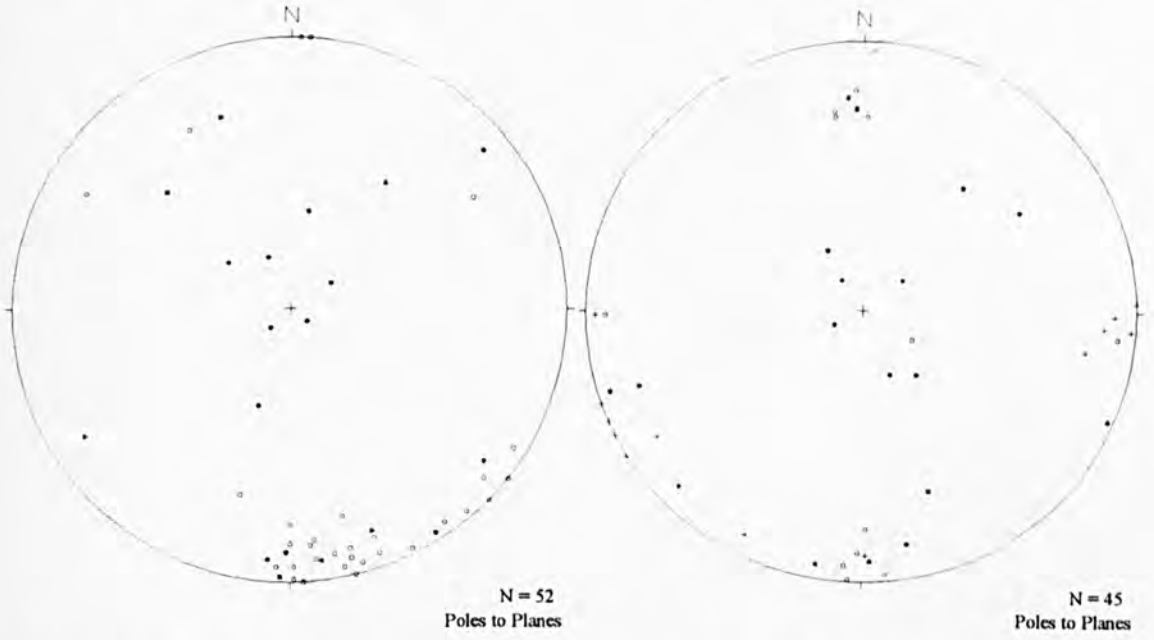

Fig. 4.4 Equal area projection for poles to planes of joint surfaces and other mineralised fractures from (a) Hingston Down and (b) Kit Hill. • = unmineralised or unaltered joints; o = fractures exhibiting greisen wall rock alteration; + = joints exhibiting kaolinisation wall rock alteration. See Fig. 4.1. for locations.

4.2.3 Interpretation of joint data

It is clear that joints and mineralised fractures observed in the field show strong preferred orientation throughout the study area. Not only are these fracture sets characterised by their orientation, but also, in many cases, by alteration of the wall rock. It can be thus assumed that fluids of varying chemistry and probably temperature were circulating within the fracture sets as they evolved. Table 4.4 is a summary of the vein and joint orientations observed in the study area.

E-W joints and greisen veins

Joints oriented E-W are dominant in the study area, and are of the same orientation as main stage mineralisation between Bodmin and Dartmoor. This is exemplified by the presence of fractures exhibiting sulphide vein fillings and greisenisation. Moore (1975) produced stress trajectory diagrams based upon the orientation of vein lodes and porphyry dykes (Fig. 4.5) which correspond well with the data presented above,

assuming that these joints and veins represent dilation fractures with their σ_2 axis oriented parallel to their length.

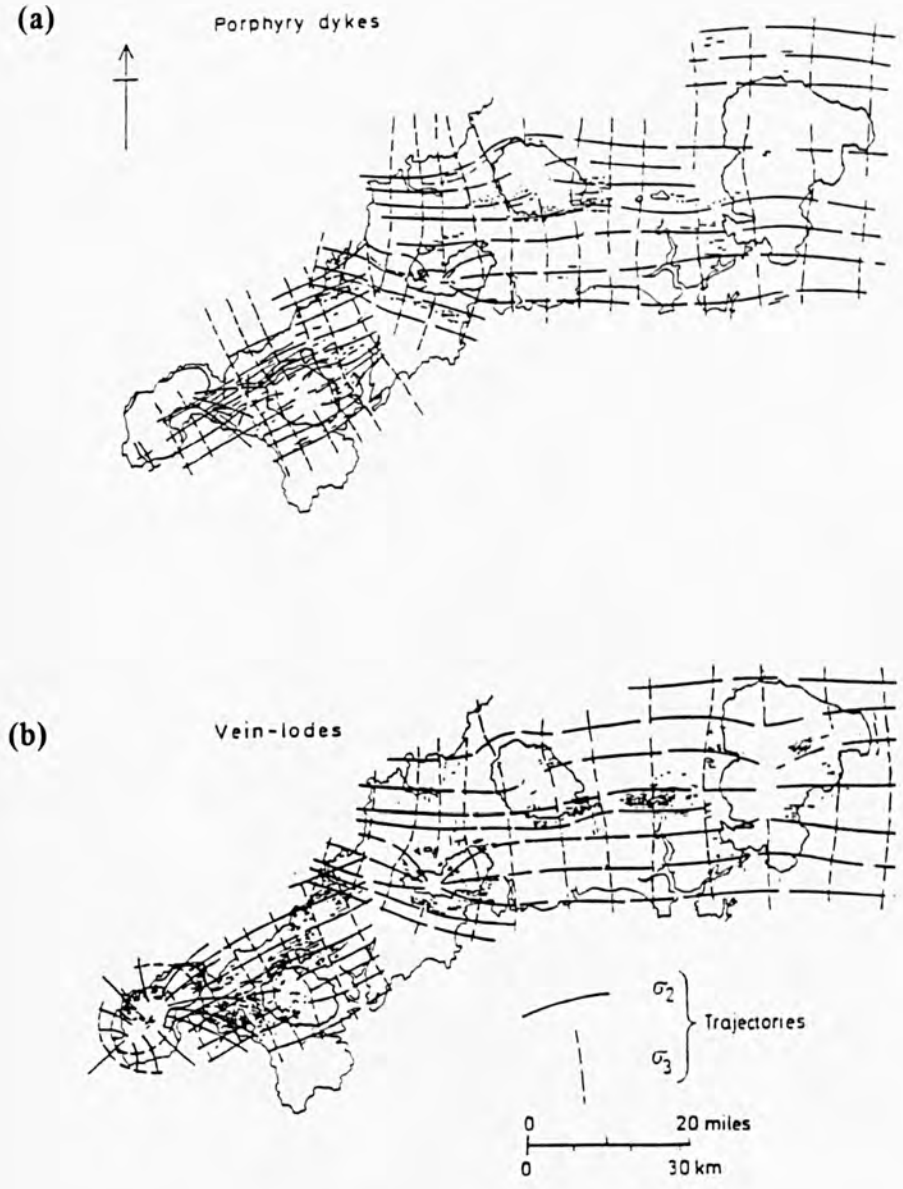

Fig. 4.5 Stress trajectory analysis after Moore (1975). (a) Porphyry dyke stress trajectory net (σ_2-σ_3 principal plane) showing important dyke outcrop traces and granite cupola outlines. (b) Vein lode trajectory net (σ_2-σ_3 principal plane) showing main vein-lodes, and cross-course vein outcrop traces.

N-S joints and kaolinised fractures

Joints and veins of kaolinised granite are also present in the study area, forming a minor set in comparison to the E-W fractures. The presence of these joint sets with orientations at 90° to each other, is common throughout the Bodmin and Dartmoor

granites, and is responsible for the formation of the classic Tor weathering patterns that may be observed at Hay Tor (SX 758 771) on Dartmoor (Bristow, 1977). Since it was evident that the zones of kaolinised granite, clearly cross-cut the greisen veins, it can be stated that the former are the youngest. The exact age of the hydrothermal fluids responsible for the kaolinisation process is not known. However, since kaolinitic clays are found within the strike-slip basins associated with other Palaeogene sediments (Edwards, 1976; Freshney *et al.*, 1982; Bristow and Robson, 1994), it may be postulated that they pre-Palaeogene in age. Further evidence for the fluids responsible for kaolinisation is presented in the next section.

Sub-horizontal joints

A third and very minor, but well-developed set of horizontal to sub-horizontal exfoliation joints are also present. This type of joint is generally ascribed to expansion of the granite due to its exhumation and unroofing (Price and Cosgrove, 1990). Dangerfield and Hawkes (1969) present evidence suggesting a possible unroofing of the Dartmoor granite before the end of the Permian. Since these low angle fractures do not exhibit any alteration, it may be implied that fluids responsible for hydrothermal alteration were not circulating during the formation of these unloading fractures.

Table 4.4 Summary of vein and joint orientations observed in the field area.

Orientation	*Alteration/mineralisation*	*age*	*probable cause*
low angle	none	Permian?	granite exhumation/unroofing
N-S	none	Permian-Tertiary	east-west extension-crustal rifting/Alpine compression
N-S	kaolinised veins 5-10cm	Permian-Tertiary	east-west extension-crustal rifting/Alpine compression
E-W	none	late/post-Variscan	north-south extension-orogenic collapse/relaxation
E-W	greisen ±minor sulphides	late/post-Variscan	north-south extension-orogenic collapse/relaxation

4.3 Microstructure and Microthermometry

The following section concerns the presentation of healed fracture orientations and characteristics together with the thermometric data from the secondary fluid inclusions contained within them. All data from which interpretations have been drawn are listed in Appendix A. The techniques involved in recording orientation and thermometric data are described in Appendices B and C. All measurements were restricted to quartz because of its relatively high abundance of fluid inclusions and the lack of strong cleavage that may affect the fracture orientations.

4.3.1 Orientation analysis

Healed fracture orientations were recorded from ten samples within the study area. The large scale sampling regime is designed to determine the orientation of FIPs over a wide area, with respect to the orientation of the regional stress axes, however detailed sampling was undertaken at Hingston Down and more detailed results are presented from this locality. Samples have mainly been prepared from horizontal sections, where it is possible to then analyse vertical or steeply dipping FIPs (see Appendix B). However, sections have also been prepared in several cases from two sections dipping at 45° in opposite directions. These sections gave a preference to shallow dipping FIPs. A few vertical sections were also prepared so that horizontal FIPs may be analysed. Only healed fractures have been analysed from granite quartz.

Summary of orientation results

Four hundred and sixty one FIP orientations were measured using sixteen thin sections from ten samples, from five localities (Appendix A; Table A1.1). Six samples were obtained from Hingston Down. Data are presented as rose plots and stereonets in Fig 4.6 and 4.7 and as raw data in Appendix A; tables A4.7-A4.15. Four main groupings of FIPs are apparent from the combined data. The most dominant are a set of E-W FIPs dipping at about 70° from the vertical. These are present at all five localities. A N-S striking set with dips varying no more than 5° from the vertical is strongly developed at Kit Hill but only weakly developed at the other localities. A NW-SE striking set is strongly developed in the combined Hingston Down samples and from samples at Lee Moor, weakly developed at two other localities (Caradon Hill and Cheesewring) but absent in the Kit Hill samples. A fourth set of FIPs, striking NE-SW and with sub-vertical dips is well developed in the Caradon Hill samples but only weakly developed (less than 5% of the population) at the other four localities.

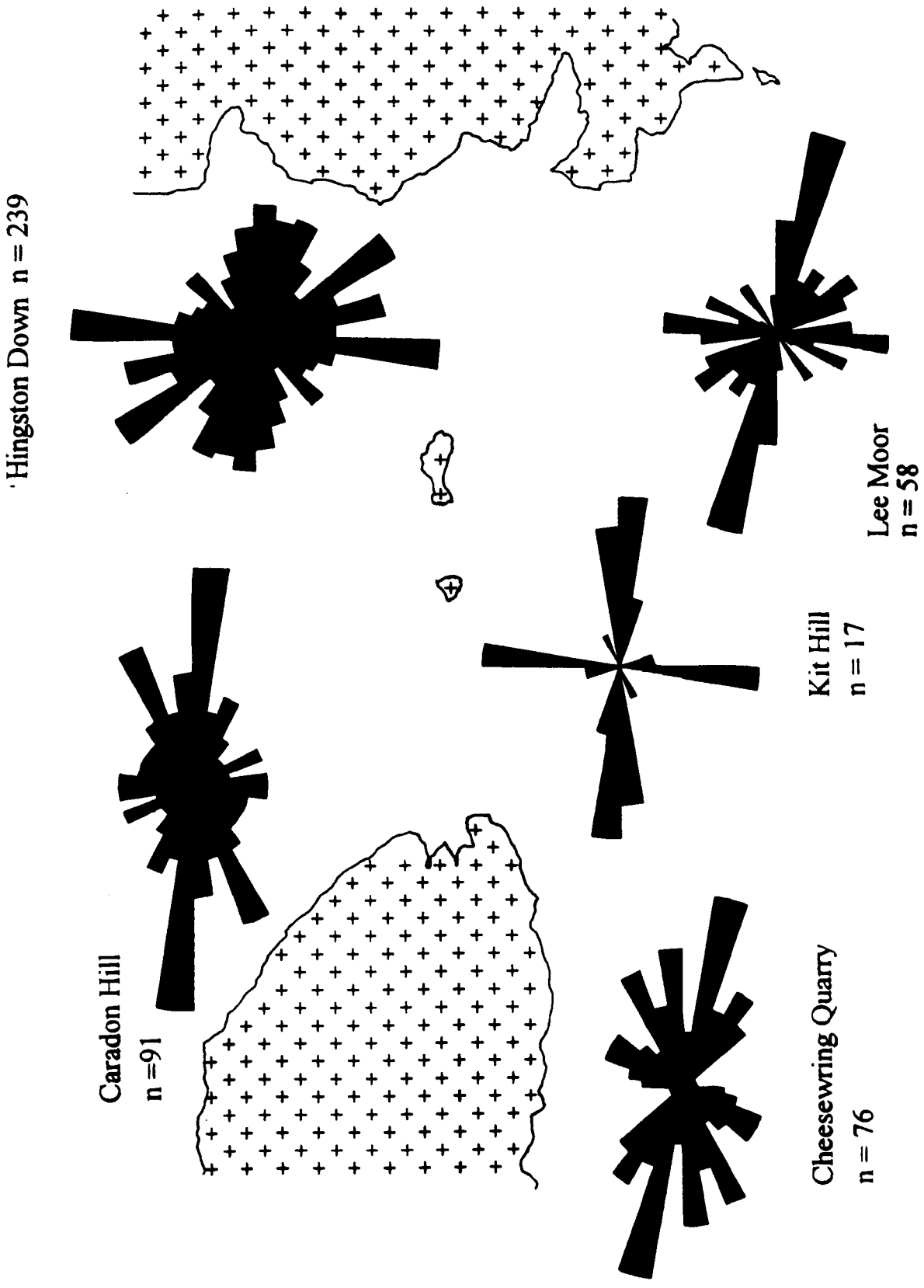

Fig. 4.6 FIP orientation data from the five sample localities within the study area. Orientation data is depicted as rose diagrams (showing strike only) illustrating relationships with vein-set trends. Geology based loosely upon Dangerfield and Hawkes (1981) and Dines (1956). Note the strong regional trend for FIPs oriented E-W. Minor FIP trends vary between sample locations illustrating the affect of local deviations in the stress regime associated with post-Variscan faulting.

Analysis of the six samples obtained from the Hingston Down granite shows a marked variation in the orientations of the FIPs between sample localities (Fig. 4.7). Data from these samples were obtained from slides cut at 45° from the horizontal and thus a large variation in the dip of the FIPs is observed. However, E-W trends are present in sample HD4 and possibly HD3 and HD6 with possible N-S trends in samples HD2 and HD5. Sample HD1 shows a possible NW-SE trend.

(a) HD1

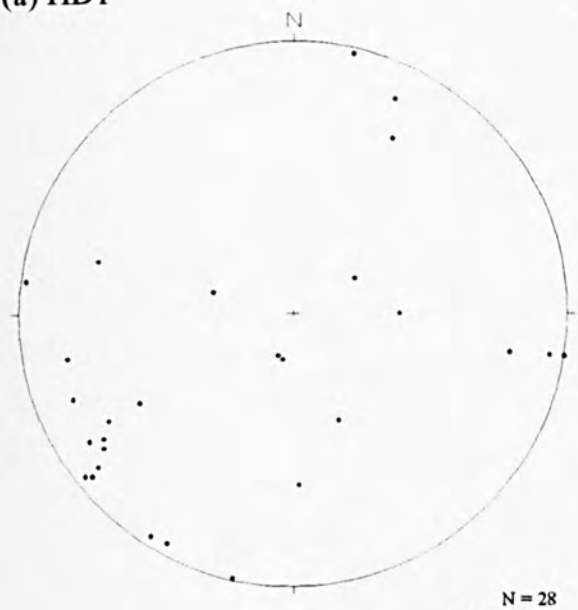

N = 28
Poles to Planes

(b) HD2

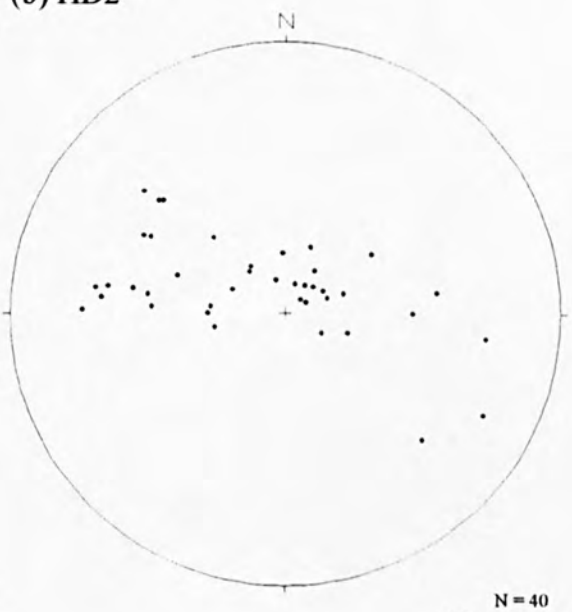

N = 40
Poles to Planes

(c) HD3

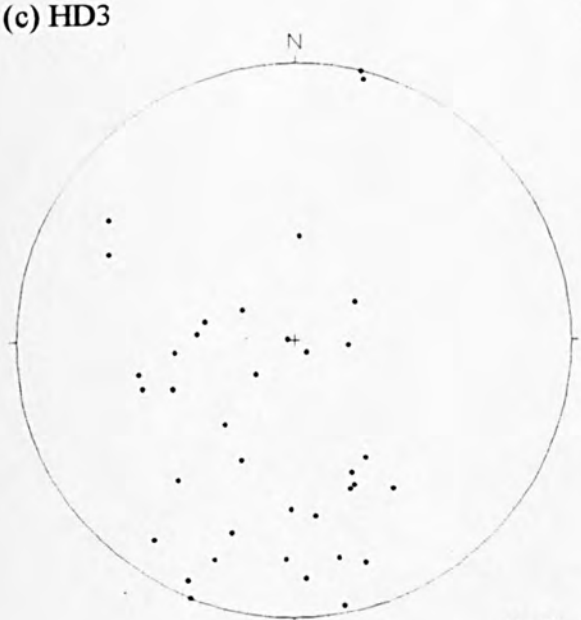

N = 37
Poles to Planes

(d) HD4

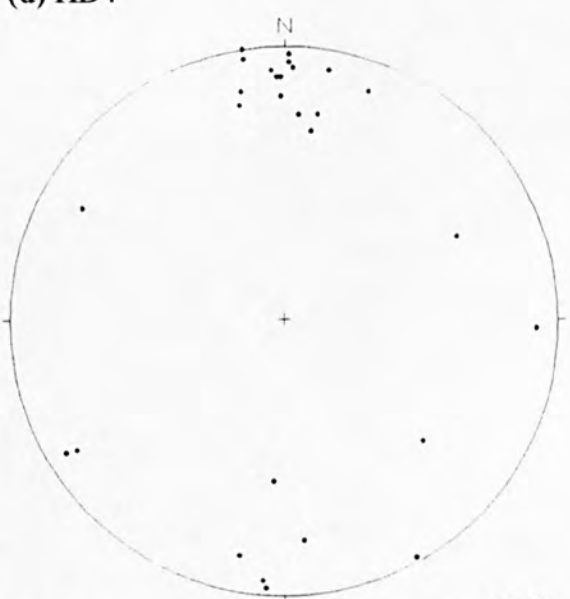

N = 28
Poles to Planes

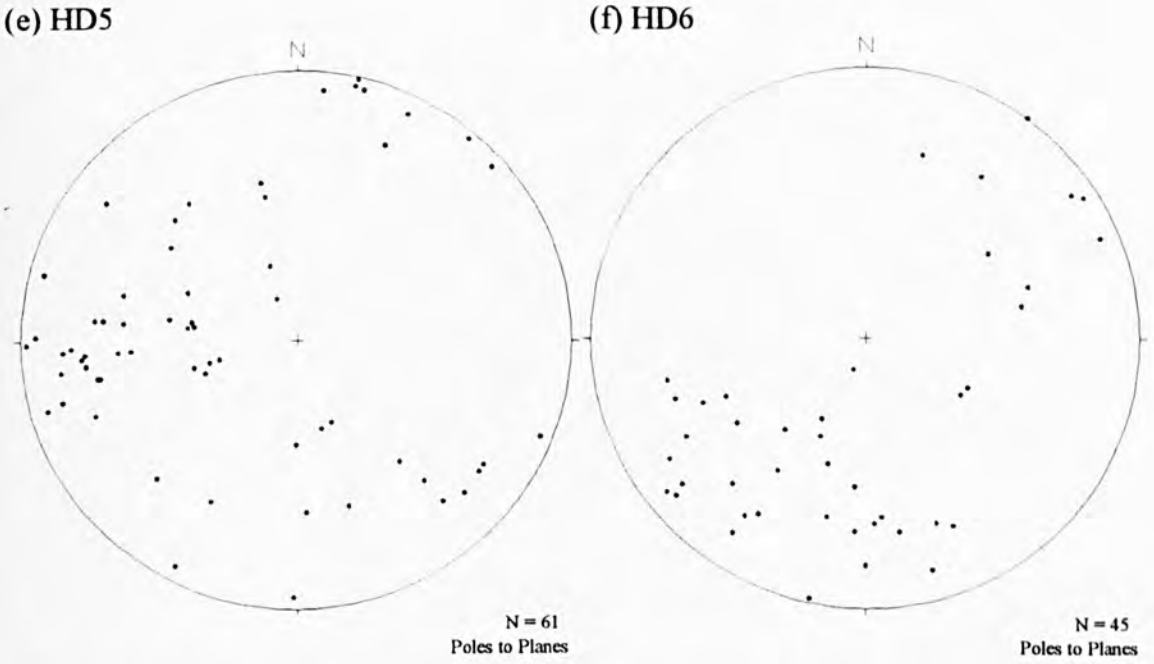

Fig. 4.7. Equal area projections showing poles to planes for FIPs from granitic quartz at the Hingston Down quarry. (a) HD1; (b) HD2; (c) HD3; (d) HD4; (e) HD5; (f) HD6. See Fig. 4.6 for location

FIP abundances

Abundance values were calculated by counting the total number of FIPs in more than one quartz crystal and then calculating the area of the crystals using a Site Systems image analysis system. FIPs were counted within a single plane of the crystal, rather than throughout the whole thickness of the section.

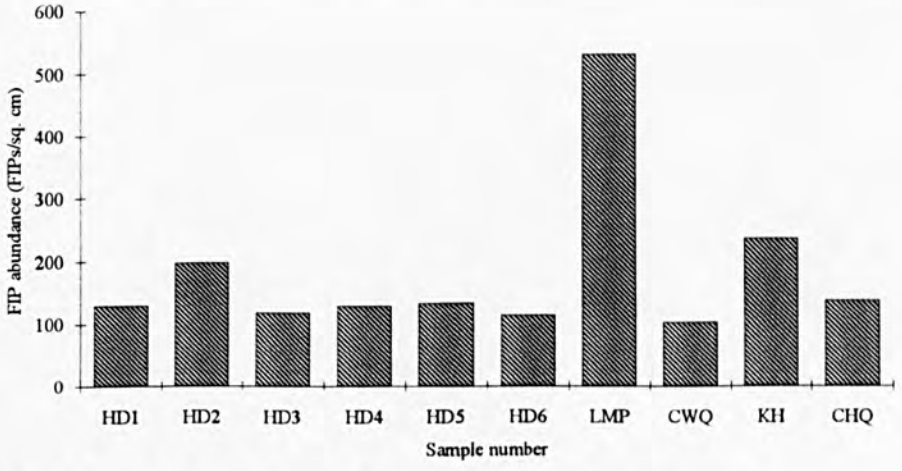

Fig 4.8. FIP abundance histogram for samples from the Bodmin-Dartmoor area.

FIP abundance between crystals, within the same samples, was generally similar. The abundance of FIPs showed a minor variation in all cases apart from the Lee Moor sample which exhibited a marked increase in FIP abundance, and the relationship between inclusion abundance and hydrothermal alteration has been observed by Alderton and

Rankin (1983) and will be discussed later. Fig 4.8 is a histogram of FIP abundances from the ten samples. FIP abundance was so pronounced in the Lee Moor sample (Plate 4.1) as to make the recording of orientation and abundance data difficult due to the presence of many low angle/horizontal healed fractures and data for this sample are only approximate. Less prominent abundance anomalies were exhibited by samples from Kit Hill and one from Hingston Down. At Kit Hill this is attributed to an increase in hydraulic fracturing in the granitic quartz, related to greisen formation (Shepherd *et al.*, 1985; Jackson *et al.*, 1989). The anomaly in the Hingston Down sample (HD2) is possibly caused by the proximity of a fault (Anders and Wiltschko 1994) to the sample location in the field, although there is no field evidence to support this.

Inter- and Intra- crystalline FIPs

The numerical relationship between the abundance of intercrystalline and intracrystalline FIPs is illustrated by Fig. 4.9. Intercrystalline FIPs are defined as those healed fractures which traverse grain boundaries, as opposed to those which do not interact with grain boundaries or terminate at them, and are defined as intracrystalline.

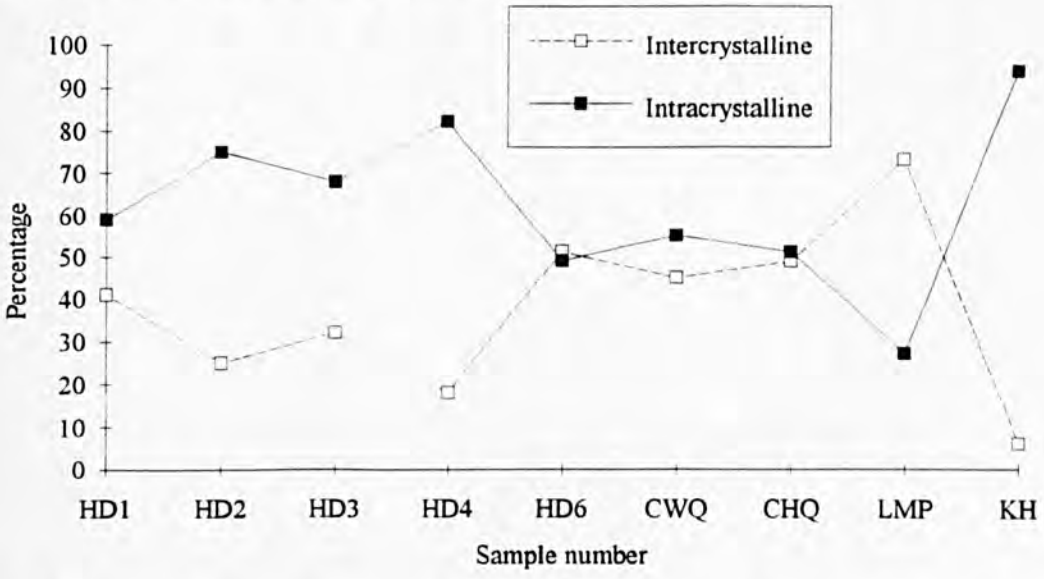

Fig. 4.9. Histogram illustrating the relative proportion (%) of intercrystalline and intracrystalline FIPs generally recorded from granitic quartz grains.

The data indicates that intracrystalline FIPs are generally the most common. Samples KH (Kit Hill) and HD4 (Hingston Down) show a pronounced development of intracrystalline FIPs. It is postulated that the bias in the Kit Hill sample is the result of hydraulic fracturing by high temperature magmatic fluids responsible for the greisenisation process (Shepherd *et al.*, 1985; Jackson *et al.*, 1989) induced by the build up of tensile forces due to differences in thermal expansion (contraction) mismatch and anisotropy (Carlson *et al.*, 1990). The Lee Moor sample was the only one to show a relatively increased proportion of intercrystalline FIPs. Orientation data from Lee Moor

Plate 4.1 Quartz crystal from Lee Moor kaolinised granite (approx. 5% kaolinite alteration) exhibiting high FIP abundance. Note the presence of intracrystalline FIPs forming two sets at 90° and the large intercrystalline shear fracture in the bottom right hand corner.

possess a strong NW-SE trend, similar (consistently discordant) to that of major strike-slip faults present in the study area, and it is implied that these FIPs represent Riedel shear orientations forming at angles of about 15° from the associated master fault (Tchalenko and Ambraseys, 1970). It is presumed that shear fractures will cross grain boundaries, unless they are oriented at a shallow angle to the propagating fracture, without a reduction in stress intensity, and thus continue to propagate into the adjacent grains (Tapponier and Brace, 1976).

It may be implied that the ratio of inter- and intra- crystalline FIPs is controlled by the grain size of the rock being analysed. Samples with a fine grain size will tend to have a greater number of intercrystalline FIPs due to the increase probability of interaction with grain boundaries. Likewise samples with a coarse grain size will tend to possess larger numbers of intracrystalline FIPs. However, the samples studied were all of similar grain size (see Table 4.5) and this is not thought to be responsible for variations in the ratios.

Table 4.5. Quartz grain size for samples from the Bodmin Dartmoor area.

Sample	HD1	HD2	HD3	HD4	HD5	HD6	KH	LMP	CHQ	CQW
Quartz grain size (mm)	1-2	1-2	1-2	2-3	2-3	1-2	4-5	5-6	3-4	4-5

4.3.2 Optical analysis of fluid inclusion population.

The following section is a brief summary of the optical characteristics of the fluid inclusion populations observed within the samples. Synoptic sketches illustrating the inclusion population and abundances are shown in Fig. 4.10. Data from the granite samples studied during the orientation analysis are provided, together with data from quartz and fluorite vein material from the Kit Hill/Hingston Down area. A classification of the inclusion types is summarised in Table 4.6, and illustrated by summary sketches in Fig. 4.11. Again data from primary inclusions have also been included for completeness.

Inclusion types - granitic quartz

Fluid inclusions occur mainly in healed fractures, or as small clusters or groups. Single, isolated inclusions are rare. Inclusions may possess a wide range in shapes, being equant, negative crystals, rounded, elongate and highly irregular. Inclusions are generally two phase, though mono phase inclusions are not uncommon. Three phase inclusions are rare, with daughter minerals generally presumed to be NaCl. Secondary or pseudosecondary inclusions comprise volumetrically up to ≈95% of the total fluid inclusion population in any given sample.

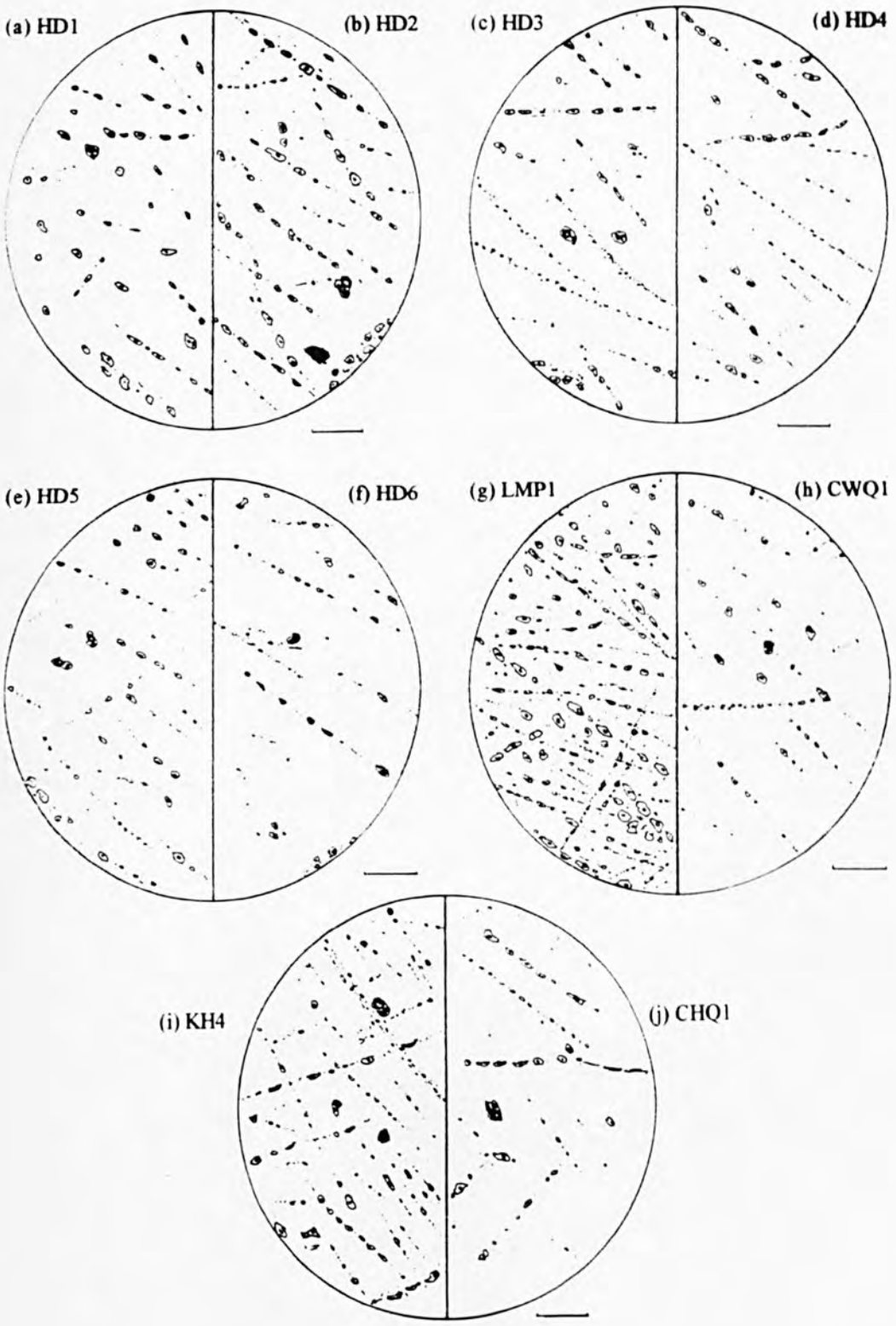

Fig. 4.10 Synoptic sketches of representative sections of ten samples from the five sample localities. (a-f) Hingston Down (HD1, HD2, HD3, HD4, HD5, HD6); (g) Lee Moor (LMP1); (h) Cheesewring Quarry (CWQ1); (i) Kit Hill (KH4); (j) Caradon Hill (CHQ1). Scale bars 40μm.

Table 4.6. Summary of fluid inclusion types observed within fresh and altered granites from Bodmin, Kit Hill, Hingston Down and Lee Moor. Data from vein quartz (Hingston Down) and fluorite vein material are also included for completeness.

Type	*Size*	*Shape*	*Occurrence*	*Phases*
Type 1	< 5μm	rounded/equant	secondary, fracture bound	generally mono-phase (*l*); rare two phase (*l* + *v*)
Type 2	5-15μm	regular/elongate	secondary, fracture bound; isolated groups	generally two phase (*l* + *v*)
Type 3	5-25μm	irregular/flattened /necked.	secondary, fracture bound, isolated groups	mono- (*l*) and two phase (*l* + *v*)
Type 4	10-20μm	rounded/equant	primary, pseudosecondary, isolated/grouped	two phase (*l* + *v*)
Type 5	5-20μm	rounded/equant	pseudosecondary/ secondary	monophase, gas rich, decrepitated
Type 6	10-25μm	rounded/equant	primary/ pseudosecondary/secondary/ fractures/grouped	three phase (*l* + *v* + *s*)

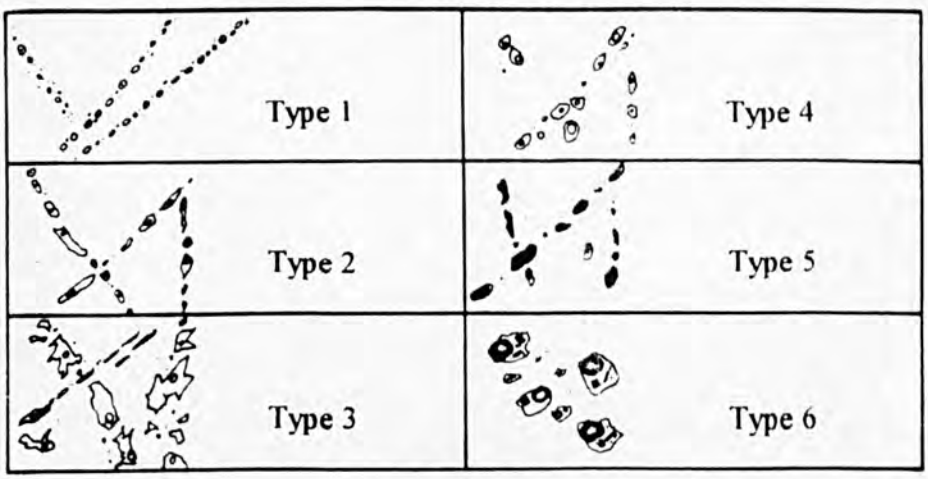

Fig. 4.12 Classification of inclusion types based upon studies of inclusion populations of granite samples from all localities.

Inclusion types - vein quartz and fluorite

Quartz was sampled from east-west trending chalcopyrite-pyrite-sphalerite veins from Hingston Down and barren east-west trending veins at Kit Hill. Inclusions from this material were generally two phase (with some monophase types), and presumed to be generally pseudosecondary types. Primary inclusions were rare and difficult to identify. Secondary fracture bound inclusions were also common. Inclusions range in size from 5-20μm and were usually rounded, equant and negative crystals in shape. Inclusions were generally less abundant in fluorite associated with galena and sphalerite from tips at Kelly

Brae. They showed a wide range in size 5-30μm, and were typically two or mono-phase. These inclusions were extremely irregular and generally occurred in healed fractures, clusters or commonly isolated.

Inclusion abundances

The abundance of FIPs has been estimated as described above. It is postulated that high inclusion abundances will correlate with high FIP abundances. Similar techniques for estimating inclusion abundances have been described by Rankin and Alderton (1982). Comparison with schematic charts of known inclusion abundances were used to make visual estimates. Although this technique was not incorporated in the present study, it is presumed that similar results would be obtained.

4.3.3 Thermometric analysis

Thermometric analysis was carried out on granite quartz (samples HD2, HD3, HD5, HD6, CWQ, KH4, LMP1), vein quartz (HD7) and vein fluorite (KH3). Measurements were generally restricted to secondary fluid inclusions representative of healed microfractures (FIPs) of a known orientation. It would then be possible to define fracture orientations utilised by a particular fluid. However, analysis of possible primary and pseudosecondary inclusions has also been included so that a complete picture of the fluid evolution can be characterised. Analysis of vein material, obtained in relation to sampling of oriented granitic material has also been undertaken. The methodology involved in thermometric analysis of secondary fluid inclusions is detailed in Appendix C. Histograms of homogenisation temperature (°C) and bulk salinity (wt. %. equiv. NaCl) are presented for the identification of modal populations, together with scatter plots (see section 4.3.4) to illustrate the possible evolution of the fluids. Salinity data from the Ternary system $NaCl\text{-}CaCl_2\text{-}H_2O$ are presented on triangular diagrams so that the bulk composition of the fluid can be estimated.

Homogenisation temperatures - granitic quartz

Thermometric analyses were undertaken on the sample CWQ, HD2, HD3, HD5, HD6, KH4 and LMP1. Homogenisation temperatures were recorded from 304 mainly secondary inclusions, giving a wide range in temperature (Th 100-440°C). Homogenisation temperatures are depicted in Fig. 4.12.

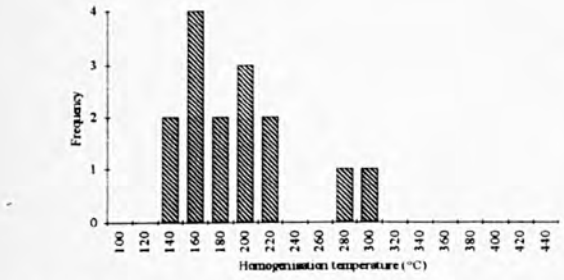

(a) HD2

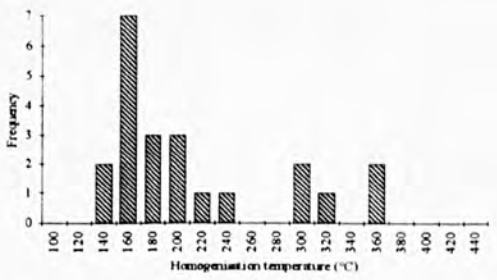

(b) HD3

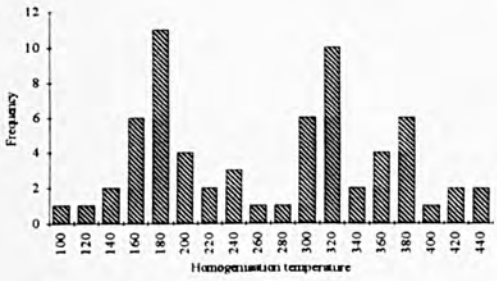

(c) HD5

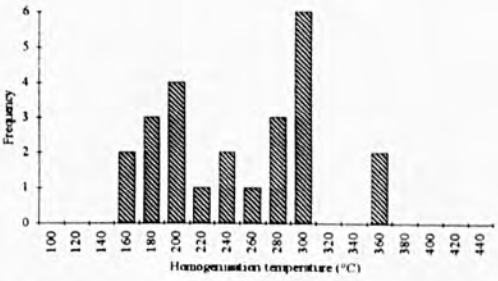

(d) HD6

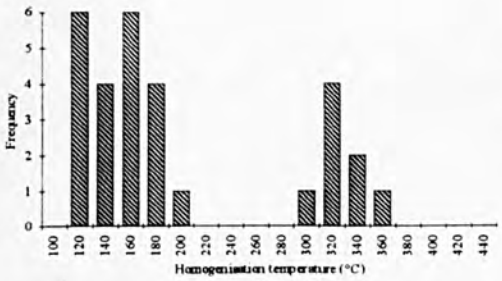

(e) KH4

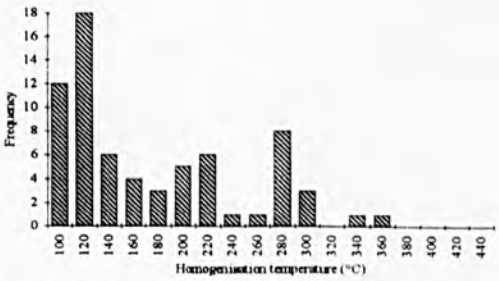

(f) LMP1

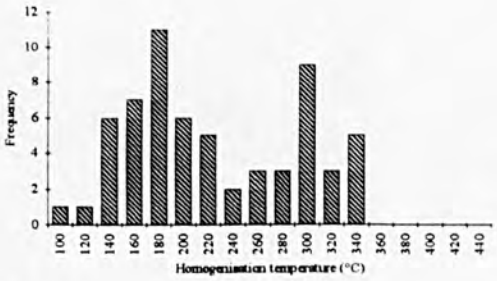

(g) CWQ1

Fig. 4.12. Histograms of homogenisation temperatures from samples of granite quartz, obtained from Hingston Down, Kit Hill, Lee Moor and Cheesewring quarry.

A wide range in temperatures was encountered, as might be expected, from the range of secondary inclusions studied. Generally, histograms illustrate a bimodal (HD5, HD6, LMP1, CWQ1, KH4) or a unimodal distribution (HD2, HD3). The Hingston Down samples possess a moderate temperature peak at around Th 140-240°C, and a possible

higher temperature peak at around Th 300°C. This is in agreement with sample CWQ1 (peaks at 180°C and 300°C), and is typical of samples collected at locations where polymetallic vein mineralisation is abundant. The unimodal distributions observed in samples HD2 and HD3 represent the lower temperature peak. Samples with a negative skew (KH4 and LMP1) have an abundance of low temperature fluids, with the skew being produced by the on-set of the monophase inclusion field at around 100°C. A high temperature peak was observed in sample KH4 at around 340-360°C. The break in the temperature range in sample KH4 is thought to be due to the lack of data, and the subjective method used during the orientation and thermometric analysis.

The bimodal distribution of the temperatures implies the presence of at least two fluids. However, since these inclusions are from healed fractures, temporally discrete fracturing episodes may have been utilised by the same fluid during a simple cooling trend, thus providing the simple two peak distribution. A comparison with the salinity and orientation data would verify the situation.

Bulk salinity - granitic quartz

Bulk salinity was determined from last melting temperatures of 254 mainly secondary inclusions. Last melting was generally restricted to ice with rare hydrohalite. Last melting of hydrohalite was observed in only a few inclusions. Eutectics were generally around -21°C, although the small size of the majority of inclusions made the recognition of these eutectics and first melt phase changes difficult. First melting temperatures lower (-47°C to -51°C) than -21°C were observed in 14 inclusions, the majority being restricted to sample KH4. The presentation and interpretation of the first melt data from these inclusions is covered below. Histograms displaying bulk salinity, expressed as wt. %. equiv. NaCl, are shown in Fig. 4.13. Salinity was determined from last ice melting temperatures using equations of state as described by Brown and Lamb (1986). Ice and hydrohalite melting data is presented in Appendix A; Tables A4.16-A4.24.

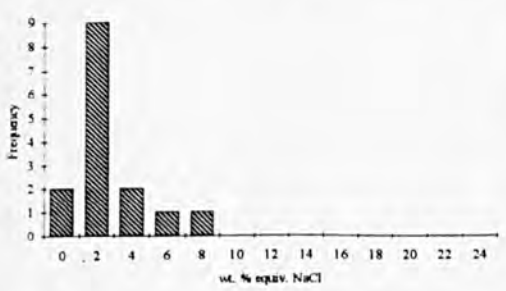

(a) HD2

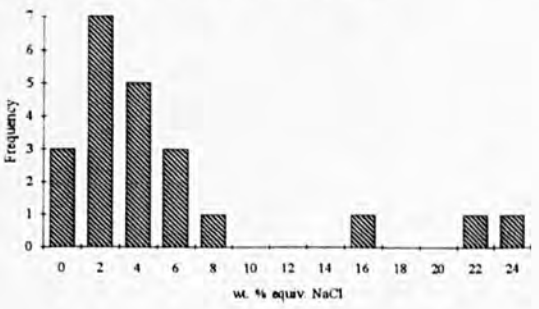

(b) HD3

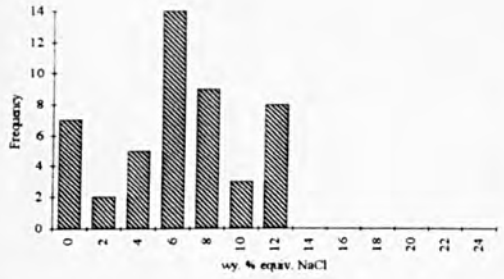

(c) HD5

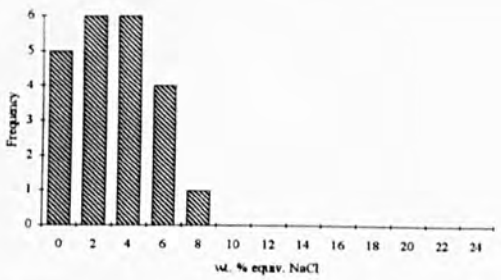

(d) HD6

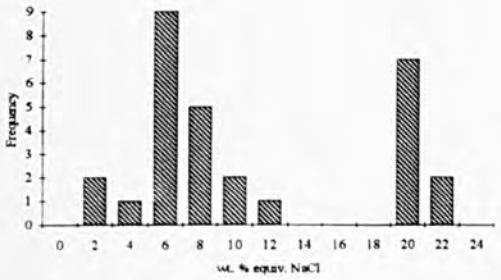

(e) KH4

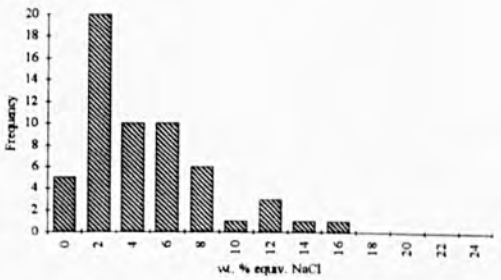

(f) LMP1

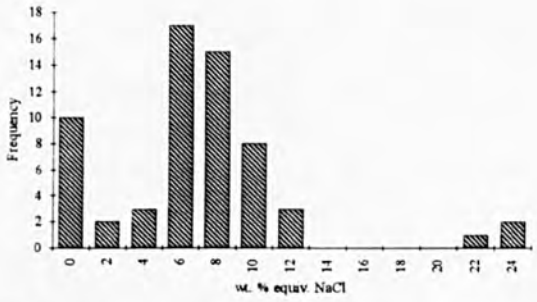

(g) CWQ1

Fig. 4.13. Frequency histograms of bulk salinity expressed as wt. %. equiv. NaCl, from secondary inclusions in granitic quartz from Hingston Down, Kit Hill, Lee Moor and Cheesewring.

The majority of the samples indicate peaks of moderate salinity fluids at around 6-8 wt. %. equiv. NaCl and/or low salinity fluids at around 0-4wt. %. equiv. NaCl. Samples HD3, KH4 and CWQ1 possess discrete groups of high salinity fluids (20-24 wt. %. equiv. NaCl). This would suggest that there are two distinct fluids, rather than progressive mixing. However, discrete fracturing events will cause a break in the record of hydrothermal continuum, and may result in the misinterpretation of the data.

Homogenisation temperatures - vein material

Homogenisation temperatures were recorded from 16 presumed primary and pseudo-secondary inclusions within quartz (based upon the conditions of Roedder (1984) for the identification of primary inclusions) associated with chalcopyrite, pyrite and sphalerite.

The quartz material was obtained in the Hingston Down quarry from an approximate E-W striking vein structure. Homogenisation temperatures were also recorded from 12 inclusions within fluorite obtained from mine dumps in the vicinity of the Kelly Brae mine, near Kit Hill. The fluorite was associated with banded sugary quartz, sphalerite and galena. Data is presented as histograms in Fig. 4.14.

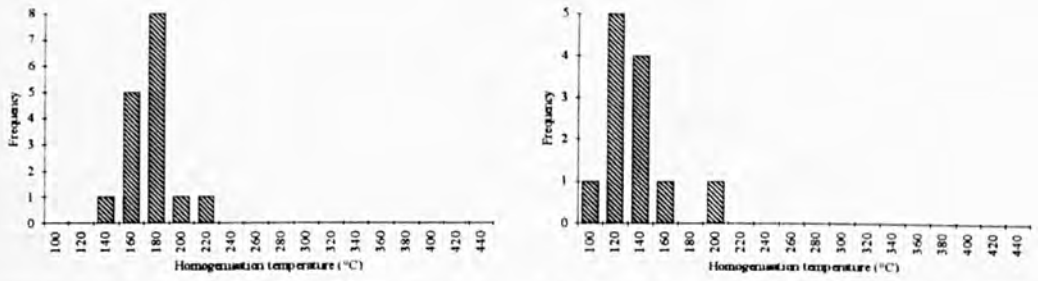

(a) HD7 (b) KH3

Fig. 4.14. Histograms of homogenisation temperatures from vein material from (a) Hingston Down, E-W polymetallic sulphide bearing quartz vein and (b) Kelly Brae, near, Kit Hill, N-S(?) lead-zinc bearing fluorite.

Data from sample HD7 shows peak frequency of homogenisation temperatures occurring around 180-190°C, which is in agreement with data from FIPs obtained at the same location and at Cheesewring and are typical of polymetallic sulphide deposition in the area. Sample KH3 depicts significantly lower homogenisation temperatures, again showing similarity with data from secondary inclusions in the Kit Hill area. The single high temperature reading is believed to be from a necked inclusion, since repeat values showed no increase that might be linked to leakage which is not uncommon in fluorite.

Bulk salinity - vein material

Last ice melting temperatures were recorded from 14 inclusions in sample HD7 and from 10 in sample KH3. These were mainly primary and pseudosecondary inclusions. Eutectics in sample HD7 were restricted to -21°C, however, in sample KH3 first melt data was recorded at around -50°C in 9 inclusions. This was attributed to the presence of $CaCl_2$ as a salt component in the fluid. Melting in these inclusions proceeded via hydrohalite and then ice. Histograms representing the bulk salinity are illustrated in Fig. 4.15.

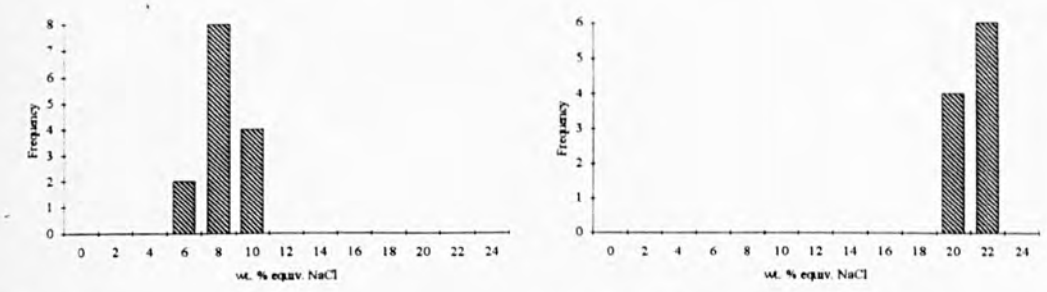

(a) HD7 (b) KH3

Fig. 4.15. Histograms depicting bulk salinity expressed as wt. % equiv. NaCl based on last ice melting data from samples of vein material (a) Hingston Down and (b) Kit Hill.

It is clear from the above data that the fluids responsible for the formation of the two veins were of differing salinities. Sample HD7 shows peak salinity distribution around 8wt. % equiv. NaCl compared with 22.5wt. % equiv. NaCl for sample KH3. The data from these veins compares well with salinities of secondary inclusions recorded from FIPs of known orientations in granitic quartz in the sample areas. High salinities have been recorded in samples HD3, KH4 and CWQ1 corresponding to those observed in sample KH3.

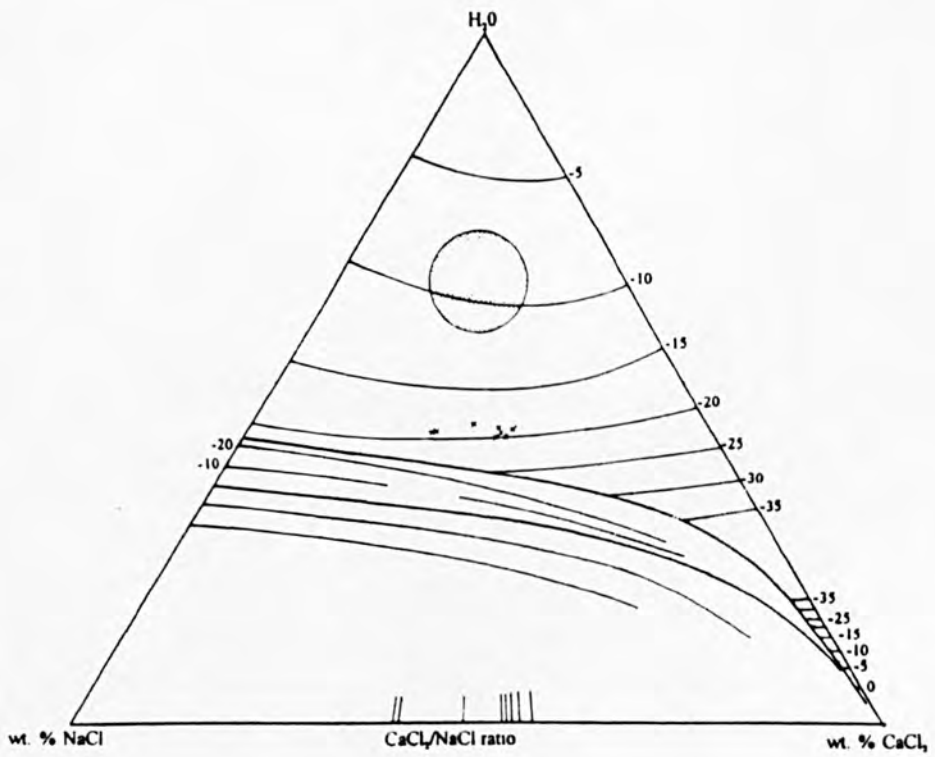

Fig. 4.16 Ternary phase diagram for the system NaCl-$CaCl_2$-H_2O. Crosses (x) mark composition of inclusions within fluorite associated with Pb-Zn mineralisation (sample KH3) with $CaCl_2$/NaCl ratios marked on the baseline. Stippled area represents overall composition of N-S vein fluorite after Shepherd and Scrivener (1987).

Based upon Tfm, Tm_{hydro} and Tm_{ice} data, the ratio of $CaCl_2$/NaCl can be found in the high salinity inclusions observed in sample KH3, using data from Borisenko (1977) and methods described by Shepherd *et al.*, (1985). Fig. 4.16 is a ternary phase diagram for the system NaCl-$CaCl_2$-H_2O, showing the melting paths, phase boundaries and composition of solid phases. Last ice melting data from inclusions in sample KH3 are plotted. The position of Tm_{hydro} the ratio of $CaCl_2$/NaCl is calculated at 1.2:1. From Fig. 4.16 it is apparent that three inclusions give lower ratios. However, the nature of the Tm_{hydro} phase boundary allows a large change in the $CaCl_2$/NaCl ratio to occur over a small temperature scale, and thus these inclusions are ignored.

4.3.4 Discussion

Microstructural and microthermometric analysis has been used to define the orientations, and abundances of FIPs, together with the temperature and chemistry of fluids that have utilised them. From a combination of this data an it should be possible to illustrate the hydrothermal evolution of the study area with respected to an evolving fracture system.

Fluid evolution

Fig 4.17 illustrates the evolution of the secondary fluid inclusion population of recorded within granitic quartz from Cheesewring, Kit Hill, Hingston Down and Lee Moor.

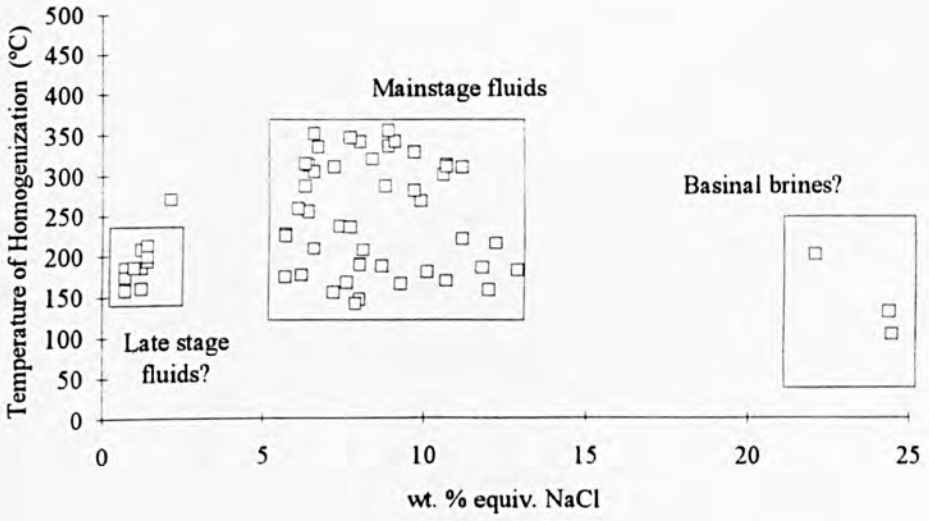

(a) Cheesewring

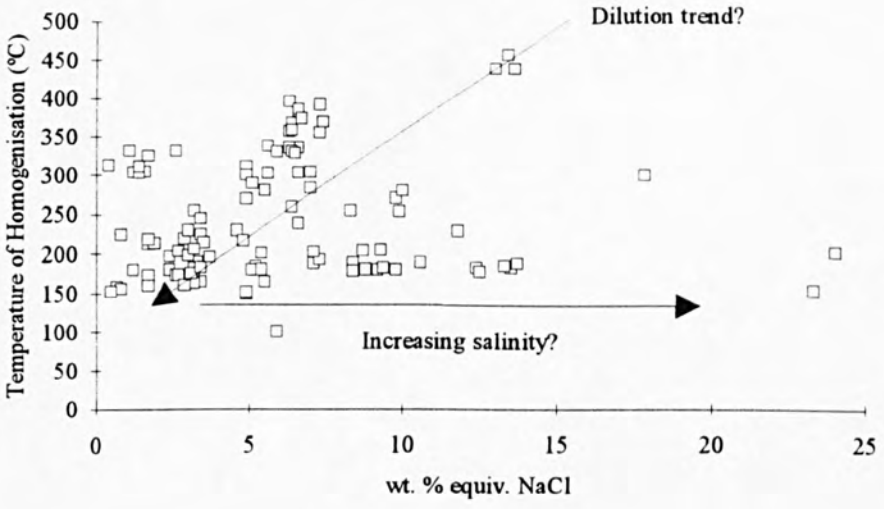

(b) Hingston Down

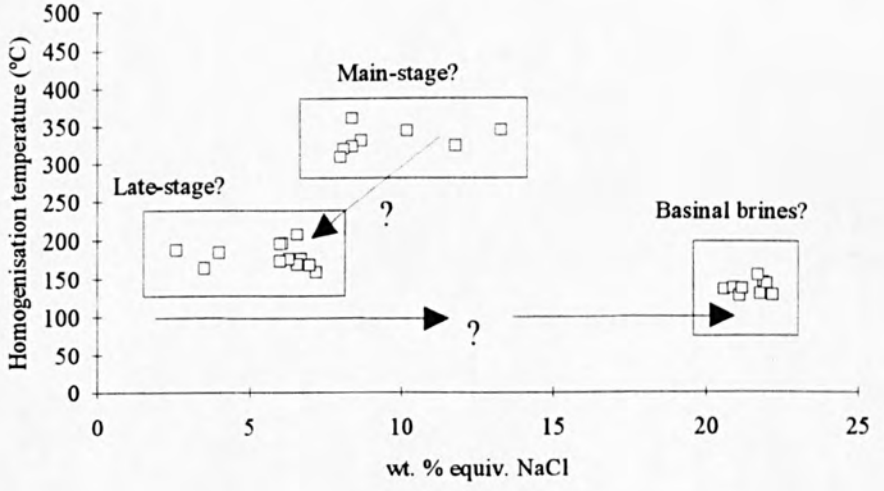

(c) Kit Hill

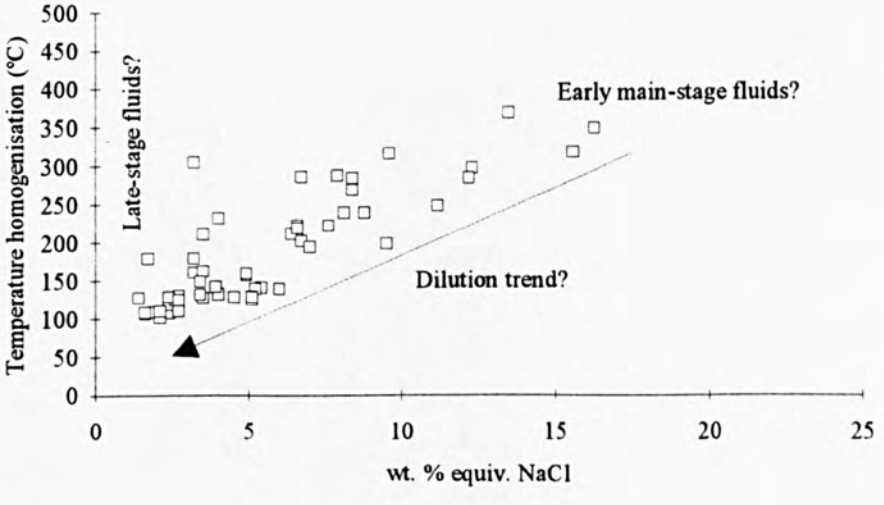

(d) Lee Moor

Fig. 4.17. Bivariate scatter plot of Th and salinity from secondary fluid inclusions in granite quartz.

The data illustrate that a wide range in the temperature and salinity of the hydrothermal fluids exists. It is also possible to imply a number of trends in the evolution of the fluids. Generally, published data from sites of mineralisation in the study area are restricted to primary inclusions related to ore deposition, providing small windows related to specific periods (Alderton, 1978; Shepherd *et al.*, 1985; Shepherd and Scrivener 1987; Clayton *et al.*, 1990; Alderton and Harmon, 1991). However, in this study, it is likely that any hydrothermal fluid active in the area will be observed and recorded, allowing a complete picture to be developed.

The majority of the secondary fluid inclusions are generally moderate to high temperature (Th 150-450°C) and low to moderate salinity (5-15wt. % equiv. NaCl) as were inclusions observed in vein quartz from sample HD7. This is in agreement with Shepherd *et al.*, (1985) and Alderton and Harmon (1991) for fluids associated with greisen bordered sheeted vein systems at Hemerdon, and for polymetallic sulphide mineralisation from the Bodmin-Dartmoor area (Shepherd *et al.*, 1985). Low temperature and low salinity fluids (Th 100-180°C; 0-5wt.% equiv. NaCl) are observed in all the sample areas, and are particularly abundant in the Lee Moor data. These fluids are similar to those identified by Alderton and Rankin (1983), thought to be responsible for the widespread late stage alteration (kaolinisation) observed in the St. Austell granite.

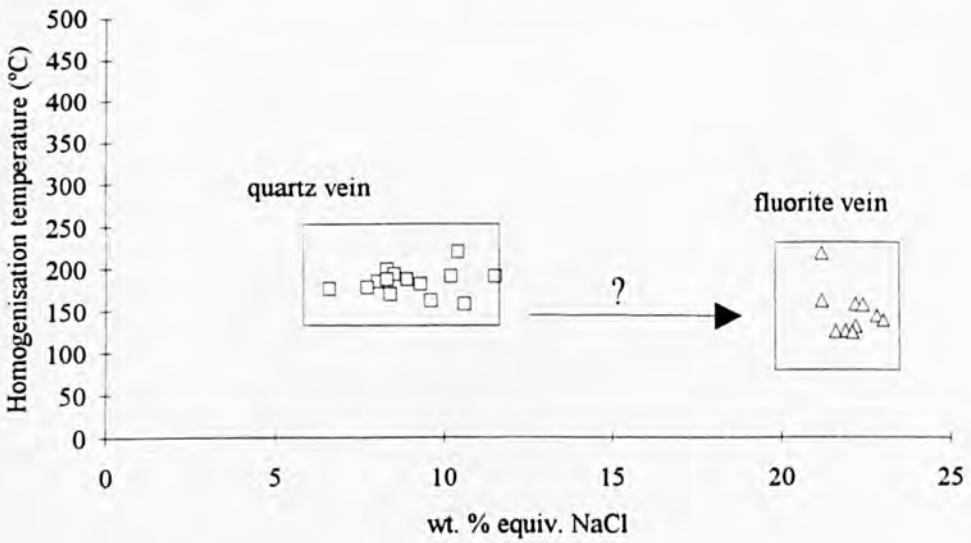

Fig 4.18. Bivariate scatter plot for inclusions from vein material in the Kit Hill and Hingston Down area. □ = Sample HD7; Δ = Sample KH3.

A third fluid was identified at Kit Hill and in a few inclusions at Hingston Down and Cheesewring. This fluid was typically low temperature (Th <150°C) and high salinity (20-24wt. % equiv. NaCl). Data from fluorite mineralisation (Fig. 4.18) shows a similar bulk salinity value, and first melt data which could not be observed in the granitic quartz, shows the presence of the $CaCl_2$. Fluid inclusion data recorded in N-S veins by Alderton (1978); Shepherd and Scrivener (1987) and Alderton and Harmon (1991) show a similar

characteristics. Shepherd and Scrivener (1987) recorded a $CaCl_2$/NaCl ratio of 1:1.1 from inclusions in the north-south veins, comparing well to data by Dominy *et al.*, (1994) who calculated a $CaCl_2$/NaCl ratio of 1:1.2 from inclusions in cross-course material at South Crofty. This is in comparison with the present study which determines a $CaCl_2$/NaCl ratio of 1.2:1.

The three broad fluid groupings may be clearly identified from data shown in Fig. 4.17a representing secondary inclusions from Cheesewring, and possibly also from data at Kit Hill (Fig. 4.17c). However, a more complicated picture is illustrated by data from Hingston Down and Lee Moor (Fig. 17b, d), where mixing trends are possibly illustrated between main-stage(?) and cooler, more dilute, late-stage(?) fluids. Data from Hingston Down also suggests an increasing salinity trend within the low temperature fluids. The absence of these trends at Kit Hill and Cheesewring may be attributed to a lack of data. However, it is also possible that open fractures were not present during the evolution of the fluids that could be utilised at these localities. This may be of particular significance for the trend between low and high salinity low temperature fluids. These fluids have been associated with cross-course mineralisation, which in turn may be related to strike-slip faulting associated with east-west extension during the Triassic (236±3Ma; Scrivener *et al.*, 1994). It is postulated that fractures containing these high salinity fluids are associated with these NW-SE striking dextral, strike-slip faults. High fluid pressures may have allowed hydraulic fractures to form parallel to σ_1 with a N-S orientation, but possibly only in proximity to areas undergoing active faulting.

(a) Kit Hill (KH4)

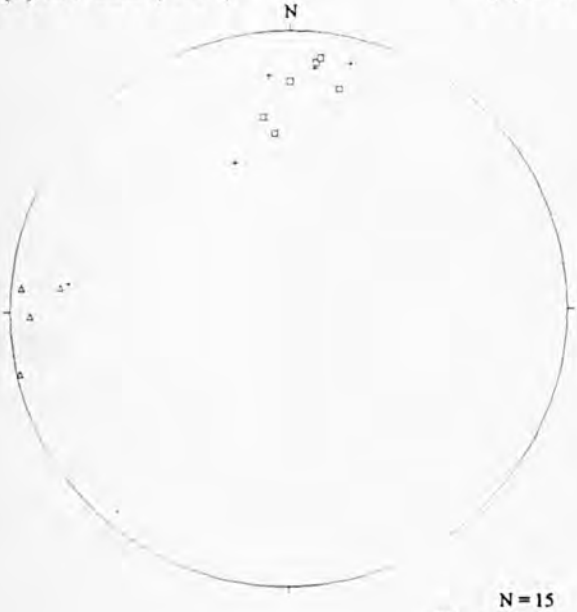

(b) Lee Moor Pit (LMP1)

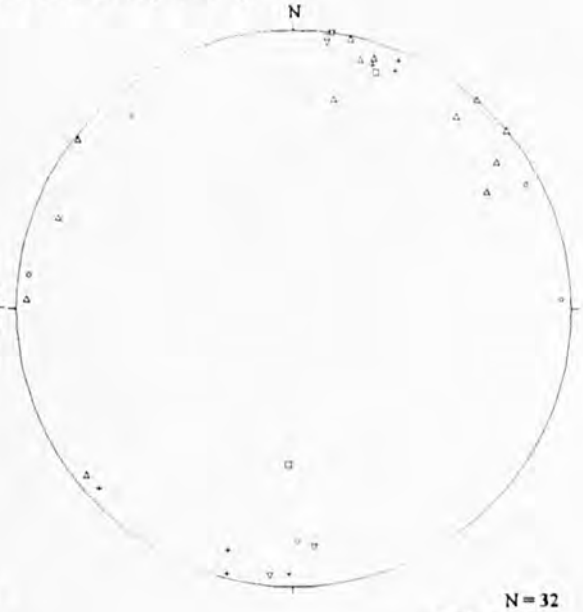

(c) Cheesewring Quarry (CWQ1)

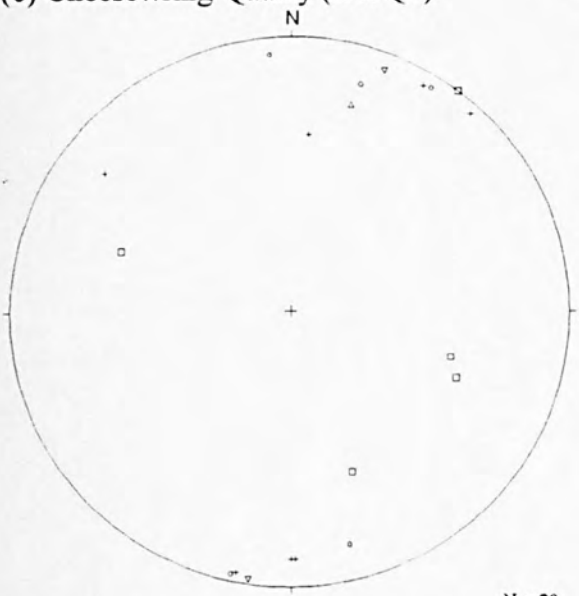

N = 20
Poles to Planes

(d) Hingston Down (HD2; 3; 5; 6)

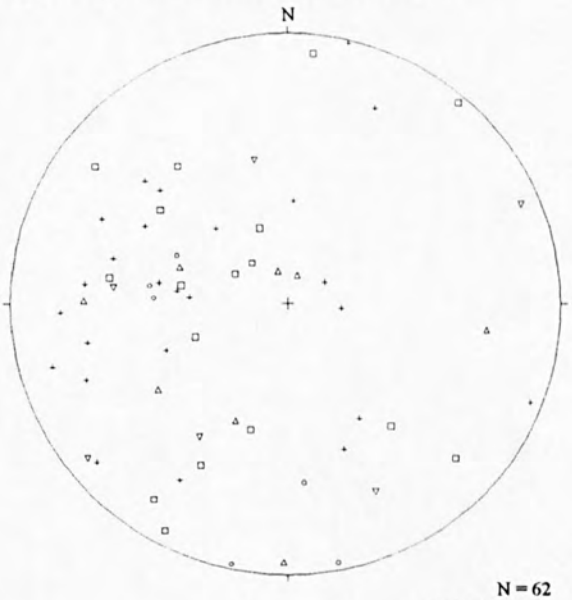

N = 62
Poles to Planes

Fig. 4.19. Equal area projections showing poles to planes of FIP orientations and homogenisation temperatures of respective secondary inclusions contained within them. $\Delta < T_h$ 150°C; + = T_h 150-200°C; O = T_h 200-250°C; $\nabla = T_h$ 250-300°C; □ > T_h 300°C.

(a) Kit Hill (KH4)

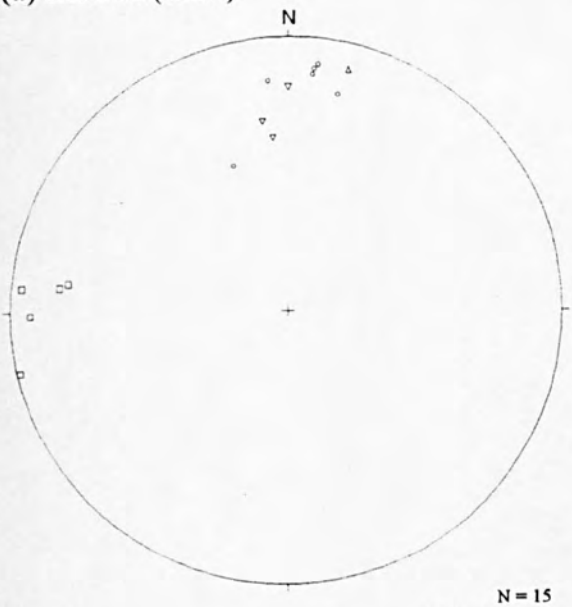

N = 15
Poles to Planes

(b) Lee Moor Pit (LMP1)

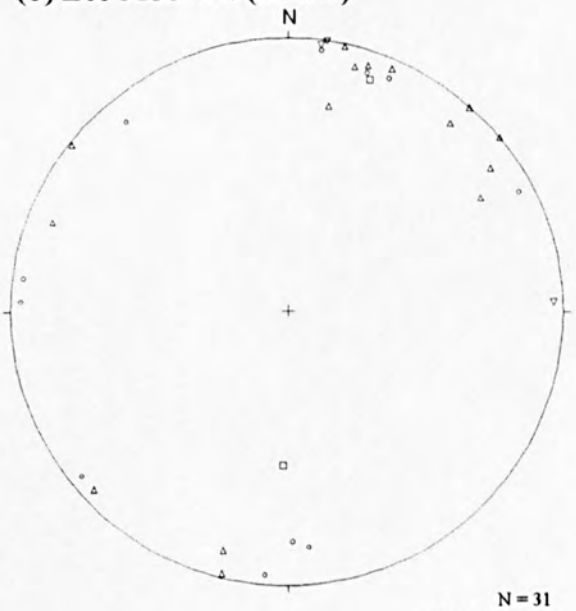

N = 31
Poles to Planes

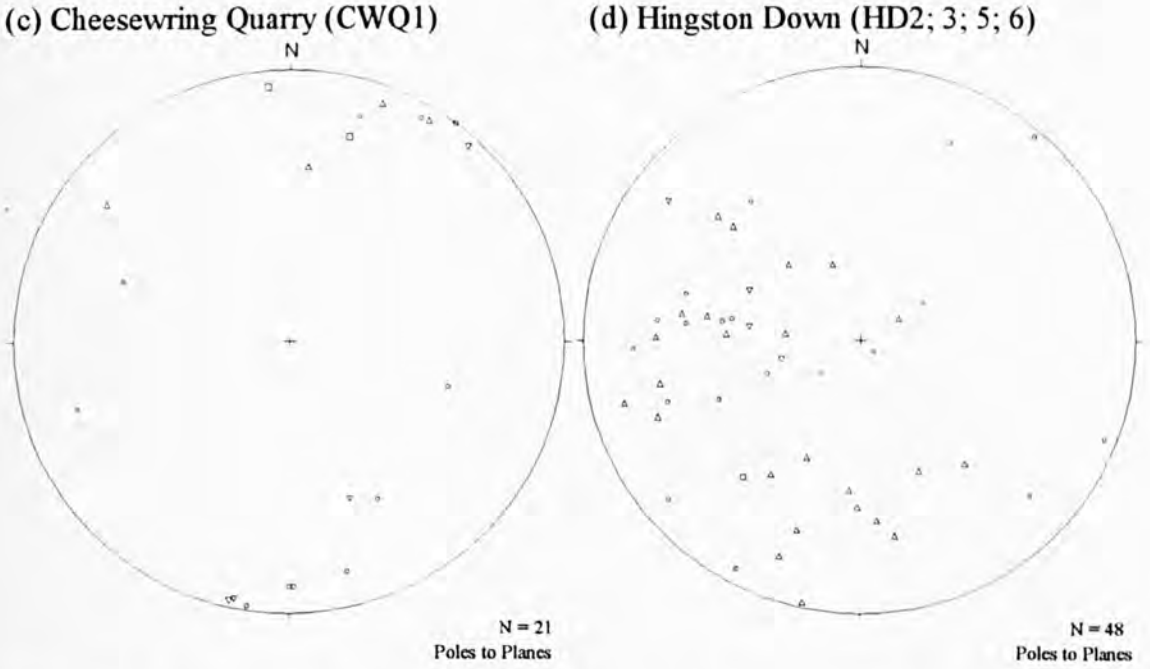

Fig. 4.20 Equal area projections showing poles to planes of FIP orientations and salinity of secondary fluid inclusions contained within them, in wt. %. equiv. NaCl. $\Delta < 5$; O = 5-10; ∇ = 10-15; $\square > 15$.

Combined orientation/thermometric data is presented in Figs. 4.19 and 4.20. Although data from Hingston Down appears to be inconsistent and fails to illustrate any strong trends, data from other localities do exhibit trends. At Kit Hill, low temperature (T_h <200°C), high salinity (> 20 wt. %. equiv. NaCl) fluids are restricted N-S oriented FIPs, whereas E-W FIPs contain varying salinity/temperature fluids. This suggests that the two fluid groups are not undergoing a mixing trend as inferred in Fig. 4.17 and inferred by Shepherd and Scrivener (1987), and are the result of two distinct fracture orientations related to a rotation of the regional stress regime. However, this picture is complicated by the trends observed at other localities, notably Lee Moor and Hingston Down. Combined orientation data from Lee Moor suggests a predominance of low temperature/low salinity fluids in FIPs with a general NW-SE orientation (thought to be related to strike-slip faults of similar orientations) with other higher salinity/temperature fluids in E-W fractures. Thus it is apparent that the striking dilution trend illustrated in Fig. 4.17d, occurred during a rotation of the stress regime, where there appears to be no break in the hydrothermal continuum. However, at Hingston Down a hydrothermal continuum between all fluids may exist. Thus, both low and high salinity (first melt data suggesting a differing provenance), low temperature fluids occur in FIPs related to dextral strike-slip faulting.

Although it is not the purpose of this study to investigate the origin of the hydrothermal fluids and no data has been presented, it is necessary to make some comment on their nature. High temperature/low to moderate salinity fluids are postulated to represent a magmatic-hydrothermal component together with a fluid derived from the surrounding

sedimentary rocks (Shepherd *et al.*, 1985). These fluids are associated with early tungsten (± tin) and main-stage mineralisation, although it was not possible to distinguish between the two components.

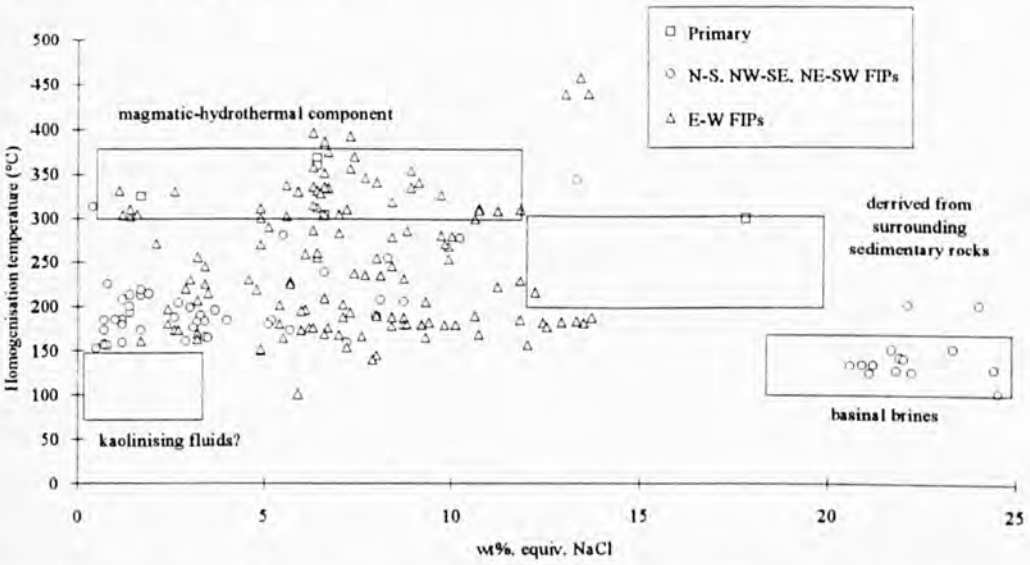

Fig. 4.21 Bivariate scatter plot of combined thermometric data from Cheesewring, Kit Hill, Hingston Down and Lee Moor. Homogenisation temperature (°C) *vs.* salinity (wt. %. equiv. NaCl). Note position of boxes related to fluid components summarised by Shepherd *et al.*, (1985) and Shepherd and Scrivener (1987) responsible for mineralisation in the study area. Note also the position of possible kaolinising fluids as described by Alderton and Rankin (1983) for the St. Austell granite.

The combined thermometric data is illustrated in Fig. 4.21 and infers different fluid compositions compared to those of Shepherd *et al.*, (1985) for the fluids responsible for early and main-stage mineralisation. A fluid component derived from the surrounding sedimentary rocks (Shepherd *et al.*, 1985) during the intrusion of the granite is not evident in the secondary inclusion data recorded in this study. However, the position of the early magmatic-hydrothermal component together with the low temperature/high salinity fluids do compare well. It should also be noted that low temperature fluids associated with widespread alteration (kaolinisation) of the St. Austell granite (Alderton and Rankin, 1983) are of substantially lower temperature than those reported here.

Orientations of microstructures vs. macrostructures

A combination of the orientation and thermometric data illustrates that the three major fluid groups may be assigned to a specific orientation in the majority of cases. Generally, fluids with properties similar to those responsible for main-stage mineralisation occur in FIPs oriented E-W. Likewise, low temperature, high salinity fluids similar to those described by Shepherd and Scrivener (1987) occur in FIPs generally oriented N-S. This answers the simple question posed in section 4.2. that FIPs do mimic the strike of regional vein and fault sets that are observed in the field. Moore (1975) projected the trajectories of the three axes of compressive stress throughout SW England based upon the orientations of elvan dykes and main stage mineralisation (Fig. 4.5). Moore (1975)

concluded that σ_2 was oriented E-W in the area between Bodmin and Dartmoor which is in agreement with the FIP orientation data. However, Moore (*op. cit.*) based these trajectories upon the orientations of normal faults, generated by crustal extension resulting from orogenic collapse (Shail and Wilkinson, 1994), whereas the majority of FIPs with a E-W orientation are have likely to been formed by thermal stresses arising from cooling of the granite and hydraulic fracturing due to high fluid pressures. This is thus in agreement with other authors (Jang *et al.*, 1989; Ren *et al.*, 1989; Jang and Wang, 1991) who state that the FIPs tend to have a preferred orientation parallel to the regional maximum principal stress axis, even though they might have been produced by local stresses developing within the granite.

FIP abundances

Ren *et al.*, (1989) states that the initial episode crack and joint formation in a granite pluton will generally be in the most intense period of fracturing in its history because of the presence of large thermal gradients and hot circulating fluids. This may be the case in granites which have relatively short cooling histories and have undergone little or no tectonic deformation. However, the Cornubian batholith is a High Heat Producing granite (Jackson *et al.*, 1989) with an extended cooling history, allowing the convection of hydrothermal fluids to occur over a long period of time. Together with substantial amounts of local brittle deformation resulting from strike-slip faulting (Dearman, 1963; Holloway and Chadwick, 1987), in some samples the majority of FIPs are ascribed to a late, low temperature period of the cooling history of the granite. An example of this situation can be inferred from the Lee Moor data. FIP abundances here may be up to four or five times greater than samples obtained elsewhere from unaltered granite (see plate 4.1). Work by Rankin and Alderton (1982) has also shown a high degree of secondary fluid inclusions in kaolinised St. Austell granite. Cox (1993) stated that granite which had been subjected to both fluids responsible for greisenisation together with late stage fluids possibly related to the kaolinisation process may contain fluid inclusions representing up to 5% of its total volume.

It is postulated that the intense hydrothermal alteration which is locally developed in the Lee Moor area is related to the very high abundance of FIPs. It is also inferred that the abundance of FIPs in the Lee Moor sample is related to brittle deformation produced by movement along the Tavistock-Modbury fault zone (Fig. 4.2). This is based upon the orientation of the FIPs being similar to the fault, and the fractures thus being regarded as Riedel shears (Tchalenko and Ambraseys 1970). Although microfracture density has been seen to decrease as a function of distance from naturally occurring faults (Brock and Engelder, 1977; Knipe and White, 1979; Kanori *et al.*, 1991), it is still not clear whether microfractures are generated during the build up of stress during the initial failure of the rock, or through subsequent post-failure fault-slip (see section 2.2.3). It is

important to clarify this point, together with periods of possible fault movement along the Tavistock-Modbury fault zone. Dearman (1963) postulated dextral wrench faulting during the Tertiary along a series of NW-SE striking strike-slip faults found throughout SW England. However, Holloway and Chadwick (1986) attributed movements along the Sticklepath-Lustleigh Fault Zone (SLFZ) to Permo-Triassic times, together with sinistral and minor dextral movements in the Tertiary. More recently, Bristow and Robson (1994) have argued that basins containing Tertiary sediments are related to transtensional and transpressional dextral strike-slip along the SLFZ during the Eocene and Oligocene.

Although it is not possible to obtain exact dates for the fractures, relative ages using cathodoluminescence may be obtained, and are discussed in more detail in Chapter 5.

Variations in the local stress regime

An important observation is that not all microfracture orientations are present in all samples. This includes samples obtained on a local scale within the Hingston Down Quarry and those obtained throughout the study area on a more regional scale. E-W oriented FIPs were present in all samples, indicating that these microfractures formed in response to regional tectonic forces, and are only slightly affected by local hetrogenities (Lespinasse and Pécher, 1986; Kowallis *et al.*, 1987; Lespinasse and Cathelineau, 1990). It may also be possible that they form irrespective of the presence of associated macro-structures, (e.g. normal faults), although it may be argued that sampling stations are all in the vicinity of varying numbers of lode-bearing faults (Fig. 4.6). FIP orientations from the Hingston Down samples indicate variations in the local stress regime, most likely to be associated with minor faults within the quarry. Lespinasse and Pécher (1986) suggest that microfracture orientations may be disturbed by the presence of large compressive faults, resulting in a local deviation of the σ_1 axis.

FIPs oriented N-S, NW-SE and NE-SW are not present at all sample locations, and are likely to be related to the presence of local faults and macrostructures. N-S oriented FIPs are associated with N-S oriented cross-course mineralisation, while NW-SE and NE-SW FIP are associated with Riedel and conjugate Riedel shear orientations considered to be the product of strike-slip faulting. It is believed these are only locally developed when in proximity of macrostructures of the same orientation. This is typically shown in the Lee Moor data, where microfracture density has been shown to be greatly increased, and also in the Kit Hill sample where the strong, clearly observed N-S oriented FIPs contain low temperature/high salinity fluids associated with cross-course mineralisation, which is locally present (Shepherd and Scrivener, 1987).

Microfracturing process

It is postulated that microfractures develop in response to stress imposed upon a rock. This stress may be thermally, hydraulically or tectonically induced (Kranz, 1983) and therefore the resulting microfractures may be thus classified. However, it is likely that a combination of these stress resulted in the formation of the varying sets of microfractures observed in the samples. Since FIPs represent fractures healed by a hydrothermal fluid, it is possible that a fluid phase played a role during the fracturing process and theoretically they may thus all be classified as hydraulic fractures (see section 2.2.2) to a certain degree. However, during this study only FIPs that are thought to have been generated by high fluid pressures, initiating the fracturing process are classified as hydraulic fractures.

Data from Kit Hill suggests that FIPs oriented E-W are generally high to moderate temperature (moderate salinity) healed fractures probably associated with early and main-stage mineralisation forming shortly after granite emplacement (Jackson *et al.*, 1989). It is therefore likely that these FIPs were generated by thermal stresses occurring in the granite due thermal expansion mismatch/anisotropy (Carlson *et al.*, 1990; Jang and Wang, 1991) rather than by thermal stress gradients (Chen and Wang, 1980) (see section 2.2.1). The thermal expansion/contraction differences of quartz and feldspar are considered to be the primary reason for the production of thermal fracturing. This results in the preferred fracturing of feldspar/quartz boundaries by intragranular fractures terminating at the grain boundary. Although this type of data was not recorded until later on in the study, results from other areas (Carrock, Fig. 3.17; Lundy and NE Dartmoor, Fig. 5.11) and temperatures of the fluids healing the fractures (generally above T_h 200°C and usually greater than T_h 300°C) suggest that they are thermal in origin.

However, high temperature sheeted vein swarms observed in the porphyry stocks at Kit Hill and Hemerdon Bal in the study area (as well as at Cligga Head in north Cornwall) are presumed to have been generated hydraulic fracturing when fluid pressures exceed the confining pressures and tensile rock strength (see section 2.1.4) (Jackson *et al.*, 1989). Jackson *et al.*, (1989) states that this is caused by a build up fluid pressure beneath or within a partly crystalline carapace, resulting in hydraulic fracturing, adiabatic decompression and separation of a low salinity vapour phase, which is also in agreement with Shepherd *et al.*, (1985) interpretation of the formation of the Hemerdon Bal deposit. However, Jackson *et al.*, (1989) also states that the regularity and spacing of the sheeted vein swarms (e.g. Cligga Head; Moore and Jackson, 1977) indicates fracturing under the influence of thermal stresses is important. The resulting early high temperature E-W oriented FIPs are generally simple planar fractures, propagating to, or from, grain boundaries but generally intragranular.

It should be noted that main-stage mineralisation occurring in the surrounding country rocks and on the edges of the granite stocks is thought to occupy normal faults related to end-Variscan extension resulting from orogenic collapse (Shail and Wilkinson, 1994). It is unlikely that these faults were formed by hydraulic fracturing. FIPs containing fluids associated with this stage of mineralisation are difficult to distinguish from the FIPs resulting from early hydraulic fracturing and sheeted vein formation. Homogenisation temperature data of fluids associated with main-stage polymetallic sulphide mineralisation (approximately 200-300°C) typically observed in E-W FIPs suggest that intragranular fracturing due thermal stresses is still important (Fredrich and Wong, 1986; Wang *et al.*, 1989). Although E-W FIPs have resulted from a combination of more than one fracturing process, it is apparent that their orientation is generally parallel to σ_1 on a regional scale (Jang *et al.*, 1989; Ren *et al.*, 1989; Jang and Wang, 1989).

However, thermometric data from Hingston Down shows a random spread, suggesting that the microfracturing process is different to that occurring at Kit Hill where a clear cut pattern is present. Sampling at Hingston Down was undertaken on a smaller scale (50-100m) allowing data to illustrate variations in the local stress regime (as stated above), possibly being influenced by small second order faults of vaying orientations. However, another possible cause for this apparently random pattern may be the occurrence of repeated fluid over-pressuring of the granite upon cooling. Microfracture development may thus be controlled by very high local stresses as opposed to lower regional stresses.

At temperatures below 200°C it is unlikely that thermal stresses in the cooling granite would be singularly responsible for the generation of fractures (Wang *et al.*, 1989). Therefore, FIPs oriented N-S, NW-SE and NE-SW, containing fluids with homogenisation temperatures below 200°C would generally have been produced by tectonic or hydraulic, rather than thermal stresses. It is postulated that N-S FIPs are produced by hydraulic fracturing, related to extensional vein formation during dextral movement of major NW-SE strike-slip faults that are present in the study area and throughout SW England (Dearman, 1963; Holloway and Chadwick, 1986). Extensional veins may form at angles close to 30° to the strike-slip fault, parallel to the σ_1 direction during faulting (Sibson, 1990) (see Fig. 2.1 and 2.8). Cross-course mineralisation in the study area and throughout SW England is typically banded in nature, indicating an episodic nature to the mineralisation (Dines, 1956; Dominy *et al.*, 1994) and is typical of the crack-seal mechanism described by Ramsay (1980). It is therefore presumed that these fractures are hydraulic in origin, with mineralisation synchronous with extension (Jackson *et al.*, 1989). Fluid pressure increases as formational brines move up-dip along NW-SE striking strike-slip faults (Shepherd *et al.*, 1985; Shepherd and Scrivener, 1987) to a point where seismic failure and active faulting occurs. This model of vein formation

is similar to the seismic pumping model described by Sibson *et al.*, 1975). Associated with the seismic failure, is the process of fault related dilatancy (Brace *et al.*, 1966; Ismail and Murray, 1976) with N-S striking microfractures forming as pre-cursor to seismic failure. Homogenisation data for these FIPs is generally <180°C, temperatures at which thermal stress fracturing is not thought to play an important role. Scrivener *et al.*, (1994) have dated N-S cross-course mineralisation in the Tamar valley at 236±3Ma suggesting a Triassic age. It may then be inferred that active dextral strike-slip faulting was therefore occurring during the same time interval, which is in agreement with Holloway and Chadwick's proposal for movement along the SLFZ from late Variscan to Permo-Triassic times.

These FIPs are then inferred to be formed by hydraulic fracturing, in orientations parallel to σ_1 during dextral strike-slip faulting. Although significant amounts of data were not observed during the early part of this study concerning the morphology of these fractures, they are thought to be typically planar features, rarely interacting with grain boundaries, being generally intracrystalline.

FIPs oriented NW-SE, and a minor set occasionally observed, oriented NE-SW are also inferred to be associated with strike-slip faulting. These fractures, characterised as Riedel shears (NW-SE) and conjugate Riedel shears (NE-SW) and contain low temperature/low salinity fluids are thought to be directly related to strike-slip faulting based upon their similar orientation to major fault zones operating in the study area. These FIPs may vary in abundance depending upon the proximity to the fault zone, and are therefore not present in all samples. Low temperatures recorded (<200°C) from the inclusions within them suggest thermal stresses would be unimportant in the fracturing process. Samples from Lee Moor have shown a high degree of intercrystalline fractures as opposed to intracrystalline, suggesting that they are mode 2 in origin. Dating of these fractures may prove to be important in further the understanding of the kaolinisation process.

4.4 Summary and conclusions

In this Chapter, FIPs have been analysed from the granites of SW England, especially related to post-Variscan deformation and fluid evolution. The formation of FIPs in the study area has been attributed to thermal, hydraulic and tectonic stresses, and is briefly summarised as follows:

Following the intrusion of the batholith, high thermal stresses and fluid pressures initiate E-W fracturing with sheeted vein formation, with orientations of the fractures governed by the onset of orogenic collapse. As the granite cooled, relaxation of Variscan compressive forces became more important, with resulting normal faults controlling

fracture and vein development, although homogenisation temperatures indicate that thermal stresses were still significant. During Triassic(?) times strike-slip faulting coupled with high fluid pressures generated by formational brines migrating up-dip form sedimentary basins to the north and south of the SW England peninsular (Shepherd and Scrivener, 1985; Scrivener *et al.*, 1994; Dominy *et al.*, 1994). Further active strike-slip faulting generated intense microfracturing in the proximity to the fault zones, possibly allowing the formation of intense argillic alteration.

4.4.1 Conclusions

Several conclusions have been drawn (discussed above) which are succinctly listed below:

(i) Fluids have been identified within secondary inclusions from granite quartz which correspond to hydrothermal fluids identified by previous authors. However, not all components have been identified.

(ii) In some cases FIPs are observed to mimic the orientations of macrostructures observed in the field, clearly observed at Kit Hill. However, other data did not show clear cut trends, so whatever processes were occuring at Kit Hill were not operating at Hingston Down. Thermometric data from within the FIPs were also not as conclusive as thought to be from work in the previous chapter.

(iii) FIPs have been characterised by their orientation, morphology and the thermometric properties of the hydrothermal fluids that healed them. However, the large scale sampling system (over a 10km between adjacent sampling points) was significantly influenced by local deviations in the stress regime. Therefore, although the major FIP trends do correspond with the macrostructures, local deviations were enough to complicate the picture.

(iv) An important observation was the anomalously high value of FIPs in sections analysed from Lee Moor, which had undergone late stage alteration. This association of FIP abundance and thus microfracturing is possibly linked to post-Variscan strike-slip faulting. However, it is not clear when the high quantity of microfractures were produced, either during failure of the granite during initial movements of the faults, or during later significant post-failure fault slip.

4.4.2 Further work

Further FIP studies and sampling around the SLFZ in NE Dartmoor and on Lundy Island will allow the clarification of theories developed during the work Kit Hill - Hingston Down area regarding:

(i) FIP morphology and occurrence.

(ii) FIP formation with respect to fractures formed by thermal, hydraulic and tectonic stresses.

(iii) Relative dating of FIPs associated with strike-slip faulting, to produce possible movement histories of the faults, using fluid evolution, fracture orientation and cathodoluminescence.

(iv) Further the understanding of the mineralisation and alteration processes that may be governed by these major strike-slip faults.

CHAPTER 5

FIP FORMATION ASSOCIATED WITH POLYPHASE STRIKE-SLIP FAULTING, GRANITE INTRUSION AND HYDROTHERMAL EVOLUTION

5.0 Introduction

Analysis of orientation and thermometric data from SW England (Chapter 4) has shown that several generations of FIPs are present, with varying orientations and thermometric properties. The generation of FIP orientations by strike-slip faulting can occur in numerous orientations, especially where polyphase (sinistral and dextral) movement is involved. The study area was chosen to define FIP orientations and morphologies associated with dextral and possibly sinistral strike-slip faulting along the Sticklepath-Lustleigh Fault Zone (SLFZ).

Orientation analysis has been undertaken in the north-east area of the Dartmoor granite where brittle deformation associated with the SLFZ is believed to be responsible for the generation of second order normal and strike-slip faults of varying orientations. The data from mainland SW England are then compared to that obtained from the Lundy granite, where FIP development is related only to stress regimes operating since the Tertiary, and possibly associated with both sinistral and dextral movements along the SLFZ.

The sampling procedure was designed to investigate the following:

(i) Characterise the morphology and orientations of FIPs associated with *mode I* (tensile) and *mode II* (shear) (see section 2.1 for definitions) fractures related to strike-slip faulting along the SLFZ. It should then be possible to discriminate between FIPs resulting from thermal, hydraulic and tectonic stresses.

(ii) As the Lundy granite is of Tertiary age, a clearer picture of FIP formation related to Tertiary to recent stress regimes may be observed. This can then be compared to brittle deformation of the earlier Dartmoor granite by the SLFZ and secondary faults associated

with it. It may then be possible to build up a movement history of the SLFZ using the orientations of FIPs, together with an idea of the evolution of hydrothermal fluids associated with the faults and the relative ages of the microfractures using cathodoluminescence.

(iii) Relate the orientation of FIPs to macrostructures of varying origins in the sampling areas. These include the Lundy Tertiary dyke swarm (possibly representing tensile magma filled fractures) and second order normal and strike-slip faults mapped in the north-eastern area of the Dartmoor granite.

5.1 Geology of the study area

The Island of Lundy in the Bristol Channel, is the most southerly expression of the British Tertiary Volcanic Province (BTVP). It lies on a possible direct line with the Sticklepath-Lustleigh Fault Zone (SLFZ) which traverses the SW England peninsular, and is responsible for the formation of several Tertiary strike-slip basins, both on- and off-shore. The geology of SW England including the Dartmoor granite and the surrounding sedimentary envelope, together with its deformational and hydrothermal history was outlined in Chapter 4. Included here is an overview of the geology of the Lundy granite and its relationship to the BTVP and the SLFZ.

5.1.1 Lundy Igneous Complex

The island of Lundy is made up of up to 90% granite with a faulted and/or intrusive contact with deformed Pilton Shales of Upper(?) Devonian age on the southerly tip of the island (Thorpe *et al.*, 1990) (Fig. 5.1). The whole complex is intruded by a NW-SE striking dyke swarm. The subsurface structure of the complex has been investigated by a variety of geophysical methods (Bott *et al.*, 1958; Cornwall, 1971; Brooks and Thompson, 1973; McCaffrey, 1993; Roberts and Smith, 1994), which have shown it to be similar to other BTVP igneous centres, with positive gravity and magnetic anomalies. These are interpreted to indicate an underlying basic intrusion at shallow depth, with a volume that is likely to be greater than that of the granite (Thorpe *et al.*, 1990).

The geology and mineralogy of the granite has been described by Dollar (1941), Edmunds *et al.*, (1979), Stone (1990) and Thorpe *et al.*, (1990) as a coarse-grained megacrystic granite containing up to 20% alkali feldspar megacrysts in a coarse-grain groundmass composed of alkali feldspar, quartz, lithium-bearing muscovite and biotite. Thorpe *et al.*, (1990) states that the granite is derived from a parental magma comprising a crustal component (similar to that of the Cornubian batholith) and a mantle component, derived from a differentiate of contemporaneous basaltic magma. Associated with the

granite intrusion is a series of dolerite-peralkaline/subalkaline trachyte/rhyolite dykes thought to have evolved from extensive fractional crystallisation from a basaltic magma chamber of complex geometry below the exposed Lundy Granite (Thorpe and Tindle, 1992).

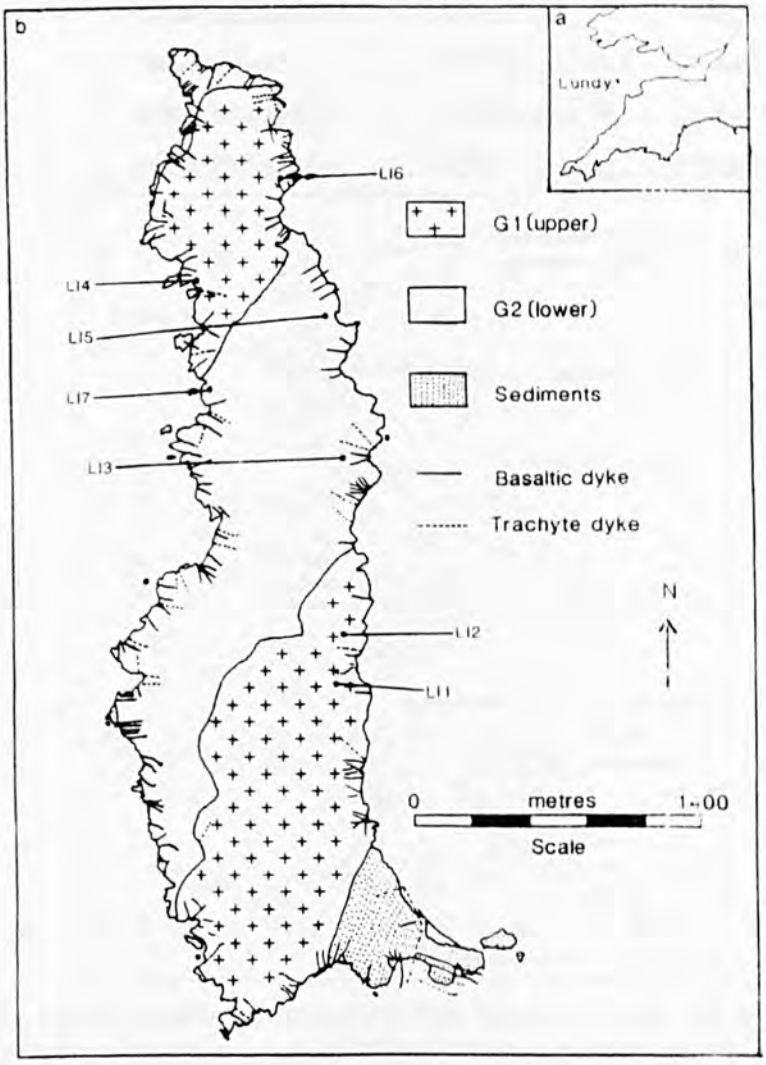

Fig 5.1. Simplified geological map of the Island of Lundy showing the main granite units, the orientation of coastal out-cropping basic and trachyte dykes and the location of sampling points (after Dollar, 1941; Thorpe *et al.*, 1990; McCaffrey *et al.*, 1993).

There is no previous published work concerning the evolution and origin of hydrothermal fluids associated with the Lundy granite with particular reference to the fluid inclusion population.

The Lundy complex has been given a Palaeocene-Eocene age (cf. time scale of Odin *et al.*, 1982) with dating by a variety of methods as shown in Table 5.1. It seems likely that the dyke swarm was emplaced soon after the emplacement of the granite (Thorpe and Tindle, 1992) with an orientation in keeping with the regional Tertiary dyke swarm trend observed in Scotland and northern Ireland (Fig. 5.2).

Table 5.1. Published ages of the Lundy granite and dyke swarm

Intrusion	*Method*	*Age (Ma)*	*Reference*
Granite	whole rock Rb-Sr biotite K-Ar	52±2	Dodson and Long (1962)
Granite	biotite Ar-Ar	50±3	Miller and Fitch (1962)
Granite	whole rock Rb-Sr	58.7±1.6	Thorpe *et al.*, (1990)
Dykes	feldspar K-Ar	44.6±1 to 54.3±1.0	Mussett *et al.*, (1976)
Dykes	whole rock K-Ar	51.9±s to 56.1±4	Edmonds *et al.*, (1979)
Dykes	whole rock Ar-Ar	56.4±3	Mussett *et al.*, (1988)

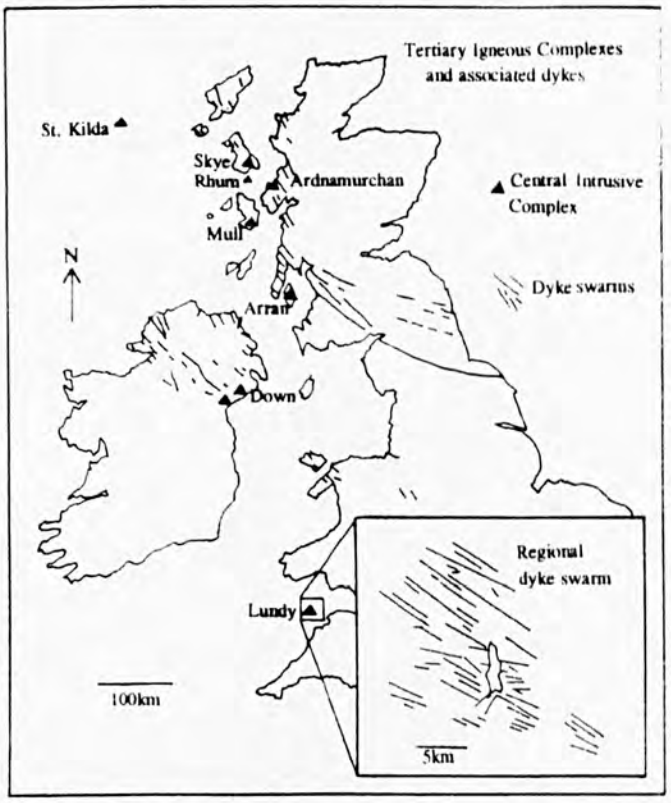

Fig 5.2. Central intrusive complexes within the British Tertiary Volcanic Province and their associated dykes. The Lundy dyke swarm (inset) is inferred from marine-based geophysical magnetic data and based on Hains *et al.*, (1983). After Roberts and Smith (1994)

5.1.2 Structure

Lundy Rhomb Horst

Arthur (1989) describes the Lundy Rhomboid Horst (Fig. 5.3 and 5.4) as a fault-bounded area of Devonian-Carboniferous strata intruded by the Tertiary Lundy Igneous Complex. Arthur (*op. cit.*) states that it originated as the Lundy Rhomb Graben, created by 28-40km of Tertiary sinistral strike-slip faulting, along the left stepping, NW-SE striking SLFZ. Subsequent minor dextral faulting on the SLFZ inverted the graben to form the Lundy Rhomb Horst. An associated pull-apart basin (Stanley Banks Basin) was

first recognised by Fletcher (1975) and later by Arthur (1989) who described it has having formed from the intersection of reactivated Hercynian NW-SE transform fault zones and reactivated E-W thrusts. During the Cenozoic, N-S tensional and compressional reactivation of the thrusts was respectively associated with transtensional development of the pull apart basin, and the transpression of the Lundy Rhomb Horst.

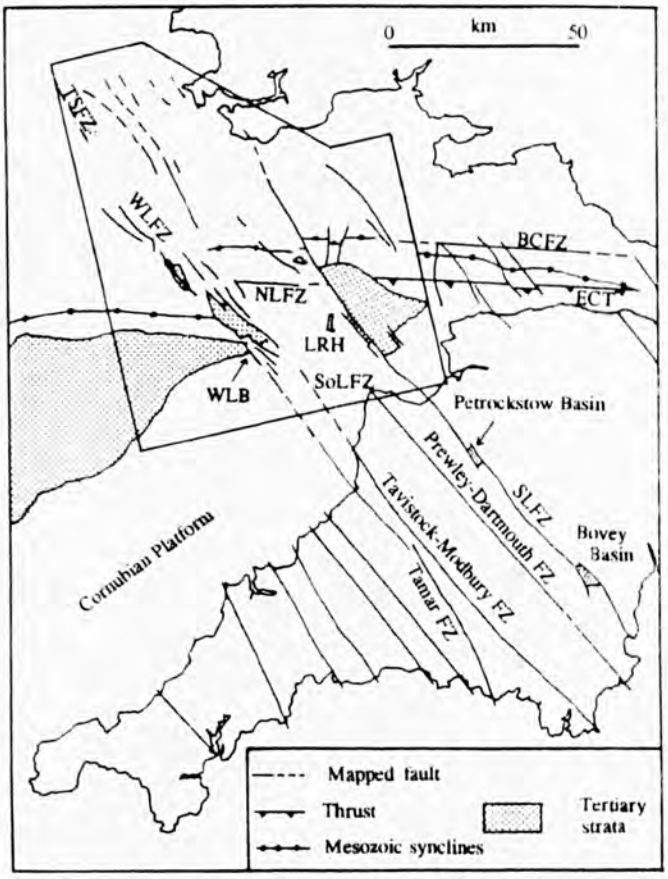

Fig. 5.3. Regional setting of the Lundy Rhomb Horst after Arthur (1989); BCFZ = Bristol Channel FZ; BCS = Bristol Channel Syncline; DB = Dutson Basin; ECT = Exmoor Cannington Thrust; FBFZ = Flimston Bay FZ; FZ = Fault Zone; GFZ = Grassholm FZ; LaB = Lamerton Basin; LRH = Lundy Rhomb Horst; NLFZ = North Lundy FZ; SBB = Stanley Banks Basin; SLFZ = Sticklepath-Lustleigh FZ; SoLFZ = South Lundy FZ; TSFZ = The Smalls FZ; WLB = West Lundy Basin; WLFZ = West Lundy FZ.

Northeast Dartmoor

The SLFZ crosses the Dartmoor granite on mainland SW England where it is responsible for the formation of the Bovey, Petrockstow and Dutson Tertiary basins (Edwards, 1976; Freshney *et al.*, 1982; Bristow *et al.*, 1992; Bristow and Robson, 1994) together with brittle faulting within the NE area of the Dartmoor granite (Blyth, 1957, Blyth, 1962) and north Devonshire (Shearman, 1967). Movement of the SLFZ and other Tertiary wrench faults was first analysed by Dearman (1963) who envisaged some 35km of Tertiary dextral offset. This was later reinterpreted by Holloway and Chadwick (1986) and Arthur (1981, 1983) as minor dextral movement in the late-Variscan and Permo-Triassic times, followed by major sinistral movement in the Tertiary. However,

more recently Bristow and Robson (1994) concluded that the basin development in SW England was the result of oblique extension produced by dextral movement along right stepping en-echelon strike-slip faults in the Eocene, followed by compression in the Oligocene, forming thrusts on the edges of the basins (Fig. 5.5).

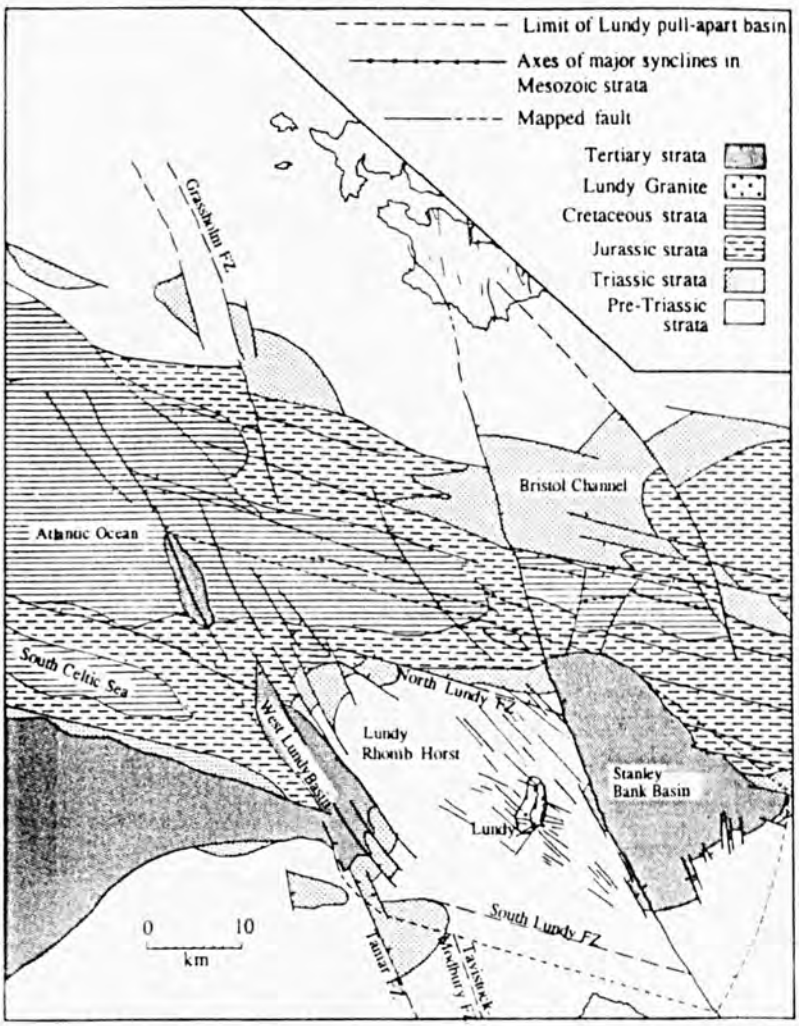

Fig. 5.4. Faulting in the Lundy area (after Arthur, 1989) illustrating Tertiary strata and faults affecting pre-Tertiary sediments. See Fig. 5.3. for location.

5.2 Sampling and the collection of field data

Sampling was undertaken on mainland SW England around the SLFZ and on Lundy Island, in the Bristol Channel. Data from Chapter 4 have demonstrated the relationship between preferred orientations of FIPs and strike-slip faulting. Although mineralisation is absent from Lundy and poorly exhibited in NE Dartmoor, FIPs related to brittle deformation by Tertiary faulting and thermal fracturing are still likely to occur.

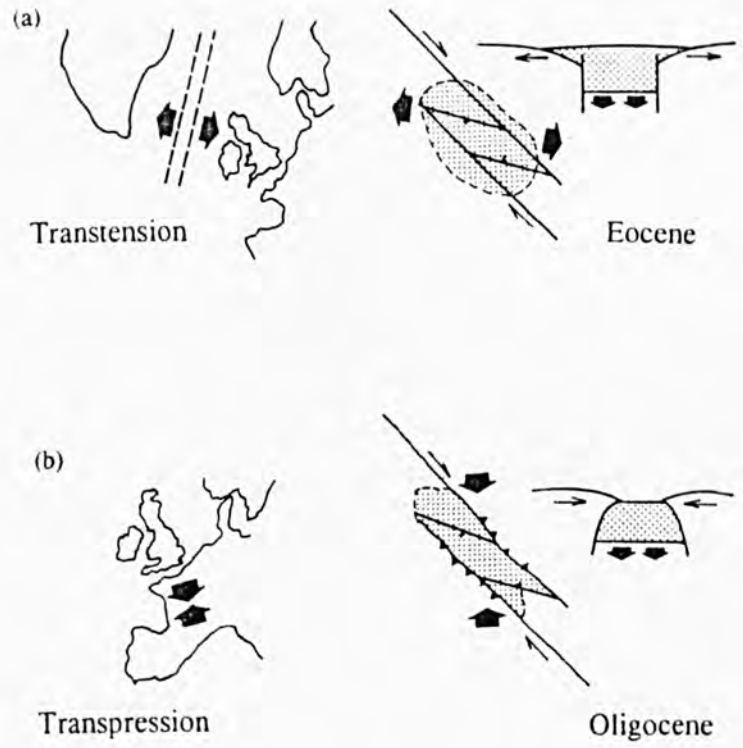

Fig. 5.5. Proposed structural evolution of Palaeogene basins in Devon (after Bristow and Robson, 1994). (a) Transtension along *en-echelon* dextral strike-slip faults associated with initial opening of the North Atlantic producers pull-apart basin within depressed area at right offset; (b) Transpression results from Alpine deformation, resulting in boundary faults to become thrusts, basins deeper further.

5.2.1 Sampling

Sampling was undertaken from disused quarries and sea cliff exposures on Lundy during four days spent in the field during June 1992 and November 1993. Oriented samples of granite were obtained from seven localities within both the Upper and Lower granites as defined by Dollar (1941) and Thorpe *et al.*, (1990) (Fig. 5.1). The samples of granite obtained showed no evidence hydrothermal alteration. Where possible, joint surveys were undertaken in proximity to the sample site. FIP orientations from Lundy will be restricted to stress regimes operating since the emplacement of the granite. This is important in constraining FIP formation associated with strike-slip faulting, and constructing a movement history of the SLFZ during the Tertiary. Data from Lundy could then be compared to that from NE Dartmoor which was designed to test the variation in abundance of FIPs related to second order faults of varying orientations (Fig. 5.6) presumed to be related deformation associated with the SLFZ.

Sampling on Dartmoor was made difficult by poor exposure. However, samples were obtained close to the SLFZ and on its western border in the vicinity of second order faults as defined by Blyth (1962). It was not possible to carry out reliable joint surveys

because of the low lying topography and poor exposure. Granite was generally fresh (apart from supergene weathering) except for sample MHD 1 which was situated directly over the SLFZ and showed evidence of high temperature alteration associated with tourmalinisation.

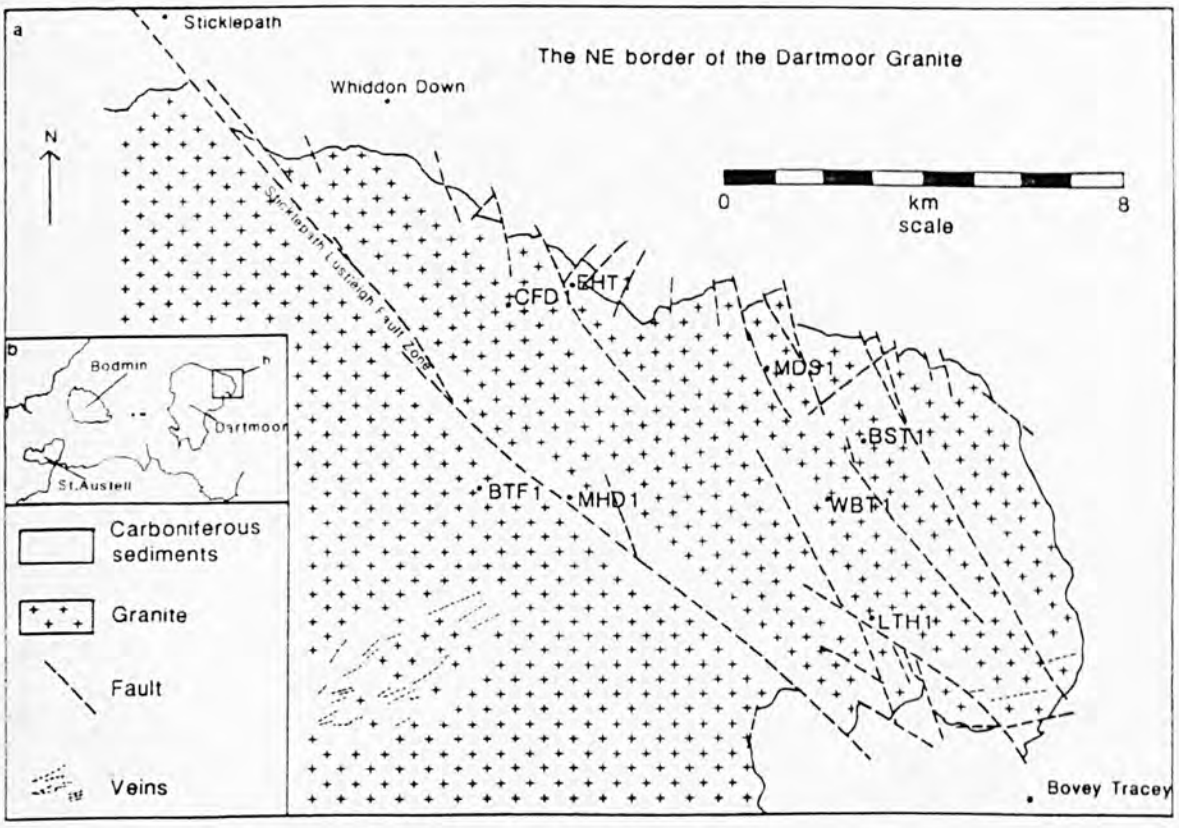

Fig. 5.6. Faulting in the NE Dartmoor area possibly related to the Sticklepath-Lustleigh FZ and relation to sampling locations (after Blythe, 1962).

5.2.2 Joint and dyke orientations

As stated above joint orientations were obtained where possible on Lundy. The dip and strike of the joint were recorded together with its form (planar/curvi-planar), fill (if present), development (length at locality) and border (alteration along the joint). The presence of slickenfibres on any joint signifies movement and the fracture is therefore classified as a fault. A total of 98 joint orientations were recorded, from four locations, together with 16 dyke and vein orientations (Appendix A, Tables A5.1).

Joint orientations-Lundy

Joint data are depicted as poles to planes in Fig. 5.7. It is evident that there are two major orientations, N-S and E-W, both steeply dipping vertical joints and a third minor low lying sub-horizontal set.

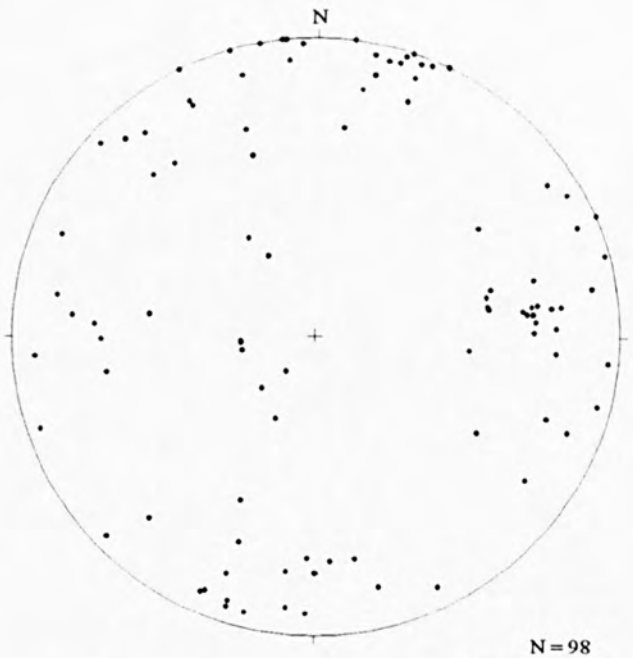

Fig. 5.7. Equal area projection of poles to planes of joint orientations within granites from four locations on the island of Lundy.

Vein and dyke orientations-Lundy

Veins were observed to contain tourmaline, were generally between 2-5mm in thickness and typically associated with iron staining and alteration of the vein walls. Dykes were fine grained aplite/granitic material and basic dolerite varieties. Orientations of veins and dykes are depicted in Fig. 5.8.

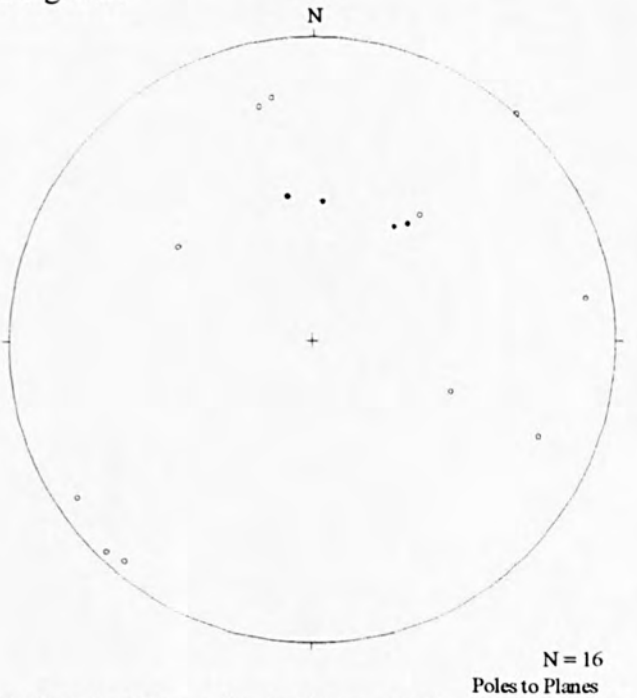

Fig. 5.8. Equal area projection depicting poles to planes of vein and dyke orientations. o = dykes; • = veins.

Orientations of both veins and dykes vary between E-W and NW-SE, and generally dip at angles between 45- and 85°.

5.2.3 Interpretation of field data

The formation of vertical to sub-vertical joint sets is likely during exhumation and unroofing of the granite (Price and Cosgrove 1990) with their orientations possibly governed by the orientation of the regional stress regime. Sub-horizontal, low-lying fractures would probably have formed in response to expansion of the granite during exhumation and un-roofing of the intrusion. Orientations of dykes (and possibly veins) is similar to the regional trend of exposed dykes and those mapped by geophysical methods as published by Arthur (1989), Hains *et al.*, (1983) and Roberts and Smith (1994). The orientation of the Lundy dyke swarm is generally similar to that of the BTVP in Northern Ireland and Northwest Scotland (Emeleus, 1982; Hains *et al.*, 1983). The emplacement of these dykes has been related to regional continental extension in a NW-SE direction (England, 1988), immediately prior to the opening of the NE Atlantic.

5.3 Microstructure and microthermometry

The following section concerns the presentation of healed fracture orientation data and characteristics together with the thermometric data from the secondary inclusions contained within them. All data from which conclusions have been drawn are listed in Appendix A, (Tables A5.2-A5.16). All techniques involved in recording orientation and thermometric data are described in Appendices B and C.

5.3.1 Orientation analysis

Healed fracture orientations have been recorded from seven samples from Lundy Island (Fig. 5.1) and six samples from NE Dartmoor (Fig. 5.6). Sampling was designed to investigate the generation of vertical healed fractures and thus all sections have been cut in the horizontal from oriented samples. Only healed fractures in quartz have been analysed. The dip and strike of the FIP, was recorded in addition to the FIP morphology (planar, curvi-planar or irregular), its development (inter- or intracrystalline), the abundance, size and shape of fluid inclusions contained within it and the propagation points/direction of the fracture. Only complete FIP morphological analysis was conducted in two samples (LI1 and LI4), which possessed a representative FIP population when compared to the total orientation data from all the samples.

Summary of orientation results

Five hundred and thirty seven FIP orientations were recorded from samples of Lundy granite, and four hundred and twenty three orientations from samples of Dartmoor granite. All FIPs have been analysed from sections cut in a horizontal plane. Four possible orientations have been identified from stereonets depicted in Fig. 5.9. Present in the Lundy samples (LI2, LI3, LI5, LI6 and LI7 and possibly LI1) are strong E-W and N-S orientations. N-S data is also apparent in samples from Dartmoor (CFD1, MHD1 and possibly WBN1). However, Dartmoor samples show predominate NW-SE (CFD1, EHT1, MHD1, WBN1, and possibly MDS1), and NE-SW (EHT1, WBN1 and LTH1) orientations. Generally the majority of FIPs dip at about 75° or greater from the horizontal.

(a) Lundy LI1

(b) Lundy LI2

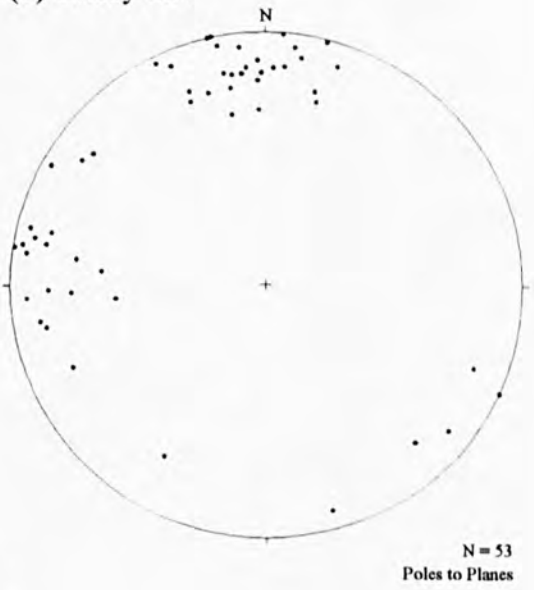

(c) Lundy LI3

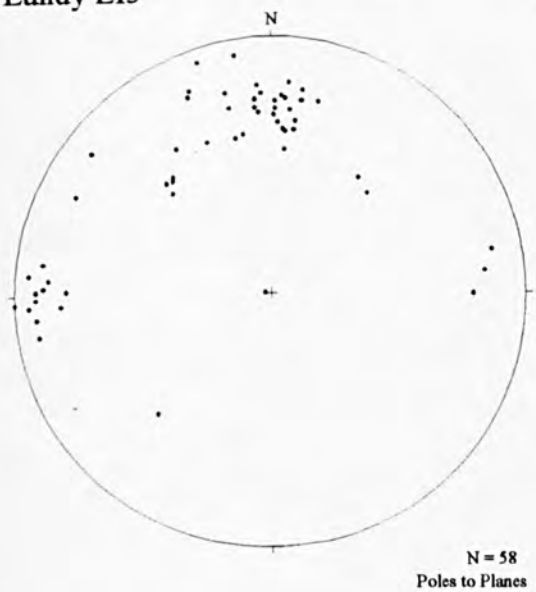

(d) Lundy LI4

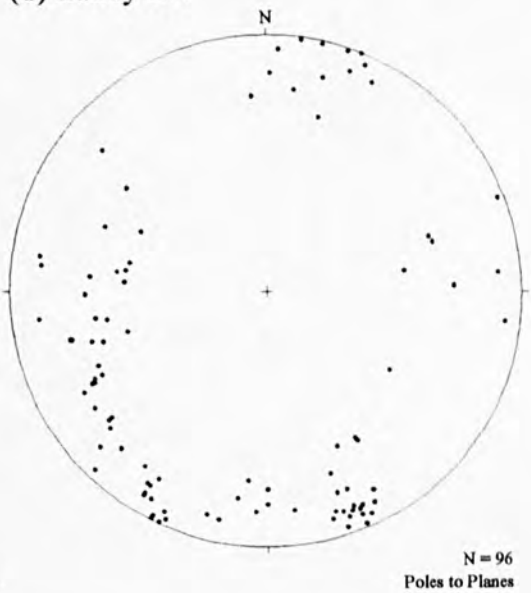

(e) Lundy LI5

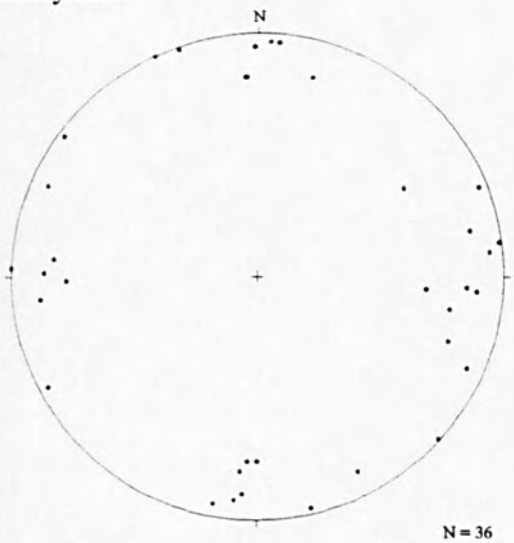

N = 36
Poles to Planes

(f) Lundy LI6

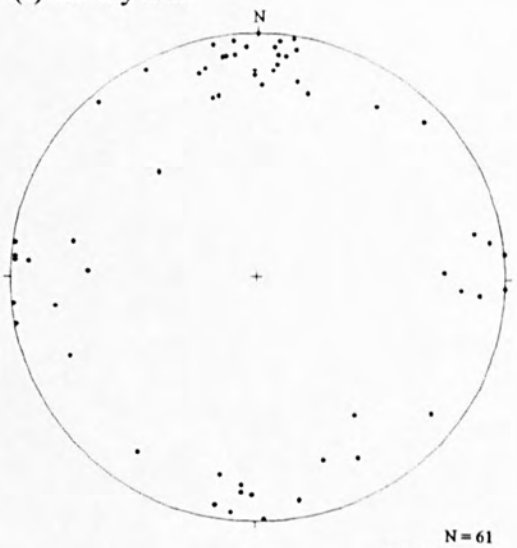

N = 61
Poles to Planes

(g) Lundy LI7

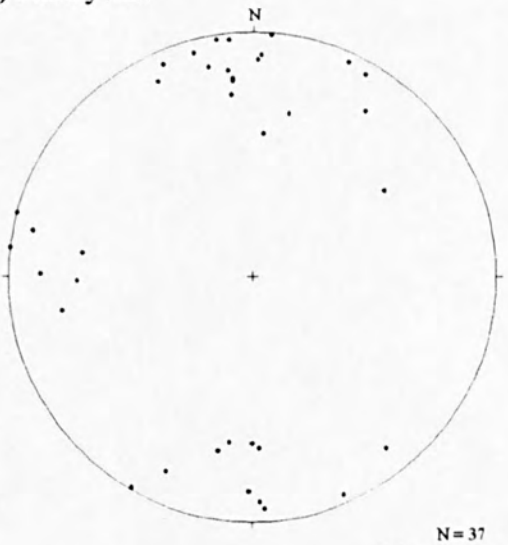

N = 37
Poles to Planes

(h) Dartmoor CFD1

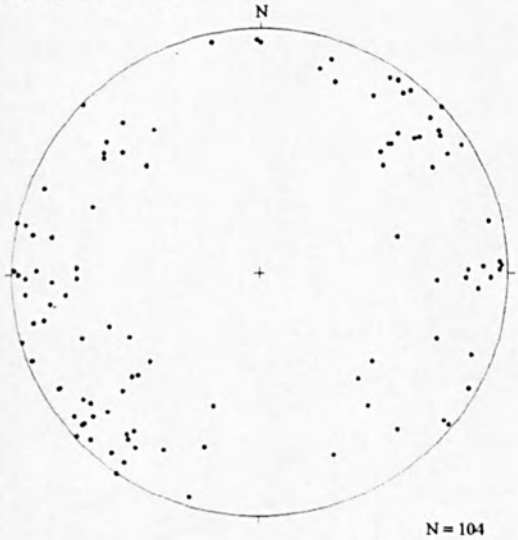

N = 104
Poles to Planes

(i) Dartmoor EHT1

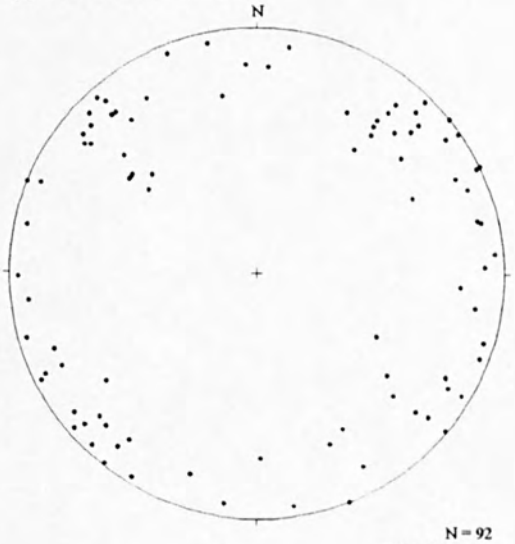

N = 92
Poles to Planes

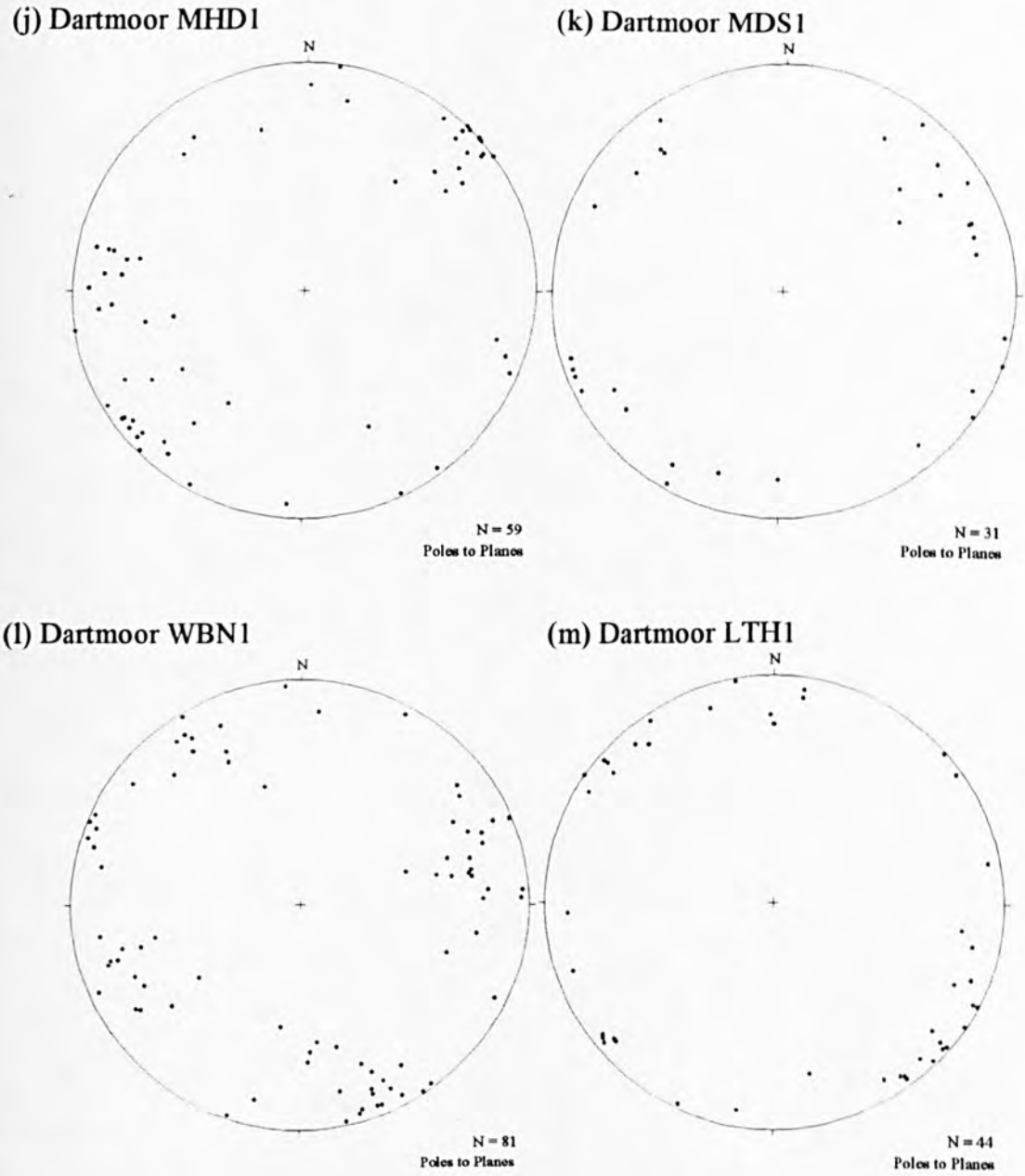

Fig. 5.9. Equal area projections showing poles to planes of FIP orientations from samples (a) LI1; (b) LI2; (c) LI3; (d) LI4; (e) LI5; (f) LI6; (g) LI7; (h) CFD1; (i) EHT1; (j) MHD1; (k) MDS1; (l) WBN1; (m) LTH1. For sample localities see Figs. 5.1 and 5.6.

5.3.2 Variations in FIP morphology with orientation

Together with orientation data, variations in the morphology of the fractures was also recorded. Morphological variations of the FIP orientations were expected, related to their varying origins and microfracturing processes. These variations include:

(i) FIP development: whether inter- or intracrystalline.

(ii) Propagation points: where the FIP initiates from and/or terminates.

(iii) FIP shape: planar, curvi-planar, sinusoidal or irregular.

(iv) Inclusions shape, size and abundance within the FIP.

These data may be plotted on a stereonet to illustrate the variation with orientation.

Inter- and intracrystalline FIPs

FIPs were classified as either intracrystalline (restricted to a single quartz crystal) or intercrystalline (crossing one or more grain boundaries). Generally, most FIPs were typically intracrystalline with intercrystalline FIPs being numerically less important. Stereonets illustrating the variation in development with orientation are illustrated in Fig. 5.10. Data for samples LI2, LI3, LI5, LI6 and LI7 was not collected in relation to the inter- and intracrsytalline nature of FIPs contained within them.

(a) Lundy LI1

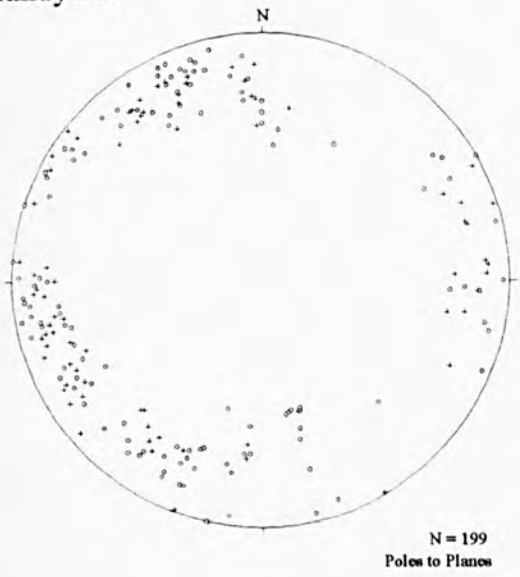

(b) Lundy LI4

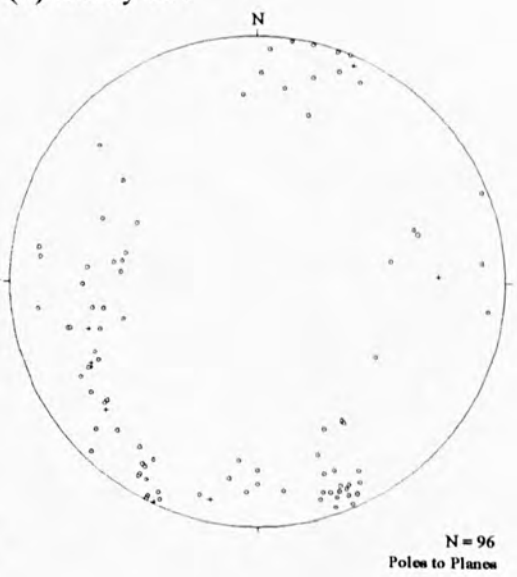

(c) Dartmoor CFD1

(d) Dartmoor EHT1

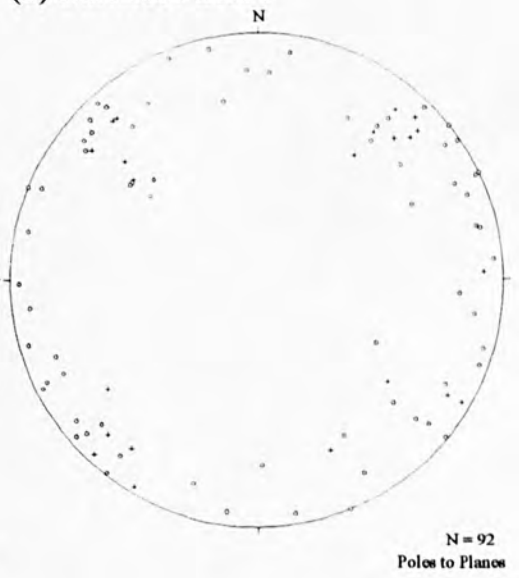

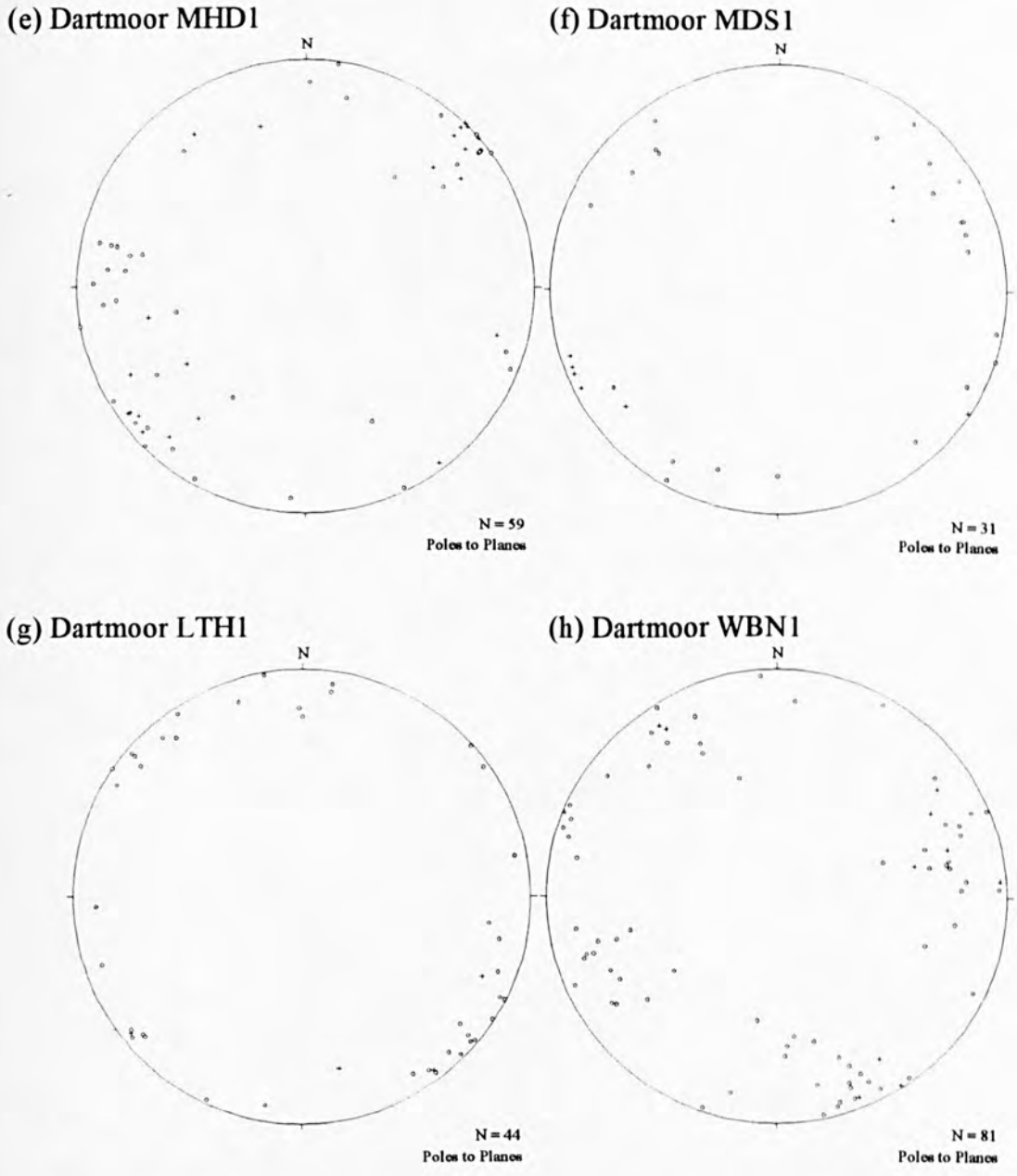

Fig. 5.10. Equal area projection showing poles to planes of FIP orientations and FIP development. + = intercrystalline FIP; O = intracrystalline FIPs. (a) LI1; (b) LI4; (c) CFD1; (d) EHT1; (e) MHD1; (f) MDS1; (g) LTH1; (h) WBN1. Refer to sample locations of Figs. 5.1 and 5.6.

From the data it is apparent that several samples possess preferred orientations of inter- and intracrystalline FIPs. In samples MHD1, EHT1 and CFD1 and possibly MDS1 intercrsytalline FIPs are generally restricted a NW-SE orientation and NE-SW orientation in sample EHT1. Intracrystalline FIPs do not generally show possible preferred orientations. No preferred orientations can be observed in the Lundy samples.

Fracture propagation

Strain resulting from thermal, tectonic and hydraulic stresses will be concentrated in varying domains within a rock due to the nature of the origins of such stresses (see Chapter 2). Therefore the propagation (and termination) point of an FIP may be related to variation in stress concentration and orientation. FIPs were grouped according to the following classification:

(i) **Isolated**: no interaction with other healed fractures or with grain boundaries.
(ii) **Grain boundary**: FIP terminates at, or propagates from, a grain boundary.
(iii) **Healed fracture**: FIP terminates at, or propagates from, another healed fracture.

(a) Lundy LI1

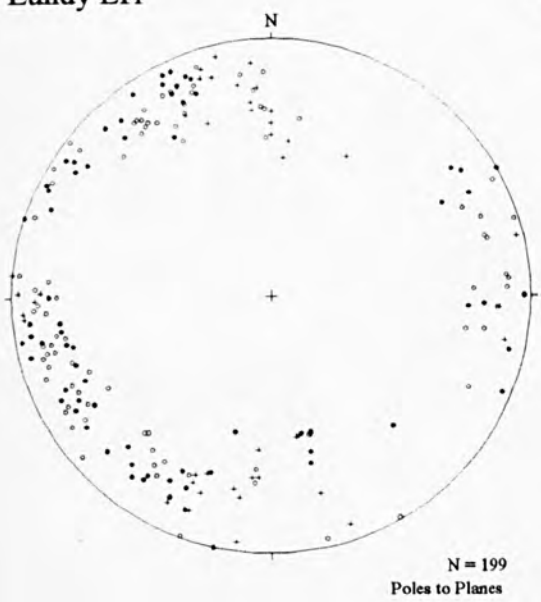

(b) Lundy LI4

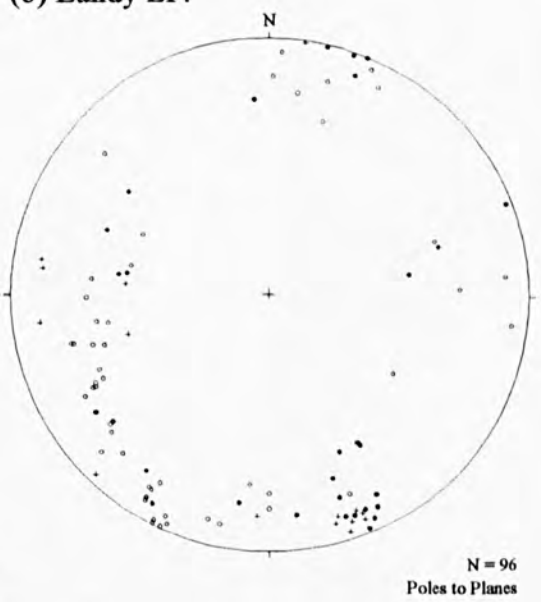

(c) Dartmoor CFD1

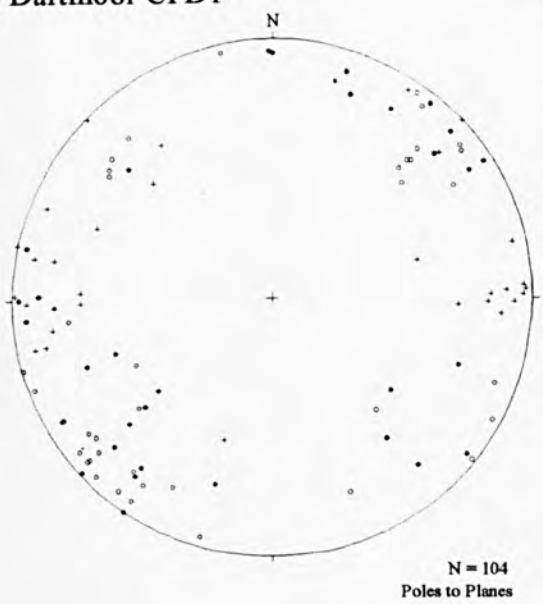

(d) Dartmoor EHT1

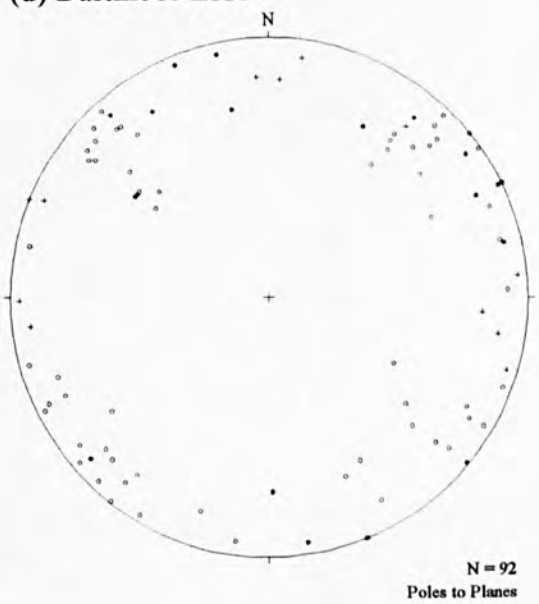

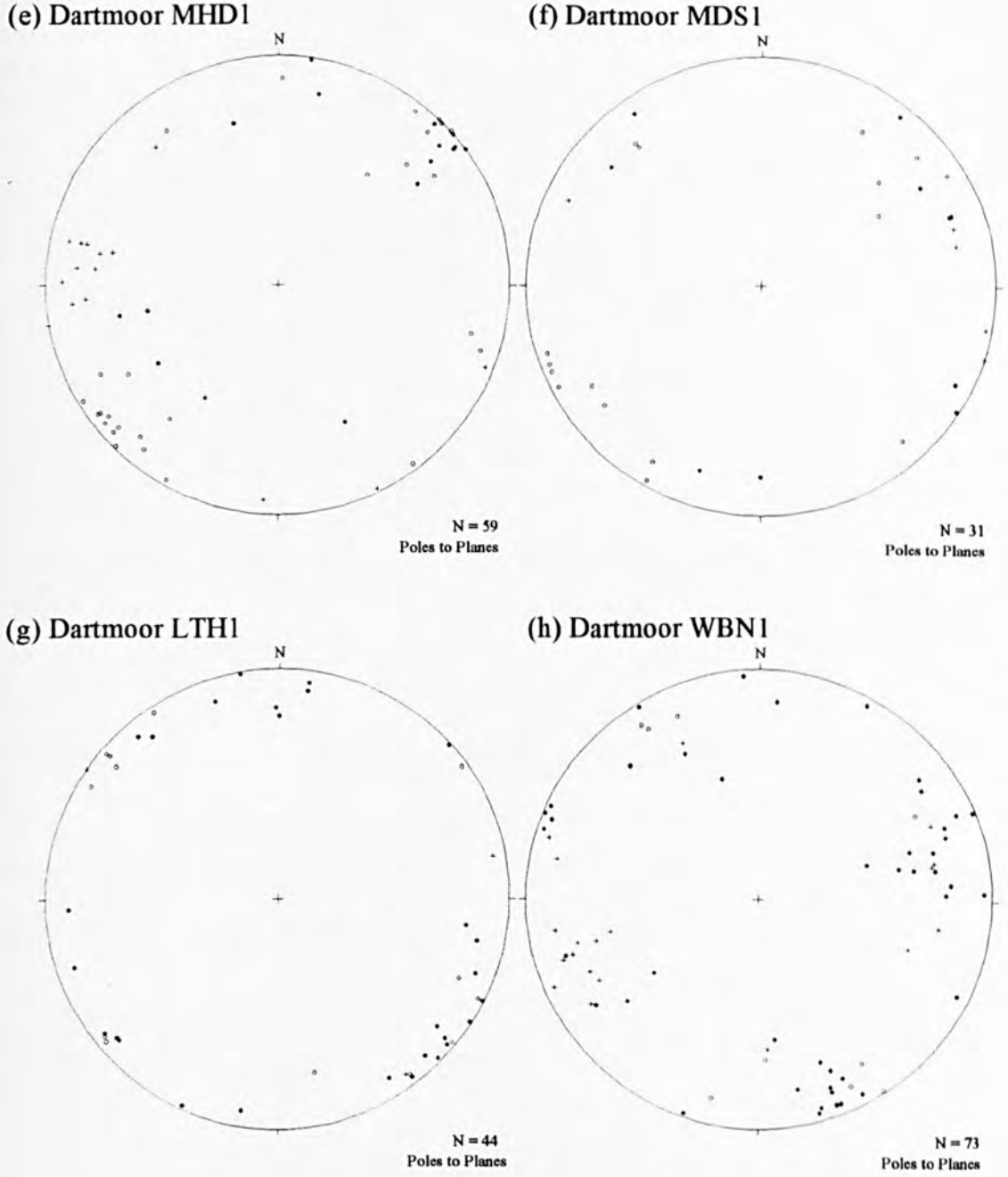

Fig. 5.11. Equal area projections showing poles to planes of FIP orientations and points of propagation and/or termination. + = isolated; O = grain boundary; • = healed fracture. (a) LI1; (b) LI4; (c) CFD1; (d) EHT1 (e) MHD1; (f) MDS1; (g) LTH1; (h) WBN1.

It is generally, not possible to ascertain the propagation direction of the healed fracture. Where an FIP interacts with both grain boundary and healed fracture, it was generally classified as a **grain boundary** type as this is the most likely place that the FIP would propagate form due to thermal and compressibility differences that may exist across a grain boundary (see section 2.2.1). Fig. 5.11 shows stereonets illustrating FIP orientation and propagation points.

From the data preferred orientations of FIPs showing a distinct grouping of propagation points are apparent in a number of cases. FIPs classified as **isolated**, typically occur in a N-S or NNE-SSW orientation (approximately N-S) in samples CFD1, EHT1, MHD1 and WBN1. In the Lundy sample LI1, **isolated** fractures have an E-W to ENE-WSW orientation, with a minor N-S orientation. FIPs terminating at, or propagating from, **grain-boundaries** typically occur in a NW-SE or NE-SW orientation as observed in samples CFD1, MHD1, WBN1 and possibly MDS1. FIPs propagating to or from other **healed-fractures** show preffered orientations in samples MHD1, LTH1, WBN1.

Fracture morphology

The morphology of all FIPs was recorded when viewed in a vertical orientation, with respect to the cross-hairs of the microscope eye-piece. Generally, the majority of FIPs were typically planar, essentially two dimensional features. However a number of other morphologies were observed (Fig. 5.12) and were classified as follows:

(i) **Planar**: essentially flat two dimensional features.
(ii) **Curvi-planar**: curved fracture or fracture with a curved propagation front.
(iii) **Sinusoidal**: FIP displaying a series of curved steps.
(iv) **Irregular**: FIP displaying irregular changes in geometry, with its orientation being difficult to record.
(v) **Complex**: FIPs displaying complex microstructural geometries that may be related to their origins.

Stereonets illustrating variation in FIP orientation in relation to planar and curvi-planar morphologies failed to show significant groupings with preferred orientations. Sinusoidal FIPs and FIPs displaying complex geometries were generally rare, and together with difficulties in recording their orientations it was not possible to produce stereonets for each sample showing the orientations for such healed fractures.

Examples of sinusoidal FIPs are shown in Plate 5.1 and Fig. 5.13. These FIPs were observed in the Lundy samples (LI1 and LI4) and samples WBN1, CFD1 and MHD1. They may be analogous to releasing/restraining bends observed in strike-slip faults (Christie-Blick and Biddle, 1985) on the macroscale, and are thus believed to represent shear (*mode II*) fractures exhibiting transtension/transpression. Examples of complex FIPs are illustrated in Plates 5.2, 5.3, 5.4 and Fig. 5.14. These geometries include left-, and right-stepping FIPs and possible duplex structures, the possible result of shear fracturing and again observed on the macro scale associated with strike-slip faults (Woodcock and Fischer, 1986; Naylor *et al.*, 1986).

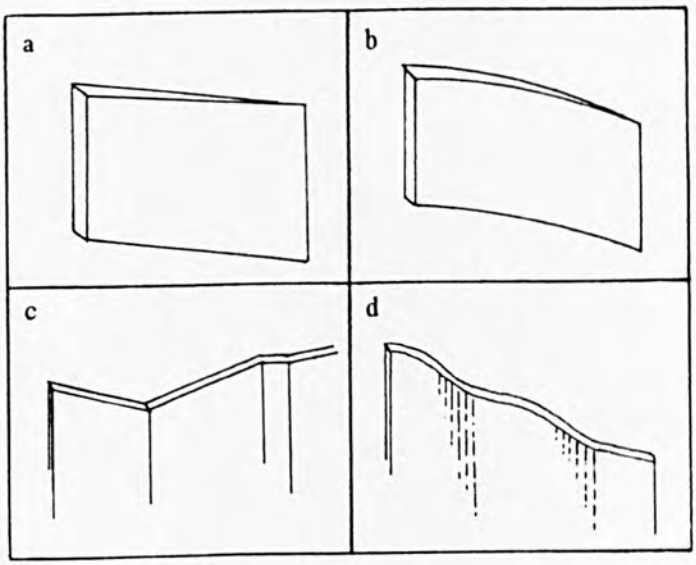

Fig. 5.12 FIP morphologies (a) planar (b) curvi-planar (c) irregular (d) sinusoidal

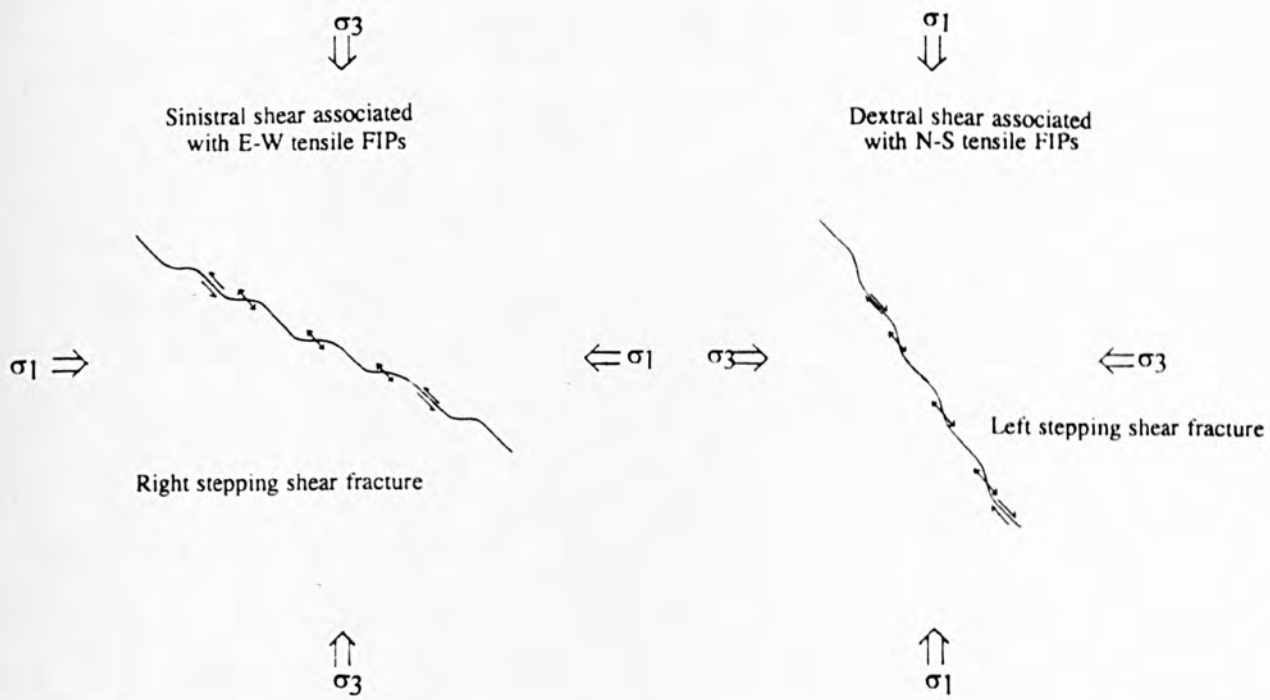

Fig. 5.13. Left and right stepping possible healed, *mode II* shear fractures and inferred principal compress stress axis directions; (a) right stepping FIP, with possible dextral movement assuming N-S oriented releasing bends represent (*mode I*) tensile segments; (b) left stepping FIP, with possible sinistral movement assuming E-W oriented releasing bends represent (*mode I*) tensile segments. FIPs observed in samples LI1, LI4, MHD1 and CFD1. Orientation of the healed shear sections generally NW-SE striking.

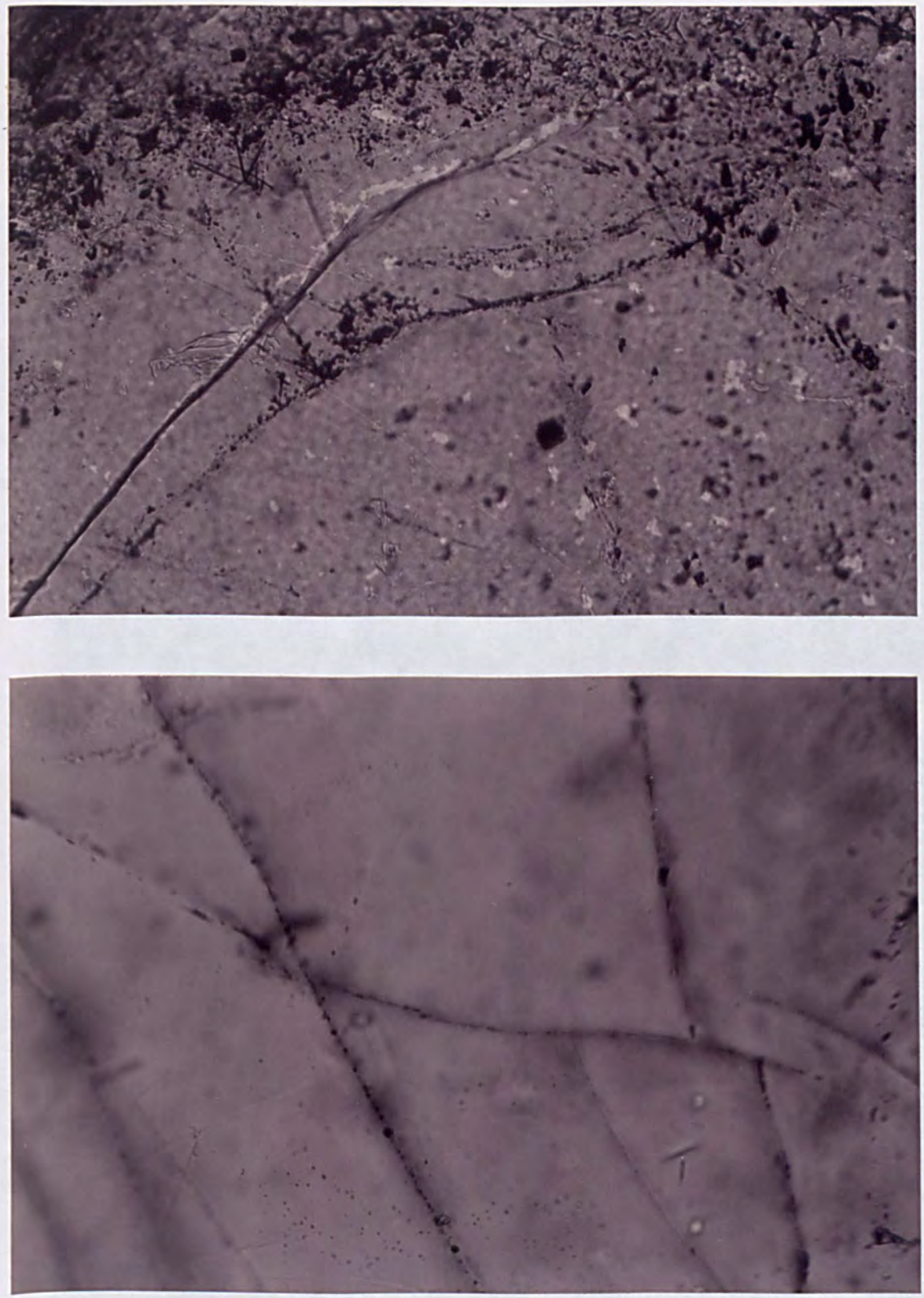

Plate 5.1a, b. FIPs exhibiting a sinusoidal morphology, analogous to a restraining/releasing bend characterised on the macroscale by strike-slip faults. Orientation of the pure shear section, suggests its origin as a Riedel shear fracture. Bar is 100μm.

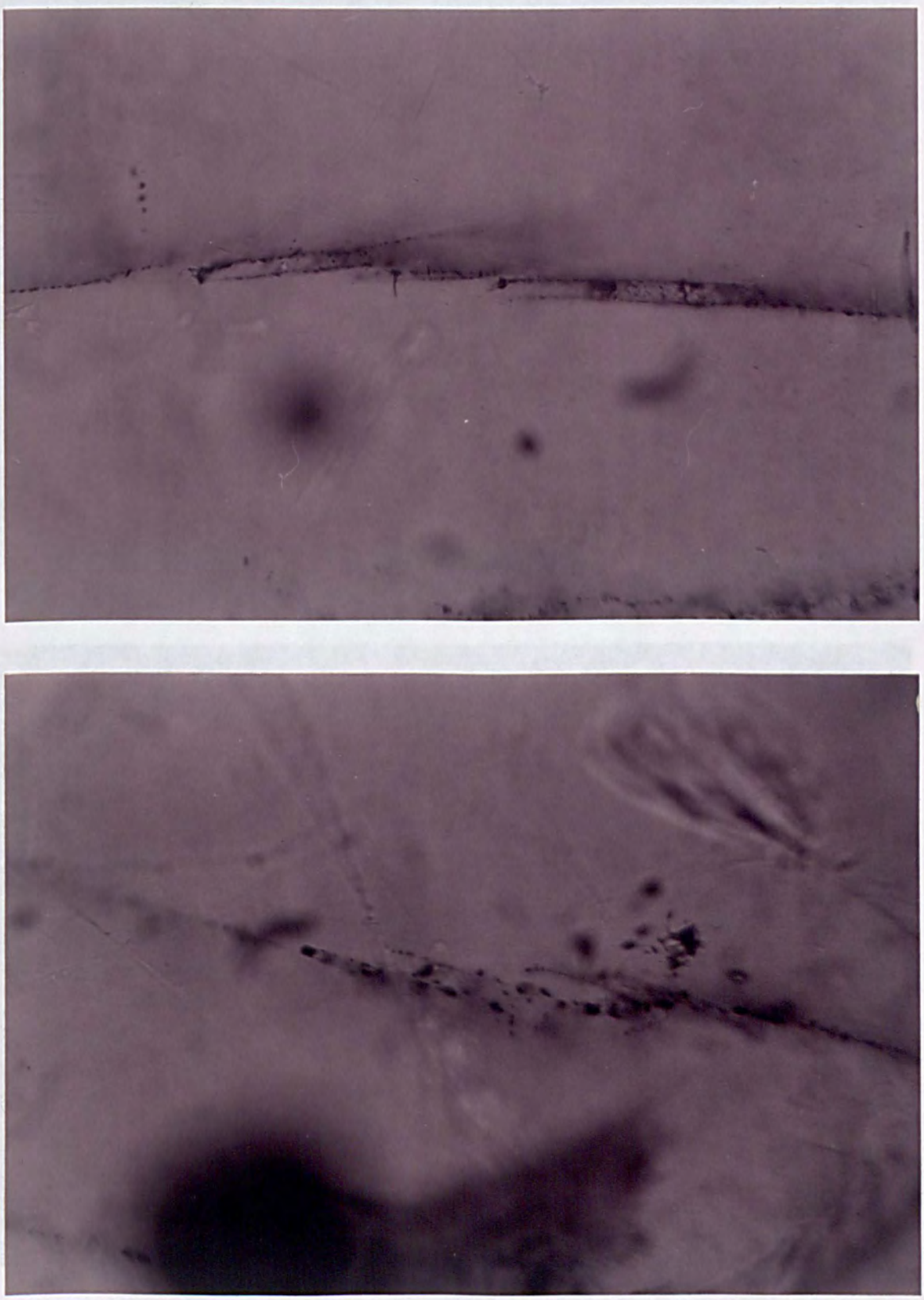

Plate 5.2a,b. FIPs exhibiting a left and right stepping morphology. Orientation of FIP suggests its origin as a Riedel shear fracture. Bar is 100μm

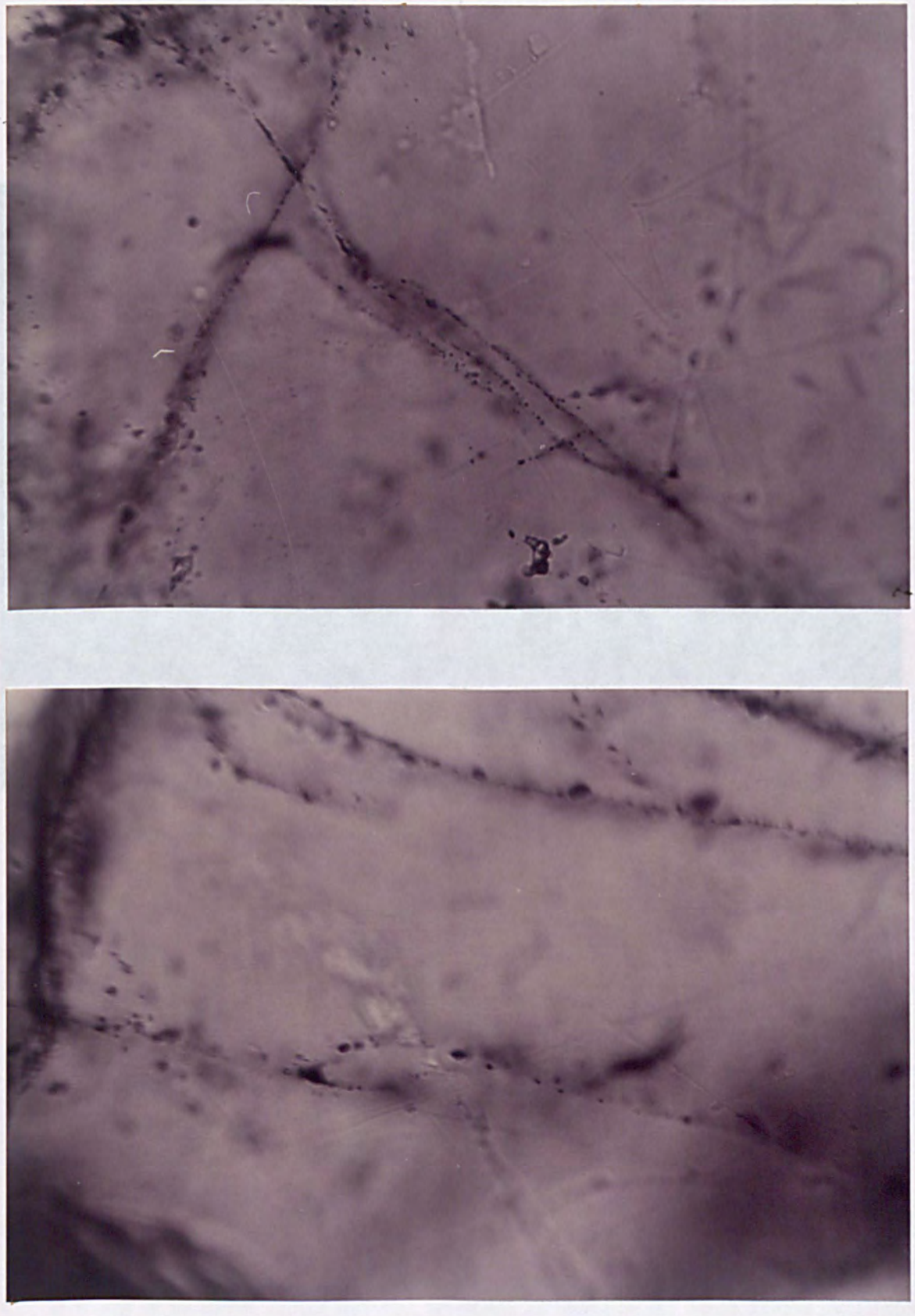

Plate 5.3a,b. Possible strike-slip duplex (terminology after Woodcock and Fischer, 1986) Orientation of FIP suggests its origin as a Riedel shear fracture. Bar is 100μm.

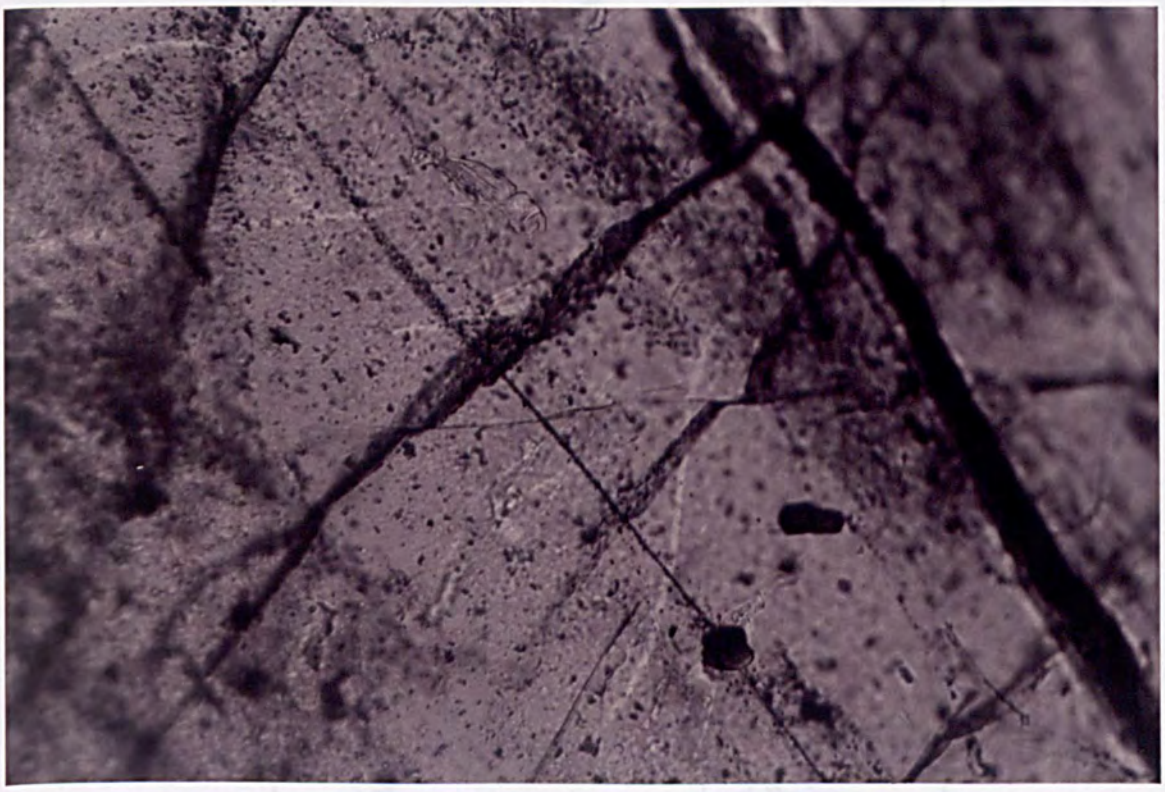

Plate 5.4. FIP illustrating sinistral shearing, shown by offset of an earlier cross-cutting fracture. Bar is 100μm.

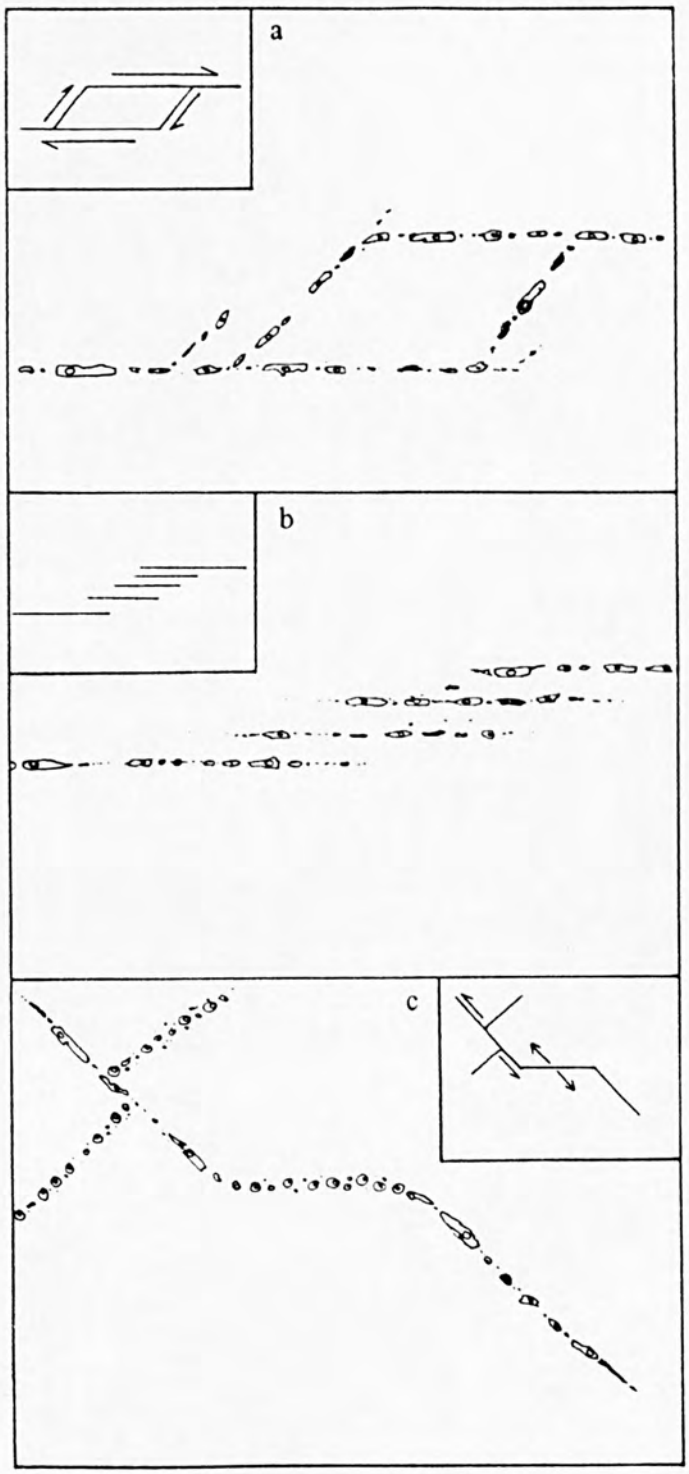

Fig. 5.14. Variation in inclusion morphologies with respect to fracture morphology. (a) Strike-slip duplex with possible movement directions observed in sample LI1. Note inclusions may form parallel to the length of the FIPs; (b) Left stepping FIP morphology again with inclusions forming parallel to the length of the FIP; (c) Sinusoidal FIP with proposed movement directions based upon the offsetting of an earlier healed fracture. Inclusions occurring in the centre section form under transtension and possess a markedly different shape to the inclusions subjected to shearing.

Inclusion shape, size and abundance within FIPs

The size and shape of secondary inclusions was also recorded within FIPs during the orientation analysis (Appendix A; Tables A5.9- A5.17). It was hoped that this data may provide an insight into the processes governing the healing of FIPs and the rate at which the healing processes occurs naturally in relation to the chemistry and temperature of the fluids and the origins and orientations of the FIPs. The size and abundance of inclusions showed a large variation between FIPs and will be discussed in more detail in section 5.3.3. However, no correlation between inclusion abundance and size could be identified in relation to FIP orientation. Variation in inclusion shape between and within FIPs of varying orientations did exist. Inclusions were categorised according to the following (more detailed classification of inclusion types is presented in section 5.3.3.):

(i) **No shape orientation**: inclusions possess no overall preferred shape orientation in respect to the FIP length.
(ii) **Parallel**: Inclusions generally form with their length parallel to the FIP.
(iii) **Perpendicular**: Inclusions generally form length perpendicular to the FIP. This type was extremely rare and has not been plotted on the stereonets.

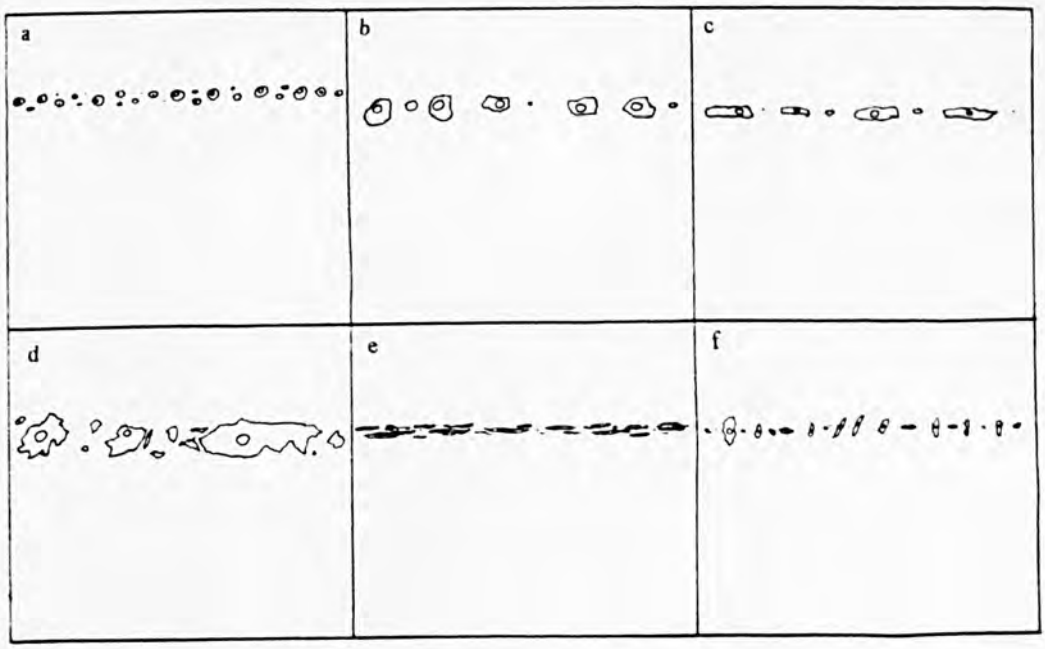

Fig. 5.15. Inclusion variation between FIPs. (a) small regular inclusions, generally <5μm in size; (b) rounded, equant, 5-15μm in size; (c) inclusions elongate parallel to FIP length, 5-20μm in size; (d) flattened, irregular or necked inclusions, 5-40μm in size, (low angle view of FIP); (e) smeared inclusions/strong shape orientation parallel to FIP length, viewed when FIP is a vertical position; (f) rare elongate inclusions, forming perpendicular to FIP length, 5-15μm.

Plates 5.5 and Fig. 5.15 illustrate preferred orientations of inclusions with respect to FIP length. Stereonets showing preferred shape orientation of secondary inclusions in relation to FIP orientation are illustrated in Fig. 5.16. Inclusions were classified when the FIP was viewed from a vertical position, parallel to the cross-hairs of the eyepiece and then compared when viewed at inclined angle (45°). A more detailed account of the actual method is presented in Appendix B.

(a) Lundy LI4

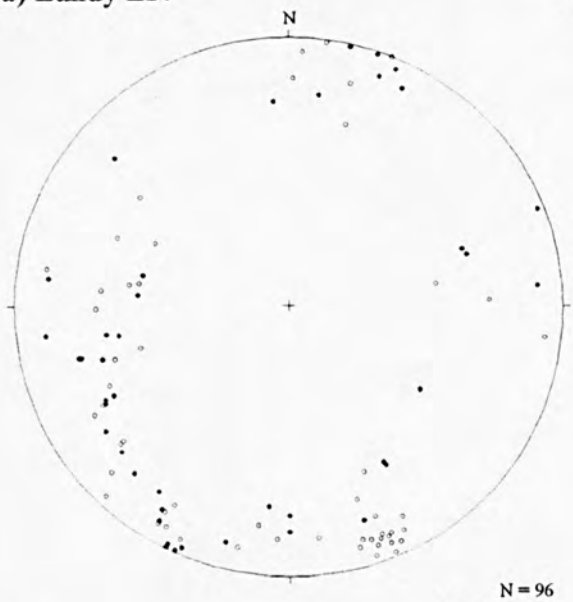

(b) Dartmoor CFD1

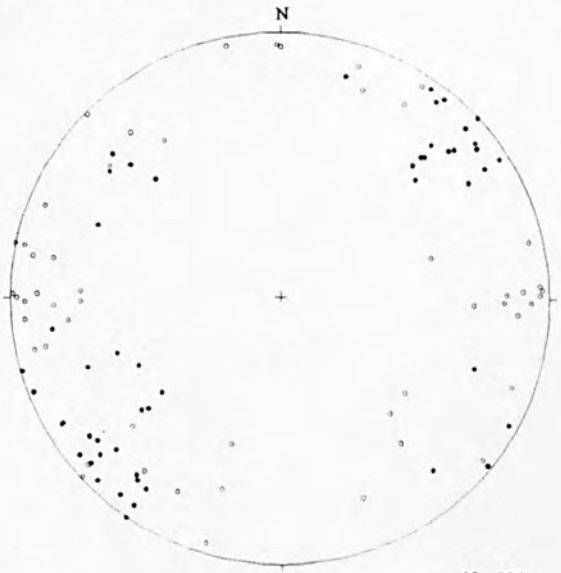

(c) Dartmoor EHT1

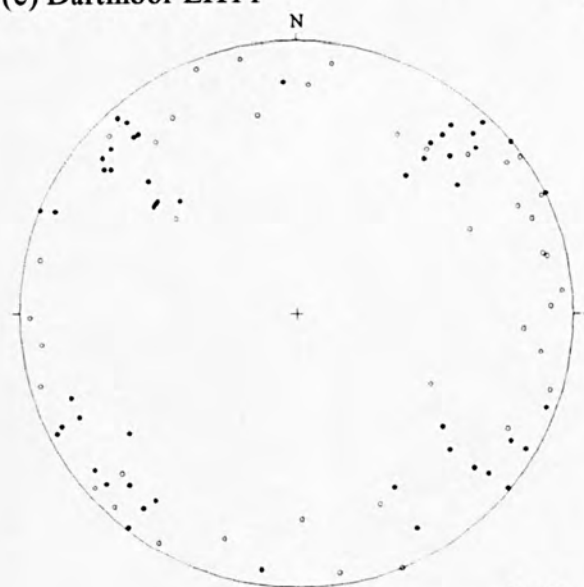

(d) Dartmoor MHD1

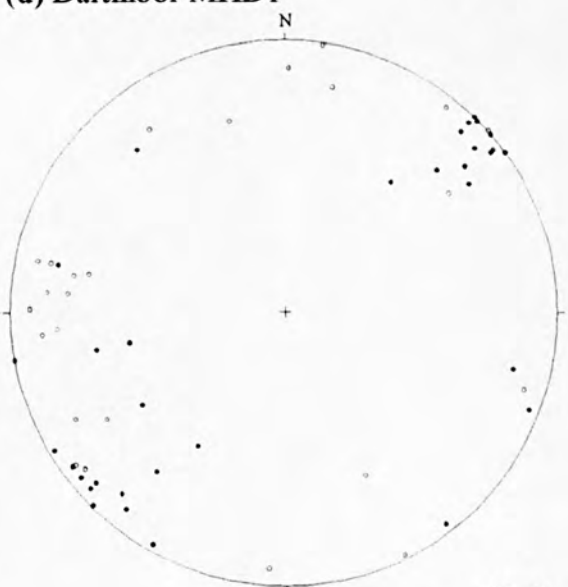

(e) Dartmoor MDS1

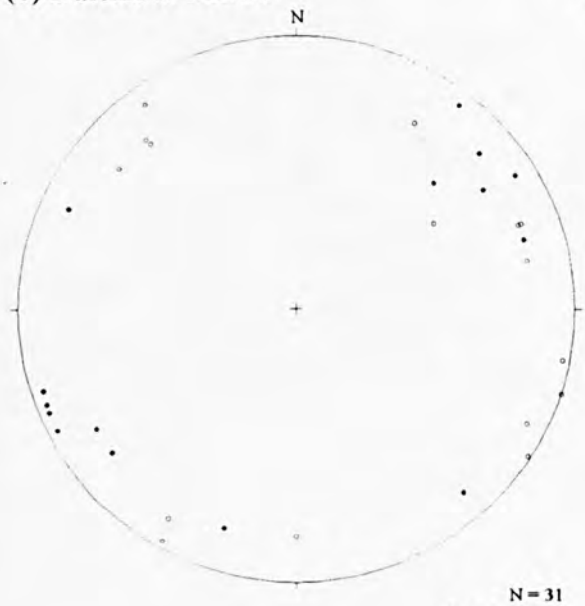

(f) Dartmoor LTH1

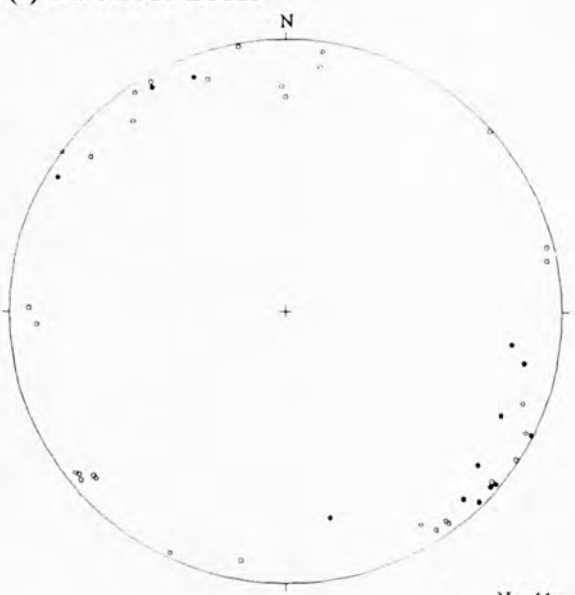

Fig. 5.16. Equal area projections showing poles to planes of FIP orientations and preferred shape orientation of secondary fluid inclusions contained within them. O = no preferred shape orientation; • = preferred shape orientation length parallel to FIP. (a) LI4; (b) CFD1; (c) EHT1; (d) MHD1; (e) MDS1; (f) LTH1. Refer to Figs. 5.1 and 5.6 for sample locations

Inclusions exhibiting a preferred shape orientation length parallel to the FIP generally occur in orientations NW-SE and NE-SW in samples MDS, EHT, MHD and possibly samples CFD and LTH. Regular inclusions, or those that did not possess a preferred shape orientation, occur typically in FIPs whose orientations are generally N-S and E-W, as observed in samples CFD and MHD. No interpretations could be drawn from samples LI1, LI4 and WBN1.

Variation in inclusion shape (together with abundance and possibly size) was observed along the length of certain FIPs. These were typically FIPs that possessed a varied orientation (i.e. curvi-planar, sinusoidal or FIPs with a complex morphology). A more detailed description of this phenomenon is given in section 5.3.3.

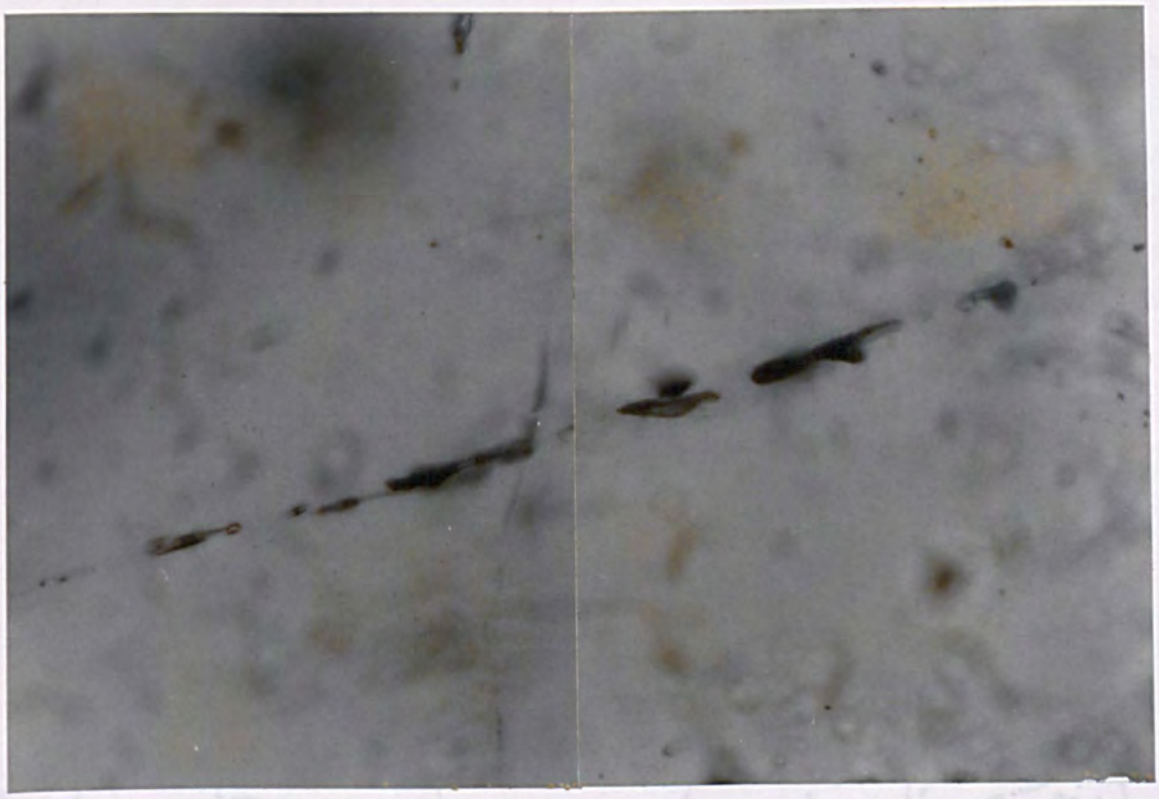

Plate 5.5. Inclusions showing a preferred orientation parallel to the length of the healed fracture. Bar is 100μm

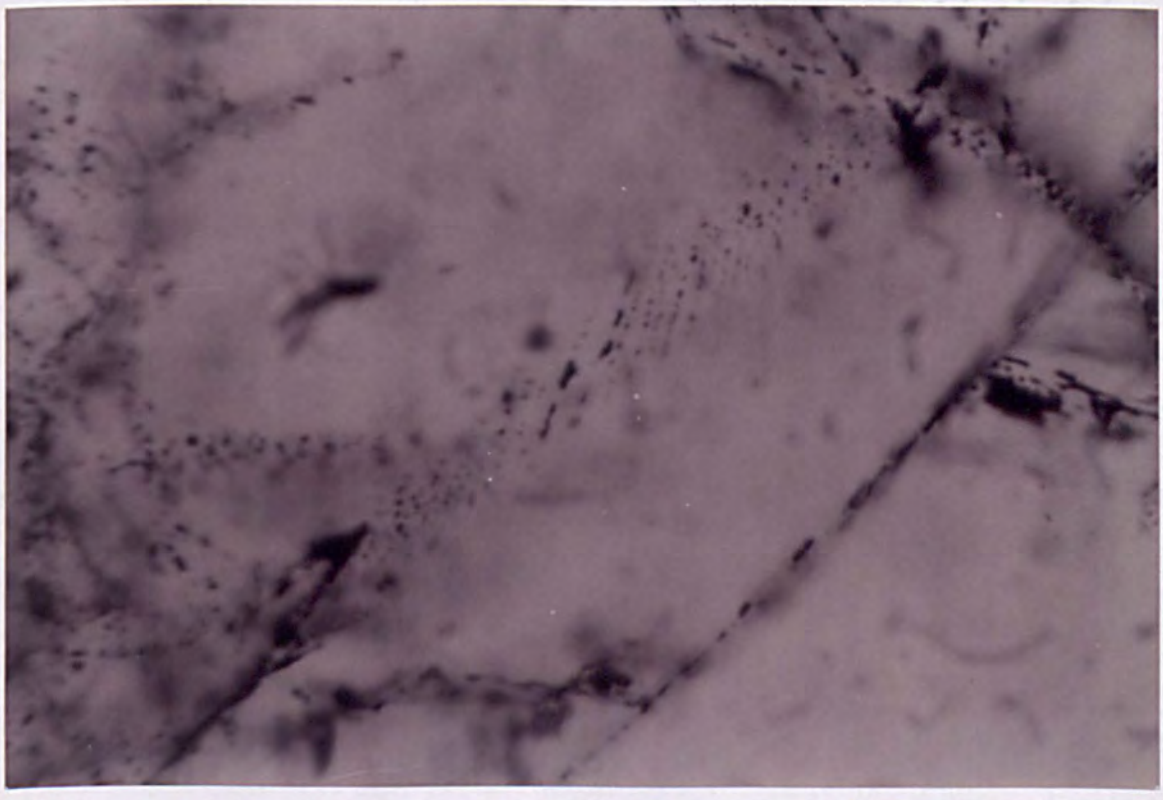

Plate 5.6. Inclusions formed perpendicular to the length of the FIP. Bar is 100μm.

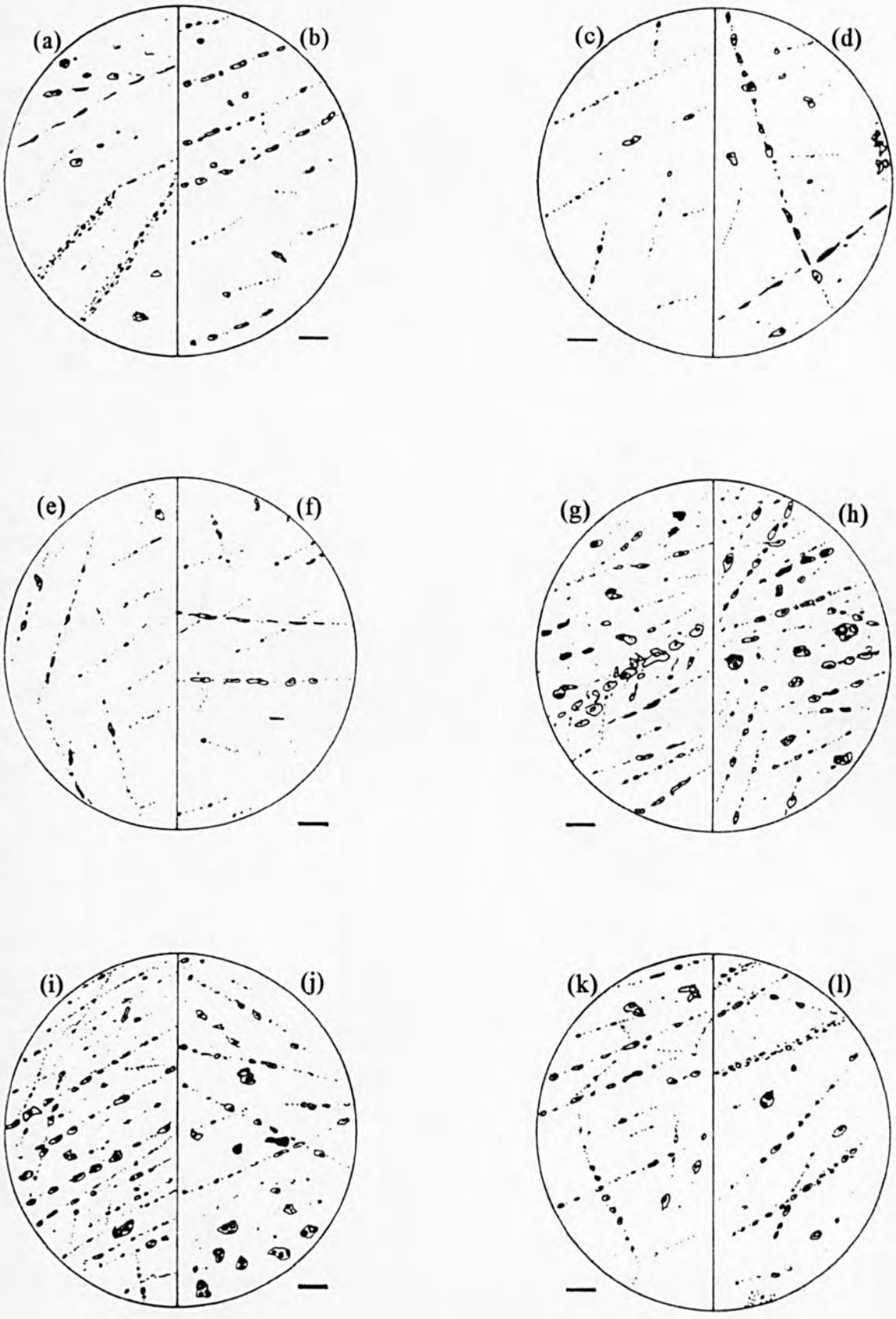

Fig. 5.17 Synoptic sketches of inclusion populations (a) LI1 (b) LI2 (c) LI3 (d) LI4 (e) LI6 (f) LI7 (g) CFD1 (h) EHT1 (i) MHD1 (j) MDS1 (k) WBN1 (l) LTH1

5.3.3 Optical Analysis of the fluid inclusion population

The following section is a brief summary of the optical characteristics of the fluid inclusion populations observed within the samples. Synoptic sketches illustrating the inclusion populations and abundances for the Lundy granite are shown in Fig. 5.17. A classification of the inclusion types is summarised in Table 5.2, and illustrated by summary sketches in Fig. 5.15. Data from primary inclusions have been included for completeness. Inclusion classification relating to the Dartmoor granite samples is presented in Chapter 4.

Table 5.2. Summary of fluid inclusion types observed within granitic quartz from Lundy island.

Type	*Size*	*Shape*	*Occurrence*	*Phases*	*Age?*
Type 1	<5μm	rounded/equant	secondary, fracture bound	generally monophase (*l*); rare two phase (*l*+*v*)	late
Type 2	5-15μm	regular/elongate	secondary, fracture bound, isolated groups	generally two phase (*l*+*v*)	early
Type 3	5-40μm	irregular/flattened /necked	secondary, fracture bound, isolated groups	generally mono (*l*) and two phase (*l*+*v*)	late
Type 4	10-25μm	rounded/equant	isolated,	two phase (*l*+*v*)	early

Four genetic types of inclusions have been identified within granitic quartz from Lundy island. The majority of inclusions observed (≈95%) are believed to be secondary or pseudo-secondary in origin. Primary inclusions are generally rare. No daughter minerals, CO_2 or gas rich inclusions were observed in any samples.

A wide range in shape, size and abundance of inclusions was observed within the fluid inclusion population. Plate 5.7 and Fig. 5.15 illustrates inclusion morphology variations within and between FIPs. Inclusions vary from small and regular to flattened and elongate, showing preferred shape orientation parallel to FIP length. Fig. 5.14a,b show preferred shape orientation of inclusions in more complex FIP morphologies, analogous to strike-slip duplex structures and left- and right-stepping shear fractures. Fig. 5.14c illustrate the variation in inclusion shape observed along the length of an FIP during a change in its orientation. Inclusions are seen to change their shape from regular and equant to possess a preferred shape orientation parallel to the FIP length. This is presumed to be related to a change in the mode of fracturing along the FIP. Fig 5.14c shows dextral offset of a later fracture suggesting the curve in the FIP represents a zone of transtension (analogous to a releasing bend). Similar observations were also recorded within the Dartmoor samples.

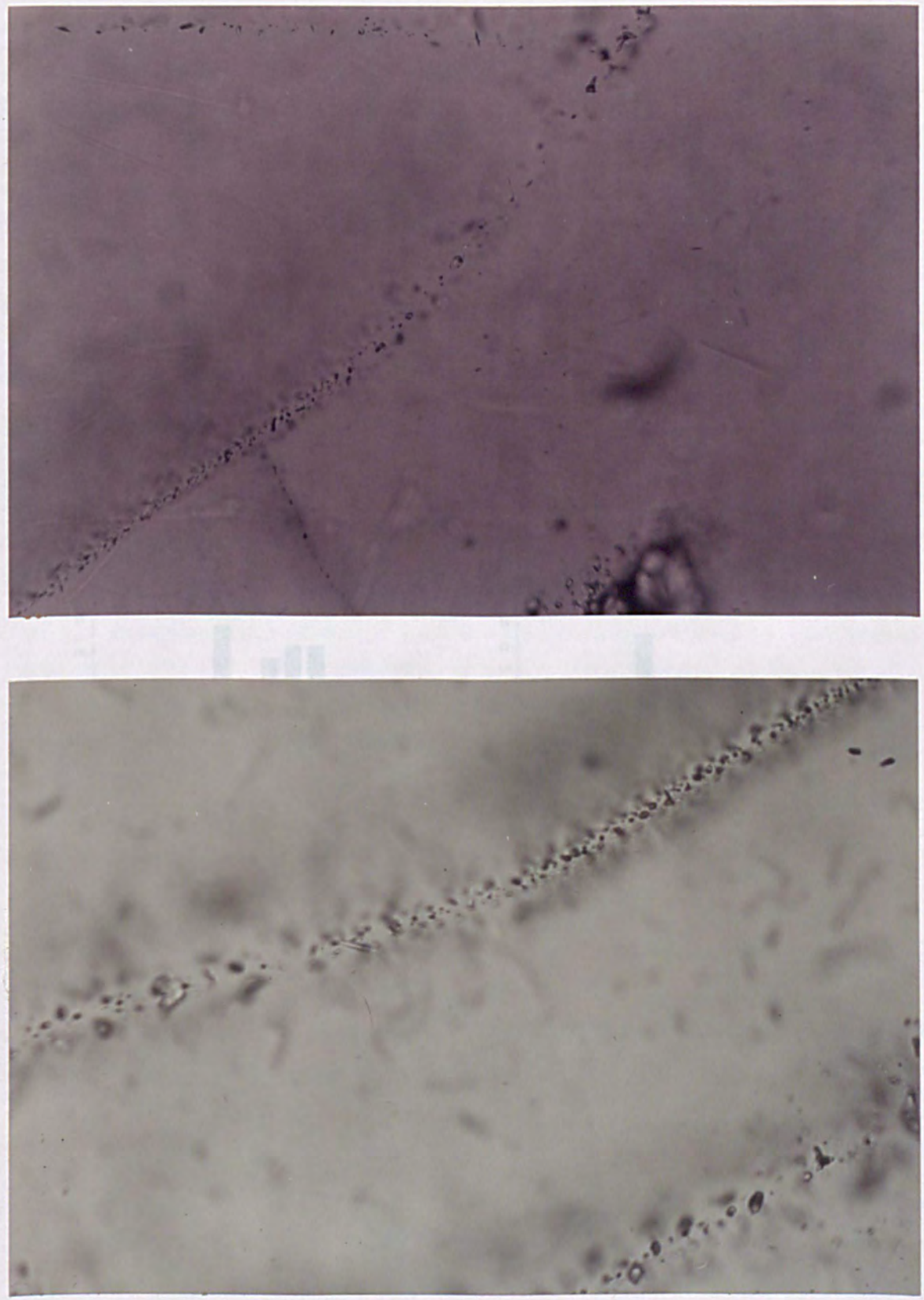

Plate 5.7a,b. FIPs in quartz exhibiting change in inclusion abundance and morphology with change in orientation. Bar is 100μm

5.3.4 Thermometric analysis (Lundy)

Thermometric analysis was restricted to secondary inclusions within FIPs of known orientation. Analysis was undertaken on samples LI1 and LI3. Data are presented as histograms of homogenisation temperature (°C) and wt. % equiv. NaCl for the identification of modal populations. Paired temperature and salinity data are presented as bivariate scatter plots to illustrate the possible evolution of the hydrothermal system. The small size (3μm) of inclusions defining certain FIPs made it impossible for data to be obtained. The observation of phase changes representing first melting was also not possible due to the low salinity and generally small size of most secondary inclusions.

Homogenisation temperatures - granitic quartz

Homogenisation temperatures were recorded for 178 secondary fluid inclusions. Homogenisation temperatures ranged from 122-395°C (for both secondary and primary inclusions) and modal ranges are shown in histograms in Fig. 5.18. Homogenisation was to the liquid state in all cases.

(a) (b)

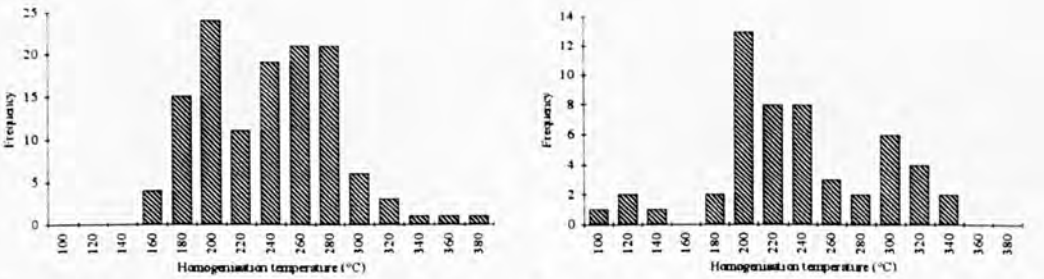

Fig. 5.18. Frequency histograms of homogenisation temperature (°C) distribution in samples (a) LI1 and (b) LI3. Data are from both primary and secondary inclusions.

The majority of the fluid inclusion data falls between 180 and 280°C, exhibiting modal peaks within this range. The high temperature peak (300-340°C) in sample LI3 represent data from primary inclusions not recorded in sample LI1. Low temperature fluids (100-140°C) were generally uncommon and only observed in sample LI3.

Bulk salinity - granitic quartz

Ice melting temperatures (Appendix A; Tables; A5.18 and A5.19) were recorded from 143 primary and secondary inclusions from samples LI1 and LI3. Salinities were calculated from last ice melting temperatures (Tlm_{ice}) and based upon equations of state produced by Brown and Lamb (1986). Salinities are expressed as wt. % equiv. NaCl as first melt data denoting the composition of the salt content was not observed. Fig. 5.19. shows histograms of salinity ranges and frequency in samples LI1 and LI3.

(a) (b)

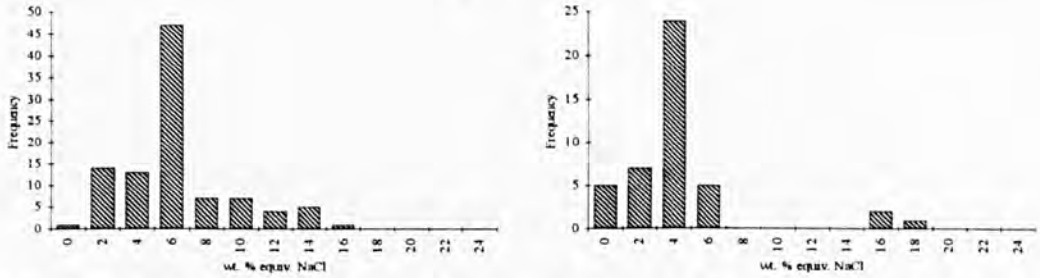

Fig. 5.19. Frequency histograms of salinity distribution, expressed as wt. % equiv. NaCl in samples (a) LI1 and (b) LI3. Data is from primary and secondary inclusions.

A wide range in salinity was observed in both samples (though discontinuous in LI3, thought to be due to lack of data) from less than 1 to 18 wt. %. equiv. NaCl. The majority of inclusions expressed salinity measurements around 4-6 wt. %. equiv. NaCl. High salinity fluids occurred mainly in early, possibly primary fluid inclusions.

5.3.5 Cathodoluminescence

The relative ages of the FIPs may be observed, based upon their cross-cutting nature. The cathodoluminescence of quartz show a wide variation in colour (or grey scaling contrasts in SEM-CL). These differences in contrast (and intensity) are the result of a complex relationship between trace elements (Al, Ti, Fe, etc.), crystal lattice defects and the state of the water (silanol, molecular) (van der Kerkhof and Behr, 1994). Thus, the healing of fractures by fluids of differing provenance may result in the FIPs being observed as lines of different contrasts.

Samples of Lundy and Dartmoor granites were analysed using CL attached to an SEM (see Appendix B for full method). Problems were encountered due to the poor luminescence intensity of the quartz in the samples, especially when compared to the luminescence of feldspar. Plate 5.8 shows a zoned quartz from Lundy (sample LI1). FIPs can be seen as dark lines crossing the quartz crystal, however, it is not possible to obtain relative dates as there is no apparent contrast in the different generations of FIPs. Plate 5.9 is feldspar from Dartmoor (sample WBN1) which luminesces more favourably than quartz. Well defined healed fractures are easily visible (rarely seen under plane polarised light) contrasting well with the background. Contrasts and intensities may also be observed between FIPs showing the relative age relationships. However, since the strong cleavage present in feldspar may have affected the orientations of the fractures, they can not be related to the major orientations of FIPs observed in quartz. However, some information, such as the presence of FIPs exhibiting shear can be observed. The large intergranular FIP which crosses the frame from top left to bottom right has offset several early FIPs (sinistrally) while later FIPs show not such offset.

Plate 5.8. SEM-CL image of a zoned quartz crystal from the Lundy granite (sample LI1). FIPs are present as dark anastomising lines. Vertical edge of frame oriented at 310°. Width of frame is 1.5mm. Grey scale contrasts between the different generations of the FIPs can not be discerned. Section cut in the horizontal plane.

Plate 5.9. SEM-CL image of a alkali feldspar from sample WBN1 (Dartmoor granite). Various generations of FIPs are easily identifiable based upon varying intensity and grey scale contrasts. Width of frame is 2mm, vertical edge aligned 000° (due north). Section cut in the horizontal plane. Note the large intergranular fracture (bottom right to top left) exhibiting dextral shear (off-setting of earlier) and possible strike-slip duplexes.

5.3.6 Discussion

The combination of microstructural and microthermometric data has been used to define the orientations of fluid pathways and the possible relative timing of the formation of these pathways. From a combination of this data it is possible to:

(i) Reconstruct the hydrothermal evolution of fluids associated with the Lundy granite.
(ii) Produce a relative history of movement along the SLFZ based upon the evolving fracture systems.
(iii) Fully characterise the morphologies and orientations of FIPs in relation to the stresses (i.e. tectonic, thermal or hydraulic) that were responsible for their formation and the mode of fracturing (shear or tensile).

Origin and evolution of the Lundy hydrothermal fluids

Although it is not the purpose of this study to characterise fully the evolution and origin of hydrothermal fluids associated with the Lundy granite some comment should be included for completeness. Field evidence and previous published accounts of the Lundy granite (Edmonds *et al.*, 1979; Thorpe *et al.*, 1990; Stone 1990) indicate that there is only minor amounts of mineralisation and hydrothermal alteration (Bromley and Holl, 1986). However, small amounts of tourmaline occurring as veins were observed with a general E-W (080-129°) orientation. The lack of significant mineralisation and alteration may be attributed to the absence of a hydrothermal system and metals in the granite or surrounding rocks. The Lundy granite may have cooled quickly enough to prohibit the creation of a convection cell allowing the circulation of hydrothermal fluids. However, Tertiary igneous centres in Scotland (e.g. Mull and Skye) do exhibit widespread hydrothermal alteration (Emeleus, 1991). Oxygen isotope studies (Taylor and Forester, 1971) infer that there must have been substantial convective circulation of meteoric waters through both the complexes and the surrounding country rocks, with the groundwaters derived mainly from the lava piles. However, there is no evidence of sub-aerial volcanic activity around the Lundy complex to provide adjacent reservoirs of meteoric waters which coupled with a far smaller volume of basic magma at depth as a heat source for a convection cell may be responsible for the absence of hydrothermal alteration.

Fluid inclusion data from secondary and possibly primary inclusions shows a wide variation in salinity and temperature, representing the trapping of hydrothermal fluids over a significant range. Fig. 5.20 shows bivariate scatter plots of homogenisation temperature and inclusion salinity inferred from ice melting temperatures for the two Lundy samples LI1 and LI3. Data was recorded generally from FIPs of a known orientation, although possible primary inclusions were also selected for analysis. Fig. 5.20a shows a possible evolutionary trend of the fluids from that of high

temperature/high salinity to low temperature/low salinity. This is generally interpreted as simple cooling and mixing with less saline fluids (Shepherd *et al.*, 1985), implying early magmatic fluids mixing with later possibly meteoric fluids, although stable isotope analysis would be required for confirmation.

(a) Lundy LI1

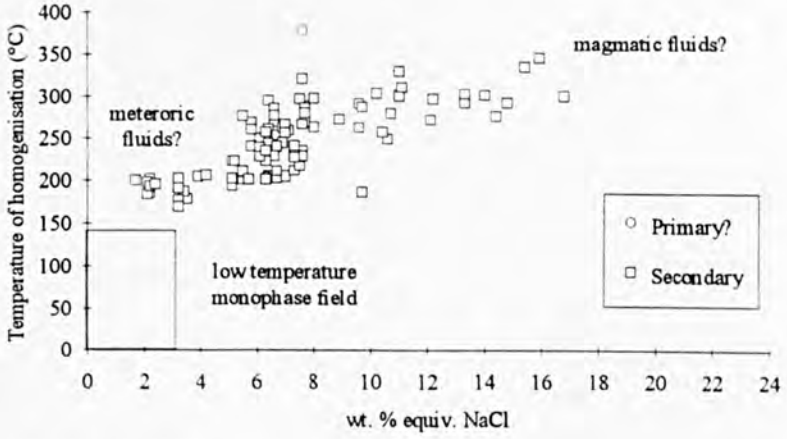

(b) Lundy LI3

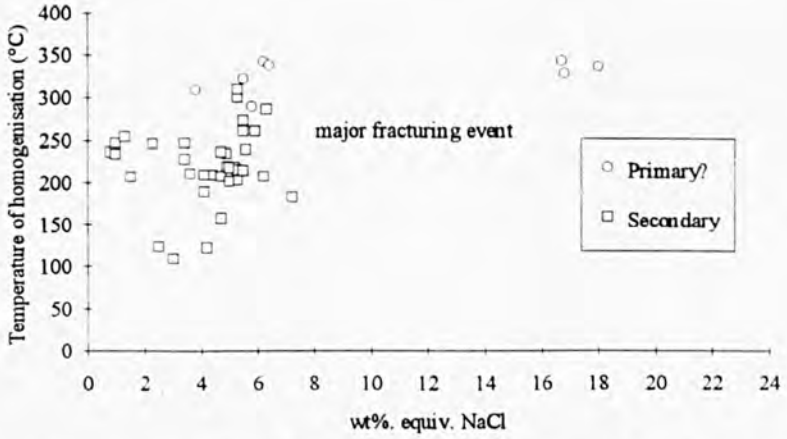

Fig. 5.20. Bivariate scatter plots of Th (°C) and salinity (wt. %. equiv. NaCl) for primary and secondary fluid inclusions from samples (a) LI1 and (b) LI3.

However, analysis of possible primary inclusions infers a fluid of approximately 18 wt. %. equiv. NaCl homogenising at temperatures close to 350°C. Emplacement depths for Scottish Tertiary igneous centres of 3-4km (Emeleus, 1991) suggest a trapping temperature for the Lundy fluids of approximately 380-420°C (Fig. 5.21), making it likely that these inclusions are primary, and may represent magmatic fluids. The majority of secondary inclusions possess homogenisation temperatures of around 200-300°C and salinities ranging from 6-8 wt. %. equiv. NaCl. At these temperatures thermal stresses would play an important role in fracture generation. Theoretical thermal stresses (Jang and Wang, 1991) of around 70-80 MPa will initiate thermal fractures when maximum and minimum regional principal stress axes associated with continental extension, granite

emplacement and basin formation are typically 150 and 50MPa respectively. Trapping temperatures for these inclusions would be above 300°C.

Thermometric data from Lundy exhibits a similar cooling trend to that from Lee Moor (4.3.4; Fig. 4.17). However, at Lee Moor an increase in fracturing occurs at around 100-150°C with salinities of 0-5 wt. %. equiv. NaCl, generally lower temperature/lower salinity than the bulk of the Lundy FIPs. This suggests the majority of the Lee Moor fractures were the result of tectonic stresses, healed by meteoric? fluids rather than thermal stresses healed by fluids with a more magmatic? component.

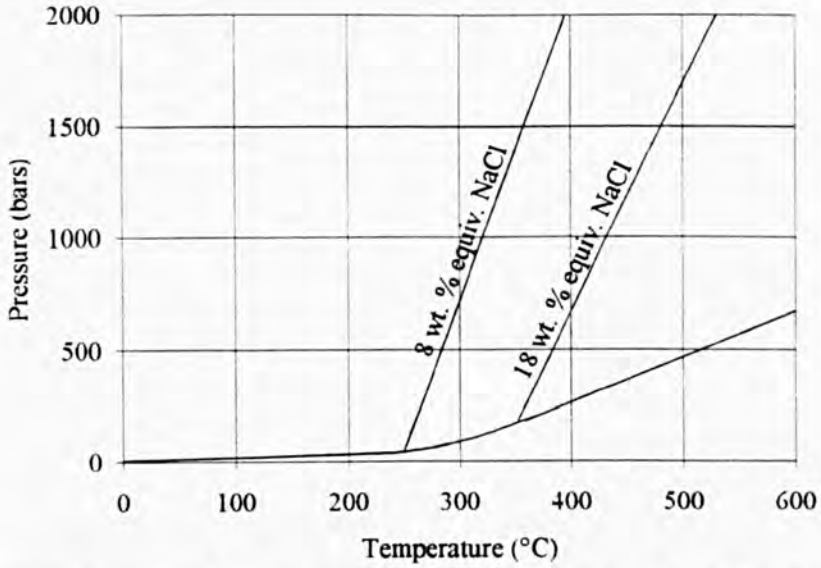

Fig. 5.21 Pressure correction diagram for inclusions representing two fluids of 8 and 18 wt. %. equiv. NaCl homogenising at 250 and 350°C respectively. See text for further explanation.

A large proportion of the secondary fluid inclusion data relates to a moderate temperature (Th 200-260°C) low to moderate salinity (4-8 wt. %. equiv. NaCl) fluid. This suggests that a significant amount of the fractures were generated during this period in the evolution of the hydrothermal fluids.

A combination of temperature and salinity data with FIP orientations (Fig. 5.22, 5.23) illustrates the fracture system orientations that were utilised during the evolution of the hydrothermal system. It can be seen from the data that a low salinity (0-6 wt. %. equiv. NaCl), low to moderate temperature (Th 100-250°C) fluid is generally found to occur in N-S NW-SE oriented FIP, as opposed to a higher salinity (> 6 wt. %. equiv. NaCl) higher temperature (Th 250-400°C) fluid which is generally restricted to NW-SE and E-W oriented FIPs.

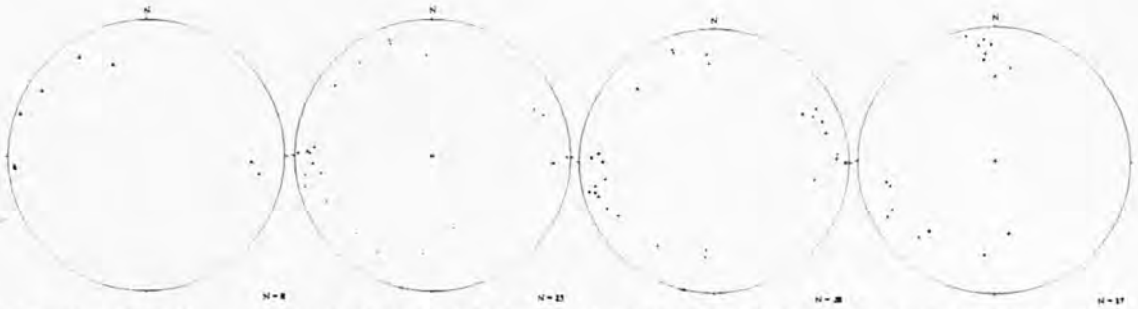

(a) Th <200°C (b) Th 201-250°C (c) Th 251-300°C (d) Th >301°C

Fig. 5.22. Equal area projection showing poles to planes of FIP orientations from sample LI1 combined with homogenisation temperature (°C) from secondary fluid inclusions contained within them.

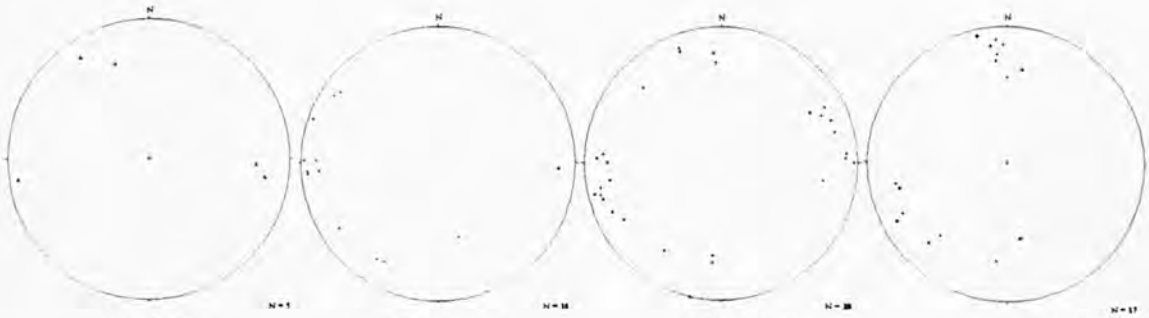

(a) 0-3 (b) 3.1-6 (d) 6.1-9 (e) >9.1

Fig. 5.23. Equal area projection showing poles to planes of FIP orientations from sample LI1 combined with salinity (wt. %. equiv. NaCl) of secondary fluid inclusions contained within them.

Based upon the evolution of the hydrothermal fluids, it is postulated that the N-S oriented FIPs are relatively younger than the E-W oriented FIPs, since the fluids contained within them are cooler and less saline. This assumes a simple cooling of the hydrothermal fluids, together with mixing with less saline fluids, during the evolution of the fracture system.

Characterisation of FIP formation

At temperatures above 200°C thermal stresses are thought to play an important role in the fracturing process (Wang *et al.*, 1989) and the formation of FIPs. Homogenisation temperature data shows that FIPs with temperatures above 250°C possess NW-SE and E-W orientations in the Lundy granite. The orientations of these FIPs does, however, suggest an affinity with a stress regime associated with sinistral movement along the SLFZ. Therefore although FIPs may be formed due to thermal stresses, their orientations are governed by the orientations of the regional stress regime. FIPs with a NW-SE orientation are inferred to be Riedel shears (*mode II* fractures) while FIPs oriented E-W are inferred to be tensile FIPs (*mode I* fractures). The morphological characteristics of these two FIP groups have been shown to be different (see 5.3.2; also

3.3.2). NW-SE oriented FIPs are typically intergranular, are rarely isolated (initiate or terminate at grain boundaries or other healed fractures) and may possess inclusions with preferred shape orientation parallel to the FIP. FIPs oriented E-W are generally intracrystalline, commonly isolated and do not exhibit a preferred shape orientation of the fluid inclusion contained within them. FIPs oriented N-S possess morphological characteristics similar to E-W FIPs, though they possess generally lower homogenisation temperatures, and are therefore thought to be less influenced by thermal stresses.

FIPs that are thought to be the result of thermal stresses developing within the cooling granite are presumed to be formed by the differences in thermal contraction\expansion of the mineral assemblage (see section 2.2.1). The principal differences occur between quartz and feldspar (Richter and Simmons, 1974; Plumb *et al.*, 1984), and as a result, a significant proportion of thermal fractures are observed propagating from quartz-feldspar grain boundaries, which possess orientations, related to the regional stress regime at the time. This is observed in several of the Dartmoor samples (Fig. 5.11) for FIPs with orientations NE-SW and NW-SE, and is generally verified by the high homogenisation temperatures that may be observed in these FIPs.

Proposed movement history of the SLFZ

It is postulated that a movement history of the Sticklepath-Lustleigh Fault Zone (SLFZ) can be inferred from the relative ages of FIP orientations observed within quartz from the Lundy and Variscan granites. Preferred FIP orientations have been shown to exist, and will be shown to be related to more than one orientation of the regional stress regime, based upon their orientation, morphology and thermometric characteristics.

There has been much discussion in the literature regarding the movement history of the SLFZ and the associated formation of sedimentary basins since the end of the Variscan orogeny, throughout the Mesozoic the Cenozoic and up to the present day. Dearman (1963) and Shearman (1967) envisaged large amounts of dextral movement during the Tertiary, which has now been discounted by more recent work by Holloway and Chadwick (1986) who proposed that the dextral movement occurred along the SLFZ from end-Variscan times though to the Permo-Triassic. Holloway and Chadwick (*op. cit.*) concluded that sinistral movement occurred during early-Tertiary times (6km) with only minor dextral movement in mid- to late-Tertiary times, based upon the shape of pull-apart basins and the formation of minor faults which may represent Riedel and conjugate Riedel shears (Fig. 5.24). This is in agreement with Arthur (1989) who described the evolution of the Lundy pull-apart basin, being created by 28-40km of Tertiary sinistral strike-slip faulting along the left stepping SLFZ. Subsequent relatively minor dextral faulting along the SLFZ resulted in the inversion of the graben to form the Lundy Rhomb Horst.

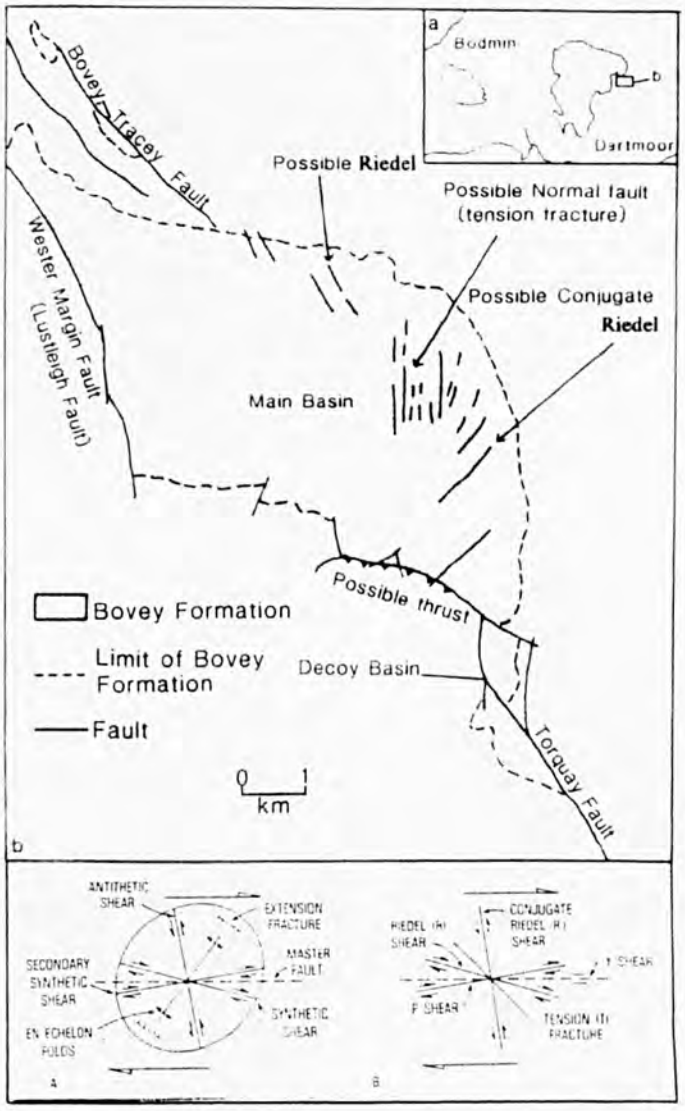

Fig. 5.24. Proposed origin of the Bovey Tracey Basin by sinistral movement along the left-stepping Lustleigh Torquay FZ. Late dextral movements may be inferred if minor faults affecting the Bovey Formation represent Riedel shears, conjugate Riedel shears and tension fractures associated with a dextral shear couple (after Holloway and Chadwick, 1986; Christie-Blick and Biddle, 1985).

The tectonic evolution of the NW Europe since the end of the Variscan orogeny is a story of rifting, basin formation, subsidence and inversion (see Ziegler 1987a, 1987b) for review). Rifting occurred in the Western Approaches Trough from Permian to Aptian times (Ziegler, 1987a), with late Oligocene to Miocene compressional deformations and inversions related to Alpine collision and possible Pyrenean deformation. The Mesozoic rift systems of the Celtic Sea-Western Approaches came into evidence during the Permo(?)-Triassic and remained active until the Aptian crustal separation of the Bay of Biscay (Ziegler, 1987c). These basins terminated to the NE along a complex set of wrench faults, the main element being the SLFZ (*op. cit.*). The South Celtic Sea-Bristol Channel basin originated due to the extensional reactivation of Hercynian thrust zones

during the Permian(?) and Triassic, with minor inversions associated with dextral strike-slip movements in the late Jurassic and early Cretaceous (Van Hoorn, 1987). The SLFZ controlled the development of the western part of the Wessex basin, and represented the reactivation of late Hercynian basement structures, and its sinistral motion throughout the late Palaeozoic and Mesozoic allowed the development of the Channel Basin (Lake and Karner, 1987)

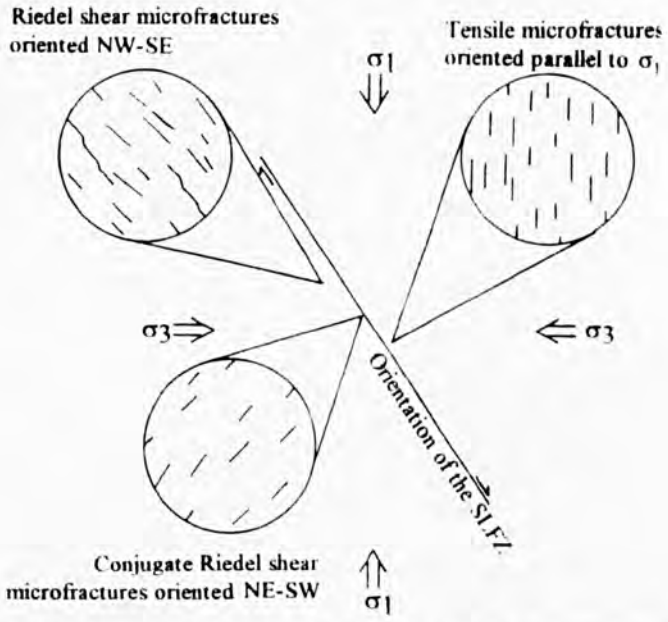

Fig. 5.25. Orientation of healed microfractures in relation to dextral movement along the NW-SE striking Sticklepath-Lustleigh Fault Zone (SLFZ). N-S FIPs represent healed tensile (*mode I*) fractures. NW-SE and NE-SW striking FIPs represent healed dilatant shear (*mode II*) Riedel and conjugate Riedel shear fractures respectively.

FIP orientation data from NE Dartmoor are generally interpreted as Riedel and conjugate Riedel shears and *mode I* extension fractures, oriented N-S associated with dextral strike-slip faulting along the SLFZ (Fig. 5.25). These FIPs have already been interpreted in Chapter 4, as Permo(?)-Triassic in age (Scrivener *et al.*, 1994). Figure 5.26 depicts the evolution of the study area and SW England during late-Variscan to Permo-Triassic times where initial Arctic-North Atlantic rifting results in dextral strike-slip movements along NW-SE reactivated Variscan Basement structures which is associated with the development of N-S cross-course mineralisation and of N-S striking FIPs (see also Chapter 4). High salinity $CaCl_2$/NaCl bearing basinal brines move up-dip along strike-slip faults from sedimentary basins (Western Approaches Trough, South Celtic Sea/Bristol Channel Graben), forming episodic hydraulic vein structures. Initial movements and deformation of the granites may result in intense microfracturing (see section 2.2.3), possibly resulting in hydrothermal argillic alteration.

The formation of E-W and N-S striking FIPs within the Lundy granite represent tensile fractures associated with sinistral and dextral shearing respectively (Christie-Blick and Biddle, 1985), forming parallel to σ_1 and perpendicular to σ_3 (Fig. 4.8). Thus, FIP

orientation data from Lundy imply that both sinistral and dextral movements along the SLFZ, and possibly other NW-SE striking strike-slip faults, have occurred since the emplacement of the granite. Based upon the evolution of fluids associated with the Lundy granite it can be inferred that the E-W FIPs are older than the N-S FIPs.

The present data is in agreement with previous work (Holloway and Chadwick, 1986; Arthur, 1989) concerning the movement history of the SLFZ during Tertiary times. The data implies that sinistral strike-slip faulting, or a stress regime conducive to sinistral strike-slip faulting was operating shortly after the emplacement of the granite. Temperature data for these E-W FIPs does suggest that some cooling of the granite took place before extensive microfracturing was induced. The granite has been dated at 58.7± 1.6Ma (Thorpe *et al.*, 1990), placing it in the mid- to late Palaeocene. Sinistral movement along the SLFZ has been inferred by Holloway and Chadwick (1986) and Arthur (1989) during Eocene-Oligocene times (Fig. 5.27). This is not in agreement with Bristow and Robson (1994), who conclude that the formation of the Bovey Tracey basin originated from dextral strike-slip movement at a right offset along the SLFZ associated with transtension in the Eocene and transpression in the Oligocene (Fig. 5.5). However, the conclusion of dextral strike-slip is based upon the interpretation of the geometry of the Bovey Basin, and does not take into account the any offshore data and structure associated with the Lundy Rhomb Horst.

Figure 5.27 illustrates the evolution of the study area during the early the tertiary. Emplacement of the Lundy granite and dyke swarm is contemporaneous with the formation of the Lundy Rhomb Graben. Sinistral movement along NW-SE striking strike-slip faults is associated with left lateral transtension along southern margin of the Bristol Channel basin, contemporaneous with Mesozoic basin inversion, early Alpine deformation and Atlantic Rifting. Development of E-W tensile striking FIPs and NW-SE striking shear FIPs in the Lundy granite are inferred to represent a sinistral shear couple with the NW-SE striking SLFZ. Movement of high salinity $CaCl_2$/NaCl bearing basinal brines is not observed in E-W FIPs in Lundy or in Dartmoor, suggesting that fluid migration ended with on-set of basin inversion.

North-South oriented FIPs, generally associated with lower temperature, lower salinity fluids observed in the Lundy granites are inferred to have formed during the mid- to late Tertiary (Fig. 5.28), associated with dextral shearing and in agreement with Holloway and Chadwick (1986) who suggest that minor faults observed within the Bovey Basin represent possible Riedel shears (and likely extension fractures for the N-S faults). This

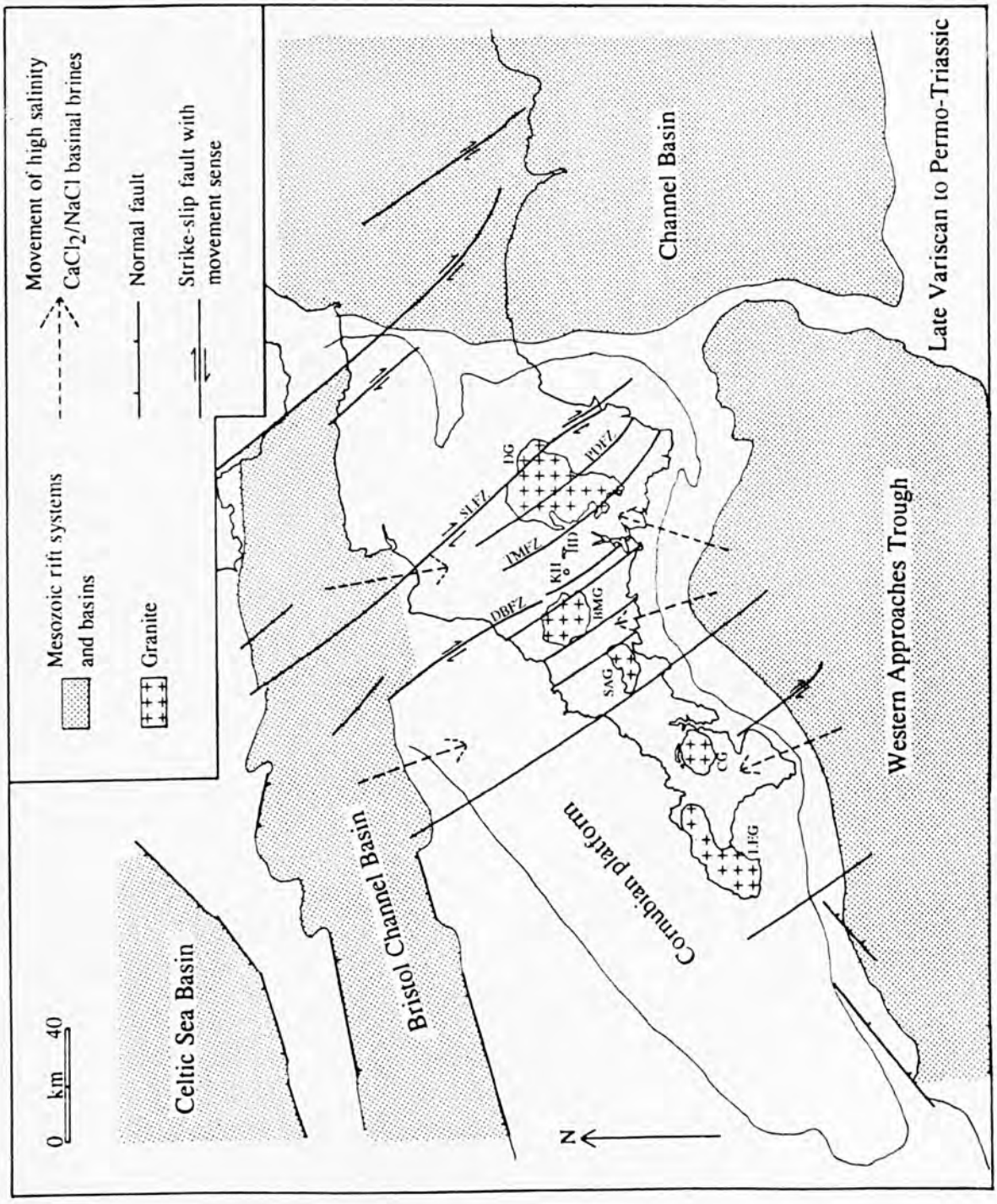

Fig. 5.26.. Evolution of the study area during late-Variscan to Permo-Triassic times. Based upon Holloway and Chadwick (1986); Lake and Karner (1987); Shepherd and Scrivener (1987); Ziegler (1987a) Ziegler (1987c); Scrivener *et al.*, (1994) and other references quoted in the text. DG = Dartmoor granite; HD = Hingston down; KH = Kit Hill; BMG = Bodmin Moor Granite; SAG = St. Austell Granite; CG = Carnmenellis Granite; LEG = Lands End Granite; SLFZ = Sticklepath-Lustleigh Fault Zone; PDFZ = Prewley-Dartmoor FZ; TMFZ = Tavistock-Modbury FZ.

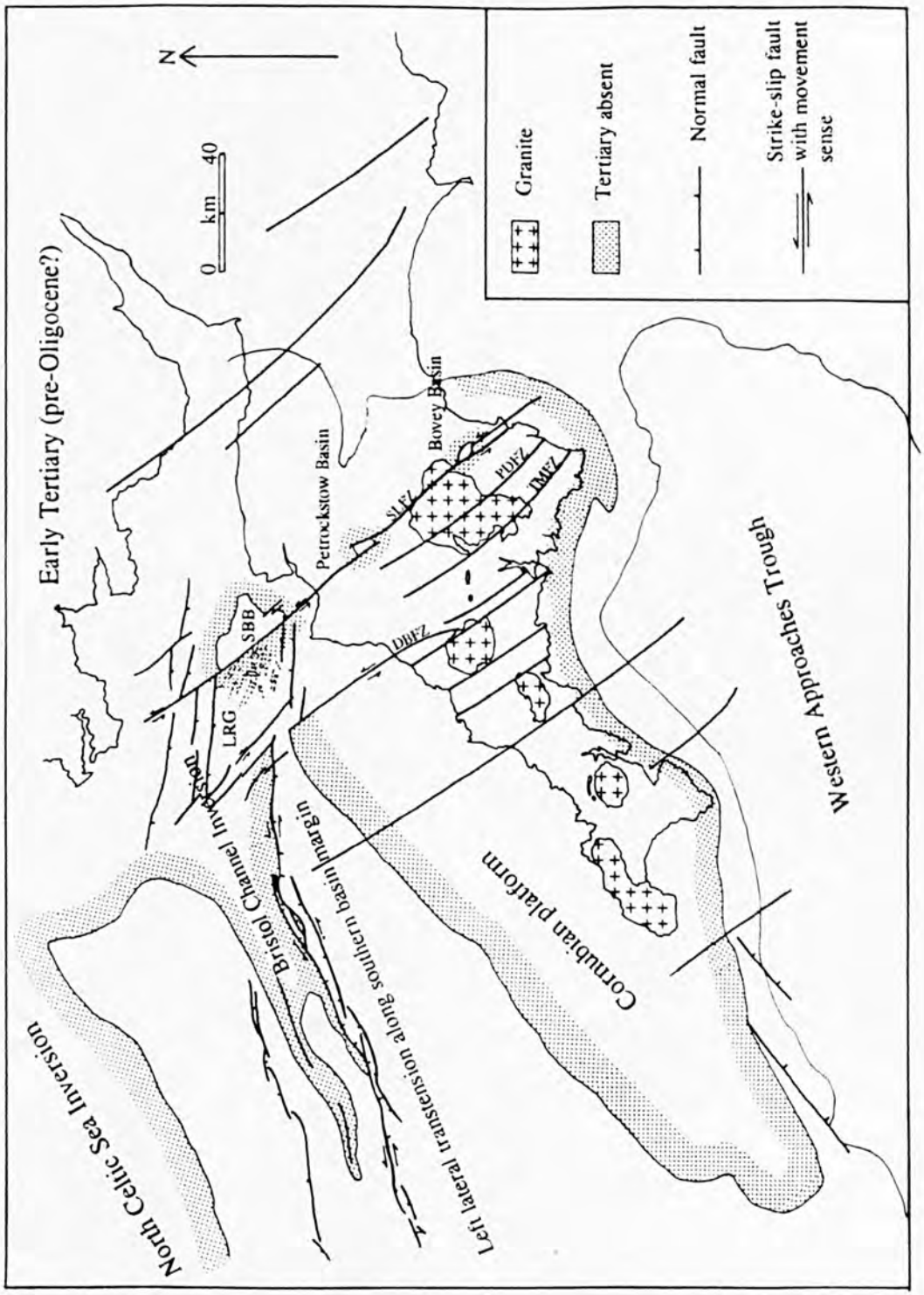

Fig. 5.27. Evolution of the study area during the early-Tertiary (Palaeocene-Oligocene?) times. Based upon Holloway and Chadwick, (1986); Lake and Karner (1987); Ziegler (1987a); Ziegler (1987b); Ziegler (1987c); Van Hoorn (1987); Arthur (1989). L = Lundy; LRG = Lundy Rhomb Graben; SBB = Stanley Banks Basin; see Fig. 5.26 for other definitions.

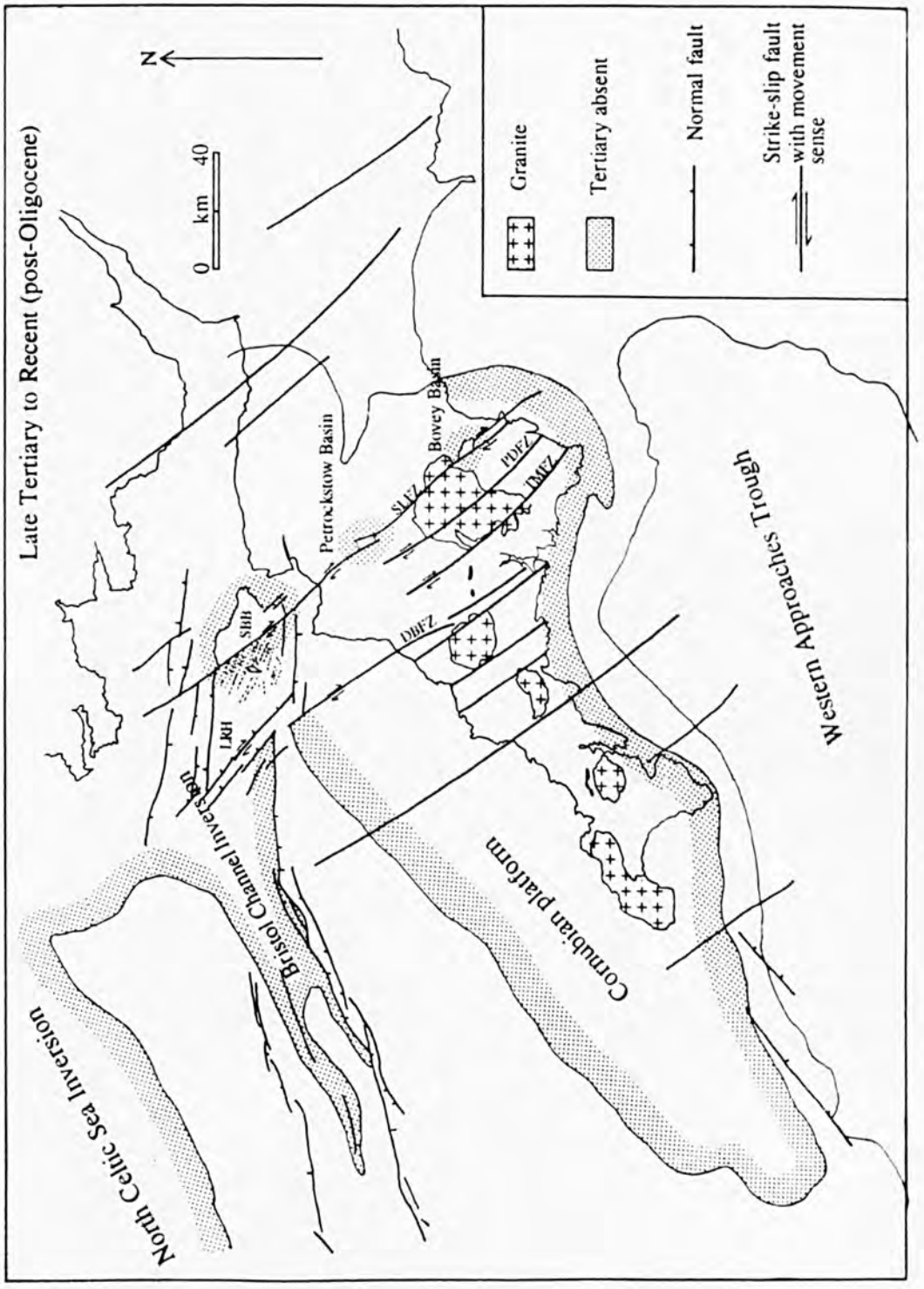

Fig. 5.28. Evolution of the study area during mid-Tertiary to Recent (post-Oligocene?) times. Based upon Holloway and Chadwick, (1986); Lake and Karner (1987); Ziegler (1987a); Ziegler (1987b); Ziegler (1987c); Van Hoorn (1987); Arthur (1989); Bristow and Robson (1994). LRH = Lundy Rhomb Horst; see Figs. 5.26 and 5.27 for other definitions.

is also in agreement with Bristow and Robson (1989) and Arthur (1989). Figure 5.28 illustrates the evolution of the study area and SW England during the mid- to late Tertiary times. Latest dextral strike-slip movements along the SLFZ result in the transformation of the Lundy Rhomb Graben into the Lundy Rhomb Horst and the deformation the Bovey Formation (of Oligocene age) in the Bovey Basin. Development of N-S striking tensile FIPs and NW-SE striking shear FIPs in the Lundy granite is inferred to represent a dextral shear couple with the NW-SE striking SLFZ.

In contradiction to the FIP data, the presence of the Lundy Dyke swarm, which post-date the granite, with ages ranging from 51.9±3Ma to 56.1±4Ma (Edmonds *et al.*, 1979) and 56.4±3 (Mussett *et al.*, 1988), imply a late Palaeocene to early Eocene age. They have an orientation consistent with the orientation of the Tertiary dyke swarm of NW Scotland and N. Ireland, striking NW-SE (Speight *et al.*, 1982).

Previous authors have shown that dykes may represent tensile hydraulic fractures (see Pollard, 1984 for review), with the magma pressure being equivalent to the fluid pressure (Delaney, 1986). It can then be inferred that the dykes formed parallel to σ_1, with their opening direction parallel to σ_3 (Fig. 5.29.), implying a slightly different orientation of the regional stress regime to that inferred by the orientation of the FIP data. This difference in orientation may be explained by the existence of a pre-existing shear fracture set associated with faulting along the SLFZ, which would open preferentially (Ramsay, 1967), as opposed to the formation of new east-west fractures. Arthur (1989) used the orientations of the Lundy dyke swarm to determine the palaeostress orientations, that was in existence during the formation of the Lundy Rhomb Graben. However, there is a considerable spread in time over the period of dyke intrusion (Table 5.1) and it is possible that there may have been variations in the palaeostress orientation during this time. It would therefore be an over simplification to suggest that the palaeostress orientation inferred from the dyke orientations was contemporaneous with that of granite intrusion and graben formation (McCaffrey *et al.*, 1993). Angular differences between the major orientations of the dyke swarm and the orientations of the E-W striking FIPs which are thought to have been formed during the same sinistral shearing event, may be explained by the presence of stress refraction due to the competence contrast between the Lundy granite and the surrounding meta-sedimentary rocks (Strömgård, 1973; McCaffrey *et al.*, 1993) However, considering the dyke swarm is of similar orientation to the dyke swarm of the British Tertiary Volcanic Province (BTVP) to the north, and Oligocene dykes on the Dingle Peninsular in west Ireland, it is likely they are related to tectonic activity along a broadly NNW-SSE striking extensional fracture (Horne and Macintyre, 1975). This suggests a NE-SW extensional stress field existing in the Palaeocene, changing to NW-SE extension in the Eocene (England, 1988). Figure 5.30 shows a summary of important events occurring within the study

area against time specifically in relation to deformation, intrusion, basin development and FIP formation.

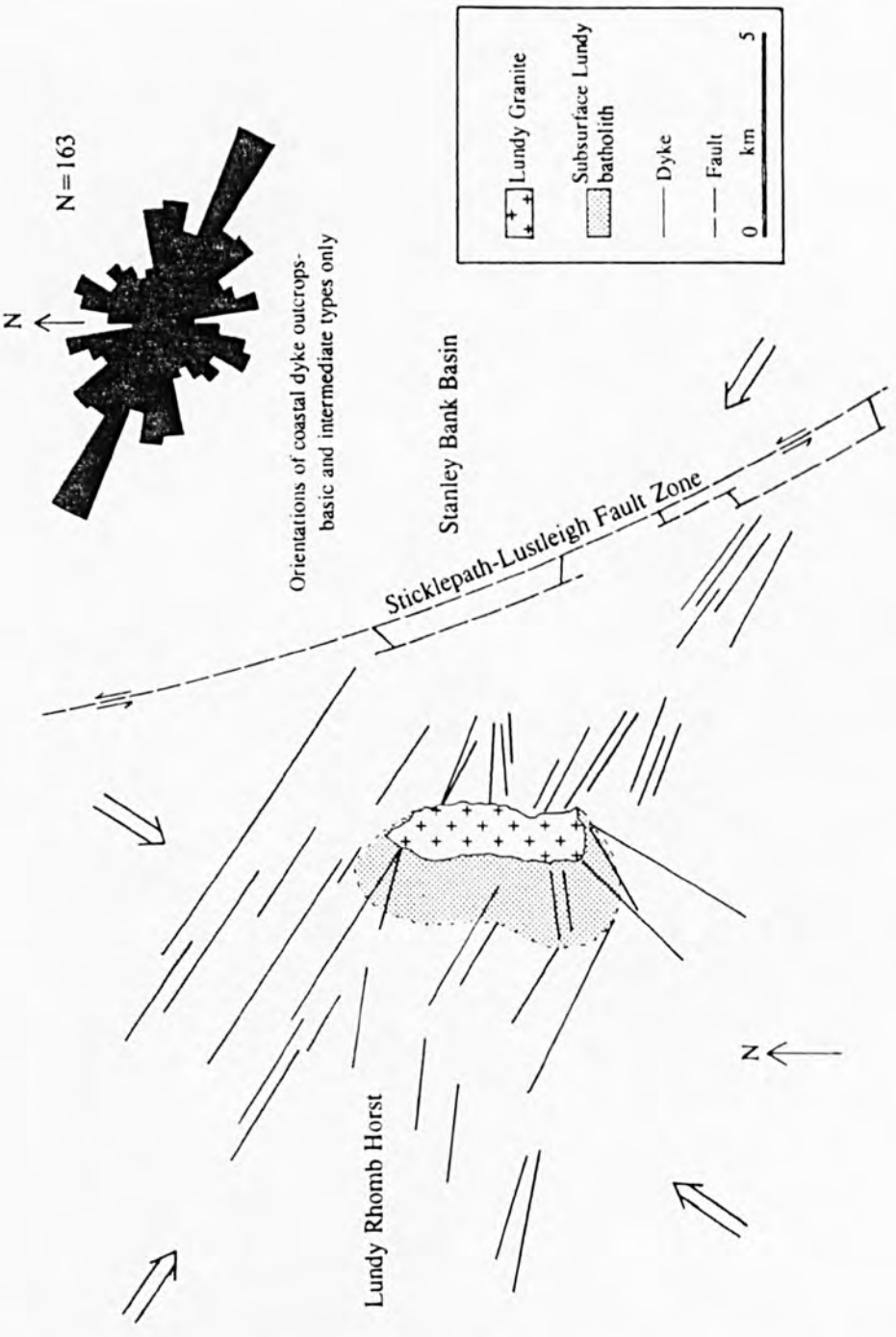

Fig. 5.29. Possible inferred orientations of the regional principal compressive stress axis during emplacement of the Lundy Dyke swarm (see text) (Hains *et al.*, 1983). Rose diagram represents the orientations of coastal dyke outcrops on Lundy (after Roberts and Smith, 1994). Assuming that dykes represent tensile fractures, a deduction of a sinistral shear couple may be inferred from the angular relationship between the orientation of the principal compressive stress axes and the orientation of the Sticklepath-Lustleigh FZ.

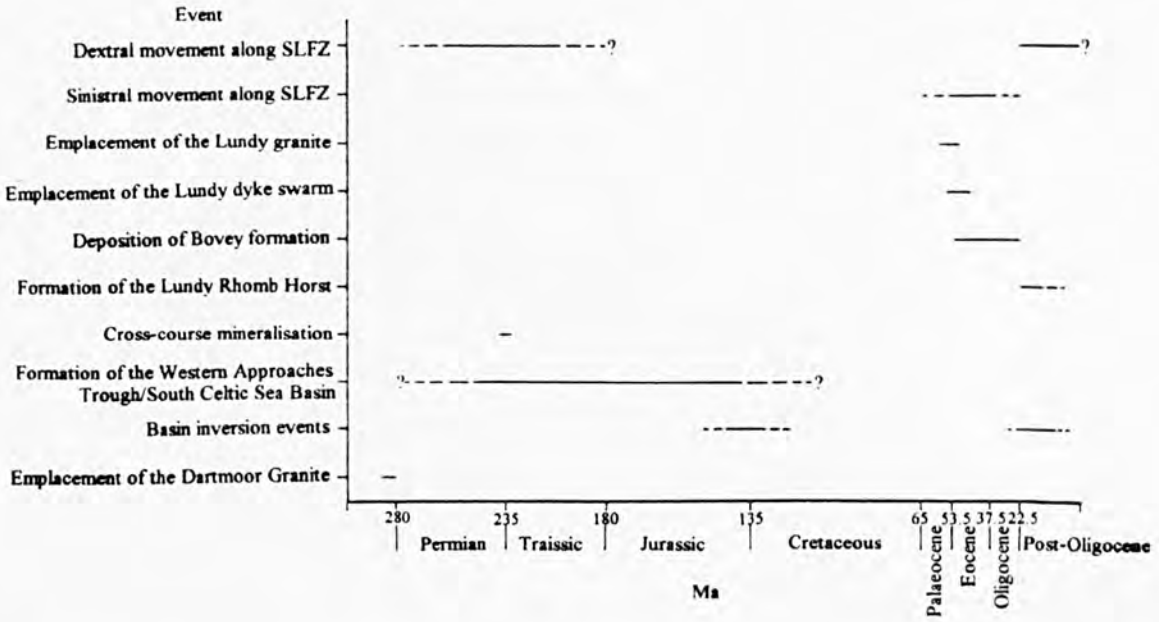

Fig. 5.30 Important events discussed in the text occurring within the study area and surrounding region since post-Variscan times.

5.4 Summary and conclusions

5.4.1 Conclusions

Fluid Inclusion Planes in granites from Lundy and NE Dartmoor have been shown to be formed to some extent by thermal stresses (see also Chapters 2 and 3), but mainly due to tectonic deformation related to the movement of the SLFZ. As a result of the orientation and thermometric analysis, the morphologies of the FIPs and the inclusions within them have also been characterised. These morphologies are inferred to be associated with the origin of the FIP together with its mode of fracturing. The following conclusions have been reached:

(i) FIPs may be characterised as tensile (*mode I*) or dilatant shear (hybrid *mode II*) fractures based upon their orientation and morphology. They may be further related to the stresses that were responsible for their formation These stresses may be classified as one of the following:

(a) thermal: related to volumetric expansivity contrasts between quartz and feldspar upon cooling of the granite

(b) hydraulic: fracturing results from high fluid pressures.

(c) tectonic: high deviatoric stresses resulting from active faulting

(ii) The presence of a preferred shape orientation of fluid inclusions in FIPs of certain orientations suggests that their shape may be related to the mode of fracturing of the FIP, together with the temperature and salinity of the fluids that healed them (see also Chapter 6 for further discussion).

(iii) Evolution of the Lundy hydrothermal fluids is illustrated as possible early high temperature magmatic-hydrothermal fluids mixing with cooler less saline (possibly meteoric) fluids. This is likely to coincide with the transformation of the Lundy Rhomb Graben into the Lundy Rhomb Horst, related to a re-orientation of the regional stress regime, based upon the formation of early E-W, and later N-S tensile fractures. The orientation of FIPs from the Lundy granite compare well with data obtained from the Dartmoor granite close to the surface trace of the SLFZ.

(iv) Orientations of tensile FIPs are related to dextral and sinistral shear couples associated with the reactivation of the SLFZ from Variscan to recent times. It is thus possible to use FIP orientations in conjunction with an evolving hydrothermal system to reconstruct the movement of a major fault.

5.4.2 Further work

Detailed analysis of FIPs from samples in proximity to a major strike-slip fault exhibiting considerable movement have been used to reconstruct its movement history. Important observations and conclusions have been made concerning the formation and characterisation of FIPs and the inclusions contained within them. The techniques outlined could be used to investigate the tectonic and thermal history of other regions where active faulting accompanies hydrothermal fluid flow. However, several points have been raised which need further clarification and are listed below:

(i) Tentative conclusions concerning the possible preferred shape orientation of inclusions within an FIP have been made in relation to its mode of fracturing. However, although a preferred shape orientation in some FIPs was observed, other inclusions in FIPs of the same or different orientations showed great morphological variations. Further analysis of these morphological variations is needed in relation to other governing factors e.g. temperature and chemistry of the fluids, age of the inclusions, the affect of later deformations or heating.

(ii) Some FIPs have been classified as the product of thermal stresses during the cooling of the granite. However, the parameters which control the formation of FIPs by thermal stresses are not yet been fully evaluated. These parameters include the temperature limits, both upper but more importantly the lower limit at which thermal stresses are not

thought to be important (an arbitrary value of 200°C was used for the Lundy granite and throughout this study), and the relationship of FIP propagation to grain boundaries (specifically quartz-feldspar boundaries).

(iii) Further work directly related this field area include the clarification of the Lundy hydrothermal fluids, specifically their origin and evolution. The use of stable isotopes would be invaluable in this respect, although the practical analysis of samples containing many inclusions of different ages would be difficult, making techniques such as crush-leach of little use.

CHAPTER 6

GENERAL DISCUSSION, OVERVIEW AND PROPOSED CLASSIFICATION SCHEME OF FIPS AND THEIR GEOLOGICAL SIGNIFICANCE.

6.0 Introduction

The previous three chapters have shown that FIPs may be used to identify the evolution of a fracture network within a changing stress regime, from granite intrusion to brittle deformation associated with the most recent tectonic movements. FIPs have been shown to be formed by stresses which possess varying origins (thermal, tectonic, and hydraulic). This chapter will attempt to characterise and classify the formation of Fluid Inclusion Planes in relation to their origins, with respect to: (i) stresses that are responsible for their generation, (ii) their mode of fracturing and, (iii) the thermo-chemical properties of the fluids that healed them. Results from all three study areas will be combined to provide a synthesis, overview and generalised classification of FIPs with special reference to the following:

(i) Characterise FIP morphologies, which have shown to be typically planar, curvi-planar or possess a more complex shape in respect to their mode of fracturing.

(ii) Characterise FIPs in relation to the stresses responsible for their origin i.e. thermal, hydraulic tectonic.

(iii) Relate the preferred shape orientations possessed by some secondary inclusions to the mode of fracturing, illustrating the importance of the thermo-chemical aspects of the fluids found within it. This is of special importance in relation to re-equilibration of the inclusion morphology, and the healing rate/fracturing rate of the FIP.

This is the first such attempt at providing a generalised model for understanding the shape and distribution of FIPs in crystalline rocks. It's potential applications (and limitations) are also discussed in this chapter.

6.1 FIP morphologies

FIP morphologies have been characterised over the previous three chapters as generally being either planar, curvi-planar, sinusoidal or complex. It has generally been implied that the type of FIP generated is related to the mode of failure of the original fracture. Generally previous studies (e.g. Kowallis *et al.*, 1987; Ren *et al.*, 1989; Lespinasse and Cathelineau 1990; Boullier *et al.*, 1991) have characterised healed microfractures as tensile cracks, forming parallel to the maximum principal stress direction (σ_1). However, in the thesis, healed fractures have been identified (see 3.3.2, plate 3.1; 4.3.1, plate 4.1, 5.3.2, plate 5.4), that are thought to possess lateral offsetting of the fracture walls, which are therefore defined as dilatant shear fractures. The proposed criteria for classifying shear microfractures includes: orientation of the FIP, offsetting of earlier fractures and the morphology of the FIP.

6.1.1 Planar FIPs

Planar, intragranular FIPs in granitic quartz are believed by the author to mostly represent healed tensile fractures. Mostly these are thought to be the product of thermal contraction mismatch/anisotropy (Carlson *et al.*, 1990) between different minerals (quartz, feldspar and biotite) due to the large thermal expansivity and compressibility contrasts (Rosenfield and Chase, 1961; Devore, 1969; Nur and Simmons, 1970; Voight and St. Pierre, 1974; Savage, 1978) but some may also be produced by dilatancy (Ismail and Murrell, 1976) prior to faulting, especially when high fluid pressures are involved (Sibson, 1990). Fig. 6.1 shows idealised tensile fractures (partly after Tapponnier and Brace, 1976) and the healed fractures most commonly observed during the course of the present study. Isolated tensile microfractures (6.1a) are generally presumed to be generated by dilatancy associated with large scale strike-slip faulting.

Large, intergranular, planar FIPs are also commonly observed (see section 3.3.2, 4.3.1 and 5.3.2). Although not as abundant as intragranular fractures, they are not uncommon. These FIPs regularly traverse one or more grain boundaries and may represent healed dilatant shear (defined here as *mode II* see 2.1.2) fractures. The lack of direct evidence for the lateral offsetting along FIPs, observed in the granites during the present study and also by other authors is discussed below (section 6.2.3).

6.1.2 Curvi-planar FIPs

FIPs with a curvi-planar morphology were commonly observed in most samples studied here. The formation of these 'curved propagation' fronts is not clear, but they may be related to changes in the orientation of stress fields on the grain scale. On a macroscale Pollard (1987) has shown that curved fractures occupied by dykes may be generated by

mixed tensile/shear (*mode I*, II) fracturing, induced by the spatial rotation of the least compressive stress about an axis parallel to the dyke periphery. This may be analogous to the formation of curved FIPs if grain rotation due to grain boundary sliding occurs during fracture propagation. It is likely that curvi-planar FIPs are generated by tectonic stresses, although it is difficult to relate their orientation to other macro-structures (as discussed in sections 3.3.2 and 5.3.2). Cotterell and Rice (1980) predict the stress intensity factors for a slightly curved or kinked crack. They postulate that this type of mixed mode (*mode I*, II) fracture is characterised by *mode I* loading conditions at the advancing tip.

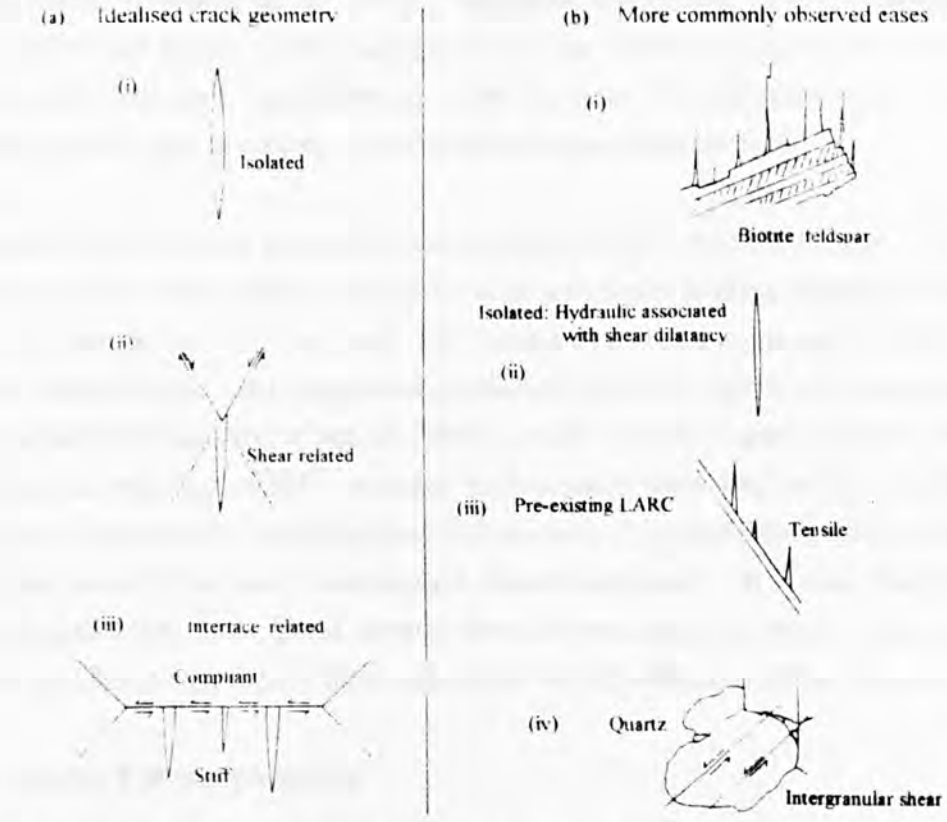

Fig. 6.1a. Idealised crack geometry (after Tapponnier and Brace; 1976). (i) Isolated, no interaction with grain boundaries and other healed fractures. (ii) Tensile FIP resulting from the interaction of two shear fractures. (iii) Tensile FIPs resulting from compressibility contrasts of adjacent minerals during grain boundary sliding. Fig.6.1b. FIPs commonly observed during course of the present study. (i) Tensile FIPs related to differences in thermal contraction of adjacent minerals. (ii) Isolated, associated with hydraulic stresses and shear dilatancy. (iii) Tensile FIPs associated with pre-existing LARC. (iv) Large shear intergranular healed fractures.

6.1.3 Sinusoidal FIPs

Sinusoidal FIPs were commonly observed in several samples (Fig. 5.12d and Plate 5.1). These are thought to represent *mode II* dilatant shear fractures. The curved segments within these FIPs are analogous to releasing bends (see Fig. 6.2a) observed in macroscopic strike-slip faults (Christie-Blick and Biddle, 1985) and are thought to represent tensile sections (or more accurately transtension) within the FIP (Fig. 6.2b).

Likewise, lateral offsetting of the fracture walls occurs along the straight sections (Fig. 6.2b(i)). It is these sections of the FIP, which have orientations similar to the orientation of major strike-slip faults, and are classified as Riedel shears. Actual lateral off-setting of other fractures and grain boundaries was only rarely observed (Plate 5.4), although direct proof was recorded in a number of cases with respect to sinusoidal FIPs (Fig. 5.14c, Plate 5.4).

Other authors have also had difficulty in observing shear fractures in rocks which have been stressed to near peak stresses (Paulding, 1965; Friedman *et al.*, 1970; Peng and Johnson, 1972; Hallbauer *et al.*, 1973; Tapponier and Brace, 1976). Tapponier and Brace, (1976) and Kranz (1983) suggested that the lack of evidence of off-setting of other fractures and grain boundaries by shear fractures was generally due to the small amounts of off-set that are likely to be exhibited (approximately 5μm).

Sinusoidal FIPs have thus generally been classified in this study as *mode II* fractures, related to tectonic deformation associated with strike-slip faulting present in the study area. It is thought unlikely that such FIPs could have been generated by thermal and hydraulic stresses alone. It is important to consider that the majority of previous studies have classified the majority, if not all FIPs as *mode I* tensile fractures and it should be stated that the majority of FIPs recorded in this study were also *mode I* fractures. It should also be noted that fractures classified as *mode II*, contain fluid inclusions and are thus hybrid *mode II* fractures, containing a tensile component. It is also likely that they have undergone the same, if not greater amount movement as *mode I* fractures (in a direction parallel to σ_3), as they have undergone lateral off-setting of the fracture walls.

6.1.4 Complex FIP morphologies

FIPs displaying more complex morphologies were also observed, albeit rarely in a number of samples. These included left and right stepping offsets (en-echelon arrays) and duplex structures (Fig. 5.3) analogous to those associated with strike-slip faults, described by Woodcock and Fischer (1986). The formation of these strike-slip duplexes may be by a process analogous to the sequential imbrication of ramps on dip-slip faults, or by the initiation of non-sequential 'Riedel' fractures at fault offsets or on straight fault segments (*op. cit.*). The orientation of these straight FIP segments has been shown to be similar to that of strike-slip faults in the sample areas, implying their *mode II* nature and possible origin as Riedel shears. Fig. 6.2b shows idealised structures associated with a dextral strike-slip system (after Woodcock and Fischer, 1986) and the morphologies of the more commonly observed FIPs. The presence of a fluid phase within the healed fractures indicates tensile opening must have occurred within these duplex structures. It is therefore unlikely that they could represent contractional structures, generated from

restraining bends. Therefore a tentative movement direction may be implied from the structures, assuming that they represent extensional features (Fig. 6.2b).

The origins of FIPs exhibiting complex morphologies are regarded as being formed by tectonic stresses, resulting from fault propagation and fault movement. There is still debate concerning the timing of microfracture development in respect to fault propagation, post-failure slip and reactivation (Hallbauer et al., 1973; Lockner and Byerlee, 1977). A relative chronology based upon the thermo-chemical characteristics of the fluids that are contained within these FIPs indicates that they may be generated during post-failure slip along the fault, as well as possibly during the initial failure of the rock as the fault propagates (see section 2.2.3).

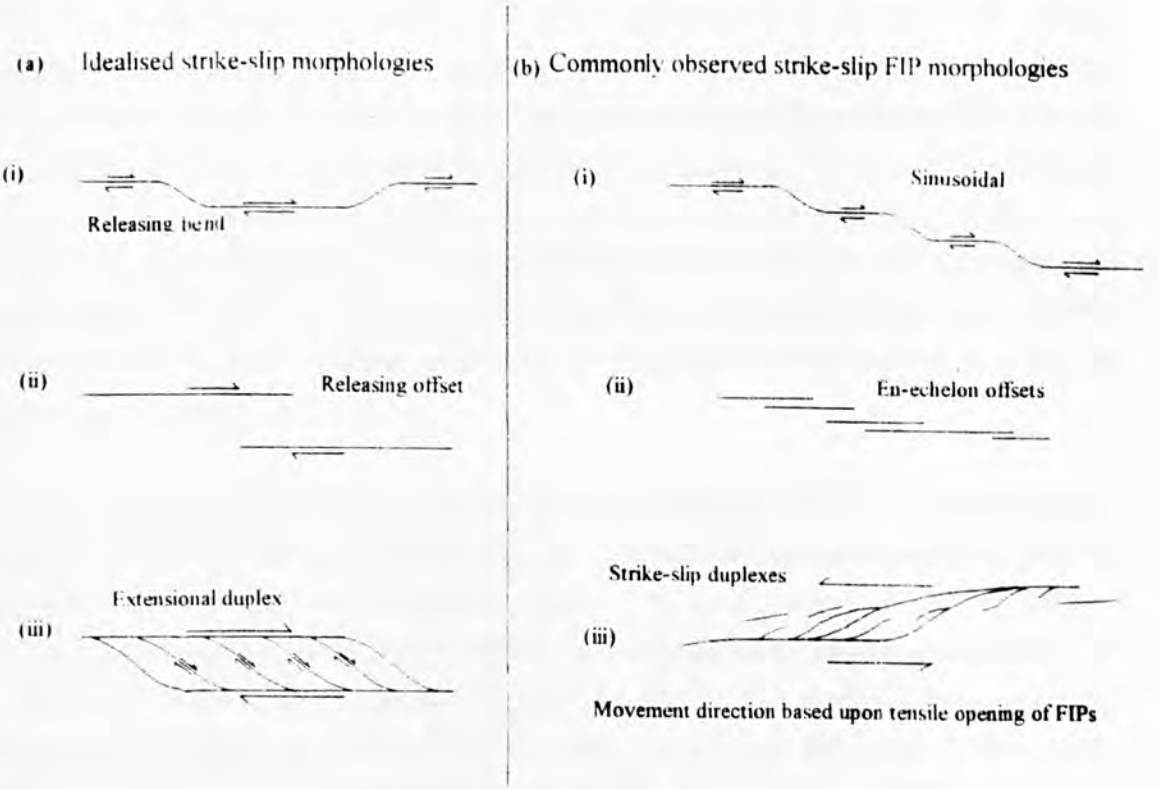

Fig. 6.2a Idealised strike-slip morphologies (after Woodcock and Fischer, 1986). Fig.6.2(b) morphologies of dilatant-shear FIPs commonly observed during the present study.

6.2 FIP origins

One of the most important conclusions of the present study is that it is possible to characterise FIPs in relation to the stresses responsible for their origin. In this study the majority of FIPs have been shown to have formed by thermal and tectonic stresses together with minor cases of hydraulic fracturing. However, it is also believed that FIPs

are generally the result of a combination of two or more of these stresses. The following section attempts to summarise the characteristics observed in FIPs which may be indicative of these stresses.

6.2.1 FIPs resulting from thermal stresses

A great many FIPs observed in quartz are potentially formed due to its differential thermal contraction compared to feldspar (see section 2.2.1). During isobaric cooling of a granite, quartz crystals surrounded by feldspar will preferentially undergo tensile fracturing since:

$$\Delta V_{QTZ} > \Delta V_{FELD}$$

where ΔV is the change in volume of quartz and feldspar (Carlson *et al.*, 1990). Resulting FIPs are believed to occur in the samples as intragranular tensile fractures (Fig. 6.1d) and are generally observed to propagate from quartz/feldspar boundaries into the quartz grain which is in agreement with Tapponnier and Brace (1976) and Fredrich and Wong (1986). Thermal fractures propagating from a quartz/feldspar boundary may traverse the entire quartz grain, although generally they are arrested after a short distance due to a decrease in stress intensity with increasing crack length (Wang *et al.*, 1989). The propagation fronts of these FIPs may be identified by the notable decrease in inclusion size towards the crack tip.

The homogenisation temperature of secondary inclusions may also be an indication of whether the FIP is a result of thermal stresses. Thermal stresses are thought to play an important role in the microfracturing process at temperatures down to 200°C. Therefore, FIPs containing inclusions exhibiting homogenisation temperatures above 200 °C may have their origins related to thermal stress. The highest homogenisation temperatures generally recorded from all the field areas were in the range of 350-440°C. With an approximate pressure correction of possibly up to 100°C (typically expected in granites cooling at depths of around 5km), trapping temperatures are still below 550°C. It is therefore presumed likely that these high temperatures FIPs are also the result of thermal contraction differences between quartz and feldspar upon cooling and not related to the α-β transition temperature of quartz at 573°C, which would result in internal stresses being generated in the quartz grain, possibly resulting in fracturing (Sterner, 1990) However, rounded opaque (or nearly opaque) inclusions believed to be vapour rich monophase types (see Figs. 3.19and 4.11) may represent early high temperature inclusions. These FIPs may be the result of fracturing and healing processes above the α -β transition temperature, and therefore the result of internal stresses within the quartz

grain. Their orientation may be related to the quartz *c*-axis (Cox, 1995, *pers. comm.*) though this is could not be demonstrated.

6.2.2 FIPs resulting from tectonic stresses

During this study, FIPs have also been characterised as being the result of tectonic stresses, or more precisely stresses occurring in the proximity to a fault, prior to or during faulting. FIPs generated by tectonic stresses may be classified as tensile or shear fractures, depending upon the type of faulting and their orientation relative to the fault. FIPs representing tensile fractures are interpreted to commonly form in areas undergoing active normal faulting associated with crustal extension. They have also been shown to form associated with strike-slip faults, especially when faulting is accompanied by high fluid pressures.

Tensile FIPs occur parallel to σ_1 and perpendicular to σ_3. They are generally simple, intracrystalline, planar fractures, terminating at grain boundaries. FIPs representing healed dilatant shear fractures are typically morphologically different. They may be planar, or possess a curvi-planar propagation front, traverse grain boundaries or possess a more complex morphology as displayed in Fig. 5.14. These are believed to represent Riedel or conjugate Riedel shear fractures (see Fig. 2.8).

The formation of FIPs as a result of associated faulting are generally restricted to the proximity (several km's) of the fault. Data from the sample areas have shown that abundances of FIPs that are the result of thermal fracturing are generally similar (Fig. 4.8) between samples. However, the presence of faulting may create anomalous FIP abundance values in samples obtained close (2-3km's; see Fig. 5.6) to the fault (see sections 2.2.3 and 4.3.1). Intense kaolinisation which is locally developed at Lee Moor on the southern edge of the Dartmoor granite may be partly attributed to the high abundance of FIPs observed. The presence of anomalous FIP abundances may thus be attributed to local faulting. Previous workers (Brock and Engelder, 1977; Chernyshev and Dearman, 1991) have shown that microfracture density decreases as a function of distance away from a fault zone. However, it is not clear whether the abundance of FIPs is related to the initial failure of the rock and the size of the deviatoric stress associated with this failure or the amount of subsequent post-failure fault-slip that has occurred. The example of Lee Moor may indicate that it is the amount of fault movement which is important for the development of high FIP abundances as it has been shown that NW-SE striking strike-slip faults in the vicinity have had a long and polyphase movement history.

6.2.3 FIPs resulting from hydraulic stresses

It is unlikely that open fractures can occur at depth without the presence of a fluid phase and thus fluid pressure is the key parameter affecting deformation within the Earth's crust (Sibson 1990) (see also 2.1.4 and 2.2.2). As FIPs represent microfractures which have been annealed by a fluid phase in a pressure solution process, it is likely that hydraulic stresses were important in maintaining the fractures open. Also, the majority of crack propagation occurs below the critical stress intensity value, and is therefore termed sub-critical crack growth (Atkinson, 1982), stress corrosion must be occurring. The rate at which stress corrosion occurs is controlled by the rate at which reagents can be brought to the crack tip. These reagents are generally water molecules.

However, during the present study, FIPs are only termed hydraulic fractures when the hydraulic stresses are presumed to be the major controlling factor of fracture development. FIPs presumed to be the result of hydraulic stress have been identified from all the field locations and their morphology and occurrence have been characterised. Hydraulic fracturing is thought to be associated with high temperature/pressure mineralisation processes at Carrock Fell (see section 3.3.5) and at Kit Hill/Hemerdon Bal (4.3.4). The nature of these FIPs makes it difficult to differentiate them from those formed by thermal stresses, as they are also generally simple, planar, intergranular fractures. They also possess high homogenisation temperatures similar to thermal fractures, and it is likely that their origin is a combination of the two stresses.

A second variety of FIPs representing hydraulic fractures has also been observed. These FIPs are thought to be associated with fault related dilatancy, representing purely tensile fractures, forming under conditions of low differential stress and high fluid pressure. These FIPs are typically intragranular, planar fractures, rarely interacting with grain boundaries, usually being isolated within the quartz grain. They have been identified associated with strike-slip faulting, with orientations parallel to σ_1 and perpendicular to σ_3 with an angle to the fault of between 30 and 60°.

6.3 Inclusion morphologies and fracture healing

The shape, size and abundance of secondary fluid inclusions contained within FIPs has regularly and systematically been recorded in FIP orientations in samples from the three study areas. The presence of a preferred shape orientation exhibited by secondary fluid inclusions has been recognised in a number of cases. It appears possible to relate these shape orientations to FIP orientations and the mode of fracturing. The following is an

attempt to further clarify the existence of the preferred orientation observed within secondary inclusions in relation to the fracturing and healing process.

6.3.1 Inclusion morphologies

Inclusions were generally classified as being regular, rounded and equant or possessing a preferred shape orientation, and were thus tubular, elongate or smeared. Generally, preferred shape orientations were observed parallel to the FIP length with those perpendicular to FIP length being extremely rare. The size and abundance of inclusions was also recorded in FIPs, although there was no apparent correlation with FIP orientation (see Tables A3.4-A3.10; A4.7-A4.15; A5.2-A5.13).

Equant, rounded and regular inclusions

These inclusions were commonly observed in many different FIP orientations, showing a diverse range in size and abundance (see Figs. 3.20; 4.10; 5.17). In many cases they have been classified as occurring in FIPs that are typically *mode I* tensile fractures. Inclusions that have undergone a post-trapping re-equilibration of their morphology are likely to have transformed into rounded and negative crystal shapes (Sterner and Bodnar, 1989). The influence of re-equilibration on inclusion morphology is discussed in more detail below.

Tubular, elongate and flattened inclusions

Inclusions exhibiting a preferred shape orientation parallel to the FIP length were not uncommon (see 5.3.2 and Plates 5.5, 5.6). Inclusions tended to exhibit elongate and tubular shapes, with the most extreme cases appearing completely flattened when the FIP was viewed in the vertical position, and highly irregular in morphology when viewed at a low angle to the eye-piece. Only a few rare observations of inclusions oriented length perpendicular to the FIP were recorded. The origin of these preferred shape orientations has been attributed to the mode of fracturing of the FIP. This is based upon the orientation of the FIPs in relation to the orientations of macro-structures in the sample areas. However, stronger evidence can be implied from the variation of inclusion shape with change in orientation along an FIP length. Fig. 5.14c shows a sinusoidal FIP, exhibiting sinistral off-setting of an earlier fracture. Inclusions are observed to change their morphology along the FIP, with equant morphologies occurring in the dilatant jog and inclusions exhibiting elongate flattened shapes along the sections undergoing dextral shear (see Fig. 5.14c and Plates 5.7a, b).

6.3.2 Implications of the fracture healing process

The following section considers at the implications that the crack healing process posses in regard to the healing of both tensile and shear fractures and the formation of the possible preferred shape orientation of secondary fluid inclusions within these healed cracks. The mechanics of the crack healing process itself are outlined in section 2.3.2.

The process by which fractures are healed (section 2.3.2), where tubular voids neck-down to become separate inclusions was first described by Lemmlein (1956) and Lemmlein and Kliya (1960) in laboratory experiments on sodium nitrate crystals. These experiments were presumably conducted without the application of differential stress (isotropic stress field). However, during the natural healing of microfractures in quartz, it is likely that the resulting fluid inclusions were formed under the influence of a external deviatoric stress. It can therefore be envisaged that inclusion morphologies were thus influenced by this stress.

The classification of FIPs as *mode I* and *mode II* fractures is based entirely upon their structural origins. However, a number of other important processes (e.g. changes in internal and external pressures in and around the fluid inclusion) may be occurring that will govern the morphology and orientation of the FIPs and fluid inclusions they contain. For inclusions to develop orientations related to the fracture opening directions, it is implicit that the rate of healing of the fractures must be occurring within the same time parameters as the fracture process. Thus factors controlling the rate of healing of a FIP will therefore have some control over the morphology of the inclusions. A number of workers (Brantley *et al.*, 1990; Brantley, 1992: Pécher, 1981; Smith & Evans, 1984; Vaughan *et al.*, 1986) have shown that the factors controlling the rate of healing include the temperature and chemistry of the fluids, the geometry of the microfracture network and the application of non-hydrostatic stresses. Even at temperatures as low as 200°C, microfractures will heal in geologically short periods of time (Brantley, 1992). Smith & Evans (1984) showed that fractures at 400°C in the presence of a fluid were completely healed within 1-2 days.

Brantley (1992) also states that the geometry of the fracture network is probably the most important control over the rate of crack healing, even more so than the chemistry of the fluids. Large interconnected microfracture networks will permit the movement of fluids, allowing widespread alteration and metasomatism of the rock and thus allowing fractures to heal quickly. It is therefore likely that these fractures will exhibit preferred shape orientations of the secondary inclusions contained within them, if their kinematic circumstances were to allow it.

The presence of a preferred shape orientation of fluid inclusions in healed microfractures has also been reported by Shelton & Orville (1980) and Smith & Evans (1984). They illustrated how fluid inclusions showed a relationship with the pre-existing fracture topography. Curvi-linear steps in the crack steps that were visible in the unhealed portions were sometimes parallel to lines of nearby fluid inclusions. Also if the fracture possessed an orientation which contained the c-axis of quartz (a possible control over the formation of microfractures since the experiments took place in a uniaxial stress field), lines of fluid inclusions were often sub-parallel to (0001). However, Fig. 5.14c shows that fluid inclusions change their orientation along the length of healed fracture, and therefore it is unlikely that they possess a relationship with the c-axis of the quartz grain that the fracture has propagated in.

Laboratory controlled experiments also demonstrate a relationship between the rate of fracture healing, the width of the fracture and the size of the inclusions. Brantley (1992) further showed how the diameter of fluid inclusions increases with the widening of the fracture aperture as the propagation tip is approached. Smith & Evans (1984) further speculated that inclusions will be smaller in narrow cracks and related this to healing rates, as narrow fractures will tend to heal more rapidly than wider ones. Data from FIPs studied in this work are in agreement with these authors, as fluid inclusions have been seen to become noticeably smaller towards the propagation front of the fracture, an observation also made by Boullier *et al.*, (1991). It can therefore be assumed that FIPs containing small inclusions experience faster healing rates than those which contain large inclusions, suggesting wider crack apertures.

6.3.3 Post-healing re-equilibration

As stated in Chapter 2, there is a large amount of existing literature concerning the re-equilibration of fluid inclusions in synthetic (Pécher, 1981; Bodnar *et al.*, 1989; Sterner and Bodnar, 1989; Boullier *et al.*, 1989) and naturally-occurring quartz (Wilkins and Barkas, 1978; Gratier and Jenatton, 1984; Hurai and Horn, 1992; Vityk *et al.*, 1994). Studies have shown that fluid inclusions may not represent closed systems regarding changes in fluid composition (Sterner *et al.*, 1993), changes in fluid density (Bodnar *et al.*, 1989) and most importantly regarding this study, changes in inclusion morphology (Vityk *et al.*, 1994). The reasons why inclusions re-equilibrate with respect to their density, morphology and composition are considered in Chapter 2 (see section 2.3.3). It has been hypothesised during this research that the morphology of fluid inclusions, can in some cases be related to the mode of fracturing of the FIPs in which they occur. Generally, changes in morphology of fluid inclusions, whether in synthetic or natural quartz are dependant on a state of internal overpressure. This state occurs when the internal pressure within an inclusion is greater than the confining pressure. In the

laboratory, this is achieved by heating the inclusion to a temperature equal to, or greater than the temperature of homogenisation (Gratier and Jenatton, 1984). This difference between confining and internal pressures is termed the effective pressure by Vityk *et al.*, (1994).

Analysis of fluid inclusion morphologies in quartz from the studied samples has shown a wide diversity. Although in the majority of FIPs inclusions appear rounded, equant, regular or irregular, there are distinct occurrences of FIPs exhibiting inclusions possessing preferred shape orientation with respect to the FIP length. These preferred shape orientations have been seen in FIPs with specific orientations as well as varying within an FIP when it shows a change in orientation. Therefore, although some inclusion morphologies may have re-equilibrated, others quite clearly have not. It is the aim of the discussion below to clarify this apparent contradiction.

Fluid inclusion data from the three sample areas (Carrock, Bodmin-Dartmoor and Lundy) suggests simple cooling histories, possibly with mixing with cooler less saline fluids. It is, therefore, unlikely that conditions could arise where earlier inclusions would be subjected to internal overpressures during heating. If re-equilibration of inclusion morphologies has occurred then it is more likely to be under conditions of internal underpressure. The possible controls for the re-equilibration of part of the inclusion population include:
(i) The temperature of formation of the inclusions.
(ii) Size of the inclusions.
(iii) Deformation episodes, particularly in relation to earlier, pre-existing inclusions.
(iv) Age of the inclusions.

The re-equilibration of inclusion morphologies in quartz in conditions of internal underpressure has been demonstrated by Sterner and Bodnar (1989) and Vityk *et al.*, (1994). However, in most of these studies the authors have concentrated on the effects of high confining pressures related to metamorphic burial and uplift, concerning primary inclusions. Re-equilibration of inclusion morphologies in these cases can result in the explosion/implosion of a large inclusion, causing a change in shape and the generation of a secondary inclusion halo/clusters. These inclusion halos or clusters may be related to fracturing of the inclusions during re-equilibration (Pécher, 1981), and were not observed in secondary inclusions from the sample areas.

Here we are considering the transformation of possible elongate inclusions (exhibiting a preferred shape orientation) into more equant regular types. In its simplest form, this type of re-equilibration is termed necking down (Roedder, 1984). An important observation regarding the presence of a preferred shape orientation in this study was that

it only occurred in inclusions which possessed homogenisation temperatures below ~250 °C. It is therefore implied that similar inclusions with homogenisation temperatures above ~250°C have undergone re-equilibration of their morphologies. However, it should be noted that this is an over-simplification of the general observations, as there were many cases where FIPs which did not possess a preferred shape orientation had similar orientations and microthermometric properties to those that did.

The size of inclusions observed in the present study was recorded in most cases and it was noted, most obviously in samples from NE Dartmoor and Lundy, that the presence of a preferred shape orientation was generally restricted to inclusions larger than 5μm and generally between 15μm and 40μm. Inclusions with sizes under 5μm were always extremely regular or rounded in shape. Vityk *et al.*, (1994) has presented research showing the influence of inclusion size on re-equilibration. Vityk demonstrated that small inclusions re-equilibrate at lower effective pressures than larger ones during deformation or crustal thickening. Inclusions of different sizes exhibited different re-equilibration features, with the intensity of the re-equilibration being inversely proportional to the size of the inclusions (Vityk *et al.*, 1994). However, these experiments were carried out over a limited time period, with instantaneous loading, and the effects of time and strain rate was not considered. This introduces the possibility that over geological time, all inclusions, regardless of size may re-equilibrate to the same extent.

The relationship of inclusions to a stress field during internal overpressuring has been demonstrated by Gratier and Jenatton (1984), also in relation to the geometric characteristics of the inclusion (length and width) and the orientation of the inclusion with respect to the c-axes of quartz. They applied a uniaxial stress of between 20-65MPa at 265°C to inclusions (Th 265°C) for a period of several months without showing a clear link to a change in shape. However, inclusions did become shorter and wider, and eventually rounder, while initially round inclusions attained a negative crystal morphology.

Finally, perhaps the simplest answer as to why some inclusions exhibit complicated, flattened or elongate morphologies is the age of the inclusions, especially when related to later hydrothermal events. Inclusions with a preferred shape orientation are linked to sinistral and dextral strike-slip faulting in samples from Lundy and NE Dartmoor. A Tertiary age for this faulting has been inferred from the orientation and temperature data, showing it to be the latest deformation event. The relationship between the re-equilibration of rounded primary inclusions whose temperature of formation was less that of highly irregular secondary inclusions (interpreted as being formed by tectonic fracturing) is demonstrated by Gratier and Jenatton (1984). The earlier rounded

inclusions would have preserved their fluid under internal overpressure, thus their shapes have changed in this respect. The later, irregular inclusions would be in equilibrium with the later thermal event, and have preserved their irregular shape (probably due to their low internal pressure). In the Lundy and NE-Dartmoor sample areas, the later secondary inclusions generally possess a Th which is lower than that of the primary inclusions. However, it is the earlier, high temperature inclusions which have undergone re-equilibration of their morphologies, possibly by conditions of internal underpressure, related to confining pressures produced by late tectonic brittle deformation.

It is not fully understood why some inclusions have undergone re-equilibration and others have not. Although the most stable inclusion morphologies are negative crystals and equant, rounded shapes which are extremely common, there is a numerically comparable population which exhibit complicated, high energy surface energy morphologies. It is envisaged that a number of potential processes are responsible for the re-equilibration of an inclusion morphology. These may include the age, size, temperature of formation, together with the nature of later deformation episodes that may affect earlier, pre-existing inclusions. The processes that may be responsible for maintaining an irregular morphology through geological time, include the stacking of dislocations, creating a high activation energy barrier, preventing further change (Sterner and Bodnar, 1989).

6.4 Conclusions and wider implications

A classification scheme has been proposed for the formation and morphological characteristics of Fluid Inclusion Planes, observed in granitic quartz. The scheme will allow the classification of FIPs or more probably sets of FIPs as follows:

(i) FIPs may be classified as dilatant (*mode I*) or dilatant shear (*mode II*) healed fractures based upon a number of factors which include; visible off-setting of grain boundaries and other healed fractures (rare), morphology of the FIP (planar, curvi-planar, sinusoidal, complex), its distribution within on the grain scale (i.e. inter- or intracrystalline) and the possible presence of a preferred shape orientation exhibited by the secondary fluid inclusions. This describes the kinematic origins of the FIP as a healed fracture and its resulting morphological characteristics.

(ii) FIPs may be described as fractures resulting from either one, or a combination of thermal, tectonic and hydraulic stresses. The origins of FIPs in respect to these stresses may described by their orientations in relation to appropriate macrofractures, their morphological characteristics, and their thermometric properties. This is important when

considering the development of FIPs resulting from a number of processes over a wide period of geological history.

This classification scheme based on FIPs from granitic quartz, may also be used in other geological terranes where processes that may be occurring can be likened to those characterised in this study.

CHAPTER 7

CONCLUSIONS, WIDER IMPLICATIONS AND FURTHER WORK

7.0 Conclusions

The following statements are the major conclusions reached as a product of this research regarding the formation, healing and morphological characteristics of Fluid Inclusion Planes from the various field areas.

(i) Fluid Inclusion Planes may possess a preferred orientation over a wide area similar to that of macrostructures observed in the field, although their orientation may be affected by local hetrogenities in the stress field caused by the presence of minor second order faults.

(ii) The morphologies and distributions of FIPs have been described and related to their origin. FIPs have been shown to planar, curvi-planar, sinusoidal, or exhibit strike-slip duplex and off-setting morphologies which may be related to their orientation together with their distribution in the quartz grain (isolated, interacts with grain boundaries or transgranular). In turn these characteristics have been used to correlate FIPs in respect to their origins (thermal, hydraulic, tectonic) and their mode of fracture (dilatant-*mode I* or shear-*mode II*)

(iii) The abundance of microfractures is typically similar within samples of unaltered granite but exhibit a marked increase within samples that show hydrothermal alteration, e.g. kaolinisation or greisenisation. This pervasive hydrothermal alteration is presumed to be clearly linked to the intense microfracture network, allowing the passage of large volumes of hydrothermal fluids. The formation of these FIPs has been shown to be related to thermal or hydraulic stresses (greisen formation) and tectonic deformation associated with active faulting (possibly related to the formation of kaolinisation).

(iv) FIPs have been classified as pure tensile, dilatant (*mode I*) and dilatant shear (*mode II*) healed microfractures. This is in contrast to other workers who have failed to recognise *mode II* microfractures, suggesting that the small amounts of shear movements would be to small to observe. However, during this study, dilatant shear fractures were characterised by their orientation, morphology, morphology of the inclusions within them, and the offsetting of grain boundaries and other healed fractures, when observed.

(v) Fluid Inclusion Planes have been classified as being the product of stresses resulting from differences in the thermal expansion behaviour of minerals (notably quartz and feldspar) in the cooling granite (thermal stress), high fluid pressures (hydraulic stress) and brittle deformation associated with active faulting (tectonic stresses). The classification of FIPs as being the product of one of these stresses is based upon their orientation, morphology and temperature of the fluid inclusions contained within them.

(vi) FIPs can be used to provide a complete picture of an area undergoing hydrothermal evolution. A complete hydrothermal continuum is illustrated through the use of secondary inclusions which may be only partly shown by the use of primary inclusions from vein material. Secondary fluid inclusions have been used to demonstrate the evolution of hydrothermal fluids on different scales. At Carrock Fell, fluid evolution and mineralisation is associated with local mineralisation, alteration and intrusion, whereas, data from the SW England covers a much larger area, relating FIPs to regional stress regimes, regional mineralisation episodes, associated with the intrusion of several granite bodies.

(vii) The morphology of secondary fluid inclusions contained within the healed fractures exhibited possible preferred orientations with respect to the fracture length. These were classified as being parallel or perpendicular (rare) to the fracture and attributed to the movement sense of the fracture. Inclusion morphologies were observed to vary between fractures of different orientations and also within fractures which were sinusoidal or exhibited other variations in geometry. However other factors controlling the inclusion morphologies include the amount of movement of the fracture during healing and the chemistry and temperature of the hydrothermal fluids which will affect the re-equilibration of the inclusion morphology.

7.1 Wider implications and further work

During this study FIPs have been analysed from quartz in granite, formed due to thermal cooling and subsequent brittle deformation. These FIPs have also been linked to ore forming and alteration processes associated with movements of hydrothermal fluids. Further research concerning the development of FIPs can therefore take two directions; (a) analysis of FIPs with regard to their origin as a result of thermal, tectonic and hydraulic stresses, perhaps in more complex geological terranes associated with significant amounts of deformation or associated or (b) analysis of FIPs with regard to their role in ore deposition, pervasive alteration and the crack healing process. Ultimately, these two lines of research will interact.

Some of the more interesting lines of research initiated by this study are listed below:

(i) It has been shown that the presence of high FIP abundances may be linked to hydrothermal pervasive alteration. This may result in widespread kaolinisation and greisenisation, although the two processes have been linked to different types of FIPs. Fluids responsible for these alteration processes may be characterised by analysis of the crack walls of FIPs that cross from quartz into feldspars. Techniques including ion microprobe can be used to show alteration of the feldspars close to the crack walls, which in turn may be related to fluids of a known temperature and salinity in FIPs of a known orientation, within the quartz.

(ii) FIPs have been characterised as being the result of thermal, tectonic or hydraulic stresses. However, at present, this classification is based only on results from granitic quartz, exhibiting thermal cooling, subsequent brittle deformation and associated high fluid pressures. Further work regarding FIP formation in more complex or just different geological situations is required to fully understand these processes. This may include FIP generation in areas undergoing regional metamorphism, associated with re-heating and burial of pre-existing quartz as well as FIP formation associated with large shear belts related to large amounts of tectonic deformation and high fluid pressures. This relationship of active strike-slip faulting and FIP formation/fault related dilatancy and high fluid pressure may be significant in the role of periodic mineralisation episodes and earthquake prediction.

(iv) FIPs have been used to tentatively reconstruct the movement history of a fault which has exhibited both sinistral and dextral polyphase movement, in conjunction with the evolution of hydrothermal fluids associated with the intrusion and cooling histories of two granite bodies.

(iii) Cathodoluminescence (CL) has been used in this study, with little success, to try and produce a relative dating of FIP formation. However, more favourable samples (which fluoresce) show that CL is a powerful tool for unravelling the story of FIP formation. Cl would be essential for the identification of healed fractures in feldspars (see Plate 5.8).

(iv) Perhaps one of the most interesting observations discussed in this study, is the presence of a preferred shape orientation present in some FIPs of certain orientations. A great deal of clarification of this phenomena is needed, especially with regard to the crack healing process and the post-depositional re-equilibration of inclusion morphology. Preferential inclusion morphologies may be related to stresses acting on the fracture subsequent to its healing. These strain energies may also be responsible for allowing some inclusions to re-equilibrate while others do not. This may be especially true for variations in inclusion morphologies within a single FIP where the stacking of dislocations provides an activation energy barrier preventing inclusion re-equilibration along certain sections of the fracture.

(v) In recent years a great deal of work has been published on the fractal dimension of faulting, vein formation and fluid flow. It is also possible that the distribution of healed microfractures in quartz may exhibit fractal behaviour. Fractal analysis of the microfracture distribution would help to illustrate the scale of fluid movement in the rocks. Although orientation is not a good fractal parameter, fracture trace lengths (in a specific frame) and density can be used and are easily measured in a thin section using a grid frame. This would be useful to illustrate the distribution of FIPs around fault zones, especially in relation to possible pervasive alteration of fluids through an interconnected microfracture network resulting in wide spread hydrothermal alteration. e.g. kaolinisation.

APPENDIX A

A1 Sampling, sample preparation and sample locations

The following is a description of the sampling techniques used both in the field and laboratory. Lists of samples, their locations (grid references) and techniques applied are presented here. Maps showing the locations of samples are located in the relevant chapter.

A1.1 Sampling procedure

Samples of mainly fresh granite (unless otherwise required) were carefully obtained from *in-situ* localities, generally being restricted to working and disused quarries, china clay pits, roadside cuttings and sea cliff exposures. Generally all samples where possible were marked with orientation lines before removal. This allowed the samples to be re-oriented in the laboratory for the marking of thin section orientations.

Sampling orientation

The following is a brief description of the procedure published by Prior *et al.*, (1987):

(i) Select a planar surface which may be easily removed
(ii) Mark on the sample whilst *in-situ* a horizontal strike line of a known orientation, generally as long as the edge of the clinometer.
(iii) Measure the dip of the surface and place a dip tick either below or above the orientation strike-line. Depending upon whether the planar surface is upright or overhanging, mark below or above the strike-line.
(iv) Carefully remove the sample, starting again if the sample markings are disrupted.

In the laboratory, the sample can be re-oriented into its original orientation:

(i) Place sample up-right in modelling clay on a turntable.
(ii) Re-orientate so that the orientation markings again comply with their real orientations

(iii) Mark a surface for cutting, generally in the horizontal or vertical
(iv) Again re-orientate the sample and mark on the section location and orientation on the cut surface.
(v) Cut section and transfer orientation marking to the glass slide.

A1.2 Thin section preparation

Thin sections were initially produced by the author at Kingston University and later by the technical department at the Royal School of Mines. The procedure is similar to that described by Shepherd *et al.*, (1985) and is briefly described below:

(i) A slice is cut containing the section marking and orientation, approximately 4-5mm in thickness.
(ii) The top is lapped and fixed to a glass slide, using a thermosetting epoxy with the orientation marking transferred to the slide, with one side of the section set against the edge for accuracy.
(iii) The section is then cut and ground to a thickness of around 100-200μm.
(iv) The underside is then polished using Al_2O_3 powder.
(v) The section is then removed and inverted so that it is now right side up in relation to the orientation markings, fixed to the slide and again polished using Al_2O_3 powder.

The section is now ready for orientation analysis. Following the orientation analysis, sections that were used to for CL were given a carbon coating.

A1.3 Sample locations and listings

A complete list of samples obtained is presented, regardless of whether they have been analysed or not (Table A1.1). Details include the locality name, sample code, material sampled, orientation of the specimen, locality grid reference and the orientation in which a section was cut from the sample. Table A1.2 shows specimens which have been analysed for microstructure, microthermometry and cathodoluminescence.

Table A1.1 Sample listings and locations

location	*code*	*sample*	*strike*	*dip*	*quad*	*G.R.*	*cut*
Wet Swine Gill	WSG1	qtz vein	002	68	E	318 321	
Caldew River	CR1	granite	280	66	S	305 305	000/00
Caldew River	CR2	granite				305 305	
Caldew River	CR3	granite	000	90		308 307	000/90
Caldew River	CR4	granite	098	70	S	310 310	000/00
Caldew River	CR5	granite	065	85	N	326 326	000/00
Grainsgill	GG1	greisen	280	79	SW	324 328	000/00
Grainsgill	GG2	greisen	274	90		323 329	000/00
Grainsgill	GG3	greisen	097	25	N	326 327	000/90
Grainsgill	GG4	greisen	185	67		325 327	000/00
Grainsgill	GG5	greisen	046	75		324 327	000/00
Sinen Gill	SG1/CR6	granite	359	87	W	297 279	000/00
Sinen Gill	SG2	granite	091	35	S	297 279	
Carrock	HDV1	qtz. vein				327 327	
Carrock	EWLZ1	calcite. vein				327 327	
Hingston Down	HD1	granite	242	39	N	410 717	000/00
Hingston Down	HD2	granite	054	85	N	410 717	000/00
Hingston Down	HD3	granite	031	65	S	410 717	000/00
Hingston Down	HD4	granite	049	78	NW	410 717	000/00
Hingston Down	HD5	granite	046	89	NW	410 717	000/00
Hingston Down	HD6	granite	340	90		410 717	000/00
Hingston Down	HD7	qtz. vein				410 717	
Kit Hill	KH1	greisen	259	85	N	375 717	
Kit Hill	KH2	greisen	073	79	S	375 717	
Kit Hill	KH3	fluorite. vein				364 707	
Kit Hill	KH4	granite	319	74	NE(OH)	375 717	
Kit Hill	KH5	granite	330	86	SW	375 717	
Poldark Mine	PO1	qtz. vein	067	71	N		000/00
Cape Cornwall	CC1	qtz. vein	333	90		352 317	
Cape Cornwall	CC2	qtz. vein	333	89	NW	352 317	000/00
Cligga Head	CH1	qtz. vein	330	85	(OH)	740 538	000/90
M'hampstead	MSW1	alt. granite	254	76	NW	720 847	
Hemerdon	HQ1	qtz. porph	227	61	N		
Birch Tor	BT1	granite	068	90	S	680 811	
Two Bridges	TB1	granite	183	90	W	609 751	
Cheesewring	CWQ1	granite	072	82	S	258 724	000/00
nr. Bearah Tor	HWQ1	granite	148	72	SW	260 744	
Corey Tor	CT1	granite	327	84	NE	231 770	
Caradon Hill	CHQ	granite	298	80	S	269 705	000/00
Kit Hill	KHVQ1	qtz. vein	265	65	S	375 716	
nr. Colcerrow	CCQ1	granite	266	90	N	065 578	
Blackpool Pit	BPP1	kaol. granite	156	90	E	980 545	000/00
Blackpool Pit	BPP2	kaol. granite	150	72	SW	980 545	000/90
Rocks Pit	RP1	kaol. granite	046	74	NW	015 584	000/00
Rocks Pit	RP2	kaol. granite	223	90	NW	018 584	000/90
Lower Tregarne	LT1	granite	177	90	E	765 297	
nr. Halvasso	HLVQ1	qtz. vein	305	85	SW	745 322	
Lamorna Cove	LC1	granite	324	76	SW	453 242	
Lamorna Cove	LC2	granite	311	90	SW	453 242	
Penberth Cove	PB1	granite	146	81	SW	403 227	
Penberth Cove	PB2	granite	173	86	SE	403 227	
Cape Cornwall	CC3	qtz. vein	328	88	W	352 317	
Kelly Brae	KB 1	fluor. vein	Not	oriented		364 707	
Burrator	BRT 1	granite					
M' hampstead	MHD1	alt. granite	081	83	S(OH)	722 848	000/00
Chagford	BTF1	granite	160	63	E	705 848	000/00

Chagford	CFD1	granite	140	58	NE	713 885	000/00
Easton	EHT1	granite	340	40	SW	726 890	000/00
Lustleigh	LTH1	granite	130	60	NE	787 821	000/00
Lustleigh	LTH2	granite	211	63	NW(OH)	787 821	000/90
Wray Barton	WBT1	granite	145	35	SW	777 846	000/00
Blackingstone	BST1	granite	126	37	SW	786 856	000/00
Blackingstone	BST2	granite	131	43	SW	786 856	000/90
Mardon Down	MDT1	granite	333	41	SW	765 872	000/00
Lee Moor Pit	LMP1	kaol. granite	280	76	N		012/50E
Lundy Island	LI1	granite	174	90	E		000/00
Lundy Island	LI2	granite	225	78	SE		000/00
Lundy Island	LI3	granite	270	64	S		267/13N
Lundy Island	LI4	granite	230	45	S		000/00
Lundy Island	LI5	granite	145	70	NE		000/90
Lundy Island	LI6	granite	028	70	E		000/90
Lundy Island	LI7	granite	268	56	N		000/00

Table A1.2 Samples and techniques applied

code	*orientation analysis*	*microthermometry*	*cathodoluminescence*
CR1	☺	☺	
CR4	☺	☺	
CR5	☺	☺	
CR6	☺	☺	
GG2	☺		
GG4	☺	☺	
GG5	☺		
HDV1		☺	
EWLZ		☺	
HD1	☺		
HD2	☺	☺	
HD3	☺	☺	
HD4	☺		☺
HD5	☺	☺	
HD6	☺	☺	
HD7		☺	
LMP1	☺	☺	☺
CHQ1	☺		☺
CWQ1	☺	☺	
KH3		☺	
KH4	☺	☺	
LI1	☺	☺	☺
LI2			
LI3		☺	
LI4	☺		☺
LI5	☺		
LI6	☺		
LI7	☺		
CFD1	☺		☺
EHT1	☺		
MHD1	☺		☺
MDS1	☺		☺
WBN1	☺		☺
LTH1	☺		

APPENDIX B

B1 Orientation analysis methodology and calibration

The following details the methods, instruments and calibration techniques used during the analysis of FIP orientations.

B1.1 Methodology

Samples were studied on a standard Leitz petrographic microscope, fitted with a Leitz universal stage. Sections were placed between two hemispheres of refractive index (1.554) close to that of the subject medium (quartz; 1.544). An immersion oil, again with a similar refractive index (1.524) was used to lubricate the samples for ease of movement and optical continuity between the hemispheres. Generally two or three quartz crystals were selected from the specimen which were then photographed using a video-printer and carefully mapped out. Images were generally recorded using a x10 objective. The orientations of all planar and non-planar FIPs were then recorded, allocated a number and their positions carefully recorded.

The recording of FIP orientations was conducted as follows:

(i) Initially, focus on the upper surface of the upper hemisphere. Position the rotary stage of the microscope until the E-W horizontal axis of the U-stage can be rotated without lateral movement being observed on the upper hemisphere. The microscope stage is then clamped and need not be altered again unless the U-stage is removed.
(ii) Clamp the N-S horizontal axis of the U-stage into the horizontal position. This is not used.
(iii) Position an FIP until it is in a vertical position and parallel to the E-W cross-hairs of the microscope. This is done by rotating the E-W horizontal axis of the U-stage until the FIP is considered to be at its most thinnest (i.e. a line). Then rotate the vertical axis of the U-stage until the FIP is parallel to the E-W cross-hairs.
(iv) Record the position of the FIP on both the horizontal and vertical axis scales. This data can then be transferred to the stereonet as described below. It must be remembered that it does not represent the dip and strike of the FIP, but its dip to the vertical and the angular difference to the E-W cross-hairs.

Data obtained from the U-stage can be directly transferred to the stereonet as follows:

(i) Rotate the transparent overlay until the North (index) arrow coincides with the number recorded on the vertical rotary axis of the U-stage.
(ii) Plot the dip recorded from the east-west horizontal axis of the U-stage along the N-S diameter of the net from the end corresponding to the U-stage orientation.

The point plotted represents a pole to plane and may be used to ascertain the dip and strike of the FIP. The orientation may be visibly checked by holding the net in a similar orientation to the U-stage and noting the movement of the pole of the FIP as it is tilted from its vertical position. A comprehensive account of the use of the universal stage together with the recording of data on a stereonet is given by Turner and Weiss (1963).

B1.2 Calibration

Systematic calibration of the U-stage technique was conducted by mathematically calculating the dip of a FIP based upon the horizontal distance from where it interacts with the top and bottom of the section and the thickness of the section (minus the thickness of the glass slide). Simple Pythagoras was then used to calculate the dip of the FIP.

APPENDIX C

C1 Thermometric analysis and calibration

The following details the methods, instruments and calibration techniques used during the thermometric analysis of fluid inclusions upon completing the orientation analysis.

C1.1 Methodology

Once the orientation data has been recorded, the samples were removed from the glass slides for thermometric analysis. It must be noted, that once removed from the slide the reference orientation is lost, although the location and orientations of individual FIPs is known. The samples were removed either by heating (approx. 90°C) the slide (in the case where thermosetting epoxy was used) or by immersion in acetone and subjected to a low power ultrasonic bath in cases where the slides were fixed with a cyanocryalate glue. The wafers were then broken to remove the individual quartz crystals. Thermometric analysis was undertaken on all FIPs where possible. However, the size of inclusions was commonly too small for analysis. Three or four inclusions were analysed where possible from each FIP of a known orientation. These were selected away from other cross-cutting FIPs which may have interacted with the inclusion fluids. FIPs were analysed in order of degree of fill, with the highest values first so that leakage could be kept to a minimum. All data points were duplicated where possible. Phase changes recorded include T_{FM}, T_{Mice}, T_H, T_{Ddiss}. Generally due to the small size of the inclusions (the majority being 3-10μm) only T_H and T_{LM} were commonly recorded.

Thermal gradients across the sample and sapphire window were considered negligable (0.1°C at 0.0°C and ~5°C at 372.4°C). Reprted microthermometric data is considered accurate ±1°C between -20-50°C, ±2°C between 50-350°C and ±4°C above 350°C.

All measurements were recorded on a Linkham THM600 and THMS600 heating/freezing stage with a working temperature range of -196 to 600°C. Heating and freezing was controlled by the TMS91 temperature controller up to August 1992 when it was replaced with the TMS92. Temperature control was manual with the TMS91 but with an auto option for cooling pump control included on the TMS92. The cooling

pump was the model LNP2, with a video text overlay connected to a Mitsubishi thermal image video-printer. All heating freezing controllers and pumps (TMS91, TMS92, LNP2, VTO232) were supplied by Linkam Scientific of Reigate, Surrey. The stage was attached to a standard Nikon binocular petrographic microscope.

C1.2 Calibration

Periodic calibration of the heating/freezing stage is an integral part off all fluid inclusion studies. Samples are placed upon a 7mm diameter sapphire window located on top of a silver block in which is located a platinum resistance sensor. As a result there is a temperature difference between the sample and the sensor. Furthermore there is an increase in the temperature difference with departure from the ambient temperature and with ageing of the sensor. This temperature difference is thus calibrated and calibration measurements applied to data recorded during phase changes observed in inclusions. The reader is referred to Linkam (1992) for a comprehensive account of the technical specifications concerning the THMS600 heating/freezing stage.

Calibration was conducted using phase changes observed in several synthetic inclusions. The temperatures at which these phase changes occur are exact physical reference points. They include the CO_2 triple point, CO_2 clathrate melting point, melting point of pure water and the critical point of pure water. The temperatures of these phase changes are listed in table C1.1. Other exact reference points may be determined from the melting points of certain pure chemicals also listed in table C1.1.

Table C1.1 Calibration materials for the Linkham THMS600 heating/freezing stage

Material	*Phase change*	*Temperature*
Synthetic CO_2-H_2O inclusion	CO_2 triple point	-56.6°C
Synthetic pure H_2O inclusion	T_{Mice}	0.0°C
Synthetic CO_2-H_2O inclusion	$T_{Mclathrate}$	+10.1°C
8-Hydroxy Quinoline	melting point	+76°C
Salicylic acid	melting point	+159°C
Sodium Nitrate	melting point	+306.8°C
Synthetic pure H_2O inclusion	H_2O critical point	372.4°C

Deviations from these reference points can be used to construct calibration curves (Fig. A1.1) which may then be used to apply error estimate for phase changes between the end members. A full list of calibration materials and their reference temperatures as well as further details concerning the calibration of heating/freezing stages is provided by Roedder (1984) and Shepherd *et al.*, (1985).

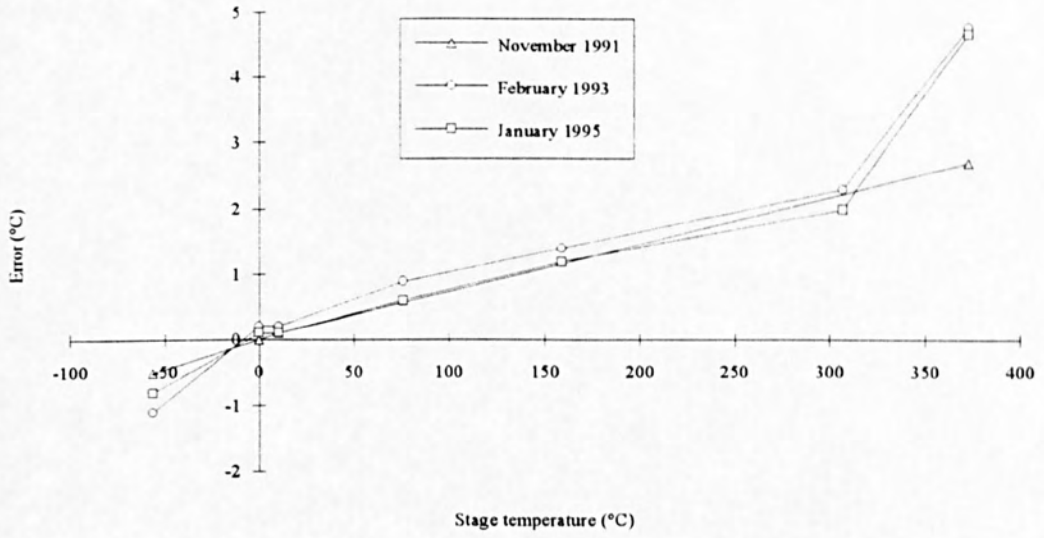

Fig. A1.1 Calibration curves for the Linkham THM600 and THMS600 heating/freezing stage.

APPENDIX D

DATA BASE

All orientation data is given as strike and dip according to the right hand rule (dipr), that the dip direction always lies to the right of the strike .e.g. 120/34 indicates the plane dips 34 degrees toward 120 degrees (120/34SE).

Table A3.1 Joint data: Grainsgill outcrop

strike	dipr	fill
260	77	unmineralised
268	68	unmineralised
153	84	unmineralised
150	84	unmineralised
155	89	unmineralised
120	85	unmineralised
55	80	qtz/muscovite
266	74	qtz/muscovite
257	81	unmineralised
259	80	unmineralised
151	74	unmineralised
304	82	unmineralised
270	75	unmineralised
264	85	unmineralised
255	82	unmineralised
1	14	unmineralised
60	10	unmineralised
270	90	unmineralised
47	12	unmineralised
21	75	qtz/muscovite
324	88	unmineralised
145	80	unmineralised
137	65	unmineralised
265	50	unmineralised
272	50	qtz/muscovite
193	71	qtz/muscovite
199	67	qtz/muscovite
187	69	qtz/muscovite
85	72	unmineralised
143	85	unmineralised
129	81	unmineralised
132	82	unmineralised
125	76	unmineralised
107	33	unmineralised
95	68	unmineralised
254	62	unmineralised
129	12	unmineralised
65	7	unmineralised
35	10	unmineralised
314	90	unmineralised
147	80	unmineralised
325	85	unmineralised
345	85	unmineralised
39	75	unmineralised
92	84	unmineralised
94	82	unmineralised
107	90	unmineralised
116	41	unmineralised
338	71	unmineralised
171	70	qtz/muscovite
137	90	unmineralised
141	80	unmineralised

Table A3.2 Joint data: Caldew River outcrop

strike	dipr
18	85
49	85
354	79
94	64
48	21
134	89
137	78
218	2
300	9
319	86
128	79
48	45
136	79
144	82
129	86
48	84
106	84
178	79
42	83
128	78
127	79
136	85
144	88
219	89
222	90
200	77
108	76
151	81
142	86
257	69
354	14
18	98
335	15
129	69
147	84
105	79
328	89
339	84
14	76
78	71
91	85
96	84
14	76
220	89
315	82
309	87
308	78
145	56
319	90
305	75
320	59
320	75

339	64	unmineralised
323	88	unmineralised
75	90	unmineralised
60	88	unmineralised
77	80	unmineralised
85	67	unmineralised
75	70	qtz/muscovite
85	80	qtz/muscovite

Table A3.3 Joint data: Brandy Gill outcrop

strike	dipr	fill
11	84	unmineralised
241	86	unmineralised
184	78	unmineralised
298	15	unmineralised
347	75	unmineralised
198	89	unmineralised
847	90	unmineralised
358	79	unmineralised
249	82	unmineralised
147	84	unmineralised
349	21	unmineralised
48	10	unmineralised
18	9	unmineralised
4	89	qtz/muscovite
48	76	unmineralised
179	84	qtz/muscovite
179	86	qtz/muscovite
184	82	unmineralised
21	90	unmineralised
358	79	unmineralised
349	76	unmineralised
15	64	unmineralised
14	82	qtz/muscovite
21	69	qtz/muscovite
28	83	unmineralised
348	86	unmineralised
126	72	unmineralised
18	59	unmineralised
0	83	unmineralised
214	71	unmineralised
94	84	qtz/muscovite
181	72	unmineralised
106	79	unmineralised
209	84	unmineralised
186	86	unmineralised
174	87	qtz/muscovite
258	74	unmineralised
174	82	unmineralised
59	69	unmineralised
213	85	qtz/muscovite
218	83	unmineralised
18	88	unmineralised
2	76	qtz/muscovite
348	74	unmineralised
134	82	unmineralised

287	89	unmineralised
359	74	qtz/muscovite
358	77	unmineralised
9	85	unmineralised
8	79	unmineralised
147	84	unmineralised
12	86	unmineralised
348	83	unmineralised
179	64	unmineralised
184	85	qtz/muscovite
183	79	qtz/muscovite
165	75	unmineralised

Table A3.4 FIP orientation data: CR1

Crystal A								
F.I.P. No	Strike	dipr	Inclusion size	Planar	Crack width	Development	Definition	Abundance
1	2	71	>5	planar	narrow	intracrystalline	well defined	few
2	14	61	varied	curvi-planar	narrow	intracrystalline	poorly defined	few
3	70	43	varied	planar	narrow	intercrystalline	well defined	many
4	84	38	<5	planar	narrow	intracrystalline	well defined	many
5	12	36	>5	planar	narrow	intracrystalline	poorly defined	few
6	88	35	<5	planar	narrow	intracrystalline	well defined	many
7	81	20	<5	curvi-planar	narrow	intracrystalline	well defined	many
8	84	36	varied	planar	narrow	intercrystalline	well defined	many
9	80	30	varied	planar	narrow	intracrystalline	well defined	many
10	103	60	varied	curvi-planar	narrow	intracrystalline	well defined	many
11	68	74	<5	planar	narrow	intracrystalline	poorly defined	few
12	80	34	varied	planar	narrow	intercrystalline	well defined	many
13	77	34	varied	planar	narrow	intercrystalline	well defined	many
14	73	87	<5	planar	narrow	intracrystalline	poorly defined	few
16	36	60	<5	curvi-planar	narrow	intracrystalline	poorly defined	few
17	19	71	<5	planar	narrow	intracrystalline	well defined	many
18	64	34	varied	planar	narrow	intercrystalline	poorly defined	few
19	66	49	varied	planar	narrow	intercrystalline	poorly defined	few
20	46	35	varied	planar	narrow	intracrystalline	poorly defined	few
Crystal B								
1	241	73	>5	irregular	narrow	intercrystalline	well defined	few
2	100	21	<5	planar	narrow	intracrystalline	well defined	many
4	240	69	varied	planar	narrow	intercrystalline	well defined	many
5	240	67	varied	planar	narrow	intercrystalline	well defined	many
6	300	24	<5	planar	narrow	intracrystalline	poorly defined	few
7	322	25	>5	planar	narrow	intracrystalline	poorly defined	few
8	245	84	<5	planar	narrow	intercrystalline	well defined	many
9	256	73	<5	curvi-planar	narrow	intracrystalline	well defined	many
10	281	65	>5	planar	narrow	intracrystalline	poorly defined	few
11	260	85	<5	irregular	narrow	intercrystalline	well defined	many
12	263	85	<5	planar	narrow	intracrystalline	poorly defined	few
13	282	63	<5	curvi-planar	narrow	intracrystalline	poorly defined	few
14	239	62	<5	planar	narrow	intercrystalline	well defined	many
15	53	64	>5	planar	narrow	intracrystalline	poorly defined	few
16	239	64	varied	planar	narrow	intercrystalline	well defined	many

Table A3.5 FIP orientation data: CR4

Crystal A

F.I.P. No.	Strike	dipr	Inclusion size	Planar	Crack width	Development	Definition	Abundance
1	218	80	<5	planar	narrow	intracrystalline	poorly defined	few
2	221	87	>5	planar	narrow	intracrystalline	poorly defined	few
3	2	82	varied	planar	narrow	intercrystalline	well defined	many
4	34	70	>5	planar	narrow	intracrystalline	well defined	many
5	2	82	<5	planar	narrow	intercrystalline	poorly defined	few
6	305	28	<5	planar	narrow	intracrystalline	poorly defined	few
7	258	54	<5	planar	narrow	intracrystalline	intercrystalline	many
8	232	67	>5	curvi-planar	narrow	intracrystalline	poorly defined	few
9	230	45	varied	planar	narrow	intracrystalline	poorly defined	few
10	313	32	<5	planar	narrow	intercrystalline	well defined	few
11	232	35	varied	curvi-planar	narrow	intercrystalline	poorly defined	many
12	230	39	varied	planar	narrow	intracrystalline	poorly defined	few
13	26	86	<5	planar	narrow	intracrystalline	well defined	few
14	25	87	>5	planar	narrow	intracrystalline	well defined	few
15	20	76	<5	curvi-planar	narrow	intracrystalline	well defined	many
16	11	63	varied	curvi-planar	narrow	intracrystalline	poorly defined	few
17	0	86	<5	planar	narrow	intracrystalline	poorly defined	few
18	17	87	>5	curvi-planar	wide	intracrystalline	poorly defined	few
19	197	70	<5	planar	narrow	intracrystalline	well defined	many
20	220	78	varied	planar	wide	intercrystalline	poorly defined	many
21	224	41	>5	planar	narrow	intracrystalline	poorly defined	few
22	1	81	<5	planar	narrow	intercrystalline	poorly defined	few
23	4	81	>5	planar	wide	intracrystalline	well defined	few
24	7	76	>5	planar	wide	intracrystalline	poorly defined	few
26	307	32	<5	planar	narrow	intracrystalline	poorly defined	few
27	0	87	<5	planar	narrow	intracrystalline	poorly defined	few
28	334	78	<5	planar	narrow	intercrystalline	well defined	many
29	305	63	varied	planar	wide	intracrystalline	poorly defined	few
30	164	72	varied	curvi-planar	narrow	intercrystalline	well defined	many
31	358	83	<5	planar	narrow	intercrystalline	well defined	few
32	223	35	>5	planar	narrow	intracrystalline	well defined	few
33	210	29	varied	planar	narrow	intracrystalline	poorly defined	few
34	342	81	<5	planar	narrow	intracrystalline	well defined	many
35	292	59	>5	planar	wide	intracrystalline	well defined	many
37	33	68	<5	planar	narrow	intercrystalline	well defined	many
38	196	73	>5	planar	wide	intercrystalline	poorly defined	few
39	204	28	>5	curvi-planar	wide	intracrystalline	poorly defined	few
40	0	80	<5	planar	narrow	intracrystalline	well defined	many
41	23	49	varied	planar	wide	intracrystalline	poorly defined	many
42	259	57	varied	planar	wide	intercrystalline	well defined	many
43	110	19	varied	planar	wide	intracrystalline	poorly defined	many
44	263	42	varied	planar	wide	intracrystalline	poorly defined	many
46	42	68	>5	planar	wide	intracrystalline	poorly defined	many
47	45	78	>5	planar	wide	intracrystalline	poorly defined	many
Crystal B								
2	33	74	<5	planar	narrow	intracrystalline	well defined	many
3	283	30	<5	planar	narrow	intracrystalline	poorly defined	few
4	293	48	<5	planar	narrow	intracrystalline	poorly defined	few
5	215	72	<5	planar	narrow	intracrystalline	well defined	many
6	25	73	>5	planar	wide	intracrystalline	poorly defined	few
7	212	89	>5	planar	wide	intercrystalline	poorly defined	few
8	343	86	<5	planar	narrow	intracrystalline	well defined	many
9	278	25	>5	curvi-planar	wide	intracrystalline	poorly defined	few
10	170	63	>5	planar	wide	intracrystalline	poorly defined	few
11	166	81	<5	planar	narrow	intercrystalline	well defined	many

12	165	71	>5	planar	wide	intracrystalline	poorly defined	few
13	348	90	<5	planar	narrow	intercrystalline	well defined	many
14	178	89	>5	planar	wide	intracrystalline	poorly defined	few
15	174	86	<5	planar	narrow	intracrystalline	well defined	many
16	0	86	varied	planar	narrow	intercrystalline	poorly defined	few
17	256	65	>5	planar	wide	intracrystalline	poorly defined	few
18	15	64	>5	planar	wide	intracrystalline	poorly defined	few
19	12	59	<5	planar	narrow	intracrystalline	well defined	many
20	184	88	<5	planar	narrow	intracrystalline	well defined	many
21	355	73	<5	planar	narrow	intracrystalline	well defined	many
22	278	71	varied	irregular	narrow	intracrystalline	poorly defined	few
23	358	71	varied	planar	narrow	intercrystalline	poorly defined	few
24	261	54	<5	planar	narrow	intracrystalline	well defined	many
25	256	54	varied	planar	narrow	intracrystalline	well defined	many
27	48	89	varied	planar	narrow	intercrystalline	well defined	many
28	213	79	varied	planar	narrow	intracrystalline	poorly defined	many
29	5	71	<5	curvi-planar	narrow	intercrystalline	well defined	few
30	4	77	<5	curvi-planar	narrow	intercrystalline	well defined	few
31	263	62	varied	planar	wide	intracrystalline	well defined	many
33	16	68	<5	planar	narrow	intracrystalline	well defined	many
34	224	54	varied	planar	wide	intercrystalline	poorly defined	many
35	184	78	>5	planar	wide	intracrystalline	poorly defined	few

Crystal C								
1	141	75	>5	planar	wide	intracrystalline	poorly defined	few
2	246	44	<5	planar	narrow	intracrystalline	well defined	many
3	239	34	>5	curvi-planar	wide	intracrystalline	poorly defined	few
4	30	67	<5	planar	narrow	intracrystalline	well defined	many
5	353	84	<5	planar	narrow	intercrystalline	well defined	many
6	183	87	<5	curvi-planar	narrow	intracrystalline	well defined	many
7	257	46	varied	planar	wide	intracrystalline	poorly defined	few
8	38	60	varied	planar	narrow	intracrystalline	well defined	many
9	40	61	varied	curvi-planar	narrow	intracrystalline	poorly defined	many
10	210	78	>5	planar	wide	intracrystalline	poorly defined	few
11	262	52	varied	planar	narrow	intracrystalline	well defined	many
12	262	54	varied	planar	narrow	intracrystalline	well defined	many
13	188	70	<5	curvi-planar	narrow	intracrystalline	well defined	many
14	139	67	>5	planar	wide	intracrystalline	poorly defined	few
15	244	37	>5	planar	narrow	intracrystalline	well defined	many
16	176	87	varied	planar	narrow	intracrystalline	poorly defined	many
17	166	81	varied	planar	wide	intracrystalline	poorly defined	many
18	18	77	<5	planar	narrow	intracrystalline	well defined	many
19	14	77	<5	planar	narrow	intercrystalline	well defined	many
20	236	45	<5	planar	narrow	intracrystalline	poorly defined	few
21	250	35	<5	curvi-planar	narrow	intracrystalline	poorly defined	few
22	253	47	<5	planar	narrow	intracrystalline	well defined	many
23	254	38	<5	planar	narrow	intracrystalline	poorly defined	few
24	156	65	varied	planar	narrow	intercrystalline	well defined	many
25	221	33	varied	curvi-planar	wide	intercrystalline	poorly defined	many
26	232	48	>5	planar	narrow	intracrystalline	poorly defined	few
27	262	36	varied	curvi-planar	narrow	intercrystalline	well defined	many
28	252	43	<5	curvi-planar	narrow	intracrystalline	well defined	many
29	244	42	varied	planar	wide	intercrystalline	well defined	many
30	241	64	varied	planar	wide	intracrystalline	well defined	many
31	246	39	varied	irregular	wide	intercrystalline	well defined	many
32	201	78	varied	curvi-planar	narrow	intercrystalline	poorly defined	few
33	15	89	varied	curvi-planar	wide	intercrystalline	well defined	many
34	199	77	varied	planar	narrow	intracrystalline	poorly defined	few

35	206	61	<5	planar	narrow	intracrystalline	poorly defined	few
36	196	74	<5	curvi-planar	wide	intracrystalline	poorly defined	many
37	33	63	varied	planar	narrow	intracrystalline	poorly defined	many
38	261	41	varied	planar	narrow	intracrystalline	well defined	many

Table A3.6 FIP orientation data: CR5

Crystal A F.I.P. No.	strike	dipr	inclusion size	planar	crack width	development	definition	abundance
1	336	84	>5	irregular	wide	intercystalline	poorly defined	few
2	167	74	varied	planar	narrow	intercystalline	well defined	many
3	340	90	>5	planar	wide	intracystalline	poorly defined	few
4	86	59	>5	planar	narrow	intracystalline	poorly defined	few
5	171	77	>5	planar	narrow	intracystalline	poorly defined	few
6	342	84	>5	planar	wide	intracystalline	poorly defined	few
7	173	75	<5	planar	narrow	intracystalline	poorly defined	few
8	174	72	<5	planar	narrow	intracystalline	poorly defined	few
9	174	77	<5	planar	narrow	intracystalline	poorly defined	few
10	174	78	<5	planar	narrow	intracystalline	poorly defined	few
11	186	82	<5	planar	narrow	intracystalline	poorly defined	few
12	120	52	varied	planar	narrow	intracystalline	poorly defined	few
13	123	58	<5	planar	narrow	intracystalline	poorly defined	few
14	124	57	<5	planar	narrow	intracystalline	poorly defined	few
15	117	79	varied	planar	narrow	intracystalline	well defined	many
16	125	78	varied	planar	wide	intercystalline	poorly defined	many
17	127	66	varied	irregular	wide	intracystalline	poorly defined	many
18	172	78	<5	planar	narrow	intracystalline	poorly defined	few
19	172	77	<5	planar	narrow	intracystalline	poorly defined	few
20	170	81	<5	planar	narrow	intracystalline	poorly defined	few
21	167	84	<5	planar	narrow	intracystalline	poorly defined	many
22	187	61	<5	curvi-planar	narrow	intercystalline	well defined	many
23	172	54	<5	planar	narrow	intracystalline	well defined	many
24	168	19	>5	planar	narrow	intracystalline	well defined	few
25	43	66	<5	planar	narrow	intracystalline	well defined	few
26	132	72	varied	curvi-planar	wide	intracystalline	poorly defined	many
27	117	81	>5	curvi-planar	wide	intercystalline	poorly defined	many
28	111	48	<5	planar	narrow	intracystalline	poorly defined	few
29	116	48	<5	planar	narrow	intracystalline	poorly defined	few
30	116	50	<5	planar	narrow	intracystalline	poorly defined	few
31	191	64	<5	planar	narrow	intracystalline	well defined	few
32	183	77	<5	planar	narrow	intracystalline	well defined	few
33	97	88	<5	curvi-planar	narrow	intercystalline	poorly defined	few
34	175	79	<5	planar	narrow	intracystalline	poorly defined	few
36	95	63	>5	curvi-planar	narrow	intracystalline	poorly defined	few
37	177	85	<5	planar	narrow	intracystalline	poorly defined	few
38	194	58	varied	planar	narrow	intercystalline	well defined	many
39	184	70	>5	planar	narrow	intracystalline	poorly defined	few
40	153	63	varied	planar	wide	intracystalline	well defined	many
42	56	67	very <5	curvi-planar	narrow	intracystalline	poorly defined	many
43	57	69	very <5	curvi-planar	narrow	intracystalline	poorly defined	many
44	48	74	very <5	curvi-planar	narrow	intracystalline	poorly defined	many
45	172	80	>5	planar	wide	intracystalline	poorly defined	few
46	170	79	>5	planar	narrow	intracystalline	poorly defined	few
47	186	70	varied	planar	wide	intracystalline	poorly defined	few
49	178	87	>5	planar	narrow	intracystalline	poorly defined	few
50	121	52	>5	curvi-planar	wide	intercystalline	poorly defined	few
51	173	89	<5	planar	narrow	intracystalline	poorly defined	few

52	185	86	>5	planar	wide	intracystalline	poorly defined	few
53	346	60	>5	planar	wide	intracystalline	poorly defined	few
54	131	63	varied	planar	narrow	intercystalline	poorly defined	few
Crystal B								
1	133	60	>5	irregular	narrow	intracystalline	well defined	few
2	169	52	>5	planar	narrow	intracystalline	well defined	few
3	188	72	>5	planar	narrow	intracystalline	poorly defined	few
4	305	74	varied	planar	narrow	intracystalline	poorly defined	many
6	146	61	<5	curvi-planar	narrow	intercystalline	well defined	many
7	72	65	varied	curvi-planar	narrow	intercystalline	well defined	many
8	288	77	>5	planar	narrow	intracystalline	poorly defined	few
9	149	51	<5	curvi-planar	narrow	intracystalline	well defined	many
10	347	67	>5	planar	wide	intracystalline	poorly defined	few
11	282	89	<5	planar	narrow	intercystalline	well defined	many
13	165	60	varied	planar	narrow	intercystalline	well defined	many
14	292	89	<5	planar	narrow	intracystalline	poorly defined	many
15	68	64	>5	curvi-planar	narrow	intracystalline	poorly defined	few
16	174	70	>5	planar	narrow	intracystalline	well defined	few
17	182	85	>5	planar	wide	intracystalline	poorly defined	many
18	98	70	varied	planar	narrow	intracystalline	well defined	few
19	256	86	varied	curvi-planar	wide	intracystalline	poorly defined	few
20	282	76	<5	planar	narrow	intracystalline	well defined	many
21	164	70	<5	planar	narrow	intracystalline	poorly defined	few
22	160	54	>5	curvi-planar	wide	intracystalline	poorly defined	few
23	344	46	>5	planar	wide	intracystalline	poorly defined	few
25	9	40	>5	planar	wide	intracystalline	poorly defined	many
26	28	30	<5	planar	narrow	intracystalline	well defined	many
27	161	78	>5	planar	wide	intracystalline	poorly defined	many
28	176	47	>5	planar	narrow	intercystalline	well defined	many
29	172	57	>5	planar	narrow	intracystalline	poorly defined	few
30	174	60	>5	planar	narrow	intercystalline	well defined	many
31	182	64	>5	planar	narrow	intercystalline	well defined	many
32	304	84	>5	curvi-planar	narrow	intercystalline	well defined	many
33	206	44	varied	planar	wide	intracystalline	well defined	many
34	190	59	varied	planar	wide	intracystalline	poorly defined	many
35	160	61	>5	planar	wide	intracystalline	poorly defined	many
37	179	37	<5	planar	narrow	intercystalline	poorly defined	many
38	166	47	varied	planar	narrow	intercystalline	poorly defined	many
39	177	53	varied	planar	narrow	intracystalline	well defined	many

Table A3.7 FIP orientation data: CR6

FIP #	strike	dipr	FIP #	strike	dipr
1	45	81	41	278	49
2	91	77	42	269	78
3	77	84	43	112	90
4	24	86	44	79	86
5	3	83	45	68	89
6	109	84	46	51	83
7	219	73	47	93	65
8	278	84	48	98	71
9	274	73	49	279	89
10	354	70	50	263	82
11	91	77	51	82	76
12	157	83	52	86	74
13	206	76	53	87	82
14	179	71	54	18	69

15	264	86	55	347	58
16	264	81	56	112	78
17	15	83	57	274	89
18	314	84	58	283	59
19	271	72	59	289	64
20	283	76	60	286	58
21	101	74	61	273	73
22	94	75	62	90	48
23	76	84	63	143	49
24	248	72	64	88	82
25	279	84	65	270	46
26	183	73	66	354	68
27	358	88	67	67	73
28	269	80	68	19	84
29	274	71	69	101	85
30	99	76	70	95	76
31	94	90	71	103	74
32	89	85	72	164	87
33	91	83			
34	126	71			
35	268	70			
36	251	45			
37	98	80			
38	94	83			
39	304	77			
40	249	72			

Table A3.8 FIP orientation data: GG2

FIP No.	strike	dipr	inclusion size	planar	crack width	development	definition	abundance
Crystal A								
1	251	88	varied	irregular	wide	intracrystalline	poorly defined	few
2	344	65	varied	planar	narrow	intracrystalline	poorly defined	few
3	328	86	<5	planar	narrow	intercrystalline	well defined	few
4	240	80	<5	curvi-planar	narrow	intercrystalline	well defined	few
5	103	78	<5	irregular	wide	intracrystalline	poorly defined	few
6	249	67	<5	curvi-planar	narrow	intracrystalline	poorly defined	many
7	30	87	>5	irregular	wide	intracrystalline	poorly defined	few
8	247	67	<5	curvi-planar	narrow	intercrystalline	well defined	few
9	254	70	<5	curvi-planar	narrow	intracrystalline	poorly defined	many
10	246	60	varied	planar	narrow	intercrystalline	well defined	many
11	62	88	<5	planar	narrow	intercrystalline	well defined	few
12	71	82	<5	curvi-planar	narrow	intercrystalline	well defined	many
13	71	81	<5	planar	narrow	intercrystalline	well defined	few
14	72	70	<5	curvi-planar	narrow	intracrystalline	poorly defined	few
15	166	70	<5	planar	narrow	intracrystalline	poorly defined	many
16	166	81	<5	planar	narrow	intracrystalline	poorly defined	many
17	340	85	varied	planar	wide	intercrystalline	well defined	many
18	80	82	<5	planar	narrow	intracrystalline	poorly defined	many
19	258	80	>5	planar	narrow	intracrystalline	poorly defined	few
20	238	71	varied	planar	narrow	intracrystalline	poorly defined	many
Crystal B								
1	76	59	<5	curvi-planar	narrow	intracrystalline	poorly defined	few
2	72	86	varied	planar	wide	intercrystalline	poorly defined	few
3	148	71	varied	planar	narrow	intracrystalline	well defined	few

4	253	79	varied	irregular	wide	intercrystalline	poorly defined	many
5	192	80	varied	planar	narrow	intercrystalline	well defined	many
6	97	68	<5	planar	narrow	intracrystalline	well defined	few
7	337	54	varied	planar	wide	intracrystalline	poorly defined	many
8	136	54	varied	curvi-planar	wide	intracrystalline	poorly defined	many
9	323	55	varied	planar	wide	intracrystalline	poorly defined	many
10	337	46	varied	planar	wide	intracrystalline	poorly defined	many
11	280	66	varied	planar	wide	intercrystalline	poorly defined	many
12	280	52	varied	planar	narrow	intracrystalline	well defined	many
13	99	73	varied	planar	narrow	intracrystalline	well defined	few
14	344	52	varied	planar	narrow	intercrystalline	well defined	many

Table A3.9 FIP orientation data: GG4

Crystal A

FIP No.	strike	dipr	inclusion size	planar	crack width	development	definition	abundance
1	144	84	<5	planar	narrow	intercrystalline	well defined	many
2	164	79	<5	curvi-planar	narrow	intracystalline	well defined	many
3	11	80	<5	planar	narrow	intracystalline	well defined	many
4	279	83	<5	planar	narrow	intracystalline	well defined	many
5	45	84	<5	planar	narrow	intracystalline	poorly defined	few
6	91	76	>5	planar	narrow	intercrystalline	well defined	many
7	184	80	>5	planar	narrow	intracystalline	poorly defined	many
8	184	78	varied	curvi-planar	narrow	intracystalline	poorly defined	many
9	15	49	<5	planar	wide	intracystalline	poorly defined	few
10	348	60	<5	planar	narrow	intercrystalline	poorly defined	few
11	246	81	varied	curvi-planar	narrow	intercrystalline	well defined	many
12	178	64	varied	curvi-planar	narrow	intercrystalline	well defined	many
13	86	87	varied	curvi-planar	narrow	intracystalline	well defined	few
14	184	61	<5	planar	narrow	intracystalline	well defined	many
15	20	87	<5	planar	narrow	intracystalline	well defined	few
16	345	70	<5	planar	narrow	intracystalline	poorly defined	many
17	2	87	<5	planar	narrow	intracystalline	poorly defined	many
18	274	73	<5	planar	wide	intracystalline	poorly defined	many
19	12	80	>5	planar	wide	intracystalline	poorly defined	few
20	187	81	>5	planar	narrow	intercrystalline	well defined	many
21	190	86	varied	planar	narrow	intracystalline	well defined	many
22	184	84	<5	planar	narrow	intercrystalline	well defined	many
23	14	83	>5	irregular	narrow	intracystalline	well defined	many
24	148	71	>5	curvi-planar	narrow	intracystalline	well defined	many
25	279	78	<5	planar	narrow	intercrystalline	well defined	many
26	315	84	<5	planar	narrow	intercrystalline	well defined	many
27	78	78	<5	planar	narrow	intracystalline	poorly defined	many
28	189	87	varied	planar	narrow	intracystalline	poorly defined	few
29	358	86	varied	planar	narrow	intercrystalline	poorly defined	many
30	96	84	varied	planar	wide	intercrystalline	well defined	many
31	18	78	varied	planar	narrow	intracystalline	poorly defined	many
32	179	81	varied	planar	narrow	intracystalline	poorly defined	few
33	165	73	<5	planar	narrow	intracystalline	well defined	few
34	89	50	<5	planar	narrow	intracystalline	well defined	few
35	241	61	<5	planar	narrow	intercrystalline	poorly defined	many
36	187	54	<5	planar	narrow	intracystalline	poorly defined	few
37	1	90	>5	curvi-planar	narrow	intercrystalline	poorly defined	few
38	6	73	>5	curvi-planar	narrow	intracystalline	poorly defined	few
39	125	61	varied	curvi-planar	narrow	intracystalline	poorly defined	few
40	139	68	<5	irregular	narrow	intercrystalline	well defined	many
41	267	74	varied	irregular	narrow	intercrystalline	well defined	many

42	352	86	<5	planar	narrow	intercrystalline	poorly defined	many
43	174	84	>5	planar	wide	intracystalline	well defined	many
44	175	76	<5	planar	wide	intracystalline	well defined	few
45	189	71	<5	planar	narrow	intracystalline	well defined	few
Crystal B								
1	12	59	<5	planar	narrow	intracystalline	well defined	many
2	9	87	<5	planar	narrow	intracystalline	well defined	many
3	276	65	>5	planar	narrow	intracystalline	well defined	many
4	307	65	>5	planar	narrow	intracystalline	poorly defined	many
5	188	54	varied	curvi-planar	narrow	intracystalline	poorly defined	few
6	323	78	varied	curvi-planar	narrow	intracystalline	poorly defined	few
7	198	90	<5	planar	narrow	intracystalline	well defined	many
8	99	76	<5	planar	narrow	intracystalline	poorly defined	few
8a	181	82	varied	planar	narrow	intercrystalline	well defined	many
8b	278	74	<5	planar	narrow	intracystalline	poorly defined	many
9	215	65	varied	curvi-planar	narrow	intercrystalline	poorly defined	few
10	359	90	>5	curvi-planar	narrow	intracystalline	well defined	many
11	4	82	>5	planar	narrow	intracystalline	well defined	many
12	109	87	<5	planar	narrow	intracystalline	poorly defined	many
13	86	84	<5	planar	narrow	intracystalline	well defined	few
14	179	86	<5	curvi-planar	narrow	intracystalline	well defined	many
15	169	72	<5	planar	narrow	intracystalline	poorly defined	few
16	200	87	<5	curvi-planar	wide	intracystalline	poorly defined	few
17	215	83	<5	curvi-planar	wide	intracystalline	well defined	many
19	359	84	<5	curvi-planar	narrow	intracystalline	well defined	many
20	359	81	<5	planar	narrow	intracystalline	well defined	many
21	80	78	varied	planar	narrow	intracystalline	well defined	many
22	14	73	varied	planar	narrow	intercrystalline	well defined	many
23	187	71	>5	irregular	narrow	intracystalline	well defined	many
24	181	74	<5	planar	narrow	intercrystalline	well defined	many
25	174	68	<5	planar	wide	intercrystalline	poorly defined	many
26	185	48	<5	planar	narrow	intercrystalline	poorly defined	few
27	15	49	<5	planar	narrow	intracystalline	poorly defined	few
28	12	64	>5	planar	narrow	intracystalline	poorly defined	many
29	82	71	<5	curvi-planar	narrow	intracystalline	well defined	many
30	129	87	<5	curvi-planar	narrow	intracystalline	poorly defined	many
31a	314	86	varied	planar	narrow	intracystalline	well defined	many
31b	314	86	<5	planar	narrow	intracystalline	poorly defined	many
32	5	65	<5	irregular	narrow	intracystalline	poorly defined	many
33	201	71	varied	curvi-planar	narrow	intracystalline	well defined	many
34	9	86	<5	planar	narrow	intracystalline	well defined	many
35	15	83	<5	planar	narrow	intracystalline	poorly defined	many
36	200	71	<5	planar	narrow	intracystalline	poorly defined	many
37	189	90	varied	planar	narrow	intracystalline	well defined	few
38	280	81	varied	planar	narrow	intercrystalline	well defined	few
39	350	69	>5	planar	wide	intercrystalline	well defined	many
40	10	54	>5	planar	narrow	intracystalline	poorly defined	many
41	9	90	varied	planar	narrow	intracystalline	well defined	many
42	301	69	<5	planar	narrow	intercrystalline	well defined	few
43	275	85	<5	planar	narrow	intercrystalline	well defined	many
44	356	86	<5	planar	narrow	intercrystalline	well defined	many
45	189	74	>5	planar	narrow	intracystalline	poorly defined	many
46	178	74	<5	curvi-planar	narrow	intracystalline	poorly defined	few
47	8	84	<5	curvi-planar	wide	intracystalline	well defined	many
48	77	89	<5	planar	narrow	intracystalline	well defined	many
49	349	87	varied	planar	narrow	intracystalline	well defined	many
51	270	85	varied	planar	narrow	intracystalline	poorly defined	many

52	198	69	<5	curvi-planar	narrow	intracystalline	poorly defined	few
53	174	71	varied	curvi-planar	wide	intercrystalline	well defined	many
54	2	73	<5	planar	narrow	intracystalline	poorly defined	many
55	198	74	<5	planar	narrow	intercrystalline	well defined	many
56	173	61	<5	planar	narrow	intercrystalline	poorly defined	few
58	100	69	<5	planar	narrow	intercrystalline	well defined	many
59	11	88	<5	planar	narrow	intracystalline	poorly defined	few
60	56	78	>5	curvi-planar	narrow	intracystalline	well defined	many
61	349	71	varied	irregular	narrow	intracystalline	poorly defined	few
62	1	67	<5	planar	narrow	intracystalline	poorly defined	few
63	23	56	<5	planar	narrow	intracystalline	well defined	many
65	81	90	<5	planar	narrow	intracystalline	poorly defined	many
66	359	74	<5	planar	narrow	intracystalline	well defined	many
67	165	88	varied	planar	narrow	intracystalline	poorly defined	few
68	178	83	<5	planar	narrow	intracystalline	poorly defined	few
69	194	84	<5	curvi-planar	narrow	intracystalline	poorly defined	many
70	89	73	<5	curvi-planar	narrow	intracystalline	poorly defined	few
71	18	71	<5	irregular	narrow	intracystalline	poorly defined	many
72	147	79	varied	curvi-planar	narrow	intracystalline	poorly defined	few
73	12	84	<5	planar	narrow	intracystalline	poorly defined	few
74	359	79	<5	planar	wide	intercrystalline	well defined	few
75	0	71	varied	planar	narrow	intercrystalline	well defined	few
76	14	58	<5	planar	narrow	intracystalline	well defined	many
77	36	90	<5	planar	narrow	intracystalline	poorly defined	many
78	15	89	<5	planar	wide	intercrystalline	well defined	many
79	174	74	<5	planar	narrow	intracystalline	poorly defined	many
80	195	65	<5	planar	narrow	intercrystalline	well defined	few
81	1	48	<5	planar	narrow	intercrystalline	well defined	few
82	94	94	>5	curvi-planar	wide	intracystalline	well defined	many
83	174	87	>5	planar	narrow	intracystalline	well defined	many

Table A3.10 FIP orientation data: GG5

Crystal A

FIP No.	strike	dipr	inclusion size	planar	crack width	development	definition	abundance
1	181	71	<5	planar	narrow	intracrystalline	well defined	few
2	186	58	<5	planar	narrow	intercrystalline	poorly defined	many
3	21	84	<5	curvi-planar	narrow	intracrystalline	well defined	many
4	87	78	varied	curvi-planar	narrow	intercrystalline	poorly defined	many
5	169	85	>5	planar	narrow	intercrystalline	well defined	many
6	11	59	<5	planar	narrow	intracrystalline	well defined	few
7	11	74	<5	planar	narrow	intracrystalline	well defined	few
8	218	63	<5	planar	wide	intercrystalline	poorly defined	few
9a	341	86	>5	planar	narrow	intercrystalline	poorly defined	many
9b	169	61	>5	planar	wide	intracrystalline	well defined	many
11	175	73	varied	planar	wide	intracrystalline	well defined	many
12	28	74	varied	curvi-planar	wide	intracrystalline	well defined	many
13	1	64	<5	planar	narrow	intercrystalline	well defined	few
14	270	59	<5	planar	narrow	intercrystalline	well defined	many
15	179	76	<5	planar	narrow	intracrystalline	well defined	many
16	184	90	<5	planar	narrow	intracrystalline	poorly defined	many
17	189	81	>5	planar	narrow	intercrystalline	well defined	many
18	91	78	<5	planar	narrow	intercrystalline	well defined	many
19	11	64	varied	planar	narrow	intracrystalline	well defined	many
21	6	79	<5	planar	narrow	intercrystalline	well defined	few
22	178	90	>5	curvi-planar	wide	intracrystalline	well defined	few
23	87	81	<5	curvi-planar	narrow	intracrystalline	well defined	many

24	1	76	<5	planar	wide	intracrystalline	well defined	few
25	358	74	<5	planar	narrow	intercrystalline	well defined	few
26	358	82	varied	planar	narrow	intercrystalline	well defined	many
27	169	71	<5	planar	narrow	intercrystalline	poorly defined	many
28	131	90	>5	planar	narrow	intercrystalline	poorly defined	many
29a	199	89	<5	planar	narrow	intracrystalline	well defined	few
29b	205	86	varied	planar	narrow	intercrystalline	well defined	many
30	267	74	varied	planar	wide	intracrystalline	well defined	many
31	278	84	<5	planar	narrow	intracrystalline	poorly defined	many
32	181	83	<5	planar	narrow	intracrystalline	poorly defined	many
33	180	81	<5	curvi-planar	narrow	intracrystalline	poorly defined	many
34	0	79	<5	planar	narrow	intracrystalline	well defined	many

Crystal B

1	10	54	>5	planar	narrow	intercrystalline	well defined	many
2	92	85	<5	planar	wide	intercrystalline	poorly defined	many
3	10	78	<5	planar	narrow	intracrystalline	poorly defined	many
4	24	46	>5	planar	narrow	intracrystalline	poorly defined	many
5	349	49	varied	planar	narrow	intracrystalline	poorly defined	many
6	355	90	varied	curvi-planar	narrow	intercrystalline	poorly defined	few
7	278	85	<5	curvi-planar	narrow	intracrystalline	well defined	few
8	184	86	<5	planar	narrow	intracrystalline	well defined	many
9	169	86	<5	curvi-planar	narrow	intracrystalline	well defined	many
10	175	75	<5	planar	narrow	intracrystalline	poorly defined	few
11	55	87	<5	planar	wide	intracrystalline	poorly defined	many
12	84	86	>5	planar	narrow	intracrystalline	well defined	many
13	187	84	>5	planar	narrow	intracrystalline	poorly defined	few
14	189	75	<5	planar	narrow	intracrystalline	well defined	few
15	174	59	>5	curvi-planar	narrow	intercrystalline	well defined	many
16	164	62	<5	planar	narrow	intercrystalline	well defined	many
17	125	86	<5	planar	narrow	intracrystalline	well defined	many
18	91	71	<5	planar	wide	intercrystalline	well defined	many
19	300	79	<5	curvi-planar	narrow	intracrystalline	poorly defined	many
20	159	85	<5	planar	wide	intercrystalline	well defined	many
21	267	85	<5	curvi-planar	narrow	intercrystalline	poorly defined	few
22	25	87	<5	planar	wide	intracrystalline	well defined	many
23	1	83	<5	planar	narrow	intercrystalline	well defined	many
24	359	69	>5	curvi-planar	narrow	intracrystalline	well defined	many
25	1	75	varied	planar	wide	intracrystalline	well defined	many
26	181	84	<5	planar	narrow	intracrystalline	well defined	many
27	189	87	>5	planar	narrow	intracrystalline	well defined	many
28	96	86	varied	planar	wide	intracrystalline	well defined	many
29	175	87	<5	planar	wide	intracrystalline	well defined	few
30	175	82	<5	planar	wide	intercrystalline	well defined	few
31	15	59	>5	planar	narrow	intercrystalline	well defined	many
32	19	49	<5	planar	narrow	intercrystalline	well defined	few
33	179	74	varied	planar	wide	intercrystalline	well defined	many
34	11	76	<5	planar	narrow	intracrystalline	well defined	many
35	183	84	<5	planar	wide	intercrystalline	well defined	many
36	359	82	<5	planar	narrow	intracrystalline	well defined	many
37	100	59	<5	planar	narrow	intercrystalline	well defined	many
38	2	68	<5	planar	narrow	intracrystalline	well defined	many
39	65	72	varied	planar	narrow	intercrystalline	well defined	few
40	79	64	varied	planar	wide	intracrystalline	poorly defined	many
41	215	74	>5	planar	narrow	intracrystalline	well defined	many
42	184	73	>5	curvi-planar	wide	intracrystalline	poorly defined	many
43	196	84	<5	planar	wide	intercrystalline	well defined	many
44	280	83	<5	planar	narrow	intercrystalline	well defined	many

45	219	78	<5	planar	narrow	intercrystalline	well defined	many
46	278	65	varied	planar	narrow	intercrystalline	well defined	few
47	90	49	>5	planar	narrow	intracrystalline	poorly defined	many
Crystal C								
1	189	81	varied	planar	wide	intracrystalline	well defined	many
2	179	71	<5	curvi-planar	narrow	intercrystalline	well defined	many
3	24	78	<5	curvi-planar	narrow	intercrystalline	poorly defined	many
4	3	90	<5	planar	narrow	intercrystalline	well defined	many
5	354	85	>5	planar	narrow	intercrystalline	well defined	many
6	187	78	<5	planar	narrow	intracrystalline	well defined	many
7	93	64	<5	planar	wide	intracrystalline	well defined	many
8	198	89	varied	planar	narrow	intercrystalline	poorly defined	many
9	187	74	<5	curvi-planar	wide	intercrystalline	well defined	few
10	186	64	<5	planar	narrow	intercrystalline	poorly defined	many
11	1	71	<5	planar	narrow	intracrystalline	well defined	many
12	21	86	<5	planar	narrow	intracrystalline	well defined	few
13	14	84	>5	planar	narrow	intercrystalline	poorly defined	many
14	198	79	>5	curvi-planar	narrow	intercrystalline	well defined	few
15	269	81	<5	planar	narrow	intracrystalline	poorly defined	few
16	86	89	varied	curvi-planar	narrow	intracrystalline	well defined	few
17	186	83	<5	curvi-planar	narrow	intercrystalline	well defined	few
18	15	81	<5	planar	wide	intercrystalline	well defined	many
20	0	85	<5	planar	narrow	intracrystalline	well defined	few
21	268	74	<5	planar	narrow	intracrystalline	well defined	many
22	1	86	<5	planar	narrow	intracrystalline	well defined	few
23	183	79	<5	planar	narrow	intercrystalline	well defined	few
24	9	73	<5	planar	narrow	intercrystalline	well defined	few
25	100	54	varied	planar	narrow	intracrystalline	well defined	many
26	29	79	varied	planar	wide	intracrystalline	well defined	many
27	68	64	>5	planar	wide	intercrystalline	well defined	many
28	172	73	<5	planar	wide	intercrystalline	well defined	few
29	171	71	<5	curvi-planar	narrow	intercrystalline	well defined	many
30	59	82	<5	planar	wide	intracrystalline	well defined	many
31	190	79	<5	planar	narrow	intracrystalline	poorly defined	many
32	54	68	<5	planar	wide	intercrystalline	poorly defined	many
33	91	74	varied	curvi-planar	narrow	intercrystalline	poorly defined	few
34	359	86	varied	planar	narrow	intercrystalline	well defined	many
35a	359	81	<5	planar	narrow	intracrystalline	well defined	many
35b	359	79	>5	curvi-planar	narrow	intracrystalline	well defined	many
36	21	47	<5	planar	wide	intracrystalline	well defined	many
37	19	90	<5	planar	wide	intercrystalline	poorly defined	many
38	178	49	<5	planar	wide	intracrystalline	well defined	many
39	54	74	<5	planar	narrow	intercrystalline	well defined	few
40	24	85	varied	planar	narrow	intracrystalline	poorly defined	few
41	0	76	<5	planar	narrow	intercrystalline	well defined	many
42	65	90	varied	planar	narrow	intercrystalline	well defined	many
43	213	89	>5	planar	wide	intercrystalline	poorly defined	many
44	96	83	<5	planar	narrow	intracrystalline	well defined	few
45	179	84	>5	planar	narrow	intracrystalline	well defined	many
46	172	79	varied	planar	wide	intercrystalline	well defined	few
47a	349	82	<5	curvi-planar	wide	intercrystalline	well defined	many
47b	189	78	<5	planar	narrow	intracrystalline	well defined	many
48	144	64	<5	curvi-planar	narrow	intracrystalline	poorly defined	many
49	20	79	varied	curvi-planar	narrow	intracrystalline	well defined	many
50	192	85	<5	planar	narrow	intercrystalline	poorly defined	many
51	8	49	>5	planar	narrow	intercrystalline	well defined	many
52	100	84	<5	planar	narrow	intracrystalline	poorly defined	few

53	181	87	<5	planar	narrow	intercrystalline	poorly defined	many

Table A3.11 Thermometric data: CR1

Crystal B				
FIP No.	Th	Tfm	Tlmice	wt%NaCl
2	132.6		-3.1	5.1
2	146.5		-3	4.9
4	263	-22	-9.8	13.7
5	214.8		-6.9	10.4
5	231			
8	156.2	-20	-2.2	3.7
8	174.3	-20		
8	179.9		-0.8	1.4
10	186.4	-40	-15.9	19.5
10	145.7	-43	-18.7	21.7
12	213.7		-10.1	14.1
13	198.2			
13	222.5		-2.1	3.5
15	143.7	-21	-1.1	1.9
15	153.6	-21	-2.1	3.5
15	172.6	-22	-1.1	1.9
16	156.1			
16	143.8		-2.6	4.3
Crystal A				
1	287.6	-21	-2.8	4.6
1	297.6			
1	312.4		-3.6	5.8
6	143.7	-22	-3.4	5.7
6	153.8	-22	-3.2	5.2
6	145.3		-3.4	5.7
8	243.7		-5.4	8.4
8	261.3		-4.4	7
10	164.3	-21	-0.9	1.6
18	187.9		-19.9	22.6
18	196.9		-16.8	20.3
19	175.9		-1.3	2.2
20	198.5		-6.8	10.2
20	235.1		-7	10.5

Table A3.12 Thermometric data: CR4

FIP No.	Th	Tfm	Tlmice	Tlmhydro	wt%NaCl
Crystal A					
3	278.5	-21	-4.4		7
3	296.4	-21	-4.4		7
3	271.1				
3	304				
4	165.6	-20	-1.2		2.1
4	173.8		-1.3		
4	148.1	-21	-1.2		2.1
5	326.8				
5	303.2	-21	-3.3		5.4
5	298	-20	-3.4		5.5
5	334.4				
13	176.7		-3.7		6
13	186.9		-3.7		6

13	202.4				
13	210	-21	-3.6		
15	212.4		-4.1		
15	208.5	-21	-3.7		6
16	237.4		-4.1		6.6
17	278.4				
17	285.9				
17	301.3				
17	295.5				
19	198.4	-21	-4.3		6.7
19	189.4	-21	-4.9		7.7
19	206.6	-22	-4.8		7.6
22	264.8		-7.8		11.5
22	273		-8.5		12.3
23	243.6	-20	-3.2		5.2
23	253.8	-20	-3.1		5.1
23	256.4		-3.2		5.2
23	239.9				
24	197.3	-21	-3.3		5.4
24	225.5	-21.5	-3.3		5.4
24	202	-21	-3.6		5.9
24	243.3	-21	-3.4		5.5
27	212				
27	243.3				
31	324.2	-21	-2.9		4.8
33	167.8	-20	-0.9		1.6
33	174.3	-22	-0.8		1.4
33	201.1	-22	-1.2		2.1
33	185.8	-21	-1.5		2.6
35	154.4	-37	-18.9		21.9
35	148	-43	-20.3		22.9
35	147.6	-50	-20.1		22.7
37	203.4		-1.2		2.1
37	167.4		-1.2		2.1
37	210.3				
38	239.2		-3.9		6.3
38	222.6		-4.1		6.6
40	271.9				
40	297.7	-21	-3.5		5.7
40	296.7	-21	-3.5		5.7
40	254.4				
42	138.2		-0.5		0.9
44	129.5	-51		-18.9	
46	269.1		-7.5		11.1
47	301.4		-5.4		8.4

Crystal B					
7	168.3	-21	-1.1		1.9
7	176.6	-20	-1		1.7
7	187				
9	143.8		-2.4		4
9	154.4		-2.4		4
9	153.7				
11	221.5	-21	-5.8		8.9
11	225.6	-21	-6.1		9.3
11	264.8				
11	237.1				
16	301.7		-3.8		6.1

16	328.4		-3.7	6
17	157.8		-2.6	4.3
17	164.9		-2.6	4.3
17	167.9			
19	235.5		-4.8	7.6
19	233.2		-4.4	7
19	217.7		-4.4	7
20	198		-5.2	8.1
24	306.8			
24	324.7			
29	267.5	-21	-4.2	6.7
29	278.3	-21	-4.2	6.7
29	258.4	-21	-4.3	7
30	316.4			
30	335.5	-21	-3.9	6.3
30	338.2	-21	-3.9	6.3
30	311.1	-22	-4.4	7
34	158.1		-0.7	1.2
35	185.9	-22	-2.1	3.5
35	179	-22	-1.9	3.2
35	175.3		-1.9	3.2
35	183.7		-1.5	2.6
Crystal C				
6	344.1	-21	-4.2	6.7
9	212.6		-6.3	9.6
9	231.8		-6.1	9.3
11	178.9	-43	-16.8	20.3
11	168.4	-48	-19.7	22.4
12	189.4		-1.2	2.1
12	196.5	-21	-1.3	2.2
13	261.1		-5.1	8
13	258.3		-4.6	7.3
13	275.3		-4.6	7.3
13	266.6		-4.8	7.6
16	245.1	-21	-3.1	5.1
16	253.4	-22	-3.7	6
16	239.9			
21	174.3	-21	-2.1	3.5
22	195.3	-22	-0.7	1.2
22	174.2	-22	-1	1.7
22	173.7			
23	201.1		-1.3	2.2
23	179.3		-1.3	2.2
30	253.2			10.6
30	257.3	-22	-7.1	9.9
30	301.4		-6.5	5.7
33	215.5	-21	-3.5	5.1
33	204	-21	-3.1	8.3
37	272.2		-5.3	21.9
38	175.5		-2.5	4.2
38	169.4		-2.3	3.9
38	173.3		-2.6	4.3

Table A3.13 Thermometric data: CR5

FIP No.	Th	Tfm	Tlmice	Tlmhydro	wt%NaCl
Crystal A					

4	134.6	-55	-19.7		22.4
4	125.8	-40	-19.4		22.2
4	127.8			-21.1	
5	243.5	-21	-5.1		8
5	246.2	-22	-5.1		8
5	239.7	-21	-5.3		8.3
9	301.4				
9	304.6	-22	-3.3		5.4
11	323.7		-6.1		9.3
11	296.9		-6		9.2
15	143.2		-21.2		23.5
15	153.1	-55	-19.5		22.3
16	200.5		-3.7		6
16	213.8				
16	206.1		-3.4		5.5
18	326.9	-20	-4.1		6.6
19	324.8				
19	337.3	-20	-4		6.4
19	328.4	-20	-4.1		6.6
19	340.3		-4.1		6.6
21	198.5		-6.1		9.3
25	254.6		-5.3		8.3
25	261.4		-5.3		8.3
25	247.5		-5.6		8.7
27	256.3	-22	-2.9		4.7
27	250.7	-22	-2.6		4.3
27	261.4	-22	-3		4.9
27	249.5				
31	289.4	-20	-2.4		4
31	296	-20	-6.3		9.6
31	281.7		-2.5		4.2
33	179.4		-2.2		3.7
33	165.7	-22	-2.4		4
33	234.4				
34	198.5		-3.4		5.5
34	187.2		-3.6		5.8
36	142.6			-17.5	
37	234.4		-5.4		8.4
37	254.1	-23			
37	237.8	-22	-5.5		8.5
39	243.8		-3.9		6.3
39	254.8		-4.1		6.6
39	243.6		-4.1		6.6
42	231.8	-21	-3.8		6.1
42	254.2		-3.4		5.5
43	213.8				
43	219.5				
43	207.4	-22	-4.4		7
43	223	-22	-4.2		6.7
50	132.6			-20.1	
50	124.7	-37	-21	-21	
54	324.6		-6		9.2
54	354.6				
54	338.9		-5.7		8.8
54	335				
Crystal B					
3	255.6	-20	-2.1		3.5

3	264.9	-21	-2.5	4.2
6	143			
6	127.7	-40	-18.5	21.6
6	143.2	-45	-18.5	21.6
7	273.8		-9.4	13.3
7	259.4	-21	-9.7	13.7
7	215.3	-21	-8.6	12.4
14	132.6	-30	-20.6	23.1
16	324.6		-2.4	4
16	327.9	-21	-2.4	4
16	298.4	-20	-2.7	4.5
17	221.1		-3.6	5.8
17	231.8		-3.7	6
25	310.6	-21	-3.1	5.1
25	334.3	-21	-2.9	4.8
25			-3.2	5.2
25	297.9		-2.9	4.8
29	198.5		-0.6	1
29	175.4		-1.1	1.9
33	254.6		-4.8	7.6
33	275.3	-21	-4.8	7.6
33	250.2		-5	7.9
34	276	-21	-6.1	9.3
38	193.9	-21	-0.9	1.6
38	212.3		-0.8	1.4
38	203.1	-21	-1.2	2.1
39	342.7	-21	-3.6	5.8
39	352.8	-22	-3.4	5.7

Table A3.14 Thermometric data: CR7

Inclusion No.	Th	Tfm	Tlmice	wt% NaCl
1	218.4		-5.4	8.4
2	247.5		-5.9	9.1
3	226.8		-6.1	9.3
4	189.4		-3.4	5.5
5	217.6		-5.7	8.8
6	218.4			
7	201.1		-4	6.4
8	241		-7.1	10.6
9	257.6		-5.9	9.1
10	228.1		-5.7	8.8
11	237.4		-8.4	12.2
12	231.1		-6.4	9.7
13	208.4		-7	10.5
14	264.1		-7.2	10.7
15	187.2		-1.5	2.6
16	238.1			
17	218		-5.8	8.9
18	242.2		-6.3	10

Table A3.15 Thermometric data: CR8

Inclusion No.	Th	Tfm	Tlmice	wt%NaCl
1	112.7		-17.2	20.6
2	108.3		-18.4	21.5
3	128.4		-18	21.2
4	109.1			
5	105		-19.4	22.2

6	124.6	-18.3	21.4
7	122.7		
8	119.6	-17.5	20.8
9	120.1	17.8	21

Table A3.16 Thermometric data: GG4

FIP No.	Th	Tfm	Tlmice	wt%NaCl
Crystal A				
1	248.3		-6.7	10.1
1	239.1		-6.6	10
1	251.4			
1	245.4		-6.6	10
2	219.1		-6.7	10.1
2	224.7		-6.4	9.7
3	237.2		-6.9	10.4
3	241.8		-7.1	10.6
3	233.5		-7.1	10.6
5	198.4		-5.1	8
5	208.6		-5	7.9
6	141.1		-1.2	2.1
7	224.8		-7	10.5
7	231			
7	229.7		-6.8	10.2
8	266.1		-8.1	11.8
13	178.2			
13	200.1		-3.1	5.1
13	169.4		-2.5	4.2
14	258.4			
14	267.1			
14	271.6			
17	348.1		-9.1	13
17	367.1		-8.7	12.5
18	134.7	-39	-18.4	21.5
21	241.2		-5.4	8.4
21	251.3		-5.8	8.9
21	245		-5.5	8.5
21	268.9		-5.5	8.5
22	301.1			
22	324.1		-11.2	15.2
23	248.1			
23	197.7		-7.7	11.4
23	267.1		-8.1	11.8
25	141.2		-1.1	1.9
25	138.1		-1.4	2.4
25	164.2		-1.2	2.1
25	139.5		-1.4	
28	257.3			
28	261.4		-7.8	11.5
28	267.3		-7.7	11.4
28	249.9		-7.7	11.4
29	347			
29	321.1			
29	300.5			
30	112.5		-18.2	21.4
30	127.1		-21.1	23.4
31	266.6			
32	241.1		-8.8	12.6

38	201.9		
38	214.2	-4.8	7.6
38	216.1	-4.3	6.9
38	228.7	-5.1	8
39	287.3	-3.9	6.3
39	294.1	-4.1	6.6
44	274.4		
45	224.3	-5.1	8
45	238.1	-6.3	10
45	247.3		

Crystal B			
1	288.1	-4.9	7.7
1	276.3	-4.8	7.6
2	231		
2	255.4	-8.8	12.6
2	241.6	-7.9	11.6
3	168.1	-2.1	3.5
3	174.1	-2.5	4.2
3	158.3	-2.4	4
5	274.2		
7	222.1	-5.4	8.4
7	234.1	-5.4	8.4
7	231.7	-5.4	8.4
8	191.6		
8	209.4	-4.1	6.6
8b	142.1	-1.1	1.9
8b	149.7	-1.4	2.4
8b	140.6	-0.9	1.6
11	297.8	-8.9	12.7
11	301	-9.4	13.3
12	332.6	-8.1	11.8
13	116.7	-20.8	23.2
13	127.4	-21	23.4
14			
14	247		
15	231.8	-5.9	9.1
20	251.7	-7.1	10.6
20	198.1	-6.9	10.4
20	247.6	-6.9	10.4
20	254.3	-7	10.5
22	228.8		
29	201.3	-4.1	6.6
29	211.7	-4.2	6.7
29	191.4	-4.2	6.7
32	248.1		
32	244.4	-6.1	9.3
32	251.9	-6.4	9.7
35	168.4	-1.2	2.1
35	187.1	-1.4	2.4
37	241.1		
38	147.9	-0.9	1.6
38	164.2	-0.7	1.2
38	168.7	-0.9	
44	204.6		
46	308.4		
46	310.7	-11.2	15.2
51	119.7	-19.1	22

53	244.1	-10.1	14.1
53	257	-10.4	14.4
60	178.3		
60	204.9	-3.1	5.1
60	202	-3.4	5.5
62	264.8		
66	224.8	-5.8	8.9
66	247.1	-5.8	8.9
68	217.5	-5.4	8.4
68	211.2	-6.1	9.3
68	234.2	-5.2	8.1
73	364.1		
74	334.2	-12.8	16.8
75	178.4	-1.4	2.4
75	164.2	-1.2	2.1
80	231.7	-7.1	10.6
80	248.4	-7.6	11.2
80	241.9		
80	228.3	-7.6	11.2
81	277.7		
82	159.4	-8.1	11.8
82	155.1	-8.1	11.8
82	200.3	-7.9	11.6
83	174.8	-2.1	3.5
83	192	-2.7	4.5
p	347.5	-8.8	12.6
p	258.7	-7.6	11.2
p	344.1	-11.2	15.2
p	367.4	-4.4	7
p	368.4	-6.8	10.2
p	254.3	-4.8	7.6
p	301.5	-9.7	13.7
p	298.3	-8	11.7
p	344	-13.1	17.1
p	268.1	-5.6	8.7
p	377.7	-13	17

Chapter 4: Data base

Table A4.1 Joint data: Caradon Hill Quarry

strike	dip	dip direction
264	66	S
346	81	E
321	90	
247	69	S
331	72	E
266	78	N
312	82	NE
270	77	N
338	88	E
270	78	N
267	76	S
349	88	E
264	71	S
142	90	
262	81	S

Table A4.2 Joint data: Cheesewring Quarry

strike	dip	dip direction	form	frequency	comment
359	88	W	planar	1-1.5m	not mineralised
360	82	W	planar	1-1.5m	not mineralised
266	75	S	planar?	1m	not mineralised
257	75	S	planar	1m	not mineralised
12	15	E	planar	1-2m	not mineralised
342	86	E	planr	1-1.5m	not mineralised
259	77	S	planar	1m	not mineralised
322	72	SW	irregular	?	not mineralised
348	16	E	planar	1-2m	not mineralised
268	78	S	planar	1m	2mm of tourmaline
322	90		planar	irregular	not mineralised
270	74	S	planar	1m	not mineralised
336	22	E	planar	1-2m	not mineralised
284	80	S	irregular	irregular	not mineralised
346	15	E	planar	1-2m	not mineralised
262	78	E	planar	1m	not mineralised
334	87	NE			
362	82	N			
347	82	W	planar	1-2m	not mineralised
262	78	N			
306	11	E	planar	1m	not mineralised
262	78	S			
1	82	W			
237	84	S			
359	85	W			
245	80	S			
252	87	S			
353	84	W			
263	76	S			
341	80	E			
255	73	N			
274	90				

333	80	W
324	90	

Table A4.3 Joint data: Hingston Down

strike	dip	fill	border	persist-ance	form	comment
228	86NW	open 2mm slick fibre	2-3 cm greisen	3m	planar	slick 10NE pitch
30	74S	open 2mm slick fibre	2cm greisen	12m	shallows	slick 30SW pitch
220	78N	open 2mm slick fibre	2cm greisen	4m	planar	
226	90	open 2mm tourmaline vein	1-2 cm greisen	12m	planar	
226	83N	open 1mm slick fibre	1-2cm weak greisen	12m	planar	slick 12NE pitch
70	64SE	filled .5cm qtz-tourmaline	no greisen	1m	planar	
216	6N	open no fill	none	10m+	undulate	
220	84N	open no fill, slight polish	2cm greisen	12m	planar	
218	90	granite 12-20cm	2-3mm tourmaline	8m	stepped	coarse granite + kspar megs
220	75N	open no fill	none	12m	planar	parallel tourmaline veins cut 9
224	90	open .5cm qtz-tourmaline	1-2cm greisen	12m	planar	close to parallel crush zone
218	78N	open no fill	none	3m	planar	on N margin of 20cm wide fracture zone
148	76E	open no fill	none	5m+	sub-planar	slight rotation (parallel to face)

Table A4.4 Joint data: Hingston Down

strike	dip	fill	border	persist-ance	form	freq	comment
212	85NW	open slick 1mm	.5cm greisen	4m	planar	2-3m	0 pitch of slick
44	52SE	open no fill	2mm?	4-5m	undulating	only 1 (rare)	slightly polished
100	30S	open no fill -1mm qtz	none	4m	wavy 10cm	?	
258	75N	qtz - tourmaline	weak greisen	15m	planar	parallel to face 0.5m	9E pitch of slick
126	48SW	open brown staining	iron stained	2m	sub-planar	only 1 (rare)	
267	90	qtz + tour + sulphides	2-3cm greisen	2-3m	planar	0.5m	
140	80SW	open clay	none	4m	planar-anastom	only 1 (rare)	
260	80N	qtz-tour + Fe oxide	1cm greisen	2m	planar	rare	mineralised
61	64S	no fill	2cm greisen	?	sub-planar	?	
263	82N	5mm	fe oxides	2m	curvi-planar	parallelto face 0.5m	possible greisen
256	90	qtz-tour-fe oxide	1mm greisen	1m	planar	?	
221	82NW	mineralised	1-2cm greisen	8m	planar	?	

Table A4.5 Joint data: Kit Hill

strike	dip	fill	form	frequency	comment
316	81NE	open	planar		weathered surfaces
333	90	open	planar		
82	64S	qtz+fluorite	planar	75cm-2m	more penetrative fractures
340	90			4-5m	joint set control quarry face
86	68S	euhedal qtz			slick: 136/53 & 118/38
336	90	open	planar		possibly polished surface
210	17NW			irregular	possible release joints
328	76NE				
342	85NE		irregular	2-5m	granite weathered along joints

82	62S	qtz-fdsp-tour	irregular	qtz-fdsp-tour veins

Table A4.6 Joint data: Kit Hill

strike	dip	form	frequency	comment
280	84		4m	defines quarry face
328	90	planar	1-5m	kaolinized along joint
336	90	planar	1-5m	kaolinized along joint
204	88N	planar		defines quarry face
70	59NE	planar		penetrative 1.5m wide zone
230	25N		0.75-4m	steep dip of horrizontal step

Table A4.7 FIP orientation data: CHQ1

F.I.P. No.	Strike	Dipr	Inclusion size	Planar	Crack width	Development	Definition	Abund.
1	201	54	varied	planar	wide	intracrystalline	poorly defined	few
2	309	66	<5	planar	narrow	intercrystalline	well defined	many
3	66	70	<5	planar	narrow	intercrystalline	well defined	many
4	104	71	<5	planar	narrow	intercrystalline	poorly defined	many
5	145	45	varied	planar	narrow	intercrystalline	poorly defined	few
6	45	59	varied	curvi-planar	wide	intracrystalline	poorly defined	few
7	45	66	varied	planar	wide	intracrystalline	poorly defined	few
8	288	49	<5	planar	narrow	intercrystalline	well defined	many
9	292	66	<5	planar	narrow	intercrystalline	well defined	many
10	297	57	varied	planar	narrow	intracrystalline	poorly defined	few
11	81	56	<5	planar	narrow	intracrystalline	well defined	many
12	94	60	<5	planar	narrow	intercrystalline	well defined	many
13	97	60	<5	planar	narrow	intercrystalline	well defined	many
14	162	44	>5	planar	wide	intercrystalline	well defined	few
15	296	66	<5	planar	narrow	intercrystalline	well defined	many
16	99	63	<5	planar	narrow	intercrystalline	well defined	many
17	188	80	varied	planar	narrow	intercrystalline	well defined	many
18	308	46	>5	planar	narrow	intercrystalline	poorly defined	few
19	99	69	<5	planar	narrow	intracrystalline	poorly defined	few
20	148	40	<5	planar	narrow	intercrystalline	well defined	many
21	183	35	>5	planar	narrow	intracrystalline	poorly defined	few
22	138	46	<5	planar	narrow	intercrystalline	well defined	many
23	298	67	<5	planar	narrow	intracrystalline	well defined	few
24	274	55	<5	planar	narrow	intracrystalline	poorly defined	few
25	138	59	varied	planar	wide	intercrystalline	poorly defined	few
26	238	86	>5	planar	narrow	intercrystalline	well defined	few
27	237	89	>5	planar	narrow	intercrystalline	well defined	few
28	177	88	<5	planar	narrow	intracrystalline	well defined	many
29	42	77	<5	planar	narrow	intracrystalline	well defined	many
30	237	79	<5	planar	narrow	intracrystalline	well defined	many
31	15	65	varied	planar	narrow	intercrystalline	well defined	few
32	82	88	varied	planar	wide	intercrystalline	poorly defined	many
33	36	59	<5	planar	narrow	intercrystalline	well defined	unhealed
34	97	68	varied	planar	wide	intracrystalline	poorly defined	few
36	357	80	>5	planar	narrow	intracrystalline	well defined	few
37	19	82	varied	planar	narrow	intracrystalline	well defined	many
38	258	82	<5	planar	narrow	intracrystalline	well defined	many
39	245	23	<5	planar	narrow	intercrystalline	well defined	many
40	286	65	varied	planar	wide	intracrystalline	poorly defined	many
41	303	71	<5	planar	narrow	intracrystalline	well defined	many
42	299	61	<5	planar	narrow	intracrystalline	well defined	many
43	258	50	varied	planar	narrow	intercrystalline	well defined	many
44	88	74	<5	planar	narrow	intercrystalline	well defined	many
45	275	87	varied	planar	narrow	intercrystalline	poorly defined	few
46	240	76	<5	planar	narrow	intercrystalline	well defined	many

47	260	73	varied	planar	narrow	intracrystalline	well defined	many
48	243	79	varied	planar	wide	intercrystalline	poorly defined	many
49	275	84	varied	planar	narrow	intercrystalline	poorly defined	few
50	25	86	>5	planar	narrow	intercrystalline	well defined	few
51	236	72	<5	planar	narrow	intercrystalline	well defined	many
52	275	55	varied	planar	narrow	intercrystalline	well defined	few
53	262	71	>5	planar	wide	intercrystalline	poorly defined	few
54	92	71	>5	planar	wide	intracrystalline	poorly defined	few
55	94	78	>5	planar	wide	intracrystalline	poorly defined	few
56	155	86	>5	planar	narrow	intercrystalline	well defined	few
57	154	83	>5	planar	narrow	intercrystalline	well defined	few
58	250	67	<5	planar	narrow	intercrystalline	well defined	many
59	157	85	>5	planar	narrow	intercrystalline	well defined	few
60	28	76	>5	planar	narrow	intercrystalline	well defined	few
61	274	86	varied	planar	narrow	intercrystalline	poorly defined	few
62	344	86	<5	curvi-planar	narrow	intercrystalline	well defined	many
63	353	84	<5	planar	narrow	intracrystalline	well defined	many
64	281	85	<5	planar	narrow	intracrystalline	well defined	many
65	240	77	<5	planar	narrow	intercrystalline	well defined	many
66	335	80	>5	planar	narrow	intercrystalline	well defined	few
67	9	81	<5	planar	narrow	intracrystalline	well defined	many
68	36	76	>5	planar	narrow	intercrystalline	poorly defined	few
69	177	72	<5	planar	narrow	intracrystalline	well defined	many
70	84	78	varied	planar	narrow	intercrystalline	well defined	few
71	372	74	<5	curvi-planar	narrow	intercrystalline	well defined	many
72	255	79	<5	planar	narrow	intracrystalline	well defined	many
73	240	74	<5	curvi-planar	narrow	intercrystalline	well defined	many
74	240	79	<5	planar	narrow	intercrystalline	poorly defined	many
75	248	75	<5	planar	narrow	intracrystalline	well defined	many
76	30	66	>5	planar	wide	intercrystalline	well defined	few

Table A4.8FIP orientation data: CWQ1

F.I.P. No.	Strike	Dip	Inclusion size	Planar	Crack width	Development	Definition	Inc. Abund.
1	85	83	<5	planar	narrow	intercrystalline	well defined	many
2	107	75	<5	planar	narrow	intercrystalline	well defined	many
3	268	85						unhealed
4	96	54	<5	planar	narrow	intracrystalline	well defined	many
5	106	67	<5	planar	narrow	intercrystalline	well defined	many
6	106	88	>5	planar	wide	intercrystalline	poorly defined	few
7	123	82						unhealed
8	122	85	<5	planar	narrow	intercrystalline	well defined	few
9	283	83	<5	planar	narrow	intracrystalline	poorly defined	few
10	291	82	<5	planar	narrow	intercrystalline	well defined	few
11	27	88	>5	planar	narrow	intracrystalline	well defined	few
12	21	83	>5	planar	wide	intracrystalline	poorly defined	few
13	20	54	>5	planar	wide	intercrystalline	well defined	few
14	204	58	>5	planar	narrow	intercrystalline	poorly defined	few
15	222	60	>5	curvi-planar	narrow	intercrystalline	poorly defined	many
16	239	59	<5	planar	narrow	intracrystalline	well defined	many
17	16	66	varied	curvi-planar	wide	intracrystalline	poorly defined	few
18	282	86	<5	planar	narrow	intracrystalline	well defined	few
19	107	88	<5	planar	narrow	intercrystalline	poorly defined	few
20	283	87	<5	planar	narrow	intercrystalline	poorly defined	many
21	290	84	<5	curvi-planar	narrow	intercrystalline	poorly defined	few
22	115	87	<5	curvi-planar	narrow	intracrystalline	poorly defined	few
23	120	84	<5	planar	narrow	intracrystalline	well defined	few
24	132	86	>5	planar	narrow	intracrystalline	poorly defined	few
25	111	83	<5	planar	narrow	intracrystalline	poorly defined	many

26	122	70	<5	planar	narrow	intercrystalline	well defined	many
27	37	72	varied	planar	wide	intracrystalline	poorly defined	few
28	18	49	<5	irregular	wide	intercrystalline	poorly defined	many
29	241	56	>5	planar	narrow	intercrystalline	well defined	many
30	261	63	<5	planar	narrow	intracrystalline	well defined	many
31	246	65	<5	planar	narrow	intercrystalline	poorly defined	many
32	245	51	varied	planar	narrow	intercrystalline	well defined	many
33	249	52	varied	planar	narrow	intercrystalline	well defined	many
34	127	90	<5	planar	narrow	intercrystalline	well defined	few
35	308	86	varied	planar	narrow	intracrystalline	poorly defined	few
36	285	84	<5	planar	narrow	intracrystalline	poorly defined	few
37	132	74	<5	planar	narrow	intracrystalline	poorly defined	few
38	122	72	<5	planar	wide	intracrystalline	poorly defined	few
39	270	79	<5	planar	wide	intracrystalline	poorly defined	many
40	269	79	<5	planar	wide	intracrystalline	poorly defined	many
41	279	88	<5	planar	wide	intracrystalline	poorly defined	many
42	266	84	<5	planar	wide	intracrystalline	poorly defined	many
43	286	89	<5	planar	wide	intracrystalline	poorly defined	many
44	202	54	<5	irregular	narrow	intercrystalline	well defined	many
45	196	50	<5	irregular	narrow	intercrystalline	well defined	many
46	342	70	<5	planar	narrow	intracrystalline	well defined	many
47	256	76	<5	planar	narrow	intracrystalline	well defined	many
48	267	75	<5	planar	narrow	intracrystalline	poorly defined	few
49	211	61	<5	planar	narrow	intracrystalline	poorly defined	few
50	214	57	<5	planar	narrow	intracrystalline	well defined	many
51	200	52	<5	irregular	narrow	intracrystalline	well defined	many
52	284	76	<5	curvi-planar	narrow	intracrystalline	poorly defined	many
53	280	67	<5	curvi-planar	narrow	intracrystalline	well defined	many
54	211	71	<5	planar	narrow	intercrystalline	well defined	many
55	211	78	<5	planar	narrow	intracrystalline	poorly defined	many
56	260	64	<5	planar	narrow	intracrystalline	well defined	many
57	285	71	<5	curvi-planar	narrow	intercrystalline	well defined	many
58	279	82	>5	planar	narrow	intracrystalline	poorly defined	few
59	69	85	<5	planar	narrow	intracrystalline	poorly defined	few
60	41	58	varied	planar	wide	intracrystalline	poorly defined	few
61	351	64	<5	curvi-planar	narrow	intracrystalline	poorly defined	few
62	6	72	varied	planar	narrow	intercrystalline	poorly defined	few
63	146	76	>5	irregular	wide	intracrystalline	poorly defined	few
64	315	71	varied	planar	narrow	intercrystalline	poorly defined	few
65	105	65	<5	planar	narrow	intercrystalline	poorly defined	few
66	108	60	<5	planar	narrow	intercrystalline	poorly defined	few
66a	264	61	<5	curvi-planar	narrow	intercrystalline	well defined	many
67	247	79	>5	planar	wide	intracrystalline	poorly defined	few
68	248	58	>5	planar	wide	intracrystalline	poorly defined	few
69	119	75	<5	planar	narrow	intracrystalline	poorly defined	few
70	317	65	<5	planar	narrow	intercrystalline	well defined	many
71	314	70	varied	planar	wide	intercrystalline	well defined	many
72	12	71	varied	planar	wide	intercrystalline	poorly defined	many
73	44	65	varied	planar	narrow	intracrystalline	well defined	few
74	229	71	<5	planar	narrow	intracrystalline	well defined	many
75	248	58	varied	curvi-planar	wide	intercrystalline	poorly defined	many
76	264	71	varied	planar	narrow	intercrystalline	well defined	many
77	256	77	varied	planar	wide	intracrystalline	poorly defined	few
78	119	67	varied	planar	wide	intercrystalline	poorly defined	many
79	264	72	varied	planar	narrow	intercrystalline	well defined	many
80	57	47	varied	planar	wide	intercrystalline	well defined	many
81	120	86	varied	planar	narrow	intercrystalline	poorly defined	few
82	244	60	<5	planar	narrow	intercrystalline	poorly defined	few

83	252	67	<5	planar	narrow	intercrystalline	poorly defined	few
84	253	70	<5	planar	narrow	intracrystalline	poorly defined	few
85	5	52	<5	planar	narrow	intercrystalline	poorly defined	few
86	214	84	<5	curvi-planar	narrow	intracrystalline	poorly defined	few
87	251	66	<5	planar	narrow	intercrystalline	well defined	many
88	153	76	>5	planar	wide	intracrystalline	poorly defined	few
89	59	58	>5	irregular	wide	intracrystalline	poorly defined	few
90	138	74	<5	curvi-planar	narrow	intracrystalline	poorly defined	few
91	256	75	<5	planar	narrow	intracrystalline	poorly defined	few

Table A4.9 FIP orientation data: HD1

F.I.P. No.	strike	dipr	inclusion size	planar	crack width	development	definition	abundance
1	299	85	>5	curvi-planar			poorly defined	
2	115	76	variety	planar		intercrystalline	well defined	abundant
3	119	63	>5	planar		intracrystalline	poorly defined	few
4	322	86	<5	curvi-planar	narrow			few
5	328	77	>5	planar	narrow	intercrystalline	well defined	few
6	330	55	>5	curvi-planar		intercrystalline	well defined	few
7	325	74	<5		narrow	intracrystalline	well defined	abundant
8	189	90	>5			intracrystalline	well defined	few
9	283	89			wide	intracrystalline	poorly defined	none
10	103	88			wide	intracrystalline	poorly defined	none
11	190	69	>5			intracrystalline	well defined	few
12	189	84	>5			intracrystalline	well defined	few
13	15	25			narrow		poorly defined	none?
14	349	73			wide	intercrystalline	poorly defined	none
15	327	72			wide	intercrystalline	poorly defined	none
16	151	21		curvi-planar	narrow		poorly defined	
18	330	67	<5		narrow		poorly defined	few
19	339	75	>5		wide	intercrystalline	well defined	few
20	268	53	<5		narrow	intracrystalline	well defined	abundant
21	180	32	<5		narrow	intracrystalline	well defined	abundant
22	291	13	<5	curvi-planar	narrow	intercrystalline	well defined	v.abundant
23	15	63	>5	curvi-planar	narrow	intercrystalline	well defined	few
24	322	80	>5			intracrystalline	poorly defined	few
25	303	86		curvi-planar			well defined	none
26	284	14	<5	planar	narrow	intracrystalline	well defined	abundant
27	321	84	>5			intracrystalline	poorly defined	few
28	7	88	<5	planar	narrow	intracrystalline	well defined	many
29	247	35	>5	planar	v.narrow	intercrystalline	well defined	few

Table A4.10 FIP orientation data: HD2

F.I.P. No.	strike	dipr	inclusion size	planar	crack width	development	definition	abundance
1	3	40	varied					
2	8	42						few
3	1	63	<5					abundant
4	223	57						few/none
5	42	52	<5	curvi-planar				abundant
6	41	58	<5	planar	narrow			abundant
7	74	10	>5					few
8	124	15	>5					few
9	5	22	<5		narrow			few
10	49	16	>5	curvi-planar		intercrystalline		few
11	160	13	<5	curvi-planar		intercrystalline		abundant
12	349	21	>5			intracrystalline		few

13	9	47	>5				poorly defined	few
14	108	9	<5	curvi-planar	narrow		well defined	abundant
15	172	46	<5		narrow		well defined	abundant
16	29	49		curvi-planar		intracrystalline		
17	24	17		irregular				none
18	47	31		planar				none
19	54	17		planar		intracrystalline		none
20	145	31		planar		intracrystalline		none
21	110	21	>5	curvi-planar			poorly defined	few
22	9	55	>5	planar		intracrystalline		few
23	30	47	>5	planar		intracrystalline		few
24	126	10	<5	curvi-planar	narrow		well defined	abundant
25	180	38		curvi-planar			well defined	none
26	149	13	<5	planar	narrow		well defined	abundant
27	187	62	>5	kinked	narrow	intracrystalline	poorly defined	few
28	153	7	<5	curvi-planar	narrow	intracrystalline	well defined	abundant
29	209	12	<5	curvi-planar	narrow	intercrystalline	well defined	abundant
30	19	34	>5		narrow	intercrystalline	poorly defined	few
31	8	59	>5		narrow	intracrystalline	poorly defined	few
32	140	6	<5	curvi-planar	narrow	intracrystalline	well defined	abundant
33	197	19	<5	planar	narrow	intracrystalline	poorly defined	few
34	136	11		irregular				few/none
35	5	57	>5	planar	wide	intracrystalline	poorly defined	few
36	0	23	v.<5	planar	v.narrow	intercrystalline	v.well defined	v.abundant
37	162	18		planar	narrow	intracrystalline	well defined	none
38	87	18	>5	planar	narrow	intracrystalline	well defined	>5
39	207	69	>5	curvi-planar	narrow		poorly defined	>5
40	43	51	>5	narrow	narrow	intracrystalline	poorly defined	>5

Table A4.11 FIP orientation data: HD3

F.I.P. No.	strike	dipr	inclusion size	planar	crack width	development	definition	abundance
1	294	39	>5	planar	narrow	intercrystalline	well defined	few
3	148	21		curvi-planar	narrow	intercrystalline	well defined	
2	249	48	<5	curvi-planar	narrow	intracrystalline	poorly defined	abundant
5	12	27	<5	planar	narrow	intracrystalline	well defined	abundant
6	267	75	>5	planar	wide	intracrystalline	poorly defined	few
7	290	73	>5	planar	narrow	intracrystalline	well defined	few
8	259	87		planar	v.narrow	intracrystalline	well defined	
9	105	87	>5	planar	narrow	intracrystalline	poorly defined	few
10	271	51	>5	curvi-planar	wide	intracrystalline	poorly defined	few
11	4	29	>5	planar	wide	intracrystalline	poorly defined	few
12	252	73	>5	planar		intracrystalline	poorly defined	few
13	246	43	<5	planar	narrow	intracrystalline	poorly defined	few
14	339	39	>5	planar	narrow	intracrystalline	poorly defined	few
15	305	77	<5	planar	narrow	intercrystalline	well defined	abundant
16	343	48	<5	planar	narrow	intracrystalline	poorly defined	abundant
17	348	48		planar	narrow	intracrystalline	poorly defined	irregular
18	33	69	<5	planar	narrow	intercrystalline	well defined	few
19	310	55	>5	planar?	wide	intercrystalline ?	poorly defined	irregular
20	238	41	>5	planar	narrow	intracrystalline	poorly defined	few
21	12	2	>5	planar	narrow	intracrystalline	well defined	few
22	272	68	<5	planar	narrow	intracrystalline	well defined	abundant
23	104	90	<5	planar	narrow	intracrystalline	poorly defined	abundant
24	288	62	<5	curvi-planar	narrow	intercrystalline	poorly defined	abundant
25	185	16	<5	planar	narrow	intracrystalline	poorly defined	abundant

26	236	54	>5	curvi-planar	narrow	v.intracrystallin e	poorly defined	few
27	320	15	<5	planar	narrow	intracrystalline	well defined	abundant
28	25	63	>5	planar	narrow	intercrystalline	well defined	few
29	310	32	<5	planar	narrow	intracrystalline	poorly defined	abundant
30	258	69	>5	planar	wide	intracrystalline	poorly defined	few
31	355	36	<5	planar	narrow	intercrystalline	v.well defined	abundant
32	222	5	<5	curvi-planar	narrow	intracrystalline	poorly defined	abundant
33	93	31	<5	curvi-planar	narrow	intracrystalline	poorly defined	abundant
34	263	54	>5	planar	wide	intercrystalline	poorly defined	few
35	294	84	>5	planar	narrow	intercrystalline	well defined	few
36	292	90	<5	planar	narrow	intercrystalline	poorly defined	abundant
37	30	18	<5	curvi-planar	narrow	intercrystalline	well defined	abundant
38	247	47	<5	planar	narrow	intracrystalline	well defined	abundant

Table A4.12 FIP orientation data: HD5

F.I.P. No.	strike	dipr	inclusion size	planar	crack width	development	definition	abundance
1	52	54	<5					abundant
2	24	36	<5					abundant
3	1	84	<5		wide			abundant
4	223	72	regular					
5	345	32	varied					
6	10	39	varied		wide			abundant
7	70	24	>5					
8	114	68	<5		narrow			abundant
9	271	85						none?
10	105	85	<5					
11	103	89						
12	346	24	<5					abundant
13	65	14	<5					abundant
14	7	33						abundant
15	298	57	<5					few
16	248	27	>5		wide			few
17	255	28	>5		wide			few
18	271	32	varied		wide			
19	315	61						few
20	357	74	<5					abundant
21	15	55						
22	6	63						
23	358	71						
24	340	29						
25	8	31						
26	6	53						
27	77	45						
28	45	53						
29	37	48						
30	96	82						
31	298	84						
32	130	87						
33	138	85						
34	346	27						
35	10	32						
36	356	66						
37	355	67						
38	36	75						
39	353	66						

40	216	71						few
41	228	59	>5					
42	77	50	<5	curvi-planar				abundant
43	228	69			wide			few
44	15	84	<5		narrow	poor		abundant
45	345	77	<5	curvi-planar				abundant
46	6	60	>5					few
47	339	67	<5					abundant
48	359	88	<5					abundant
49	116	82	<5					few
50	214	71	<5					abundant
51	230	49	>5					few
52	349	62	<5		narrow			abundant
53	356	51	>5				poor	few
54	356	55	>5				poor	few
55	267	54						none
56	103	86						none
57	344	83	>5					few
58	349	63	>5				poor	few
59	352	75	<5					abundant
60	202	85	<5					abundant
61	253	54	<5		narrow		good	abundant

Table A4.13 FIP orientation data: HD6

F.I.P. No.	strike	dipr	inclusion size	planar	crack width	development	definition	abundance
1	282	88	>5	planar	wide	intracrystalline	well defined	few
2	265	56	varied	planar	narrow	intercrystalline	poorly defined	few
3	326	47	<5	curvi-planar	narrow	intracrystalline	well defined	few
4	292	10	<5	planar	narrow	intracrystalline	well defined	abundant
5	303	49	<5	planar	narrow	intercrystalline	poorly defined	abundant
6	338	54	>5	planar	narrow	intercrystalline	well defined	few
8	260	62	<5	curvi-planar	narrow	intercrystalline	well defined	abundant
9	320	79	varied	planar	narrow	intercrystalline	well defined	abundant
10	157	82	>5	planar	narrow	intracrystalline	well defined	few
11	245	65	varied	planar	narrow	intercrystalline	poorly defined	few
12	342	62	>5	planar	narrow	intracrystalline	poorly defined	few
13	322	81	>5	planar	narrow	intracrystalline	poorly defined	few
14	348	63	>5	planar	narrow	intercrystalline	well defined	few
15	286	40	>5	planar	narrow	intercrystalline	poorly defined	few
16	267	58	varied	curvi-planar	narrow	v.intercrystalline	poorly defined	few
17	249	62	>5	planar	narrow	intracrystalline	well defined	few
18	168	48	<5	planar	narrow	poorly developd	well defined	abundant
19	331	64	>5	planar	wide	intracrystalline	poorly defined	few
20	145	81	>5	planar	wide	intercrystalline	well defined	abundant
21	312	62	<5	planar	narrow	intercrystalline	well defined	abundant
22	294	33	<5	planar	narrow	intercrystalline	poorly defined	abundant
23	270	73	>5	irregular	wide	intracrystalline	poorly defined	abundant
24	211	33	varied	planar	wide	intercrystalline	poorly defined	few
25	147	84	>5	planar	narrow	intracrystalline	poor;y defined	few
26	273	61	>5	curvi-planar	narrow	intracrystalline	well defined	few
27	206	34	>5	planar	narrow	intracrystalline	well defined	few
28	321	75	>5	planar	wide	intercrystalline	poorly defined	few
29	254	78	<5	planar	narrow	intercrystalline	poorly defined	abundant
30	107	60	<5	curvi-planar	narrow	intercrystalline	poorly defined	abundant
31	145	45	>5	planar	narrow	intracrystalline	well defined	>5
32	274	46	varied	planar	wide	intracrystalline	poorly defined	few

33	301	65	>5	planar	v.wide	intracrystalline	v.poorly defined	abundant
34	301	65	>5	planar	v.wide	intracrystalline	v.poorly defined	abundant
35	304	68	varied	planar	narrow	intercrystalline	poorly defined	few
36	298	28	>5	planar	narrow	intracrystalline	intercrystalline	abundant
37	337	46	>5	planar	narrow	intracrystalline	poorly defined	few
38	304	76	>5	planar	narrow	intracrystalline	poorly defined	few
39	162	52	>5	planar	narrow	intracrystalline	poorly defined	few
40	311	37	>5	curvi-planar	narrow	intercrystalline	poorly defined	few
41	328	73	>5	planar	v.wide	intercrystalline	v.poorly defined	abundant
42	328	73	>5	planar	v.wide	intercrystalline	v.poorly defined	abundant
43	282	57	>5	planar	narrow	intercrystalline	poorly defined	few
44	125	62	varied	planar	wide	intercrystalline	v.poorly defined	abundant
45	125	62	varied	planar	wide	intercrystalline	v.poorly defined	abundant
46	126	90	varied	planar	wide	intracrystalline	v.poorly defined	abundant

Table A4.14 FIP orientation data: KH4

F.I.P. No.	Strike	Dip	Inclusion size	Planar	Crack width	Development	Definition	Abund.
1	96	76	>5	planar	narrow	intercrystalline	poorly defined	few
2	96	78	>5	planar	narrow	intercrystalline	poorly defined	few
3	85	73	>5	planar	wide	intracrystalline	poorly defined	few
4	85	53	>5	planar	narrow	intercrystalline	poorly defined	few
5	80	71	varied	planar	narrow	intercrystalline	poorly defined	many
6	104	80	<5	planar	narrow	intracrystalline	poorly defined	few
7	97	80	<5	planar	narrow	intracrystalline	poorly defined	few
8	103	70	varied	curvi-planar	narrow	intercrystalline	well defined	many
9	69	47	varied	planar	narrow	intracrystalline	poorly defined	many
10	347	89	varied	planar	narrow	intracrystalline	well defined	many
11	92	64	<5	planar	narrow	intercrystalline	well defined	many
12	90	71	varied	curvi-planar	narrow	intercrystalline	poorly defined	few
13	82	59	>5	planar	wide	intracrystalline	poorly defined	few
14	359	82	varied	planar	wide	intracrystalline	poorly defined	many
15	5	86	varied	planar	wide	intracrystalline	poorly defined	many
16	6	72	varied	planar	wide	intracrystalline	poorly defined	many
17	7	69	varied	planar	wide	intracrystalline	poorly defined	many

Table A4.15 FIP orientation data: LMP1

F.I.P. No.	Strike	Dip	Inclusion size	Planar	Crack width	Development	Definition	Abund
1	269	73	>5	planar	narrow	intercrystalline	well defined	many
2	150	76	>5	planar	wide	intercrystalline	poorly defined	few
3	144	79	varied	planar	wide	intercrystalline	poorly defined	many
4	149	70	>5	irregular	narrow	intracrystalline	poorly defined	many
6	4	85	>5	planar	narrow	intercrystalline	poorly defined	few
7	2	86	varied	curvi-planar	narrow	intracrystalline	poorly defined	few
8	109	79	varied	planar	narrow	intracrystalline	poorly defined	few
9	158	79	varied	planar	narrow	intercrystalline	well defined	many
10	10	89	<5	planar	wide	intracrystalline	poorly defined	many
11	57	88	<5	planar	narrow	intracrystalline	poorly defined	many
12	105	82	varied	planar	narrow	intracrystalline	poorly defined	few
13	123	83	varied	planar	narrow	intracrystalline	poorly defined	many
14	287	87	<5	planar	narrow	intracrystalline	poorly defined	many
15	265	75	>5	curvi-planar	narrow	intracrystalline	poorly defined	few
16	113	86	varied	planar	wide	intracrystalline	poorly defined	many
17	172	58	unhealed	planar	narrow	intercrystalline	well defined	unhealed
18	3	80	<5	planar	narrow	intercrystalline	poorly defined	many
19	2	81	<5	planar	narrow	intercrystalline	poorly defined	many

20	38	89	varied	planar	narrow	intracrystalline	poorly defined	few
21	50	83	varied	planar	narrow	intracrystalline	poorly defined	few
22	108	84	varied	planar	narrow	intercrystalline	poorly defined	few
23	101	66	varied	planar	wide	intercrystalline	poorly defined	many
24	178	86	>5	planar	narrow	intercrystalline	poorly defined	few
25	7	86	varied	planar	narrow	intracrystalline	poorly defined	many
26	21	80	>5	curvi-planar	narrow	intercrystalline	poorly defined	few
27	121	83	varied	curvi-planar	narrow	intracrystalline	poorly defined	many
28	103	82	varied	planar	narrow	intracrystalline	poorly defined	few
29	113	82	varied	planar	narrow	intracrystalline	poorly defined	few
30	203	89	<5	planar	narrow	intracrystalline	poorly defined	many
31	205	88	<5	planar	narrow	intracrystalline	poorly defined	many
32	97	88	varied	planar	narrow	intracrystalline	poorly defined	many
33	50	80	<5	planar	narrow	intracrystalline	poorly defined	many
34	102	89	varied	irregular	wide	intercrystalline	poorly defined	many
35	275	86	<5	planar	narrow	intracrystalline	well defined	many
36	284	88	varied	irregular	wide	intercrystalline	poorly defined	many
37	297	77	<5	planar	narrow	intercrystalline	well defined	many
38	350	76	<5	planar	narrow	intercrystalline	well defined	many
39	355	81	>5	planar	narrow	intercrystalline	poorly defined	few
40	195	86	>5	planar	narrow	intracrystalline	poorly defined	few
41	140	90	<5	planar	narrow	intracrystalline	poorly defined	many
42	97	86	>5	planar	narrow	intracrystalline	poorly defined	few
43	321	85	>5	planar	narrow	intercrystalline	poorly defined	few
44	127	90	>5	planar	narrow	intercrystalline	poorly defined	few
45	330	80	<5	planar	narrow	intercrystalline	well defined	many
46	152	84	varied	planar	wide	intercrystalline	well defined	many
47	108	81	<5	planar	narrow	intercrystalline	well defined	many
48	321	88	sheared	planar	wide	intercrystalline	poorly defined	unhealed
49	130	80	varied	planar	wide	intracrystalline	poorly defined	many
50	126	82	varied	planar	wide	intracrystalline	poorly defined	many
51	272	47	>5	planar	wide	intercrystalline	well defined	many
52	280	45	>5	planar	wide	intercrystalline	well defined	many
53	317	85	<5	planar	narrow	intracrystalline	well defined	many
54	98	90	varied	planar	narrow	intracrystalline	poorly defined	few
55	285	79	varied	planar	narrow	intracrystalline	poorly defined	few
56	271	85	varied	planar	narrow	intercrystalline	poorly defined	many
57	131	90	varied	planar	wide	intracrystalline	poorly defined	many
58	28	90	sheared	curvi-planar	narrow	intracrystalline	well defined	many

Table A4.16 Thermometric data: CWQ1

FIP No.	Th	Tfm	Tlm	wt%NaCl
1	202		-19.2	22.1
23	188.7		-5.1	8
23	173.2		-3.5	5.7
24	221.5		-7.6	11.2
24	168.5		-7.2	10.7
27	185.3		-0.7	1.2
27	193.4		-0.8	1.4
27	184.9		-0.4	0.7
39	154		-4.5	7.2
39	189.4		-5.1	8
39	191.1			
40	145.6		-5.1	8
40	164.7		-6.1	9.3
40	187.4		-5.6	8.7
41	268.1		-6.5	9.9

41	281.2		-6.4	9.7
47	208.7		-4.1	6.6
47	166.4		-4.8	7.6
47	227		-3.5	5.7
47	224.8		-3.5	5.7
47	175.4		-4.2	6.2
2	140.2		-5	7.9
2	236.9		-4.7	7.4
2	235.4		-4.9	7.7
4	159.5		-0.7	1.2
4	173.2		-0.4	0.7
4	156.9		-0.4	0.7
5	102.3	~-35	-22.7	24.5
5	130.1	~-40	-22.5	24.4
8	207.5		-0.7	1.2
8	185.5		-0.6	1
8	199.8		-0.8	1.4
8	212.4		-0.8	1.4
18	156.8		-8.2	12
18	179.4		-6.7	10.1
20	182.5		-9	12.9
20	215.5		-8.4	12.2
20	185.4		-8.1	11.8
25	270.4		-1.2	2.1
44	206.9		-5.2	8.1
44	286.4		-5.7	8.8
44	319.1		-5.4	8.4
44	335.7		-5.8	8.9
45	340.8		-5.1	8
45	327.6		-6.4	9.7
45	341		-5.9	9.1
45	354.2		-5.8	8.9
33	300.1		-7.1	10.6
33	312.1		-7.2	10.7
33	309.1		-7.6	11.2
33	310.4		-7.2	10.7
34	254.7		-4	6.4
34	258.3		-3.8	6.1
34	286.3		-3.9	6.3
34	335		-4.2	6.7
34	351.2		-4.1	6.6
29	312.1		-4	6.4
29	303.6		-4.1	6.6
29	314.2		-3.9	6.3
29	309.8		-4.5	7.2
13	346.2		-4.9	7.7

Table A4.17 Thermometric data: HD2

FIP No.	Th	Tfm	Tlm	wt%NaCl
3	150.2		-3	4.9
1	224.3		-2	3.4
1	214.6		-2.1	3.5
1	219.2		-1.7	2.9
2	204.5		-5.6	8.7
5	238.5		-4.1	6.6
5	180.1		-1.4	2.4
5	169.7		-1.9	3.2

6	280.4		-3.4	5.5
6	173.2		-1.5	2.6
6	173.5		-1.5	2.6
13	196.7		-1.4	2.4
7	115.4			
9	360.1		-0.4	0.7
14	125.4			
16	165.4			
18	173.3		-1.6	2.7
22	312.7		-0.2	0.4
26	152.4			
26	158.4		-0.4	0.7
27	106.8			
27	119.2	-35	-25.6	
27			-23.8	
27	119.3		-23.4	
30	100.4			

Table A4.18 Thermometric data: HD3

F.I.P. No.	Th	Tfm	Tlm	wt%NaCl
1	203		-1.6	2.7
1	165		-2	3.4
3	151.9		-3	4.9
3	164.2		-3.4	5.5
3	180.3		-3.3	5.4
7	255.3		-1.9	3.2
7	160.3		-1	1.7
10	163		-1.9	3.2
10	206.2		-1.9	3.2
10	229.3		-1.8	3
13	198		-1.8	3
24	172.9		-1	1.7
27	178.2		-5.4	8.4
32	184.2		-3.2	5.2
32	179.1		-3.1	5.1
36	347.5			
19	202.1	<-30	-22	24
19	152.9	-45	-20.9	23.3
prim	303	-21	-4.1	6.6
prim	325.1		-1	1.7
prim	368.5		-4	6.4
prim	301.5		-13.9	17.8
prim	360		-4	6.4
prim	401.2			
prim	383.6			
prim	455			
prim	406			

Table A4.19 Thermometric data: HD5

FIP No.	Th	Tfm	Tlm	wt%NaCL
1	311		-2.9	4.9
1	358		-3.8	6.3
1	337.9		-3.4	5.6
1	302		-3.4	5.6
2	228.9		-8.1	11.8

2	204.8	-6.1	9.3
4	335.8	-4.2	6.6
4	336	-3.9	6.3
4	331.8	-4	6.4
4	330.7	-3.7	5.9
4	329	-4.1	6.5
6	179.5	-6	9.2
7	303.9	-0.7	1.2
7	331.8	-0.6	1.1
8	189.3	-7.1	10.6
8	196.8		
8	178.8		
8	173.6		
9	132		
14	182.4	-8.6	12.4
14	177.2	-8.7	12.5
12	182.4	-9.5	13.5
12	184.8	-9.3	13.3
12	187.9	-9.7	13.7
16	323.2		
21	100.5	-3.7	5.9
21	187.9	-4.4	7.1
21	192.7	-4.6	7.3
22	259.8	-4	6.4
22	173.7		
22	203.1		
23	179.3	-6.4	9.8
23	182.4	-6.2	9.4
24	396.5	-3.8	6.3
24	392.6	-4.6	7.3
24	388.8		
24	372		
26	253.2	-6.5	9.9
26	271.1	-6.4	9.8
26	280.2	-6.6	10
27	248.5		
27	303.6		
29	329.9		
29	368.1		
30	412.3		
30	380.6		
30	377		
30	365.1		
31	356.4	-4.6	7.3
31	383.5	-4.2	6.6
31	301		
31	429.5		
32	386.5	-4.2	6.6
35	303.2		
38	440.1	-9.6	13.6
38	458.5	-9.4	13.4
38	439.7	-9.1	13
45	189.4	-2	3.3
45	212.3	-1	1.7
47	155.7	-0.5	0.8
47	179.3	-0.7	1.2
47	138.5		

47	224.3	-0.5	0.8
60	179.7	-5.6	8.7
60	180.1	-5.7	8.8
60	188.6	-5.4	8.4
58	152.8	-0.3	0.5
58	202.4	-4.5	7.1
51	331.1	-1.5	2.6

Table A4.20 Thermometric data: HD6

F.I.P. No.	Th	Tlm	Tlm	wt%NaCl
8	182.4		-1.9	3.2
8	175.4		-1.8	3.1
8	160.5		-1.7	2.9
2	213.2		-1.1	1.9
2	218.1		-1	1.7
3	145.4			
1	200.9		-3.4	5.4
1	229.2		-2.8	4.6
1	217.3		-2.9	4.8
5	244.3		-2	3.4
5	269.2		-3	4.9
9	304.2		-4.4	7
9	300.1		-3	4.9
9	283.4		-4.4	7
10	284.2			
10	307.3			
12	254		-5.3	8.3
12	289.8		-5.1	5.1
14	304.2		-0.9	1.6
14	301.9		-0.8	1.4
14	310.4		-0.8	1.4
32	183.2		-2	3.4
32	195.7		-2.2	3.7
37	375		-4.2	6.7
37	370.4		-4.7	7.4

Table A4.21 Thermometric data: HD7

Inclusion #	Th	Tfm	Tlmice	wt%NaCl
1	158.7		-7.1	10.6
2	169.9		-5.4	8.4
3	184.6		-5.1	8
4	182		-6.1	9.3
5	199.2		-5.3	8.3
6	193.1		-5.5	8.5
7	202			
8	176.7		-4.1	6.6
9	177.9		-4.9	7.7
10	220.1		-6.9	10.4
11	190.8		-7.8	11.5
12	187.2		-5.3	8.3
13	177.8			
14	162.4		-6.3	9.6
15	191.2		-6.8	10.2
16	186.9		-5.8	8.9

Table A4.22 Thermometric data: KH3

Th	Tfm	Tmice	Tmhydro	wt%NaCl
143.3	-48	-20.2	-25.7	22.8
156.9		-19.4	-23.8	22.2
216.2	-50	-18	-24.5	21.2
125	-50	-18.5		21.6
138.3	-45	-20.5	-24.8	23
147.9				
131.1		-19.4	-23.7	22.2
156.6	-45	-19.6	-25.4	22.4
125.7	-51	-18.9	-25.3	21.9
117.4	-51			
161.2	-47	-19.3		21.2
124.3	-50	-19.2	-26.1	22.1

Table A4.23 Thermometric data: KH4

FIP. No.	Th	Tfm	Tlm	Tmhydro	NaClwt%
1	158.7		-4.5		7.2
1	175.6		-4.2		6.7
1	167.8		-4.4		7
2	331.4		-5.6		8.7
2	324.1		-5.4		8.4
3	195.9		-3.8		6.1
3	194.7		-3.7		6
3	208		-4.1		6.6
4	324.5		-8.1		11.8
6	187.2		-1.5		2.6
6	164.3		-2.1		3.5
6	184.4		-2.4		4
7	361.8		-5.4		8.4
8	321.1		-5.2		8.1
8	309.4		-5.1		8
9	168.5		-4.1		6.6
9	175.8		-3.9		6.3
9	173.2		-3.7		6
10	126.2	~-35	-19.4		22.2
12	345.5		-9.4		13.3
13	344.6		-6.8		10.2
14	134.2	~-35	-17.2		20.6
14	135.5	~-40	-17.6		20.9
14	125.8	~-40	-17.9		21.1
15	143.2	-51	-18.9	-25.2	21.9
15	134.7	~-35	-18		21.2
15	128.3	~-35	-18.8		21.8
16	141.6	~-35	-16.5		22
17	152.4	-51	-18.7	-24.9	21.7

Table A4.24 Thermometric data: LMP1

FIP #	Th	Tfm	Tlmice	wt% NaCl
1	212.5		-4.1	6.6
1	222.2		-4.1	6.6
1	210.9		-4	6.4
1	218.4		-4.1	6.6
2	347.2		-12.3	16.3
3	105.6		-0.9	1.6
3	108.4		-1.2	2.1
3	109.1		-1.1	1.9

3	107.5	-1.4	2.4
3	118.2		
3	117.5		
4	121.4	-1.6	2.7
4	129.2	-1.6	2.7
6	286.4	-4.2	6.7
6	288.6		
7	157	-3	4.9
7	139.1	-3.7	6
7	160.4		
7	141.2	-3.3	5.4
7	138.4	-3.2	5.2
12	127.5	-0.8	1.4
12	134.2		
12	114.2		
12	117.9	-1.4	2.4
12	124.3	-1.5	2.6
13	367.8	-9.6	13.5
16	294.2		
16	287.6	-5	7.9
16	315.2	-6.3	9.6
18	284.1	-5.4	8.4
18	268.5	-5.4	8.4
18	239.4	-5.7	8.8
20	131.6	-2.4	4
22	127.4	-2.1	3.5
23	131.1	-2	3.4
23	142.1	-2.3	3.9
23	128.4		
24	248.1	-7.6	11.2
25	239.7	-5.2	8.1
26	108.1	-0.9	1.6
27	304.4	-1.9	3.2
27	315.9	-11.6	15.6
27	297.8		
29	198.4	-6.2	9.5
33	201.7	-4.3	6.7
34	127.8	-1.4	2.4
34	129.1		
35	159.8	-1.9	3.2
35	161.4	-2.1	3.5
35	148.3	-2	3.4
36	178.8	-1.9	3.2
41	124.6	-3.1	5.1
41	128.1	-2.7	4.5
43	297.2	-8.5	12.3
46	284.2	-8.4	12.2
46	194.1	-4.4	7
47	222.6	-4.8	7.6
49	101	-1.2	2.1
49	109.7	-1.2	2.1
53	210	-2.1	3.5
53	231.8	-2.4	4
53	227.2		
54	128.8	-3.1	5.1
54	127.8	-3.1	5.1
54	159.5	-3	4.9
55	178.6	-1	1.7

56	198.4		
57	109.4	-1.6	2.7
57	124.3	-1.6	2.7

Chapter 5: Data base

Table A5.1 Joint data: Lundy Island

Joint No.	strike	dip	quad	development	planar
Location 1					
1	201	78	w	well developed	planar
2	256	75	n	poorly developed	planar
3	295	25	n	poorly developed	planar
4	270	68	n	poorly developed	irregular
5	316	85	ne	well developed	curvi-planar
6	277	68	n	well developed	planar
7	290	62	n	well developed	planar
8	215	73	w	poorly developed	planar
9	266	64	n	well developed	planar
10	60	25	s	well developed	irregular
11	79	90		well developed	planar
12	272	63	n	well developed	planar
13	211	52	nw	well developed	planar
14	260	64	n	well developed	planar
15	164	88	w	poorly developed	planar
16	146	80	w	well developed	planar
17	170	81	w	well developed	planar
18	71	54	s	poorly developed	planar
19	341	85	e	poorly developed	planar
20	150	84	w	poorly developed	planar
21	185	86	w	poorly developed	curvi-planar
22	294	50	n	well developed	planar
23	56	32	se	well developed	planar
24	157	82	w	well developed	planar
25	244	82	n	well developed	planar
26	97	60	s	well developed	planar
27	46	80	s	poorly developed	planar
dyke 1	203	70	w	acidic	
dyke 2	171	80	w	acidic	
Locality 2					
1	284	84	n	well developed	planar
2	101	86	s	well developed	curvi-planar
3	165	50	w	well developed	planar
4	110	87	s	poorly developed	planar
5	293	81	n	well developed	planar
6	167	48	w	well developed	planar
7	112	88	s	well developed	planar
8	115	90		well developed	planar
9	107	88	s	well developed	planar
10	194	85	w	well developed	irregular
11	276	80	n	well developed	planar
12	5	69	e	well developed	irregular
13	8	46	e	poorly developed	irregular
14	171	48	w	well developed	planar
15	106	85	s	well developed	planar
16	356	82	e	well developed	planar
17	110	73	s	well developed	planar
18	108	90		well developed	planar
19	45	65	se	poorly developed	irregular

20	104	85	s	well developed	planar
21	170	48	w	well developed	planar
22	51	63	se	poorly developed	irregular
dyke 1	130	45	s	acidic	
dyke 2	130	45	s	acidic	

Locality 3					
1	100	73	s	poorly developed	curvi-planar
2	84	82	s	poorly developed	planar
3	146	54	w	poorly developed	planar
4	290	73	n	well developed	planar
5	165	63	w	poorly developed	planar
6	355	20	e	poorly developed	planar
7	63	90		poorly developed	planar
8	83	90		poorly developed	planar
9	357	20	e	poorly developed	irregular
10	355	20	e	poorly developed	irregular
11	200	70	w	poorly developed	planar
12	350	20	e	well developed	planar
13	172	61	w	well developed	planar
14	42	85	se	well developed	planar
15	288	84	n	poorly developed	planar
16	185	42	w	well developed	planar
17	22	79	e	poorly developed	planar
18	62	78	se	well developed	planar
19	73	90		poorly developed	planar
20	294	82	n	well developed	planar
21	288	82	n	poorly developed	planar
22	173	58	w	well developed	planar
23	174	59	w	well developed	planar
24	50	77	se	poorly developed	curvi-planar
25	9	75	s	well developed	curvi-planar
26	62	76	s	well developed	planar
27	174	61	w	well developed	planar
28	184	68	w	well developed	planar
29	110	82	s	well developed	planar
30	179	61	w	well developed	planar
31	102	79	s	well developed	planar
dyke 1	200	40	w	acidic	

Locality 4					
tourm. vn.	94	38	s		
dyke 1	77	68	s	acidic	
dyke 2	80	70	s	acidic	

Locality 5					
tourm. vn.	80	40	s		
tourm. vn.	129	41	sw		
tourm. vn.	125	38	sw		

Locality 6

dyke 1	35	45	se	acidic	

Locality 7					
dyke 1	310	85	ne	acidic	
dyke 2	314	87	ne	acidic	
dyke 3	132	90		acidic	
dyke 4	326	82	ne	acidic	

Locality 3b					
1	350	59	e	poorly developed	planar
2	172	63	w	well developed	planar
3	176	62	w	well developed	planar
4	97	90		poorly developed	irregular
5	173	70	w	well developed	planar
6	178	68	w	well developed	planar
7	316	20	ne	poorly developed	planar
8	74	80	s	well developed	curvi-planar
9	310	12	ne	well developed	irregular
10	87	88	s	well developed	curvi-planar
11	156	90		poorly developed	curvi-planar
12	359	60	e	well developed	planar
13	312	70	ne	poorly developed	curvi-planar
14	173	67	w	well developed	planar
15	3	62	e	poorly developed	planar
16	84	90		poorly developed	planar
17	272	82	n	poorly developed	planar
18	71	62	e	well developed	planar

Table A5.2 FIP orientation data: LI1

Inclusion No.	strike	dip	inclusion size	planar	crack width	development	definition	abundance
Crystal A								
1	56	77	<5	cuvi-planar	narrow	intercrystalline	well defined	many
2	327	75	<5	planar	narrow	intercrystalline	well defined	many
3	178	80	<5	planar	narrow	intercrystalline	poorly defined	few
4	308	77	varied	cuvi-planar	narrow	intracrystalline	well defined	many
5	87	63	>5	cuvi-planar	narrow	intercrystalline	poorly defined	few
6	38	83	<5	cuvi-planar	narrow	intercrystalline	poorly defined	few
7	275	62	<5	cuvi-planar	narrow	intercrystalline	poorly defined	few
8	275	57	<5	cuvi-planar	narrow	intercrystalline	poorly defined	few
9	88	62	<5	planar	narrow	intercrystalline	poorly defined	few
10	70	61	<5	planar	narrow	intracrystalline	poorly defined	few
11	274	60	<5	planar	narrow	intracrystalline	poorly defined	few
12	283	90	>5	planar	wide	intracrystalline	poorly defined	few
13	75	77	<5	irregular	narrow	intracrystalline	well defined	few
15	303	71	varied	planar	narrow	intercrystalline	well defined	many
16	303	65	varied	planar	narrow	intercrystalline	well defined	many
17	297	76	varied	planar	wide	intercrystalline	well defined	many
18	59	62	varied	irregular	wide	intracrystalline	well defined	many
19	299	70	>5	planar	wide	intracrystalline	poorly defined	many
20	297	76	<5	cuvi-planar	narrow	intracrystalline	well defined	many
21	31	88	<5	planar	narrow	intercrystalline	poorly defined	few
22	70	76	<5	planar	narrow	intercrystalline	well defined	many
23	64	78	<5	cuvi-planar	narrow	intercrystalline	well defined	many
24	310	73	varied	cuvi-planar	narrow	intracrystalline	well defined	many
25	118	52	>5	planar	wide	intracrystalline	poorly defined	few

26	279	68	varied	planar	narrow	intracrystalline	poorly defined	few
27	73	81	<5	curvi-planar	narrow	intracrystalline	poorly defined	few
28	72	78	<5	planar	narrow	intracrystalline	poorly defined	few
29	5	87	varied	curvi-planar	narrow	intercrystalline	well defined	many
30	22	81	<5	planar	narrow	intracrystalline	poorly defined	few
31	48	73	<5	planar	narrow	intracrystalline	well defined	many
32	66	71	<5	curvi-planar	narrow	intercrystalline	well defined	many
33	55	72	<5	curvi-planar	narrow	intercrystalline	well defined	many
34	38	88	<5	curvi-planar	narrow	intercrystalline	well defined	many
35	275	50	varied	planar	narrow	intracrystalline	poorly defined	few
36	320	85	varied	planar	narrow	intercrystalline	well defined	many
37	278	86	<5	planar	narrow	intracrystalline	poorly defined	few
38	291	78	<5	planar	narrow	intracrystalline	poorly defined	few
39	251	83	<5	planar	narrow	intracrystalline	poorly defined	few
40	334	79	varied	planar	narrow	intracrystalline	well defined	many

Crystal B								
1	345	80	<5	planar	narrow	intercrystalline	well defined	many
2	343	79	<5	planar	narrow	intercrystalline	well defined	many
3	82	76	<5	planar	narrow	intercrystalline	well defined	many
4	77	85	<5	curvi-planar	narrow	intracrystalline	well defined	many
5	144	74	>5	planar	narrow	intracrystalline	well defined	few
6	146	77	irregular	planar	narrow	intracrystalline	well defined	many
7	327	81	<5	planar	narrow	intercrystalline	well defined	many
8	36	77	<5	curvi-planar	narrow	intracrystalline	well defined	many
9	88	76	varied	curvi-planar	narrow	intercrystalline	well defined	many
10	351	83	<5	planar	narrow	intracrystalline	well defined	many
11	325	76	<5	curvi-planar	narrow	intracrystalline	poorly defined	few
12	227	58	varied	planar	narrow	intracrystalline	well defined	many
13	65	67	varied	curvi-planar	narrow	intracrystalline	well defined	many
14	183	76	<5	curvi-planar	narrow	intercrystalline	well defined	many
15	84	65	<5	planar	narrow	intracrystalline	well defined	many
16	86	70	varied	curvi-planar	narrow	intracrystalline	well defined	many
17	290	70	varied	curvi-planar	narrow	intracrystalline	poorly defined	many
18	152	86	varied	curvi-planar	narrow	intercrystalline	poorly defined	few
19	19	86	irregular	planar	narrow	intercrystalline	poorly defined	few
20	334	72	<5	planar	narrow	intercrystalline	well defined	many
21	44	68	varied	curvi-planar	narrow	intercrystalline	well defined	many
22	317	76	<5	planar	narrow	intracrystalline	well defined	many
23	64	77	varied	planar	narrow	intracrystalline	poorly defined	few
24	4	75	<5	planar	narrow	intercrystalline	well defined	many
25	85	80	varied	curvi-planar	narrow	intracrystalline	well defined	few
26	205	73	<5	curvi-planar	narrow	intercrystalline	well defined	few
27	2	80	varied	planar	narrow	intercrystalline	well defined	many
28	150	90	varied	planar	narrow	intracrystalline	well defined	many
29	293	67	>5	planar	narrow	intracrystalline	poorly defined	few
30	166	87	<5	planar	narrow	intracrystalline	well defined	many
31	355	85	irregular	planar	narrow	intracrystalline	poorly defined	many
32	356	85	<5	planar	narrow	intracrystalline	poorly defined	few
33	1	87	<5	curvi-planar	narrow	intracrystalline	well defined	few
34	1	78	<5	curvi-planar	narrow	intracrystalline	well defined	few
35	159	75	<5	planar	narrow	intercrystalline	well defined	many
36	155	70	<5	planar	narrow	intercrystalline	well defined	many
37	151	64	<5	curvi-planar	narrow	intracrystalline	well defined	many
38	297	78	<5	curvi-planar	narrow	intracrystalline	well defined	few/many
39	346	85	<5	planar	narrow	intracrystalline	well defined	many
40	330	71	<5	planar	narrow	intercrystalline	well defined	many
41	336	76	<5	planar	narrow	intracrystalline	well defined	many

42	332	73	varied	planar	narrow	intracrystalline	well defined	many
43	350	73	>5	planar	narrow	intercrystalline	well defined	few
44	183	77	>5	planar	narrow	intracrystalline	well defined	few
45	293	64	<5	planar	narrow	intracrystalline	poorly defined	few
46	312	60	varied	planar	narrow	intercrystalline	well defined	many
47	276	60	varied	planar	narrow	intracrystalline	well defined	many
48	295	65	varied	planar	narrow	intercrystalline	well defined	few
49a	331	80	varied	curvi-planar	narrow	intercrystalline	well defined	many
49b	313	61	varied	planar	narrow	intercrystalline	well defined	many
50	290	62	varied	planar	narrow	intracrystalline	well defined	few
51	260	46	>5	planar	wide	intracrystalline	well defined	many
52	294	70	<5	planar	narrow	intracrystalline	well defined	few
53	297	65	<5	curvi-planar	narrow	intracrystalline	poorly defined	few
54	305	75	varied	curvi-planar	narrow	intracrystalline	poorly defined	few
55	305	73	varied	planar	narrow	intracrystalline	poorly defined	many
56	259	46	irregular	planar	wide	intracrystalline	well defined	many
57	255	46	varied	planar	wide	intercrystalline	well defined	many
58	33	79	<5	curvi-planar	wide	intracrystalline	poorly defined	many
59	256	68	<5	planar	narrow	intracrystalline	well defined	many
60	152	75	<5	planar	narrow	intracrystalline	well defined	many
61	165	75	<5	planar	narrow	intercrystalline	well defined	many
62	308	64	varied	curvi-planar	narrow	intercrystalline	well defined	many
63	349	70	varied	planar	narrow	intercrystalline	well defined	many
64	332	78	varied	planar	narrow	intercrystalline	well defined	many
65	162	88	varied	planar	narrow	intercrystalline	well defined	many
66	314	69	<5	planar	narrow	intracrystalline	poorly defined	many
67	346	68	varied	planar	narrow	intracrystalline	poorly defined	many
68	26	85	<5	curvi-planar	wide	intracrystalline	poorly defined	many
69	50	79	<5	planar	narrow	intracrystalline	poorly defined	few
70	66	79	<5	planar	narrow	intracrystalline	poorly defined	few
71	66	72	<5	planar	narrow	intracrystalline	poorly defined	few
72	340	82	varied	planar	narrow	intercrystalline	well defined	many
73	56	85	varied	curvi-planar	wide	intracrystalline	poorly defined	many
74	34	85	varied	irregular	narrow	intracrystalline	poorly defined	many
75	69	81	varied	planar	narrow	intracrystalline	well defined	few
76	66	85	varied	planar	narrow	intracrystalline	well defined	few
77	70	79	<5	planar	narrow	intracrystalline	well defined	few
78	164	74	<5	planar	narrow	intercrystalline	well defined	many
79	176	81	<5	planar	narrow	intercrystalline	well defined	many
80	254	46	varied	planar	narrow	intracrystalline	well defined	many
81	256	52	varied	planar	wide	intracrystalline	well defined	many
82	346	75	<5	planar	narrow	intercrystalline	well defined	many
83	85	69	<5	irregular	narrow	intercrystalline	well defined	many
84	342	70	varied	curvi-planar	narrow	intercrystalline	well defined	many
85	5	90	varied	planar	wide	intracrystalline	poorly defined	many
86	289	61	varied	planar	narrow	intracrystalline	poorly defined	many
87	354	83	<5	planar	narrow	intracrystalline	well defined	few
88	90	61	varied	planar	narrow	intracrystalline	well defined	many
89	18	90	<5	planar	narrow	intracrystalline	well defined	few
90	350	87	<5	curvi-planar	narrow	intracrystalline	well defined	many
91	346	78	varied	planar	narrow	intercrystalline	well defined	many
92	341	69	varied	curvi-planar	narrow	intracrystalline	well defined	many
93	349	79	varied	planar	narrow	intracrystalline	well defined	many
94	63	82	varied	curvi-planar	narrow	intracrystalline	well defined	few
95	347	70	varied	planar	narrow	intercrystalline	well defined	many
96	258	45	varied	planar	wide	intracrystalline	poorly defined	many
97	353	71	varied	curvi-planar	narrow	intracrystalline	poorly defined	many
98	305	68	<5	planar	narrow	intercrystalline	well defined	many

99	348	76	<5	planar	narrow	intercrystalline	well defined	many
100a	329	69	<5	planar	narrow	intracrystalline	well defined	many
100b	95	45	irregular	planar	narrow	intracrystalline	well defined	many
101	357	81	varied	planar	wide	intercrystalline	poorly defined	many
102	0	75	<5	planar	narrow	intracrystalline	well defined	many
103	84	62	<5	planar	narrow	intracrystalline	well defined	many
104	61	59	<5	curvi-planar	narrow	intercrystalline	well defined	many
105	88	52	varied	planar	narrow	intercrystalline	well defined	many
106	285	45	<5	planar	narrow	intracrystalline	well defined	many
107	96	51	varied	planar	wide	intracrystalline	well defined	many
108	90	57	<5	planar	narrow	intracrystalline	well defined	many
109	203	86	<5	planar	narrow	intracrystalline	well defined	many
110	27	87	varied	planar	narrow	intracrystalline	well defined	few
111	292	78	<5	planar	narrow	intracrystalline	poorly defined	few
112	35	82	varied	curvi-planar	narrow	intracrystalline	well defined	few
113a	182	71	>5	planar	narrow	intracrystalline	well defined	few
113b	336	68	varied	planar	narrow	intracrystalline	well defined	many
114	240	89	<5	curvi-planar	narrow	intercrystalline	well defined	many
115	62	78	varied	irregular	narrow	intercrystalline	well defined	many
116	64	85	varied	curvi-planar	narrow	intracrystalline	well defined	many
117a	69	74	varied	planar	narrow	intercrystalline	well defined	many
117b	254	45	varied	planar	wide	intracrystalline	poorly defined	many
118	356	76	varied	planar	narrow	intercrystalline	well defined	many
119	0	72	>5	irregular	narrow	intercrystalline	poorly defined	many
120	81	72	<5	planar	narrow	intracrystalline	poorly defined	few
121	70	73	<5	planar	narrow	intracrystalline	well defined	few
122	291	89	varied	curvi-planar	narrow	intercrystalline	well defined	many
123	281	65	varied	curvi-planar	narrow	intracrystalline	well defined	few
124	330	76	varied	planar	narrow	intracrystalline	well defined	many
125a	257	56	varied	planar	narrow	intracrystalline	poorly defined	many
125b	351	71	varied	curvi-planar	narrow	intercrystalline	well defined	many
126a	99	59	varied	planar	narrow	intracrystalline	poorly defined	many
126b	359	80	varied	planar	narrow	intracrystalline	well defined	few
127	343	79	varied	planar	narrow	intercrystalline	well defined	many
128	358	79	<5	planar	narrow	intercrystalline	well defined	many
129	46	81	varied	planar	narrow	intracrystalline	well defined	few
130	338	65	varied	curvi-planar	narrow	intercrystalline	well defined	many/few
131	348	79	<5	curvi-planar	narrow	intracrystalline	well defined	many
132	331	61	varied	curvi-planar	narrow	intracrystalline	well defined	few
133	57	70	<5	planar	narrow	intracrystalline	well defined	many
134	336	73	varied	planar	narrow	intercrystalline	well defined	few
135	53	75	varied	planar	wide	intercrystalline	well defined	few
136	61	65	<5	planar	narrow	intracrystalline	well defined	many
137	65	68	varied	curvi-planar	narrow	intercrystalline	well defined	many/few
138	28	85	varied	curvi-planar	narrow	intercrystalline	well defined	many/few
139	54	71	varied	curvi-planar	narrow	intercrystalline	well defined	many/few
140	257	86	varied	curvi-planar	wide	intracrystalline	poorly defined	few
141	180	87	varied	curvi-planar	narrow	intracrystalline	well defined	few
142	193	83	<5	curvi-planar	narrow	intracrystalline	well defined	many
143	191	81	<5	curvi-planar	narrow	intracrystalline	well defined	many
144	190	65	varied	curvi-planar	narrow	intercrystalline	well defined	many
146	175	80	varied	planar	narrow	intercrystalline	well defined	many
147	52	75	<5	curvi-planar	narrow	intercrystalline	well defined	many
148	178	67	>5	planar	narrow	intercrystalline	well defined	few
149	54	74	<5	planar	narrow	intracrystalline	well defined	few
150	90	53	<5	planar	narrow	intracrystalline	well defined	many
151	52	70	<5	curvi-planar	narrow	intercrystalline	well defined	many
152	72	83	varied	planar	narrow	intracrystalline	well defined	few

153	52	70	varied	planar	narrow	intercrystalline	well defined	few
154	183	65	varied	planar	wide	intracrystalline	poorly defined	few
155	189	72	varied	curvi-planar	narrow	intercrystalline	well defined	many/few

Table A5.3 FIP orientation data LI2

FIP	strike	dipr
1	88	78
2	97	84
3	358	65
4	104	89
5	8	84
6	202	76
7	337	71
8	88	70
9	10	86
10	85	75
11	79	74
12	67	83
13	68	67
14	88	59
15	92	75
16	99	80
17	357	83
18	359	74
19	104	68
20	30	86
21	69	71
22	219	80
23	254	82
24	95	76
25	84	73
26	78	90
27	8	64
28	79	58
29	11	76
30	84	84
31	89	73
32	94	89
33	14	84
34	349	76
35	64	87
36	351	78
37	105	64
38	205	90
39	77	90
40	301	67
41	9	89
42	38	74
43	74	68
44	227	73
45	12	81
46	108	80
47	81	73
48	80	68
49	35	76
50	5	54
51	374	75

Table A5.4 FIP orientation data LI3

FIP	strike	dipr
1	85	62
2	94	65
3	77	69
4	94	65
5	91	64
6	67	72
7	68	74
8	85	65
9	2	78
10	92	56
11	127	47
12	77	63
13	6	2
14	96	61
15	93	66
16	95	47
17	27	74
18	350	81
19	358	90
20	95	53
21	98	54
22	134	45
23	67	54
24	77	52
25	1	69
26	86	60
27	49	49
28	50	50
29	50	50
30	4	76
31	359	81
32	57	57
33	46	46
34	91	61
35	81	83
36	72	84
37	357	71
38	99	65
39	94	54
40	104	66
41	87	67
42	80	53
43	86	70
44	47	50
45	1	81
46	8	79
47	314	54
48	99	69
49	95	71
50	354	81
51	180	68

52	355	49
53	79	86

52	169	77
53	5	84
54	174	73
55	91	59
56	357	84
57	98	57
58	38	78

Table A5.5 FIP orientation data: LI4

FIP No.	strike	dip	planar	development	abundance	crack width	boundary	inclusion size
Crystal A								
1	326	6	planar	intracrystalline	few	narrow		varied
2	18	9	planar	intracrystalline	few	narrow		<5
3	315	15	curvi-planar	intercrystalline	many	narrow		<5
4	23	6	planar	intracrystalline	many	wide		<5
5	339	2	planar	intracrystalline	few	narrow		<5
6	295	20	curvi-planar	intracrystalline	many	narrow		varied
7	312	29	planar	intercrystalline	many	wide		varied
8	305	32	planar	intracrystalline	few	narrow		varied
9	294	37	curvi-planar	intracrystalline	many	narrow		<5
10	324	22	curvi-planar	intracrystalline	many	narrow		<5
11	324	13	planar	intercrystalline	many	narrow		varied
12	333	13	planar	intracrystalline	many	narrow		<5
13	343	14	planar	intracrystalline	few	narrow		<5
14	326	22	curvi-planar	intracrystalline	few	wide		varied
15	305	23	curvi-planar	intercrystalline	few	narrow		varied
16	310	37	curvi-planar	intercrystalline	many	narrow		varied
17	309	18	curvi-planar	intercrystalline	few	narrow		varied
18	18	33	curvi-planar	intracrystalline	many	narrow		<5
19	312	39	curvi-planar	intercrystalline	many	narrow		<5
20	20	16	planar	intracrystalline	many	narrow		varied
Crystal B								
1	343	56	curvi-planar	intracrystalline	few	narrow	gb-	varied
2	213	47	irregular	intracrystalline	many	narrow	gb-	<5
3	359	60	curvi-planar	intracrystalline	many	narrow	gb-	<5
4	333	61	planar	intracrystalline	many	narrow	gb-	<5
5	251	80	planar	intracrystalline	many	narrow	hc-hc	<5
6	246	56	planar	intracrystalline	many	narrow	hc-hc	<5
7	249	81	planar	intracrystalline	many	narrow	hc-hc	<5
8	346	68	planar	intracrystalline	many	narrow	gb-hc	<5
9a	321	68	planar	intracrystalline	many	narrow	gb-	varied
9b	321	67	planar	intracrystalline	many	narrow	hc-	varied
10	158	87	planar	intracrystalline	few	narrow	hc-	>5
11	333	64	curvi-planar	intercrystalline	many	narrow	gb-gb	varied
12	243	81	planar	intracrystalline	many	narrow	hc-hc	<5
13	305	72	planar	intracrystalline	many	narrow	hc-hc	varied
14a	247	81	planar	intracrystalline	many	narrow	iso	<5
14b	250	83	planar	intracrystalline	many	narrow	iso	<5
15a	245	85	planar	intracrystalline	many	narrow	hc-hc	<5
15b	247	88	curvi-planar	intracrystalline	many	narrow	hc-	<5
15c	346	67	planar	intracrystalline	many	narrow	gb-hc	varied
16	332	65	curvi-planar	intercrystalline	many	narrow	trans	varied
17	114	86	curvi-planar	intercrystalline	many	narrow	gb-	<5
18	295	89	planar	intercrystalline	many	narrow	gb-	<5
19	313	72	curvi-planar	intracrystalline	many	narrow	gb-hc	varied

20	326	70	planar	intracrystalline	many	narrow	hc-hc	varied
21a	332	66	curvi-planar	intracrystalline	many	narrow	gb-	<5
21b	251	87	planar	intracrystalline	many	narrow	hc-	<5
22	246	80	planar	intracrystalline	many	narrow	hc-hc	<5
23	249	81	planar	intracrystalline	many	narrow	hc-	<5
24	300	73	curvi-planar	intracrystalline	many	narrow	gb-	varied
25	317	78	planar	intracrystalline	many	narrow	gb-	<5
26	270	66	planar	intracrystalline	many	narrow	gb-	varied
27	98	68	planar	intracrystalline	many	narrow	gb-	varied
28	301	77	curvi-planar	intracrystalline	many	narrow	gb-gb	<5
29	319	70	curvi-planar	intercrystalline	many	narrow	trans	varied
30	254	82	planar	intracrystalline	many	narrow	iso	<5
31	248	79	planar	intracrystalline	many	narrow	iso	<5
32	253	79	planar	intracrystalline	many	narrow	iso	<5
33	336	61	planar	intracrystalline	many	narrow	gb-	<5
35	9	78	planar	intracrystalline	few	wide	iso	>5
36	4	46	curvi-planar	intracrystalline	many	wide	iso	varied
37	247	84	planar	intracrystalline	many	narrow	hc-	<5
38a	314	86	curvi-planar	intracrystalline	many	narrow	iso	<5
38b	353	78	curvi-planar	intracrystalline	many	narrow	iso	<5
39	86	65	curvi-planar	intracrystalline	many	wide	hc-hc	varied
40	350	53	planar	intracrystalline	many	narrow	gb-	varied
41	175	80	planar	intracrystalline	many	narrow	gb-	varied
42	163	57	planar	intracrystalline	few	narrow	hc-hc	>5
43	239	56	curvi-planar	intracrystalline	many	narrow	hc-	varied
44	161	56	irregular	intracrystalline	many	narrow	gb-hc	varied
45	344	60	curvi-planar	intercrystalline	many	narrow	gb-	varied
46	9	46	planar	intracrystalline	many	wide	hc-hc	varied
47	7	77	planar	intracrystalline	few	wide	iso	>5
48	187	83	curvi-planar	intracrystalline	many	narrow	gb-hc	<5
49	263	75	planar	intracrystalline	many	narrow	hc-hc	<5
51	41	73	planar	intracrystalline	many	narrow	hc-gb	varied
52	178	62	planar	intercrystalline	few	narrow	gb-gb	varied
54	278	70	curvi-planar	intracrystalline	many	narrow	hc-	<5
55	273	75	planar	intracrystalline	many	narrow	iso	<5
56	344	47	planar	intracrystalline	few	narrow		>5
57	301	81	curvi-planar	intracrystalline	many	narrow	gb-	<5
58	302	77	planar	intracrystalline	many	narrow	gb-	<5
59	351	57	planar	intracrystalline	many	narrow	gb-hc	varied
61	22	57	planar	intracrystalline	few	narrow	hc-hc	>5
62	171	45	planar	intracrystalline	few	wide	hc-hc	>5
63	112	90	planar	intracrystalline	many	narrow	hc-hc	<5
64	26	45	planar	intracrystalline	few	narrow	gb-	varied
65	37	57	irregular	intracrystalline	many	narrow	hc-	varied
66	12	45	planar	intracrystalline	many	narrow		varied
67	297	88	curvi-planar	intracrystalline	many	narrow	gb-hc	varied
68	295	84	curvi-planar	intracrystalline	many	narrow	gb-hc	<5
69	294	87	planar	intracrystalline	few	narrow	gb-	<5
70a	299	82	planar	intracrystalline	few	narrow	hc-	varied
70b	239	57	planar	intracrystalline	many	narrow	hc-	<5
71	301	82	planar	intracrystalline	few	narrow	gb-	varied
72	282	80	planar	intercrystalline	many	narrow	gb-gb	<5
73	294	87	planar	intracrystalline	few	narrow	gb-	>5
74	285	79	planar	intracrystalline	few	narrow	gb-	>5
75	242	76	planar	intracrystalline	many	narrow	hc-	<5
76	109	89	curvi-planar	intracrystalline	few	narrow	hc-	<5
77	103	89	curvi-planar	intracrystalline	few	narrow	hc-	<5
78	8	49	planar	intracrystalline	many	narrow	hc-hc	varied

79	248	72	curvi-planar	intracrystalline	many	narrow	gb-	<5
80	331	70	planar	intracrystalline	many	wide	gb-hc	varied
81	91	74	curvi-planar	intracrystalline	many	narrow	gb-	<5
82	111	81	planar	intracrystalline	few	narrow	hc-	varied
83	251	64	planar	intracrystalline	many	narrow	hc-	<5
84	276	63	curvi-planar	intracrystalline	few	narrow	gb-hc	varied
85	251	72	irregular	intracrystalline	many	wide	hc-	varied
86	117	80	planar	intracrystalline	many	narrow	gb-	<5
87	105	75	planar	intracrystalline	many	narrow	gb-	<5
88	297	89	curvi-planar	intracrystalline	many	narrow	iso	varied
89	98	89	planar	intracrystalline	many	narrow	gb-	<5
90	93	84	curvi-planar	intracrystalline	many	narrow	gb-	<5
91	107	60	planar	intracrystalline	many	narrow	gb-	<5
92	5	58	planar	intracrystalline	few	wide	gb-	>5
93	270	72	planar	intracrystalline	many	narrow		<5

Table A5.6 FIP orientation data LI5

FIP	strike	dipr
1	184	78
2	273	65
3	36	87
4	65	90
5	183	74
6	105	73
7	243	79
8	276	81
9	95	86
10	359	67
11	149	58
12	332	86
13	86	71
14	222	89
15	168	77
16	174	84
17	199	71
18	354	78
19	204	82
20	93	86
21	270	65
22	274	78
23	184	58
24	2	90
25	257	87
26	281	84
27	71	89
28	87	71
29	190	68
30	275	69
31	5	72
32	1	76
33	158	86
34	89	84
35	172	89
36	23	82

Table A5.7 FIP orientation data LI6

FIP	strike	dipr
1	95	77
2	2	58
3	84	87
4	280	84
5	89	72
6	11	65
7	94	74
8	4	82
9	97	81
10	184	79
11	274	74
12	82	81
13	136	82
14	48	86
15	81	81
16	183	71
17	78	65
18	47	49
19	101	71
20	235	58
21	178	64
22	98	89
23	259	82
24	241	73
25	76	77
26	74	76
27	89	74
28	4	88
29	95	87
30	94	84
31	174	90
32	105	67
33	5	88
34	99	84
35	274	77
36	91	68
37	182	90

Table A5.8 FIP orientation data LI7

FIP	strike	dipr
1	84	87
2	67	84
3	294	76
4	83	64
5	91	78
6	359	61
7	281	62
8	102	58
9	12	81
10	114	86
11	64	78
12	15	90
13	84	71
14	1	76
15	75	84
16	78	77
17	268	81
18	81	88
19	7	90
20	247	86
21	270	58
22	83	74
23	350	68
24	124	71
25	271	77
26	84	70
27	119	84
28	300	89
29	92	80
30	8	60
31	278	58
32	94	89
33	94	49
34	268	60
35	147	54
36	232	78
37	267	84

38	354	89
39	87	84
40	280	71
41	76	65
42	81	81
43	304	75
44	337	71
45	250	68
46	352	71
47	268	89
48	79	87
49	62	86
50	95	81
51	349	89
52	90	90
53	218	78
54	89	74
55	276	86
56	84	81
57	168	78
58	124	74
59	8	89
60	171	84
61	271	78

Table A5.9 FIP orientation data: CFD1

FIP No.	strike	dipr	size	planar	devlopment	abundance	crack width	boundary	pso
Crystal A									
1	181	82	<5	planar	intragranular	many	narrow	iso	none
2	167	84	<5	planar	intragranular	many	narrow	iso	none
3	179	73	<5	planar	intragranular	many	narrow	iso	none
4	322	84	<5	curvi-planar	intergranular	many	narrow	gb-gb	parallel
5	138	56	<5	planar	intragranular	many	narrow	gb-	parallel
6	129	86	varied	planar	intragranular	many	narrow	hc-	parallel
7	48	72	<5	planar	intragranular	many	narrow	gb-hc	none
8	38	69	<5	planar	intragranular	many	narrow	gb-	none
9	22	62	<5	planar	intragranular	many	narrow	iso	parallel
10	322	75	<5	curvi-planar	intergranular	many	wide	gb-hc	parallel
11	1	79	>5	planar	intragranular	few	narrow	hc-hc	none
12	309	84	<5	curvi-planar	intragranular	many	narrow	gb-gb	parallel
13	339	88	<5	curvi-planar	intergranular	many	narrow	gb-	parallel
14	352	74	<5	planar	intragranular	many	narrow	iso	parallel
15a	134	63	>5	curvi-planar	intragranular	few	wide	gb-hc	parallel
15b	134	59	>5	curvi-planar	intragranular	many	narrow	gb-hc	parallel
16	1	89	<5	planar	intragranular	many	narrow	iso	none
17	137	90	<5	planar	intragranular	many	narrow	iso	parallel
18	319	84	<5	planar	intragranular	many	narrow	gb-hc	none
20	308	71	varied	planar	intragranular	many	narrow	hc-	none
21a	324	77	<5	curvi-planar	intergranular	many	narrow	gb-	parallel
21b	321	56	varied	curvi-planar	intergranular	many	narrow	gb-	parallel
22	355	84	varied	planar	intragranular	many	narrow	hc-	none
23	289	48	<5	irregular	intragranular	many	narrow	iso	none
Crystal B									
1	334	49	<5	curvi-planar	intragranular	many	narrow	gb-hc	parallel
2	165	48	<5	planar	intragranular	many	narrow	iso	none

3	179	86	<5	planar	intragranular	many	narrow	iso	none
5	178	87	<5	planar	intragranular	many	wide	iso	none
6	122	75	>5	curvi-planar	intragranular	many	narrow	hc-hc	none
7	147	79	varied	curvi-planar	intergranular	few	narrow	hc-	parallel
8	287	86	<5	planar	intragranular	many	narrow	gb-gb	none
9	315	86	<5	curvi-planar	intergranular	many	narrow	gb-	parallel
10	359	84	<5	planar	intragranular	many	narrow	iso	none
11	44	89	<5	curvi-planar	intragranular	many	narrow	iso	none
12	44	54	<5	curvi-planar	intragranular	many	narrow	iso	parallel
13	108	81	>5	curvi-planar	intragranular	many	wide	hc-	none
14	111	73	<5	curvi-planar	intragranular	few	narrow	hc-	none
15	42	64	<5	curvi-planar	intragranular	many	narrow	hc-hc	parallel
16	37	68	<5	curvi-planar	intergranular	few	narrow	gb-	parallel
17	10	74	<5	planar	intragranular	many	narrow	iso	none
18	209	86	<5	curvi-planar	intragranular	many	narrow	gb-	parallel
19	330	82	<5	curvi-planar	intragranular	many	narrow	gb-	parallel
20	309	74	<5	curvi-planar	intragranular	many	narrow	gb-	parallel
21	359	63	<5	planar	intragranular	many	narrow	iso	none
22	147	86	varied	curvi-planar	intragranular	few	narrow	hc-hc	parallel
23	0	87	<5	planar	intragranular	many	narrow	hc-	none
24	134	69	<5	planar	intragranular	many	narrow	gb-hc	parallel
25	2	63	<5	planar	intragranular	many	narrow	iso	none
26	219	85	<5	planar	intragranular	many	narrow	hc-hc	none
27	218	48	<5	curvi-planar	intragranular	many	wide	hc-	none
28	318	89	>5	curvi-planar	intragranular	many	narrow	hc-	none
29	344	89	<5	planar	intergranular	many	narrow	gb-	parallel
30	341	54	<5	planar	intragranular	few	narrow	hc-hc	parallel
31	248	69	<5	curvi-planar	intergranular	many	narrow	gb-	none
32	135	64	<5	curvi-planar	intragranular	few	narrow	gb-gb	parallel
34	317	72	>5	curvi-planar	intragranular	many	wide	hc-hc	parallel
35	184	77	<5	planar	intragranular	few	narrow	iso	none
36	219	88	<5	curvi-planar	intragranular	few	narrow	gb-	parallel
37	227	49	<5	curvi-planar	intragranular	many	narrow	gb-	none
38	22	83	<5	planar	intragranular	many	narrow	iso	none
39	177	86	varied	planar	intragranular	many	narrow	iso	none
40	123	85	<5	planar	intragranular	many	narrow	iso	none
41a	305	76	<5	planar	intragranular	many	narrow	gb-	parallel
41b	305	90	<5	planar	intragranular	many	narrow	gb-hc	parallel
41c	305	84	<5	planar	intragranular	few	narrow	gb-hc	parallel
42	358	73	>5	planar	intragranular	many	narrow	hc-	none
43	89	85	<5	curvi-planar	intragranular	few	narrow	hc-	none
45	178	79	>5	planar	intragranular	many	narrow	iso	none
46	229	74	<5	curvi-planar	intragranular	many	narrow	hc-	parallel
47	201	81	<5	curvi-planar	intergranular	many	narrow	gb-	none
48	298	71	<5	planar	intragranular	many	narrow	gb-hc	none
49	12	86	<5	planar	intragranular	many	wide	hc-	none
50	139	74	<5	curvi-planar	intragranular	many	narrow	iso	parallel
51	125	86	<5	curvi-planar	intergranular	few	narrow	gb-	parallel
52	128	83	<5	curvi-planar	intergranular	few	narrow	gb-	parallel
53	41	71	<5	curvi-planar	intragranular	many	narrow	gb-hc	parallel
54	340	65	varied	curvi-planar	intragranular	many	narrow	hc-hc	parallel
55	231	59	<5	curvi-planar	intragranular	many	narrow	hc-	none
56	320	54	varied	curvi-planar	intragranular	many	narrow	hc-	parallel
57	321	47	<5	curvi-planar	intragranular	many	narrow	hc-	parallel
58	78	86	>5	planar	intragranular	many	narrow	gb-	none

1	12	90	<5	planar	intragranular	many	narrow	iso	none
2	10	82	<5	planar	intragranular	many	wide	iso	none
3	319	78	<5	planar	intragranular	few	narrow	gb-hc	parallel
4	330	83	<5	planar	intragranular	many	narrow	hc-hc	parallel
5	106	76	<5	planar	intragranular	many	narrow	hc-	parallel
6	287	64	>5	planar	intragranular	many	narrow	hc-	none
7	319	62	<5	planar	intragranular	many	narrow	hc-	none
8	354	68	<5	planar	intragranular	few	narrow	gb-	none
9	138	72	>5	planar	intragranular	many	narrow	hc-hc	parallel
10	148	71	<5	planar	intragranular	many	narrow	gb-hc	parallel
12	54	62	varied	planar	intragranular	many	narrow	iso	none
13	137	83	<5	planar	intragranular	many	narrow	hc-hc	parallel
14	141	82	>5	curvi-planar	intergranular	many	narrow	gb-	parallel
16	142	81	<5	curvi-planar	intergranular	few	narrow	gb-	parallel
17	200	65	<5	planar	intragranular	many	narrow	hc-hc	parallel
18a	348	78	>5	planar	intragranular	many	narrow	iso	none
18b	348	82	<5	planar	intragranular	many	narrow	iso	none
19	90	84	<5	planar	intragranular	many	narrow	hc-hc	none
20	181	72	<5	planar	intragranular	many	narrow	iso	none
21	319	83	<5	planar	intergranular	many	narrow	gb-	parallel
22	305	90	<5	curvi-planar	intragranular	many	narrow	hc-	parallel
23	308	75	<5	planar	intragranular	many	narrow	hc-	parallel
24	182	61	<5	curvi-planar	intragranular	many	narrow	iso	none

Table A5.10 FIP orientation data: EHT1

FIP No.	strike	dipr	size	planar	development	crack width	abundance	boundary	pso
Crystal A									
1	221	74	<5	planar	intragranular	narrow	many	gb-	parallel
2	154	88	<5	planar	intragranular	narrow	many	hc-hc	none
3	93	73	<5	planar	intragranular	narrow	many	iso	none
4	134	69	varied	curvi-planar	intergranular	narrow	many	gb-gb	parallel
5	129	62	>5	planar	intragranular	narrow	many	gb-gb	parallel
6	301	87	<5	curvi-planar	intergranular	narrow	many	gb-gb	none
7	313	86	<5	curvi-planar	intergranular	narrow	many	gb-hc	none
8	184	71	<5	planar	intragranular	narrow	few	iso	none
9	39	79	>5	planar	intragranular	wide	many	gb-	parallel
10	44	83	<5	curvi-planar	intragranular	narrow	many	gb-	none
11	141	64	<5	planar	intragranular	narrow	many	gb-hc	parallel
12	22	90	>5	planar	intragranular	narrow	many	iso	parallel
13	23	84	varied	planar	intragranular	narrow	many	iso	parallel
14	137	74	<5	curvi-planar	intergranular	narrow	many	gb-hc	none
15	175	86	<5	planar	intragranular	narrow	many	iso	none
16	353	82	>5	planar	intragranular	narrow	few	iso	none
17	128	68	<5	irregular	intragranular	narrow	many	gb-	parallel
18a	220	79	<5	curvi-planar	intragranular	wide	many	gb-hc	parallel
18b	220	89	<5	curvi-planar	intragranular	narrow	many	hc-hc	parallel
19	78	85	<5	planar	intragranular	narrow	many	hc-hc	none
20	38	46	<5	planar	intragranular	narrow	many	gb-	none
21	42	79	varied	planar	intragranular	narrow	many	gb-hc	parallel
22	261	85	>5	planar	intragranular	narrow	many	hc-hc	none
Crystal B									
1	137	78	<5	curvi-planar	intergranular	wide	many	gb-gb	parallel
2	128	54	<5	curvi-planar	intergranular	narrow	many	gb-	parallel
3	154	90	<5	planar	intragranular	narrow	many	hc-hc	parallel
4	197	85	<5	planar	intragranular	narrow	many	iso	none

5	158	81	<5	planar	intragranular	narrow	few	gb-	none
6	209	76	>5	planar	intragranular	narrow	many	gb-	none
7	318	82	<5	planar	intragranular	narrow	many	hc-	parallel
8	49	76	<5	planar	intergranular	narrow	many	gb-gb	parallel
9	247	64	<5	curvi-planar	intergranular	wide	many	gb-hc	none
10	129	78	varied	curvi-planar	intergranular	narrow	few	hc-hc	parallel
11	322	82	<5	planar	intragranular	narrow	many	gb-gb	parallel
12	319	86	<5	curvi-planar	intragranular	narrow	many	gb-	none
13	134	87	<5	curvi-planar	intragranular	narrow	few	gb-	parallel
14	154	78	>5	planar	intragranular	narrow	many	hc-hc	none
16	145	89	<5	curvi-planar	intragranular	narrow	many	gb-	none
17	141	90	<5	curvi-planar	intragranular	narrow	many	gb-	parallel
18	44	49	<5	planar	intragranular	narrow	many	gb-	parallel
19	39	54	<5	planar	intergranular	narrow	many	gb-	parallel
20	37	76	<5	planar	intragranular	narrow	many	gb-hc	parallel
21	218	56	varied	planar	intergranular	narrow	many	gb-gb	parallel
22	211	79	varied	planar	intergranular	narrow	many	gb-gb	parallel
23	48	86	varied	planar	intragranular	narrow	many	gb-	parallel
24	222	63	<5	curvi-planar	intragranular	narrow	many	gb-hc	parallel
25	269	64	varied	planar	intragranular	narrow	many	hc-hc	none
26a	68	86	>5	planar	intragranular	narrow	many	hc-	none
26b	317	75	<5	curvi-planar	intragranular	narrow	few	gb-	none
26c	307	74	<5	curvi-planar	intergranular	narrow	few	hc-gb	parallel
28	141	90	<5	planar	intragranular	narrow	many	gb-	parallel
29	128	65	varied	curvi-planar	intergranular	narrow	few	gb-hc	none
30	167	82	varied	planar	intragranular	narrow	many	hc-hc	none
31	166	81	<5	planar	intragranular	narrow	many	gb-	none
32	201	86	>5	planar	intragranular	narrow	many	gb-	parallel
33	87	74	<5	planar	intragranular	narrow	few	iso	parallel
34	49	82	<5	curvi-planar	intergranular	narrow	many	gb-gb	parallel
35	38	74	<5	curvi-planar	intergranular	narrow	many	gb-	parallel
36	51	69	varied	planar	intragranular	narrow	many	gb-	none
37	288	75	>5	planar	intragranular	narrow	many	gb-	none
38	241	78	<5	planar	intragranular	narrow	few	gb-hc	parallel
39	144	83	<5	planar	intragranular	narrow	many	hc-hc	none
40	42	61	>5	curvi-planar	intergranular	wide	many	gb-hc	parallel
42	79	63	<5	planar	intragranular	narrow	many	hc-	none
44	334	84	<5	planar	intragranular	narrow	few	gb-	parallel
45	334	76	varied	curvi-planar	intragranular	narrow	few	gb-	parallel
46	154	59	>5	planar	intragranular	narrow	many	gb-hc	none
47	211	86	>5	curvi-planar	intergranular	narrow	many	gb-hc	parallel
48	37	54	>5	curvi-planar	intragranular	narrow	few	hc-	parallel
49	189	78	<5	planar	intragranular	narrow	many	iso	none
51	314	76	<5	curvi-planar	intergranular	narrow	many	gb-	parallel
52	49	82	<5	planar	intragranular	narrow	many	hc-hc	none
53	278	84	<5	planar	intragranular	narrow	many	gb-gb	parallel
54	38	54	varied	planar	intragranular	narrow	many	hc-	parallel
55	359	86	<5	planar	intragranular	narrow	many	iso	none
56	12	84	<5	planar	intragranular	narrow	few	gb-	none
57	333	87	<5	planar	intragranular	narrow	many	gb-	parallel
58	339	76	varied	planar	intragranular	narrow	many	gb-	parallel
59	324	64	varied	curvi-planar	intergranular	narrow	many	gb-hc	parallel
60	129	73	varied	curvi-planar	intragranular	narrow	many	iso	parallel
61	134	81	<5	planar	intergranular	wide	many	gb-hc	parallel
62	208	45	<5	planar	intragranular	narrow	many	gb-	none
63	248	90	>5	planar	intragranular	narrow	many	gb-	none
64	344	86	>5	planar	intragranular	wide	many	gb-	none
65	178	81	<5	curvi-planar	intergranular	narrow	few	gb-hc	none

66	58	73	<5	planar	intragranular	narrow	many	hc-	none
67	119	64	<5	planar	intragranular	narrow	many	hc-	none
68	241	61	<5	curvi-planar	intragranular	narrow	many	gb-	parallel
71	98	82	>5	planar	intragranular	narrow	few	iso	none
73	48	76	>5	curvi-planar	intergranular	narrow	many	gb-hc	parallel
74	308	79	<5	planar	intragranular	narrow	many	gb-	parallel
75	308	89	<5	planar	intragranular	narrow	few	gb-	parallel

Table A5.11 FIP orientation data: LTH1

FIP No.	strike	dip	size	planar	crack width	development	abundance	boundary
1	321	85	>5	planar	narrow	intercrystalline	few	trans
2	220	88	varied	planar	narrow	intracrystalline	few	gb-hc
3	56	87	<5	planar	narrow	intracrystalline	many	hc-gb
4	138	89	<5	planar	narrow	intracrystalline	few	hc-
5	52	78	<5	planar	narrow	intracrystalline	many	hc-
6	318	81	varied	planar	narrow	intracrystalline	few	hc-hc
7	319	81	varied	planar	narrow	intracrystalline	few	hc-hc
8	322	84	<5	planar	narrow	intracrystalline	many	hc-
9	341	82	varied	planar	narrow	intracrystalline	few	hc-hc
10	258	66	varied	irregular	narrow	intercrystalline	many	gb-gb
11	80	89	<5	planar	narrow	intracrystalline	few	hc-
12	227	83	<5	planar	narrow	intracrystalline	few	
13	220	84	>5	planar	narrow	intracrystalline	few	hc-hc
14	90	68	<5	planar	narrow	intracrystalline	few	hc-hc
15	89	72	>5	planar	narrow	intracrystalline	few	hc-hc
16	295	88	<5	curvi-planar	narrow	intracrystalline	many	hc-hc
21	233	85	>5	planar	narrow	intercrystalline	few	trans
22	98	80	<5	planar	narrow	intracrystalline	many	hc-
23	280	82	<5	planar	narrow	intracrystalline	many	hc-hc
24	192	77	varied	planar	narrow	intracrystalline	few	hc-hc
26	357	79	<5	planar	narrow	intracrystalline	many	hc-hc
27	31	84	varied	planar	narrow	intracrystalline	few	gb-hc
28	40	87	varied	planar	narrow	intracrystalline	few	gb-hc
29	40	85	>5	planar	wide	intracrystalline	few	hc-gb
32	39	80	varied	planar	narrow	intracrystalline	few	hc-gb
33	72	79	<5	planar	narrow	intracrystalline	many	hc-
34	221	87	<5	planar	narrow	intracrystalline	few	hc-
35	169	84	<5	curvi-planar	narrow	intracrystalline	few	iso
36	98	84	<5	planar	narrow	intracrystalline	many	hc-
37	233	87	<5	planar	narrow	intracrystalline	few	hc-hc
38	49	82	varied	curvi-planar	narrow	intracrystalline	few	hc-
39	213	89	varied	planar	narrow	intracrystalline	few	hc-hc
40a	188	71	varied	planar	narrow	intracrystalline	few	hc-
40b	201	81	varied	curvi-planar	wide	intracrystalline	few	hc-hc
42	320	86	<5	planar	narrow	intracrystalline	few	hc-gb
43	225	88	<5	planar	narrow	intracrystalline	many	hc-hc
44	204	75	<5	curvi-planar	narrow	intercrystalline	many	gb-
45	234	84	<5	curvi-planar	narrow	intracrystalline	many	iso
46	238	81	>5	planar	narrow	intracrystalline	few	hc-
47	219	78	<5	curvi-planar	narrow	intracrystalline	few	hc-hc
48	207	87	<5	curvi-planar	narrow	intracrystalline	few	gb-
52	144	87	<5	planar	narrow	intracrystalline	few	gb-
54	207	89	varied	planar	narrow	intracrystalline	few	hc-hc
56	34	90	>5	planar	narrow	intracrystalline	few	iso

Table A5.12 FIP orientation data: MDS1

FIP No.	strike	dipr	size	planar	development	crack width	abundance	boundary	pso

Crystal A									
1	300	87	<5	planar	intragranular	narrow	many	gb-	none
2	342	85	<5	planar	intergranular	narrow	many	gb-hc	parallel
3	322	73	<5	curvi-planar	intergranular	narrow	many	gb-hc	parallel
4	122	69	varied	planar	intragranular	narrow	many	gb-	none
5	159	74	<5	planar	intragranular	wide	many	hc-hc	none
6	159	75	<5	planar	intragranular	narrow	few	hc-hc	none
7	148	82	>5	planar	intragranular	narrow	many	gb-gb	parallel
8	339	86	varied	curvi-planar	intergranular	narrow	many	gb-gb	parallel
9	301	78	<5	planar	intragranular	narrow	many	gb-gb	none
10	49	69	<5	planar	intragranular	narrow	many	gb-	none
11	54	82	<5	planar	intragranular	wide	many	hc-	none
12	163	74	<5	curvi-planar	intragranular	narrow	many	iso	parallel
13	24	79	>5	curvi-planar	intragranular	narrow	many	iso	parallel
14	139	76	<5	planar	intragranular	narrow	few	gb-	parallel
15	147	69	<5	planar	intragranular	narrow	many	hc-hc	parallel
16	213	89	<5	irregular	intergranular	narrow	many	hc-hc	none
17	49	71	>5	planar	intragranular	narrow	many	gb-gb	none
18	288	73	<5	planar	intragranular	wide	many	hc-	parallel
19	228	79	varied	planar	intragranular	narrow	many	gb-	parallel
20	207	82	<5	planar	intragranular	narrow	many	hc-hc	none
21	191	87	<5	planar	intragranular	narrow	many	iso	none
22	168	73	<5	planar	intragranular	narrow	many	iso	none
24	148	49	<5	curvi-planar	intergranular	wide	few	gb-gb	none
25	137	57	>5	planar	intergranular	narrow	few	gb-	parallel
26	270	72	<5	planar	intragranular	narrow	few	hc-hc	none
27	333	86	<5	planar	intergranular	narrow	many	gb-	parallel
28	198	90	>5	planar	intragranular	narrow	many	iso	none
29	329	73	<5	planar	intragranular	narrow	many	gb-	parallel
30	337	86	<5	curvi-planar	intergranular	narrow	few	gb-	parallel
31	128	84	<5	planar	intragranular	wide	many	hc-hc	parallel
32	39	71	<5	planar	intragranular	narrow	many	hc-	none

Table A5.13 FIP orientation data: MHD1

FIP No.	strike	dipr	size	planar	development	crack width	abundance	boundary	pso
Crystal A									
1	318	82	<5	curvi-planar	intragranular	narrow	few	gb-	parallel
2	309	64	>5	curvi-planar	intergranular	narrow	many	gb-	parallel
3	356	72	<5	planar	intragranular	narrow	many	iso	none
4	300	87	<5	planar	intragranular	narrow	many	gb-	parallel
5	321	85	>5	planar	intragranular	narrow	many	gb-	parallel
6	137	65	>5	planar	intergranular	wide	few	gb-	parallel
7	139	81	varied	planar	intergranular	narrow	many	hc-hc	parallel
8	102	74	<5	planar	intragranular	narrow	few	hc-hc	none
9	274	83	<5	curvi-planar	intragranular	wide	many	iso	none
10	12	76	>5	curvi-planar	intragranular	narrow	many	iso	none
11	309	81	<5	planar	intragranular	narrow	many	gb-	parallel
12	138	90	>5	planar	intragranular	narrow	few	gb-	none
13	5	76	>5	curvi-planar	intragranular	narrow	many	iso	none
14	134	87	varied	planar	intergranular	narrow	many	hc-hc	parallel
15	128	85	varied	planar	intragranular	narrow	many	gc-hc	none
16	91	79	<5	planar	intragranular	narrow	few	gb-	none
18	129	51	varied	planar	intragranular	wide	many	gb-	parallel
19	98	89	<5	planar	intragranular	wide	few	hc-hc	none
20	142	87	varied	curvi-planar	intragranular	narrow	many	hc-hc	none
21	135	90	<5	irregular	intergranular	narrow	many	gb-hc	parallel

22	329	65	<5	planar	intragranular	narrow	few	gb-	none
23	329	88	<5	planar	intragranular	narrow	few	gb-	parallel
24	11	62	<5	planar	intragranular	narrow	many	iso	none
25	12	81	<5	planar	intragranular	narrow	many	iso	none
26	194	75	<5	planar	intergranular	narrow	few	gb-hc	parallel
27	141	74	<5	planar	intragranular	narrow	many	hc-hc	parallel
28a	142	85	>5	planar	intragranular	narrow	many	hc-hc	parallel
28b	142	86	>5	curvi-planar	intragranular	narrow	many	hc-	parallel
29	244	88	<5	curvi-planar	intragranular	narrow	many	iso	none
30	54	72	>5	planar	intergranular	narrow	few	gb-	none
31	322	82	>5	planar	intergranular	narrow	few	gb-gb	none
32	12	73	>5	curvi-planar	intragranular	narrow	many	iso	parallel
33	139	90	varied	planar	intergranular	narrow	many	hc-hc	parallel
35	327	52	varied	planar	intergranular	narrow	many	hc-hc	parallel
37	349	48	<5	planar	intragranular	wide	many	hc-hc	parallel
38a	324	84	varied	planar	intergranular	narrow	many	gb-	none
38b	324	85	<5	planar	intergranular	narrow	many	gb-	parallel
39	350	90	<5	planar	intragranular	narrow	few	iso	none
40	144	90	<5	planar	intragranular	narrow	many	gb-hc	parallel
41	74	62	>5	planar	intergranular	wide	many	hc-hc	none
42	48	69	varied	planar	intragranular	narrow	many	iso	parallel
43	312	78	varied	irregular	intergranular	narrow	few	gb-	parallel
44	1	82	<5	planar	intragranular	narrow	many	iso	none
45	198	81	>5	curvi-planar	intragranular	narrow	many	gb-hc	none
46	349	59	<5	curvi-planar	intergranular	narrow	many	hc-hc	parallel
47	145	71	<5	planar	intergranular	narrow	many	gb-gb	parallel
48	144	63	>5	planar	intragranular	narrow	few	hc-	none
49	303	49	>5	planar	intragranular	narrow	many	hc-	parallel
50	233	87	varied	curvi-planar	intergranular	narrow	few	gb-gb	parallel
51	315	89	>5	planar	intragranular	narrow	many	gb-hc	parallel
52	202	86	>5	planar	intragranular	narrow	many	iso	parallel
53	10	67	varied	planar	intragranular	narrow	many	iso	none
54	5	68	>5	irregular	intragranular	narrow	many	iso	none
55	333	75	>5	planar	intergranular	narrow	many	gb-	none
56	134	82	>5	planar	intergranular	narrow	many	gb-	parallel
58	134	90	>5	curvi-planar	intergranular	narrow	few	gb-	parallel
59	244	56	<5	planar	intragranular	narrow	many	hc-hc	none
60	355	78	<5	planar	intragranular	narrow	many	iso	none
61	318	85	<5	planar	intergranular	narrow	many	gb-	parallel

Table A5.14 FIP orientation data: WBN1

FIP No.	strike	dip	size	planar	development	crack width	abundance	boundary
Crystal A								
1	244	80	varied	planar	intracrystalline	narrow	few	gb-
2	238	73	<5	curvi-planar	intercystalline	narrow	many	gb-hc
3	283	78	<5	planar	intracrystalline	narrow	many	gb
4	53	80	>5	irregular	intracrystalline	wide	few	
5a	258	88	varied	planar	intracrystalline	narrow	few	
5b	164	66	varied	planar	intercystalline	narrow	few/many	hc-hc
6a	158	74	<5	planar	intracrystalline	narrow	many	hc-
6b	178	69	varied	curvi-planar	intracrystalline	narrow	few	hc
6c	178	86	<5	planar	intracrystalline	narrow	few	hc-
7	64	64	<5	curvi-planar	intracrystalline	narrow	many	gb-
8	162	40	varied	planar	intracrystalline	narrow	many	hc-
9	167	51	varied	planar	intercystalline	narrow	many	hc-
10	342	77	varied	planar	intracrystalline	narrow	many	iso
11	151	65	>5	planar	intercystalline	wide	few	gb-hc

12	247	70	<5	planar	intracrystalline	narrow	few	hc-
13	249	79	<5	planar	intracrystalline	narrow	many	hc-hc
14	249	85	<5	planar	intracrystalline	narrow	few	hc-
15a	86	87	varied	irregular	intracrystalline	narrow	many	hc-
15b	289	88	<5	curvi-planar	intracrystalline	narrow	few	hc-hc
16	57	77	varied	curvi-planar	intercystalline	narrow	many	gb-
17	176	87	<5	curvi-planar	intercystalline	narrow	many	
18	21	85	>5	planar	intracrystalline	narrow	few	hc-
19	279	46	>5	curvi-planar	intracrystalline	wide	few	
20	234	88	<5	planar	intracrystalline	narrow	few	
21	18	87	>5	planar	intracrystalline	narrow	few	hc-
22	156	81	<5	planar	intracrystalline	narrow	many	hc-hc
23	249	65	varied	curvi-planar	intracrystalline	narrow	many	hc-
24	162	57	<5	planar	intracrystalline	narrow	many	hc-hc
25	95	75	<5	curvi-planar	intracrystalline	narrow	many	hc-
26	253	84	<5	planar	intracrystalline	narrow	many	hc-hc
27	58	88	<5	planar	intracrystalline	narrow	many	hc-
28	256	55	>5	planar	intracrystalline	narrow	few	
29	73	45	varied	planar	intracrystalline	narrow	many	oc-
30	118	86	varied	planar	intracrystalline	wide	many	hc-oc
31								
32	169	57	<5	planar	intracrystalline	narrow	many	hc-hc
33	145	73	varied	planar	intercystalline	wide	many	oc-hc
34	175	71	varied	planar	intracrystalline	narrow	many	hc-oc
35	22	89	>5	planar	intercystalline	wide	many	hc-
36	263	52	>5	planar	intracrystalline	narrow	few	hc-hc
37	326	73	>5	planar	intracrystalline	wide	few	oc-
39	206	84	>5	planar	intracrystalline	narrow	few	oc-oc
40	24	88	>5	planar	intracrystalline	narrow	few	hc-hc
42	161	73	varied	curvi-planar	intracrystalline	narrow	few	hc-
43	170	65	varied	curvi-planar	intracrystalline	narrow	few	hc-
44	343	75	<5	planar	intracrystalline	narrow	many	hc-
45a	327	74	<5	planar	intracrystalline	narrow	many	iso
45b	346	69	<5	planar	intracrystalline	narrow	many	iso
45c	351	77	<5	planar	intracrystalline	narrow	many	iso
47	345	61	<5	planar	intracrystalline	narrow	many	iso
48	237	89	varied	planar	intercystalline	wide	many	trans
49	242	85	varied	planar	intracrystalline	narrow	many	oc-hc
50	66	76	varied	planar	intracrystalline	narrow	many	gb-
51	46	69	varied	curvi-planar	intracrystalline	narrow	many	hc-hc
52	142	75	varied	planar	intracrystalline	narrow	few	hc-hc
53	267	60	<5	planar	intracrystalline	narrow	few	trans
54	324	46	varied	planar	intracrystalline	narrow	few	hc-
56	324	46	<5	planar	intracrystalline	narrow	few	hc-hc
57	332	66	<5	irregular	intracrystalline	narrow	many	iso
58	321	61	<5	planar	intracrystalline	narrow	many	hc-
59	248	85	<5	curvi-planar	intercystalline	narrow	many	hc-hc
60	245	75	<5	planar	intracrystalline	narrow	few	hc-hc
61	157	89	varied	curvi-planar	intracrystalline	narrow	many	hc-
62	249	77	<5	planar	intracrystalline	narrow	few	hc-
63	266	56	<5	planar	intracrystalline	narrow	few	iso
64	16	83	<5	planar	intracrystalline	narrow	few	iso
68	336	85	<5	curvi-planar	intracrystalline	wide	many	iso
69	336	68	<5	planar	intracrystalline	wide	many	iso
71	189	67	varied	planar	intracrystalline	wide	many	iso
72	198	57	varied	planar	intracrystalline	wide	few	iso
73	343	72	varied	planar	intracrystalline	wide	few	iso
74	36	80						

75	55	72	>5	planar	intracrystalline	wide	few	
76	169	64	<5	planar	intracrystalline	narrow	many	iso
77	168	65	<5	planar	intracrystalline	narrow	many	iso
78	156	69	<5	curvi-planar	intracrystalline	narrow	few	iso
80	63	60	<5	curvi-planar	intracrystalline	narrow	few	hc-hc
81	254	86	<5	planar	intracrystalline	narrow	many	hc-
82	258	74	<5	planar	intracrystalline	narrow	many	hc-
83	347	55	>5	planar	intracrystalline	wide	few	iso
84	56	80	varied	planar	intercystalline	narrow	few	hc-gb
85	11	77	varied	planar	intracrystalline	wide	few	iso

Table A5.15 Thermometric data: LI1

FIP #	Th	Tfm	Tlm	wt%NaCl
Crystal A				
1	199.2		-1.3	2.2
1	201.4		-1.3	2.2
2	280			
2	280.9			
2	269.6		-3.6	5.8
3	270.2		-4.1	6.6
3	295.7		-4	6.4
3	285.1		-4.1	6.6
5	236.3		-5	7.6
5	205.2		-4.4	7
5	212.4		-4.6	7.3
5	216.9		-4.7	7.5
7	240.3		-4.2	6.7
7	255.8		-3.9	6.3
7	250.4		-3.8	6.1
8	261.5		-4	6.4
10	199.8		-1	1.7
10	186.1		-1.3	2.2
12	229.3		-5	7.6
14	243.2			
14	215.6			
14	210.8			
15	277.9		-3.4	5.5
16	260.1		-4.5	7.1
16	270.8			
16	290.2		-4.9	7.7
16	298		-4.7	7.5
19	260.5		-3.6	5.8
19	241.3		-3.6	5.8
22	205.3		-4	6.4
22	204		-4	6.4
	232.3		-5	7.6
	395.7			
	379.1		-5	7.6
Crystal B				
1	264.3		-5.1	8
1	254.1			
2	271.1		-4.9	7.7
2	284.2			
3	278.4		-10.4	14.4

4	294.1	-10.8	14.8
8	202.1	-3.4	5.5
8	210.1	-3.4	5.5
9	250.1	-7.1	10.6
9	258.4	-6.9	10.4
10	184.3	-1.2	2.1
10	187.2		
10	197.8	-1.2	2.1
11	263.4		
14	204.2	-2.3	3.9
14	223.1	-3.1	5.1
15	305.2	-6.8	10.2
16	322.4	-5	7.6
16	287.4	-4.9	7.7
16	299.1		
19	194.2	-3.1	5.1
19	202.4	-3.1	5.1
20	293.1	-6.3	9.6
20	287.1		
21	274.1	-5.8	8.9
21	258.1		
21	269.4		
24	204.8	-4.1	6.6
25	288.8	-6.4	9.7
27	236.7	-4.6	7.3
27	241.9	-4.6	7.3
27	228.1	-4.6	7.3
31	178.6	-2.1	3.5
31	187.2	-2	3.4
32	177.2	-1.9	3.2
32	169.4	-1.9	3.2
33	201.8	-1.9	3.2
34	211.3	-3.4	5.5
35	229.1	-4.1	6.6
35	187.2		
35	254.1	-4.2	6.7
36	245.3	-4.3	6.9
37	263.1	-4.3	6.9
37		-4.4	7
39	203	-4.2	6.7
40	211.6	-4.2	6.7
40	224.1	-3.9	6.3
40	208.4		
41	268	-4.8	7.6
44	223.3	-3.2	5.2
46	263.4	-6.5	9.6
47	336.4	-11.4	15.4
47	347.1	-11.9	15.9
51	294.1	-9.4	13.3
56	281.3	-7.2	10.7
58	191.1	-1.9	3.2
58	174.2		
58	187.4		
60	298.3	-5.1	8
61	286.4		
61	298.1		
61	281.2	-4.9	7.7
63	331.6	-7.4	11

64	302.1	-7.4	11
64	312.4	-7.5	11.1
66	187.2	-6.4	9.7
67	298.3	-8.4	12.2
67	278.2		
77	201.3	-3.9	6.3
79	244.1	-4	6.4
79	258.9		
80	201.4	-3.5	5.7
80	201		
83	274	-8.3	12.1
118	215.1		
118	206.2	-2.5	4.2
119	240	-3.8	6.1
119	257.4	-3.9	6.3
119	264.7		
125b	229	-3.8	6.1
126a	304.3	-9.4	13.3
126a	303.1	-10	14
131	286.1	-4.1	6.6
131	278.2	-4.1	6.6
134	241		
141	236.1	-3.9	6.3
144	241	-4.2	6.7
144	267.4	-4.3	7
144	257.1	-4.3	7
147	211.3		
150	302.4	-12.8	16.8
154	193.2	-1.3	2.2
154	190.1		
155	196.1	-1.4	2.4

Table A5.16 Thermometric data: LI3

Inclusion No.	Th	Tfm	Tlmice	wt%NaCl
1	209.6		-2.7	4.4
2	251.3			
3	203.5		-3.3	5.3
4	183.7		-4.6	7.2
5	289.1		-3.6	5.8
6	217.8		-3.2	5.2
7	215.6		-3.3	5.3
8	214.3		-3.4	5.5
9	247.4			
10	229.3			
11	227.9			
12	300.1		-3.3	5.3
13	309.4		-3.3	5.3
14	207.1		-0.9	1.5
15	210.5		-2.2	3.6
16	209.3		-2.5	4.1
17	207.4		-3.9	6.2
18	337.4		-14.3	18
19	235.5		-0.5	0.8
20	261.1		-3.4	5.5
21	273.2		-3.4	5.5
22	238.5		-3.5	5.6

23	218.9	-3	4.9
24	207.4	-2.9	4.7
25	234.4	-3	4.9
26	261.2	-3.7	5.9
27	247.1	-0.6	1
28	303.9		
29	246		
30	254.3	-0.8	1.3
31	233.2	-0.6	1
32	343.9	-12.8	16.7
33	245.5	-1.4	2.3
34	259.4		
35	328.5	-12.9	16.8
36	122.5	-2.6	4.2
37	189.6	-2.5	4.1
38	109.3	-1.8	3
39	124.2	-1.5	2.5
40	246.3	-2.1	3.4
41	202.2	-3.1	5
42	217.7	-3.1	5
43	310.4	-3.3	5.3
44	321.8	-3.4	5.5
45	227.8	-2.1	3.4
46	309.1	-2.3	3.8
47	311.9		
48	343	-3.9	6.2
49	338.6	-4	6.4
50	235.5	-2.9	4.7
51	157.5	-2.9	4.7
52	285.9	-4	6.3

REFERENCES

Abou-Sayed, A.S. and Brechtel, C.E. (1978) In Situ Stress Determination by Hydrofracturing: A Fracture Mechanics Aproach. *J. Geophys. Res.*, **83**, 2851-2862.

Alderton, D.H.M. and Rankin, A.H. (1983) The character and evolution of hydrothermal fluids associated with the kaolinised St. Austell granite, SW England. *J. Geol. Soc. Lond.*, **140**, 297-309.

Alderton, D.H.M. and Harmon, R.S. (1991) Fluid inclusion and stable isotope evidence for the origin of mineralising fluids in south-west England. *Min. Mag.*, **55**, 605-611.

Alderton, D.H.M. (1978) Fluid inclusion data for lead-zinc ores from south-west England. *Trans. Inst. Min. Metall.*, **87**, B132-135.

Anders, M.H. and Wiltschko, D.V. (1994) Microfracturing, paleostress and the growth of faults. *J. Struct. Geol.*, **16**, 795-815.

Anderson, A.J., Clark, A.H., Ma, X.-P., Palmer, G.R., MacArthur, J.D. and Roedder, E. (1989) Proton induced X-ray and gamma-ray emission analysis of unopened fluid inclusions. *Econ. Geol.*, **84**, 924-939.

Anderson, E.M. (1937) The dynamics of formation of cone sheets, ring dykes and cauldron subsidences. *Proc. R. Soc. Edinb.*, **56**, 128-157.

Anderson, J.L. (1945) Deformation planes and crystallographic directions in quartz. *Geol. Soc. Ammer. Bull.*, **56**, 409-430.

Anderton, R., Bridges, P.H., Leeder, M.R. and Selwood, B.W. (1979) *A Dynamic Stratigraphy of the British Isles*. George Allen and Unwin, 301pp.

Appleton, J.D. and Wadge, A.J. (1976) Investigation of tungsten and other mineralisation associated with the Skiddaw Granite, near Carrock Mine, Cumbria. *Miner. Recon. Progam. Rep. Inst. Geol. Sci.*, **7**.

Arthur, M.J. (1989) The Cenozoic evolution of the Lundy Pull-Apart Basin into the Lundy Rhomb Horst. *Geol. Mag.*, **126**, 187-198.

Arthur, M.J. (1982) Investigations of geophysical anomaly in the Hereford area of the Welsh Borderland. *Institute of Geological Sciences, Applied Geophysics Unit report 122.* 196pp.

Arthur, M.J. (1983) Late Precambrian-Tertiary Transcurrent Faulting and Plate Margin Activity in SW Britain. *Abstract*, 2nd Deep Geology Workshop, Cambridge University, 11.

Atkinson, B.K. (1982) Subcritical crack propagation in rocks: theory, experimental results and applications. *J Struct. Geol.*, **4**, 41-56.

Aviles, C.A., Scholz, C.H. and Boatwright, J. (1987) Fractal analysis applied to characteristic segments of the San Andreas Fault. *J. Geophys. Res.*, **92**, 331-344.

Ball, T.K., Fortey, N.J. and Shepherd, T.J. (1985) Mineralisation at the Carrock Fell Tungsten Mine, N.England: Paragenetic, fluid inclusion and geochemical study. *Mineral. Deposita*, **20**, 57-65.

Bamford, D., Faber, S., Jacob, B., Kaminski, W., Nunn, K., Prdehl, C., Fuchs, C., King, R. and Wilmore, P. (1976) Lithospheric Siesmic Profile in Britain, I: Preliminary results. *Geophys. J. R. astr. Soc.*, **44**, 146-160.

Barnes, H.L. (1967) *Geochemistry of Hydrothermal Ore Deposits.* Rinehart and Winston, 670pp.

Batzle, W.F. and Simmons, G. (1976) Microfractures in rocks from two geothermal areas. *Earth and Planet. Sci. Lett.*, **30,** 71-93.

Beach, A. (1975) The geometry of en-échelon vein arrays. *Tectonophysics,* **28,** 245-263.

Binns, P.R. and Bodnar, R.J. (1986) Decrepitation behavior of fluid inclusions in quartz at one atmosphere confining pressure. *Transactions of the American Geophysical Union,* **67,** 399. (abstr.).

Blyth, F.G.H. (1957) The Lustleigh fault in north-east Dartmoor. *Geol. Mag.*, **94,** 291-296.

Blyth, F.G.H. (1962) The structure of the north-eastern tract of the Dartmoor granite. *J. Geol. Soc. Lond.*, **118,** 435-453.

Blythe, F.G.H. (1957) The Lustleigh Fault in North-East Dartmoor. *Geol. Mag.*, **94,** 291-296.

Blythe, F.G.H. (1962) The structure of the north-eastern tract of the Dartmoor Granite. *Quart. Jour. Geol. Soc. Lond.*, **118,** 435-453.

Bodnar, R.J., Binns, P.R. and Hall, D.L. (1989) Synthetic fluid inclusions. VI. Quantitative assessment of the decrepitation characteristics of fluid inclusions in quartz at one atmosphere confining pressure. *J. Metamorphic. Geol.*, **7,** 229-242.

Bodnar, R.J. (1989) Fluid inclusion evidence for the physical and chemical conditions of petroleum generation in the Miocene and Monterey Formation of California, USA (abstr) ECROFI X, London, 10-11,

Boiron, M.C., Cathelineau, M., Essarraj, S. and Lespinasse, M. (1991) Characterisation of the relationships between deformation, fluid migration and Au deposition in quartz veins: Methedology and modelling. In: *Brasil Gold'91* (ed. E.A. Laderia), Balkema, Rotterdam, 637-643.

Bombolakis, E.G. (1964) Photoelastic investigation of brittle crack growth within a field of uniaxial compression. *Tectonphysics,* **1,** 343-351.

Borisenko, (1977) Study of the salt composition of solutions in gas-liquid inclusions in minerals by the cryometric method. *Soviet Geol. and Geophys.*, **18,** 11-19.

Bott, M.H.P., Day, A.A. and Mason-Smith, D. (1958) The geological interpretation of gravity and magnetic surveys in Devon and Cornwall, *R. Soc. Lond. Phil. Trans.*, **251,** 161-191.

Bott, M.H.P. and Scott, P. (1964) Recent geophysical studies in southwest England. In: *Present views on some aspects of geology of Cornwall and Devon,* (eds. K.F.G. Hosking and G.J. Shrimpton), R. Geol. Soc. Cornwall, 150th Anniv. Vol., 25-44.

Bott, M.H.P., Day, A.A. and Masson Smith, D. (1958) The geological interpretation of gravity and magnetic surveys in Devon and Cornwall. *Phil. Trans. R. Soc. Lond.*, **251,** 161-191.

Bott, M.H.P. (1974) The geological interpretation of a gravity survey of the English Lake District and the Vale of Eden. *J. Geol. Soc. Lond.*, **130,** 309-331.

Bottrell, S.H. and Yardley, B.W.D. (1987) A modified crush leach method for the analysis of fluid inclusion electrolytes (abstr), ECROFI IX, 15-16.

Boullier, A-M., Michot, G., Pécher, A. and Barres, O. (1989) Diffusion and/or plastic deformation around fluid inclusions in synthetic quartz: new investigations. In *Fluid movements, elements transport and the composition of the crust.* (eds. D. Bridgewater), NATO ASI Series, Kluwer Pub group, Dordrecht, 345-360.

Boullier, A-M. and Robert, F. (1992) Palaeosciesmic events recorded in Archean gold-quartz vein networks, Val d'Or, Albiti, Quebec, Canada. *J. Struct. Geol.*, **14**, 1161-1179.

Brace, W.F., Paulding, B.W. and Scholz, C.H. (1966) Dilatancy in the fracture of crystalline rocks. *J. Geophys. Res.*, **71**, 3939-3953.

Bramall, A. and Harwood, H.F. (1923) The Dartmoor granite: its mineralogy, structure and petrology. *Min Mag.*, **20**, 39-53.

Brantley, S.L., Evans, B., Hickman, S.H. and Crerar, D.A. (1990) Healing of microcracks in quartz: Implications for fluid flow. *Geology*, **18**, 136-139.

Brantley, S.L. (1992) The effect of fluid chemistry on quartz microcrack lifetimes. *Earth Planet. Science Letts.*, **113**, 145-156.

Bray, C.J. and Spooner, E.T.C. (1983) Sheeted vein Sn-W mineralisation and greisenisation associated with economic kaolinisation, Goonbarrow china clay pit, St. Austell, Cornwall, England: geologic relationships and geochronology. *Econ. Geol.*, **78**, 1064-1089.

Bray, C.J. (1980) Mineralisation, greisenisation and kaolinisation at Goonbarrow china clay pit, Cornwall, UK. Unpubl. Ph.D. Thesis, University of Oxford.

Bredhoeft, J.D., Wolff, R.G., Keys, W.S. and Shuter, E. (1976) Hydraulic fracturing to determine the regional in situ stress field, Piceance Basin, Colorado. *Geol. Soc. Am. Bull.*, **87**, 250-258.

Bristow, C.M. and Hughes, D.E. (1971) A Tertiary thrust fault on the southern margin of the Bovey Basin. *Geol. Mag.*, **108**, 61-68.

Bristow, C.M. (1977) A review of the evidence for the origin of the kaolin deposits in SW England. *Proc. 8th. Int. Kaolin. Symposium, Madrid, Rome*, **K-2**, 19pp.

Bristow, C.M. and Robson, J.L. (1994) Palaeogene basin development in Devon. *Trans. Inst. Min. Metall.*, **103**, B163-B174.

Bristow, C.M., Palmer, Q.G. and Pirrie, D. (1992) Palaeogene basin development: new evidence form the southern Petrockstow basin, Devon. *Proc. Ussher Soc.*, **8**, 19-22.

Brock, W.G. and Engelder, T. (1977) Deformation associated with movement of the Muddy Mountain overthrust in the Buffington window, southeatern Nevada. *Bull. Geol. Soc. Am.*, **88**, 1667-1677.

Bromley, A.V. and Holl, J. (1986) Tin mineralisation in southwest England. In: *Mineral processing at a crossroads.* Proceedings of NATO ASI Conference No. 117, 195-262.

Bromley, A.V. (1989) *The Cornubian Orefield.* International Association of Gechemistry and Cosmochemistry, 6th International Symposium on Water-Rcok Interaction, Malvern, UK, Field Guide, Camborne School of Mines, Redruth.

Brooks, M. and Thompson, M.S. (1973) The geological interpretation of a gravity survey of the Bristol Channel. *J. Geol. Soc. Lond.*, **129**, 245-274.

Brown and Lamb (1989) P-V-T properties of fluids in the system H2O-CO2-NaCl: New graphical presentations and imlpications for fluid inclusion studies. *Geochem. Cosmochem Acta.*, **53**, 345-356.

Bull, B.W. (1982) Geology and Mineralisation of an area around Tavistock, South-west England. *Unpubl. Ph.D. Thesis.*, Univ. of Exeter.

Burnham, C.W. (1979) Magmas and Hydrothermal fluids. In: *Geochemistry of Hydrothmal Ore Deposits.* (ed. H.L. Barnes), Wiley, New York, 71-136.

Carlson, S.R., Wu, M. and Wang, H.F. (1990) Micromechanical Modeling of Thermal Cracking in Granite. *Am. Geophys. Union*, **56**, 37-48.

Carter, N.L. and Kirby, S.H. (1978) Transient creep and semi-brittle behaviour of crystalline rocks. *Pure Appl. Geophys.*, **116**, 807-839.

Cathelinau, M., Lespinasse, M., Bastoul, A.M., Bernard, C. and Leroy, J. (1990) Fluid migration during contact metamorphism: the use of oriented fluid inclusion trails for a time/space reconstruction . *Min. Mag.*, **54**, 169-182.

Chandler, P and Isaac, K.P. (1982) The geological setting, geochemistry and significance of Lower Carboniferous basic volcanic rocks in central south-west England. *Proc. Ussher Soc.*, **5**, 279-288.

Charoy, B. (1981) Post-magmatic processes in south-est England and Brittany. *Proc. Ussher Soc.*, **5**, 101-115.

Charoy, B. (1986) The Genesis of the Cornubian batholith (South West England): the example of the Carnmenellis pluton. *J. Petrol.*, **27**, 571-604.

Chen, Y. and Wang, C-y. (1980) Thermally induced acoustic emmission in Westerly granite. *Geophys. Res. Lett.*, **7**, 1089-1092.

Chen, Y., Clark, A.H., Farrar, E., Wastneys, H.A.H.P., Hodgson, M.J. and Bromley, A.V. (1993) Diachronous and independent histories of plutonism and mineralisation in the Cornubian Batholith, southwest England. *J. Geol. Soc. Lond.*, **150**, 1183-1191.

Chernyshev, S.N. and Dearman, W.R. (1991) *Rock Fractures*. Butterworth-Heinemann, London.

Chernyshev, S.N. and Dearman, W.R., Nakai, S., Shepherd, T.J. and Scivener, R.C. (1990) Single mineral SM-Nd dating of fluorite mineraliastion in Cornwall, England. *Geol. Soc. Am. Abs. Progs.*, **22**, A223.

Chesley, J.T., Halliday, A.N. and Scivener, R.C. (1991) Samarium-neodymium direct dating of fluorite mineralisation. *Science*, **252**, 949-951.

Chesley, J.T., Halliday, A.N., Snee, L.W., Mezger, K., Shepherd, T.J. and Scrivener, R.C. (1993) Thermochronology of the Cornubian batholith in southwest England: Implications for pluton emplacement and protracted hydrothermal mineralisation. *Geochem. Cosmochem. Acta.*, **57**, 1817-1835.

Christie-Blick, N. and Biddle, K.T. (1985) Deformation and basin formation along strike-slip faults. In: *Strike-Slip Deformation, Basin Formation and Sedimentation* (eds. K.T. Biddle and N. Christie-Blick). Society of Economic Palaeontologists and Mineralogists Special Publication, **37**, 1-34.

Clayton, R.E., Scrivener, R.C. and Stanley, C.J. (1990) Mineralogical and preliminary fluid inclusion studies of lead-antimony mineralisation in north Cornwall. *Proc. Ussher Soc.*, **7**, 258-262.

Conrad, R.E. and Friedman, M. (1976) Microscopic feather fractures in the faulting process. *Tectonophysics*. **33**, 187-198.

Cooper, M.P. and Stanley, C.J. (1990) Minerals of the English Lake District: Caldbeck Fells. Natural History Museum, London, 160pp.

Cornwall, J.D. (1971) Geophysics of the Bristol Channel area. Proc. Geol. Soc. Lond., 1664, 286-289.

Cotterell, B. and Rice, J.R. (1980) Slightly curved or kinked cracks. *Int. J. of Fracture*, **16**, 155-169.

Cox, S.F. and Etheridge, M.A. (1983) Crack-seal fibre growth mechanisms and their significance in the development of oriented layer silicate microstructures. *Tectonophysics*, **92**, 147-170.

Cox, W.R., Rankin, A.H., Alderton, D.H.M. and Grocott, J. (1993) Microstructural and fluid controls on the formation of kaolinised granite at Goonbarrow china clay pit, SW England. *Archiwum Mineralogiczne*. ECROFI XII conference abstr, Warsaw, Poland, 50-51.

Crampin, S., McGonigle, R. and Ando, M. (1986) Extensive-dilatancy anisotropy beneath Mt. Hood, Oregon and the effect of aspect ratio on seismic velocities through aligned cracks. *J. Geophys. Res.*, **91**, 12,703-12,710.

Crampin, S. (1987) Geological and industrial implications of extensive-dilatancy anisotropy. *Nature*, **328**, 491-496.

Crawford, M.L. (1981) Fluid inclusions in metamorphic rocks-low and medium grade. In: *Fluid Inclusions: Applications to Petrology Short Course Handbook, vol. 6.* (eds. E.D. Ghent, L.S. Hollister and M.L. Crawford). Mineral Association of Canada, Calgary, 157-181.

Dagger, G.W. (1977) Controls of copper mineralisation at Coniston, English, Lake District. *Geol. Mag.*, **144**, 195-202.

Dangerfield, J. and Hawkes, J.R. (1981) The Variscan granites of south-west England: additional information. *Proc. Ussher Soc.*, **5**, 116-120.

Dangerfield, J. and Hawkes, J.R. (1969) Unroofing of the Dartmoor granite and possible consequences with regard to mineralisation. *Proc. Ussher Soc.*, **2**, 122-131.

Darbyshire, D.P.F. and Shepherd, T.J. (1985) Chronology of granite magmatism and associated mineralisation, SW England. *J. Geol. Soc. Lond.*, **142**, 1159-1177.

Darbyshire, D.P.F. and Shepherd, T.J. (1987) The Variscan granites of SW England: additional information. *Proc. Ussher. Soc.*, **4**, 431-438.

Davis, W.J. and Williams-Jones, A.E. (1985) A fluid inclusion study of the porphyry-greisen, tungsten-molybdenum deposit at Mount Pleasant, New Brunswick, Canada. *Miner. Deposita*, **20**, 94-101.

Dearman, W.R. (1963) Wrench-faulting in Cornwall and South Devon. *Proc. Geol. Assoc. Lond.*, **74**, 265-87.

Dearman, W.R., Fresney, E.C., Selwood, E.B., Simpson, S., Stone, M. and Taylor, R.T. (1971) Symposium on the structure of SW England. *Proc. Ussher Soc.*, **2**, 220-264.

Delaney, P.T., Pollard, D.D., Ziony, J.I. and McKee, E.H. (1986) Field relations between Dikes and Joints: Emplacement Processes and Paleostress Analysis. *J. Geophys. Res.*, **91**, 4920-4938.

Devore, G.W. (1969) Differential thermal contractions and conpressibilities as a cause for mineral fracturing and anealing. *Contrib. Geol.*, **8**, 21-36.

Dewey, J.F. (1988) Extesional collapse of oroegns. *Tectonics*, **7**, 1123-1139.

Dietrich and Ramsay (1980) Opening processes of veins from the Helvetic nappes. *Conf. on the Effect of Deformation on Rocks. (Abst.)* Univ. of Göttingen, Göttingen, 85-87.

Dineley, D.L. (1992) Devonian. In: *The Geology of England and Wales.* 179-201.

Dines, H.G. (1956) The metalliferous mining region of south-west England. *Geol. Survey Gt. Britaim Mem.*, 795pp.

Dodson, M.H. and Long, L.E. (1962) Age of the Lundy Granite, Bristol Channel. *Nature*, **195**, 975-976.

Dollar, A.T.J. (1941) The Lundy complex: its petrology and tectonics. *Quart. J. Geol. Soc. Lond.*, **97**, 39-77.

Dominy, S.C., Scrivener, R.C., Le Boutillier, N., Bussell, M.A. and Halls, C. (1994) Crosscourses in the South Crofty Mine, Cornwall: Further studies of paragenesis and structure. *Proc. Ussher Soc.*, **8**, 237-241.

Dominy, S.C. (1993) The Geology and Genesis of the China Clay Deposits of Southwest England with Particular Reference to their Commercial Properties. *Unpubl. Ph.D. Thesis*, Kingston University, 302pp.

Durrance, E.M., Bromley, A.V., Bristow, C.M., Heath, M.J. and Penman, J.M. (1982) Hydrothermal circulation and post-magmatic changes in granites of south-west England. *Proc. Ussher Soc.*, **5**, 304-320.

Eadington, P.J. and Wilkins, R.W.T. (1980) The origin, interpretation and chemical analysis of fluid inclusions in minerals. *Technical Communication No. 69*, Institute of Earth Resources, CSIRO, North Ryde, Australia.

Eastwood, T., Hollingworth, S.E., Rose, W.C.C. and Trotter, F.M. (1968) Geology of the country around Cockermouth and Caldbeck. *Mem. Geol. Surv.*, H.M.S.O., London, 298pp.

Edmonds, E.A., Williams, B.J. and Taylor, R.T. (1979) Geology of Bideford and Lundy Island. *Memoir of the Geological Survey of Great Britain*, Sheet 292, London, H.M.S.O., 143pp.

Edmunds, E.A., McKeown, M.C. and Williams, M. (1969) British Regional Geology: South-West England. National Environmental Research Council, 130pp.

Edmunds, W.M., Andrews, J.N., Burgess, W.G., Kay, R.L.F. and Lee, D.J. (1984) The evolution of saline and thermal groundwaters in the Carnmenellis granite. *Min. Mag.*, **48**, 407-424.

Edwards, R.A. (1976) Tertiary sediments and structure of the Bovey basin, south Devon. *Proc. Geol. Assoc.*, **87**, 1-26.

Emeleus, C.H. (1982) The central complexes. In: *Igneous Rocks of the British Isles*. (ed. D.S. Sutherland), John Wiley and Sons, Chichester, 369-414.

Emeleus, C.H. (1991) Tertiary Igneous Activity. In: *Geology of Scotland*. (ed. G.Y. Craig) The Geological Society, London, 455-502.

Engelder, T. (1974) Cataclasis and the generation of fault gouge. *Bull. Geol. Soc. Am.*, **85**, 1515-1522.

England, R.W. (1988) The early Tertiary stress regime in NW Britain: evidence from the patterns of volcanic activity. In: *Early Tertiary Volcanism and the opening of the NE Atlantic*, (eds. A.C. Morton and L.M. Parson) Geol. Soc. Spec. Pub. **39**, 381-389.

Etchcopar, A., Vasseur, G. and Daignieres, M. (1981) An inverse problem in microtectonics for the determination of stress tensors from fault striation analysis. *J. Struct. Geol.*, **3**, 51-65.

Evans, A.G., (1978) Microfracture from thermal expansion anisotropy, I, Single phase systems. *Acta Metall.*, **26**, 1845-1853.

Evans, A.M. (1993) *Ore Geology and Indutrial Minerals, An Introduction*. Blackwell Scientific Publications, 390pp.

Ewart, A. (1962) Hydrothermal alteration in the Carrock Fell area, Cumberland, England. *Geol. Mag.*, **99**, 1-8.

Finlayson, A.M. (1910) The ore bearing pegmatites of Carrock Fell. *Geol. Mag.*, **7**, 19-28.

Firman, R.J. (1978) Epigenetic mineralisation. In: *The Geology of the Lake District.* (ed. F. Moseley). *York. Geol. Soc.*, 226-241.

Firman, R.J. and Lee, M.K. (1986) Age and structure in the concealed English Lake District and its probable influence on subsequent sedimentation, tectonics and mineralisation. In: *Geology in the real world, the Kingsley Dunham volume.* (eds. R.W. Nesbitt and I. Nicholl). *Trans. Inst. Min. Metall.*, London, 117-127.

Fitton, J.G. and Hughes, D.J. (1970) Volcanism and plate tectonics in the British Ordovician. *Earth Planet. Sci. Lett.*, **8**, 223-228.

Fletcher, B.N. (1975) A new Tertiary basin east of Lundy Island. *J. Geol. Soc. Lond.*, **131**, 223-225.

Floyd, P.A. (1972) Geoghemistry, Origin and Tectonic Environment of the Basic and Acidic Rocks of Cornubia, England. *Proc. Geol. Assoc.*, **83**, 385-404.

Fortey, N.J., Ingham, J.D., Skilton, B.R.H., Young, B. and Shepherd, T.J. (1984) Antimony mineralisation at Wet Swine Gill, Caldbeck Fells, Cumbria. *Proc. York. Geol. Soc.*, **45**, 59-65.

Frantz, J.D., Mao, H.K., Zhang, Y.G., Wu, Y., Thompson, A.C., Underwood, J.H., Giauque, R.D., Jones, K.W., and Rivers, M.L. (1988) Analysis of fluid inclusions by X-ray fluorescence using synchrotron radiation. *Chem. Geology*, **69**, 325-244.

Fredrich, J.T. and Wong, T-f. (1986) Micromechanics of thermally induced cracking in three crustal rocks. *J. Geophys. Res.*, **91**, 12,743-12,764.

Freshney, E.C., Edwards, R.A., Isaac, K.P., Witte, G., Wilkinson, G.C., Boulter, M.C. and Bain, J.A. (1982) A Tertiary basin at Dutson, near Launceston, Cornwall, England. *Proc. Geol. Assoc.*, **93**, 395-402.

Friedman, M. (1969) Structural analysis of fractures in cores from the Saticoy field, Ventura Co., California. *Bull. Am. Ass. Petrol. Geol.*, **53**, 367-389.

Friedman, M. and Logan, J.M. (1970) Microscopic feather fractures. *Bull. Geol. Soc. Am.*, **81**, 3417-3420.

Fu, Y. and Evans, AG. (1985) Some effects of microcracks on the mechanical properties of brittle solids - 1. Stress, strain relations. *Acta Metall.*, **33**, 1515-1523.

Fyfe, W.S., Price, N.J. and Thompson, A.B. (1978) *Fluids in the Earth's Crust.* Elsverier, Amsterdam, pp383.

Fyfe, W.S. (1985) Fluids, tectonics and crustal deformation, *Tectonics*, **119**, 29-36.

Gallagher, J.J., Friedman, M., Handin, J. and Sowers, G.M. (1974) Experimental studies relating to microfractures in sandstone. *Tectonophysics*, **21**, 203-247.

Ghosh, P.K. (1927) The petrology of the Bodmin Moor granite (eastern part), Cornwall. *Min. Mag.*, **21**, 285-308.

Gibbs, A. (1984) Structural evolution of extensional basin margins. *J. Geol. Soc. Lond.*, **141**, 609-620.

Gratier, J.P. and Jenatton, L. (1984) Deformation by solution-deposition, and re-equilibration of fluid inclusions in crystals depending on temperature, internal pressure and stress. *J. Struct. Geol.*, **6**, 189-200.

Griffith, A.A. (1920) The phenomenon of rupture and flow in solids. *Phil. Trans. Roy. Soc. London*, **221**, 163-197.

Guihaumou, N., Szydlowski, N. and Pradier, B. (1989) Characterisation of hydrocarbon fluid inclusions by infra red and fluorescence microsoectrometry (abstr), ECROFI X, London, 40.

Guilbert, J.M. and Park, C.F. (1986) The Geology of Ore Deposits, Freeman and Company, New York, 985.

Gustafason, L.B. and Hunt, J.P. (1975) The porphyry coppper deposit at El Salvador, Chile. *Econ. Geol.*, **70**, 857-912.

Hains, B.A., Edmonds, E.A., Briden, J.C. and Tappin, T.R. (1983). *Lundy, Solid Geological Map, Sheet 51N-06W, (1:250000).* Southhampton: Ordnance Survey for Institute of Geological Sciences.

Hallbauer, D.K., Wagner, H. and Cook, N.G. (1973) Some observations concerning the microscopic and mechanical behaviour of quartzite specimens in stiff, triaxial compression tests. *Int. J. Rock. Mech. Min. Sci.*, **10**, 713-726.

Hancock, P.L. (1972) The analysis of en-échelon veins. *Geol. Mag.*, **109**, 269-276.

Hancock, P.L. (1973) Shear zones and veins in the Carboniferous Limestone near the Observatory, Clifton, Bristol. *Proc. Bristol Nat. Soc.*, **32**, 297-306.

Hancock, P.L. (1985) Brittle microtectonics: principles and practices. *J. Struct. Geol.*, **7**, 437-457.

Harding, T.P., Vierbuchen, R.C. and Christie-Blick, N. (1985) Structural styles, plate-tectonic settings and hydrocarbon traps of divergent (transtensional) wrench faults. In: *Strike-Slip Deformation, Basin Formation and Sedimentation* (eds. K.T. Biddle and N. Christie-Blick). Society of Economic Palaeontologists and Mineralogists Special Publication, **37**, 51-77.

Harker, A. (1894) Carrck Fell. A study in the variation of igneous rock masses: Part I. The Gabbro. Quart. *J. Geol. Soc. Lond.*, **50**, 311-317.

Harris, P. and Dagger, G.W. (1987) The intrusion of the Carrock Fell Gabbro Series (Cumbria) as a sub-horizontal body. *Proc. York. Geol. Soc.*, **46**, 371-380.

Hawkes, J.R. (1982) The Dartmoor Granite and later volcanic rocks. In: *The Geology of Devon, Exeter*, 85-116.

Hecht, C.A. (1992) The Variscan evolution of the Culm Basin, south-west England. *Proc. Ussher. Soc.*, **8**, 33-38.

Hicks, H. (1884) On the Cambrian conglomerates resting upon and in the vicinity of some pre-Cambrain rocks (the so-called intrusive masses in Anglesey and Caernarvonshire. *Geol. Soc. Lond. J.*, **40**, 187-199.

Hitchen, C.S. (1934) The Skiddaw slates and its residual products. *Quart. J. Geol. Soc. Lond.*, **90**, 158-200.

Hollister, L.S. (1981) Information intrinsically available from fluid inclusions. In: *Fluid Inclusions: Applications to Petrology, Short Course Handbook*, vol. **6**, (eds. E.D. Ghent, L.S. Hollister and M.L. Crawford), pp. 1-12, Mineral Association of Canada.

Holloway, S and Chadwick, R.A. (1986) The Sticklepath-Lustleigh fault zone: Tertiary sinistral reactivation of a Variscan strike-slip fault. *Jour. Geol. Soc. Lond.*, **143**, 447-452.

Horne and Macintyre (1975)

Hunter, R.H. (1980) The petrology and geochemistry of the Carrock fell gabbro-granophyre complex, Cumbria. *Unpubl. Ph.D. thesis*, Univ. Durham.

Hurai, V. and Horn, E-E (1992) A boundary layer-induced immiscibility in naturally re-requilibrated H_2O-CO_2-NaCl inclusions from metamorphic quartz (Western Carpathians, Czechoslovakia), *Contrib. Min. Petrol.*, **112**, 414-427.

Ineson, P.R. and Mitchell, J.G. (1974) K-Ar isotopic age determinations from some Lake District mineral localities. *Geol. Mag.*, **111**, 521-537.

Inglis, C.E. (1913) Stresses in a Plate due to the Presence of Cracks and Sharp Corners: *R. Inst. of Naval Architects Trans.*, **55**, 219-230.

Ingraffea, A.R. (1987) Theory of crack initiation and propagation in rock. In: *Fracture mechanics of Rock*, (ed. B.K. Atkinson), Academic Press, 71-110.

Ingraffea, A.R. and Gerstle, W. (1984) In: *Application of Fracture Mechanics to Cementitious Composites*, (ed. S.P. Shah), Martinus Nijhoff, The Hague, 171-209.

Isaac, K.P., Turner, P.J. and Stewart, I.J. (1982) The evolution of the Hercynides of central SW England. *J. Geol. Soc. Lond.*, **139**, 521-531.

Ismail, I.A.H. and Murrell, S.A.F. (1976) Dilatancy and the strength of rock containing pore water under undrained conditions. *Geophys. J.R. Astr. Soc.*, **44**, 107-134.

Jackson, N.J., Willis-Richards, J., Manning, D.A.C. and Sams, M.S. (1989) Evolution of the Cornubian Ore Field, Southwest England: Part II. Mineral Deposits and Ore-Forming Processes. *Econ. Geol.*, **84**, 1101-1133.

Jackson, N.J., Halliday, A.N., Sheppard, S.M.F. and Mitchell, J.G. (1982) Hydrothermal activity in the St. Just mining district, Cornwall, England. In: *Metallisation associated with acid magmatism*. (ed. A.M. Evans), Chichester, Wiley, 137-179.

Jackson, D. (1978) The Skiddaw Group. In: *The Geology of the Lake District*, (ed. F. Moseley). *York. Geol. Soc.*, 79-98.

Jackson, N.J. and Rankin, A.H. (1976) Fluid inclusions at St. Michaels Mount. *Proc. Ussher Soc.*, **3**, 430-434.

Jang, B-A., Wang, H.F., Ren, X. and Kowallis, B.J. (1989) Precambrian paleostress from healed microcracks and fluid inclusions in the Wolf River bathoilith of central Wisconsin. *Geol. Soc. Am. Bull.*, **101**, 1457-1464.

Jang, B-A. and Wang, H.F. (1991) Micromechanical Modelling of Healed Crack Orientations as a Paleostress Indicator: Application To Precambrian Granite From Illonois And Wisconsin. *J. Geophys. Res.*, **96**, 19,655-19,664.

Jones, E. (1985) Petrography and geochemistry of fluid inclusions in mineralised granites: applications to exploration. *Unpubl. Ph.D. thesis*, Univ. of London.

Kanaori, Y., Yairi, K. and Ishida, T. (1991) Grain boundary microcracking of granitic rocks from the northeastern region of the Atotsugawa fault, central Japan: SEM backscattered electron images. *Eng. Geol.*, **30**, 221-235.

Knapp, R.B. and Knight, J.E. (1977) Differential thermal expansion of pore fluids: Fracture propagation and microearthquake production in hot pluton environments. *Journal of Geophysical Research*, **82**, 2515-2522.

Knipe, R.J. and White, S.H. (1979) Deformation in low grade shear zones in the Old Red Sandstone, SW Wales. *J. Struct. Geol.* **1**, 53-66.

Kowallis, B.J., Wang, H.F. and Jang, B-A. (1987) Healed microcrack orientations in granite from Illonois borehole UPH-3 and their relationship to the rock's stress history. *Tectonophysics*, **135**, 297-306.

Kranz, R.L. (1979) Crack-crack and crack-pore interactions in stressed granite. *Int. J. Rock. Mech. Min. Sci.*, **16**, 37-47.

Kranz, R.L. (1983) Microcracks in rocks: a review. *Tectonophysics*, **100**, 449-480.

Lake, S.D. and Karner, G.D. (1987) The structure and evolution of the Wessex Basin, southern England: an example of inversion tectonics. *Tectonophysics*, **137**, 347-378.

Laubech, S.E. (1989) Paleostress indicators from the preferred orientation of closed microfractures (fluid-inclusion-planes) in sandstone, east Texas basin, U.S.A. *J. Struct. Geol.*, **11**, 603-611.

Lemmlein, G. (1956) Formation of fluid inclusions and their use in geological thermometry, *Geochemistry*, **6**, 630-642.

Lemmlein, G.G. and Kliya, M.O. (1960) Distinctive features of the healing of a crack in a crystal under conditions of declining temperature. (Transl.), *Int. Geol. Rev.*, **2**, 125-128.

Leroy, J. (1979) Contribution à étalommage de la pression interne des inclusions fluides lors de la décrépitation. *Bull. Mineral. Cristallogr.*, **102**, 584-593.

Lespinasse, M. and Cathelineau, M. (1990) Fluid percolations in a fault zone: a study of fluid inclusion planes in the St. Sylvestre granite, Northwest Massif Central, France. *Tectonophysics*, **184**, 173-187.

Lespinasse, M. and Pêcher, A. (1986) Microfracturing and regional stress field: a study of the preferred orientations of the fluid-inclusion planes in a granite from the Massif Central, France. *J. Struct. Geol.*, **8**, 169-180.

Lespinasse, M., Cathelineau, M. and Poty, B. (1991) Time/space reconstruction of fluid percolation in fault systems: The use of fluid inclusion planes. In: Source, Transport and Deposition of Metals, (eds. Pagel and Leroy), Balkema, Rotterdam, 465-468.

Lockner, D. and Byerlee, J.D. (1977) Hydrofracture in Weber Sandstone at high confining pressures and differential stress. *J. Geophys. Res.*, **82**, 2018-2026.

Lowell, J.D. and Guilbert, J.M. (1970) Lateral and vertical alteration-mineralisation zoning in porphyry ore deposits. *Econ. Geol.*, **65**, 373-408.

Maaskant, P. (1986) Electron probe microanalysis of unopened fluid inclusions, a semiquantitive approach. *Neues Jahrb. Miner.*, **7**, 297-304.

Mandelbrot, B.B. (1983) *The fractal geometry of nature*. W.H. Freeman, New York.

McCaffrey, R., Stewart, S., Dalzell, P., McCaffrey, L. and McElroy, J. (1993) A reconnaissance magnetic survey of the Lundy Tertiary Igneous Complex, Bristol Channel. *Proc. Ussher Soc.*, **8**, 193-197.

McClay, K. and Price, N.J. (1981) *Thrust and Nappe Tectonics*. Special Publication 9. Geological Society London.

Meere, P.A. (1985) High and low density fluids in a quartz vein from the Irish Variscides. *J. Struct. Geol.*, **17**, 435-446.

Miller, J.A. and Fitch, F.J. (1962) Age of the Lundy granites. *Nature*, **195**, 553-555.

Miller, J.A. (1961) The Potassium-argon ages of the Skiddaw and Eskdale Granites. *Geophys. Journ.*, **6**, 391-393.

Millward, D., Moseley, F. and Soper, N.J. (1978) The Eycott and Borrowdale Volcanic Rocks In: *The Geology of the Lake District*, (ed. F. Moseley). *York. Geol. Soc.*, 99-120.

Mitchell, A.H.G. (1974) Southwest England granites: Magmatism and tin mineralisation in a post-collision tectonic setting. *Inst. Min. Metall. Trans.*, **83**, B95-97.

Moorbath, S. (1962) Lead isotope abundance studies on mineral occurrences in the British Isles. *Phil. Trans. R. Soc. Lond.*, **254**, 295-360.

Moore, J.M. (1975) A mechanical interpretation of the vein and dyke systems of the SW England orefield. *Mineral. Deposit.*, **10**, 374-388.

Moore, J.M. and Jackson, N.J. (1977) Structure and mineralisation in the Cligga granite stock, SW England. *J. Geol. Soc. Lond.*, **133**, 467-480.

Moseley, F. (1978) The Geology of the English Lake District: An introductory Review. In: *The Geology of the Lake District*, (ed. F. Moseley). *York. Geol. Soc.*, 1-16.

Mosher, S., Berger, R.L. and Anderson, D.E. (1975) Fracturing charactering of two granites. *Rock Mech.*, **7**, 167-176.

Mussett, A.E., Dagley, P. and Eckford, M. (1976) The British Tertiary Igneous Province: Palaeomagnetism and Ages of Dykes, Lundy Island, Bristol Channel. *Geophys. J. R. astr. Soc.*, **46**, 595-603.

Mussett, A.E., Dagley, P. and Skelhorn, R.R. (1988) Time and duration of the British Tertiary Volcanic Province. In: *Early Tertiary Volcanism and the opening of the NE Atlantic*, (eds. A.C. Morton and L.M. Parson) Geol. Soc. Spec. Pub. **39**, 337-348.

Naylor, M.A., Mandl, G. and Sijpesteijn, C.H.K. (1986) Fault geometries in basement-induced wrench faulting under different initial stress states. *J. Struct. Geol.*, **8**, 737-752.

Norman, T.N. (1961) The geology of the Silurian strata in the Blawith area, Furness. *Unpubl. Ph.D. thesis*, Univ. of Birmingham.

Norton, D.L. (1982) Fluid and heat transport phenomena typical of copper-bearing pluton environments, In *Advances in geology of the porphyry copper deposits*. Tuscon, University of Arizona Press, 59-72.

Nur, A. and Simmons, G. (1970) The origin of small cracks in igneous rocks. *Int. J. Rock. Mech. Min. Sci.*, **7**, 307-314.

Nur, A. and Booker, J.R. (1972) Aftershocks caused by pore fluid flow. *Science*, **175**, 885.

O'Brien, C., Plant, J.A., Simpson, P.R. and Tarney, J. (1985) The geochemistry, metsomitism and petrogenesis of the granites of the English Lake District. *J. Geol. Soc. Lond.*, **142**, 1139-1157.

O'Grady M.R., Bodnar, R.J., Hellgeth, J.W., Conroy, C.M., Taylor, L.T. and Knight, C.L. (1989) Fourier-transform infrared (FITR) microspectrometry of individual petroleum baering fluid inclusions in geological samples. *Microbeam analysis-1989* (ed. P.E. Russell), San Francisco Press Inc., 579-582.

Odin, G.S., Curry, D., Gale, N.H. aand Kennedy, W.J. (1982) The Phanerozoic time scale in 1981. In: *Numerical Dating in Stratigraphy* (ed. G.S.Odin), John Wiley and Sons, Chichester, 957-960.

Okubo, P.G. and Aki, K. (1987) Fractal Geometry in the San Andreas Fault System. *J. Geophys. Res.*, **92**, 345-355.

Olsson, W. and Peng, S. (1976) Microcrack nucleation in marble. *Int. J. Rock Mech. Min. Sci.*, **18**, 53-59.

Paulding, B.W. (1965) Crack growth during brittle fracture in compression, MIT Ph.D. thesis, 184pp.

Pearce, J.A., Harris, N.B.W. and Tindle, A.G. (1984) Trace element discrimination diagrams for the interpretation of granitic rocks. *J. Petrol.*, **25**, 956-983.

Pécher, A. and Boullier, A-M. (1984) Evolution à pression et température élevées d'inclusions dans un quartz synthétique. *Bull Minéral*, **107**, 139-153.

Pécher, A. (1981) Experimental decrepitation and re-equilibration of fluid inclusions in synthetic quartz. *Tectonphysics*, **78**, 567-583.

Pécher, A., Lespinasse, M. and Leroy, J. (1985) Relations between fluid inclusion trails and regional stress field: a tool for fluid chronology - An example of an intragranitic uranium ore deposit (northwest Massif Central, France) *Lithos*, **18**, 229-37.

Peng, S. and Johnson, A.M. (1972) Crack growth and faulting in cylindrical specimens of Chelmsford granite. *Int. J. Rock. Mech. Min. Sci.*, **9**, 37-86.

Phillips, W.J. (1972) Hydraulic fracturing and mineralisation. *J. Geol. Soc. Lond.*, **128**, 337-359.

Phillips, W.J. (1986) Hydraulic fracturing effects in the formation of mineral deposits. *Trans. Instn. Min. Metall.*, **95**, B17-B24.

Plumb, R., Engelder, T. and Yale, D. (1984) Near-Surface in Situ Stress 3. Correlation With Microcrack Fabric Within The New Hampshire Granites. *J. Geophys. Res.*, **89**, 9350-9364.

Pollard, D.D., Segall, P. and Delaney, P.T. (1982) Formation and interpretation of dilatant echelon cracks. *Geol. Soc. Am. Bull.*, **93**, 1291-1303.

Pollard, D.D. (1976) On the form and stability of open hydraulic fractures in the Earth's crust. *Geophysical Research Letters*, **3**, 513-516.

Pollard, D.D. (1987) Elementary Fracture Mechanics Apllied to the Structural Interpretation of Dikes. In: *Mafic dyke swarms*, (eds. H.C. Halls and W.F. Fahrig), Geological Association of Canada, Special Paper 34, 5-24.

Pollard, D.D. and Holzhausen, G. (1979) On the Mechanical Interaction between a Fluid-filled Fracture and the Earth's Surface. *Tectonophysics*, **53**, 27-57.

Price, N.J. and Cosgrove, J.W. (1990) *Analysis of Geological Structures*. Cambridge University Press, 502pp.

Prior, D.J., Knipe, R.J., Bates, M.F., Grant, N.T., Law, R.D., Lloyd, G.E., Welbon, A., Agar, S.M., Brodie, K.H., Maddock, R.H., Rutter, E.H., White, S.H., Bell, T.H., Ferguson, C.C. & Wheeler, J. (1987) Orientations of Specimens: Essential data for all fields of geology. *Geology*, **15**, 829-831.

Ragan, D.M. (1985) *Structural Geolgy: An introduction to geometric techniques, 3rd edn.* Wiley, 393pp.

Ramsay, J.G. (1967) *Folding and fracturing in rocks*. Mcgraw-Hill, New York.

Ramsay, J.G. (1980) The crack-seal mechanism of deformation. *Nature*, **244**, 135-139.

Ramsay, J.G. and Graham, R.H. (1970) Strain variations in shear belts. *Can. J. Earth Sci.* **7**, 786-813.

Ramsay, J.G. and Huber, M.I. (1983) *The Techniques of Modern Structural Geology, Vol. 1, Strain analysis.* Academic Press, London, 307pp.

Ramsay, J.G. and Huber, M.I. (1987) *The Techniques of Modern Structural Geology, Vol. 2, Folds and Fractures.* Academic Press, 700pp.

Rankin, A.H. and Alderton, D.H.M. (1982) Fluid inclusion studies on mineralised granites of the British Isles: an assessment of their use in the exploration for mineral deposits associated with granitic rocks. *Final report, Contract 041 MPP UK,* 168pp.

Rankin, A.H. and Alderton, D.H.M. (1983) Fluid inclusion petrography of SW England granites and its potential in mineral exploration. *Mineral. Deposita,* **18,** 335-347.

Rankin, A.H. and Alderton, D.H.M. (1985) Fluids in granites from southwest England. In:. *High heat production (HHP) granites, hydrothermal circulation and ore genesis.*, London, Inst. Mining Metallurgy, 287-299.

Rankin, A.H. (1988) Fluid Inclusion Steam aureoles associated with Granite-hosted Mineralisation. *Mem. Geol. Soc. India.*, **11,** 45-58.

Rankin, A.H., Ramsey, M.H., Coles, B., Van Langevelde, F. and Thomas, C.R. (1992) The composition of hypersaline, iron-rich granitic fluids based on laser-ICP and Synchrotron-XRF microprobe analysis of individual fluid inclusions in topaz, Mole granite, eastern Australia. *Geochim. Cosmochim. Acta,* **56,** 67-79.

Ren, X., Kowallis, B.J. and Best, M.G. (1989) Paleostress history of the Basin and Range province in western Utah and eastern Nevada from healed microfracture orientations in granites. *Geology,* **17,** 487-490.

Richter, D and Simmons, G. (1974) Thermal Expansion Behaviour of Igneous Rocks. *Int. J. Rock. Mech. Min. Sci.*, **11,** 403-411.

Riedel, W. (1929) Zur Mechanik geologischer Brucherscheinungen. *Zent. Min. Geol. Pal.* **1929,** 354-368.

Roberts, D.E. (1977) The structure of the Skiddaw Slates in the Blencathra-Mungrisdale area, Cumbria. *Geol. J.*, **12,** 33-58.

Roberts, D.E. (1983) Metasomitism and the formation of greisen in Grainsgill, Cumbria, England. *Geol. J.*, **18,** 43-52.

Roberts C.L. and Smith, S.G. (1994) A new magnetic survey of Lundy Island, Bristol Channel. *Proc. Ussher Soc.*, **8,** 293-297.

Robson, G.R. and Barr, K.G. (1964) The effect of stress on faulting and minor intrusions in the vicinity of a magma body. *Bull. Volcanol.*, **27,** 315-330.

Roedder, E (1962) Studies of fluid inclusions I: Low temperature application of a dual-purpose freezing and heating stage. *Econ. Geol.*, **57,** 1045-1061.

Roedder, E. (1981) Origin of fluid inclusions and changes that occur after trapping, In *Fluid Inclusions: Applications to Petrology, Short Course Handbook*, vol. **6**, (eds. E.D. Ghent, L.S. Hollister and M.L. Crawford), pp. 101-137, Mineral Association of Canada, Calgary.

Roedder, E. (1984) *Fluid Inclusions. Reviews in Mineralogy No. 12.* Mineral. Soc. Amer. 644pp.

Roedder, E (1990) Fluid inclusion analysis-Prologue and epilogue. *Geochim. Cosmochim. Acta,* **54,** 495-507.

Rosenfeld, J.L. and Chase, A.B. (1961) Pressure and temperature of crystallisation from clastic effects around solid inclusions in minerals?. *Am. J. Sci.*, **259**, 519-541.

Rundle, C.C. (1979) Ordovician intrusions in the English Lake District. *J. Geol. Soc. Lond.*, **136**, 29-38.

Russell, M.J. (1976) A possible Lower Permian age for the onset of ocean floor spreading in the northern Atlantic. *Scott. J. Geol.*, **12**, 315-323.

Russell, M.J. (1978) Downward excavating hydrothermal cells and Irish-type ore deposits: importance of an underlying thick Caledonian prism. *Trans. Inst. Min. Metall.*, **87**, 168-171.

Savage, W.Z. (1978) The development of residual stress in cooling rock bodies. *Geophys. Res. Lett.*, **5(8)**, 633-636.

Schiffries, C.M. (1990) Liquid-absent, aqueous fluid inclusions and phase eqilibria in the system $CaCl_2$-NaCl-H_2O. *Geochim. Cosmochim. Acta.* **54**, 611-619.

Scholz, C.H. (1968) Microfracturing and inelastic deformation of rock in compression. *J. Geophys. Res.*, **73**, 1417-1432.

Scholz, C.H., Sykes, L.R. and Aggarwal, Y.P. (1973) Earthquake prediction: a physical basis. *Science*, **181**, 803-10.

Scrivener, R.C., Darbyshire, R.T. & Shepherd, T.J. (1994) Timing and significance of cross-course mineralisation in SW England. *J. Geol. Soc. Lond.*, **151**, 587-590.

Secor, D.T. (1965) Role of fluid pressure in jointing. *Am. J. Sci.*, **263**, 633-646.

Secor, D.T. (1968) Mechanics of natural extension functioning at depth in the Earth's crust. *Geol. Surv. Paper Can.*, **Pap., 68**, 52.

Secor, D.T. and Pollard, D.D. (1975) On the stability of open hydraulic fractures in the Earth's crust. *Geophysical Research Letters.* **2**, 510-513.

Segall, P. and Pollard, D.D. (1983) Nucleation and Growth of Strike-Slip Faults in Granite. *J. Geophys. Res.* **88**, 555-568.

Seitz, J.C., Pasteris, J.D. and Wopenka, B. (1987) Characterisation of CO_2-CH_4-H_2O fluid inclusions by microthermometry and laser Raman spectroscopy: Inferences for clathrate and fluid equlibria. *Geochim. Cosmochim. Acta.*, **51**, 1651-1664.

Seitz, J.C. and Pasteris, J.D. (1990) Theoretical and practical aspects of differential partitioning of gases by clathrate hydrates in fluid inclusions. *Geochim. Cosmochim. Acta.*, **54**, 631-639.

Selwood, E.B. (1990) A reveiw of basin development in central south-west England. *Proc. Ussher Soc.*, **7**, 199-205.

Sengör, A.M.C., Görür, N. and Saroglu, F. (1985)Strike-slip faulting and related basin formation in zones of tectonic escape: Turkey as a case study. In: *Strike-Slip Deformation, Basin Formation and Sedimentation* (eds. K.T. Biddle and N. Christie-Blick). Society of Economic Palaeontologists and Mineralogists Special Publication, **37**, 227-264.

Shackleton, R.M., Ries, A.C. and Coward, M.P. (1982) An interpretation of Variscan structures in SW England. *J. Geol. Soc. Lond.*, **139**, 533-541.

Shail, R.K. and Wilkinson, J.J. (1994) Late- to post-Variscan extensional tectonics in south Cornwall. *Proc. Ussher Soc.*, **8**, 262-270.

Shearman, D.J. (1967) On Tertiary Fault Movements in North Devonshire. *Proc. Geol. Assoc.*, **78**, 555-566.

Shelton, K.L. and Orville, P.M. Formation of synthetic fluid inclusions in natural quartz. *American Mineralogist*, **65**, 1233-1236.

Shepherd, T.J. (1990) Geological link between fluid inclusions, dilatant microcracks and the paleostress field. *J. Geophys. Res.*, **95**, 11,115-11,120.

Shepherd, T.J., Miller, M.F., Scrivener, R.C. and Darbyshire, D.P.F. (1985) Hydrothermal fluid evolution in relation to mineralisation in Southwest England with special reference to the Dartmoor-Bodmin area. In:. *High heat production (HHP) granites, hydrothermal circulation and ore genesis.*, London, Inst. Mining Metallurgy, 345-364.

Shepherd, T.J. and Scrivener, R.C. (1987) Role of basinal brines in the genesis of polymetallic vein deposits, Kit Hill - Gunnislake area, SW England. *Proc. Ussher. Soc.*, **6**, 491-497.

Shepherd, T.J., Beckinsale, R.D., Rundle, C.C. and Durham, J. (1976) Genesis of Carrock Fell tungsten deposits, Cumbria: fluid inclusion and isotopic study. *Trans. Inst. Min. Metall.*, **85**, 63-73.

Shepherd, T.J. and Waters, P. (1984) Fluid Inclusion Gas Studies, Carrock Fell Tungsten Deposit, England: Implications for Regional Exploration. *Mineral. Deposita*, **19**, 304-314.

Shepherd, T.J. and Chenery, S.R. (1993) Chemical characterisation of single inclusions by laser ablation microprobe-inductively coupled plasma-mass spectrometry (abstr), ECROFI XII, 194.

Shepherd, T.J., Rankin, A.H. and Alderton, D.H.M. (1985) *A Practical Guide to Fluid Inclusion Studies*. Blackie and Son, Glasgow.

Sheppard, S.M.F. (1977) The Cornubian Batholith, Southwest England: D/H and $^{18}O/^{16}O$ studies of kaolinite and other alteration minerals. *J. Geol. Soc. Lond.*, **133**, 573-591.

Sibson, R.H. (1981) Fluid flow accompanying faulting: field evidence and models. In: *Earthquake prediction: an International Review*, (eds. D.W. Simpson and P.G. Richards). *Am. Geophys. Union Mon., Maurice Ewing Series* **4**, 593-603.

Sibson, R.H. (1990) Faulting and fluid flow. In: *MAC Short Course on Crustal Fluids* (ed. B.E. Nesbitt), **18**, 93-132.

Sibson, R.H., Moore, J. McM. and Rankin, A.H. (1975) Siesmic pumping-a hydrothermal fluid transport mechanism. *J. Geol. Soc. Lond.*, **131**, 653-659.

Sibson, R.H. (1988) High-angle reverse faults, fluid pressure cycling and mesothermal gold-quartz deposits. *Geology*, **16**, 551-555.

Simmons, G. and Richter, D. (1976) Microcracks in rock. In: *The Physics and Chemistry of Minerals and Rocks*. (ed. R.G.J. Strens) Wiley, New York. 105-137.

Simpson, P.R., Brown, G.C., Plant, J. and Ostle, D. (1979) Uranium mineralisation and granite magmatism in the British Isles. *R. Soc. Lond. Phil. Trans.*, **A291**, 385-412.

Smith, D.L. and Evans, B. (1984) Diffusional crack healing in quartz. *J. Geophys. Res.*, **89**, 4125-4135.

Soper, N.J. and Moseley, F. (1978) Structure. In: *The Geology of the Lake District*, (ed. F. Moseley). *York. Geol. Soc.*, 45-67.

Speight, J.M., Skelhorn, R.R., Sloan, T., Knapp, R.J. (1982) The dyke swarms of Scotland. In: *Igneous Rocks of the British Isles*, (ed. D.S. Sutherland), John Wiley and Sons, 449-459.

Spetzler, H. and Mizutani, H. (1987) Predicting failure in rocks and its implications for predicting earthquakes. *Tectonophysics*, **138**, 109-113.

Sprunt, E.S. and Nur, A. (1979) Microcracks and healing in granites: New evidence from cathodoluminescence. *Science*, **205**, 495-497.

Stanley, C.J. and Vaughan, D.J. (1982) Copper, lead, zinc and cobalt mineralisation in the English Lake District: classification, conditions of formation and genesis. *J. Geol. Soc. Lond.*, **139**, 569-579.

Stanley, C.J. (1979) Mineralogical studies of copper, lead, zinc and cobalt mineralisation in the English Lake District. *Unpubl. Ph.D. thesis*, Univ. of Aston.

Sterner, S.M. (1990) An *in situ* fracturing procedure for fluid inclusion synthesis. (*Abstr.*) PACROFI III, p85.

Sterner, S.M. (1994) Kinetics of crack healing and fluid inclusion trapping in minerals. *Fifth Pan-Amer. Conf. on Research on Fluid Inclusions*, 104.

Sterner, S.M. and Bodnar, R.J. (1986) Re-equilibration of fluid inclusions in quartz at elevated temperatures and pressures: The role of H_2O diffusion (abstr.). *Transactions of the American Geophysical Union*, **67**, 407.

Sterner, S.M. and Bodnar, R.J. (1989) Synthetic fluid inclusions-VII. Re-equilibration of fluid inclusions in quartz during laboratory-simulated metamorphic burial and uplift. *J. Metamorphic Geol.*, **7**, 243-260.

Sterner, S.M., Hall, D.L. and Bodnar, R.J. (1988) Post-entrapment compositional changes in fluid inclusions: Experimental evidence for water diffusion in quartz. *Geological Society of America Abstracts with Programs*, **20**, 100.

Stone, M. (1990) The Lundy granite: a geochemical and petrogenetic comparison with Hercynian and Tertiary granites. *Min. Mag.*, **54**, 431-446.

Strömgård, K.E. (1973) Stress distribution during formation of boudinage and pressure shadows. *Tectonphysics*, **16**, 215-248.

Sylvester, A.G. (1988) Strike-slip faults. *Geol. Soc. Am. Bull.*, **100**, 1666-1703.

Tapponier, P. and Brace, W.F. (1976) Development of stress-induced microcracks in Westerlt Granite. *Int. J.Roch Mech. Min. Sci.*, **13**, 103-112.

Taylor, H.P. and Forester, R.W. (1971) Low-^{18}O igneous rocks from the intrusive complexes of Skye, Mull, and Ardnamurchan, western Scotland. *J. Petrol.*, **12**, 465-497.

Tchalenko, J.S. (1970) Similarities between shear zones of different magnitudes. *Bull. Geol. Soc. Am.*, **81**, 1625-1640.

Tchalenko, J.S. and Ambraseys, N.N. (1970) Structural analysis of the Dasht-e-Bayaz (Iran) earthquake fractures. *Geol. Soc. Am. Bull.*, **81**, 41-60.

Teufel, L.W. (1981) Pore volume changes during frictional sliding of simulated faults. In: *Mechanical Behviour of Crustal Rocks, The Handin Volume. Am. Geophys. Un. Geophys. Monogr.*, **24**, 135-145.

Thomas, A.L. and Pollard, D.D. (1993) The geometry of echelon fractures in rock: implications from laboratory and numerical experiments. *J. Struct. Geol.*, **15**, 323-334.

Thorpe, R.S. and Tindle, A.G. (1992) Petrology and Petrogenesis of a Tertiary bimodal dolerite-peralkaline/subalkaline trachyte/rhyolite association from Lundy, Bristol Channel, UK. *Geological Jour.*, **27**, 101-117.

Thorpe, R.S., Tindle, A.G. and Gledhill, A. (1990) The Pertrology and Origin of the Tertiary Lundy Granite (Bristol Channel, UK). *J. Petrol.* **31,** 1370-1406.

Titley, S.R. and Beane, R.E. (1981) Porphyry copper deposits. *Econ. Geol.*, **75th Anniv. Vol.,** 214-269.

Titley, S.R. (1982) *Advances in Geology of the Porphryr Copper Deposits, South-western North America.* Tuscon: Univ. Ariz. Press, 560pp.

Touret, J. (1981) Fluid inclusions in high grade metamorphic rocks. In: *Fluid Inclusions: Applications to Petrology Short Course Handbook, vol. 6.* (eds. E.D. Ghent, L.S. Hollister and M.L. Crawford). Mineral Association of Canada, Calgary, 182-208.

Turcotte, D.L. (1992) *Fractals and Chaos in Geology and Geophysics.* Cambridge University Press, Cambridge.

Turner, P.J. (1984) Hercynian high-angle fault zones between Dartmoor and Bodmin Moor. *Proc. Ussher Soc.* **6,** 60-67.

Turner, F.J. and Wiess, L.E. (1963) Structural analysis of metamorphic tectonites. McGraw Hill, 545pp.

Tuttle, O.F. (1949) Structural petrology of planes of liquid inclusions. *J. Geol.*, **57,** 331-356.

van den Kerkhof, A.M. and Behr, H.-J. (1994) Cathodoluminescence studies of quartz as a tool for the interpretation of fluid inclusion transposition. *Abstract,* PACROFI V, Mexico, 108.

Van der Molen, I. (1981) The shift of the α-β transition temperature of quartz associated with the thermal expansion of granite at high pressure, *Tectonophysics,* **73,** 323-342.

Van Hise, C.R. (1890) Pre-Cambrian of the Black Hills. *Geol. Soc. Am. Bull.*, **1,** 216-218.

Van Hoorn, B. (1987) The South Celtic Sea/Bristol Channel Basin: origin, deformation and inversion history. *Tectonophysics,* **137,** 309-334.

Van Reenen, D.D., Pretorius, A.I. and Roering, C. (1994) Characterisation of fluids involved with gold mineralisation and with regional high-temperature retrogression of granulites in the Limpopo Belt, South Africa. *Geochim. Cosmochim. Acta.*

Vaughan, P.J., Moore, D.E., Morrow, C.A. and Byerlee, J.D. (1986) Role of Cracks in Progressive Permeability Reduction During Flow of Heated Aqueous Fluids Through Granite. *J. Geophys. Res.*, **91,** 7517-7530.

Vityk, M.O., Bodnar, R.J. and Schmidt, C.S. (1994) Fluid inclusions as tectonothermobarometers: Relation between pressure-temperature history and re-equilibration morphology during crustal thickening. *Geology,* **22,** 731-734.

Voight, B. and St. Pierre, B.H.P. (1974) Stress history and rock stress. In: *Advances in Rock Mechanics.* International Society for Rock Mechanics, Denver, Colarado, 580-582.

Vollbrecht, A., Rust, S. and Weber, K. (1991) Development of microcracks in granites during cooling and uplift: examples from the Variscan basement in NE Bavaria, Germany. *J. Struct. Geol.*, **13,** 787-799.

Vry, J., Brown, P.E., Kyle, P. and Zhang, Z. (1987) Application of micro-FITR spectroscopy to the study of fluid inclusions (abstr), *Eos,* **68,** 1538.

Wadge, A.J., Gale, N.H., Beckinsale, R.D. and Rundle, C.C. (1978) A Rb-Sr isochron age for the Shap Granite. *Proc. York. Geol. Soc.*, **42,** 297-305.

Wallace, S.R. (1991) Model development: porphyry molybdenum deposits. *Econ. Geol.*, **8**, 207-224

Walsh, J.J. and Watterson, J. (1993) Fractal analysis of fracture patterns using the standard box-counting technique: valid and invalid methodologies.

Walsh, J.J., Watterson, J. and Yeilding, G. (1991) The importance of small-scale faulting in regional extension. *Nature*, **351**, 391-393.

Wang, H.F. and Heard, H.C. (1985) Prediction of elastic moduli via crack density in pressurised and thermally stressed rock. *J. Geophys. Res.*, **90**, 10,342-10,350.

Wang, H.F., Bonner, P.B., Carlson, S.R., Kowallis, B.J. and Heard, H.C. (1989) Thermal Stress Cracking in Granite. *J. Geophys. Res.*, **94**, 1745-1758.

Ward, C.D., McArthur, J.M. and Walsh, J.N. (1992) Rare earth element behaviour during evolution and alteration of the Dartmoor granite, SW England. *J. Petrol.*, **33**, 785-815.

Warr, L.N. (1988) The deformational history of the area north-west of the Bodmin Moor granite, north Cornwall. *Proc. Ussher Soc.*, **7**, 67-72.

Watson, J.V., Fowler, M.B., Plant, J.A. and Simpson, P.R. (1984) Variscan and Caledonian comparisons: Late orogenic granites. *Proc. Ussher Soc.*, **6**, 2-12.

Wilkins, R.W.T. and Barkas, J.P. (1978) Fluid Inclusions, Deformation and Recrystallization in Granite Tectonites. *Contrib. Mineral. Petrol.*, **65**, 293-299.

Willis-Richards, J. and Jackson, N.J. (1989) Evolution of the Cornubian Orefield, Southwest England: Part I. Batholith Modeling and Ore Distribution. *Econ Geol.*, **84**, 1078-1100.

Wise, D.U. (1964) Microjointing in basement, middle Rocky Mountains of Montana and Wyoming. *Geol. Soc. Amer. Bull.*, **75**, 287-306.

Woodcock, N.H. and Fischer, M. (1986) Strike-slip duplexes. *J. Struct. Geol.* **8**, 725-736.

Wu, C.Cm., Freiman, S.W., Rice, R.W. and Mecholsky, J.J. (1978) Microstructural aspects of crack propagation in ceramics. *J. Mater. Sci.*, **13**, 2659-2670.

Yielding, G., Walsh, J.J. and Watterson, J. (1992) The prediction of small-scale faulting in reservoirs. *First Break*, **10**, 449-460.

Ziegler, P.A. (1987a) Evolution of the Western Approaches Trough. *Tectonophysics*, **137**, 341-346.

Ziegler, P.A. (1987b) Compressional intra-plate deformations in the Alpine foreland - an introduction. *Tectonophysics*, **137**, 1-5.

Ziegler, P.A. (1987c) Celtic Sea - Western Approaches area: an overview. *Tectonophysics*, **137**, 285-289.